Seabed scour around marine structures in mixed and layered sediments

Ms Kate Emily Porter

UCL

EngD

I, Kate Emily Porter confirm that the work presented in this thesis is my own. Where information has been derived from other sources, I confirm that this has been indicated in the thesis.

Signed,

Kate Porter

Kate Porter

Abstract

The inherent uncertainty in the prediction of seabed scour depth at offshore structures such as wind turbines is currently a significant barrier to realising optimised, cost effective foundation design. One significant aspect thought to contribute to this uncertainty which has not been extensively studied is the variation in the sediment properties in the marine environment where sediment beds often consist of complex mixtures of materials stratified with depth.

This research project encompasses the design and execution of an extensive laboratory study investigating this aspect of the scour problem. Two uniformly graded sands were used to build a range of simplified mixed and layered sediment beds, as a first step to improving understanding of scour behaviour in these situations. A variety of hydrodynamic conditions including unidirectional current, tidal and wave-current flows were tested to ensure relevance to the marine environment. As part of the experiment design a detailed review of scour measurement techniques was conducted leading to the implementation of a photogrammetry system which delivered high resolution, high accuracy scour hole profiles.

This study has led to a number of original results. In a layered bed of fine sand overlying coarse sand interaction effects at the grain scale resulted in an enhancement of scour depth in the underlying coarse sand. Bimodally distributed mixed sands were found to alter significantly the scour time development curve. Novel scour tests under a spring-neap tidal cycle in the clear water regime indicated a considerable lengthening of the time to equilibrium. A review of prediction methodologies was undertaken and modifications proposed to take into account the research outcomes.

This project has demonstrated that the configuration of the sediment bed is highly influential on scour development, and will contribute towards the future development of more sophisticated design models for implementation in industry.

Index

List of tables

List of figures

Section 2

Section 4

Section 6

Figure 6.8 Comparison of layered and uniform sand tests under unidirectional current in the small flume, fine over coarse sand layered test with 55 mm upper layer thickness.

Figure 6.9 Comparison of layered and uniform sand tests under unidirectional current in the small flume, fine over coarse sand layered test with 40 mm upper layer thickness.

Figure 6.10 Comparison of fine over coarse sand layered bed and uniform sand tests under unidirectional current in the small flume, T-1 test series, 40 mm pile, V=19.2 cm/s.

Figure 6.11 Comparison of fine over coarse sand layered bed and uniform sand tests under unidirectional current in the coastal flume, V=24.1 cm/s.

Figure 6.12 Comparison of fine over coarse sand layered bed and uniform sand tests under unidirectional current in small flume with no scour enhancement in the lower coarse sand layer, V=19.2 cm/s, 40 mm pile.

Figure 6.13 Comparison of fine over coarse sand layered bed and uniform sand tests under unidirectional current in small flume with no scour enhancement in the lower coarse sand layer, 40 mm pile.

Figure 6.14 Quasi-equilibrium scour depth versus upper layer thickness in the layered (fine sand overlying coarse sand) and uniform sand tests under unidirectional current.

Figure 6.15 Comparison of scour development in uniform fine and coarse sands with a layered bed of coarse sand overlying fine sand under unidirectional current in the small flume, V=25.3 cm/s, 40mm pile.

Figure 6.16 Layered beds with three sand layers, 40-10-50 mm thick, plotted alongside the uniform fine and coarse sand tests under unidirectional current in the small flume, with 40 mm pile.

Figure 6.17 Comparison of fine-coarse-fine sand layered test with superposed fine and coarse sand curves for the relevant layers (under unidirectional current in the small flume).

Figure 6.18 Comparison of coarse-fine-coarse sand layered test with superposed fine and coarse sand curves for the relevant layers (under unidirectional current in the small flume).

Figure 6.19 Unidirectional current scour tests in the small flume in fine-coarse mixed sand beds, with 40 mm pile.

Figure 6.20 Unidirectional current scour tests in the small flume in fine-coarse mixed sand beds, test series T-1, 40mm pile, 19.2 cm/s.

Figure 6.21 Unidirectional current scour tests in the coastal flume in 50%-50% fine-coarse sand mixed bed.

Figure 6.22 Quasi-equilibrium scour depth plotted against percentage of fine sand in the fine-coarse mixed beds under unidirectional current, with uniform coarse and fine sands plotted at 0% and 100% respectively.

Section 7

Appendix 2

Appendix 3

Appendix 4

Nomenclature

Length Parameters

D	Pile diameter
h	Water depth
H	Wave height
A	Amplitude of wave orbital motion at bed
λ	Wavelength
A_s	Cross-sectional area of structure
A_f	Cross-sectional area of flume
B	Flume width
L_u	Upper layer thickness in layered sand bed
S	Scour depth
S_e	Equilibrium scour depth
S_{qe}	Quasi-equilibrium scour depth
$S_{e,m}$	Equilibrium scour depth in mixed sand
$S_{e,uc}$	Equilibrium scour depth in uniform coarse sand
$S_{e,layered}$	Equilibrium scour depth in layered sand bed (fine sand overlying coarse sand)
$S_{e,Ll}$	Equilibrium scour depth that would be reached in a uniform bed of the lower layer sand type from a two-layered bed
$S_{e,Lu}$	Equilibrium scour depth that would be reached in a uniform bed of the upper layer sand type from a two-layered bed
S_c	Scour depth under the current component in wave-current flow
S_f	Final scour depth recorded i.e. at end of test run time
$S(t)$	Scour depth as a function of time

Time Parameters

t	Time
t_e	Time to equilibrium scour depth
t_{qe}	Time to quasi-equilibrium scour depth
T_c	Characteristic scour timescale
$T_{c,current}$	Characteristic scour timescale in current
$T_{c,waves}$	Characteristic scour timescale in waves
T^*	Non-dimensional scour timescale
T	Wave period
t_B	Time at which $S/D = A_2 S_e/D$

Flow Parameters

V	Depth averaged streamwise ambient flow velocity
V_{cr}	Critical depth averaged velocity for sediment entrainment
V_a	Critical velocity for bed armour layer
V_{lp}	Velocity required for peak equilibrium scour depth in live bed regime
U_{bed}	Near-bed velocity
U_m	Maximum bottom orbital velocity in waves
U_c	Depth-averaged streamwise velocity of current component in combined wave-current flow
U_{cw}	Representative streamwise velocity in combined wave-current flow
U_w	Depth-averaged streamwise velocity in waves
$u(z)$	Streamwise velocity as a function of depth
u^*	Shear velocity
u^*_{cr}	Critical shear velocity for sediment entrainment
τ	Bed shear stress
τ_{cr}	Critical bed shear stress for initiation of sediment motion
τ_{max}	Maximum bed shear stress
τ_{mean}	Mean bed shear stress
τ_{wave}	Bed shear stress in waves
$\tau_{current}$	Bed shear stress for current component in wave-current flow
C_D	Drag coefficient
f_w	Wave friction factor
C_r	Wave reflection coefficient
ø	Angle between wave and current directions in wave-current flow

Sediment parameters

d_{50}	Median grain size
d_{10}	Grain size at which 10% of particles are smaller
d_{90}	Grain size at which 90% of particles are smaller
d_{84}	Grain size at which 84% of particles are smaller
d_{16}	Grain size at which 16% of particles are smaller
d_{60}	Grain size at which 60% of particles are smaller
d_{95}	Grain size at which 95% of particles are smaller
d_5	Grain size at which 5% of particles are smaller
d_{25}	Grain size at which 25% of particles are smaller
d_{75}	Grain size at which 75% of particles are smaller
d_{95}	Grain size at which 95% of particles are smaller

d_{99}	Grain size at which 99% of particles are smaller
d_{85}	Grain size at which 85% of particles are smaller
φ	Angle of repose of sediment
D_{cfm}	Sediment coarseness factor
σ_g	Geometric standard deviation of sediment grain size distribution
C_u	Sediment uniformity coefficient
θ	Shields parameter
θ_{crit}	Critical Shields parameter for incipient motion of sediment
K_{mob}	Sediment mobility number
w_s	Sediment fall velocity
D^*	Dimensionless grain size
ρ_b	Bulk density
ρ_s	Sediment density
$s(=\rho_s/\rho)$	Relative density (specific gravity)
z_0	Roughness length

Non-dimensional parameters

V/V_{cr}	Flow intensity
h/D	Flow shallowness
S/D	Non-dimensional scour depth
S_e/D	Non-dimensional equilibrium scour depth
S_e/D_{pred}	Non-dimensional equilibrium scour depth obtained from prediction equation
S_e/D_{exp}	Non-dimensional equilibrium scour depth measured from experiment
Z	Relative scour depth
Re	Reynolds number
Re_λ	Boundary layer Reynolds number
Re_D	Pile Reynolds number
Fr	Froude number
F_d	Densimetric Froude number
F_{di}	Inception densimetric Froude number for initiation of clear water scour
F_{dt}	Threshold densimetric Froude number for initiation of live bed scour
KC	Keulegan-Carpenter number
KC_{wc}	KC number for combined wave-current flow
KC_{wave}	KC number of the wave component in wave-current flow
D/λ	Diffraction parameter

Constants

g	Gravitational acceleration
υ	Kinematic viscosity
κ	Von Karman constant
ρ	Fluid density

Empirical coefficient or curve fitting coefficient

A_1, A_2	Empirical coefficient or curve fitting coefficient
a_1, a_2, a_3, a_4	Empirical coefficient or curve fitting coefficient
K_1, K_2, K_3, K_4	Empirical coefficient or curve fitting coefficient
K_A	Empirical coefficient or curve fitting coefficient
n	Empirical coefficient or curve fitting coefficient
P_1, P_2	Empirical coefficient or curve fitting coefficient
K_v,	Empirical factor to account for flow intensity
K_h	Empirical factor to account for flow depth
K_{hD}	Empirical factor to account for flow shallowness
K_d	Empirical factor to account for sediment size
K_σ	Empirical factor to account for sediment gradation
K_s	Empirical factor to account for pier shape (=1 for cylindrical pile)
K_α	Empirical factor to account for pier alignment (=1 for cylindrical pile)
K_G	Empirical factor to account for channel geometry (=1 for cylindrical pile)
K_t	Empirical factor to account for scour timescale

Echosounder Nomenclature

β	Beamwidth for circular transducer
d	Sensor diameter

Permeabiilty Nomenclature

k	Coefficient of permeability
A_x	Cross-sectional area of test section
a_x	Cross-sectional area of standpipe in falling head permeameter test
L	Length of test section in constant head permeameter test
h_0	Initial head level in falling head permeameter test
h_1	Final head level in falling head permeameter test
q	Flow rate
Δh	Head difference in constant head permeameter test

Photogrammetry Nomenclature

$\mathbf{X}_A$	3D coordinates of the object points

$\mathbf{X}_o$	3D coordinates of the camera position
μ	Scaling factor
$\mathbf{x}_a$	2D coordinates of points in the image plane
c	Principle distance
R	Rotation matrix
ω, ϕ, κ	Rotation angles about the x, y and z axes respectively
xideal, yideal	Theoretical coordinates of a point in the image plane
xmeas, ymeas	Actual coordinates of a point in the image plane
δr_x, δr_y	Radial lens distortions in x and y directions
δt_x, δt_y	Tangential lens distortions in x and y directions
a_o	Orthogonality factor
a_a	Affinity factor

List of publications for the project

Porter, K., Harris, J., Simons, R., 2015. Discussion of "Time Development of Scour around a Cylinder in Simulated Tidal Currents" by David J. McGovern, Suzana Ilic, Andrew M. Folkard, Stuart J. McLelland, and Brendan J. Murphy. Journal of Hydraulic Engineering, 141(7).

Porter, K., Simons, R. and Harris, J., 2014. Comparison of three techniques for scour depth measurement: photogrammetry, echosounder profiling and a calibrated pile. 34th International Conference on Coastal Engineering, 15th-20th June, Seoul, Korea.

Porter, K., Harris, J. and Simons, R., 2014. Laboratory investigation of scour development through a spring-neap tidal cycle. 7th International Conference on Scour and Erosion, 2-4th December, Perth, Australia.

Ferradosa, T., Taveira-Pinto, F., Neves, L., Simons, R. and Porter, K., 2014. Scour around marine foundations in layered sediments: a mathematical modelling approach. 3rd IAHR Europe Congress, Porto, Portugal.

Harris, J., Whitehouse, R., Porter, K. and Simons, R., 2013. Scour development through time: modelling scour in layered soils. ASME 2013 32nd International Conference on Ocean, Offshore and Arctic Engineering, Volume 5: Ocean Engineering, 9-14th June, Nantes, France.

Green, J., Davies, A., Bowers, D., Zhu, F., Ward, S. and Porter, K., 2013. Briefing: Young Coastal Scientists and Engineers Conference 2012. Proceedings of the ICE – Maritime Engineering, 166(3).

Porter, K., Simons, R. and Harris, J., 2012. Scour development in layered sediments – a laboratory study. 6th International Conference on Scour and Erosion, 29-31st August, Paris, France.

Porter, K., Harris, J., Simons, R. and Ferradosa, T., 2012. Scour development in complex sediment beds. 33rd International Conference on Coastal Engineering, 1-6th July, Santander, Spain.

Acknowledgments

Thanks very much to the EPSRC and HR Wallingford for funding this research project. Many thanks to Prof. Richard Simons (UCL) and Dr. John Harris (HR Wallingford) who provided excellent supervision of the research. A special thanks also to Leslie Ansdell for his invaluable help with numerous aspects of the laboratory tests and to Keith Harvey and all those in the technical team who helped with preparing the model, installing (and removing) the false bed for each experimental programme and for helping me with the painful task of moving 1.5 tonnes of sand for each change of bed condition!

1. Introduction

This research project initiated from industry recognition of the need to better understand scour in the marine environment. The project was jointly funded by HR Wallingford and the EPSRC and therefore took its initial direction from discussion with HR Wallingford to ascertain core areas in which research would be particularly beneficial for the design of offshore structures.

Fundamentally, this project is concerned with improving understanding of the scour process around marine structures. While this research is relevant to a range of structures, particular attention is given to the application to offshore wind turbine monopile foundations in order to align with the current priority in industry. As will be shown in the literature review, Section 2, there is a gap in existing research regarding the effect of mixed and layered sediment beds on scour time development and maximum scour depth. Heterogeneous sediment beds consisting of sand mixtures with a range of grain sizes or with grain size stratification with depth are commonly encountered in the field (see Section 2.5) yet research has predominantly focused on scour in uniformly graded sand beds (see Section 2.2). This project aims to address this gap in the research by conducting an extensive laboratory investigation of scour in mixed and layered sand beds under a range of hydrodynamic conditions applicable to the marine environment.

The thesis begins by introducing the scour topic, and the context and motivations for the research, before presenting the research question in Section 1.3. The literature review follows in Section 2 in which the core knowledge is outlined and the gaps in the research are identified in order to inform the specifics of this project. A detailed breakdown of the research question is then given in Section 3 based on the conclusions from the literature review, and the project scope and limitations are defined. The methodology for the project is presented in Section 4 detailing the experimental design and some preliminary tests; the full test programme is provided in Section 5. The main findings of the laboratory study are presented in Section 6. A more in-depth discussion of the results follows in Section 7. The results are first compared with existing knowledge before a physical understanding of the novel results is developed, and an assessment is made of the suitability of existing prediction equations in light of the new findings. An evaluation of the methodology is included in Section 7.4 and recommendations for future work are given in Section 7.5. Concluding statements are delivered in Section 8.

1.1 Background

Scour occurs at structures situated in flowing water where there is potential for seabed sediments to be eroded. The presence of the structure results in changes to the flow patterns in its vicinity, causing an increase in shear stress at the seabed, providing the necessary force to entrain sediment particles from the seabed local to the foundation of the structure. Over time as more sediment is transported downstream a scour hole forms at the base of the structure. This can have severe consequences for the stability of the structure due to exposure or undermining of the foundation leading to structural failure in extreme cases with substantial associated financial losses as well as potentially loss of life. Failures of bridge structures due to scour have

been numerous, see Prendergast and Gavin (2014) for a more detailed review and Coleman and Melville (2001) for examples of bridge failures due to scour in New Zealand. For deep monopile foundations even if stability is not affected, the fatigue life of the structure may be significantly reduced (Van Der Tempel et al., 2004), resulting in further expenditure on maintenance and remedial measures.

Scour occurs at many types of structures in rivers and coastal environments. Scour at bridge piers has been studied quite extensively, the findings from which will be presented in Section 2.2 of the literature review, also see Melville (2008) for a review of bridge scour. However, more recently the focus has turned to scour in the coastal environment due to the increasing number of projects relating to installation of offshore wind turbine structures in these areas. The relatively shallow water depths, highly dynamic flows and often sandy seabeds have meant that scour has been prevalent at many farms (see Section 2.5 for further details).

Currently two methods are used to mitigate scour. The foundation can be designed to take into account the likely depth of scour, i.e. make the foundation deeper, or scour protection can be placed at the structure e.g. rock armour. However, both methods add considerable expense to the project. The latter has also had a limited success rate, due to a variety of failure mechanisms (see Chiew, 2008; De Vos et al., 2011; Whitehouse et al., 2011; Sumer and Nielsen, 2013). Scour protection can be laid prior to scouring or once a scour hole has formed. In both cases secondary scour can occur around the edge of the protection which may affect its stability and fitness for purpose. One way to reduce secondary scour around backfilled armour material is to ascertain the volume of armour required to just fill the scour hole. However, this requires accurate knowledge of the scour depth at a given time at the structure. Knowledge of the maximum scour depth at the structure is also required to size appropriately the foundation if no scour protection measures are used. The scour depth that will occur at the structure must be known with high certainty to avoid overdesign of the foundation, or conversely under-design of the foundation, both of which add considerable cost to the project.

Unfortunately existing approaches for scour prediction do not enable a high level of accuracy to be achieved in many cases, severely limiting the optimisation of foundation design. Modelling the scour process in the marine environment is particularly difficult due to the complex nature and high variability of the flow conditions imposed by waves, storms and tidal flows, as well as complexities in the seabeds which often consist of highly variable material (see literature review Section 2.5 for further details). Scour models have been predominantly based on simplified laboratory testing of scour around basic structure shapes, in uniform sands and under constant unidirectional flow, so conditions that are more realistic for the marine environment have not yet been fully incorporated into the equations (see Section 2.6).

The scour process has proven difficult to model even under simplified conditions because it involves fluid-structure-sediment interaction. This makes it a multidisciplinary problem, drawing on areas such as hydrodynamics, sediment transport and soil mechanics. Limitations in these fields feed into the scour problem; an example of this is the empirical nature of sediment

transport modelling. Furthermore, there are a substantial number of variables affecting the scour process. The individual effects of these on the scour process can be difficult to separate and additional interaction effects between sets of variables add further complexity for modelling. Fluid-structure-sediment interaction is difficult to model numerically because of the linkages between fluid-structure and fluid-sediment models and the requirement for continual updating of boundary conditions as the scour hole develops.

Further research to improve understanding of scour and to begin to understand the effects that more complex conditions have on the scour process would lead to a reduction in uncertainty in the prediction of scour, enabling greater optimisation of foundation design and considerable cost savings.

Reduction in project costs is particularly important for the offshore wind energy industry because of the need to compete with more traditional, cost effective technologies such as oil and gas.

1.2 Context

Now that the problem and research motivations have been introduced this section identifies the wider context of the research. The relevance and impact of the research is highlighted through discussion of the offshore wind energy industry.

The offshore wind energy industry has grown rapidly in the last decade, particularly in Europe. The UK is currently the world leader in offshore wind energy, with 4 gigawatts installed capacity (The Crown Estate, 2015). This has stemmed from the setting of targets for reduction in carbon emissions in the EU and UK, with key milestones to be achieved in 2020 (DECC, 2011) and through to 2030 (European Commission, 2014). Wind energy has been identified as a key sector for meeting these targets, because it is one of the more developed and proven renewable technologies. Offshore wind has significant political advantages over onshore wind because it avoids noise and visual pollution. Furthermore, the wind climate is generally superior offshore where wind speeds are higher and more stable (Estaban et al., 2011; Bilgili et al., 2011). The lack of space and noise constraints offshore enables bigger, more efficient turbines to be built. However, offshore deployment is considerably more expensive than land-based construction, and so finding ways to reduce costs in these projects is imperative to achieving cost competitiveness with other technologies and to reduce the reliance of the industry on government incentives (see Green and Vasilakos, 2011 for more information on the economics of offshore wind).

In the UK, 3 phases of offshore wind turbine deployments have been organised. Stages 1 and 2 are now operational. Phase 3 deployments are mostly in the planning phase, but some have been consented and are due to start construction as early as 2016. Phase 3 sites will be considerably bigger in scale as well as located further offshore (see RenewableUK, 2015 for further details). Offshore wind energy is concurrently rapidly developing in Northern Europe,

particularly in Germany and Denmark (EWEA, 2015). Interest in offshore wind is also gathering globally, particularly in the USA and East Asia (GWEC, 2015).

The continued commitment to developing offshore wind with deployments planned well into the future shows the direct relevance and potential impact research into the scour problem can have both immediately and in the longer term. Furthermore, research at this stage is crucial to sustaining the UK's position as leader in the field. Maintaining the lead in the field will further develop the industry promoting economic growth and providing opportunities for expanding research and consulting services as interest in developing offshore wind grows globally.

1.3 Research question overview

This section provides an outline of the research question to define the focus of the literature review which follows in Section 2. A detailed research question will be formulated in Section 3 from the conclusions of the literature review.

The overarching objective of this research project is to improve understanding of the scour development process. As has been explained above (and will be discussed in greater detail in the literature review, Section 2), current scour prediction equations are limited at least partly because they do not take into account a variety of factors that have the potential to affect scour depth. The influence of realistic sediment beds consisting of mixtures and layers of materials was identified in conjunction with HR Wallingford as a key area for investigation.

The aim of this project is to design and conduct an extensive laboratory investigation of scour development in a range of sediment beds to fill this gap in the research. In order for the research to be relevant to the marine environment testing will include a range of hydrodynamic conditions. A secondary aim of the project is to gain new insights into scour in tidal and wave-current flows, as these have been studied less extensively in the scour literature. The results are then compared with existing prediction methodologies to develop preliminary methods for incorporating the new findings. The success of the project depends on the design of a comprehensive and high quality experiment methodology and measurement techniques capable of measuring the sediment and flow properties, and the scour depth development through time.

Therefore, the main areas that will be focussed on in the literature review are:

- understanding of scour in complex sediments, particularly layered and mixed materials
- understanding of the scour process in complex hydrodynamic conditions relevant to the marine environment (wave-current interaction, tidal flow)
- understanding of the methodologies and limitations in existing prediction methods both for scour time development and equilibrium scour depth in order to assess how uncertainty can be reduced and new findings for complex sediments can be incorporated

- experimental modelling approaches and measurement techniques in order to develop a robust laboratory set-up

To enable in-depth investigation of scour in mixed and layered sediment beds, it is necessary to set some limitations to the range of conditions tested in the laboratory. Firstly only one type of structure will be used in the study - the cylindrical monopile. This will provide a baseline for understanding scour in complex sediment beds and enable direct comparison with the literature which has predominantly focused on this type of structure. Also, the monopile is a popular design and likely to continue to be used in the field in shallow to medium water depths where wind farms are commonly located. Secondly, the study will focus on non-cohesive sediments (median grain size of the sediment, $d_{50} > 0.1$ mm) as scour is generally more prevalent in sands compared to clays (Whitehouse, 2006), and this will serve as a baseline case for future extension to cohesive materials.

2. Literature review

The intention of this literature review is to provide an overview of the scour issue, and to identify the gaps in understanding in order to demonstrate the ways in which this project can contribute to the research field. The review begins by introducing some basic concepts and terminology in Section 2.1 before detailing the key relationships between parameters that are understood to influence the scour process, which have been analysed mostly through laboratory testing, in Section 2.2. Those aspects which have been less extensively addressed will then be discussed in Sections 2.3 and 2.4 which relate to the influence of the hydrodynamic and sediment properties on scour development. Section 2.5 focuses on observations of scour at wind turbine foundations in the field, providing the context and justification for this research to be conducted. A discussion of scour modelling and prediction techniques follows in Section 2.6, highlighting the current gaps between research and design. Lastly the methodology for scour research is considered in Section 2.7, including issues for scour measurement and experiment design in the laboratory.

2.1 Understanding scour – basic concepts

The purpose of this section is to introduce the basic concepts and relationships between parameters. Key terms will be defined before detailed discussion of scour mechanisms and the interaction processes between the soil, structure and fluid.

2.1.1 Key terms and definitions

As discussed in Section 1, scour is the erosion of sediment from around the foundation of a structure situated in flowing water, such as in river and coastal environments. Images of the scour process at different points through time around a cylinder are shown in Figure 2.1. Under unchanging flow conditions (such as a unidirectional current with constant depth-averaged velocity) the scour process evolves through time with a distinctive curve when considering the increase in scour hole depth (Sumer and Fredsøe, 2002a). The shape of a typical scour depth time development curve is given in Figure 2.2. It is clear that the scour process begins rapidly, but slows over time, until a plateau is eventually reached. This is known as the equilibrium scour depth, and signifies that the depth of the scour hole has stabilised and reached a maximum value under the given unchanging conditions.

Dargahi (1990) conducted a detailed study of the shape of a scour hole. Under unidirectional current the scour hole is asymmetrical in the streamwise direction with a steeper upstream slope and shallower downstream slope (Link et al., 2008). The upstream slope angle is typically about equal to the angle of repose of the sediment (Hoffmans and Verheij, 1994).

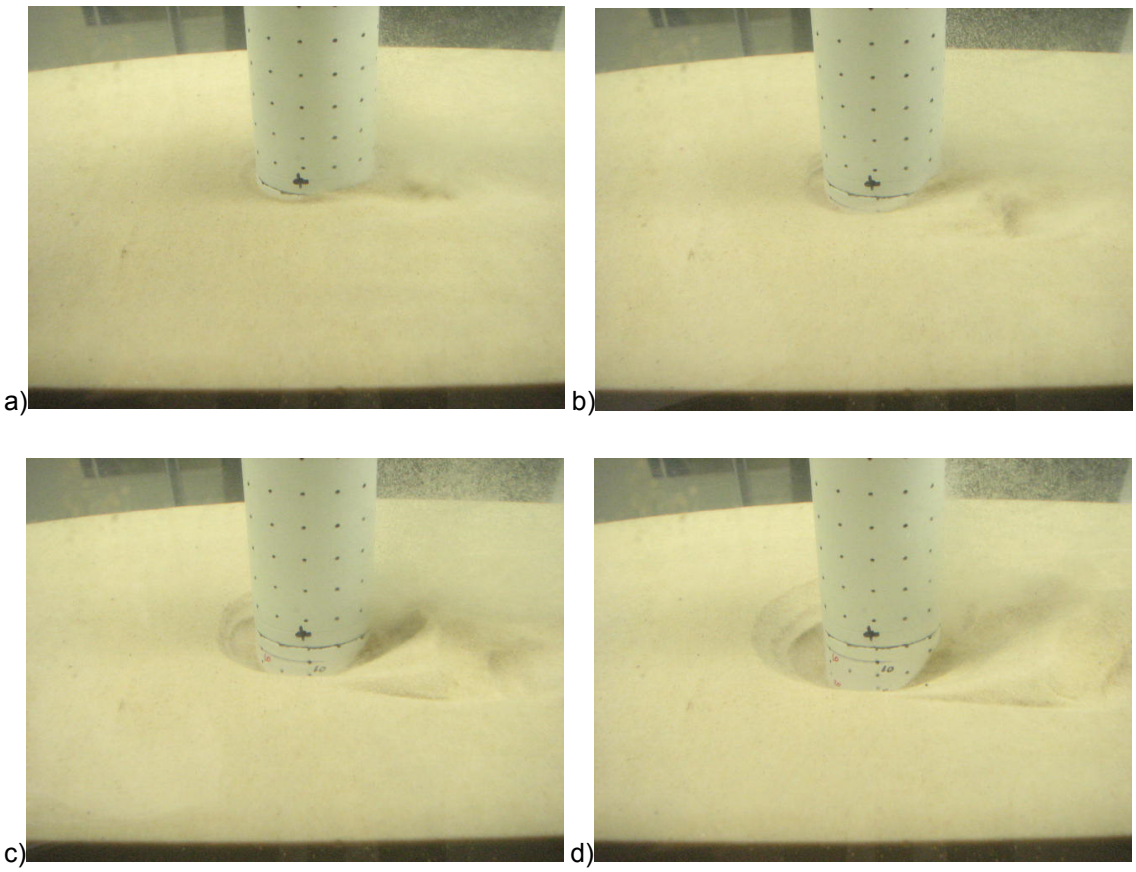

Figure 2.1 Initial stages of scour development at a cylindrical pile: a) 3 s b) 15 s c) 42 s d) 105 s after the initiation of scour.

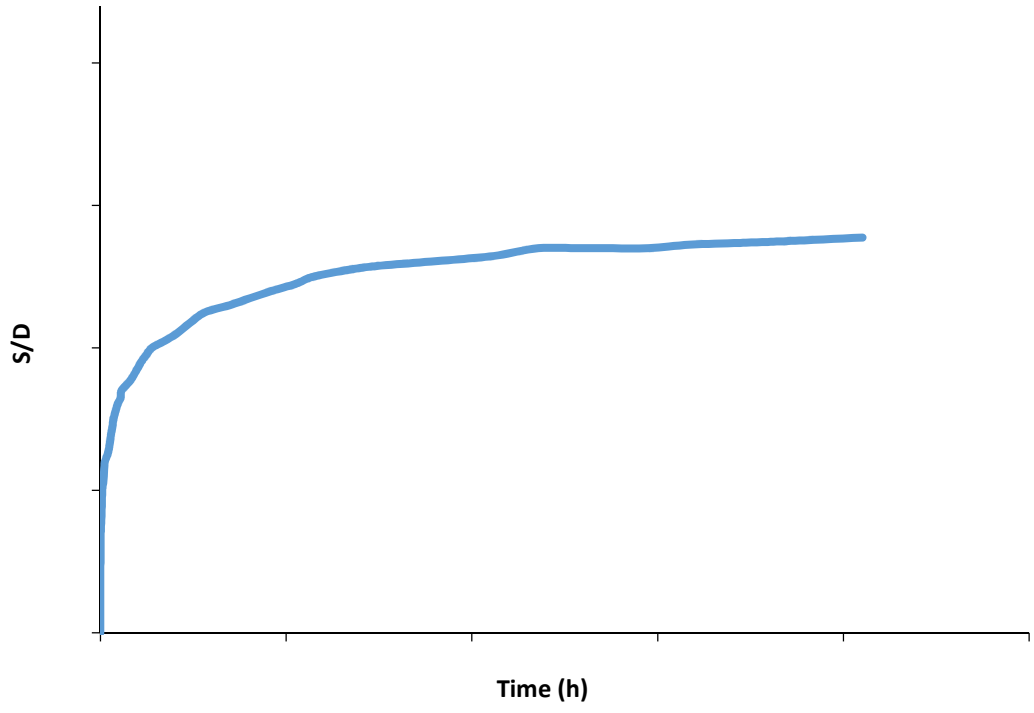

Figure 2.2 Typical scour depth development curve at a cylindrical pile in uniform sediment under unidirectional current.

Scour is essentially a sediment transport problem, but with the added complication of the presence of a structure. Soulsby (1997) provides an excellent review of the subject. Sediment is transported when the force of the flowing water (represented as a bed shear stress) is sufficient to overcome both the weight of the particle, and friction between adjacent sediment particles. White (1940) described the balance of forces on a sediment particle, defining the conditions at which it will just start to move on a flat bed, known as initiation of motion. Shields (1936) conducted extensive laboratory testing of this, and adopted the non-dimensional critical Shields parameter to describe the conditions in which a given sediment would start to move. This can also be described in terms of a critical bed shear stress which can be related to a critical depth-averaged velocity, which is a more practical parameter for use in design, see Appendix 2 for details of these formulae.

While Shields' approach is commonly adopted, a variety of other formulae and approaches for modelling initiation of particle motion have been offered, see Beheshti and Ataie-Ashtiani (2008) and Paphitis (2001) for a review of these. The range of methods indicates that there are limitations in the understanding of the sediment entrainment process and consequently a degree of empiricism is used in these methods. Scatter is also induced when comparing these models with data due to the difficulty of consistently defining the point of incipient motion experimentally (Paphitis, 2001). According to Le Roux (2005) the critical shear stress is dependent on grain size, shape and density, boundary roughness and internal friction angle, the bed slope angle and the flow velocity (laminar or turbulent, uni-directional or oscillatory). Zanke (2003) found that turbulence was also an important parameter for sediment entrainment. However, precise relationships have not been established for each of these effects, and many approaches do not take all of these factors into account, for example the effect of grain shape is not included in Shields' method. These limitations are important to consider in terms of empirical and analytical scour modelling approaches (see Section 2.6 for further discussion).

Another key concept for scour is the definition of two different sediment transport regimes. If scour occurs at the structure, but the ambient shear stress on the flat bed away from the pile is also large enough to entrain sediment then the regime is termed 'live bed'. If scour occurs at the structure but in the far field the shear stress is not large enough to entrain sediment then the conditions are known as 'clear water'. In the first case there is an influx of sediment from the flat bed in and out of the scour hole, but in the second case there is not, and this results in fundamentally different scour behaviours (see Section 2.2).

A final concept to note is that scour directly around a structure is termed 'local scour' which is the focus of this study. Other types of scour such as general and contraction scour will not be discussed (see Melville and Coleman, 2000 for details of these).

2.1.2 Scour mechanisms

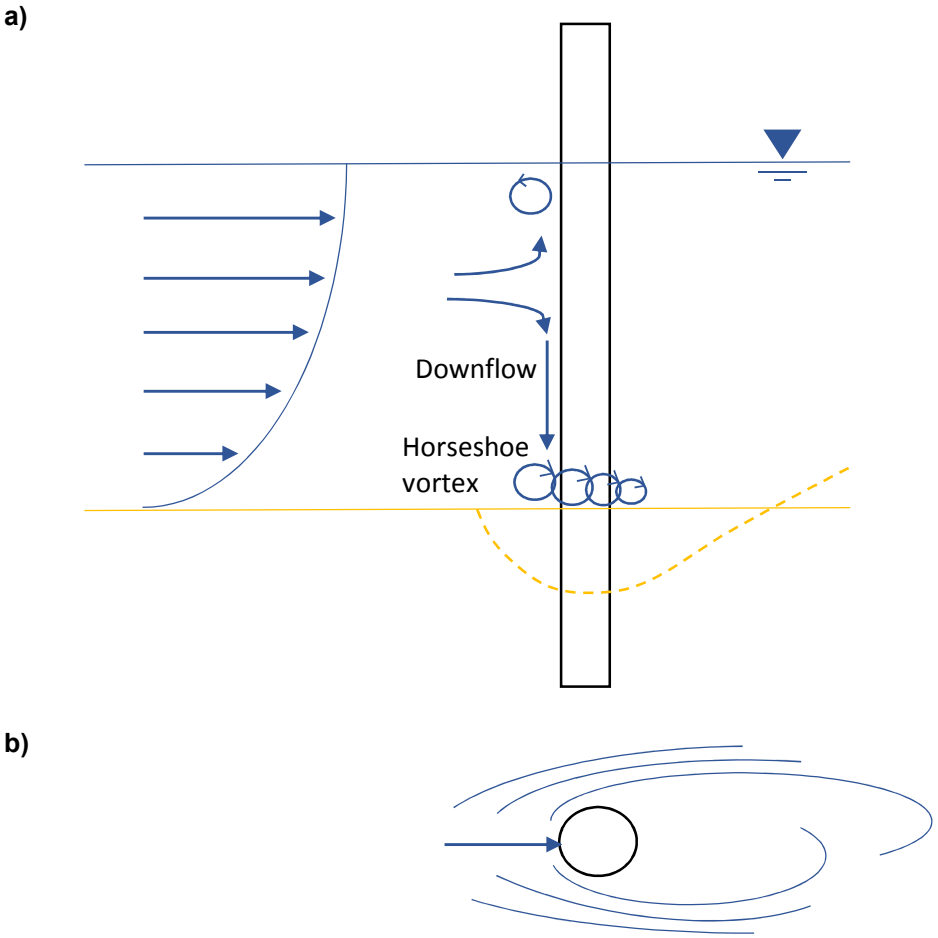

Figure 2.3 Diagram of scour mechanisms and flow around a cylinder a) vertical plane showing velocity profile, downflow, horseshoe vortex and developing scour hole b) plan view showing contraction of streamlines, separation of flow and wake vortices around the cylinder.

Now that the basic terms have been established this section will discuss in detail the mechanisms for scour in terms of the flow-structure-sediment interaction processes. As mentioned previously the presence of the structure causes alteration to the ambient flow patterns. This results in an amplification of bed shear stress in the vicinity of the structure resulting in the entrainment of sediment. The main alterations to the flow are described in Figure 2.3. There are two distinctive mechanisms for scour. Firstly, the fluid is brought to rest at the upstream side of the structure, resulting in a high pressure region compared to downstream, accelerating the flow to a maximum velocity at the sides of the structure (contraction of streamlines), and leading to separation of flow, vortex shedding and formation of a wake region behind the cylinder (see Sarpkaya and Isaacson, 1981 and Sumer and Fredsøe, 2006 for more detailed discussion of flow around cylinders). Secondly a pressure gradient forms vertically down the upstream face of the structure due to the difference in flow velocity between upper layers of fluid in the free stream and lower layers of fluid in the boundary layer which are

retarded by friction with the bed. The streamwise flow velocity varies with depth as shown in Figure 2.3. The vertical pressure gradient at the structure causes a downflow which separates at the bed where its path is blocked, resulting in horseshoe vortex formation. Flow acceleration and vortex formation increase the bed shear stress and sediment transport capacity of the flow (Roulund et al., 2005). As long as the enhancement in bed shear stress is above a threshold value for entrainment of the sediment (such as that described by Shields see Section 2.1.1), then erosion will occur at the structure. A detailed description of the scour process and mechanisms is provided by Niedoroda and Dalton (1982) and Guo (2012).

2.1.3 The horseshoe vortex system

The horseshoe vortex is the primary mechanism for scouring in currents (Whitehouse, 1998), being more significant than the contraction of streamlines and wake vortices. These are discussed in more detail in relation to scour in waves in Section 2.3.3. A detailed treatment of the horseshoe vortex system on a flat bed around a cylinder is given by Baker (1979) and Baker (1980).

The mechanism for entrainment of sediment by the horseshoe vortex system is described by Graf and Yulistiyanto (1998). The upstream flow on the bed near the pile (counter current) is responsible for initiating motion of the particles, and the main vortex is responsible for transportation of those particles downstream.

The strength of the horseshoe vortex depends on the strength of the downflow which in turn depends on the bed boundary layer profile, so that bed shear stress under the horseshoe vortex and consequently scour depth increase with increasing steepness of the gradient in the boundary layer and as the thickness of the boundary layer relative to the pile diameter increases (Roulund et al., 2005). The boundary layer gradient also increases with bed roughness because of the greater frictional effect on the lower layers of fluid (Ahmed and Rajaratnam, 1998). Campbell et al. (2005) found that sediment transported as bed-load also increased the gradient in the velocity profile and altered the mean flow velocity by affecting the bed roughness and level of turbulence in the flow.

The downflow at the cylinder has been investigated by Dargahi (1989), Raudkivi (1986) and Unger and Hager (2007) who found that it does not vary through time as scour depth increases. However, the horseshoe vortex is not time invariant as it is affected by the development of the scour hole. The time evolution of the horseshoe vortex during scouring has been studied by Dey and Raikar (2007a), Veerappadevaru et al. (2011), Dey (1996) and Unger and Hager (2007). It has been shown that the size of the horseshoe vortex core increases as the scour hole develops (Dey and Raikar, 2007a), and Veerappadevaru et al. (2011) measured the weakening of the vortex in terms of a reduction in its rotational speed. The decrease in horseshoe vortex strength with increasing scour depth explains the shape of the scour time development curve. The resulting change in bed shear stress with depth has been measured by Dey and Raikar (2007a) who found that bed shear stress initially increased before decreasing with depth until it

was about equal to or just under the critical value (in agreement with Graf and Istiarto, 2002), at which point the equilibrium condition has been reached and no further scouring occurs.

The horseshoe vortex is strongly related to the pile Reynolds number. Graf and Yulistiyanto (1998) found that the horseshoe vortex was stronger and closer to the base of the cylinder at higher approach flow velocity (or flow Reynolds number), but the dimension of the vortices is dependent only on the pile diameter (Dargahi, 1989).

In terms of the maximum amplification of bed shear stress under the horseshoe vortex, a range of values have been reported. Ahmed and Rajaratnam (1998) measured an amplification of 13.5 and Roulund et al. (2005) found it was amplified by a factor of 10. Whitehouse (1998) notes that a bed shear stress amplification factor of 4 is expected from potential flow theory, but that a range of amplification factors up to 12 have been measured in laboratory studies. There is a need for further investigation of this to better define the effect of a full range of parameters on bed shear stress amplification at the pile and to improve understanding of the relationship between horseshoe vortex strength and bed shear stress. Bed shear stress is difficult to measure directly in the laboratory which presents a barrier to research in this area.

The structure of the horseshoe vortex has been investigated by Link et al. (2008) and Dargahi (1989) who found that up to five vortices could be present in the system and that the number of vortices increases with increasing Reynolds number. Unger and Hager (2005) found that the number of vortices reduced with increasing scour depth. Unger and Hager (2007) also noted a difference in the initial horseshoe vortex which only developed into the full system once the scour hole was more developed. They found that sediment entrainment began at the pile sides due to the acceleration of flow caused by the contraction of streamlines around the pile, while the initial horseshoe vortex upstream of the pile was too weak to induce scouring. The deepest part of the scour hole moved upstream around the pile to the pile front as the horseshoe vortex became fully established.

The horseshoe vortex spatial characteristics have been investigated by Graf and Yulistiyanto (1998) and Kumar et al. (2012) who found that the horseshoe vortex system decays in strength as it stretches around the cylinder in the horizontal plane in the downstream direction. This explains why the deepest part of the scour hole is found on the upstream side of the cylinder once the horseshoe vortex system is fully established.

A final point to note is the short term variability of the horseshoe vortex strength and position. Apsilidis et al. (2012) showed how the position of the primary horseshoe vortex moves towards and away from the cylinder aperiodically as the wall-extracted vorticity fluctuates, influencing the sediment entrainment and transport processes.

2.1.4 Concluding remarks on scour mechanisms

While the horseshoe vortex and flow patterns around a cylinder have been studied in some detail, it should be noted that many studies employed a smooth flat bed to investigate this (e.g. Graf and Yulistiyanto, 1998; Apsilidis et al., 2010) or a rough flat bed (e.g. Dargahi, 1989).

Distinctly fewer studies have been conducted to investigate flow patterns in the presence of a scour hole (Barbhuiya and Dey, 2003; Arkhipov, 1984; Ahmed and Rajaratnam, 1998; Graf and Istiarto, 2002; Istiarto and Graf, 2001; Isiarto, 2001; Kirkil et al. 2007; Kirkil et al. 2008). These studies only consider an equilibrium scour hole due to the difficulties in determining suitable measurement techniques to monitor the transient flow patterns as the scour hole develops, although a few researchers, Melville (1975), Dey and Raikar (2007a), Unger and Hager (2007) and Roulund et al. (2005) developed methodologies in order to do this. Ahmed and Rajaratnam (1998) found that the downflow was stronger over a scour hole than over a flat rough bed demonstrating the significant effect that the scour hole can have on the flow. These types of measurements also enabled Roulund et al. (2005) to identify an additional mechanism for scouring under the vortex due to the erosion at the foot of the upstream scour hole slope which causes sand avalanching effects. The relatively small number of studies means that the range and number of parameters that have been tested is limited and consequently there are still gaps in the research relating to full understanding of the effects of certain parameters on the flow patterns during scouring.

2.2 Influence of parameters

This section details the influence of a range of parameters on the scour process. These have not been studied extensively in terms of the effect on the horseshoe vortex or flow field. Instead these have been investigated primarily in terms of the effect on the depth of the scour hole which is more easily measured and hence more suitable as a design parameter. The most extensively investigated parameters in the scour problem are the flow velocity, pile diameter, grain size and water depth. These are the key dimensional parameters for the simple case under consideration in this section (cylindrical pile, uniform sediment, unidirectional current). However, it is often more useful to think of these non-dimensionally in order to understand the problem in terms of the relative change in behaviour of one parameter compared to another. In this respect the Reynolds and Froude numbers will also be discussed.

2.2.1 Pile diameter

One of the most influential variables on scour depth is the pile diameter, which is used extensively to normalise the scour depth enabling data from different piles to be collapsed onto one curve. This is because the scour depth increases approximately linearly with pile diameter (Raudkivi and Ettema, 1983). Raudkivi and Ettema (1983) also found that the time to equilibrium scour depth increases with pile diameter because the scour hole volume is proportional to the cube of the pile diameter and hence larger piles have larger scour holes which take longer to erode.

It is difficult to treat the pile diameter as a separate variable because a change in pile diameter often instigates a change to the ratios of other parameters such as flow shallowness (D/h), relative roughness (D/d_{50}), Euler and Reynolds numbers (V^2/gD and VD/ν), and rate of scour development (Melville, 2008). The effects of these parameters on scour are discussed in more detail in the following sections. It should be noted that equivalence in scour depth when

normalised by pile diameter is only found in certain ranges of these parameters, and this is often not the case when comparing small scale laboratory studies with field scale, making direct comparison difficult, see Section 2.7.4 for more detailed discussion of laboratory scaling considerations.

2.2.2 Velocity

When discussing the relationship between ambient depth-averaged velocity and scour depth, it is important to differentiate between the clear water and live bed regimes. The use of a non-dimensional velocity parameter, $V_i=V/V_{cr}$, known as flow intensity which describes the velocity condition in respect to the critical velocity for the sediment, distinguishes between the live bed and clear water regimes depending on whether the flow intensity is above or below 1. The use of flow intensity rather than flow velocity not only takes into account regime change but also enables data from different sediment sizes which have different critical flow velocities to be collapsed onto one curve. Some researchers prefer to normalise shear stress or shear velocity parameters with the corresponding critical value (see Imberger et al., 1982 for discussion of this) as these are the true drivers for scour, but the trends are essentially equivalent, and the velocity intensity parameter is more commonly used due to ease of measurement.

Raudkivi and Ettema (1983), Melville (2002), Melville and Sutherland (1988), Melville (1984), Chiew (1984) and Sheppard and Miller (2006) present conceptual graphs of velocity or flow intensity versus scour depth, showing how scour depth increases with velocity through the clear water regime up to the critical velocity. The scour depth then starts to decrease as velocity increases through the first part of the live bed regime. A similar graph is given in Raudkivi (1986), but the relationship is extended further into the live bed regime to show the occurrence of a second peak in scour depth. The reduction in scour depth with velocity in the live bed regime is due to the migration of bedforms through the scour hole (Melville 1984). Melville (2008) found that the second peak occurs when ripples no longer form on the bed due to the higher capacity for sediment transport, known as the transition flat bed stage, but in uniform sediment the live bed peak is smaller than the peak at critical velocity, as there is still a flux of sediment through the scour hole.

Melville (2008), Elliot and Baker (1985), Chiew (1984), Raudkivi and Ettema (1983) and Raudkivi (1986) reported that the equilibrium scour depth increases almost linearly with flow velocity through the clear water regime. Melville (1984) plotted a large set of laboratory data which despite some scatter demonstrates this trend clearly.

Melville (2008) showed that the timescale of the scour process also increases linearly in the clear water regime to a peak at critical velocity, before decreasing through the live bed regime mirroring the scour depth trend and indicating that larger scour holes take longer to erode (as already mentioned in Section 2.2.1).

At very low flow velocity scour will not occur because the shear stress at the structure will not be increased above the critical value. There is some disagreement as to the point at which scour is

initiated as velocity is increased. Raudkivi (1986) defines the threshold for scouring as 0.6 V/V_{cr}, Melville (2008) as 0.3 V/V_{cr}, and Sheppard et al. (2011a) between 0.3 - 0.4 V/V_{cr}, where V is the ambient depth-averaged flow velocity, and V_{cr} is the ambient depth-averaged flow velocity that would result in initiation of sediment motion on the bed. There is also considerable scatter in the data used to define these values (see Melville and Sutherland, 1988) and although these differences are potentially due to discrepancies in the scour depth and critical velocity measurement methodologies it probably indicates the importance of other variables on the scour initiation condition which have yet to be investigated as this aspect is considered less important for design.

2.2.3 Water depth

Water depth is most usefully considered non-dimensionally in comparison to the width of the pile. For shallow water depths compared to the pile diameter, equilibrium scour depth increases with water depth, but scour depth becomes independent of water depth in deeper conditions (Melville, 2002; Melville, 2008; Yanmaz and Altinbilek, 1991; Lança et al., 2013a). Raudkivi (1986) noted that this trend occurs in both the clear water and live bed regimes.

Chiew (1984) describes how the reduction in equilibrium scour depth in shallow water is due to the proximity of the surface roller which interferes with the downflow and horseshoe vortex systems. Melville and Sutherland (1988) explain how the opposite directions of rotation of the surface and horseshoe vortices result in a decrease in vortex strength.

There is some disagreement as to the point at which scour becomes independent of water depth. Mueller and Wagner (2002) and Chiew (1984) define it as when the ratio of water depth to pile diameter, h/D>4, Melville and Sutherland (1988) and Raudkivi and Ettema (1983) at around h/D=3, and in the study of Melville (2002) independence appears to have been achieved by 2 h/D. Chiew (1984) found that the point at which scour becomes independent of water depth depends on the ratio of pile diameter to median grain size of the sediment, D/d_{50} (this parameter is discussed in the following section), because for a constant value of flow intensity the flow velocity will be lower over a fine sand bed than a coarse sand bed and hence the stagnation pressure and vortex interaction at the pile is less significant. The considerable scatter in the S_e/D (where S_e is the equilibrium scour depth) versus h/D plots (see for example Lança et al., 2013; Yanmaz and Altinbilek, 1991) also contributes to the difficulty in defining the point of independence and suggests that a wider range of parameters are likely to be of influence.

Chiew (1984) notes that it is essential to keep the shear velocity ratio, u^*/u^*_{cr}, constant to observe an increase in scour depth with increasing water depth for shallow flows. If the flow rate is instead kept constant then the bed shear stress will decrease as water depth increases hence reducing the potential for scour. Despite keeping the flow intensity parameter constant, opposing results were reported by Link and Zanke (2004a) and Link and Zanke (2004b) who found that scour depth decreased with increasing h/D, in both clear water and live bed conditions. It is currently unclear as to the reason for this, suggesting that further investigation of the relationship between water depth and scour depth is warranted.

Raudkivi and Ettema (1983) noted that it is difficult to change water depth without changing the ratios of other parameters, and this may alter the apparent relationship between scour depth and water depth. One must be careful to understand and separate these effects in order to discern the vortex interaction mechanism that reduces scour depth as the proximity of the two vortices increases with decreasing water depth.

2.2.4 Grain size

The effect of sediment grain size on scour depth is partly taken into account by using the V/V_{cr} parameter, but additional effects on scour depth depending on the ratio of the grain size to the pile diameter have also been determined. It is generally agreed that equilibrium scour depth decreases with decreasing ratio of D/d_{50} for small values of D/d_{50} (Raikar and Dey, 2005; Raudkivi and Ettema, 1983; Raudkivi, 1986; Melville and Sutherland, 1988; Lee and Sturm, 2009) so that if the grain size is very large compared to the pile diameter erosion is impeded as a significant amount of energy from the downflow is dissipated in the coarse bed material (Raudkivi and Ettema, 1983).

There is some disagreement as to when this effect becomes negligible, but commonly a value of $D/d_{50}=25$ is taken (Lee and Sturm, 2009; Raikar and Dey, 2005) or $D/d_{50}=50$ (Raudkivi, 1986; Melville and Sutherland, 1988; Melville, 2008). However, Sheppard et al. (2004) reported that the influence of D/d_{50} on the scour process ceases somewhere in the range of 25-100 D/d_{50}.

This is linked to some disagreement as to the relationship with equilibrium scour depth at larger values of D/d_{50}. Lee and Sturm (2009) and Sheppard et al. (2004) reported a decrease in scour depth with increasing D/d_{50} beyond $D/d_{50}>25$, until independence of D/d_{50} at around $D/d_{50}=100$. However, Lança et al. (2013a) found that scour depth decreased over a larger range of D/d_{50} from 100-1000. In contrast, Raudkivi and Ettema (1983) and Raikar and Dey (2005), found no dependence on D/d_{50} once $D/d_{50}>25$-50. The effects of several parameters were removed from the data set used by Lee and Sturm (2009), which may partly explain the discrepancies between these studies. Despite this there is still considerable scatter in their data indicating that the dependence on D/d_{50} in this range is fairly weak. The influence of other factors not removed from the data may be important such as bedforms in ripple forming sediments reducing the scour depth for larger values of D/d_{50} (Chiew, 1984), see Section 2.7.4 for further discussion of ripple effects.

Lee and Sturm (2009) link the variation in S_e/D with D/d_{50} to the effect of D/d_{50} on the horseshoe vortex system in terms of the ratio of vertical to streamwise turbulence fluctuations. At $D/d_{50}=25$ the ratio is such that it enables both the entrainment and transport of sediment. At higher values of D/d_{50} more sediment is entrained but less can be transported, whereas at lower values of D/d_{50} sediment entrainment is reduced.

In terms of the scour timescale Melville (2008) reported that the time to equilibrium increases with D/d_{50} up to $D/d_{50}=100$. This may be a reflection of the timescale increasing with pile diameter and decreasing with increasing d_{50} rather than a direct dependence on the ratio of

grain size to pile diameter, as in general as the scour hole size increases (at larger piles and in finer sediments), the scouring process takes longer.

2.2.5 Froude number

The Froude number, $V/\sqrt{(gh)}$, represents the ratio of the inertial to external (gravitational) forces in the fluid. The Froude number has the potential to affect the scour process because it influences the water surface profile and hence the flow field around the pile (see Ting et al., 2001). However, the effect of Froude number on the flow patterns around the pile in relation to the scour problem has not been investigated in detail in the laboratory.

Most scour studies are conducted in the subcritical regime ($Fr<1$) because this is usually representative of the conditions in the marine environment. Within this regime, it is expected that scour depth will increase with Froude number (Richardson and Davis, 2001) although this trend may be more directly linked to the flow velocity. Conversely the trend may not be observed in shallow flows where the h/D parameter dominates. Chiew (1984) notes that using Froude number as the only parameterisation for the effect of the flow on scour is limited because the relationship with the sediment is not considered (i.e. the clear water-live bed regime change in not modelled). As noted by Raudkivi (1986), the use of the flow intensity parameter instead of Froude number enables data from different sediments to be collapsed onto the same curve. However, a consensus has not been reached as to whether to use the flow intensity parameter or Froude number when formulating scour prediction equations, see Section 2.6 for further discussion.

2.2.6 Reynolds number

The Reynolds number, VD/ν (where V is the ambient depth-averaged velocity, D is the pile diameter and ν is the kinematic viscosity), represents the ratio of inertial to viscous forces in the fluid, which determines whether the flow is laminar or turbulent, the separation point of boundary layers (on the bed and around the pile) and the vortex shedding and wake patterns. The relationship between Reynolds number and the horseshoe vortex was discussed in Section 2.1.3 demonstrating the potential importance of Reynolds number as a parameter for scour.

At low Reynolds numbers ($Re<500$) scour depth is expected to increase with Reynolds number due to the increasing strength of the horseshoe vortex (Ting et al., 2001; Roulund et al., 2005). However, Ettema et al. (1998) state that once the Reynolds number is high enough for fully developed turbulent flow to persist, there is little dependence of the horseshoe vortex system on Reynolds number. This is true in the subcritical range of the pile Reynolds number between 1000 and $3x10^5$, although according to Sumer et al. (1993) at the top of this range there may be a small decrease in scour depth with increasing Reynolds number from 10^5 to $3x10^5$ (transition from subcritical to supercritical flow) as the position of the separation point around the pile changes.

Ettema et al. (2006) reported a different result, that scour depth increased if the Reynolds number was reduced by decreasing the pile diameter while keeping flow velocity constant.

Melville (2008) attributed this to the influence of Reynolds number on the frequency of vortex shedding, with a higher frequency of eddies at narrower piles. Melville (2008), Ettema et al. (1998) and Ettema et al. (2006) also used the Euler number, V^2/gD to describe this effect. The non-dimensional scour depth increases with increasing Euler number due to the relatively stronger eddies at smaller pile diameters. As this effect is related to small pile diameters it may be most prevalent in the laboratory and is therefore discussed in greater detail in respect to laboratory 'scale effects' in Section 2.7.4.

As noted in Section 2.1.4 scour research is limited by the lack of full understanding of the effects of parameters on the flow patterns at the pile. It is clear from this review that measurements of the flow patterns for a range of Reynolds, Froude and Euler number would be beneficial to better understand the scour process over a wider range of values.

2.3 Scour in complex hydrodynamics: time-varying, tidal and wave flows

The previous section established the basic concepts, scour mechanisms and the principle parameters that influence the process. However, this project is concerned with scour in more complex hydrodynamic conditions and sediment beds, aspects which have not been so extensively studied. This section sets out what is currently understood about scour in velocity varying and tidal flows, in waves, and in combined wave-current conditions, before the effects of sediment non-uniformity, bed stratification and a range of sediment properties are considered in Section 2.4. Where gaps exist in the research these will be highlighted in view of the project objectives.

2.3.1 Time-varying (unidirectional) current

The research in the previous section was concerned with scour under constant ambient flow conditions. However, in the field the flow velocity is often time varying due to flood or storm surge events, tidal cycles and changing wave fields so it is important to understand the effect that this has on the scour process.

Scour in unidirectional time-varying flow in the form of a variety of hydrograph shapes has been investigated by Kothyari et al. (1992), López et al. (2014), Borghei et al. (2012) and Chang et al. (2004), and a more extensive investigation of this was conducted by Chreties et al. (2013). These studies consistently show that regardless of the order, magnitude or duration of the flow variations the scour development is equivalent to that found in steady flow under the same conditions and from the appropriate depth, if in the clear water regime, with uniform sediment and structure shape. It is not yet known if this result extends to the live bed regime, or if it is valid for non-uniform sediments and structure shapes, or bi-directional flows.

2.3.2 Tidal flow

Only a few laboratory scour studies have been conducted in tidal flow (Simons et al., 2007; Jensen et al., 2006; Margheritini et al., 2006; Escarameia, 1998; Escarameia and May, 1999; May and Escarameia, 2002; Mcgovern et al., 2014; Zhao and Wang, 2009; Zhao et al., 2003).

This is probably due to the difficulty of replicating this type of flow in the laboratory, as both water depth and velocity are required to vary continuously and flow direction reverses periodically. Continuous variation of just one of these parameters can be practically difficult in laboratory facilities depending on the mechanics of flume operation. Because of this, most of the studies approximate tidal flow to a square wave so that velocity and water depth are kept constant and the only variable is the flow direction. This has the advantage of allowing separation of variables to better understand the problem, but it means that the work is limited in terms of fully representing the influence of tidal flow on scour that would be present in the field.

Probably the most extensive study of tidal scour to date is that of Escarameia (1998), also discussed in Escarameia and May (1999) and May and Escarameia (2002). In these studies a key variable for scour depth was determined to be the length of the tidal cycle with equilibrium scour depth increasing with tidal cycle length, although in general they found that scour depth was reduced compared to scour in unidirectional current, a result which is supported in most of the other studies. However, Margheritini et al. (2006) found that scour depths were similar in reversing and unidirectional flow, and Jensen et al. (2006) found that scour depth was greater in tidal flow than in unidirectional current, although they noted some uncertainty in the measurements due to correcting for a general lowering of the bed (global scour). These tests were for live bed conditions, which may explain the difference in the findings compared to the other studies which were in the clear water regime. Escarameia (1998) attributes the smaller scour depth in clear water reversing flow to the presence of downstream ripples and bedforms triggered by the deposition zone behind the pile, because these are situated on the upstream side of the pile once the flow direction is reversed. Similarly Mcgovern et al. (2014) reported that infilling occurred from the mound of deposited sediment downstream of the scour hole once this was located on the upstream side of the scour hole after flow reversal (also noted by Simons et al., 2007). Mcgovern et al. (2014) reported that this infilling caused a delay to scour development and a reduction in scour depth. This is an interesting result, because it is unclear as to whether this is characteristic of processes in the field considering the likely unrepresentative scale of such ripples in small scale laboratory experiments. Scale effects of ripples are discussed in greater detail in Section 2.7.4. In the live bed regime, ripples migrate through the scour hole in both reversing and unidirectional flows which may explain the smaller difference in scour depth between these.

These studies consistently show that the equilibrium scour depth is reached after only a few tidal cycles so that the scour timescale is much shorter than in unidirectional flow. This may also be a consequence of the ripple effects in a similar way that scour in unidirectional current is quicker in live bed conditions compared to in the clear water regime (see Section 2.2.2).

Another interesting effect of tidal flows is the resulting change to the shape of the scour hole. Margheritini et al. (2006) found that initially the slope angle remained steepest on the upstream side so that it alternated with each flow reversal, but after a few cycles the two sides became symmetrical, and compared to the scour hole shape in unidirectional current the slope angles were shallower and the eroded volume was larger. This is in agreement with the findings of

Mcgovern et al. (2014) who reported that the slope angles were typically about 10 degrees under tidal current.

A few researchers have investigated the influence of some of the more complex aspects of tidal flows on scour development. Zhao and Wang (2009) investigated tidal asymmetry by employing a weaker velocity in one direction of a square wave reversing flow. May and Escarameia (2002) conducted scour tests under sinusoidally varying flow but without water depth variation, and only at a square foundation. McGovern et al. (2014) conducted a single scour test in which both water depth and velocity were varied in tandem, but with a significantly simplified signal consisting of just three step changes in the parameters per half cycle. One issue with these tests is determining a suitable unidirectional current test for comparison to enable appropriate conclusions to be made as to whether the tidal flow has resulted in an increase or decrease in equilibrium scour depth. McGovern et al. (2014) compared their tidal flow test to a unidirectional current test set equal to the maximum velocity in the tidal test (live bed) but with a slightly different water depth to any of those used in the tidal test. May and Escarameia (2002) altered the length of the tidal cycle so that the discharge per half cycle in the sinusoidal tidal test was equal to that in a square wave reversing test run at the maximum velocity employed in the tidal test. These comparisons led to the conclusion that scour depth was considerably less in the velocity varying tidal tests, but this may well be because a considerable portion of the velocity varying flow in each half cycle was below the threshold for the initiation of scour or the velocity was considerably reduced compared to the square wave or unidirectional current test used for comparison.

To date tidal scour studies have been limited due to the small number of tests conducted, the short duration of tests and the significant simplifications made to the tidal signal. Consequently several research gaps for scour in tidal flows can be identified:

- Effect of spring-neap cycles
- Combined flow asymmetry, water depth and sinusoidal velocity variation
- Different tidal patterns (diurnal, semi-diurnal etc.)
- Variation in flood and ebb flow directions from 180 degrees
- Tidal flows combined with waves
- Impact of ripples and infilling on the scour process

2.3.3 Scour in waves

Scour in waves is somewhat different to that in a current because wave flow causes substantial alterations to the flow field around the structure and hence to the scour mechanisms. Under a unidirectional current the boundary layer has the time and distance to become fully developed, but this is not the case in waves where due to the oscillatory flow the boundary layer development is confined to half of the wave period. The thinner boundary layer under the wave results in a much weaker downflow and horseshoe vortex system around the pile, so that the main mechanism responsible for scour in waves is actually the acceleration of flow around the pile sides and the wake vortices (Niedoroda and Dalton, 1982; Dey et al., 2006).

This change in scour mechanism is generally agreed to result in a reduction in scour depth compared to in a unidirectional current with depth-averaged velocity equal to the maximum bottom orbital velocity under the wave (Jensen et al., 2006; Raaijmakers and Rudolph, 2008; Sumer et al., 1992), as the horseshoe vortex mechanism is a stronger mechanism for scouring than the wake vortices.

An important parameter identified for scour in waves in live bed conditions is the KC number, U_mT/D (where U_m is the maximum bottom orbital velocity, T is the wave period and D is the pile diameter), with equilibrium scour depth increasing with KC number (Petersen et al., 2012, Sumer and Fredsøe, 2002a). As the ratio of the wave excursion to pile diameter increases the horseshoe vortex system will gradually become more dominant so that at high KC numbers scour in waves tends towards the steady current value. Sumer et al. (1992) found that S_e/D became independent of KC number once KC>100, as the wave period was sufficiently increased to enable the horseshoe vortex system to be fully established within each half-cycle. Sumer et al. (1992) and Faraci et al. (2000) investigated the effect of KC number on the scour mechanisms using flow visualisation techniques. Sumer et al. (1992) found that neither the horseshoe vortex nor the vortex shedding mechanisms occurred if KC<6 and hence concluded that scour does not occur in waves below this value. Furthermore Faraci et al. (2000) found that no scour occurred if the boundary Reynolds number, Re_λ<50, as at this point the boundary layer becomes too thin to generate a horseshoe vortex.

However, studies by Baglio et al. (2001), Sumer and Fredsøe (2001b), Sumer and Fredsøe (2002b), Larsen (2004) and Khalfin (2007) have shown that a small amount of scour can occur in waves with KC<6, as flow is still accelerated around the pile sides (Baglio et al., 2001). Sumer and Fredsøe (2001b) also conducted a study of scour at low KC numbers in order to determine if diffraction effects are important for scour. They found that steady streaming (mean flow at the pile not equal to zero) due to wave reflection in the radial direction induced scouring below KC=6, but ultimately the scour depths were small, $S_e/D \leq 0.05$. The scour depth increased with the diffraction parameter, D/λ and the KC number. Khalfin (2007) obtained larger scour depths of $S_e/D \leq 0.2$ at low KC numbers. They attributed this to the use of non-rippling coarser sediment, and they obtained smaller scour depths in finer, rippling sediment. This is an interesting result as it demonstrates the significance of ripples on scour development, and there is a potential issue if these do not scale representatively in the laboratory compared to the field (see Section 2.7.4).

In the clear water regime, the KC number and also the flow intensity (or Shields parameter) have been found to be important for scour with scour depth increasing with Shields parameter to a peak at critical velocity in a similar manner to that in unidirectional current (Umeda, 2011). However, there is some disagreement as to the relationship in the live bed regime as Sumer et al. (1992) found only a weak dependence on Shields parameter, but the data of Hatton (2006) indicated (with some scatter) that scour depth increased with increasing Shields parameter in live bed conditions.

The scour hole shape is quite different in waves compared to in a current. Kobayashi and Oda (1994) found that in the clear water regime the maximum scour depth was situated up to 1 pile diameter downstream from the cylinder, corresponding with the wake vortex scour mechanism. This was most pronounced for low KC numbers, indicating that the erosion and deposition patterns depend on the KC number due to the associated changes in vortex patterns and separation point around the cylinder (Neidoroda and Dalton, 1982).

Scour studies in waves have employed a variety of wave types. Carreiras et al. (2000) found that scour in non-linear waves was equivalent to that in linear waves if a modified definition for wave velocity in the KC number was used. Hatton (2006) and Sumer and Fredsøe (2001a) found that the scour process was equivalent between regular and irregular waves, however, Prepernau et al. (2008) suggested using alternative definitions for U_m and T in order to achieve this result. Although there may not be agreement in terms of the best definitions of parameters, it is clear that the overall trends are consistent between these cases.

2.3.4 Wave-current flow

Wave-current interaction effects are complex and the focus of much research; see Wolf and Prandle (1999) for a more in-depth discussion of this topic. Non-linear interaction effects between the wave and current components produce a distinctive boundary layer and velocity profile in wave-current flows (Olabarrieta et al., 2010), and consequently the flow patterns around the pile and scour mechanisms in wave-current flows are altered compared to the wave alone or current alone cases.

Sumer and Fredsøe (2001a) introduced the parameter

$$U_{cw} = U_c/(U_c+U_m) \quad (2.1)$$

to represent the ratio of the wave and current components in wave-current flows. They found that in the live bed regime scour depth increases with U_{cw} up to the steady current value, as the current component becomes more dominant and the strength of the horseshoe vortex increases. This means that in live bed conditions the equilibrium scour depth is always expected to be less when a wave is added to a current than in that current alone. This is in agreement with Breusers (1971), Rudolph and Bos (2006), Bijker and Bruyn (1988) and Chen et al. (2012).

In contrast, Eadie and Herbich (1986) and Kawata and Yoshito (1988) found that adding a wave to a current increased the equilibrium scour depth. This difference may be explained by a change in scour behaviour between the clear water and live bed regimes. This is probably due to the presence of ripples in the live bed regime, and Kawata and Yoshito (1988) observed that scour depth decreased once ripples started to form on the bed.

Qi and Gao (2014b) investigated the transition between the clear water and live bed regimes by adding a wave to a clear water current which resulted in live bed conditions under the combined wave-current flow. They found that in this case the scour depth was still increased when the wave was added, but that there was little difference in scour depth when they added a wave to

a live bed current. In general they noted that the scour depth under wave and current was greater than the linear sum of the scour depths in the individual wave and current cases.

It is important to consider in greater detail the effect of having a wave-dominated or current-dominated flow. In wave dominated conditions the flow direction reverses every half cycle, resulting in an alteration to the scour hole geometry compared to in current dominated conditions where the flow direction does not change (Niedoroda and Dalton, 1982). Niedoroda and Dalton (1982) note that when the current and wave velocities are equal, the situation is difficult to evaluate and has not been studied extensively. However, study of flow around cylinders has indicated that unique vortex patterns occur under this condition with a KC number about equal to 10 (Grass et al. 1985), and a peak in the drag force occurs (Mackwood et al., 1997). It has not yet been considered how these aspects might affect the scour process.

Similarly to scour in waves, the KC number has been identified as an important parameter for wave-current scour, with equilibrium scour depth increasing with KC number (Petersen et al., 2012). In terms of the scour timescale Petersen et al. (2012) found that it increases with KC number in wave dominated flows (as it did with wave only scour), but KC number does not affect the scour timescale in current dominated conditions. The timescale was also found to decrease as Shields parameter increased. Breusers (1972) and Niedoroda and Dalton (1982) found that the scour rate is faster in wave-current flow compared to in unidirectional current and Qi and Gao (2014b) reported that the scour rate in wave-current flow was faster than both scour in wave alone and current alone cases.

One aspect that requires clarity for scour in wave-current combinations is the set of parameters used in the comparative unidirectional current case. In many studies (see above) the wave-current case is compared to the unidirectional current prior to adding the wave, so that the maximum velocity under the current is smaller than the maximum velocity in the wave-current flow. However, some studies have compared a current with velocity equal to the maximum combined velocity in the wave-current combination. Niedoroda and Dalton (1982) found that in this case the scour depth was always less in the wave-current flow in both live bed and clear water regimes, because of the reduction in strength of the horseshoe vortex which is disrupted by the oscillatory motion of the wave component.

Similarly to wave scour, no difference in scour behaviour has been found between random and regular waves in wave-current flows (Eadie and Herbich, 1986). Sumer and Fredsøe (2001a) found that there was little difference to scour if the waves were parallel or perpendicular to the current direction. However, Ong et al. (2012) and Ong et al. (2013) presented initial results using a stochastic approach that indicated there may be a difference in scour development under short and long crested waves, but this is yet to be tested in the laboratory.

2.3.5 Breaking waves

Very few studies have investigated the effect of breaking waves on scour depth. Nielsen et al. (2012) found that in live bed conditions the maximum scour depth was less than in a

unidirectional current but was significantly larger than under non-breaking waves. They determined that the pile diameter, height of breaking wave at the break point, wavelength, and distance between the break point and the pile influenced the process. Bijker and Bruyn (1988) found that breaking waves added to a current increased the scour depth compared to that current on its own.

One issue with tests in breaking waves in live bed conditions is the difficulty in measuring the scour depth and datum level due to the extensive movement of the bed (Carreiras et al., 2000). This aspect is likely to affect the conclusions as to whether scour depth in breaking waves is greater or less than in a current (Jensen et al., 2006).

2.3.6 Backfilling

Backfilling is the opposite of scouring, where sediment is deposited into the scour hole resulting in a reduction in scour depth. This occurs in the live bed regime, and can be caused by a change in the hydrodynamic conditions, such as running waves after a scour hole has been formed by a current.

Sumer et al. (2013) found that the scour depth was reduced to the same equilibrium depth after backfilling as the equilibrium scour depth that would be reached from a flat bed under the same flow conditions, but the timescale to equilibrium was different. They found that the backfilling timescale was larger than the scour timescale for small KC but smaller for large KC. Hartvig et al. (2010) reported that the backfilling process is about 10 times slower than scouring. However, Rudolph et al. (2008) note that the rate of backfilling is about 10 to 100 times the scour rate. Backfilling is likely to be important in marine environments where changes in hydrodynamic conditions are common.

2.3.7 Concluding remarks on scour in wave-current flows

This review has shown that research into scour in wave-current flows has been somewhat less extensive than in other conditions. In particular only a few studies have considered wave-current scour in the clear water regime, and the relationship between parameters such as KC number and flow intensity in clear water conditions are not fully understood.

There is also some disagreement as to whether scour depth can be larger in a wave-current combination than in the current alone and the differences in this regard between the two sediment transport regimes would be worth further investigation.

Finally it would be interesting to study the effects of different vortex patterns on sediment transport as the KC number and the ratio of wave and current components vary. In particular it was identified that the impact of wave-current flows with equal wave and current components has not been fully investigated.

2.4 Sediments

In the uniform sediment scour studies discussed thus far, only d_{50}, the median grain size of the sediment has been viewed to be important in describing the influence of the sediment on the scour process. This section discusses the literature relating to scour in sediments other than the uniform sands which many studies are limited to, and investigates the influence that a wider range of sediment properties may have on the scour process. As will become apparent in this section, there is currently a significant lack of research into the impacts of many of the sediment properties on scour. This is probably because scour research is usually approached purely from a hydrodynamics or sediment transport perspective rather than as a geotechnical problem. De Vriend and Barends (2006) and Heibaum (2002) discuss some of the issues associated with ignoring the geotechnical aspects. In particular they highlight the likely importance of pore water pressure in scouring mechanisms, which, along with other sediment properties are not usually monitored in scour experiments.

Where investigation into the effect of the sediment parameters on scour has been conducted it has principally been concerned with the effect of non-uniformity in the sediment gradation on scour depth. This is closely linked to the process of bed armouring which has also received some attention in the scour literature, both in terms of scour in non-uniform sediments and scour in layered sediment beds with a layer of uniform coarse armouring material overlying a uniform finer sand. The available research on these topics is reviewed in Sections 2.4.1 and 2.4.4, before the few studies that have investigated other aspects of sediment effects on scour are presented.

2.4.1 Scour in non-uniform sediments

Non-uniform sands are characterised by a wider distribution of grain sizes, and are typically parameterised by the geometric standard deviation of the sediment grain distribution:

$$\sigma_g = \sqrt{\frac{d_{84}}{d_{16}}} \tag{2.2}$$

where d_{84} and d_{16} are the sieve sizes for which 84% and 16% of grains will pass through respectively. The geometric standard deviation is used to define non-uniformity because sediments are often approximated as having a log-normal distribution; see Wu et al. (2004) for explanation of the use of the log-normal distribution to model sediments, and Molinas (2003) for discussion of some of the limitations of this model when applied to natural sediments. Some studies have used alternative definitions of the geometric standard deviation. For example Chiew (1984) used $\sigma_g=d_{84}/d_{50}$ which is appropriate if the coarse fraction is dominant (Raudkivi, 1986), although in a true log-normal distribution this would be identical to the geometric standard deviation as defined previously. Note that $\sigma_g=d_{50}/d_{16}$ and $\sigma_g=0.5*(d_{84}/d_{50}+d_{50}/d_{16})$ are also equivalent in a log-normal distribution (Molinas, 2003). Raudkivi (1998) presents a wider range of formulas used to classify sediments such as the uniformity coefficient, $C_u=D_{60}/D_{10}$, and Whitehouse et al. (2010b) reported that the sediment is uniform if $C_u<5$.

There is some uncertainty as to the point at which a sediment should be classified as non-uniform in terms of its effect on scour. Melville and Sutherland (1988) defined uniform sands as having σ_g<1.3 and Raikar and Dey (2005) and Dey and Barbhuiya (2005) defined non-uniform sediment as having σ_g>1.4, although Chiew and Melville (1989) and Raudkivi (1986) found that the effects of sediment gradation on scour were negligible if σ_g<2.

There is general agreement in the literature that when comparing a uniformly graded sediment with a non-uniform sediment where both have the same d_{50} value, the scour depth will be less in the non-uniform sediment, and the scour depth decreases as the non-uniformity of the sediment increases (Raudkivi and Ettema, 1983; Melville and Sutherland, 1988; Molinas and Noshi, 1999; Oliveto and Hager, 2002; Dey and Barbhuiya, 2005; Raikar and Dey, 2005; Melville, 2008; Guo, 2012).

Molinas and Noshi (1999) found that the reduction in scour depth with increasing sediment non-uniformity is a function of the flow intensity parameter. Melville and Sutherland (1988), Melville (2008) and Raudkivi (1986) provide schematics of the effect of sediment non-uniformity on the relationship between flow intensity and equilibrium scour depth. As velocity intensity increases the scour depth linearly increases up to a first maximum, then decreases before further increasing through the live bed regime to a second peak (in a similar manner to that in uniform sand, see Section 2.2.2, although the scour depth is less in the non-uniform sands). The height of the first peak reduces with increasing sediment non-uniformity and the position of the peak moves to the right so that the peak occurs at a higher flow intensity than it does in the uniform sand, where the peak coincides with the critical velocity for the sediment. In contrast the second peak in the live bed regime is in the same location and of the same height in the uniform and non-uniform sands. In the non-uniform sand this means that the live bed peak is actually higher than the first peak once the non-uniformity parameter increases sufficiently. Chiew and Melville (1989) concluded that the shift of the first peak to higher flow intensity in the non-uniform sands is due to bed armouring. This is an effect which acts to increase the sediment's resistance to erosion so that a greater shear stress (and hence flow intensity) is required for incipient motion of the particles. The position of the peak is aligned with the new threshold condition for the sediment. Once flow velocity increases so that every grain size in the sediment mixture is mobile, sediment non-uniformity has little effect on scour (Melville, 2008). This explains why the second peak in the live bed regime is similar in the uniform and non-uniform cases.

The bed armouring process is described by Shen and Lu (1983), Borah (1989), Bettess (2002), Dey and Barbhuiya (2005), and Froehlich (1995). Bed armouring occurs under a flow condition in which not all of the particle sizes in a mixture can be transported. The finer sediment is preferentially removed from the bed and consequently the median size of the surface sediment layer becomes coarser and coarser as the finer more mobile particles are entrained leaving behind the larger particles. Chang et al. (2004) measured this change in distribution in the upper layer of sediment by collecting sediment cores from the bed. Once the armour layer has formed it will protect underlying finer material from erosion.

Armour layers can be classified as stable or unstable, depending on whether they are mobile or static under a given condition. Froehlich (1995) states that the stability of the armour layer will depend on its thickness, the non-uniformity of the sediment, and the ambient flow conditions. Due to the difference between local shear stress at the structure in the scour problem compared to the ambient condition on the flat bed away from the pile, the armouring process may occur both in the scour hole and on the flat bed or only at one of these locations, and the properties of the armour layer and its stability may be different between the two locations.

As with uniform sediment, the change in the relationship between velocity intensity and equilibrium scour depth in non-uniform soils as the bed transitions between the clear water and live bed regimes is linked to the development and migration of ripples along the bed. However, an interesting effect specific to sand with σ_g=1.5 was observed by Raudkivi and Ettema (1983). In this case ripples were prevented from forming on the bed due to the formation of a grain thick armour layer and the scour depth was increased beyond that in a uniform sediment where ripples did form. However, as σ_g was increased beyond this value an armour layer formed in the scour hole, reducing the equilibrium scour depth below that in the uniform sediment once more.

Another aspect affecting the scour depth in non-uniform sand is whether there is a continual supply of sediment from upstream. As the bed armours, if there is still an influx of fine grains from the upstream bed then scour depth is reduced compared to in uniform sand due to ripples passing through the scour hole creating a dynamic equilibrium condition. However, if the sediment feed dries up then ripples will diminish and the scour depth will tend towards that in uniform sand equating to the armour layer that has formed (Chiew and Melville, 1989; Raudkivi, 1986; Chiew, 1984; Melville and Sutherland, 1988).

2.4.2 Sediment distribution shape effect on scour

Most scour studies have used sediments with log-normal distributions. However, Molinas (2003) tested sediments with different distribution shapes but with the same σ_g and d_{50} values in order to consider the effect of sediment coarseness on scour. He found that the velocity for initiation of scour was independent of the coarse fraction in the sediment, but the scour depth was reduced as the coarse fraction increased. This is an important study as it shows that the scour process in non-uniform sediments depends on not only the σ_g parameter but also the shape of the grain size distribution. Therefore, it would be interesting to study the effects on scour of a wider range of distribution shapes.

Guney et al. (2011) conducted scour tests using a mixed sand and gravel bed, with a bimodal distribution. Although this study is limited because the scour depth is not compared with other non-uniform or uniform sediments, Guney et al. did observe interesting deposition patterns with the two types of sediment segregating as the scour hole developed. However, they do not discuss what influence this has on the scour process.

2.4.3 Incipient motion of non-uniform sediment

In order to understand the behaviour of non-uniform soils in the scour problem it is important to consider the mechanisms of incipient motion and sediment transport for these materials more generally in terms of the sediment transport research, especially seeing as the scour literature is quite sparse in this respect. These types of sediments are still undergoing research in the field of sediment transport, demonstrating that this is a complex problem. As noted by Yang et al. (2010), the physical processes of sediment transport in non-uniform sediment have not been described analytically yet, and one reason for the considerable scatter in empirical methods such as the Shields diagram is the complex effects induced by grain non-uniformity (Buscombe and Conley, 2012).

Paphitis (2001) states that the incipient motion of sediment depends on sorting and packing, particle exposure, bed configuration, particle orientation, pivoting angles, particle shape variations, bed slope, ratio of flow depth to particle diameter and bed armouring. Additionally Yang et al. (2010) list particle size, density, and sheltering from other particles as key parameters that influence initiation of motion. Some of these parameters relate directly to non-uniform soils and will be discussed in this section but others apply to both uniform and non-uniform materials (see previous discussion in Section 2.1.1).

One mechanism that is unique to entrainment in non-uniform sediments and hence is likely to influence scour development in these materials is the exposure and sheltering of grains. Exposure and sheltering effects are caused by alterations to the flow patterns in close proximity to the bed due to the variability in the grain size (Wörman, 1992). This causes particles to be entrained at a different shear stress than would be required in a uniform bed of that grain size. Larger grains are more exposed in a non-uniform sand, because of the smaller grain sizes in their vicinity, and the more the grains protrude, the lower the shear stress needed to move them (Shen and Lu, 1983). Saadi (2008) notes that the exposure of grains is dependent on the mixture of grain sizes, and may also vary in time. For example as fine particles are eroded from between the coarser particles this may result in an increase in exposure of the coarse particles.

Shen and Lu (1983) describe how in the viscous sublayer the fine particles are not subjected to the same lift forces as they are in a uniformly sized bed due to larger particles sheltering them. This sheltering effect of the finer grain sizes increases their resistance to erosion so that a higher shear stress is required to entrain them.

Therefore, in non-uniform sediments the incipient motion of each size fraction is influenced by the other sizes in the mixture, so that in general fine grains are entrained at a higher shear stress and coarser particles at a lower shear stress than in a uniform bed of that grain size (Hossain and Sarker, 2006; Shen and Lu, 1983; Saadi, 2008). Hossain and Sarker (2006) note that this means in some non-uniform sediments all of the particle sizes are entrained at about the same shear stress, but in others incipient motion of different grain sizes within the mixture occurs at different shear stresses (and bed armouring effects are observed).

Wilcock (1993) investigated the difference in incipient motion characteristics for a range of distribution shapes including skewed, lognormal, rectangular, and weakly and fully bimodal. The individual grain sizes in the mixtures were consistently entrained at about the same shear stress, apart from in the fully bimodal case where the two grain sizes were entrained at separate shear stresses due to the substantial difference in grain size in this case. Kuhnle (1993) reported that the incipient motion of bimodal sediments depends on the absolute size of the sediment, the relative size of each fraction, the separation in sizes between the two modes, the proportion in each mode and the fraction of sediment sizes contained between the two modes.

Another interesting effect in bimodal sands was observed by Wilcock et al. (2001) who reported that in bimodal sand-gravel mixtures bed armouring did not occur. They attributed this to the sediment structure increasing the entrainability of the gravel fraction. However, Kuhnle (1993) determined that the change in bed roughness was responsible for the movement of the fine particles at higher shear stress and the coarse particles at lower shear stress in bimodal mixtures.

This review has highlighted some significant research gaps for scour in non-uniform sands:

- The hydrodynamic conditions used in non-uniform sand experiments have been limited (no wave or wave-current tests)
- Most studies have used log-normally distributed non-uniform sediment and the effects of other distribution shapes have not been studied extensively
- There is no agreement on the parameters to define sediment non-uniformity, which shows a lack of understanding of the underlying physical processes

2.4.4 Layered sands - with an armour layer

Bed armouring can be a transient process created by preferential entrainment of finer material from the surface layer of a non-uniform sediment (as discussed previously). However, bed armouring can also be present when a bed is stratified with a layer of coarse (armouring) material overlying finer sediment. This case has been studied by a few researchers in the laboratory by layering a uniform coarse sand over a uniform fine sand.

Raudkivi and Ettema (1985) identified four cases for scour in this type of layered armoured bed, depending on the flow intensity, the ratio of the grain sizes between the two layers, and the layer thickness, and depending on these factors the equilibrium scour depth could be either smaller or greater in the underlying fine sand compared to a uniform bed of that fine sand i.e. without the presence of the armour layer. Dey and Raikar (2007b) agreed with these findings but presented an alternative classification system consisting of three cases for scour. These cases broadly depend on whether the armour layer stays intact under the flow conditions, or if and how it is breached either locally to the pile, or a longer way downstream and upstream of the pile. In general the thicker the armour layer and the greater the difference in grain size, the smaller the scour depth in the lower fine sand layer.

In the cases in which scour depth in the fine sand is reduced by the armour layer, the larger particles start to fall into the scour hole once the amour layer is breached (Kothyari et al., 1992) creating what Dey and Raikar (2007b) term a secondary armour layer in the scour hole which limits further scouring.

However, at higher flow intensity Dey and Raikar (2007b) note that a secondary armour layer does not form in the scour hole, (if the difference in grain size between the layers is not too large) as the amplification of bed shear stress at the structure enables the armour material to be scoured, but the armour layer is still in the clear water regime on the ambient bed. In this case the armour layer enables an extension of 'clear water' conditions for the underlying fine sand, because general movement of the bed and bed rippling is inhibited by the stability of the armour layer. This results in an increase in scour depth compared to the peak scour depth that can be obtained in a uniform bed of the fine sand. However, if flow intensity is further increased the armour layer will also reach the live bed regime on the flat bed and the equilibrium scour depth will be reduced.

2.4.5 Layered sands – other configurations

It is difficult to find studies that have investigated layered beds other than with an overlying armour layer at a cylindrical pile (see previous section). However, Govsha and Gjunsburgs (2012) presented a study of scour in a stratified bed at guide banks in a river and in Gjunsburgs et al. (2014) at an abutment. The layered bed tested was of two layers with fine sand overlying coarse sand. They suggested that the scour depth development could be predicted by changing the sediment parameters to coincide with each layer. However, the agreement with the experimental data in the lower layer appears to be reduced compared to that in the upper layer using this method. This study was limited by the small number of tests conducted and the two sand layers were assumed to scour independently, so a more extensive study of scour in layered sands would be warranted to understand the scour behaviour in a wider range of layered bed configurations and flow conditions, and to investigate the potential for additional influences on the scour process due to interaction effects at the sediment grain scale in stratified beds.

2.4.6 Effects of other soil parameters

A number of parameters were listed in Section 2.4.3 that are thought to influence sediment transport, and hence these are likely to also influence the scour process (Harris, 2003). Very few scour studies have looked into these aspects, so sediment transport studies have also been reviewed to consider the likely impacts of these parameters on the scour process and highlight the limitations in understanding.

a) Bulk density

Bulk density, or porosity of a sediment (the two are linearly related) is a property of a bed of sediment rather than of individual grains. It takes into account both the density of the sand material and the amount of space or voids between particles. Consequently bulk density is not a

material property but varies with degree of compaction. Porosity decreases with increasing sediment non-uniformity as the greater range of sizes of particles can fit more closely together than uniformly sized grains (McLachlan and Brown, 2006).

Briaud et al. (2001) found that bulk density is likely to affect the incipient motion of a sediment and Govindasamy et al. (2008) note that sediment becomes less erodible with increasing compaction and increasing bulk density, especially if the soil is well graded.

Higher porosity also means that the downflow energy is dissipated more in the bed (Raikar and Dey, 2005). This affects the equilibrium scour depth when the grain size is large compared to the pile diameter (as was discussed previously in Section 2.2.4).

Sumer et al. (2004) and Sumer et al. (2007) investigated the effects of bulk density on the scour process by conducting experiments in two silt beds of different density under waves. They found that the denser silt resulted in a larger scour depth. This counter-intuitive result is probably caused by cohesive effects and Sumer suggested it was due to an increase in the angle of friction for the denser material. It is probable that a different result would be obtained in cohesionless sands.

Another study that has considered the bulk density of sediment in a scour hole is that of Sørensen et al. (2012). They noticed a significant increase in bulk density of backfilled material compared to the original sediment, but they did not consider the effect that this would have on future scouring, only the effect that it had on structural stability. This study is interesting because it demonstrates that changes in bulk density can occur during the scour process, but further research is needed to ascertain what impact this has.

b) Permeability

Permeability is a measure of how easily water moves through the sediment. This depends on the connectedness of void spaces and grain size. Permeability increases with increasing median grain size, and non-uniform sediments are less permeable than uniform sediments (Blanco, 2003). Permeability is influenced by the shape of grains, their packing, orientation and grain size distribution (Soulsby, 1997). Permeability affects the rate of dissipation of excess pore pressures in the soil (Cheng et al., 2014a) and consequently the entrainment of sediment under waves (Soulsby, 1997) but it is not known if and how permeability affects the scour process.

c) Particle shape

The shape of the grains affects the threshold of motion of a sediment, with rounded particles being more mobile than angular and flat particles because of increased interlocking effects between the particles (Gomez, 1994). Grain shape also affects porosity as irregular shapes have poorer packing and hence higher porosity (Selley, 2000). These two aspects demonstrate some of the complexities in modelling incipient motion, as in a sediment with irregular grains one effect acts to increase erodibility (increasing porosity) while the other decreases it

(increasing interlocking effects), and it is difficult to understand how these aspects interact. The effects of particle shape on scour development have yet to be investigated.

d) Pore pressure

Heibaum (2002) describes how the pore pressures in the soil will fluctuate under unsteady flows due to turbulence, vortices, and waves, and this will influence the stability of the soil skeleton. However, laboratory studies have predominantly focused on the effect of waves on pore pressures in the seabed with regards to the liquefaction process and burial of pipelines (Sumer et al. 2006a; Sumer et al. 2006b; Sumer and Fredsøe, 2002a). Qi et al. (2012) present one of the few studies in which pore pressures were monitored during scour testing at a cylindrical pile, and noted that the upward seepage force may increase the propensity for sand to be scoured. However, the interaction between the flow patterns around the pile and the pore pressures, and how this influences scour development is still poorly understood.

2.4.7 Concluding remarks on scour in complex sediments

This section has shown that studies of scour in non-uniform and stratified sediments have predominantly been conducted under unidirectional current, and so extension of this work to other flow conditions would be necessary for applicability to the marine environment.

For non-uniform sands the limited range of sediment distribution shapes considered in the research was highlighted, while for layered beds, investigation of a wider range of bed configurations would be interesting.

In order to understand scour development in more realistic conditions the effects of heterogeneity in the bed need to be considered, and there is a distinct lack of research into the effects of the sediment properties on the scour process.

2.5 Field Data

Now that the laboratory based scour research deemed relevant to this project has been presented, this section provides an overview of the scour problem in the context of realistic marine conditions through discussion of data from offshore windfarms in European waters. A comparison of the field data with the laboratory data is then made in Section 2.5.1 in order to assess the current limitations in understanding and priorities for further research.

Obtaining field data in general is not straightforward. There are two aspects to obtaining usable field data, one relates to measurement of the hydrodynamics, the other to the monitoring of scour depth at the structure. In terms of the hydrodynamics one must rely on organisations to put in place the measurement infrastructure and to publish the data. Analysis of wave data in UK waters is given in Boukhanovsky et al. (2007) and Woolf et al. (2003). While these data sets are not specific to offshore windfarm sites, they do provide an overview of typical conditions and can be used to inform the design of laboratory experiments to ensure the parameters are within the appropriate range.

Similarly, scour depth data is difficult to acquire because it depends on monitoring equipment being deployed, and this data being made public. Often at windfarm sites seabed bathymetry data is collected from one-off acoustic surveys or a sequence of surveys carried out months or years apart (Rudolph et al., 2008; Stahlmann and Schlurmann, 2010; Raaijmakers et al., 2010). The significant length of time between surveys means that the dynamic scour process is simply not captured. Higher frequency monitoring of scour depth over a limited duration has been conducted in a few cases by fixing equipment to the pile, see Dixen et al. (2012a), however this is prone to damage if left in place for a long period, and maintenance will be required adding expense. As yet, the limited duration of deployment has meant that neither the initial scour stages nor the long-term scour depth evolution have been captured in any detail. The complexity and expense of monitoring scour depth in the field are significant barriers to obtaining comprehensive data sets.

The field environment is characterised by changing conditions over many scales, and this will affect the scour development. Therefore, at any given survey point it is difficult to determine whether the scour hole is in an equilibrium or transient condition. If comprehensive hydrodynamic data was available for the site, an attempt could be made to correlate this to the scour survey, but there is seldom a comprehensive flow measurement system in close proximity to the scour data, and in the few cases where tandem systems have been installed the deployment time or data captured has been limited, see Lu et al. (2008), Rudolph et al. (2008), Dixen et al (2012a). Scour protection installed at piles also reduces the amount of available scour data. These points demonstrate why in reality it is difficult to use field data directly to advance understanding of the scour process.

One reason to study the field data is to improve the experiment design so that conditions in the laboratory are representative of those in the field. Whitehouse et al. (2008), Whitehouse et al. (2010b), ABPmer Ltd et al. (2010), Matutano et al. (2013), Harris et al. (2011), DECC (2008) and Dixen et al. (2012a) have provided descriptions of some of the existing windfarm sites around the UK and across Europe including flow conditions, typical pile diameters, water depths and seabed properties as well as measured scour depths in some cases. The key facts from these studies are shown in Table 2.1.

What is clear from reviewing these papers is the significant level of variation of the hydrodynamics, soil properties and scour depths between sites. Furthermore there is substantial variation in the soil properties within a site in the horizontal plane and with depth into the seabed, with mixtures as well as distinctly different layers of materials common. Further information regarding soil layering in the field is given in Harris et al. (2010b), Whitehouse et al. (2008), Mengé and Gunst (2008) and Harris and Whitehouse (2012). This variation in soil properties is likely to be the reason for also observing highly variable scour depths over one site, seeing as the hydrodynamic conditions are fairly consistent at this scale. This demonstrates the importance of conducting research into the effects of sediment properties on scour depth so as to advance understanding of scour behaviour in the field.

Table 2.1 Summary of field conditions at offshore wind farms.

Pile description	The majority of turbines have steel monopile foundations between 4-5 m in diameter.
Water depths	Up to 30 m. The water depth at Burbo bank and Robin Rigg sites is up to around 10 m, while the water depth at Lynn and Inner Dowsing is between 18-26 m.
Hydrodynamics	Sites vary from tidal- to wave-dominated, and breaking waves are common at Kentish flats farm. Typical peak tidal currents are in the range of 1-1.5 m/s but can be as much as 2 m/s (Robin Rigg). Wave heights are in the range of 4-8 m with a period typically around 10 seconds but with varying return period (1 year at Barrow and Burbo Bank, but 50 years at Princess Amalia). Asymmetry is common in the tidal flows; Robin Rigg has a 7 hour ebb and 5 hour flood, and the peak ebb and flood flows are 0.9 m/s and 0.7 m/s respectively at Kentish flats.
Soils	The seabed usually consists of surficial sediment deposits and dense clay or rock strata underneath. The upper layers of sediment often consist of mixtures of materials including fine to medium sands, gravels, clay and silt, and shells and seaweed may be prevalent. Some sites do have sediments with a more uniform nature (Robin Rigg is fine-medium sand). The density of the material is quite variable, for example the surface layer consists of loose to medium dense sand at the Princess Amalia site.
Scour depths	Scour depth, S, typically in the range of 2-6 m (0.5-1.3 S/D) but it is noted that scour depth is limited at some sites by underlying clay. A maximum non-dimensional scour depth of 1.8 S/D was recorded at Robin Rigg and Scroby sands, and 1.7 S/D at Gunfleet sands. Very small scour depths of up to 0.125 S/D were recorded at some piles at North Hoyle. The scour depth varied significantly between different piles at Scroby sands, from 0-7 m.

Very few studies have captured scour time development in the marine environment. Whitehouse et al. (2010a) plotted scour depth through time for several piles at Barrow offshore windfarm, but the data points are 3 - 6 months apart with the scour depth both increasing and decreasing between measurement points, indicating variable hydrodynamic conditions during that time. Whitehouse et al. (2011) and Rudolph et al. (2008) plotted some unique scour depth data through time from the N7 site, with measurements collected close enough to the installation date to enable the more familiar scour development curve (i.e. an increasing function but with reducing gradient) to be observed. Harris et al. (2011) plotted single measurements of scour depth from different sites in terms of time after installation. The data is quite scattered but there is evidence of the expected scour development trend here also.

Scour hole extents have also been measured in the field (Dixen et al., 2012a; Harris et al., 2011). Harris et al. (2011) found that scour hole slope angles tended to be shallower than the angle of repose of the sediment, and symmetrical upstream and downstream of the pile with slope angles of approximately 10 degrees at the bottom of the scour hole, in agreement with the findings of McGovern et al. (2014), Section 2.3.2, for scour in tidal flows. Harris et al. (2011) suggest that the change in scour hole shape is due to the hydrodynamics of the site but note that more research is needed to understand properly scour hole shape development. Rudolph et al. (2008) reported that scour extents were significantly wider and the slope angle was shallower in the field compared to in the laboratory. However, they propose that this is due to greater levels of turbulence in the field causing sediment to remain in suspension for longer. In contrast scour holes at Gunfleet sands windfarm were found to be asymmetric in the direction of flow, in closer agreement with laboratory studies under unidirectional current (Hoffmans and Verheij, 1994). Therefore, further investigation into the effects of a range of parameters on the scour hole shape would be useful to understand these differences in the field.

2.5.1 Comparison of laboratory and field data

A few studies have made comparisons between parameters for scour in the field and those in the laboratory. Guo et al. (2012), Whitehouse et al (2010a), Whitehouse et al (2011) and DECC (2008) plotted h/D or water depth versus S/D for laboratory and field data. Commonly, the data are so scattered that it is difficult to determine if the trends found in the laboratory are also observed in the field, but it can be seen that both data sets populate a similar range of values, Guo et al. (2012).

Mueller and Wagner (2002) plotted a range of parameters including S/D versus V/V_{cr}, D/d_{50} and h/D for bridge scour data compared with laboratory data. Again there is significant scatter in the data, but for the V/V_{cr} and h/D versus S/D graphs the envelope curves fitted to the laboratory data seem also to be valid for the field data.

One reason for the scatter in the field data in the above comparisons is that it is difficult to separate variables in the field data and multiple parameters will be varying in tandem. Secondly, scatter will be due to the field data not necessarily representing an equilibrium condition due to the changing flow parameters.

An alternative to this comparison is to take a case study approach. Lee et al. (2004) compared laboratory scour depth data with field data for a bridge during a specific flood event, which resulted in reasonable agreement. This shows that laboratory studies can be informative and can successfully model the scour process. However, this approach does not produce results that will be applicable to a wider range of sites.

Harris and Whitehouse (2014) plotted field data from only sandy sites against the laboratory data of Sheppard et al. (2011a) and found that, although with some scatter, there was a clear exponentially decreasing trend so that scour depth relative to water depth decreased with increasing water depth relative to pile diameter. This is interesting as it is the opposite to the

results most commonly reported in the literature, except for that of Link and Zanke (2004a). Harris and Whitehouse (2014) also point out that the laboratory data is for unidirectional flow but the field data relates to tidal sites yet both data sets are in agreement, thereby suggesting that scour depths can be equivalent under these flow conditions in contrast with the findings of the clear water tidal scour studies discussed in Section 2.3.2.

Jensen et al. (2006) made a comparison of field data from Scroby sands windfarm and Otzumer windfarm with laboratory data of tidal flows (Escarameia, 1998; Jensen et al., 2006), as well as unidirectional current (Sheppard 2003). Similarly to Harris and Whitehouse (2014) they found that there was substantial overlap between the tidal data from the field sites and the unidirectional current data from the laboratory so that it does not appear that scour depth under unidirectional flow is greater than under tidal flow as has been commonly suggested based on experimental data (see Section 2.3.2). This could be due to a difference in behaviour under clear water and live bed conditions, or due to other factors yet to be investigated such as the influence of bedforms, flow asymmetry, and spring-neap cycles. This is clearly an area in which further research would be useful.

This section has demonstrated the inherent difficulty in validating experimental work. The conditions in the field are more complex than tested, both in terms of steady state complexities (i.e. heterogeneous sediment beds) but also due to the dynamic nature of the sites including changing hydrodynamic conditions, 3D effects in the flow, and migrating sandwaves. Without an understanding of how these complexities affect the scour process it will not be possible to accurately model scour development in the field.

2.6 Scour Prediction

This section discusses the approaches to predicting scour depth. Modelling can be broadly split into three categories: ones with a basis in the physics of the problem (analytical or numerical), those that are based on experimental data and so are a combination of descriptions of physical processes and regression analysis (empirical or semi-empirical approaches), and ones that are purely based on finding a best fit to the data (algorithm style/neural networks). Deng and Cai (2010) provide a comprehensive review of the range of scour prediction methods in the context of bridge scour.

Overviews of numerical modelling of scour are given by Sumer (2004, 2007, 2008). While numerical modelling is an active area of research and is developing rapidly, there are currently some key limitations to this approach:

- difficulties with modelling turbulence and the free surface
- assumptions made in terms of the scour hole shape as it develops
- reliance on sediment transport formulas which have their own limitations (discussed previously in Section 2.1.1)
- the compromise between model resolution and computational time reduces the accuracy of the solution

These limitations mean that even in simple conditions the agreement between the numerical model and laboratory data may be limited, see Baranya et al. (2014). Most methods combine a hydrodynamic model to calculate bed shear stress with a morphology model to represent scour development. Simplified analytical equations based on this approach have also been offered (Mia and Nago, 2003; Veerappadevaru et al., 2012; Kothyari et al., 1992; Kothyari and Kumar, 2012). These reduce the computation time but have the same limitations in terms of the model assumptions. For this project numerical methods are not suitable because of the complex conditions to be investigated.

A wide range of neural network algorithms have been utilised by numerous researchers in recent years in an attempt to find a solution to the scour prediction problem (Bateni et al. 2007; Ismail et al., 2013; Azamathulla et al., 2010; Pal et al., 2012; Laucelli and Giustolosi, 2011; Najafzadeh et al., 2013; Akib et al., 2014; Hong et al., 2012; Ayoubloo et al., 2010; Kaya, 2010). Because of the difficulties in defining physical relationships between parameters analytically, this method uses an algorithm to define a best fit relationship between a set of inputs and outputs. While this means that no assumptions are made about the physical processes that might limit the model, it also means that the relationship determined between the parameters has no immediate physical meaning. The solution is dependent on the input parameters, the selected functional form/algorithm type, and the data used (i.e. field, laboratory, live bed, clear water) which are selected by the user. While a close fit may be achieved with the calibration data, the agreement is likely to reduce when the results are applied to a different data set, as the model is unlikely to be a true representation of the scour process.

Empirical approaches to scour prediction are the most widely used in design. This is probably because of their ease of use, applicability to a wide range of conditions and greater confidence in quantifying their performance. These approaches are somewhat similar to neural networks in that they are based on experiment data (and in some cases also field data), but consideration is given to the physical processes, in combination with the use of empirical constants. Because of the applicability to design, this type of modelling will be the focus in this project. A review of empirical prediction methods is given in the following section.

Empirical approaches can be split into two categories:

- approaches that provide a prediction of equilibrium scour depth only
- approaches that predict scour development over time

The first of these is discussed in Sections 2.6.1 – 2.6.4, and the second in Sections 2.6.5 - 2.6.7.

2.6.1 Equilibrium scour predictors

When reviewing the literature on empirical equilibrium scour predictors it is clear that there are a considerable number of formulas and range of formulations in terms of the mathematical functions and the choice of parameters. It is not the aim of this section to detail every approach, but instead key differences will be discussed. For further details and a comprehensive list of

prediction equations see Sheppard et al. (2011a). Some of the equations are also given in Appendix 4.

The simplest approaches to equilibrium scour depth prediction are based on only one variable, the pile diameter, being linearly proportional to equilibrium scour depth (Neill, 1973; Sumer and Fredsøe, 2002a). The equation of Sumer and Fredsøe is as follows:

$$\frac{S_e}{D} = 1.3 \tag{2.3}$$

Sumer and Fredsøe (2002a) defined the standard deviation as 0.7 S_e/D for their equation indicating the considerable potential for improvement of this method.

Another simple approach was offered by Shen et al. (1969) who treated scour depth only as a function of Reynolds number:

$$S_e = 0.000223 \left(\frac{VD}{\nu}\right)^{0.619} \tag{2.4}$$

Following the discussion in Section 2.2.6 it is not thought that Reynolds number is an important parameter for scour within the subcritical range. Therefore, it is more likely that this equation is simply representing scour depth as a function of pile diameter and flow velocity.

The approaches mentioned thus far have not included any influence of the sediment properties. Hancu (1971) and Breusers et al. (1977) included the velocity intensity parameter in their equations in order to account for the propensity for a particular sediment to erode under a given flow condition. Breusers' equation is given as (for the clear water regime):

$$\frac{S_e}{D} = \left(\frac{2V}{V_{cr}} - 1\right)\left[2\tanh\left(\frac{h}{D}\right)\right] K_1 K_2 \tag{2.5}$$

Hancu's formula also contains the Euler number whereas Breusers' equation accounts for flow shallowness. These choices probably reflect the parameter ranges in their respective laboratory studies.

Breusers' approach as well as that of Melville and Sutherland (1988) and Sheppard et al. (2011a, 2011b) is based on the flow intensity concept but also employs a set of K factors in the equation to account for a greater range of effects including structure shape and alignment, sediment size and water depth.

Melville's approach is interesting because it is based on envelope curves fitted to the data rather than best fit lines so that conservatism is built into the approach. While the agreement with data will therefore be reduced, this approach is potentially more useful in design. Conservatism can also be introduced by applying safety factors, so it is not necessarily beneficial to include conservatism in the original equation. Instead the main criteria for use of a prediction equation in design is the level of certainty in its performance over a full range of conditions.

Jain (1981) and Richardson and Davis (2001) use the Froude number as an alternative to the Reynolds number or V/V_{cr} parameter to represent the influence of velocity on scour depth. Both of these methods also take into account flow shallowness and the equation of Richardson and Davis (2001) uses the k factor approach to include the influence of pier shape and alignment and bed rippling condition (a way of accounting for clear water and live bed regimes). Their equation is given as:

$$\frac{S_e}{D} = 2.0K_1K_2K_3K_4\left(\frac{h}{D}\right)^{0.35}Fr^{0.43} \quad (2.6)$$

Where h is the water depth, D is the pile diameter, Fr is the Froude number, and K_1, K_2, K_3, K_4 are factors used to incorporate the effects of pier geometry and bed condition, see Appendix 4 for further details.

The problem with using Froude number instead of flow intensity is that the same scour depth will be predicted regardless of the sediment grain size. However, this approach was designed to be conservative, meaning that the agreement will be closest with data for the most severe scour conditions, i.e. in fine sands. The Richardson and Davis (2001) equation (known as HEC-18) is frequently used in design due to its conservatism. Even though it can be excessively conservative in some conditions, Ghosn and Wang (2003) suggest that a safety factor of 2 should be added to HEC-18 because of its poor reliability. This issue is also discussed by Briaud et al. (2014) who propose that an additional safety factor is used in certain scour conditions. This highlights the substantial level of uncertainty in even the most conservative of prediction approaches. Guo et al. (2012) and Calappi et al. (2010), have developed modifications to the HEC-18 formula to try to reduce the level of conservatism. These have not replaced the HEC-18 formula in design, because while the level of conservatism has been reduced, the uncertainty hasn't.

Most comparisons of laboratory and field data with prediction equations are characterised by significant scatter for both bridge and marine scour (Den Boon et al., 2004; Briaud, 2002). Several authors have made comparisons between a range of equilibrium scour prediction equations. Perhaps the most comprehensive of these is that of Sheppard et al. (2011a, 2011b), but also see Melville and Sutherland (1988), Johnson (1995), Jensen et al (2006), and Høgedal and Hald (2005). Some equations tend to over-predict while others under-predict scour depth, with Melville's approach consistently being the most conservative. However, for a given equation scour depths are commonly found to be both over and under-predicted when compared to a range of data (Matutano et al., 2013). For example, despite the fairly uniform sandy seabed at Scroby sands windfarm Jensen et al. (2006) found that neither the approach of Breusers, Sumer, Richardson and Davis nor Sheppard enveloped all of the data points. This is difficult for design because of the need for conservatism. These comparisons demonstrate the shortcomings of present prediction methods; that they do not deliver the level of accuracy that would indicate full understanding of the scour process.

2.6.2 Scour prediction in complex flows

Sumer et al. (1993) and Petersen et al. (2012) modified Sumer's original equation to model scour in waves and wave-current combinations in the live bed regime by including dependence on the KC parameter and also on the U_{cw} parameter in the case of wave-current flows (Appendix 4). Rudolph and Bos (2006) offer an alternative wave-current scour equation based on the same parameters but with a different formulation. Qi and Gao (2014a) developed an equation for scour in wave-current flows based on the Froude number rather than KC number.

Few studies have addressed prediction of equilibrium scour depth in tidal flows, apart from May and Escarameia (2002) who offered an equation based on Melville's approach. This incorporated a parameter to reflect the tidal cycle duration relative to the scour timescale, however, this approach has not been validated.

2.6.3 Modelling approaches for complex sediments

Annandale and Smith (2001) provided an approach for scour prediction in complex soils based on the erodibility index method detailed in Annandale (1995). The approach is also discussed in Harris et al. (2010b) who note that while this method was developed for rock scouring, it can also be applied to scour depth calculation in layered marine soils. An erodibility index is calculated for each soil type with depth and compared to the stream power at that depth which is a function of the equilibrium scour depth calculated for example using the HEC-18 formula. Therefore, this approach is limited by the performance of HEC-18, the relationship between stream-power and depth and classification of the soil parameters.

The erodibility method is also discussed by Govindasamy et al. (2008), Briaud et al. (1999), and Briaud (2002). Erosion tests on soil core samples are used to construct a chart of shear stress versus erosion rate. This is then incorporated into established prediction techniques, thereby sharing their limitations. Importantly, each of these approaches assumes that there are no interaction effects between the different layers of sediment with depth.

A variety of approaches have been used to incorporate effects of sediment non-uniformity into prediction equations. One method is to define an effective sediment size to replace the d_{50} parameter so that the scour depth reached in the non-uniform sediment is modelled by the size of uniform sand which would attain an equivalent scour depth. However, different definitions for effective sediment size have been suggested demonstrating the difficulty of obtaining close agreement with this approach (Lim, 1994; Kothyari et al., 1992). Melville and Sutherland (1988) also defined an effective sediment size but additionally altered the definition of flow intensity to account for the increase in critical velocity due to bed armouring.

Molinas (2003) developed a representative grain size for non-uniform sediment based on the size of the coarse fraction and developed a K 'reduction' factor to account for the influence of the coarse fraction on scour depth. Similarly Den Boon et al. (2004), Raikar and Dey (2009) and Richardson and Davis (2001) developed factors that could be incorporated into existing prediction equations to take into account sediment non-uniformity and bed armouring effects,

although in the HEC-18 formula sediment gradation effects are only taken into account for coarser sands where d_{50}>2 mm and d_{95}>20 mm.

2.6.4 Concluding remarks for equilibrium scour prediction

The wide range of equilibrium scour predictors indicates that the scour process cannot be comprehensively modelled to account for the full range of conditions experienced in the field. Clearly there is a gap in the research in terms of understanding:

- The parameters that are important for scour
- How to non-dimensionalise parameters
- The correct relationships between parameters
- For wave-current flows, how to define the combined velocity from wave and current components
- For mixed sediments how to define non-uniformity and bed armouring effects

Representation of scour in the clear water regime is also lacking in the wave and wave-current formulae. The focus on live bed conditions is probably due to the prevalence of this regime in the field, however, better understanding of scour in the clear water regime may help to improve modelling in the live bed regime also.

2.6.5 Prediction of scour time development

As with the equilibrium scour predictors there is no consensus in the literature as to an approach for modelling the time development of scour, and again many different equations are offered. These are also reviewed in Sheppard et al. (2011a) and the details of some of the equations are given in Appendix 4. This section will outline the different methodologies and discuss the limitations associated with a range of approaches.

Scour time prediction methods can be classified as those that are fully predictive techniques that provide a solution from a simple set of measureable input parameters, and those techniques that require empirical adjustment of the parameters in order to fit the data. The latter will be termed ‘curve fitting techniques’.

Firstly considering fully predictive methods, Melville and Chiew (1999), Melville (2002) and Melville and Coleman (2000) extended their equilibrium scour prediction model by adding a K time factor, defined as:

$$K_t = exp\left\{-0.03\left|\frac{V_{cr}}{V} ln\left(\frac{t}{t_e}\right)\right|^{1.6}\right\} \quad (2.7)$$

This method is therefore still based on flow intensity and is still designed to be conservative due to the use of envelope curves. The time factor follows an exponential function and depends on the time to equilibrium parameter which they defined using flow intensity and pile diameter.

Oliveto and Hager (2002) and Hager et al. (2002) developed an equation based on a log function and with Froude number rather than flow intensity:

$$Z = 0.068{F_d}^{1.5}\log(T_c) \quad (2.8)$$

where $Z = \frac{S}{(D^{2/3}h^{1/3})}$.

However, they used the densimetric particle Froude number, F_d, in which the length scale is based on the sediment grain size, thereby accounting for sediment parameters in a similar way to the flow intensity parameter. The equation is a function of a timescale parameter defined from σ_g, median grain size, pile diameter, water depth and relative gravity ((s-1)*g).

Lança et al. (2013a) provide another equation based on an exponential function which was first used by Franzetti et al. (1982):

$$\frac{S}{S_e} = 1 - e^{[-a_1(Vt/D)^{a_2}]} \quad (2.9)$$

but with new parameterised definitions for the original empirical constants, a_1 and a_2, in the equation. This equation is different to the others in that it does not have a 'timescale' parameter or a flow intensity concept because it was formulated from a limited range of data (at critical velocity). Therefore, this equation is unlikely to be suitable when applied to a wider range of data sets. The equation is a function of the equilibrium scour depth parameter, and this must be calculated using a standard approach (see Section 2.6.1) which may significantly limit the model performance.

The approach applied by Sumer and Fredsøe (2002a), Sumer et al. (1992), Sumer et al. (1993), Petersen et al. (2012) and Whitehouse (1998) is probably the most well-known approach for scour time development modelling:

$$S(t) = S_e\left[1 - \left(e^{-t/T_c}\right)^n\right] \quad (2.10)$$

This simple equation is also based on an exponential function and requires knowledge of the equilibrium scour depth and a timescale parameter, T_c. A variety of approaches have been offered to obtain the timescale parameter, from curve fitting techniques such as the time at which a line drawn tangent to the scour time curve at time t = 0 intersects a line marking the equilibrium scour depth (Sumer and Fredsøe, 2002a), or defining the timescale as 63% of the time to equilibrium (Whitehouse, 1998). Petersen et al. (2012) presented a method which does not require prior knowledge of the scour curve or equilibrium time by defining a non-dimensional timescale parameter which they related empirically to the dimensional timescale used in the scour time prediction equation. Clearly there is not currently a consensus on how best to model this aspect of the scour problem.

In summary, the main limitations of these approaches are:

- reliance on knowledge of the equilibrium scour depth, and/or the equilibrium time parameter
- dependence on the accuracy of the equilibrium scour predictor used to obtain S_e
- the correct definition of a timescale parameter or equilibrium time

- the mathematical function used and the relationships between parameters
- the choice of parameters used in the equation to represent the scour development process

In terms of curve fitting approaches, Borghei et al. (2011) used a trial and error approach to determine which mathematical function could best represent the scour development curve. They concluded that a power function was more appropriate than a logarithmic function. They devised a new scour time development equation:

$$S(t) = S_e \left[1 - e^{a_1 \left(\frac{t}{t_e}\right)^{a_2}}\right] \tag{2.11}$$

However, this did not include definitions for the empirical coefficients, a_1 and a_2, so these must be selected based on the fit to data, which limits the predictive capabilities of this approach.

Sheppard et al. (2004) suggested two different equations that can be used to model the scour development curve in a range of conditions by adjusting the coefficients. One uses exponential functions, while the other is a linear formulation (Appendix 4). The purpose of these equations is to enable extrapolation of laboratory curves to equilibrium scour depth, so that tests in the laboratory don't need to be run for such long durations. Sheppard et al. (2004) note that there is a minimum test duration in order for the curve fitting to result in accurate equilibrium scour depths, in agreement with Simarro-Grande and Martin-Vide (2004), see Section 2.7.4. However, there is uncertainty in this approach which is exacerbated by the use of two different equations without determining the situations in which each formula should be applied.

Another approach employed by a few researchers is to model different parts of the scour development curve with different functions. While this necessitates a more complex equation, it enables assessment of whether one of the limitations of other prediction approaches is due to the scour depth not following the same function throughout its progress. There is physical evidence for this in terms of changes in the development of the horseshoe vortex and bed shear stress with depth, as was discussed in Section 2.1.3.

Talebi et al. (2004) concluded that the initial part of the curve is almost linear, so proposed modelling the scour curve with a linear function followed by an exponential function. Chang et al. (2004) split the scour development curve into three separate models, with a linear function for the initial section, followed by two different exponential formulations. No definitions for the empirical constants in these approaches were offered. Guo (2014) produced a combined equation that models the first part of the scour curve with a power law, the second part with a logarithmic function and the final part with an exponential function. The full equation can be written in the form:

$$t = -T_c \left[\frac{S}{S_e} + \frac{S^2}{2{S_e}^2} + \frac{S^3}{3(D\tan\varphi+1){S_e}^3} + ln\left(1 - \frac{S}{S_e}\right)\right] \tag{2.12}$$

This equation uses the equilibrium scour depth and a characteristic time as input parameters; the latter is reported to be a little smaller than the equilibrium time, but again is not fully defined.

Sheppard et al. (2011a) found that there was no consistency in the results when comparing a range of scour time development prediction methods and all of the approaches tested had relatively large errors. Sheppard et al. (2011a) discounted the approaches of Sumer and Fredsøe (2002a) and Chang et al. (2004) after a preliminary comparison indicated that the errors were particularly large in these equations.

2.6.6 Scour time prediction in complex hydrodynamics and sediments

Sumer and Fredsøe (2002a) present an extension to their time prediction equation to apply to scour development in waves by adjusting the non-dimensional timescale parameter to be a function of KC number and Shields parameter. Similarly Rudolph et al. (2008) modified Sumer's method to predict scour in waves or currents by altering the definition of the timescale parameter depending on each of these conditions. Rudolph et al. included the sediment mobility number in the definition, so that the influence of the sediment size on the scour process is taken into account (Appendix 4). However, they note that this is an order of magnitude approach.

Scour development in time-varying unidirectional flow has been modelled by linear superposition of scour time predictions for each change in hydrodynamic condition (Chang et al., 2014b) following the findings from laboratory studies of scour development in these flows (see Section 2.3.1). In terms of designing for the marine environment Harris et al. (2010a) developed a time stepping model based on the equilibrium scour depth equation of Breusers et al. (1977) and Sumer's scour time prediction equation, that enabled varying hydrodynamic conditions to be input. Time varying field hydrodynamics have also been input into models by Dixen et al. (2012a) and Rudolph et al. (2008). While the agreement with data has been shown to be reasonable for a few cases, the full validity of these approaches has yet to be assessed.

Few methods incorporate effects of complex soils in the prediction of scour time development directly. Instead these are taken into account through the use of the S_e (equilibrium scour depth) parameter, assuming that the scour curve in non-uniform sediment is equivalent to that in a uniform sand with the same equilibrium scour depth.

2.6.7 Concluding remarks on scour prediction

The wide range of prediction methodologies demonstrates that there is no universally accepted approach to scour prediction. Scour prediction is challenging because the scour process is influenced by many different parameters, and without a full understanding of these, as has been demonstrated in Sections 2.2 and 2.3 it is difficult to derive a prediction methodology that is comprehensive enough to perform satisfactorily in design. This highlights the limitations in knowledge and understanding of scour, and the need for further research in order to improve the prediction methods which are so crucial for optimized foundation design.

2.7 Research methodology

As has been shown in this literature review the scour research is predominantly based on laboratory measurements, but other research approaches have also been employed, including

analytical and numerical modelling, regression analysis and field studies. This section presents the justification for the laboratory based approach chosen for this project and then reviews some of the aspects in the literature pertinent to this methodology.

2.7.1 Research approaches

Given the limitations of the analytical approaches for scour modelling and the use of empiricism in at least some parts of the solution (see Section 2.6), investigation of more complex conditions for scour relating to the soil and hydrodynamic parameters would currently be difficult using this approach. Instead laboratory testing is determined to be the most appropriate method to meet the aims of this project because it enables complex interaction effects between parameters to be observed.

Zevenbergen et al. (2004) listed the main advantages of laboratory testing:

- None of the simplifications integral to numerical modelling are needed
- Scale modelling is cheaper and more practical than field studies
- Scale modelling enables better control of parameters than is possible in the field
- Laboratory testing results in qualitative, insightful results at the same time as quantitative measurement of parameters

2.7.2 Laboratory testing

Before presenting the full details of the experiment design for the laboratory flumes in Section 4, it is important to first discuss those aspects which required research in order to implement. In particular, a detailed review of measurement techniques for scour monitoring in the laboratory was conducted (Section 2.7.3). Other aspects of the test procedures also needed to be considered in order to fully understand the limitations of laboratory testing and the potential influence of a range of factors on the tests, these are discussed in Section 2.7.4.

2.7.3 Scour measurement techniques

On inspection of the literature, many different techniques have been used to measure scour depth development in the laboratory. No single technique is ideally configured for this application, and so various configurations have been proposed that suit the specific tests and laboratory facilities of each study. This section summarises the main techniques and seeks to highlight the advantages and disadvantages of each so that the most suitable techniques can be determined for use in this project.

a) Scales

Probably the simplest measurement technique in the literature is to attach or mark a scale onto the pile itself. Appendix 1 details those studies which have used this technique, in a variety of configurations. As well as being cheap and simple to set-up and collect measurements, it has the advantage of measuring both time development of scour and the equilibrium scour depth.

Another advantage is the capability of this system to be completely nonintrusive, although some of the more complex automated techniques lose this advantage (Lin et al., 2005; Kong et al., 2013; Babu et al. (2002, 2003a, b)).

The temporal resolution of this technique is also excellent. However, the vertical depth resolution varies depending on the system used.

The main disadvantage of this technique is that it is a point measurement so the scour hole shape and extent are not measured, although some researchers have placed multiple scales around the pile to monitor scour depth at more than one point (Chaudhuri and Debnath, 2013; Sheppard et al., 2004). Sumer and Fredsøe (2001b) used a set of measurement pins to monitor scour depth across the scour hole. However, this is an intrusive technique and scour is likely to occur local to each pin making it difficult to measure the true bed level.

Note that the type of system used depends on the scale of the laboratory facilities and it will not be possible to set-up monitoring equipment such as cameras inside small diameter piles.

b) Point gauge

Mechanical point gauges generally consist of a thin probe with a pointed end which is slid vertically relative to a fixed scale until the point is just touching the sand. The depth of the bed can then be read off the scale, although some digital point gauges have also been developed (Akib et al., 2014). The point gauge systems described in the literature for scour measurement are detailed in Appendix 1.

The main advantages of this technique are its simple and cost effective set-up, and the high precision of measurements which can be taken at any point on the bed. Therefore, in contrast to pile scales the point gauge can be used to collect 3D profiles of the scour hole. However, a point gauge has to be traversed to take multiple measurements and repositioning the gauge in the z direction takes time. The time taken to collect a bed profile will be long compared to the rate of scour development and consequently a bed profile collected in this way during a running test cannot be approximated as an 'instantaneous' scour hole. Many authors resort to only taking measurements at a small number of points on the bed (Hager et al., 2002; Li et al., 2002), or only considering the equilibrium condition (Sturm and Janjua, 1994; Whitehouse et al., 2006; Eadie and Herbich, 1986; Thompson and McCarrick, 2010; Babu et al., 2002; Debnath and Chaudhuri, 2010).

Another issue with point gauges is that they can be intrusive to the experiment. Unless the diameter of the submerged part of the probe is very small a scour hole local to the gauge may form if measurements are collected while the flow is running. It is also very easy to disturb the bed by overshooting the gauge, especially where bedforms obscure the bed level at the location of the probe. Ballio and Radice (2003) attempted to reduce intrusivity by using an optical non-contact probe. While this did not directly contact the bed, it needed to be in close proximity to it and the sensor diameter was such that it was still likely to cause disturbance to the flow (see Appendix 1).

c) Echosounder

An echosounder measures the time taken for sound waves to be reflected from the bed and received back at the sensor. As the speed of sound in water is known, the distance travelled can be calculated. The emitted sound wave spreads out as it travels through the water so that the beam has a conical shape. This means that rather than being reflected from a point on the bed, it intersects a small area known as the beam footprint from which it derives a single depth reading. The size of this area depends on the distance that the beam has travelled (proximity of sensor to bed) as well as the size and specifications of the sensor. According to De Jong et al. (2002) the beamwidth for a circular transducer is approximately:

$$\beta = 65\frac{\lambda}{d} \tag{2.13}$$

where d is the sensor diameter and λ is the wavelength of the transmitted signal. Therefore, for a given wavelength (or frequency) the smaller the transducer diameter, the larger the beamwidth. This is unfortunate in terms of small-scale laboratory work where both a small beam footprint is needed so that the horizontal resolution is acceptable and a small sensor diameter is necessary to reduce the level of disturbance to the flow, so this can only be achieved by using high frequency sensors. A plot to illustrate the difference in depth measurement between wide and narrow beam echosounders is given in IHB (2005), and Thorne and Hanes (2002) provide a comprehensive review of acoustic measurement techniques. Also see De Jong et al. (2002) for discussion of the wider issues for echosounder technology.

Because of the compromise between sensor diameter and horizontal resolution, acoustic sensors are more suited to use in the field or in large-scale laboratory studies (Stahlmann and Schlurmann, 2010; Sheppard and Miller, 2006), where larger sensor sizes and beam footprints are acceptable. Despite these limitations echosounders have also been used in small-scale laboratory facilities and a review of the studies employing echosounders for scour measurement is given in Appendix 1.

The loss of horizontal resolution due to the relatively large size of the beam footprint in comparison to the scale of the bedforms in the laboratory can be significant. Dingler et al. (1977) compared measurements collected with a point gauge and an echosounder. They found that while the accuracy was similar on a flat bed the accuracy of the echosounder measurements decreased over a sloping bed. Best and Ashworth (1994) also reported erratic measurements over sudden slope changes and Shepherd (1996) noted that steep ripples and edges of small stones were not measured accurately. Loss of accuracy can also be induced by noise (Dingler et al., 1977) and by reflections from suspended particles (Mcgovern et al., 2014) which may be problematic in live bed conditions and in the initial stages of scouring in clear water conditions.

Echosounders can be traversed in a similar manner to a point gauge to map the bed. One of the main advantages of echosounders is that they do not need to be in close proximity to the bed so they have the potential to be significantly less intrusive than point gauges (assuming the sensor

is not very large), and echosounders can be traversed at significantly faster speeds because the vertical position does not need to be altered. Despite this the time required to collect a bed profile may still be long compared to the rate of scour, especially in the initial stages of testing. Some authors have collected profiles only at the equilibrium stage (Chen et al., 2012; Lee and Sturm, 2009) while others have used more than one sensor to record simultaneous depth measurements at different locations (WenGang and FuPing, 2014; McGovern et al., 2012; Guney et al., 2012; Guney et al, 2011; Stahlmann and Schlurmann, 2010; Sheppard and Miller, 2006). It is difficult to determine the level of intrusiveness of the sensors in many of the studies as the sensor dimensions and submergence depth are often not reported.

d) Laser

Laser probes have also been used for scour depth measurement in the laboratory. Similarly to the echosounder systems, laser probes provide point measurements from a reasonable distance away from the bed and can be attached to a traverse to facilitate 3D bed profiling. For information on the different types of laser distance sensors see Marszalec and Marszalec (1994).

The scour studies employing laser distance sensors in the laboratory are detailed in Appendix 1. As with the point gauge and echosounder techniques there is a wide range of system configurations.

The fine horizontal resolution achievable with laser probes is a significant advantage compared to using an echosounder. Lasers have a footprint of about 1 mm on the bed, which is an order of magnitude smaller than the resolution that can be obtained with an echosounder. Mlaenik et al. (2004) quantified the performance of a laser probe by collecting measurements over a series of objects of known dimensions. While the agreement in this study was excellent, some issues with measurement accuracy in scour studies have been reported by Jensen et al. (2006) and Hartvig et al. (2010) due to the pile causing interference with the backscattered light.

In most of the studies employing laser distance sensors (Stahlmann and Schlurmann, 2010; Margheritini et al., 2006; Jensen et al., 2006; Hartvig et al., 2010; Zhao et al., 2010; Unger and Hager, 2007) see Appendix 1, the flow is paused or drained prior to collecting measurements. Many studies do not report the dimensions of the sensor, but in the few that do the dimensions are quite substantial, so these systems are likely to be more intrusive to an experiment than echosounder devices if operated while the test is running. Link (2006) developed a fully non-intrusive system by traversing a horizontally aligned laser inside the pile, although this places constraints on the areas of the surrounding bed that can be measured and is limited by the pile diameter. This makes laser sensors (as with echosounders) perhaps more appropriate for use in larger scale facilities.

e) Photogrammetry

Photogrammetry is a technique whereby 3D measurements of an object are obtained from photographs of the object. The 3D object coordinates can be computed from the 2D image

coordinates by establishing a geometric relationship between them using the principal of colinearity; that light travels in a straight line from the point on the object through the camera to the point on the image plane. A detailed description of the underlying theory for photogrammetry is given in Mikhail et al. (2001) and Cooper and Robson (1996), and the mathematical computation for this method is summarised in Appendix 8.

Due to the number of unknowns compared to the number of equations in this method, a calibration step is necessary in order to compute some of the parameters specific to the camera used (focal length etc.) by initially photographing an object with known coordinates. Once the camera parameters have been determined, the equations can be solved if at least two images of the object points to be computed are available. However, a more rigorous solution is obtained by simultaneously processing the coordinates of many points in the object space from a large number of photographs taken from different orientations. This is known as bundle adjustment.

While the above method is an explicit method because all of the variables have physical meaning, there are alternative implicit methods for computing the 3D coordinates from the images using a linear direct transformation or the two-step method (see Wei and Ma, 1994 and Mikhail et al., 2001 for details of these). However, the bundle adjustment method is generally considered to be the most accurate (Remondino and Fraser, 2006). Salvi et al. (2002) and Remondino and Fraser (2006) provide further discussion of the differences in the computational methods and camera calibration techniques.

There has been increasing interest in using photogrammetry for scour measurement in the laboratory, however as noted by Shepherd (1996) photogrammetry still requires development for use in this application, because of the departure from the colinearity principal caused by the air-glass-water interfaces if the cameras are set up outside of the flume. A comprehensive solution to account for refraction of light through media interfaces has yet to be adopted in the field of photogrammetry, although some methods have been proposed. Chari and Sturm (2009) note that as a result of this, refraction is either ignored, included as an aberration to perspective imaging (i.e. in a similar way to lens distortion modelling, see Appendix 8), or a correction is made by using iterative optimisation. Kotowski (1988) states that the presence of refractive surfaces between the object and camera may cause too much of a deviation from the colinearity principle to be appropriately modelled in this way, but if the refractions are small, or close to the camera and symmetrical this may not be an issue; for example this works well for underwater cameras (Agrawal et al., 2012; Mulsow, 2010; Kotowski, 1988).

A method for accounting for refraction was proposed by Kotowski (1988). He suggested a physically based approach known as ray tracing, where the paths of individual light rays between the object and image are modelled following Snell's law. Muslow (2010) notes that this method is problematic because the direction in which light travels from a point on the object is unknown and an iterative method is needed to find a solution, which is reliant on deriving appropriate algorithms to increase the chance of solution convergence.

Compared to the other measurement techniques discussed in this section, 3D multi-media photogrammetry has the significant advantage of being completely nonintrusive as the equipment can be set up from outside the basin, while also providing instantaneous measurement of many points over an area during testing, thereby negating the need for slow traversing systems and pausing the flow. As refractive photogrammetry is an area of ongoing research, only a few authors have attempted to use photogrammetry systems in the laboratory, and a variety of compromises have been made for successful application of the technique to scour measurement. The known studies are listed in Appendix 1.

It is clear from the table in Appendix 1 that to date no systems have attained the optimum level of temporal and spatial resolution simultaneously with a nonintrusive system. Although Baglio et al. (2000), Baglio et al. (2001), Baglio and Foti (2003), Baglio et al. (2005) and Sumer et al. (2013) configured a system to monitor scour development during testing from outside of the flume, the algorithms used do not account for refraction effects and consequently the accuracy of the solution is reduced. Higher accuracy techniques have compromised by collecting measurements with the flow paused or drained (Raaijmakers at al., 2012; Umeda et al., 2008; Rosier et al., 2004), or alternatively the spatial coverage has been reduced to 2-dimensional profiling (Huang et al., 2010).

f) Concluding remarks on scour measurement

This section has reviewed the main techniques for scour measurement in the laboratory comprising pile scales, point gauges, echosounders, laser distance sensors and photogrammetry. While photogrammetry has the potential to provide nonintrusive, high precision, high resolution measurements of many points on the bed instantaneously, a system capable of properly accounting for refraction while enabling time development of scour to be captured has to date not been accomplished. The lack of development of a workable and robust solution for dealing with refraction indicates that this technique would require significant development prior to successful implementation in the laboratory, or compromises would need to be made in terms of the operational performance. Laser distance sensors and echosounders have the potential to be reasonably nonintrusive if the sensor diameter is small, but this has to be balanced by the resolution and expense of the device. Point gauges may be more precise but it is considerably more time consuming to collect a bed profile, and none of these three methods enable simultaneous measurement of a number of points on the bed. The pile scale is a nonintrusive and simple system providing scour depth measurement at high temporal resolution, but does not allow the scour hole shape development to be captured. The scale of the laboratory facilities has been shown to be important for choosing an appropriate measurement technique depending on its dimensions and resolution, and affecting the placement and configuration of equipment.

2.7.4 Other considerations for experimental work

In this section the limitations of laboratory testing are considered and aspects which will aid experiment design are discussed.

a) Scaling experiments for the laboratory

In order to model correctly the processes in the field at smaller scale in the laboratory, consideration should be given as to how to scale correctly the different parameters to ensure similitude in the model. As discussed by Heller (2011) the principle is that geometric, kinematic, and dynamic similarity must be maintained, so that all length scales, flow patterns and ratios of forces between prototype and model are constant including inertia, gravity, viscosity, surface tension, elastic compression and pressure (Fowler, 1993).

Hughes (1993) provides a comprehensive discussion of scaling for the laboratory and presents the derivation of a set of non-dimensional parameters from the continuity and Navier-Stokes equations: the Strouhal, Froude, Reynolds, Weber, Cauchy and Euler numbers. These must remain constant for perfect similitude between the model and field scales.

However, as discussed by Payne (2008) it is not easy to scale the Froude and Reynolds numbers at the same time because the fluid viscosity and gravity are usually constant between model and prototype. These could be changed by using a centrifuge or a different liquid but this is difficult in practice. Instead a commonly adopted solution is to determine the dominant forces in the given situation and ensure that these are scaled correctly.

Fowler (1993) states that for coastal modelling inertia and gravity forces are usually dominant hence it is most important to scale Froude number correctly. Heller (2011) notes that scaling based on the Froude parameter is suitable where friction effects are negligible or for highly turbulent phenomena since the energy dissipation depends mainly on the turbulent shear stress terms which are correctly modelled by Froude scaling. Reynolds scaling becomes important in air, or in laminar boundary layer problems.

The impact of the incorrect scaling of Reynolds number in the laboratory is expected to be small if the boundary layer is in the fully rough turbulent regime, where viscous effects are generally confined to the boundary layer and independent of Reynolds number (Heller, 2011). However, a study by Huang et al. (2009) indicated that the lack of similitude in Reynolds number may affect scour experiments due to differences in the level of turbulence in the flow field altering the sediment transport characteristics.

The lack of Reynolds number similitude may be more apparent in wave flows. The effect of this was demonstrated by Prepernau et al. (2008) who ran large scale wave scour tests and found that the non-dimensionalised scour depth was consistently larger than that in the small-scale tests of Sumer et al. (1992).

b) Issues with sediment scaling in the laboratory

Consideration also needs to be given as to how to scale correctly the sediment properties. Hughes (1993) discusses criteria for sediment scaling and derives a set of non-dimensional parameters that should be conserved between the prototype and model: grain Reynolds number, densimetric Froude number, relative length, relative fall speed, and relative density.

This is difficult in practice because of conflicts between the fall velocity of the sediment and geometric scaling requirements (Sutherland and Whitehouse, 1998). In the scour problem it is generally expected that bedload is the dominant sediment transport process rather than suspended load and therefore it is the geometric scaling that is important (Fowler, 1993). This also satisfies the Froude scaling requirements discussed in the previous section. However, there is an issue with geometric scaling of sediment grain size if it is reduced to less than about 0.08 mm in the laboratory because of the introduction of cohesive effects (Hughes, 1993). Furthermore, if the sediment size is reduced to below about 0.6 mm a ripple forming sediment will be used to model a non-rippling sediment (Jehanno et al., 2012).

One commonly adopted solution for these issues is to instead ensure similitude of the Shields parameter (Whitehouse, 1998). This results in the use of a larger grain size in the laboratory than would be determined from geometric scaling considerations thereby avoiding cohesive effects, and ensures that the correct sediment transport regime is observed in the laboratory (clear water or live bed conditions), but the compromise with this method is that the flow velocity will be faster than that specified by Froude scaling.

Another option discussed by Jehanno et al. (2012) is to use a lighter material to model the sediment so that the critical velocity is correctly represented, adhering to Froude scaling. However, Sutherland and Whitehouse (1998) note that when using lightweight sediment, due to the lower density and larger diameter of the particles the effects of pressure gradients on the flow within the bed will be more apparent.

The lack of similitude for all parameters can cause distortions to the size of scour depth and to the timescale of the process in experiments (Sumer et al., 2001), particularly due to differences in Reynolds number, bed roughness, pile roughness, bed ripples, wave-soil interaction, and incoming flow turbulence (Sumer 2004). Sumer (2004) notes that the best way to reduce scale effects is to run larger scale experiments, or experiments can be conducted at a range of scales to try to quantify the effects on the scour process.

It is often noted that scour depths tend to be larger compared to the pile diameter in the laboratory than in the field because of the relatively larger grain size and increased flow velocity to maintain similitude of the Shields parameter, resulting in differences in the flow patterns around the cylinder (Ettema et al., 1998). Ettema et al. (2006) and Kirkil et al. (2004) used ADV measurements to show that small cylinders shed more frequent, stronger eddies with a higher capacity for sediment transport than larger cylinders in the same flow conditions. Ettema et al. (1998) also note that the Euler number is larger in the laboratory than in the field so that there is a steeper pressure gradient in the flow at smaller cylinders, and Lee and Sturm (2008) attribute the larger scour depths in the laboratory to the larger D/d_{50} ratio. They concluded that the sediment entrainment and transport processes in the scour hole are linked to the frequency of the horseshoe vortex fluctuations, which they found to depend on D/d_{50}. Each of these aspects contributes to the differences in the processes between small and large scale. However, it is

currently uncertain as to how these aspects interact with each other and which are the dominant processes and the situations in which these occur.

Sumer et al., (2001) note that laboratory tests do not have to be seen as scaled down models from prototype but instead as investigations of basic processes, so that regardless of the scaling issues laboratory testing is a valuable first step towards understanding the scour problem.

c) Ripples and bed forms

One issue ensuing from the scaling considerations to discuss further is the formation of ripples on the sediment bed. Kawata and Yoshito (1988) found that the ripple dimensions are usually considerably smaller than the dimensions of the scour hole in the field whereas in the laboratory ripples are often of a similar order of magnitude to the scour hole when the sediment is not scaled geometrically (Sutherland and Whitehouse, 1998). Although the existence of a ripple induced scale effect in the laboratory is well known, the impacts of this on scour development have so far proven difficult to quantify (Ettema et al., 1998). The various influences ripples have on scour tests are discussed in this section.

Ettema et al. (1998) note that sediments have a propensity to ripple if the grain size is less than about 0.6 mm because the particles are small relative to the viscous sublayer. According to Coleman and Melville (1996) ripples start to form on a mobile bed as random pile ups of sediment build up, trapping further sediment. When the ripple approaches the bed roughness height, ripples begin to be generated at preferred spacings downstream. The wavelength of the ripples is a function of the sediment size, which explains the relatively larger ripple dimensions in the laboratory when geometric similitude of the grain size is not observed in experiments.

Melville (1984) found that the scour depth was significantly smaller in ripple forming sediments than in non-rippling sediments under a unidirectional current close to critical velocity due to the change in bed roughness and the migration of ripples through the scour hole, although further into the live bed regime the ripples were washed out and the scour depth coincided with that in non-rippling sediments again. Khalfin (2007) reported that scour depth was similarly reduced in ripple forming sediment compared to non-rippling sediments in waves.

Prepernau et al. (2008) noted that it can be difficult to distinguish between the scour patterns and ripple formation around the pile in the laboratory, which has consequences for the accuracy of scour measurement, and may explain differing results in some studies. Sutherland and Whitehouse (1998) suggested that the influence of ripples located at some distance from the pile may be negligible as the amplification of shear stress at the pile may be sufficient to cancel out any effect. Sumer et al. (1992) reported that there was little difference in scour depth in the live bed regime when the ripple dimensions were varied, although they did not compare these results with non-rippling sediment.

Yoon (2004) found that the dimensions of bedforms generated downstream of a pile decrease with increasing pile diameter, and that the bedform dimensions are dependent on the Froude number, implying that in the laboratory the effects of ripples will vary with the test conditions.

Ripples also influence the flow patterns by increasing turbulence in the near bed region and altering the velocity profile (Fredsøe et al., 1999), and in wave flows ripples increase wave reflection (Dalrymple and Kirby, 1986). While it is probable that these aspects will have additional impacts on scour development these have yet to be quantified.

d) Global scour and depth degradation

Another sediment transport process that can affect scour development in the live bed regime is a general lowering of the bed level from the initial height, making scour depth difficult to determine. This occurs when there is a lack of upstream sediment to replenish the downstream section as sediment is transported along the flume.

In the design of live bed scour tests it is important to consider this effect as it is an inherently different process to the scour induced by the structure. Bed lowering can be prevented by having adequate sediment upstream of the structure compared to the timescale of the scour tests (Roulund et al., 2005; Sumer et al., 2013) or by introducing a sediment feed (Sheppard and Miller, 2006; Chiew, 1984; Melville, 1984). Otherwise bed degradation can be taken into account when measuring scour depth by adjusting the datum level to coincide with the global scour level (Dey et al., 2008; Prepernau et al., 2008).

e) Blockage and side wall effects

In the design of flume studies it is important to consider the effect of the proximity of the flume walls on the experiment. Blockage effects occur when the flow is accelerated due to a reduction in cross-sectional area. This will occur in scour studies if the pile is overly large relative to the width of the flume, resulting in contraction scour. Whitehouse (1998) states that blockage effects will be negligible when

$$\frac{A_s}{A_f} < 0.167 \tag{2.14}$$

where A_s in the cross sectional area of the structure and A_f is the cross sectional area of the flume. However Hager et al. (2002) found that a higher ratio of D/B<0.65 was adequate, where D is the diameter of the pile and B is the width of the flume. In contrast Chiew (1984) recommended using a smaller ratio of D/B<0.1. Ballio et al. (2009) conducted a series of tests with different blockage ratios. For the most part there was little change to the scour depth when D/B<0.33, and there was no change to the scour depth once D/B<0.1-0.17 so there is reasonable agreement between these studies.

The proximity of the structure to a wall may also impact the tests, causing flow acceleration and changes to the wake structure. Based on potential flow theory Sumer and Fredsøe (1997)

calculated that the wall effect is negligible in wave flows once the distance to the wall is greater than 1 pile diameter, and 1-2 pile diameters in currents.

A further consideration is the distance of the circumference of the scour hole from the flume walls. Interestingly few studies report these dimensions and there is little information on the impact that the proximity to the wall may have on scour hole development.

f) Interaction of two piles

A similar issue to interaction between the pile and the flume wall is the interaction of one pile with another pile. Consideration of this point will establish whether two piles can be tested simultaneously in the same flume without affecting each other, thereby increasing the efficiency of the test programme.

Zdravkovich (1987) conducted an extensive study of flow around many different arrangements of cylinders on a flat bed, in the subcritical regime. For two piles side by side in the cross stream direction there was no interference once the separation distance between the pile centres was greater than about 4-5 pile diameters.

Only a few studies have considered the effect of pile spacing on scour depth. Under unidirectional current in the clear water regime Ataie-Ashtiani and Beheshti (2006) and Beg (2010) agree that the effect on scour depth is much reduced once the separation distance is 2-4 pile diameters. Full independence occurred at about 6-7 pile diameters according to Ataie-Ashtiani and Beheshti (2006) and Elliot and Baker (1985) but at 8-10 pile diameters according to Beg (2010).

Sumer and Fredsøe (1998) investigated how the interaction effects between piles impacted the scour depth in waves. They found that the piles acted independently at a separation distance of only 2 pile diameters, although only one flow condition was tested.

g) Criteria for reaching equilibrium scour depth in the laboratory

The gradual decrease in the rate or scouring in the later stages of the process makes it difficult to assess when a scour test has reached a true equilibrium condition. However, this issue has largely been ignored in the literature. One method that has been implemented is to reduce the test duration and use a predictive curve to extrapolate the data to an equilibrium condition (McGovern et al., 2014; Sheppard et al., 2004). However, Simarro-Grande and Martin-Vide (2004) demonstrated that extrapolation of short duration tests is likely to result in significant error using existing scour time development equations.

To address this issue some researchers have devised criteria defining an equilibrium or quasi-equilibrium condition at which experiments can be ended consistently. The different approaches are given in Table 2.2.

It is clear from Table 2.2 that there is not a general consensus as to an approach to adopt and the criteria differ in terms of whether they are a function of the grain size or pile diameter, and the timescale over which they apply.

A more comprehensive investigation of the equilibrium scour condition has been conducted by Simarro et al. (2011) by running very long duration experiments. They concluded that the criteria of Cardoso and Bettess (1999) and Melville and Chiew (1999) can lead to significant error, because in some tests a noticeable increase in scour depth occurred after these criteria were reached.

A new perspective on this problem is given by Chreties et al. (2008). They developed a different approach to scour testing to enable the equilibrium condition to be found in a much shorter timescale by conducting tests initially at a faster flow velocity before reducing the velocity until an equilibrium condition was achieved at the desired scour depth. However, this approach is only applicable if the time development of scour is not of interest. Also it is unknown if it is valid in the live bed regime or under different hydrodynamic conditions such as waves.

Table 2.2 Test stopping criteria used in the scour literature.

Paper	**Criteria**
Link et al. (2006) Link and Zanke (2004b)	d_{50} per hour
Melville and Chiew (1999) (also used by Umeda et al., 2008)	0.05 D in 24 hours
Cardoso and Bettess (1999)	Start of flat line on log plot
Fael et al. (2006)	2 d_{50} in 24 hours
Grimaldi et al. (2009)	0.05 D/3 in 24 hours
Lança et al. (2013a)	2 mm in 24 hours (approx. 2 d_{50})

h) Effect of pausing experiments

The measurement technique tables in Appendix 1 demonstrate that it is common for scour tests to be paused at regular intervals for bed profiling or other practical reasons and it is important to consider the effect this may have on the tests. Only a few authors have commented on this point. Zanke et al. (2011) found that the scour depth was reduced by up to about 0.8 S/D when tests were paused in live bed conditions. Hartvig et al. (2010) also noticed a reduction in scour depth during live bed tests of a few millimetres when the flow was paused due to settlement of suspended sediment. However, in clear water conditions Unger and Hager (2007) concluded from preliminary testing that pausing the test did not affect the experimental results, probably due to the smaller volume of suspended material in this regime.

2.8 Summary

This literature review has discussed the core parameters that influence the scour process, scour under different hydrodynamic conditions and the effect of the sediment bed configuration and properties on scour development. It was demonstrated that there is a significant gap between field measurements of scour and scour prediction techniques based on either laboratory data or analytical models. The need for further research is clear in order to bridge this gap and reduce uncertainty in prediction techniques, to enable a decrease in the level of conservatism in current approaches for the design of marine structures. Key gaps identified in the research were as follows:

- Scour in complex sediments
    - mixed materials with different distributions
    - layered beds with finer material overlying coarser material or multiple layers
    - effects of sediment properties on scour: bulk density, permeability, pore pressure
- Scour in more complex tidal flows (spring-neap cycles)
- Scour in wave-current flow in the clear water regime
- The effect of the variation in vortex patterns on scour in wave-current combinations
- Prediction approaches for scour in complex sediment beds and hydrodynamic conditions

The chapter finished by reviewing a range of issues for laboratory modelling of scour providing the background for the development of the research methodology for this project which is detailed in Section 4.

3. Aims and objectives

The general scope of the project was outlined in Section 1.3. This section will present the aims and objectives of the project on a more detailed level taking into account the findings from the literature review.

The overall research aim is to improve understanding of scour development in complex, realistic conditions. The main focus is on the sediment bed, as this has been shown to be highly variable in the field (see Section 2.5), and this is probably a key factor for the discrepancies between field measurements and prediction methods. It was shown in Section 2.4 that more complex aspects of sediments have been investigated in terms of a general sediment non-uniformity parameter and the concept of bed armouring. However, more detailed study of the influence of the distribution shape of mixed sediments, and layered beds without an armour layer have largely been overlooked. In terms of complex sediment beds this research will complement and add to the literature by:

- Focusing on the effect of bi-modal and varying grain size distribution shape in sediment mixtures rather than testing log-normal distributed non-uniform sediments
- Focusing on layered beds with fine sand overlying coarse sand to investigate interaction effects other than bed armouring
- Investigating the effects of sediment properties on scour such as bulk density and permeability
- Investigating the sediment mixing processes within the scour hole and scour hole shape development to illuminate an understanding of new scour mechanisms related to sediment properties
- Presenting design guidance on the impact of the above through indicative adjustments to empirical formulae, as these aspects are not currently included in design approaches

To provide a reasonably comprehensive assessment of the above objectives, it is important that the tests are conducted over a range of hydrodynamic conditions in order for the results to be applicable to a number of cases in the marine environment. However, it was concluded in Section 2.3 that there are still many gaps in the research regarding scour under complex flows. Therefore, a secondary focus of the project is to also improve understanding of scour in more complex hydrodynamic conditions before combining the first and second parts of the research together to improve understanding of scour in mixed and layered sediments under a range of hydrodynamic conditions. In particular, in Section 2.3.2 it was identified that knowledge of the scour process in tidal flows is limited. Secondly for scour in wave-current flows there was a lack of agreement as to whether a wave added to a current enhances or reduces scour depth, and only limited data was available in the clear water regime for scour. These aspects lead to the following secondary research questions:

- Does adding a wave to a current increase or reduce scour depth compared to the current alone?
- What are the key parameters and trends in the clear water regime in wave-current flow?

- Does the vortex pattern have an impact on scour development in wave-current flow? Are there particular wave-current combinations that result in enhanced sediment transport around the structure due to the wake patterns?
- In tidal flow what is the effect on scour development of a spring-neap cycle where flow varies within and between cycles?
- In tidal flow tests what are the effects of upstream ripples on scour development in the laboratory?

In order to meet these objectives an extensive laboratory study has been conducted, the design of which will be detailed in Section 4. Prior to starting the testing it is important to ensure a robust methodology is in place. Section 2.7 provided justification for the experimental methodology for this project. However, it was also shown that there are a variety of issues associated with laboratory studies of scour. These present a number of objectives and areas for development that must be met in this project to ensure a robust methodology:

- Determine or develop suitable measurement systems to monitor scour depth and scour hole shape in the laboratory. Can a comprehensive measurement system be tested and validated to help to standardise measurement techniques and to improve the quality and dimensionality of the data (i.e. 3D scour hole shape rather than point measurements)?
- Determine suitable methods for investigating sediment interaction effects and mixing processes in the scour hole
- Determine methodology for simulating complex spring-neap tidal cycles in the laboratory
- Investigate the scaling issues created in the laboratory, building on current understanding and providing confidence in the relevance of the research to the field scale

To meet these aims and objectives in practice, the scope of the project needs to be further refined. Firstly it was decided to at least initially place limits on the types of sediment beds that would be tested, to enable a more systematic study and separation of variables. Therefore, two sand sizes were selected from which to construct a variety of mixed and layered sediment beds, also making these more directly comparable with uniform sand beds. In terms of the hydrodynamics the main constraint is to limit the majority of testing to the clear water regime, so as to prevent ripple scaling effects from being significant and because of practical difficulties with providing a constant influx of upstream material in live bed conditions. Scour is likely to be most severe under clear water conditions close to the critical velocity for the sediment so this limitation will not reduce the importance of the research. In order to assess scale effects, two flumes of different dimensions are used and a selection of pile diameters tested, with multiple independent piles located within the same flume during a test (see Section 4.2.1 for assessment of the feasibility of this). The following points set out the detailed scope of the project:

- The work will be constrained to testing cylindrical surface piercing monopile foundations
- Only non-cohesive sands will be tested

- Two uniform sand grain sizes will be selected which will be mixed together or layered in a range of configurations
- Two flumes will be employed with different dimensions, one smaller scale, one larger scale
- Tests will be limited to the clear water regime
- A range of pile diameters will be tested
- A range of unidirectional flow velocities will be tested
- In layered beds the layer thickness, number of layers and order of layers will be varied
- In mixed beds the proportion of the two sands will be varied
- Tests will be conducted in a variety of waves, wave-current combinations, constant velocity reversing flow and time-varying tidal flow (spring-neap cycle)
- The uniform sands will be tested under each flow condition for direct comparison with the mixed and layered cases and for validation of the methodology through comparison with the literature
- The key variables to be monitored are: ambient velocity, water surface elevation, sediment properties, time development of scour depth and scour hole shape to enable thorough comparison with prediction equations and literature studies

4. Methodology

The methodology for this project is to investigate the scour process experimentally through the use of scaled model tests in laboratory flumes. This method is adopted because of the complex situations to be examined which, as discussed in Section 2.6 are difficult to model numerically or analytically. Experimental work will enable the fundamental physics of the problem to be studied in a controlled way through careful selection of parameters.

Due to the scaling issues mentioned in Section 2.7.4 it is not envisaged that the results from the laboratory work will be directly applicable to the field situation, instead the research should be viewed as one stage in the progression of understanding of the scour process in more complex, realistic environments. Nonetheless, the scale effects will be quantified where possible in order to maximise the insight that can be gained from the work. To facilitate the study of scale effects and ensure the results are applicable to a range of scales, two laboratory flumes of different dimensions were chosen for use in the project, one at small scale and one at a medium scale. The small flume had the advantage of being a more practical environment for conducting the tests, while the dimensions of the larger flume were similar to many of those used in the literature, so that direct comparison between studies would be possible. In the larger of the two flumes, further assessment of scale effects was made from the simultaneous testing of two piles of different diameters, as the flume was wide enough for two piles to be situated side by side in the cross-stream direction without any interference (see calculation in Section 4.2.1). This allowed a greater range of parameters to be tested without extending the timescale of the test programme. A range of hydrodynamic conditions were tested in the medium scale flume, including wave and current combinations, complex tidal flows and unidirectional current. Only unidirectional current tests were conducted in the small scale flume.

Due to practical considerations the entire test programme was constrained to the clear water regime. This prevented large quantities of suspended sediment infiltrating the pumps in the medium scale flume facility, and avoided the need for a complex sediment feed or recirculation system to be fitted upstream. One advantage of confining the tests to the clear water regime is that the development of ripples and ripple migration through the scour hole which can cause a significant scaling issue was avoided (see Section 2.7.4). Restricting the tests to the clear water regime is also justified because this allowed testing of the most severe case for scour, which is expected to occur in the clear water regime close to the critical velocity of the sediment before a condition of general sediment transport occurs on the bed. Another practical constraint that affected the test design was that for health and safety reasons the flumes had to be switched off overnight.

It was not possible to carry out repetitions of each test as is standard practice in a laboratory because of the long timescale of a scour test. Therefore, another method was required to provide confidence in the results. This was achieved through comparison of control tests with other studies, repetition of tests at different scales and repetition of the initial stage of some of

the tests. In this way the experiment methodology was verified, and the repeatability and uncertainty of the test results was assessed. This aspect is dealt with in Section 6.10.

This section specifies the experiment design, flume set-up, and test procedures, as well as the preliminary tests which informed the development of these. The differences in the scale and operational systems between the two flumes made it necessary for the experimental set-up to be somewhat different in the two cases, so the design of the experiments in both of the flumes will be discussed separately. The theoretical basis for the choice of parametric values in the tests will be outlined and typical values of these parameters in the field will be given to provide an indication of the scale of the tests. Following on from the discussion in Section 2.7.3, the choice of measurement techniques and the development of these systems will also be detailed.

4.1 Experiment design

4.1.1 Small flume facility

The small scale flume facility used in this study (which will henceforth be termed the 'small flume') is located in the Civil Engineering fluids laboratory at University College London. It is a 10 m long, 30 cm wide and 35 cm deep glass walled flume. The experimental design and flume dimensions are shown in Figure 4.1. Flow through the channel is controlled by a constant head tank above the flume and a combination of valves and weir gates. A pump supplies the water from an underground sump to the constant head tank. The excess water flows over a weir in the tank and directly back to the sump. Water enters the flume from the constant head tank via a series of pipes. The discharge of water from the constant head tank to the flume is controlled by a valve in the pipe just beneath the tank. Water flows through this valve and along a pipe running parallel with the flume underneath the main channel. The direction in which water flows along the flume is controlled by opening one of two valves that are positioned at either end of this pipe.

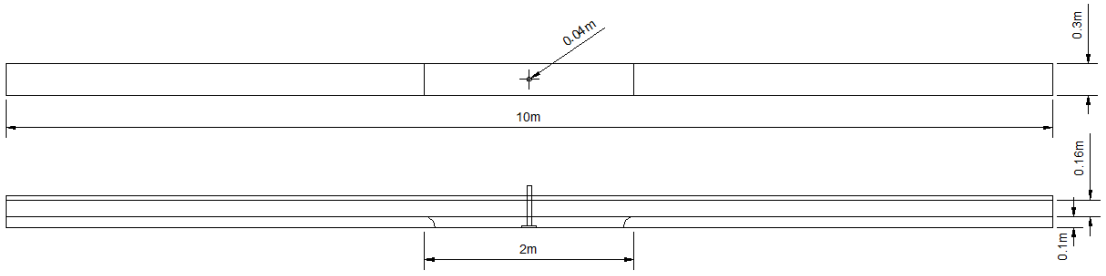

Figure 4.1 Schematic of test set-up in small flume.

Control of the flume water depth and flow rate was facilitated through the valve settings and the use of weir gates at both ends of the flume. An adjustable weir gate was located at the downstream end of the flume so that, using an iterative approach, the valve on the constant head tank and the height of the adjustable weir gate could be positioned to achieve the desired flow rate and water depth, with the valve underneath the flume left fully open. Once the design conditions were obtained, identical flow conditions were ensured each time the flume was

switched on/off by leaving the constant head tank valve and weir gates in the same positions and opening or closing fully the valve underneath the flume. This procedure was developed following preliminary testing in which the upper valve was realigned each time the flow was paused and re-started which resulted in a small change in flow velocity, thereby affecting future scour development (see preliminary test R.2 Appendix 3).

When the flume was switched off overnight, it was important that some water was retained in the flume above the level of the sand to prevent disturbances to the bed that would be caused by the draining process and de-saturation of the sand. The weir gates were fixed in place with a waterproof silicone sealant thereby preventing water from draining below the level of the lower section of the adjustable gate. This arrangement resulted in the water level holding at about 6 cm above the sand. Retaining water in the flume was also important so that the restart process would not have an impact on the test due to a surge of water along the flume as the valve was reopened. This occurred in preliminary test R.5, Appendix 3 where there is a noticeable discontinuity in the scour curve at the point at which the test was paused, with a sudden increase in scour depth due to the surge of water. From the preliminary testing it was found that as long as the valve was opened slowly the effect on the test was minimal, as shown in Appendix 3 where in the main test series the scour curves continue on smoothly either side of the test pauses. Following this procedure it took approximately 2 minutes to re-start the experiment. This length of time is small compared to the timescale of the scour process during the later stages of scouring so was not considered to be of significance. However, this is not true in the initial stages of scour testing. Consequently the flow was not paused until a test had been running for at least 4 hours.

Only unidirectional currents were operated in this flume because it would have been difficult to reposition the weir gates for the reverse flow direction as they were sealed in position, and also due to the iterative nature of the method for positioning the weir gate levels to obtain the required flow. Therefore, in practice it would be difficult to run the flow in the opposite direction while at the same time ensuring repeatability of the flow conditions.

The test set-up consisted of a layer of sand placed in the flume around a scale model of the foundation structure. For practical reasons, the loose sand bed only occupied the central 2 m section of the flume. The sand was held in place with a ‘false bed’ section on either side preventing the flume from having to be filled with sand along its entire length, and ensuring a level and controlled approach section. The loose sand bed was smoothed flush with the false bed sections to maintain a constant bed level. The transition to the sand bed was made smoother by attaching a rounded sloping section to the false bed so that the height of the false bed reduced gradually at the start of the sand bed. The false bed sections were made of plastic and screwed to the base of the flume to hold them in place. The surfaces were painted with varnish so that a thin layer of sand could be stuck to them. This fixed roughness aided in the development of a consistent boundary layer at the test section and an even transition between the false bed and real sand section. Due to scaling considerations, a rough turbulent boundary

layer was preferable at the test section to reduce issues associated with ignoring Reynolds scaling (see Section 2.7.4).

Dong et al. (1992) found that the turbulent boundary layer is established within a distance of 20 h (h = water depth) from the entrance of the flume over a rough bed, but that the boundary layer continues to adjust for a further distance of 20-30 h. However, Bonakdari et al. (2014) noted that a wide range of entrance lengths have been reported in the literature, from 55-130 h for smooth beds and between 50-140 h for rough beds although it is generally agreed that bed roughness reduces the entrance length. Bonakdari attributes the range of values to differences in defining fully developed turbulent flow:

- when a characteristic boundary layer thickness parameter becomes constant
- when the mean velocity profile along the centreline of the flume becomes constant
- once the mean velocity profile across the width of the channel is unchanging

In the present test programme the available entrance length (approx. 30 h) was constrained by the length of the flume and so it was important to incorporate a rough bed upstream of the model to promote quick transition to a turbulent boundary layer. The coarsest sediment used in the tests was chosen to roughen the false bed sections. While ideally the sand glued to the false bed sections would be the same sand as used in the test section, it was impractical to change this multiple times during a test series. The streamwise velocity profile was measured upstream and downstream of the pile location to assess the state of the boundary layer at the test section, and the velocity profiles were observed to be unchanging in this region, see Appendix 10. The boundary layer was also found to be similar over the different sand types used in the test bed, probably because the majority of the approach section (i.e. the rough false bed) was the same for each test (Appendix 10).

The model pile was made from cylindrical ceramic water pipe of the desired diameter. This was a rigid material so that the pile was assumed to be stationary under the test flow conditions, and no vibrations of the pile were observed during testing. The surface was considered to be smooth, but note that the tests were found to be insensitive to pile roughness in the parameter ranges tested (see Section 4.1.2 for a more detailed discussion of this point). The pile was screwed into a 10 mm thick flat plastic base board and positioned in the centre of the flume prior to placing sand around it (Figure 4.2).

Before placing sand in the flume section it was soaked in water to reduce the quantity of trapped air in the test section. It was assumed that the sand bed was fully saturated so that complex effects of partially saturated material were not considered.

A test was set up by first filling the flume until the water level was above the level of the false bed, so that the sand would be kept saturated when placed in the flume. The sand was then placed carefully around the pile until the section was full. As the sand was introduced in the flume it was gently mixed to prevent stratification of the material due to the variation in settling velocities of different grain sizes in water. The sand bed was in a loose state and was not

compacted apart from for one specific test (test R.28, Appendix 3) where the effect of the sand bed density was investigated. For this test the bed was vibrated using a concrete poker to increase the bulk density. Further sand was added as the volume reduced and this process was repeated until the full depth of the sand section was compacted.

In all tests the bed level was smoothed flush with the false bed section using a scraping device that rolled along rails above the flume (Figure 4.2). This consisted of a flat scraper mounted on a vertical arm the height of which could be adjusted. This was manually pulled across the sand bed until the sand surface was as smooth and level as possible. The pile section was split into two sections that screwed together at the height of the false bed so that while the smoothing device was being operated it could run straight over the top of the bottom pile section ensuring the sand was smooth in the vicinity of the pile. Where a layered sand bed was tested, the height of the smoothing device was lowered to the desired depth and the sand layer smoothed in the same way, before the next layer of sand was placed on top and the smoothing process repeated. For these tests the pile was split into multiple sections that screwed together at the height of each sand layer. Any excess sand after smoothing was removed from the flume prior to running the test. Figure 4.2 illustrates the different stages of the test set-up.

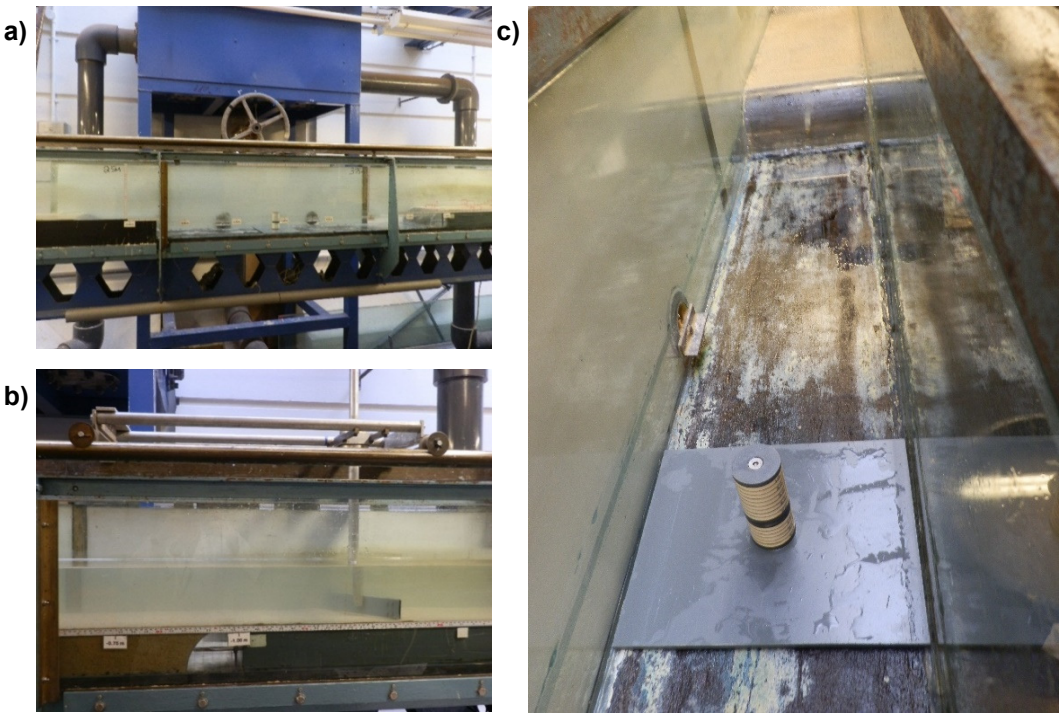

Figure 4.2 Test set-up procedure in the small flume a) false bed and empty test section b) smoothing device c) base pile section.

To start an experiment, the valve underneath the flume was opened gradually until the pre-set flow condition and water level were reached. It was observed in the initial tests, R.X.1, R.X.2, R.X.3, (see Appendix 3) that with the pile in place during start-up scour occurred before the design flow velocity and water depth were obtained. Therefore, in future tests the upper section of the pile was only screwed into place once the flow conditions had finished adjusting. The

preliminary experiments (test series P-1 and P-2) showed that this approach enabled a near instantaneous start to the test, see Figure 4.3.

While the experiments were designed to be in the clear water regime, and in theory ripples would not develop on the bed upstream of the scour hole, the preliminary experiments revealed that ripples did gradually form during the tests, in agreement with the discussion about rippling sediments in Section 2.7.4. This was triggered by any slight unevenness in the smoothed sand bed, but was mostly due to a small discrepancy between the flat false bed and the rounded end section. This meant that the ripples were initiated in the far field relative to the pile, and so while initially this did not impact scour development, over time these ripples migrated downstream, eventually affecting the shape of the scour hole and the scour depth as they migrated past the pile. This is shown in the scour curves in preliminary tests R.2, R.4, R.7, Appendix 3 where there is a departure from the expected trend in the latter part of the curves. As ripples do not scale correctly in the laboratory and inhibit scour development (see Section 2.7.4) the effect of ripples in the clear water regime were removed in the main test series by carefully smoothing out the upstream ripples while the test was paused (i.e. overnight).

The influence of the downstream bedforms on scour development was also considered. In test R.N.27 the downstream dunes were smoothed out, but leaving the scour hole intact, once the test had reached a quasi-equilibrium condition. The test was then continued and it was found that there was no change to scour development, see Appendix 3. This indicates that at this stage of the test, scour depth is not influenced by the shape of the downstream bedforms or at least that the downstream bedforms are not hindering scour development.

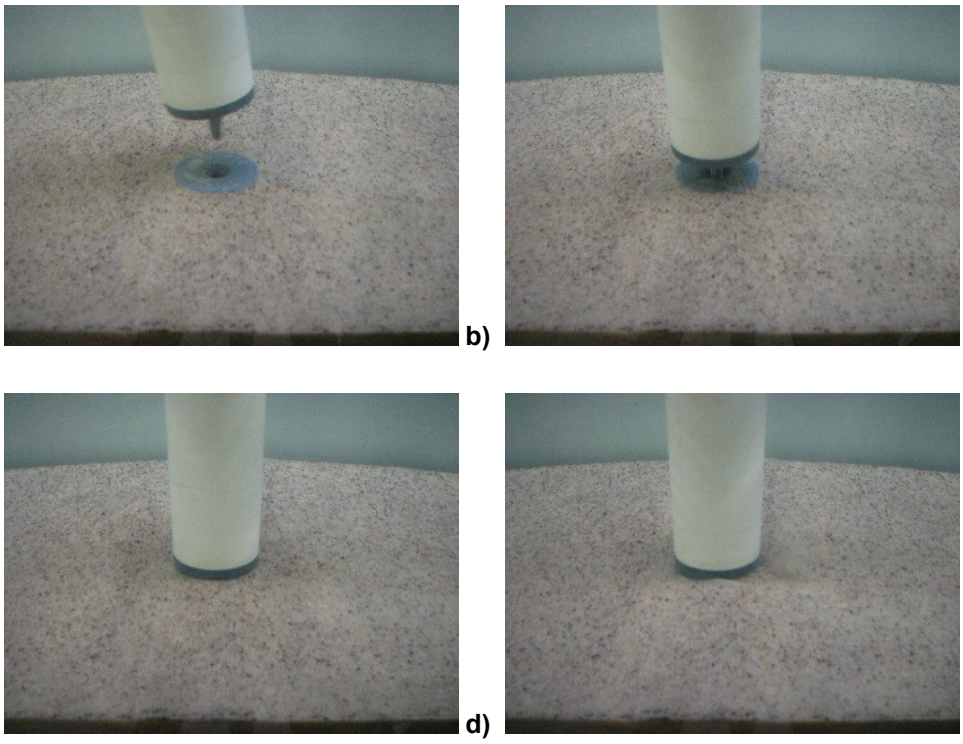

Figure 4.3 Test start-up procedure in the small flume with flow running, but scour initiates only once the pile is screwed into place.

In some tests in situ measurements of the density of the sand bed were collected. This enabled comparison of the consistency of the bed set-up between tests and investigation of the spatial variability of bulk density within a test. Nine round lidless plastic containers were placed at a variety of locations in the sand bed during its preparation. The containers were 46.4 mm deep with an internal diameter of 87.2 mm, giving a volume of 277 cm^3. Figure 4.4 shows the layout of the containers in plan and elevation.

Figure 4.4 Density pot layout in the small flume (not to scale).

For practical reasons the exact coordinates of each container were difficult to fix. Instead once each container had been placed in the flume, its x and y position was measured using a ruler (Appendix 5). The smoothing device was used to create a level surface in the sand bed to position each container at the required depth. Sand was placed into the flume in a similar way to the tests without the buried pots, and without any compaction (except in test R.28 where a concrete poker was used). The containers were located in the far field of the test bed relative to the pile to reduce possible disturbances to the scour process due to the impermeability of the pots, and at a depth where they would not become uncovered during the scour tests. Once a test had been completed, the water was drained to the level of the sand and each container was carefully extracted from the flume without disturbing its contents. A steel rule was used to gently level the surface of the container by scraping off the excess sand. Each of the containers was immediately weighed before placing them in an oven on a low heat to remove the water from the sand. The samples were then weighed again so that the dry bulk density of the samples could be calculated.

4.1.2 Medium scale flume

The medium scale flume, known as the ‘Coastal flume’ is based in the Mechanical Engineering department at University College London. The flume is glass-walled, 1.2 m wide, 1 m deep and 20 m long. Active-absorption, Piston-type wave makers are positioned at either end of the flume so that while one is generating waves the other actively absorbs waves to reduce wave reflection. Pumps are situated under one end of the flume and can be run in forward or reverse to drive a recirculating current in either direction along the flume. The current inlet and outlet are situated in the floor in front of the wave paddles at either end of the flume, and are connected to the pipe running underneath the flume to the pumps. The motor speed of the pump is controlled

electronically by selecting the desired percentage of the maximum speed the motor can run at. The flume is filled from a tap located above the flume and the water remains in the flume as long as the outlet valve beneath the flume is shut. Therefore, the water level holds constant regardless of whether the pump is running (unlike in the small flume facility). Once the desired water level is attained, the flow is started by simply choosing the required motor speed.

Waves are controlled electronically using Edinburgh Designs' WaveSynthesiser and Wave Runtime softwares. For regular waves, only the wave amplitude and frequency values need to be selected; otherwise more complex wave patterns can be programmed. The wave amplitude was calibrated by adjusting the gain parameter iteratively in the software so that the selected wave height in the software matched the measurement of wave height in the flume. This was necessary due to the presence of the false bed which affected the waves propagating over it. It was anticipated that the test set-up may induce wave reflection and the degree of wave reflection was estimated following the method of Goda and Suzuki (1976) using two wave probes. The reflection coefficient was found to be no more than C_r=0.16. The results of the wave reflection analysis are given in Appendix 9.

The experimental set-up (shown in Figure 4.5) was similar in principle to that in the small flume. A false bed was constructed to run either side of a section of loose sand. Due to the layout of the flume however, ramps were needed at the far ends of the false bed sections to provide smooth transition to the base level of the flume. The false bed and ramps were constructed from marine plywood sheets with 12 mm thickness. The false bed sections were held in place by sticking them to the flume base and side walls with Silicone sealant. Sediment traps were built into the false bed as the flume did not have a system in place for preventing sediment from reaching the pumps where it could cause serious damage. The flume layout was symmetrical with ramps and sediment traps at both ends of the flume so that flow could be run in either direction in a consistent manner.

The sediment traps were designed based on the assumption that the majority of material would be travelling as bedload by the time it reached the sediment trap. The greatest distance required for suspended particles to settle out was estimated based on the fall velocity of the smallest particle size (d_{50}=0.2 mm) which would just be caught in the trap, when starting from a height equal to 70% of the water column just downstream of the pile. This calculation ignores complex factors such as the presence of wake turbulence and the effects of downstream bedforms on sediment transport but provided a baseline from which to determine the downstream location and width of the trap. The calculation is detailed in Appendix 2. The traps were covered with a metal perforated plate with holes of 5 mm diameter. This was meant to reduce as much as possible the influence of the traps on the flow and waves propagating over them while still allowing sediment to easily pass through to the trap. In the preliminary test series P-3 (Appendix 3) before the success of the sediment traps had been verified in the flume, the current inlet and outlet were covered with a sheet of steel mesh of 0.1 mm aperture to provide further protection to the pumps. However, in practice these created several problems. As was expected, the sheets reduced the flow velocity. Although this could be accounted for if

the reduction was constant during testing, because the sheets became blocked over time with very fine particles the velocity reduction varied with time. It was also difficult to secure the sheets effectively and in some of the initial tests the sheet became partially unattached from the inlet, resulting in a change in flow conditions. The sediment trap design was proven to be successful during the initial testing as sediment was deposited upstream but not downstream of the traps. Therefore the steel mesh did not need to be utilised in the main test series.

As with the small scale flume, a thin layer of the coarse sand was glued using varnish to the flat false bed sections either side of the loose sand bed, following the same reasoning as discussed in Section 4.1.1. Sand was not glued to the parts of the false bed and ramps beyond the sediment traps as their presence disrupted continuity in the bed roughness.

The dimensions of the false bed section and ramp slope angles were restricted by the location of the current inlet and outlet, and the depth of the false bed (which is discussed in Section 4.2.1). Within these constraints the main criterion was to ensure that the flat bed sections were long enough to allow the boundary layer to develop fully before reaching the piles. The flume was a little short (only 12 m in-between the current inlet and outlet) so some compromises had to be made. Ideally the ramps would have been set at a shallower gradient to reduce their influence on wave propagation. However, these effects can be taken into account in the analysis by measuring the actual surface elevation and velocity profiles under the waves in the flume rather than relying on the programmed wave parameters.

Two piles of different diameters were tested simultaneously in this flume to help quantify scale effects, and so that a greater number of parameters could be tested in the given time. The larger of the two piles was placed at the nearside of the flume as it was of greatest interest, and a smaller pile was placed at the far side of the flume. As the access to this location was limited, only basic monitoring of the small pile was feasible (see Section 4.4 for details of the measurement techniques employed). In order for this set-up to be successful, the two piles needed to be positioned in the flume so that there would be no interaction between them. The cross-stream separation distance was set equal to 9 times the largest pile diameter (0.09 m), following the discussion in Section 2.7.4 where it was found that piles acted independently at a separation distance of 7 pile diameters. Using a value of 9 pile diameters provided extra space to accommodate the uncertainty in this value and ensure that there would be no interference under any condition. The choice of pile diameters and locations of the piles are discussed in Section 4.2.1.

The larger pile was made from ceramic pipe in the same manner as those used in the small flume, but the smaller diameter pile was made of thick walled plastic tube. The piles were screwed into a marine plywood base board.

A rough pile was employed under two flow conditions (unidirectional current and wave-current flow) to simulate a higher pile Reynolds number in comparison with a smooth pile of the same diameter, in order to assess the influence of pile Reynolds number on the scour process but with all other test parameters constant. The diameter of the rough pile was reduced to 48.3 mm

before being painted with varnish and rolled in sand so that the diameter was consistent with the smooth pile once the roughness elements had been added. The coarse sand was passed through 1000 micron and 850 micron sieves so that only this fraction was used to coat the pile with uniform roughness. The pile was carefully rubbed down and re-rolled as required to produce an even sand layer of single grain thickness on the pile surface. It was determined that the scour behaviour was unaffected by the pile roughness and hence pile Reynolds number in the range that was tested (subcritical Reynolds number regime) and therefore the pile roughness is not an important factor in the methodology. The full analysis of these tests is given in Appendix 3.

The tests were set up in a similar way to those in the small flume. The sand was pre-soaked and the flume filled with water to a level just above the false bed before the sand was added to the central 3 m section. The pile was split into sections so that the sand could be smoothed at the depth of the sand layers and at the false bed level. As the flume was not equipped with rails running along the tops of the walls, the method of smoothing had to be adapted for this flume. A sheet of marine plywood was glued to the flume wall on each side of the sand bed with a height equal to the false bed sections so that a plastic scraper could run along these boards to smooth the sand at the correct level. A secondary board was fitted to the first board at the required depth for the layered tests.

The sand bed was smoothed by a person located within the flume. It was smoothed methodically from one end to the other, and the sand had to be walked on to do this. In the layered tests where a similar approach would have resulted in disturbance of the lower sand layer when the upper layer was smoothed, a dividing board was fitted in-between the two piles running parallel with the flume walls (see Figure 4.5). This provided the level for the smoother to run along on the other side of the main pile, but importantly meant the smoothing could be completed from the far side of the divider, without walking on the smoothed lower sand layer. Consequently layered tests could not be set up around the smaller pile, but in any case this would not have been practical because different layer thicknesses would have been needed at each pile in the same test. Once the bed was smoothed to a point just past the piles, the upper portions of the piles were screwed into place before the rest of the bed was levelled. The smaller pile was held rigid by fixing a cross-bar to the top of the pile (above the water level) which was clamped to the side of the flume. In the preliminary tests no vibrations of the larger pile were observed and so it was considered to be rigid without extra support.

A solid scraper was used to smooth the bed in the initial tests. However, this resulted in the generation of large scale vortices as it was pulled through the water which disturbed the sand bed. In the main series of tests this was mitigated by using a perforated plastic sheet to smooth the bed. Handles were attached to the smoothing device so that it could also be used from a platform above the flume, and with the full depth of water in place. This enabled small sections of the bed such as where ripples had developed upstream of the piles during the tests to be re-smoothed while the test was paused but without draining the water, following the methodology for removal of ripples in the small flume (Figure 4.6).

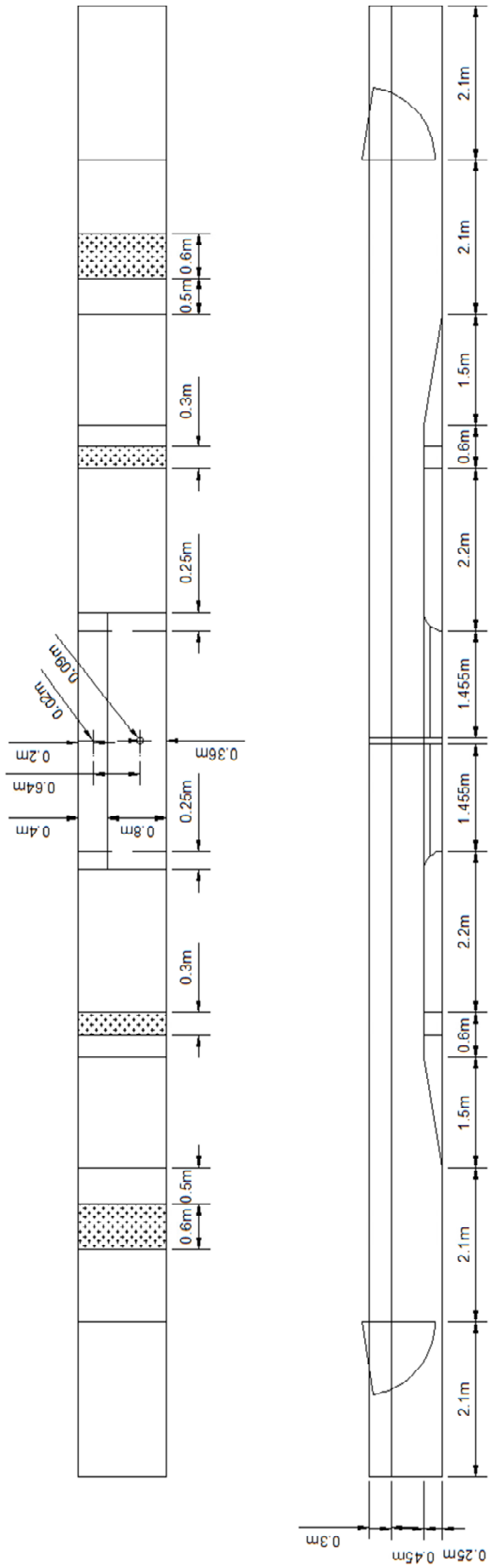

Figure 4.5 Plan view and side elevation of experimental set-up in the coastal flume.

In contrast to the small flume methodology, the water level was topped up to the required depth with the full height of pile already in place at the end of the smoothing process. Scour was not initiated around the piles during this procedure because the inflow rate was slow (it took approx. 45 min to fill the flume), and there was no recirculation in the flume during this time (pumps not switched on).

Once the desired water level was reached, the test was begun by simply switching on the motor and/or the wave paddles. This resulted in a near instantaneous start to the test, bearing in mind that there is a short warm up time before the motor runs at the desired speed or the wave paddles produce the programmed wave pattern. However, the finite start-up and power-down times ensured that the transition was gentle enough to prevent surge wave effects from occurring. Tests were paused overnight by simply switching off the motor and wave paddles, which did not cause the water level to drop as was the case in the small flume.

In the wave-current tests the waves were initiated before the current was switched on because it took longer for the waves to settle. However, the current was always switched off before the waves when pausing a test. This helped to reduce the influence of the finite time of the start-up and shut-down procedures as waves on their own were expected to cause less scour. For this reason the test start and stop times were recorded to coincide with the current.

a) 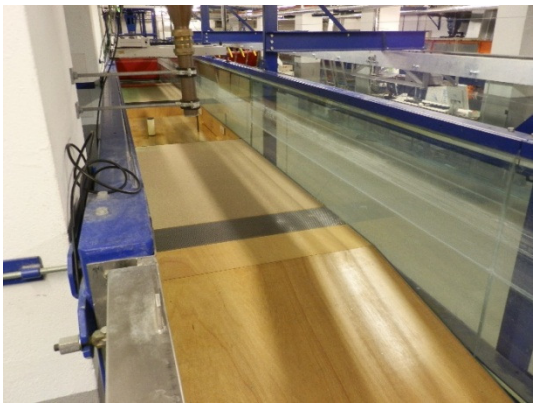 **b)** 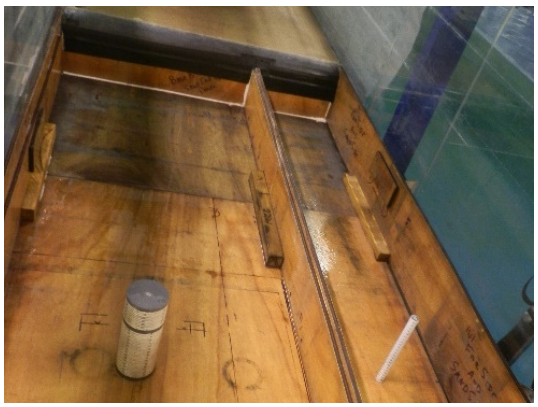

c) 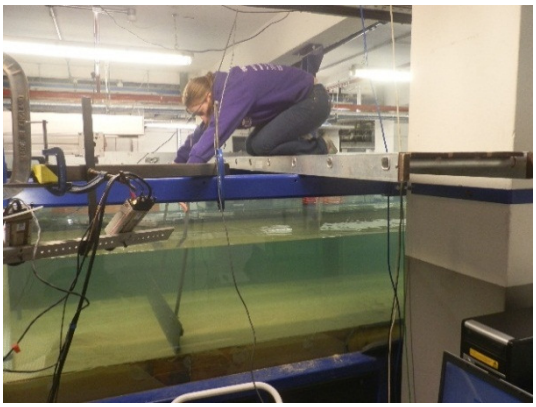 **d)** 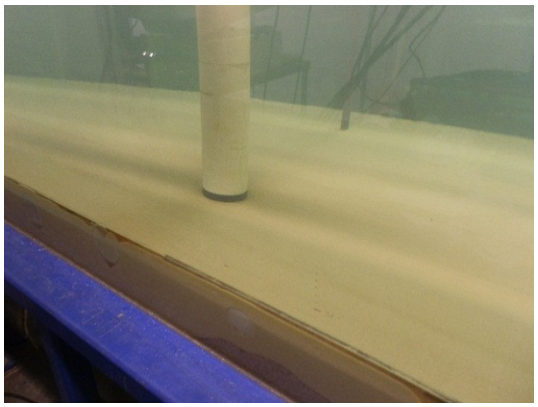

Figure 4.6 Test set-up and procedures in the coastal flume a) false bed section including sediment trap b) base sections of piles and dividers for bed smoothing levels c) smoothing device d) smoothed sand bed prior to start of test.

4.1.3 Ending a test

Following the discussion of test stopping criteria in Section 2.7.4, and given the time constraints in this project the test duration would have been too long to enable a full programme of experiments to be conducted if the longest criteria were used, especially because the tests could not be run overnight. However, those criteria which specified a much shorter test duration would result in stopping the tests when the scour depth was clearly still increasing. Therefore, a new criterion was developed to maximise the length of the experiments within the time constraints, defining a quasi-equilibrium condition. The scour tests were stopped when a maximum of 0.025 S/D of scour occurred in 6 hours (i.e. 1 mm of scour at the 40 mm pile, ≈2 mm of scour at the 90 mm pile, and ≈0mm of scour at the 20 mm pile). This was a fairly arbitrary condition in terms of scour development but offered a degree of consistency between the tests. A few tests were run for a considerably longer period, allowing analysis of scour time development in the latter stages and assessment of the suitability of the stopping criterion, see Section. 7.1.9.

4.2 Choice of test parameter values

4.2.1 Pile diameter, water depth and bed depth

The main criterion for determining the pile diameter was to ensure the blockage effect would not be significant (see Section 2.7.4) and that the water depth to pile diameter ratio would be sufficiently large so as not to be an important parameter (see Section 2.2.3). The largest pile diameter that fitted with these conditions was then chosen to reduce scale effects as much as possible. In the small flume initially the limits for these conditions were applied so that a 50 mm diameter pile and a water depth of 15 cm were tested. This gave a blockage ratio of 1/6 (the limit proposed by Whitehouse, 1998) and water depth ratio of 3, both of which are less conservative than some authors recommend in the literature. The sand bed was 10 cm deep so that the scour could equal up to 2 pile diameters in depth, which is often considered to be the maximum possible scour depth. However, in this set-up the scour depth came very close to reaching the bottom of the flume in preliminary test R.1. Therefore, a 40 mm pile diameter was selected so that 2.5 pile diameters of scour could be accommodated. With a water depth of 16 cm this also improved the ratio of water depth to pile diameter so that the more conservative criterion of Whitehouse (1998) was observed (h/D=4). These dimensions also reduced the blockage ratio, which is sensible considering the limits are only indicative. For the most part the water depth and pile diameter dimensions were held constant in this flume, but a 25 mm pile diameter was used in one case (test R.9) to assess the effect of the pile diameter on scour depth in comparison with the 40 mm and 50 mm piles. A full list of parameters for each test is given in table 5.1, and the dimensions of the test set-up are shown in Figure 4.1.

A similar approach was employed in the larger flume for parameter sizing. However, based on the experiences in the small scale flume, in the coastal flume a slightly greater degree of conservatism in the parameter values was applied compared to the limiting criteria of Whitehouse (1998). Also the clearance required for waves had to be taken into account so that

the maximum water level was situated approximately 25 cm from the top of the flume. The false bed depth was set to accommodate 2.5 pile diameters of scour, with a small amount of extra allowance so that scouring would not be influenced by the impermeable flume bottom. Using an iterative process, an optimal combination of dimensions for the false bed, pile diameter and water depth was obtained. This resulted in a pile diameter of 9 cm, water depth of 45 cm and a 25 cm depth of sand bed, giving a water depth to pile diameter ratio of 5. Using a 9 cm pile diameter meant there was room to add a second pile in the cross-stream direction (as mentioned in Section 4.1.2). The blockage criterion was still satisfied with the addition of a 2 cm diameter pile. The placement of the piles relative to the flume walls was based on the expected maximum width of the scour hole, so that the centre of the larger pile was located at a distance of 4 pile diameters from the side wall. The smaller pile was located at a distance of 20 cm from the wall so that it would be situated outside of the horizontal boundary layer. This positioning facilitated a suitable separation distance between the two piles as discussed in Section 4.1.2.

In one test series (C-2) the 9 cm pile was replaced with a 5 cm pile so that it would be possible to test a specific combination of wave-current parameters. Also, the 2 cm pile was swapped with a 5 cm pile in a few experiments so that two 5 cm piles were tested side by side to investigate the effect of pile roughness (see previous discussion in Section 4.1.2). In these cases the nearside pile was located in the same position as the 9 cm pile but the pile on the far side of the flume was located 5 cm further from the far wall compared to the position of the 2 cm pile to allow room for the larger scour hole around this pile. The parameters for each test conducted in this flume are given in Table 5.2 and the details of the flume set-up are shown in Figure 4.5.

4.2.2 Current velocity

The velocity for the tests was designed to be in the clear water regime, and although a range of velocities were tested, in particular velocities close to critical needed to be investigated as this was expected to be the most severe case for scouring. The critical velocity for each of the sediments in both of the flumes was estimated theoretically using the method of Soulsby and Clarke (2005) in conjunction with the method of Soulsby (1997) for determining the critical Shields parameter. This method was found to agree well with observations of initiation of sediment movement in the flumes, and provided a consistent method to determine critical conditions for current, wave and wave-current flows. The details of these calculations are presented in Appendix 2. To avoid extensive ripple formation upstream of the scour hole the velocity was set between 80-90% of the critical value in many of the tests. The ambient flow conditions required for initiation of scour at the structure were also determined, following the criterion of Whitehouse (1998) ($\tau/\tau_{cr}>0.25$). This set the lower limit of the velocity range for the tests.

4.2.3 Wave design

In the main series of tests regular waves were used, although irregular waves based on the Pierson-Moskowitz spectrum were employed in some of the preliminary tests in the P-3 test series, see Appendix 3 for further details. Linear wave theory was used to provide a simple

method for estimating the design parameters (Appendix 2). The actual wave height and velocity profiles under the waves were then measured in the flume prior to testing.

The parameters that needed to be selected for wave design were the wave amplitude and frequency. The maximum orbital velocity at the bed under the wave was calculated and this was checked against the critical velocity computed using the Soulsby and Clarke (2005) method (Appendix 2). The KC number also needed to be defined, being a particularly important parameter for scour in waves (see Section 2.3.3). Calculations were run for a range of amplitude and frequency combinations for the two pile diameters to determine the best compromise between KC number and wave orbital velocity, as a high KC number but clear water conditions were desired. This was difficult in practice for the larger pile given that there were limitations to the frequency that the wave paddles could operate at. This meant that some of the preliminary wave tests were conducted in the live bed scour regime, while in the main series of tests the pile diameter was reduced to resolve this issue as discussed previously in Section 4.2.1.

4.2.4 Wave-current design

The Soulsby and Clarke (2005) method was also used to calculate the critical velocity for the combined wave-current cases and the main series of tests were designed to be in the clear water regime. The wave-current design procedure is detailed in Appendix 2. The main series of wave-current tests investigated the transition between wave-dominated and current-dominated flow, including a case in which the velocities of the wave and current components were set equal, at a combined wave-current KC number of 10 to investigate possible effects on the sediment transport and scour process of the unique vortex patterns under these conditions found previously by Grass et al. (1985) for flow around cylinders.

4.2.5 Tidal flow

Two types of tidal flow signal were studied during the test programme. The different tidal signals are shown schematically in Figures 4.7 and 4.8. The simplest consisted of a square wave pattern so that the velocity was held at a constant value in the forward and reverse directions. This provided a means to investigate the influence of flow reversal as an isolated parameter in direct comparison with unidirectional flow tests at the same velocity. Six cycles were run for these tests, based on the literature review where equilibrium scour depth was found to be achieved after only 2 or 3 cycles (see Section 2.3.2). The cycle length was determined from Froude scaling of field dimensions, resulting in a 48 minute half cycle. However, for the layered test a 130 minute half cycle was used to ensure that scour would reach the lower sand layer prior to flow reversal, and enabling investigation of the effect of cycle length on scour depth through comparison of these tests.

The second tidal flow case was designed to model a full spring-neap cycle. A real tidal signal from the field was scaled for the laboratory by equating the RMS based on the peak value from each half cycle to the current velocity used in the unidirectional current test in test series C-1.

The signal was simplified into discrete velocity steps, as the flume was not set up to run complex velocity signals automatically. Each velocity step consisted of 5 original data points. These were arranged so that a step was always centred on the peak value in each half cycle, resulting in 7 or 8 velocity changes per half cycle. The steps at the start and end of each half cycle were slightly shorter and varied in length to coincide with the small variation in the length of each half cycle in the real tidal signal. As can be seen in Figure 4.8 the tidal signal contained a small degree of asymmetry between the flood and ebb tides which was replicated in the tests. To operate the tidal signal in the flume the relevant motor speed was selected manually at the time prescribed by the simplified spring-neap pattern. The motor speed was calibrated by plotting the motor speed against the depth-averaged velocity obtained from in-flume measurements, see Appendix 10. This resulted in a linear relationship between the parameters. However, there was some scatter in the data, so the velocity was also measured during these tests to check for consistency (see Appendix 10 for comparison of the design and measured signals). Note that similarly to the reversing current tests the scaled cycle length for the spring-neap tests was approximately 48 minutes per half cycle.

One important difference in the methodology for the tidal tests compared to the studies reported in the literature review, Section 2.3.2, was that the downstream bed was resmoothed prior to flow reversal each time so that the new upstream side was flat. Note that the deposition dune immediately downstream of the scour hole was left intact, only the farstream bedforms were removed. This enabled assessment of the influence of ripples on tidal scour tests in the laboratory through comparison with the findings in the literature where bedforms were left to develop.

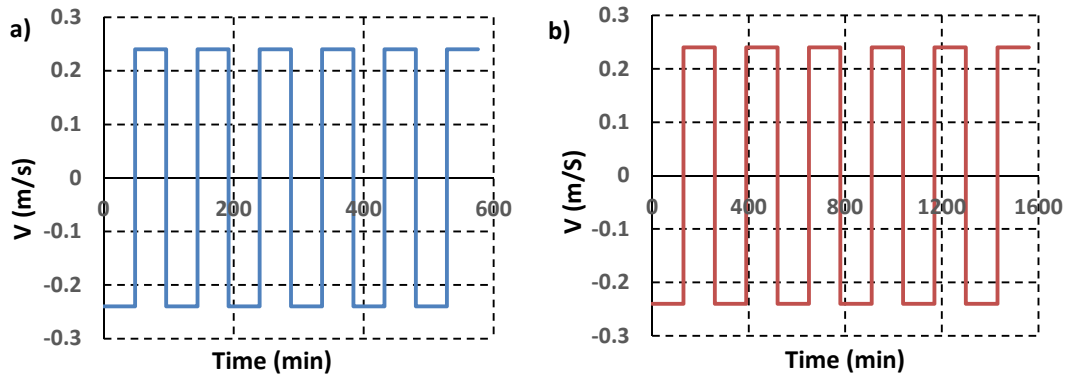

Figure 4.7 Depth-averaged ambient current velocity for square wave reversing flow signal, a) 48 min half cycle b) 130 min half cycle.

a)

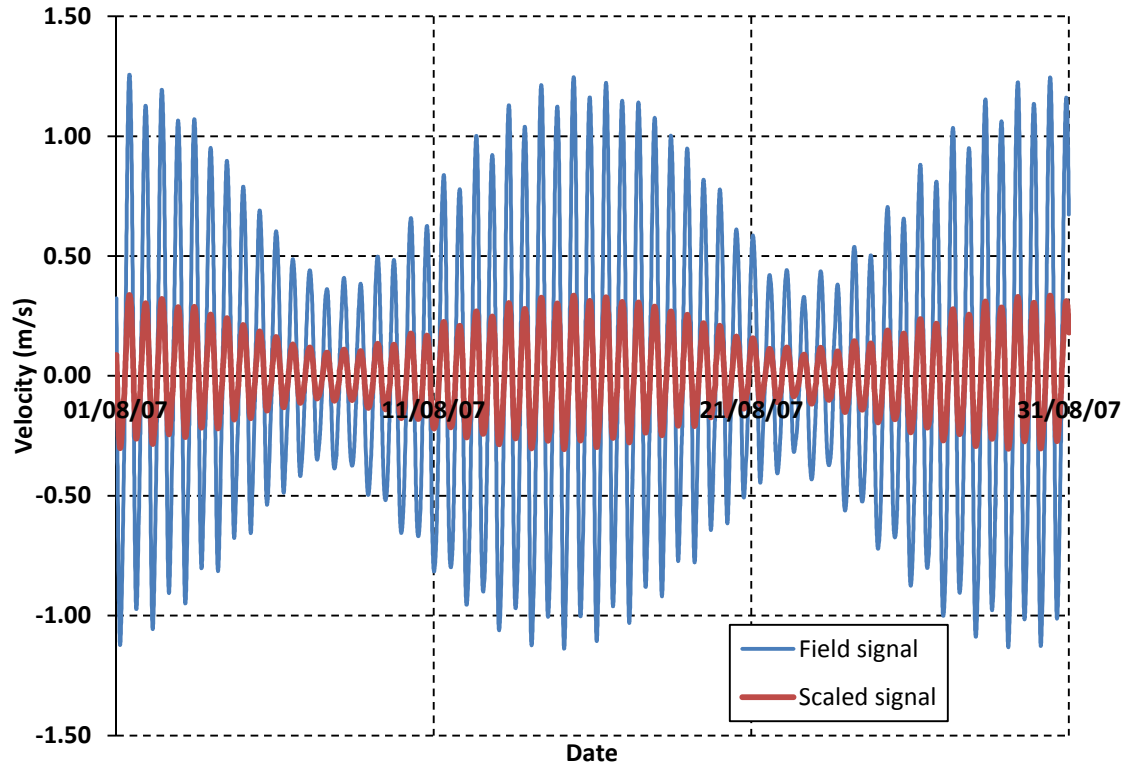

b)

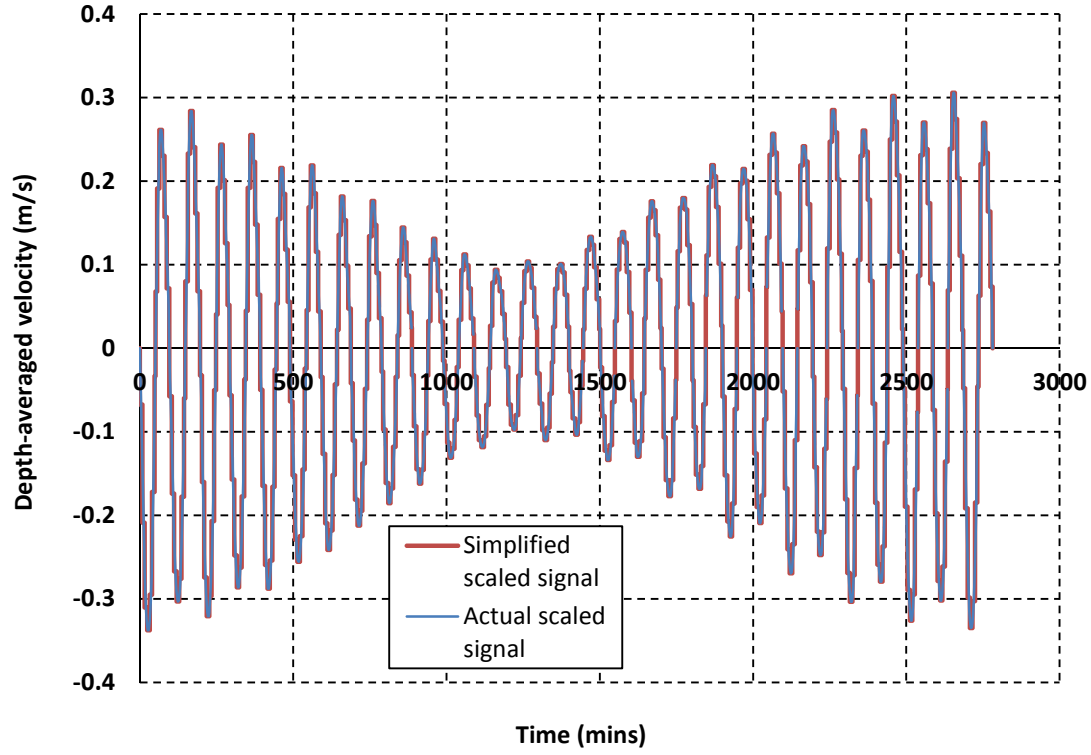

Figure 4.8 Spring-neap tidal cycle a) signal measured in the field compared to scaled signal based on the RMS of the peaks b) simplified, stepped tidal signal compared with original scaled signal.

4.2.6 Scaling parameters

A further consideration for choosing the water depth, pile diameter and flow parameters was their relationship with typical field values. Nominal field parameters were chosen for comparison based on the findings in Section 2.5 of the literature review. The field values were linked to the flume dimensions using Froude scaling (see Section 2.7.4), to give an indication of the applicability of the experiment design. However, it should be remembered that it is not the aim for these laboratory tests to be directly compared with the field. The typical field dimensions that were used are given in Table 4.1 along with the scaled laboratory values. Note that this scaling does not apply in the same way to the smaller pile in the large flume, where the water depth to pile diameter ratio is significantly higher. This scaling is only approximate as it does not take into account the sediment sizing which is discussed in the next section. The wave parameters were also not scaled directly from typical field values because of the need to remain in the clear water regime.

Table 4.1 Typical field and laboratory parameters to give an idea of the scale of the laboratory experiments in the two flumes

Parameter	Field	Coastal flume experiments (1:55 scale)	Small flume experiments (1:125 scale)
Water depth	20-25 m	45 cm	16 cm
Pile diameter	5 m	9 cm	4 cm
Velocity	1.8-2.7 m/s	24 cm/s	24 cm/s
Tidal cycle duration	12 hours	1.6 hours	-

4.3 Sediments

4.3.1 Sediment size and distribution

The sand size was selected so that it would not exhibit cohesive behaviour, so the median grain size of the sand could not be smaller than about 0.1 mm. As discussed in Section 2.7.4 this means that the ratio of grain size to other parameters in the experiments will be larger than those in the field. This is one shortcoming of laboratory testing and there is no solution to this other than to attempt to quantify the effect that this has.

The aim of this study was to investigate scour in different bed configurations such as stratified and mixed sediments. Therefore, two uniformly graded sands were chosen, of different sizes but so that both would scour under clear water conditions (i.e. if the difference in grain size was large, one might be in live bed conditions before scour initiation even occurred in the other sand). This resulted in choosing sands with median grain sizes approximately equal to 0.2 mm and 0.6 mm. It should be noted that initial testing was conducted with materials readily available in the laboratory, which happened to be 0.2 mm and 0.5 mm sands. For the main test series new washed Silica sands were sourced at 0.2 mm and 0.6 mm; the data sheets supplied with these sands are given in Appendix 2.

Layered beds and mixed beds were constructed from these two sands. For the mixed tests the two sands were combined in a variety of proportions. Where a sand mixture was required for testing in the small flume, the appropriate proportions of the dry base sands were measured out by mass. Once the correct proportions of the sand types had been measured, they were carefully combined while dry to ensure they were as evenly mixed as possible, before water was added to saturate the mixture. For practical reasons, only one sand mixture was tested in the larger flume (50% fine – 50% coarse). This would help verify the results in the smaller flume, and extend the mixed sand results to a greater range of hydrodynamic conditions. In this case due to the large volume required the mixture was blended off-site by the supplier.

The grain size distributions for each of the sands used in the laboratory were measured and compared with the data from the manufacturer, see Section 6.8.4. The sand was sieved by passing a sand sample through a series of sieves from larger to smaller mesh size and then weighing the sand caught in each of the sieves. The sample mass was measured prior to sieving and compared with the combined total of the weighed sand fractions from the sieves so that the losses during sieving could be quantified (and error calculated). Sieve sizes were selected at approximately 0.1 mm steps but this depended on what was available in the laboratory. The sand in each sieve was shaken through into the next sieve until there were visually very few grains still falling through. The sand retained in the sieve was emptied into a container for weighing. Sand grains that were stuck in the sieve mesh but that could be tapped out were added to the container before it was weighed.

Due to the manual sieving method used in the laboratory it was expected that a slightly smaller proportion of sand would pass through each sieve than in a more rigorous testing procedure as the sieves were not shaken for as long or as quickly as in an automated process. However, the close agreement between the distributions measured (see Section 6.8.4) from several samples of the same sand type demonstrated a high level of consistency in the approach.

4.3.2 Sediment bulk density

The bulk density of the sand both wet and dry, compacted and uncompacted was measured prior to the experiments. A specified quantity of each sand was weighed and placed in a container marked with a volume scale. The sand was either left loose, or compacted by shaking the container and using a solid plastic rod to compact and flatten the surface. In each case the volume of sand in the container was recorded. To measure the density of wet sand a known volume of dry sand was mixed in the container with a known volume of water. The water volume was chosen so that the sediment was completely submerged beneath the water in the container. The volume of sediment was again read from the scale. As with the in situ density measurements (see Section 6.8.1) the mass of the water was removed in the calculation so that an equivalent dry density is given for the wet density condition.

4.3.3 Sediment permeability

A second parameter measured externally to the tests was the permeability of the sands. This was measured in a permeameter. A permeameter works by measuring the flow rate of water through a sample of the sand placed in a vertical tube, which in these tests had a diameter of 3 cm. Each of the uniform and mixed sands was tested. There are two methods available; the falling head test, and the constant head test. Both methods were implemented in this study to help quantify the error in the results. These tests are fairly standard and are described in detail by Murthy (2002). The details of the permeability calculations using each method are given in Appendix 5.

The top of the permeameter tube is either connected to a constant head tank, or to a vertical tube with an attached scale. The flow from the bottom of the permeameter can be connected to a drain or directed into a calibrated container to measure discharge in the constant head test. Two piezometer tubes attached to the sample section at different heights provide the head readings for the constant head test. Foam with permeability an order of magnitude higher than the sands to be tested was placed in the bottom of the permeameter and in the ends of the attached piezometer tubes to prevent sand from escaping, while not influencing the measured permeability of the sand.

To set up a test, the permeameter tube was first filled with water so that the sand would be properly saturated as it was placed in the tube. To prevent stratification of the sediment in the permeameter due to a range of fall velocities in the sample, a small quantity of the sand was placed in the tube at a time so that it could be carefully re-mixed in situ.

4.3.4 Core sampling

A core sampling method was devised to facilitate analysis of the change in sediment grain distribution in the sand bed at different depths and locations. This was especially relevant to the tests involving stratified or mixed sand beds. The cores were collected at the end of a test.

Due to the small scale of the tests, it was not possible to purchase off the shelf coring equipment of the desired dimensions. Instead the equipment was developed at UCL. Initially in test series P-2, readily available metal tubes were used to investigate the practicalities of such a technique. These had an internal diameter of 19 mm and wall thickness of 3 mm. The end of the tube that was inserted into the bed was tapered over a depth of 5 mm so that the wall thickness at the end of the tube was 1 mm. After clarifying that this technique was feasible, clear plastic tubes were chosen instead of the metal ones so that visual insights could also be gained. The tubes had an internal diameter of 26 mm and wall thickness of 3 mm with the ends tapered in a similar manner to the original metal tubes. While these tubes provided a useful means to observe the sand cores, in the final version of the technique, used in the R-3 test series, thinner walled copper tubing of 0.9 mm wall thickness and 26.2 mm internal diameter was selected to reduce as much as possible the disturbance to the bed as the cores were inserted.

In the initial method water was left in the flume when the cores were inserted, as would be the case in a real streambed. However, as the sand had very little resistance to the cores in this arrangement, the final methodology (used in test series R-3) involved very slowly draining the water below the surface level of the sediment (so the draining process did not disturb the bed) and then inserting the cores into the sand which was now able to hold its shape better. Note that the agreement between the results from the different coring techniques was shown to be reasonable, see Appendix 6.

Figure 4.9 shows the layout of the core samples around the pile. The exact locations of each tube varied from test to test, see Appendix 6. Once the cores had been inserted the sand around the tubes was excavated. Each tube was carefully slid onto a thin plastic sheet and then lifted out of the flume. Once the cores had been removed from the flume, observations of the sand pattern were recorded in the case of the plastic tubes. In all cases the sand was then removed from the tubes in 1 cm sections. A 1 cm thick plastic disk of slightly smaller diameter than the tube connected to a plastic handle was used to push the sand out of the tube. In order to do this the water content of the sand within the tube was adjusted by carefully adding water into the top of the tube so that the particles held together as they were removed. A 1 cm scale was marked onto the handle of the plunger. Once it had moved one centimetre the displaced sand was put into a container by levelling the end of the sample tube with a metal rule. This process was repeated for the rest of the sample. The 1 cm sections were dried out and sieved to provide a measure of the grain size distribution. Due to the small size of each sample only 3 sieves were used with mesh sizes of 420, 600 and 850 microns so that the sand was grouped into 4 grain size bandings. Based on the grading curves for the two sizes of sand used in the test programme, the smallest mesh size was chosen to act as a separation point between the fine and coarse sand distributions, see Figures 6.92 and 6.93, Section 6.8.4 where it can be seen that less than 3% of the coarse sand distribution is finer and less than 1% of the fine sand distribution is coarser than the 420 micron sieve aperture. Therefore, the smallest banding was considered to be the original fine sand and the other grain size bandings together were the coarse sand. The two largest sieve sizes divided the coarse sand into three sections, to help assess processes such as the development of bed armouring during the tests.

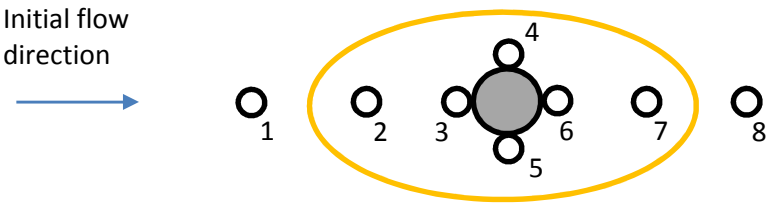

Figure 4.9 General layout of core samples taken from the scour hole at end of test.

The core sample technique was used in both flumes. However, the technique was much more effective in the small flume, as considerable force was needed to insert the tubes into the deeper false bed section in the larger flume. This resulted in them needing to be hammered in, the vibrations causing further disturbance to the samples. Consequently the compression of the samples was more evident and it was more difficult to remove the sand from the tubes.

4.4. Scour measurement

After the discussion of scour measurement techniques in Section 2.7.3, a suitable scour measurement system had to be selected. It was important to consider the requirements of the system in the given laboratory setting and relating to the specific test programme and objectives. It was desirable to investigate 3D aspects of scour hole development as these may be important for characterising the scour process, especially in more complex sediment beds and hydrodynamic conditions. This is also important when considering the basic way in which the scour hole shape evolution is currently characterised in state of the art analytical models (see Section 2.6).

To summarise, the criteria for the ideal measurement system in this context is:

- Non-intrusive - no equipment in the flow (or equipment is very small), no pausing the flow or draining the water
- Instantaneous and simultaneous measurement of multiple points covering the scour hole and surrounding area, or the whole measurement area covered during a small change in time
- Measurements at 1 cm intervals or finer in the horizontal plane
- Vertical resolution of about 1 mm or finer
- Accurate to 1 mm or better in both horizontal and vertical
- Temporal resolution from seconds to hours

Due to the relatively small scale of the tests, some of the measurement options were impractical where the equipment placed in the flow would be large relative to the pile. Positioning a camera or other equipment such as stepper motors inside the pile was not very practical considering the pile diameter would be as small as 20-40 mm for many of the tests. The resolution and accuracy requirements stated above are also a consequence of the test scale. Note that the above requirements can be relaxed slightly for the larger scale flume, so that slightly coarser measurement resolution and slightly lower accuracy would be acceptable.

Point gauge methods were ruled out because of their intrusiveness and due to the length of time required to collect a 3D bed profile. Techniques using a plastic sheet on the flow surface were discounted because of the need to run waves in some of the tests. As it was not essential to automate the measurement process, more complex pile scale systems such as those involving steel wires were of little benefit and were likely to be more intrusive than a simpler approach. The techniques left for consideration were the simple pile scale systems, small echo or laser devices with minimal equipment submergence, and photogrammetry techniques.

The optimum technique identified in Section 2.7.3 was (multimedia) photogrammetry, as this is the only technique with the potential to meet all of the above requirements. However, to the author's knowledge this type of system has yet to be successfully implemented in the scour literature because refraction has not been properly accounted for, resulting in a compromise in

terms of the measurement accuracy. Therefore, this technique would need further development and validation before it could be used with confidence.

Because of the uncertainty in the performance of photogrammetry systems, it was important to consider the merits of the other options for scour measurement. Laser and echosounder distance sensors have been used quite extensively in fluids laboratories and are standard technologies. Assuming a device with small enough dimensions without unacceptable loss of resolution could be found within budget then this would provide a reasonable compromise to the requirements. Commercial echosounder devices were found to fit these constraints more so than laser systems; the latter having larger dimensions and being considerably more expensive.

The limitations of these systems – that measurements are affected by suspended sediment and poor visibility, and have reduced operability in close proximity to the pile – made it prudent to also employ the simple pile scale method to deliver measurements close to the pile and especially in the very initial stages of scour at high frequency.

This led to the decision to use several methods for scour depth measurement in the flume simultaneously, so as to have confidence in the results through cross-validation and so that the strengths of each method could be combined to obtain all of the required information. The three techniques that were used are discussed in the following sections.

4.4.1 Echosounder

Initial testing of acoustic devices was conducted to determine their potential. An ADV sensor was used for this purpose which was readily available in the laboratory and includes a basic distance measurement. Comparison between the ADV and a point gauge was conducted in the small flume over a sand bed, but there was poor agreement between the two techniques, see Porter (2011) for further discussion of this. This was most likely due to the large size of the ADV's beam footprint. Therefore, a search was conducted to find a sensor with higher specifications. While laser sensors were also explored there were none to hand for initial testing, and either the dimensions of the device or the high cost meant that in the circumstances it was an echosounder device that best matched the requirements.

An echosounder device was purchased that had been designed specifically for small-scale testing in fluids laboratories such as for measuring bed profiles. The echosounder had been designed with reasonably small dimensions but with high frequency to maintain good resolution on the bed. According to the manufacturer, the General Acoustics Ultralab UWS echosounder has vertical resolution of 1 mm with accuracy equal to 1% of the measured value. The echosounder frequency is 1 MHz with a beam angle of less than 3 degrees. The sensor has a 30 mm diameter, and only the surface of the sensor needs to be in contact with the water in order to take measurements. In these experiments a submergence depth of the sensor face of 1-2 mm below still water level was employed.

The echosounder is connected to a data box which outputs the depth measurement in real time at a user selected frequency (i.e. 0.1 s). Alternatively the box can be connected to a data logger

so that the signal is recorded directly to a computer. In this case the output is a voltage signal and the echosounder must be calibrated to equate the voltage signal with distance measurement. The calibration is straightforward as there is a linear relationship between the voltage and depth measurements (the calibration methodology is detailed later in the section).

A range of settings can be adjusted on the data box. The main parameters that need to be specified are the minimum and maximum measuring distances, the measurement window and the delay time so that the signal processing is optimised for the experiment. If the settings are not adjusted correctly the signal may be very noisy or it may not output a reading at all (e.g. if the measurements are outside of the programmed minimum and maximum distances). With the right settings it is possible to measure depths between 2 cm and 15 m.

The set-up of the echosounder system was different in the two flumes. In the larger flume the x and y positioning of the echosounder was computer controlled by fixing the echosounder to a traverse sitting over the flume. In the smaller flume this was not possible so the echosounder was traversed manually. In both cases the echosounder was attached to a metal rod of approximately 10 mm diameter via a custom made holder. This provided it with a degree of stiffness to reduce vibration of the sensor and enabled it to be positioned so that the sensor face was parallel to the flat bed. Due to the width of the holder and the radius of the sensor the closest the centre of the echosounder could be placed to the edge of the pile was 2 cm. The echosounder sensor and its set-up in each of the flumes is illustrated in Figure 4.10.

In the small flume the echosounder was clamped via the rod to a board above the flume. The echosounder was used to measure profiles along the centreline of the scour hole in the streamwise direction at 1 cm intervals. Once the cross-stream position had been set by clamping the echosounder in the required position, the echosounder could be moved in the streamwise direction by simply sliding the board along the flume wall. The board was lifted over the pile to switch between upstream and downstream measurements. The streamwise position was determined by fixing a rule along the rail above the flume so that the board could be moved the correct distance relative to the scale. At each measurement point the recording on the box was noted. As there was considerable variation in the reading when the echosounder was stationary, the maximum depth reading over a 30 second period was recorded. The maximum rather than an average depth was taken because of the tendency for the readings to relate to reflections from suspended particles. This approach resulted in good agreement between the echosounder and pile scale measurements in the small flume (see Section 4.4.5). The sensor face was approximately 16 cm from the flat bed level. This meant that the beam footprint diameter was just over 8 mm on the flat bed.

In the larger flume the metal rod was fixed to an x-y traverse. The sensor was positioned approximately 45 cm from the flat bed level, giving a beam footprint diameter of nearly 24 mm. It should be noted that as the scour hole deepens the beam footprint diameter will increase. For example for a 10 cm deep scour hole in this flume the beam footprint diameter will increase to

almost 29 mm. The beam footprint will also be larger on an inclined slope relative to the echosounder orientation.

The echosounder data were recorded straight to a computer via a data logger, so the signal had to be calibrated prior to analysis. The calibration was completed with the full depth of water in the flume. 10 plastic blocks, the widths of which were measured with high precision callipers were stacked one at a time on the bottom of the flume (70 cm from the echosounder). Each block was approximately 2.5 cm thick. 10 seconds of echosounder data was collected as each block was added to the stack. The depth reading on the echosounder box was also recorded for cross-checking. The known depths (calculated from the block heights) were plotted against the voltage readings and a best fit was obtained to give a linear equation for conversion between the voltage and depth readings. It is important to note that the calibration is dependent on the values of the parameters programmed into the echosounder box, so these were not changed during a test series.

a) 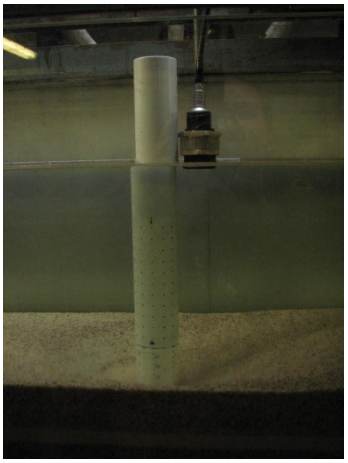 b) 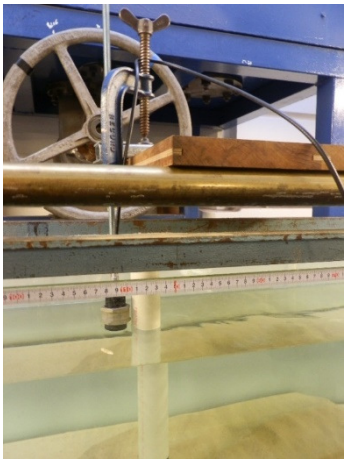 c) 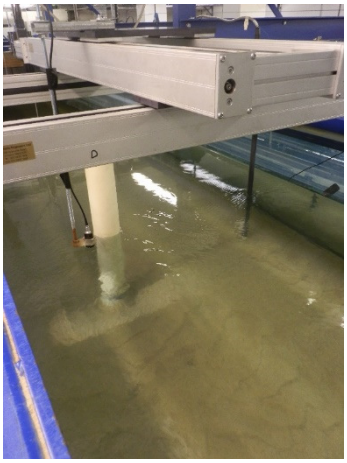

Figure 4.10 Echosounder sensor with mounting, a) in the small flume b) in the small flume showing mounting board c) in the coastal flume with traverse.

The traverse was controlled electronically. A matrix of x-y positions was input to the software so that the echosounder would automatically travel on a specified path. To reduce the time taken to complete one profile, measurements were limited to 2D profiles along the centreline of the scour hole initially (similar to those in the small flume). A complete map of the scour hole was obtained in the final stages of a test, see Figure 4.11.

The speed of the traverse and the waiting time at each position could be specified in the software. A compromise had to be made between the time taken for a profile to be completed and the accuracy of the depth measurement. Therefore, the echosounder was paused for just 1 s at each measurement point so that 10 depth readings were obtained at each location. The traverse speed was initially set at 5 mm/s but in later tests this was increased to 10 mm/s. While a faster speed would have been preferable to reduce the profiling time, increasing the speed beyond this value resulted in large vibrations of the echosounder at each stopping point.

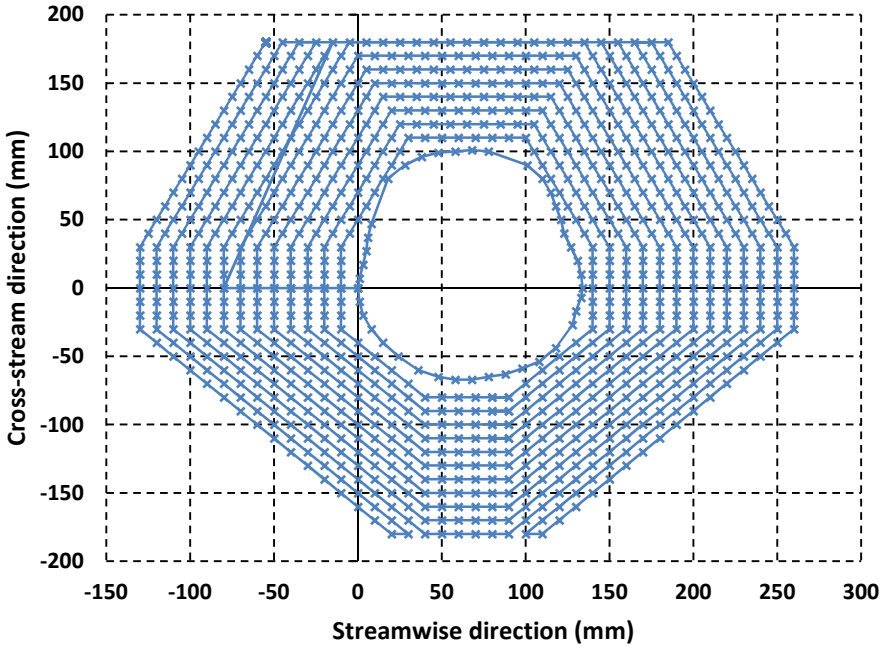

Figure 4.11 Traverse matrix for 3D echosounder profiling in the coastal flume

The echosounder data stream was not connected to the same software as the traverse. Therefore, synchronising the location data with the depth signal was difficult. They were synchronised approximately by starting both pieces of equipment at roughly the same time using two computer mice. However, the data was synchronised more rigorously at the analysis stage, by examining the shape of the echosounder signal (flat or sloping) to determine when the echosounder first started moving.

Once the start of the echosounder signal and the matrix had been lined up, the next stage of data processing was to compute a time history of the traverse matrix based on the traverse speed and the distances between the measurement points. Taking into account the 1 second stopping time at each point, this gave the time at which the echosounder was at each position in the matrix. The data at each location could then be pulled out of the echosounder time history signal. Following the method in the small flume the maximum values were plotted against the x-y position to produce 3D profiles of the depth measurements.

One complexity during the analysis was that after following the above method there was still a discrepancy between the x-y positions and the depth readings. An investigation was conducted to determine if this was due to a difference between the true speed of the traverse and the specified value. A laser pointer was attached to the traverse and moved to a series of positions. At each point a mark was carefully made on the floor. The location of the laser dot relative to the marked points was then filmed as it completed the traverse path. A high resolution clock was positioned in view of the camera so that the true traverse speed could be calculated from the time taken to travel the known distances between the markers. The distances between the marked points on the floor were measured to check for consistency with the programmed

coordinates, which was the case. The markers were positioned to include single axis and combined axis movement of the traverse in both forward and reverse directions.

The results indicated that the programmed traverse speed was linked only to the axis travelling the furthest distance during two axis movement and not to the direct path travelled between two points, as was assumed in the first analysis. By basing the speed calculation on the distance that the longest axis travelled to move between points the discrepancy in the data was significantly reduced. However, a small discrepancy between the traverse and echosounder readings was still evident. This small discrepancy added up into one that was noticeable in the signal over the long traverse pattern. A systematic correction was applied to the calculated position times to account for this, based on evidence from the video analysis as well as the length of the time discrepancy over the full matrix. The output results were checked against other techniques and visual observations to ensure they were sensible, see Section 4.4.5.

As the echosounder records the distance between the sensor and the bed, a datum had to be defined to convert the data into a scour depth. The echosounder was set over the flat sand bed to record the datum level. In the case of the small flume the variation in the flat bed was only 1 mm. However, in the larger flume an average value from a profile of the flat bed was used as there was slightly more deviation in the sand level at this scale.

4.4.2 Photogrammetry

To develop a working photogrammetry system, several aspects had to be considered. These included the practical set-up of the system such as the camera positioning and mounting, lighting and measurement targets. Data acquisition and image processing had to be investigated and a method for dealing with refraction needed to be determined.

The computational side was approached through the use of a software package, VMS version 8.5 (Vision Measurement System) that was developed by Robson and Shortis (2012). This software was chosen as the first author is based at UCL facilitating the provision of in-house training and support as well as detailed discussion of practical aspects and the refraction issue. This software uses the bundle adjustment method (see Section 2.7.3 and Appendix 8 for full description of the method). Using an existing software package has the significant advantage that it is tried and tested, and removes the need for manual image processing or writing code from scratch which would be time consuming. However, this software does not explicitly take into account refraction through surfaces between the camera and the object. The implications of this will be discussed after the equipment set-up is detailed.

Initially two high resolution CCD Kodak MegaPlus ES1.0 cameras were positioned outside of the small flume (and 4 cameras at the larger flume) to photograph the scour hole during testing through the air-glass-water interface, as this was the system that had the most potential for scour measurement in terms of meeting all of the requirements. As discussed in Section 2.7.3 a minimum of two photographs are required to solve the colinearity equation, so a minimum of two cameras were needed in a system obtaining dynamic measurements through simultaneous

image capture. The two cameras were mounted at a steep downward looking angle (at least 45 degrees to the horizontal) in order to provide the best possible coverage of the deepest scour holes. They were positioned so that their optical axes crossed towards the back of the scour hole to maximise the image quality over the area to be measured. The cameras were connected to a computer via a frame grabber for image acquisition. A trigger box was used to control the image capture and synchronisation of the two cameras. The image acquisition software was set to run with an external trigger and an internal trigger on the trigger box was set to the required frequency for image capture. To establish points for measurement in the images a grid of dots was projected through the flume wall onto the bed. A film projector was readily available for this function and was a cheaper option compared to the diffractive lasers used in some other studies (Section 2.7.3). The dot size that was projected was controlled through careful positioning of the projector and design of the grid system printed onto the slide. Using projected markers avoided the need to use image matching software, the capabilities of which were likely to be limited due to the featureless nature of the fine sand bed. A pair of lamps were used to enhance the ambient lighting as the best image quality was obtained with a small aperture setting (less light allowed into the camera).

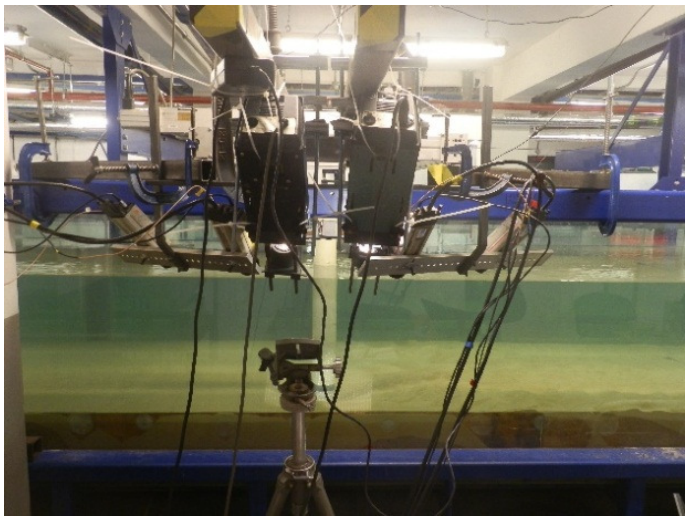

Figure 4.12 Photogrammetry technique set-up at the coastal flume.

This set-up produced images during the scour tests of suitable quality, with excellent spatial coverage and frequency. The remaining issue was how to calibrate the cameras to account for refraction.

Several options were investigated:

1. Calibrate the cameras ex situ and ignore the refractive plane in the in situ measurements

For this solution the intrinsic calibration parameters of the cameras were calculated a priori by photographing a carefully designed calibration plate made of a square sheet of glass. The sheet was painted mat black with reflective dot targets positioned on one face. The coordinates of the dots were known with a high level of accuracy from another measurement system. The

calibration plane was photographed with both cameras from a range of positions and orientations relative to the plane. These photographs along with the known coordinates of the targets were entered into the VMS software and a bundle adjustment calculation was run to obtain the lens distortions and other camera parameters. The intrinsic parameters were identical between the calibration and the flume measurements because the focal length was kept fixed by applying tape to the adjusters so that they could not be moved accidentally. The solution at the flume was made possible by placing a small number of targets of known coordinates on the front wall of the flume (i.e. no refractive planes between the targets and the camera). These targets provided enough information for computation of the camera orientation parameters relative to the flume. Along with the intrinsic camera parameters and image observations the unknown 3D coordinates of the scour hole could then be calculated in the bundle adjustment.

2. Calibrate the cameras in situ and implicitly account for refraction

For this option the calibration was completed with the cameras in place next to the flume prior to running the scour tests. A calibration cube with a series of targets of known coordinates was placed underwater in the flume in view of the cameras. The position and orientation of the cube was varied while a series of photographs were taken with the cameras in the fixed position. The known coordinates along with the measured image coordinates of the calibration cube targets were input and a bundle adjustment computation was run to obtain the camera orientations and intrinsic parameters. The idea was to obtain a best fit to the calibration cube in this method. Apart from computing the standard camera parameters iteratively in the solution (lens distortions etc.) a further set of up to 10 parameters can also be input into the bundle adjustment to help improve the fit between the computed and real target coordinates, thereby implicitly taking into account the additional effects of the refractive flume wall.

The calibration cube is shown in Figure 4.13. The sides of the calibration cube were 30 cm long. Lines of white dots on a black background were printed, laminated and fixed to the calibration cube to make up the targets. Prior to the camera calibration the coordinates of the markers on the calibration cube needed to be measured to ascertain the known coordinates needed for the calibration. Initial estimates using callipers were refined using a standard photogrammetry solution. This was conducted outside of the flume (i.e. no refraction issue) with a Nikon D3200 DSLR camera, in order to establish the coordinates of the calibration points with high accuracy. The first option discussed above established that as expected there was a need to account for refraction as the distortions in the computed solution were large, although it was possible to compute a solution (solution was convergent). However, the distortions were too large for the method to be appropriate for scour measurement.

The second option was designed to incorporate refraction in a similar manner to accounting for lens distortion through an additional set of parameters that would be computed as a best fit in the bundle adjustment. It was hoped that this would provide at least a reasonable approximation between the real and computed coordinates in the object space. While some degree of compromise in terms of accuracy was expected, this method was preferable because of its

simplicity as it did not require software development. Unfortunately a convergent solution in the bundle adjustment could not be obtained as the initial estimates of the parameters were too inaccurate and the distortion too severe. A range of options were investigated to obtain a convergent solution, including switching between a 2 and 4 camera system, running the calibration for one image pair only so that the calibration cube did not move relative to the refractive plane, and a trial and error approach was implemented for selection of the combination of additional parameters used in the calculation. Using only one pair of images did enable a solution to be obtained for the camera calibration parameters and camera orientations. However, when this solution was used to measure a real scour hole, the errors were very large and an acceptable solution using this method could not be obtained.

a) 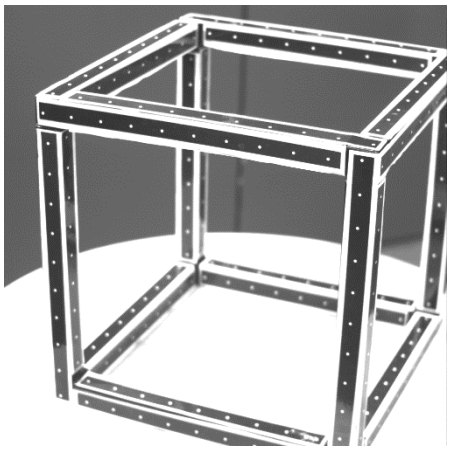 b) 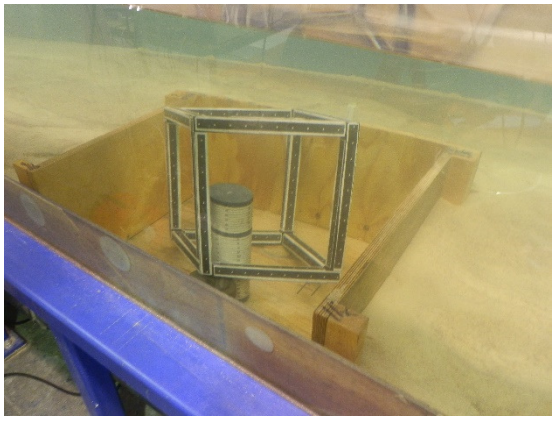

Figure 4.13 Calibration of photogrammetry system in the Coastal flume a) calibration cube b) in-flume calibration.

Consequently this approach had to be revised and the remaining options considered were as follows:

1. Extend the software to incorporate a physical model for refraction

This could be based on the ray-tracing method discussed in Section 2.7.3. Although this method has been shown to be feasible it would be complex to implement, as it relies on an iterative solution to calculate refraction which would require extensive code development. As discussed in Section 2.7.3 there are circumstances in which a solution cannot be obtained from this method, and other aspects may reduce the accuracy of the solution such as having very steep angles between the cameras and the refractive planes. Therefore, although plausible, an accurate solution would not be guaranteed.

2. Compromise in terms of the measurement system requirements

This required a rethink of the system requirements in terms of intrusiveness, time resolution, spatial coverage, or accuracy.

The first of these options was considered high risk as results could not be guaranteed and the feasibility was an issue considering the timeframe of the project. Therefore, the second option

was chosen. One way to deal with the refraction issue was to switch to using underwater cameras. As discussed in Section 2.7.3 underwater cameras can be successfully calibrated in the standard way because the refractive distortions are symmetrical. This would still enable most of the desired measurement system requirements to be maintained, but would compromise in terms of intrusiveness.

The use of underwater cameras was first investigated in terms of the feasibility of image capture during testing (dynamic measurements). The size of the existing Kodak cameras and the fact that they would need a waterproof housing would result in a large amount of equipment in the water. If positioned downstream of the pile this would not interfere with the experiment except in wave tests where reflections could be an issue or tidal flows where the downstream side changed with every half cycle. Another option was to switch to using smaller cameras. However, it was difficult to source small cameras within budget that could be synchronised accurately. Furthermore, the field of view of the cameras would need to be assessed to determine if the scour hole could be viewed without placing the cameras in intrusive locations.

An alternative compromise to the requirements was to only take photographs when the flow was paused. This meant firstly that any size of camera could be used without affecting the level of intrusiveness, and secondly only one camera was needed as a series of pictures could be taken while the scour hole was stationary. This also meant that a large number of photographs could be taken of the scour hole which would promote a robust bundle adjustment calculation due to a high level of redundancy. As the system was one which can be fully accommodated by the VMS software, accuracy was also expected to be excellent. As mentioned in Section 4.1 the tests had to be paused periodically to re-smooth bed ripples, overnight, and before flow reversal in the tidal experiments. By taking photogrammetry measurements at these points, the new system compromised only in terms of the frequency of measurements.

A specifically designed, relatively inexpensive underwater camera, (Canon PowerShot D20) was purchased. Critically, the focus could be set manually so that it did not change between photographs, making it possible to calibrate the camera in the usual way. Photographs were taken all the way around the pile using a range of roll angles to enable a robust computation. The camera was hand held and submerged just beneath the water surface so that it did not result in any disturbance of the bed. Calibration was conducted by marking a matrix of dots of known coordinates onto the pile prior to running the tests. As the targets were in situ during the experiments the calibration could be obtained from the same photograph sets used for the scour hole measurement.

The measurement points in the scour hole were consistent with the earlier technique using projectors. Digital projectors were used in the final set-up, so that the clarity of the dots was improved (brighter and more defined). The most suitable dot size and spacing could be easily determined in situ by making adjustments to the computer file that was being projected. In the larger flume two projectors were used to cover the required area, in the smaller flume only one projector was needed. The projector was positioned at a steep angle of at least 45 degrees to

the horizontal to provide the best possible coverage on the nearside scour hole slope which faced away from the projectors. In this way only a small area of the scour hole slope did not contain any measurement points, as well as a small shadow zone directly behind the pile.

a)

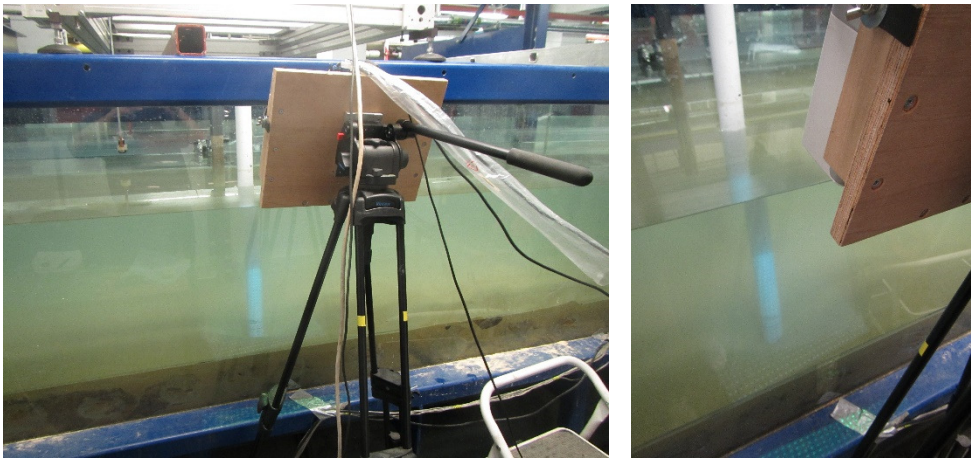

b)

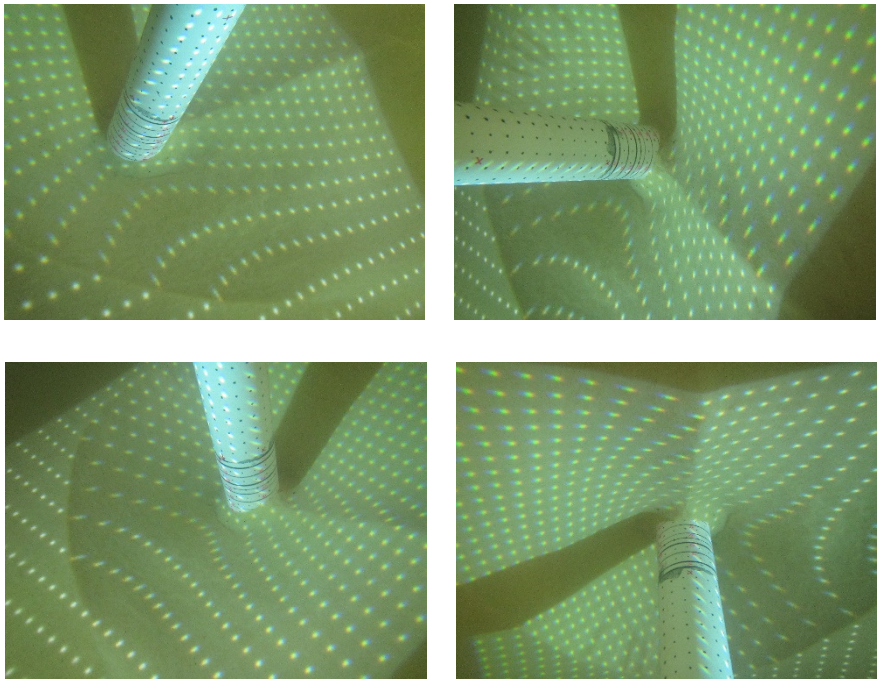

Figure 4.14 Photogrammetry technique in the coastal flume a) final set-up with digital projector b) example underwater images used in the analysis.

To increase the accuracy of the solution, only the known targets on the pile were used in a first stage solution to obtain the camera parameters. In the second stage the unknown dots on the bed were computed. This prevented dots that were less defined due to the projection angle relative to the sand bed profile from influencing the computation of the camera parameters. In this way the scour hole profile was successfully computed in both flumes and this was the final photogrammetry system adopted. The set-up and example images are shown in Figure 4.14.

Post processing of each photogrammetry solution was required to output 3D plots of the bed profiles in the correct coordinate system. The coordinate system in the photogrammetry

software cannot be fixed because of small adjustments made in the solution to the coordinates of the known points. Therefore, coordinate transformations had to be applied to align the bed profiles with the coordinate system adopted in the flume, with the x axis in the streamwise direction and the z axis vertical. The profiles were also translated so that the (0,0,0) point coincided with the initial bed level, and the centre of the pile. 2D profiles were obtained from the 3D bed profiles using a linear interpolation function in Matlab.

4.4.3 Pile scale

Initially a scale was attached to the pile by gluing a thin acetate sheet around the cylinder which had a 1 mm scale printed on it. However, problems arose with the sheet becoming detached from the pile during trial tests, eventually influencing the deposition patterns in the scour hole. It was also difficult to read the scale clearly due to its fine resolution. So for the final experimental design this system was revised to marking a scale onto the pile directly. A lathe was used to mark concentric circles around the pile with a thin tipped marker pen at 5 mm intervals (see Figure 4.15a).

In some of the later series of tests in which the final photogrammetry system was implemented the scale was incorporated into the pattern of dots that were marked onto the pile as targets. A stencil of the required dot matrix was made by drilling the pattern into an acetate sheet using a 0.5 mm drill bit in the case of the smaller scale tests, and a 1 mm drill bit for the larger flume so that the dots were suitably sized in the photographs. The sheet was then wrapped around the pile and spray painted to mark the dots onto the pile through the stencil. Once the paint was dry the stencil was removed. The dot pattern included vertical lines of dots at 5 mm intervals to coincide with the base section of the pile, and the scale was marked at several discrete positions around the pile circumference (Figure 4.15b).

a) 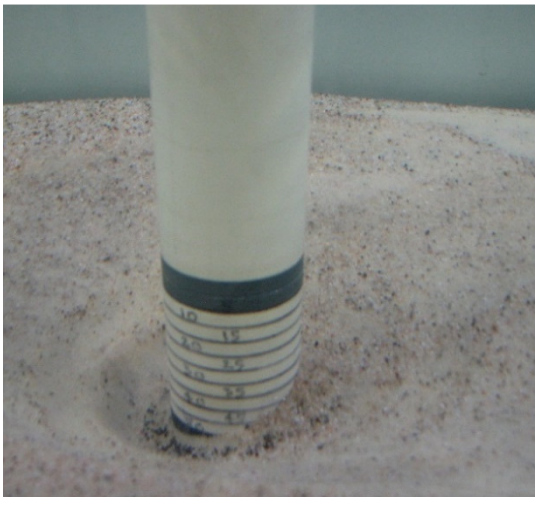 b) 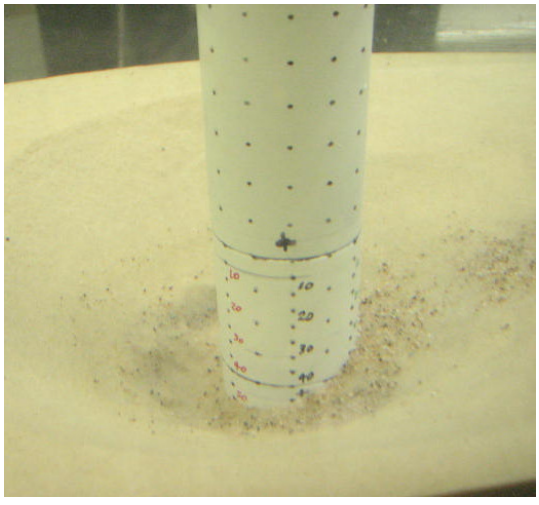

Figure 4.15 Pile scales in the small flume a) concentric circle scale marked onto the pile b) dot scale marked onto the pile.

The scour depth data from the pile scale was collected through visual observations, supported by video recording and still images. The frequency of the measurements depended on the rate

of scouring. The first part of the test was observed continuously with scour depth recorded at approximately 30 second intervals. Later in the tests the scour depth was checked hourly. The 5 mm scale enabled scour depth to be estimated by eye to the nearest millimetre with a reasonable degree of accuracy. The scour depth of the deepest point at the pile was recorded, which was located at the upstream face of the pile apart from during the initial phase of the test where scour depth was deeper at the pile sides.

4.4.4 Observational recordings

Interesting processes and unusual features observed during the tests were recorded by making notes and taking photographs and videos. Time lapse photography was also used to aid in the monitoring of scour depth from the pile scale, see Figure 4.16. The camera was set up on a tripod outside of the flume and connected to a computer. The frequency of photographs could be set in the image capture software. Photographs were acquired at 3 second intervals initially, and every 5 minutes once the rate of scour had reduced. In the larger flume this method was employed to monitor scour progress around the small pile, as the scale could not be observed directly due to the pile being located at the far side of the flume with limited access. In the small flume these photographs were not relied upon for measuring the scour depth but instead provided a record, guaranteeing the integrity of the data as well as allowing further qualitative insight to be gained post-test.

a) 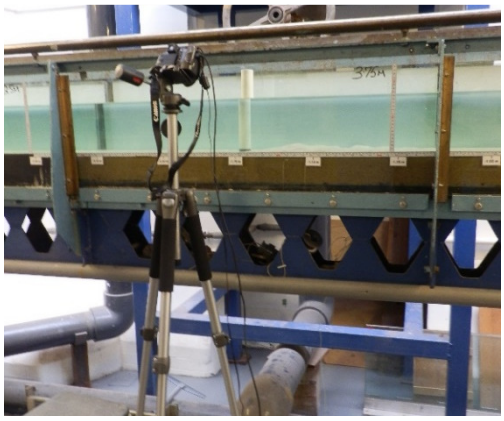 b) 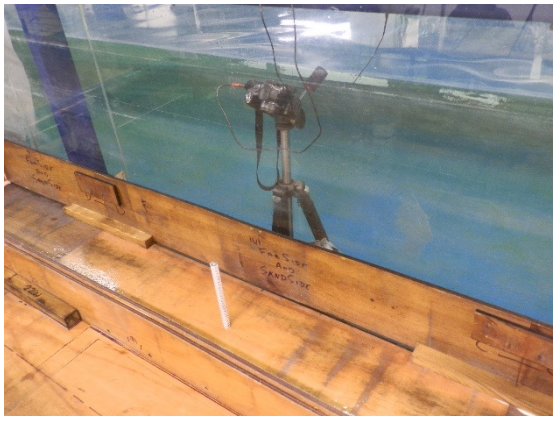

Figure 4.16 a) Time lapse photography in the small flume b) Time lapse photography to monitor the small pile in the coastal flume.

4.4.5 Comparison of measurement techniques

To determine the suitability of the three measurement techniques detailed above for use in the two flumes and to have confidence in the results a comparison was undertaken of measurements between the systems in both flumes.

In the small flume an echosounder profile taken in the streamwise direction along the centreline of the flume was compared with a 2D profile of the same scour hole interpolated from the 3D bed profile obtained with the photogrammetry system. The measurement on the pile scale was

also recorded at the same time. The comparison of the three techniques is shown in Figure 4.17.

In the small flume it was not possible to collect measurements in close proximity to the pile with either the echosounder or photogrammetry techniques, however, if the profiles are extrapolated to the location of the pile it can be seen that there is good agreement between these profiles and the pile scale measurement.

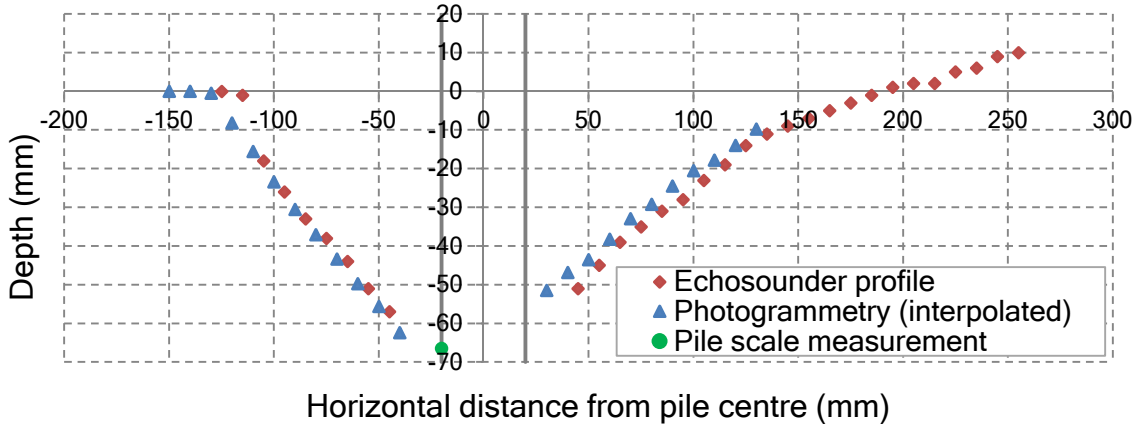

Figure 4.17 Comparison of echosounder and photogrammetry scour hole profiles with the pile scale measurement from test R.19 in the small flume.

The photogrammetry and echosounder profiles are also in good agreement with each other, particularly on the upstream side of the pile. However, there is a more significant discrepancy between the profiles towards the top of the upstream scour hole slope.

This aspect was investigated by traversing the echosounder across the upstream edge of the scour hole in small increments. It was found that the echosounder output a step change in depth rather than a smooth transition as it crossed the edge of the scour hole. This can be linked to the size of the beam footprint of the echosounder. A stronger signal is obtained from a flat bed than a sloping bed, so as soon as the edge of the flat bed comes into range this is the value that is output rather than an average of the depth over the footprint area. This results in the edge of the scour hole appearing to be closer to the pile than it should be, seen in Figure 4.17 in comparison to the photogrammetry profile.

The small difference in the profiles on the downstream side of the pile in Figure 4.17 may be due to small discrepancies in the alignment of the echosounder compared to the photogrammetry system. A small offset in terms of the x or y position or a slight rotation of the echosounder sensor from horizontal would account for the difference.

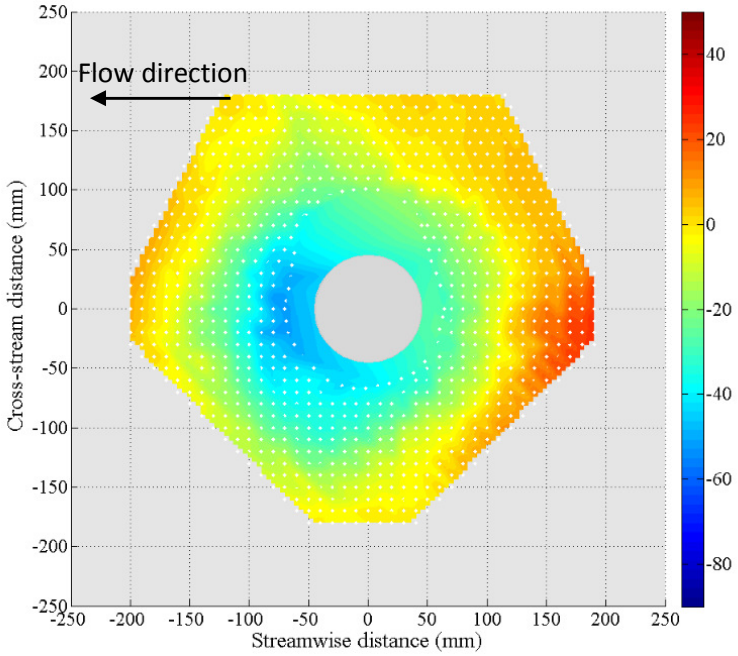

a)

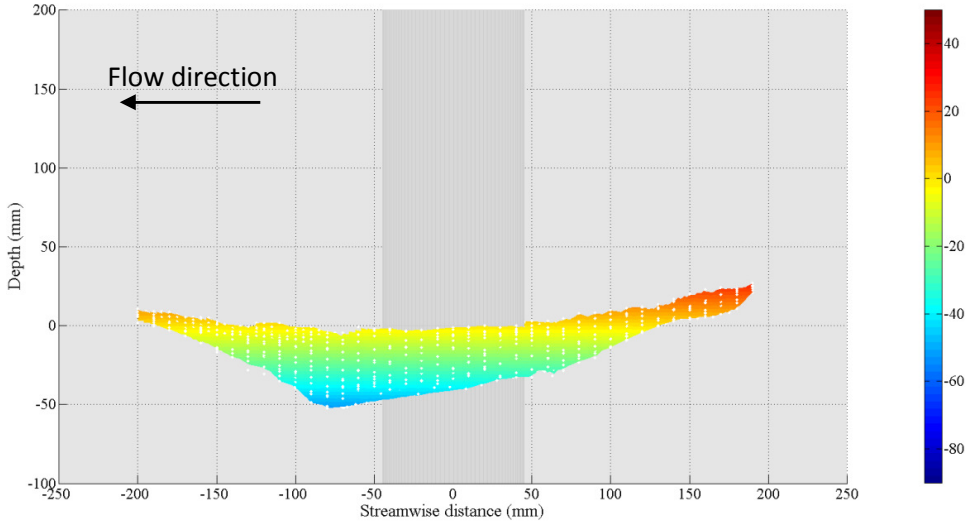

b)

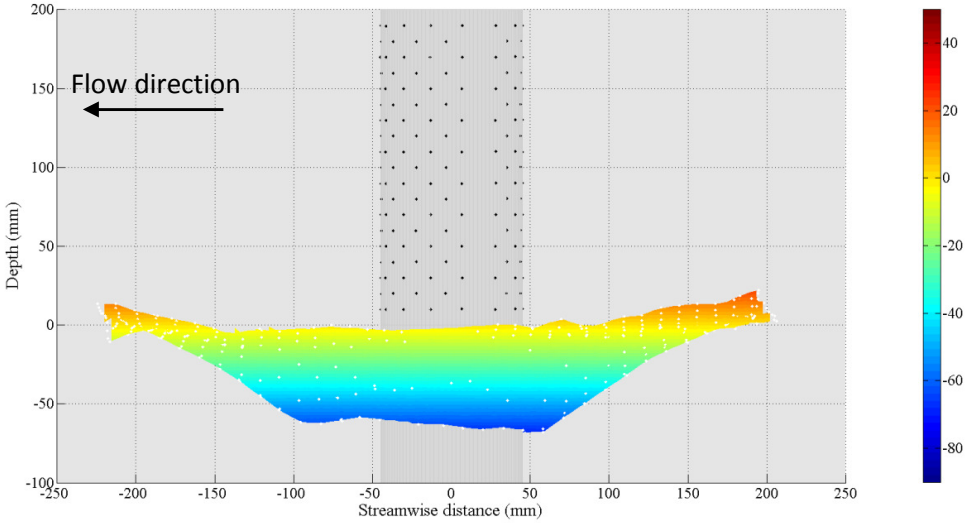

c)

Figure 4.18 Echosounder profile of scour hole in coastal flume at end of test C.90.19 a) plan view b) side elevation c) photogrammetry profile for comparison

The level of agreement between the three techniques in this flume provides confidence in the results. While the photogrammetry technique has the better resolution and accuracy it could not be used as extensively because of the limitation that the flow needed to be paused. Therefore, the echosounder was used as the primary measurement system during tests in this flume for measuring 2D scour hole profiles. This system also has the advantage of quicker data processing time compared to the photogrammetry method. A final check of the reliability of the echosounder technique in the small flume was made during tests R.29.1, R.29.2, R.29.3 and R.29.4 which were repeated under the same conditions, enabling repeat scour hole profiles to be collected. Very close agreement was found for each of the comparisons (see Appendix 7).

In the large flume excellent agreement was also found between the interpolated 2D photogrammetry profiles and the pile scale readings. In this flume the photogrammetry was able to measure almost adjacent to the edge of the pile so direct comparison with the pile scale was possible. The comparisons are shown in Figures 6.67 - 6.68, Section 6.

While the photogrammetry and pile scale were in close agreement in the large flume, this was not found to be the case for the echosounder system. Figure 4.18 shows a 3D profile of the scour hole measured with the echosounder at the end of test C.90.19. The same scour hole measured using the photogrammetry technique is shown in Figure 4.18c and in Figure 4.21b alongside a photograph of the scour hole.

It is clear qualitatively when comparing the profiles from the two techniques that there are significant differences between the scour hole profile shapes. In particular the region in close proximity to the pile is much shallower in the echosounder profile than it is in the photogrammetry profile. Furthermore the deepest part of the scour hole is on the left hand side of the pile in the echosounder profile but this does not match observations of the scour hole and pile scale or the photogrammetry profile in which the scour hole is deepest on the right hand side of the pile. To analyse these differences a direct comparison of the measurements interpolated from the echosounder and photogrammetry profiles at the same locations is shown in an identity plot in Figure 4.19.

It is clear in Figure 4.19 that the echosounder is systematically recording shallower scour depths than the photogrammetry system. This was also found to be the case when comparing ADV depth readings with point gauge measurements in the small flume (Porter, 2011). This is a consequence of the larger size of the beam footprint which results in poor measurement accuracy over steeply sloping sections of the bed. The measured points that are in closest agreement in Figure 4.18 are close to the zero depth, which is the initial, flat bed level. The shorter measurement window (1 s) used in this flume compared to measurements in the smaller flume is also likely to be a factor in the poor agreement between the two techniques. Note that in Figure 4.19 the photogrammetry and echosounder measurements in the small flume are also plotted against each other demonstrating the much closer agreement achieved at the smaller scale.

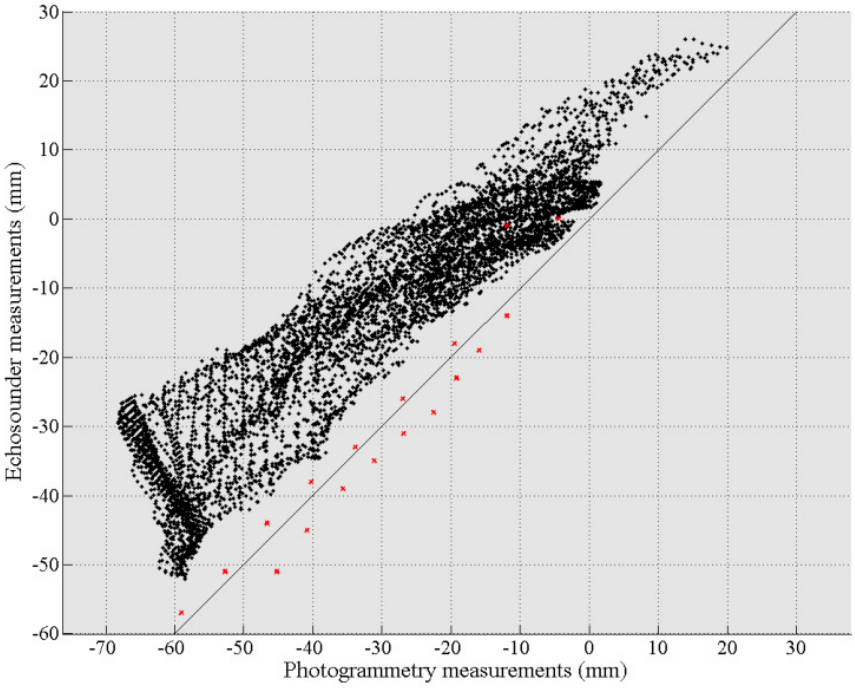

Figure 4.19 Identity plot of photogrammetry versus echosounder measurements of the 3D scour hole profile at the end of test C.90.19 (black) and echosounder measurements compared to photogrammetry measurements in the small flume from test R.19 (red).

As discussed in Section 4.4.1 a substantial amount of post-processing was needed in order to plot the echosounder 3D profile due to the synchronisation of separate data streams. Another possible reason for the poor agreement between the techniques may be persisting synchronisation errors. As was discussed in Section 4.4.1 a small error was noted after synchronisation and so an additional correction was applied. One way to assess the persistence of synchronisation errors is to consider the features of an unaligned profile due to poor synchronisation. The traverse matrix moved in a spiral starting at the closest point to the upstream (left hand) side of the pile in Figure 4.18 and moving in an anti-clockwise direction. Therefore, an issue with synchronisation of the data streams would be less apparent in the region closer to the pile, and increase in significance at the outer extremities of the scour hole. Furthermore, a systematic error in the synchronisation would result in a shift of each circle of measurement points relative to the next in a visually recognisable pattern (as was seen prior to applying the final correction to the synchronisation see Figure 4.20). This indicates at least qualitatively that the synchronisation has been successful in Figure 4.18.

This suggests that the synchronisation issue is not solely responsible for the significant differences in the 3D echosounder profile compared to the photogrammetry profile. The larger beam footprint and shortened data acquisition time compared to measurements in the smaller flume are the key factors that have resulted in poor representation of the deepest sections of the scour hole. Due to the poor quality of the echosounder data in the coastal flume, further processing was not undertaken, and instead the photogrammetry technique which has shown

excellent agreement with the pile scale measurements was used as the primary system for profiling the scour hole in the larger flume.

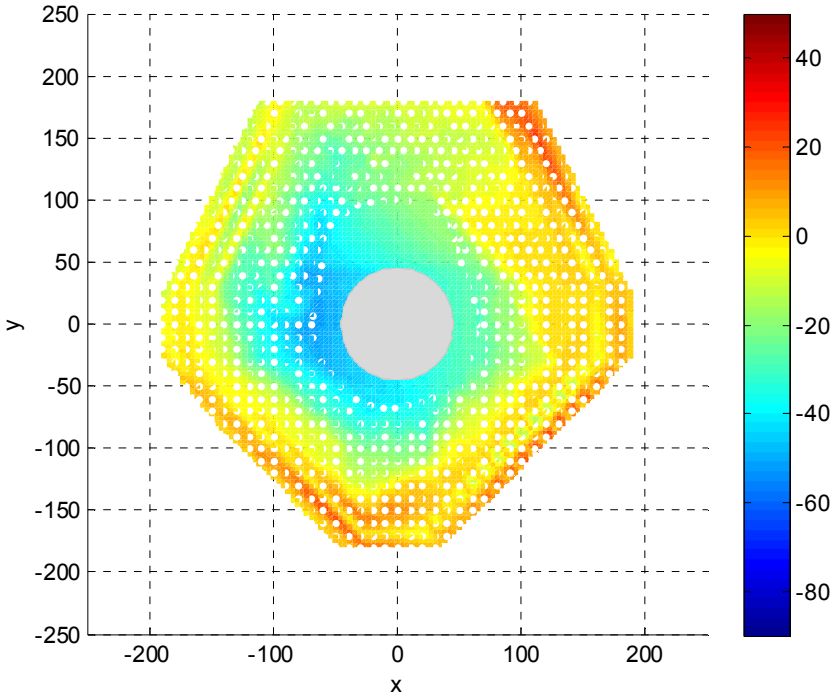

Figure 4.20 Echosounder profile without final synchronisation correction

a)

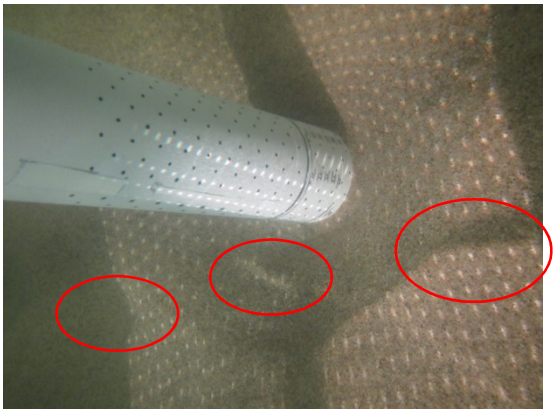

b)

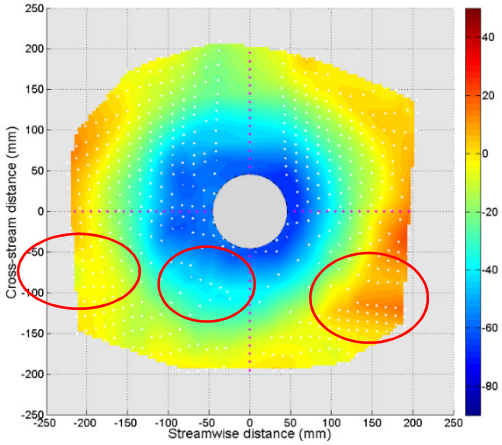

Figure 4.21 Comparison of photogrammetry and visual observations of features in the scour hole a) photograph of the scour hole that was profiled with the echosounder and photogrammetry techniques at the end of test C.90.19 b) photogrammetry profile of the scour hole shown in a) with matching features identified (red circles).

A final check of the photogrammetry data was made by qualitative comparison with scour hole features observed in photographs. A photograph of the same scour hole profiled by the echosounder and photogrammetry techniques is shown in Figure 4.21a, alongside the photogrammetry profile (Figure 4.21b). The photogrammetry technique successfully captures

the finer details of the scour hole for example the small depressions and ridges marked in Figure 4.21a are visible in the correct locations in Figure 4.21b demonstrating the excellent resolution of the photogrammetry technique.

4.5 Velocity measurement

It was important to measure the ambient flow velocity for each test condition as neither facility provided explicit specification of the velocity (velocity control is based on valves and weir gates in the small flume and on motor speed in the larger flume). Therefore, only through in situ measurement could the flume be set up to be consistent with the design velocity for each test.

The vertical profile of streamwise velocity was measured in the flumes prior to each test series or change in flow condition. This prevented interference between the velocity measurement equipment and the scour process. By removing the upper section of the pile, the ambient flow could be measured in the central section of the flume over a flat sand bed. This meant that the velocity measurements were not influenced by the pile wake or bedforms. In the larger flume the ambient velocity profiles were collected at the locations of both of the piles to check the uniformity of the flow across the width of the flume. The depth-averaged velocity was calculated from the velocity profiles using the trapezium rule (see Soulsby, 1997).

In some cases the velocity was also monitored during the tests with the measurement equipment situated downstream of the pile. While these measurements were affected by the pile wake, this provided an indication that the flow conditions were consistent for the duration of the tests and between experiments. In the tidal tests the equipment was located upstream of the pile for half of each cycle as it was impractical to switch the location of the equipment with each flow reversal. As these tests were run in the larger flume, the effect of the equipment on the scour process should be minor as the equipment was placed in the far field away from the pile, the probe was small relative to the pile diameter, and in any case there was a greater level of background turbulence in the flow. It was particularly important to measure the flow velocity during the spring-neap tidal tests as the calibration between motor speed and flow velocity contained a degree of uncertainty (see previous discussion in Section 4.2.5). Measurements were taken 18 cm above the bed to provide an estimate of the depth-averaged streamwise velocity during these tests. Good agreement was found between the measured and design values, see Appendix 10.

Initially, a propeller meter was used for velocity measurement in the small flume. The probe was mounted over the flume and was positioned vertically in the water column by aligning it with a ruler attached to the outside of the flume. While propeller meters provide a quick and simple method of measuring velocity and the small size of the equipment means that disturbance to the ambient flow will be small, it was found that there was considerable discrepancy in the measurements between the four propeller meter probes available in the laboratory. To avoid the time consuming process of re-calibrating the probes and because of other issues such as poor resolution of measurements in proximity to the bed this method was rejected in favour of other techniques which are discussed in the following paragraphs. Note that this technique was

employed in the preliminary test series P-1 but sensible velocity readings could not be obtained due to an issue with the calibration parameters programmed into the data box. Therefore, an estimate of the depth-averaged velocity for these tests was obtained from comparison of the results with those from the other test series, see Section 7.1.1.

One technique used in both flumes was Acoustic Doppler Velocimetry (ADV). A Nortek Vectrino+ system was used. This was more successful in the larger flume, as in the smaller flume the signal was often very noisy due to reflections from the glass flume walls which, because of the small flume dimensions were always in close proximity to the sensor. ADV requires seeding particles to be introduced into the flow which reflect the acoustic signal from the probe. This allows measurement of the particle velocity using the Doppler shift principle. This technique was more suited to measuring the ambient flow prior to scour testing as the large amount of seeding required to obtain a high signal to noise ratio clouded the water to such an extent that during the tests the reduction in visibility would be too great for observational recording of the scour depth from the pile scale. Therefore, the signal quality was somewhat reduced when ADV was implemented during tests due to the reduction in the volume of seeding that could be used. This was particularly evident in the preliminary test series P-3, Appendix 3.

During post-processing of the data, the signal quality was checked to determine its suitability for use. In the main test series data spikes were removed from the data using a simple cut-off, but data that was very noisy was discarded. The ADV system calculates the velocity of particles within a measurement volume of approximately 1 cm^3 located 5 cm beneath the sensor. Therefore, it is not suited to taking high resolution measurements near the bed, and measurements within a few centimetres of the water surface are not possible with a downward looking probe.

The ADV probe was fixed to a vertical bar above the flume. Holes were drilled into the bar at 1 cm intervals which enabled accurate vertical positioning of the probe by simply moving it up or down the required number of holes. To obtain a representative average velocity profile, at each measurement position the velocity was recorded for a minimum of 2 minutes to account for the turbulence in the flow. Velocity recordings lasted a minimum of 4 minutes at each position for wave or wave-current profiles.

Due to the limitations of the propeller meters and ADV probes in the small flume, Laser Doppler Velocimetry was also employed in this facility (Figure 4.22). This was not practical in the larger flume for health and safety reasons. LDV works on the same principle as ADV in that it measures the velocity of seeding particles in the water using the Doppler shift principle, except that it emits light waves instead of sound waves. This difference enables the measurement volume to be much smaller than for an ADV system and is of the order of 1 mm^3. The laser is positioned outside of the flume on a traverse so that the measurements are non-intrusive. High-resolution, near-bed measurements can be collected, so it is well suited to producing detailed vertical velocity profiles from which estimates of bed shear stress can be obtained (Appendix 10).

a) 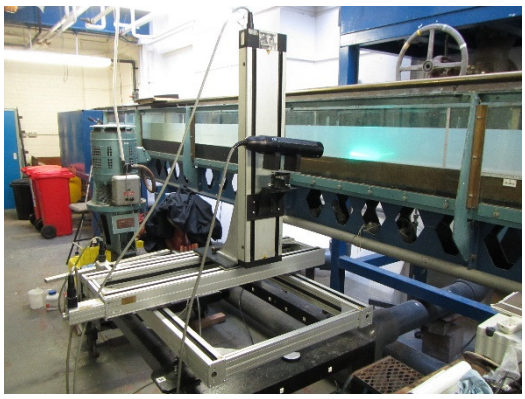 b) 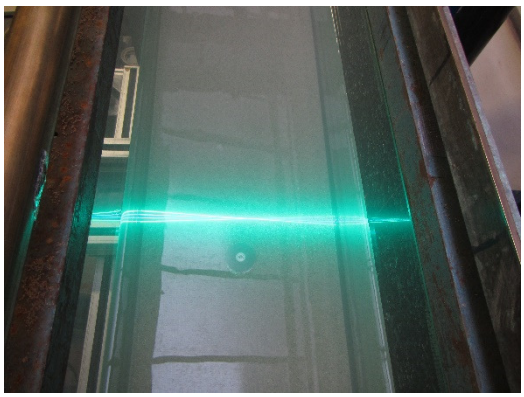

Figure 4.22 a) LDV system set-up at small flume, b) laser positioned to measure streamwise velocity on the flume centreline 5 cm upstream of the pile section over a flat sand bed prior to scour testing.

The techniques described above were used to measure only the ambient or far field flow. However, one experiment (test R.25) was conducted to investigate the flow properties in the vicinity of the pile during scour development. A flow visualisation technique was used to provide qualitative information about the flow processes. Polystyrene balls were added to the water as seeding. A vertical laser light sheet was positioned above the centreline of the flume aligned with the streamwise direction running either side of the pile. A camera was set up on a tripod next to the flume to photograph the reflections from the seeding particles travelling through the laser sheet. The exposure time had to be adjusted on the camera so that the particles were displayed as streaks in the images, providing qualitative insight into the speed and direction of the flow. The lighting had to be carefully managed by covering the outside of the flume with black cardboard sheets to leave a single viewing window at the pile where the camera was situated under a black cloth canopy. While this technique enabled interesting insights to be gained (see Section 6.7.1), over time the polystyrene balls clogged the filters at either end of the flume channel, resulting in an increase in water depth and a reduction in velocity during the test, see Appendix 3 for further discussion. This meant that the technique could not be used to investigate scouring under controlled conditions.

4.6 Water depth measurement

Water depth was measured by attaching a ruler to the external wall of the flume in the central section close to where the pile was situated. In the wave tests the water level was monitored during experiments using a set of resistance-type wave gauges. These were distributed along the flume both upstream and downstream of the pile location (see Figure 4.23), so that the effects of the false bed, sand ripples, scour hole and piles on the waves could be quantified. The probes were placed at set distances from the wave paddles and to each other to enable calculation of the reflection coefficient following the method of Goda and Suzuki (1976).

The wave probes were connected to a data logger so that the voltage signal from each probe was recorded directly to a computer. Prior to starting the waves, the signal was recorded with the probes positioned at a series of known vertical heights relative to the still water level to

provide the information necessary for calibration. The wave probes were held in position on a custom made mounting that enabled vertical position adjustment via a series of holes drilled at 1 cm intervals. Calibration was completed with the wave paddles switched on and powered up so that there would be no change in still water level between the calibration and the experiment. The probes were calibrated at the start of each day of testing because of the sensitivity of the probes to the still water level, water temperature and other parameters that affect electrical conductivity in water. The calibration relationship was linear so that a conversion equation could be easily obtained by plotting the voltage signal against the known water level. The calibration data are given in Appendix 9.

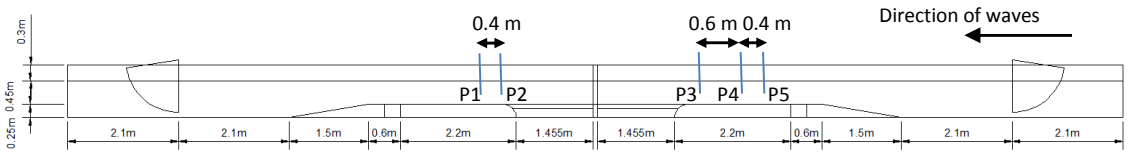

Figure 4.23 Layout of wave probes and wave probe naming convention (P1-P5) (not to scale).

5. Test programme

Following the testing criteria set out in the project aims and objectives (Section 3) the test programme was designed to cover a range of flow conditions for uniform, layered and mixed sand beds. To constrain the problem, two sand sizes were selected which for the purposes of this project were termed 'fine sand' and 'coarse sand' with d_{50} values of 0.2 mm and 0.6 mm respectively. These two sands were used to create a variety of layered and mixed sand bed configurations in the test programme. This enabled a number of interesting results to be obtained which will be presented in the next chapter, so the constraint of using only two sands did not need to be widened within this project.

For the layered sand beds, the majority of tests consisted of a 2-layer configuration with an upper fine sand layer and lower coarse sand layer, as this combination has been seldom investigated in the literature (see Section 2.4). The main variable for these tests was the thickness of the upper layer.

For the mixed sand beds, the fine and coarse sands were combined in a variety of ratios, as the key parameter to be varied, resulting in a range of bimodalities in the mixture, and a range of sediment non-uniformity parameters.

For tests under unidirectional flow, a range of velocities in the clear water regime were tested for each of the uniform, layered and mixed sands. A selection of tests were also repeated in the larger flume to enable assessment of scale effects and check for consistency in the test methodology.

Tidal and wave-current flows were also tested in the large flume for a selection of uniform, layered and mixed sand beds. Reversing flow tests consisted of constant velocity in each direction. Two tests were conducted with a spring-neap tidal cycle (coarse sand and layered bed). This consisted of asymmetric, velocity varying flow but with constant water depth. A set of wave-current tests were conducted in clear water conditions to enable investigation of this less studied regime for wave-current scour. Investigation of the effect of wake patterns on the scour process was incorporated into this test series by conducting one test with $KC_{wc}>10$, one with $KC_{wc}<10$ and one with $KC_{wc}=10$ (following the discussion in Section 2.3.4).

Each test set was designed to enable direct comparison between the standard and novel cases. Therefore, each flow condition consisted of testing in the uniform sands as well as in the mixed and layered sands to determine the differences. In the wave-current cases, tests were also conducted under the wave alone and current alone conditions for this reason. For tests in tidal flow, the velocity was set so as to enable consistent comparison between unidirectional, constant velocity reversing and spring-neap cycle tests.

The core parts of the test programme are described as follows:

- Baseline tests in uniform fine and coarse sands for comparison with literature in unidirectional flow
- Extending these tests to the large flume and to reversing flow, wave, and wave-current flow
- Layered bed tests with fine sand overlying coarse sand with a variety of upper layer depths in unidirectional flow
- Other layered bed configurations: coarse sand overlying fine sand and 3-layer tests in unidirectional flow
- Extending selected layered cases to the larger flume in unidirectional current and reversing, tidal and wave-current flows
- Mixed bed tests consisting of varying proportions of fine and coarse sand in unidirectional flow
- Selected mixed tests extended to the large flume in unidirectional current, reversing and wave-current flows

The programme of tests conducted in the small flume is detailed in Table 5.1, and the main series of tests in the larger flume are presented in Table 5.2. Each test is assigned to a test series, and given an individual test number. These will be used to reference specific groups of tests and individual tests in the following chapters. The parameters for each test are shown and a brief description is included to indicate the motivation for running each test. Comments are noted where additional factors need to be considered when analysing the results of a given test. More extensive descriptions of each test including the results of that test are given in Appendix 3. Also see Appendix 3 for details of further sets of initial and preliminary tests that were run in each flume but were excluded from the main analysis.

Table 5.1 Small flume tests. Note that all of these tests were run under unidirectional current with a water depth of 0.16 m, except test series P-1 which had a water depth of 0.15 m.

Test Series	Description	Test Number	Diameter of pile (mm)	Description of sand bed	Depth-averaged velocity (cm/s)	Notes	Time to eq (h)	Eq depth (S_e/D)	Final time (h)	Final depth (S_f/D)
P-1	Preliminary layered and uniform sand tests	R.1	50	Fine	21.5	Velocity measurement issue – estimated from Figure 7.1. Small amount of ripple development	-	-	15.8	1.68
		R.2	50	Layered: 50 mm fine overlying 50 mm coarse			-	-	12.0	1.34
		R.3	50	Coarse			-	-	14.3	1.32
P-2	2nd set of preliminary layered and uniform sand tests with layers in different orders	R.4	40	Fine	25.3	Ripple development	-	-	13.5	2.03
		R.5	40	Coarse		-	-	-	12.3	1.58
		R.6	40	Layered: 40 mm coarse overlying 60 mm fine		-	-	-	19.4	1.70
		R.7	40	Layered: 40 mm fine overlying 60 mm coarse		Ripple development	-	-	14.4	1.53
D-1	Influence of pile diameter	R.8	50	Coarse		Short duration test	-	-	3.9	1.40
		R.9	25	Coarse		Short duration test	-	-	1.6	1.44

T-1	Layered tests with varying layer depth, mixed tests with varying percentage of fine-coarse sand, and uniform sand tests	R.T.1/ R.T.2	40	Layered: 25 mm fine overlying 75 mm coarse	19.2	Repeated test, see discussion in Section 6.10	-	-	15.0	1.10
		R.T.3	40	Layered: 10 mm fine overlying 90 mm coarse		-	-	-	15.0	1.08
		R.T.4	40	Coarse		-	-	-	12.0	0.93
		R.T.5	40	Layered: 40 mm fine overlying 60 mm coarse		-	14.0	1.18	17.7	1.18
		R.T.6	40	Fine		-	-	-	18.0	1.50
		R.T.7	40	Mixed: 25% coarse, 75% fine		-	-	-	18.0	1.20
		R.T.8/ R.T.11	40	Mixed: 50% coarse, 50% fine		Repeated test, see discussion in Section 6.10	-	-	14.7	1.13
		R.T.9	40	Mixed: 75% coarse, 25% fine		-	11.0	0.75	16.9	0.75
		R.T.10	40	Layered: 55 mm fine overlying 45 mm coarse		-	15.5	1.38	16.5	1.38

R-1	Extension of series T-1	R.10	40	Mixed: 10% coarse, 90% fine	19.2	-	27.3	1.38	29.5	1.38
		R.11	40	Mixed: 90% coarse, 10% fine		-	17.1	0.76	17.2	0.76
		R.12	40	Coarse		Repeated test of R.T.4, see discussion in Section 6.1.3 and 7.2.2	-	-	23.4	0.89
R-2	Investigation of linear trend in 50%-50% mixed sands at different flow velocities and comparison with uniform sand tests	R.13/ R.14	40	Mixed: 50% coarse, 50% fine (offsite blend)	23.9	Start-up issue in test R.13, see Appendix 3	-	-	24.4	1.60
		R.15	40	Mixed: 50% coarse, 50% fine (in house blend)		-	-	-	22.2	1.50
		R.16	40	Coarse		-	21.4	1.40	21.8	1.40
		R.17	40	Fine		-	24.5	1.90	30.3	1.95
		R.18	40	Mixed: 50% coarse, 50% fine	18.3	-	-	-	21.9	1.04

R-3	Additional layered, mixed and uniform sand tests to extend previous results to greater range of flow velocities and bed configurations	R.19	40	Layered: 55 mm fine overlying 45 mm coarse	23.3	-	-	-	24.4	1.69
		R.20	40	Layered: 40 mm fine sand overlying 10 mm coarse sand, overlying 50 mm fine sand		-	-	-	24.4	1.64
		R.21	40	Layered: 40 mm coarse sand overlying 10 mm fine sand, overlying 50 mm coarse sand		-	17.8	1.38	20.5	1.39
		R.22/ R.24	40	Layered: 70mm fine sand overlying 30 mm coarse sand		Sand contamination issue in R.22 see Appendix 3	17.5	1.74	21.0	1.78
		R.23	40	Mixed: 90% coarse, 10% fine		-	21.8	1.41	23.8	1.41
		R.25/26/ R.N.27	40	Coarse		Filter blockage issue, see Appendix 3	26.3	1.47	28.0	1.48
		R.28	40	Dense coarse sand		-	-	-	30.2	1.45
		R.29 (1,2,3,4)	40	Layered: 40 mm fine overlying 60 mm coarse		-	27.3	1.60	28.2	1.61

Table 5.2 Coastal flume tests. Note that the pile diameter is included in the test number (90, 20 or 50 mm and R for rough pile). Water depth = 45 cm for all of the tests.

Test Series	Description	Test number	Flow type	Sands used	Flow parameters	Time to eq (h)	Eq depth (S_e/D)	Final time (h)	Final depth (S_f/D)
C-1	Uniform, mixed and layered tests, under unidirectional, constant velocity reversing and spring-neap flows.	C.90.10	Unidirectional	Coarse	24.1 cm/s	39.3	1.08	52.7	1.11
		C.20.10	Unidirectional	Coarse	22.6 cm/s	21.0	1.40	44.1	1.50
		C.90.11	Unidirectional	Layered: 70 mm fine overlying 180 mm coarse	24.1 cm/s	54.8	1.34	72.8	1.41
		C.20.11	Unidirectional	Fine	22.6 cm/s	25.6	1.90	72.4	2.20
		C.90.12	Reversing	Layered: 70 mm fine overlying 180 mm coarse	Forward: 24.1 cm/s,				
					Reverse: 23.9 cm/s				
		C.20.12	Reversing	Fine	Forward: 22.6 cm/s,				
					Reverse: 21.7 cm/s				
		C.90.13	Unidirectional	Mixed: 50% coarse, 50% fine	24.1 cm/s	56.2	1.31	75.2	1.34
		C.20.13	Unidirectional	Mixed: 50% coarse, 50% fine	22.6 cm/s	21.6	1.45	22.0	1.45
		C.90.14	Reversing	Mixed: 50% coarse, 50% fine	Forward: 24.1 cm/s,				
					Reverse: 23.9 cm/s				

C-1	Uniform, mixed and layered tests, under unidirectional, constant velocity reversing and spring-neap flows.	C.20.14	Reversing	Mixed: 50% coarse, 50% fine	Forward: 22.6 cm/s,				
					Reverse: 21.7 cm/s				
		C.90.15	Unidirectional	Fine	24.1 cm/s	79.7	1.53	79.7	1.53
		C.20.15	Unidirectional	Fine	22.6 cm/s	25.0	1.80	80.7	2.05
		C.90.18	Reversing	Coarse	Forward: 24.1 cm/s,				
					Reverse: 23.9 cm/s				
		C.20.18	Reversing	Coarse	Forward: 22.6 cm/s,				
					Reverse: 21.7 cm/s				
		C.90.19	Spring-neap	Coarse	See Figure 4.8				
		C.20.19	Spring-neap	Coarse	See Figure 4.8				
		C.90.21	Spring-neap	Layered: 70 mm fine overlying 180 mm coarse	See Figure 4.8				
		C.20.21	Spring-neap	Fine	See Figure 4.8				

C-2	Clear water wave-current tests in uniform, mixed and layered sands, and comparison with wave alone and current alone tests. Investigation of scour at KC_{wc} = 10. Check of pile Reynolds number/ roughness effect.	C.50.22	Wave	Coarse	4.7 cm, 2.5 s,	-	-	0.5	0.00
		C.20.22			KC = 11.3				
		C.50.23	Wave	Coarse	4.7 cm, 2.5 s,	-	-	0.5	0.00
		C.20.23			KC = 4.5				
		C.50.24	Current	Coarse	4.5 cm/s	-	-	0.5	0.00
		C.20.24	Current	Coarse	4.2 cm/s	-	-	0.5	0.00
			Current	Coarse	9.2 cm/s	-	-	0.5	0.00
			Current	Coarse	8.4 cm/s	-	-	0.5	0.00
		C.50.25	Current	Coarse	13.5 cm/s	-	-	3.5	0.06
		C.20.25	Current	Coarse	12.7 cm/s	-	-	3.5	0.00
		C.50.26	Wave-current	Coarse	Current: 4.5 cm/s	-	-	4.5	0.08
					Wave: 4.7 cm, 2.5 s, KC_{wc} = 6.8				
		C.20.26	Wave-current	Coarse	Current: 4.2 cm/s	-	-	4.5	0.00
					Wave: 4.7 cm, 2.5 s, KC_{wc} = 16.5				
		C.50.27	Wave-current	Coarse	Current: 9.2 cm/s	-	-	4.5	0.15
					Wave: 4.7 cm, 2.5 s, KC_{wc} = 9.1				

C-2	Clear water wave-current tests in uniform, mixed and layered sands, and comparison with wave alone and current alone tests. Investigation of scour at KC_{wc} = 10. Check of pile Reynolds number/ roughness effect.	C.20.27	Wave-current	Coarse	Current: 8.4 cm/s Wave: 4.7 cm, 2.5 s, KC_{wc} = 21.8	-	-	4.5	0.00
		C.50.28	Wave-current	Coarse	Current: 13.5 cm/s Wave: 4.7 cm, 2.5 s, KC_{wc} = 11.3	30.1	0.50	30.1	0.50
		C.20.28	Wave-current	coarse	Current: 12.7 cm/s Wave: 4.7 cm, 2.5 s, KC_{wc} = 27.1	18.4	0.70	30.1	0.75
		C.50.29	Wave-current	Layered: 30 mm fine overlying 220 mm coarse	Current: 13.5 cm/s Wave: 4.7 cm, 2.5 s, KC_{wc} = 11.3	10.3	0.67	10.8	0.67
		C.20.29	Wave-current	Fine	Current: 12.7 cm/s Wave: 4.7 cm, 2.5 s, KC_{wc} = 27.1	10.6	1.05	10.8	1.05
		C.50.30	Wave-current	Mixed: 50% coarse, 50% fine	Current: 13.5 cm/s Wave: 4.7 cm, 2.5 s, KC_{wc} = 11.3	23.2	0.69	24.4	0.69
		C.20.30	Wave-current	Mixed: 50% coarse, 50% fine	Current: 12.7 cm/s Wave 4.7 cm, 2.5 s, KC_{wc} = 27.1	-	-	24.3	0.95
		C.50.31	Wave-current	Fine	Current: 13.5 cm/s Wave: 4.7 cm, 2.5 s, KC_{wc} = 11.3	41.0	1.29	42.2	1.29
		C.50R.31	Wave-current	Fine	Current: 12.7 cm/s Wave: 4.7 cm, 2.5 s, KC_{wc} = 10.9	32.8	1.06	41.1	1.08
		C.50.32	Current	Fine	24.1 cm/s	-	-	15.2	1.53
		C.50R.32	Current	Fine	22.6 cm/s	-	-	14.6	1.32

6. Results

In this section the main findings from the laboratory tests are presented. The key results will be discussed in greater detail in Section 7 in order to establish the causes and make comparison of the scour behaviours under the different conditions tested. The results section begins by presenting the measurements of time development of scour depth at the pile. The results are subdivided into flow type, starting with the tests in unidirectional current, then moving on to the tests in reversing and tidal flow, before presenting the results from the wave and wave-current tests. In each flow case the results are further divided by sediment type: fine sand, coarse sand, layered sand beds and mixed sand beds. Following the scour depth-time development results, the outcomes from the echosounder and photogrammetry techniques are presented. Finally the laboratory work investigating the sediment parameters and flow properties is detailed. These aspects will be brought together in the discussion section thereby developing an in-depth understanding of the results presented in this section.

6.1 Unidirectional current tests

6.1.1 Uniform sand tests

A set of control tests were conducted under a unidirectional current in uniform sand in order to verify the experimental methodology and measurement techniques through comparison of the results with those available in the literature. These tests were also designed to provide a basis for comparison of tests conducted at later stages of the test programme where the sediment parameters and flow conditions were varied.

The unidirectional current scour tests that were conducted are shown in Figures 6.1-6.4. For ease of visualisation, the results are displayed separately by flume and by sediment type (fine or coarse sand).

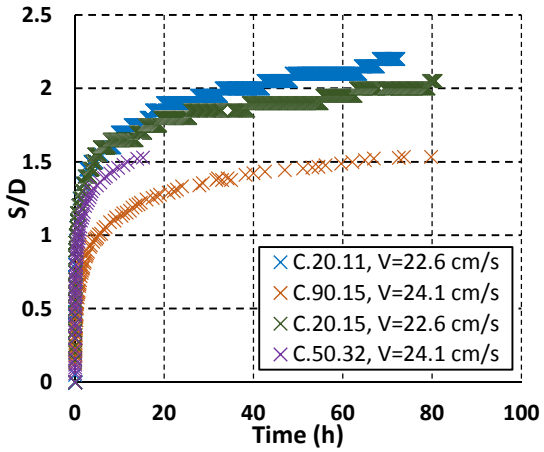

Figure 6.1 Unidirectional current scour tests in the coastal flume in fine sand, with 20, 50 and 90 mm piles.

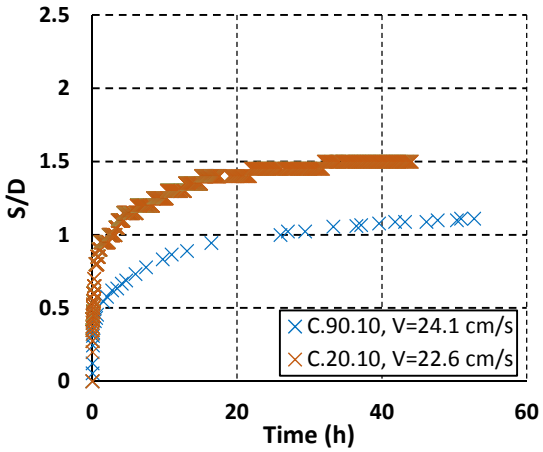

Figure 6.2 Unidirectional current scour tests in the coastal flume in coarse sand, with 20 and 90 mm piles.

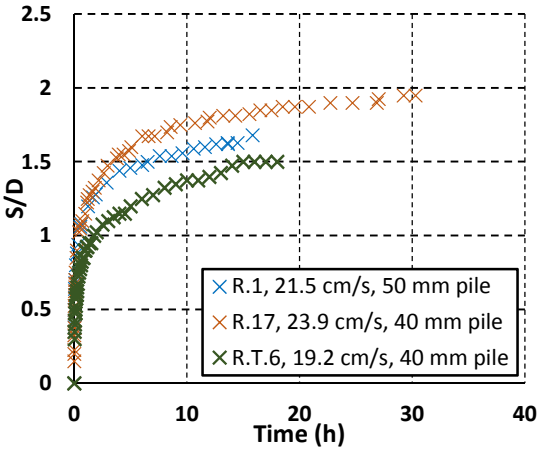

Figure 6.3 Unidirectional current scour tests in the small flume in fine sand.

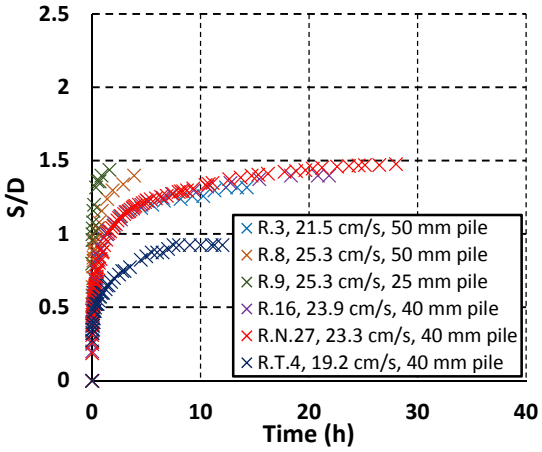

Figure 6.4 Unidirectional current scour tests in the small flume in coarse sand.

The tests shown in Figures 6.1-6.4 follow the expected scour development trend (an increasing function with decreasing gradient) in agreement with the literature, demonstrating in general the success of the test methodology. A more detailed comparison with results from the literature will be given in Section 7.1 of the discussion chapter to ascertain the level of agreement in terms of the relationship with flow intensity and other key variables.

While the general trend (increasing function with decreasing gradient) is similar between the tests, the time scale of the scour process and the maximum scour depth differ considerably between the tests in Figures 6.1-6.4. This is due to the variation between the tests of a range of parameters such as the flow velocity, grain size and pile diameter. The most severe scour case is shown to be a scour depth of 2.2 times the pile diameter. This occurred at the 20 mm pile in the larger of the two flumes. A scour depth of 2 times the pile diameter was approached in the smaller flume at the 40 mm pile. These values are within the range of scour depths reported in the literature (Whitehouse, 1998). In comparison across the tests, the largest scour depths were attained in the fine sand rather than the coarser sand, and the largest scour depths occurred at the highest flow velocities tested, within the clear water regime, following the reported literature results (see Section 2.2). In general the results are in agreement with the expected trends in terms of scaling, pile diameter, sand grain size and velocity. These aspects will be discussed in greater detail including a more quantitative comparison with the literature and standard prediction equations in Sections 7.1 and 7.3 of the discussion chapter.

The quasi-equilibrium scour depth defined for each test is another interesting parameter to consider. Apart from a few tests which were run for a shorter duration due to time constraints (e.g. tests R.8, R.9, C.50.32) the remaining tests were stopped at the earliest once the change in scour depth was less than 0.025 S/D in a 6 hour period, as specified in the methodology Section 4.1.3. The quasi-equilibrium condition for each test is given in Tables 5.1 and 5.2. Where time constraints allowed, tests were run for longer than this criterion and the full length of the tests is also given in Tables 5.1 and 5.2 (and shown in Figures 6.1-6.4). The quasi-equilibrium condition is important when making comparisons between tests, to provide

consistency in terms of a maximum scour depth parameter. It is important to note that at the defined point of quasi-equilibrium, although the curves are considerably flatter, scour depth development has certainly not stopped entirely. Furthermore, for those tests which were continued for a considerable amount of time beyond the point of quasi-equilibrium, the scour depth continued to develop quite substantially. In particular in tests C.20.10, C.20.11 and C.20.15 which were run for the longest duration compared to the timescale of the scour process, the scour depth continued to increase slowly right to the end of the tests. This means that a true equilibrium condition was not reached in any of the tests. A more in depth analysis of the time to equilibrium parameter is given in Section 7.1.9. An evaluation of the stopping criteria in the literature in comparison with the one used for these tests is also included.

6.1.2 Layered sand tests

Following the presentation of the baseline uniform sand tests, the results of the tests in layered sand beds (Section 6.1.2) and mixed sand beds (Section 6.1.3) under unidirectional current are described.

The layered sand tests with fine sand overlying coarse sand in unidirectional flow are plotted in Figures 6.5-6.7. The time development curves follow the expected trend (increasing function with decreasing gradient), and similarly to the uniform sand scour tests the spread in scour depths between the layered tests can be linked to a number of variables including the flow velocity and pile diameter. Unique to these tests is a clear dependency on the depth of the upper layer, with scour depth increasing with upper layer thickness.

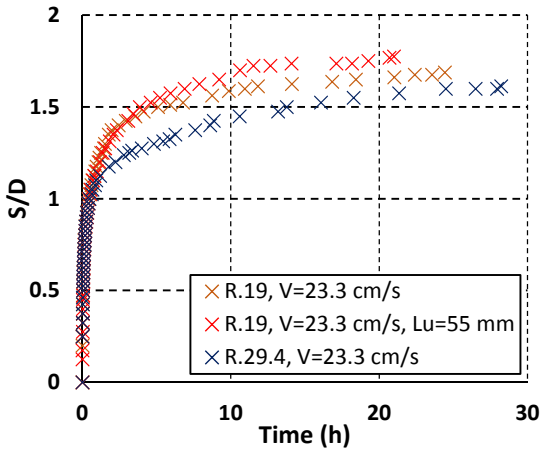

Figure 6.5 Unidirectional current scour tests in the small flume in layered sand beds with fine sand overlying coarse sand, 40 mm pile.

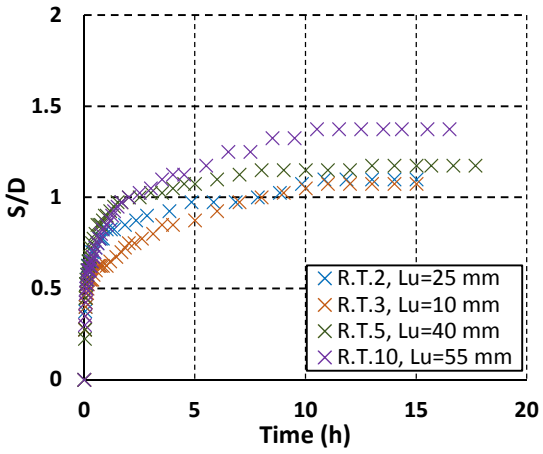

Figure 6.6 Unidirectional current scour tests in the small flume in layered sand beds with fine sand overlying coarse sand, test series T-1, 40 mm pile, V=19.2 cm/s.

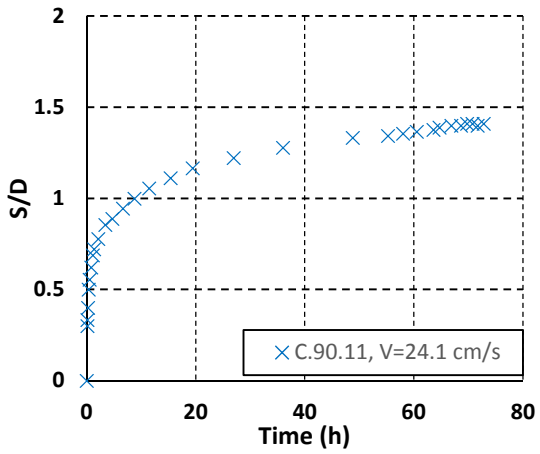

Figure 6.7 Unidirectional current scour test in the coastal flume in a layered sand bed with fine sand overlying coarse sand, 70mm upper layer depth.

The key question to consider for the layered sand tests is whether or not the scour behaviour is equivalent in these tests to the uniform sand tests. In other words, can the appropriate sections of the curves for the uniform fine and coarse sand tests under the same conditions simply be added together to correctly model the layered sand case as has previously been assumed in the literature (see Sections 2.4.5 and 2.6.3). In order to assess this, Figures 6.8-6.11 show each layered case plotted alongside the fine sand and coarse sand tests conducted under the same test conditions. To aid the comparison with the layered beds, in Figures 6.8-6.11 the section of the uniform coarse sand curve starting from the depth of the interface between the layers has been translated so that the start time is equal to the time at which the same depth is reached in the layered case. Close agreement of the translated curve with the layered test would indicate that the scour process is equivalent between the layered and uniform sand tests.

In Figures 6.8-6.11 it can be seen that for each case the uniform fine sand curve and the first part of the layered sand curve, which is at this point scouring through the upper fine sand layer, are in good agreement (i.e. within the measurement uncertainty, see Section 6.10), up to the depth at which the interface between the layers is reached.

In contrast, in Figures 6.8-6.11 the scour development through the lower coarse sand layer in these layered tests does not follow the same scour development curve as it did from the same depth in the uniform coarse sand test. In fact, in the layered tests once the lower coarse sand layer is reached the scour development is appreciably quicker, and leads to a deeper quasi-equilibrium scour depth than in the uniform coarse sand test. This is a new and very significant result as it demonstrates that there is a fundamental change to scour behaviour due to sand layering which has not previously been identified. In the cases shown in Figures 6.8-6.11 this has resulted in a deeper scour depth than one would anticipate from assuming scour depth can be calculated based on the uniform fine and coarse sand test behaviours, hence this approach would lead to non-conservative predictions. This key result will be discussed further in Section 7.2.1 where the reasons for this change in scour development will be explored in relation to interaction effects between the two sands at the grain scale.

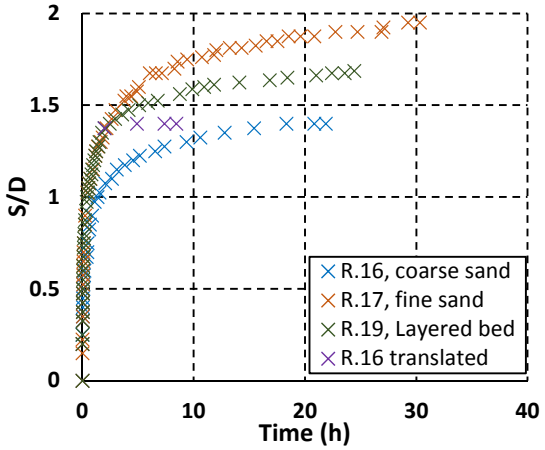

Figure 6.8 Comparison of layered and uniform sand tests under unidirectional current in the small flume, fine over coarse sand layered test with 55 mm upper layer thickness.

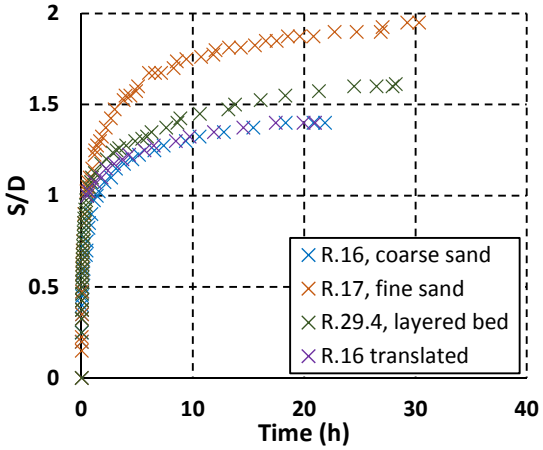

Figure 6.9 Comparison of layered and uniform sand tests under unidirectional current in the small flume, fine over coarse sand layered test with 40 mm upper layer thickness.

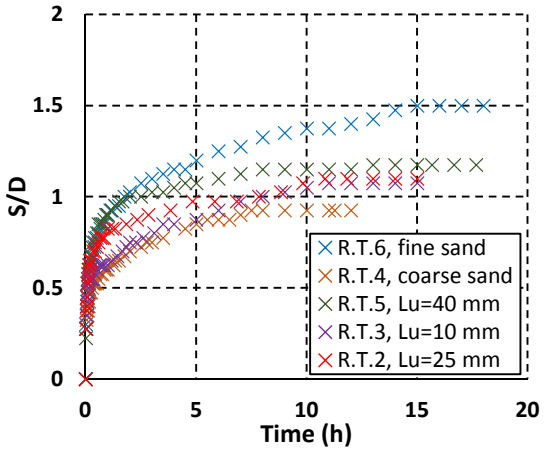

Figure 6.10 Comparison of fine over coarse sand layered bed and uniform sand tests under unidirectional current in the small flume, T-1 test series, 40 mm pile, V=19.2 cm/s.

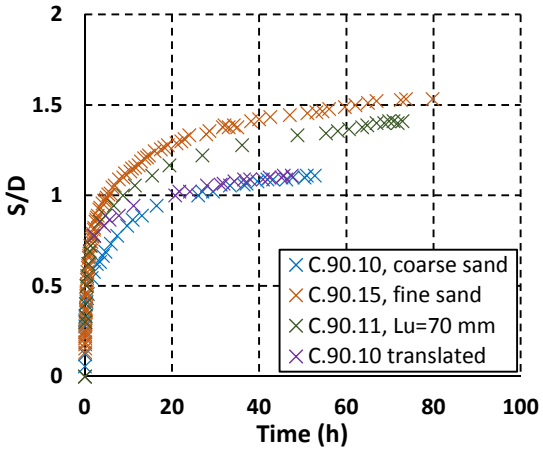

Figure 6.11 Comparison of fine over coarse sand layered bed and uniform sand tests under unidirectional current in the coastal flume, V=24.1 cm/s.

Note that this trend was also observed in the preliminary test series P-1 and P-2 prior to the development of ripples upstream of the scour hole (see Appendix 3).

While the trend of scour depth enhancement in the lower layer of coarse sand has been observed for a range of upper layer depths and flow velocities, not all of the layered beds tested exhibited this trend. Specifically, in the bed configurations with the thickest upper fine sand layers scour did not continue once the interface between the fine and coarse sand layers was

reached. Figures 6.12 and 6.13 show these tests in comparison with the appropriate uniform fine and coarse sand curves.

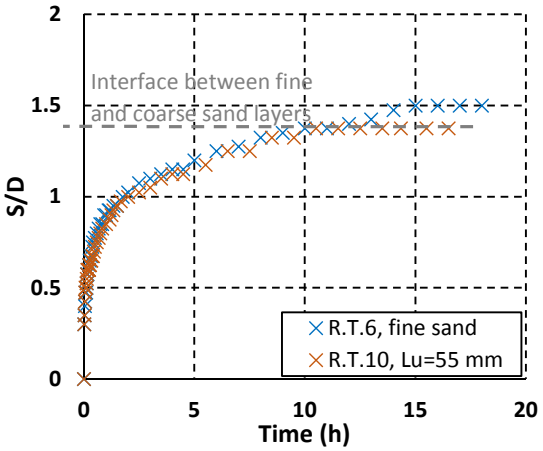

Figure 6.12 Comparison of fine over coarse sand layered bed and uniform sand tests under unidirectional current in small flume with no scour enhancement in the lower coarse sand layer, V=19.2 cm/s, 40 mm pile.

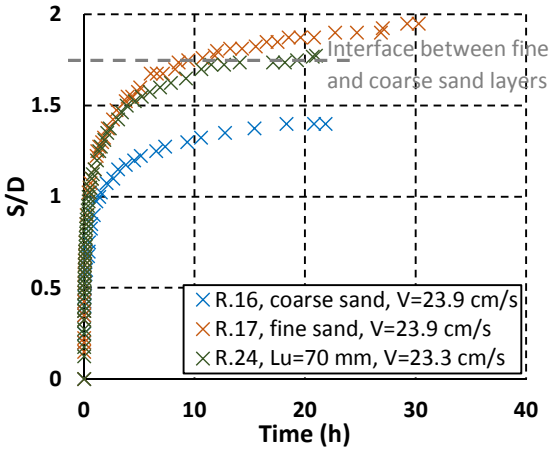

Figure 6.13 Comparison of fine over coarse sand layered bed and uniform sand tests under unidirectional current in small flume with no scour enhancement in the lower coarse sand layer, 40 mm pile.

To describe this relationship between layer depth and scour depth more comprehensively, each of the layered sand tests are plotted together in Figure 6.14, where for each of the tests the quasi-equilibrium scour depth is plotted against the upper layer thickness. Note that both axes are non-dimensionalised by the pile diameter, to enable fairer comparison of the results conducted under different conditions. The quasi-equilibrium scour depths reached in the uniform fine and coarse sands are also plotted in Figure 6.14. The upper layer depth parameter in the uniform coarse sand tests is set equal to zero, and in the uniform fine sand tests the upper layer depth parameter is defined as equal to the equilibrium scour depth. The tests are divided by test series in Figure 6.14, with each set run at a different flow velocity.

Two trend lines are also displayed in Figure 6.14. One marks the equilibrium scour depth reached in the uniform coarse sand case for each set of tests. The other trend line marks the points at which the equilibrium scour depth is equal to the upper layer depth, thus the uniform fine sand tests lie on this line. If the scour development in the layered cases was equivalent to that expected from superposition of the relevant sections of the uniform fine and coarse sand tests, all of the points would fall onto one of these two trend lines. Where the layered cases sit above the first trend line and to the left of the second trend line it means that the scour depth in these tests cannot be modelled simply by superposition of the uniform tests, and in fact enhancement of scour depth in the lower layer of coarse sand has occurred. In Figure 6.14 it can be seen that for the smaller layer thicknesses scour is enhanced in the lower layer of coarse sand, but as the layer depth increases there comes a point at which the quasi-equilibrium depth reached in the layered cases starts to coincide with the second trend line.

This means that the scour depth is now equal to the depth of the interface between the two sand layers and there is no longer any scour in the lower layer. In these cases superposition of the uniform curves would be appropriate. The point at which the relationship between upper layer depth and equilibrium scour depth changes to coincide with the second trend line is likely due to the diminishing strength of the horseshoe vortex with depth, and this will be analysed in greater detail in Section 7.2.1.

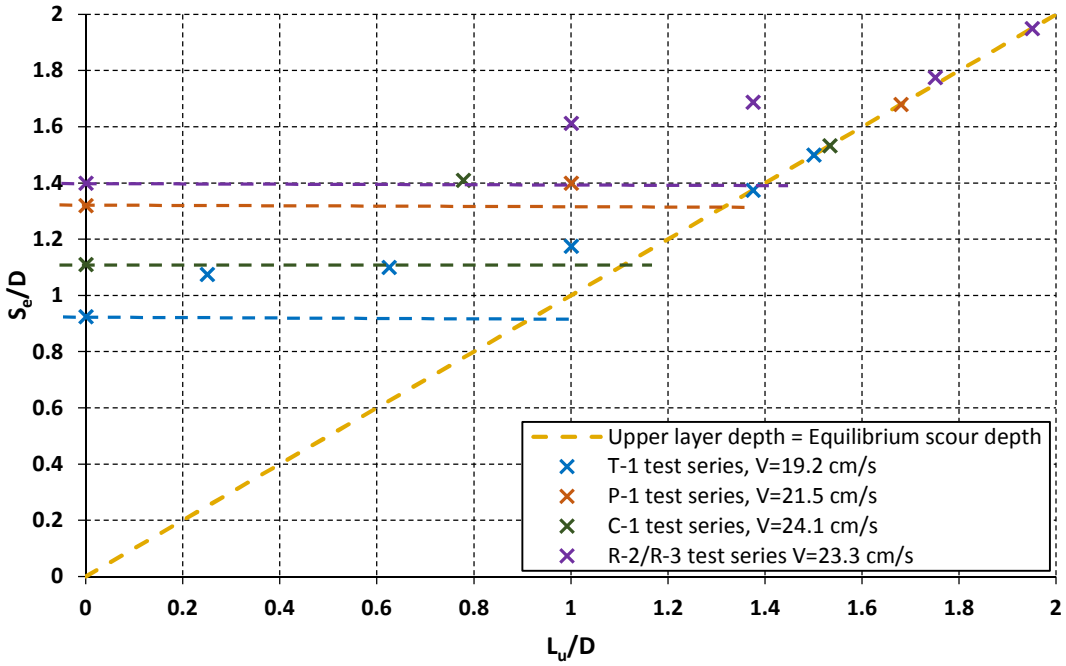

Figure 6.14 Quasi-equilibrium scour depth versus upper layer thickness (L_u) in the layered (fine sand overlying coarse sand) and uniform sand tests under unidirectional current.

In Figure 6.14 the relationship between upper layer thickness and scour depth is similar in the four test series conducted at different flow velocities. This demonstrates that the new findings are repeatable, and valid for a range of flow conditions within the clear water regime. While qualitatively the trends are in good agreement, quantitatively there is some variation in the amount of scour enhancement that occurred in the lower sand layer. For example in test series C-1 the scour depth in the layered test is somewhat larger compared to the uniform coarse sand test than it is in similar layered sand tests at the other flow velocities. The C-1 test series was run in the larger flume and so the differences in other parameters such as water depth and the change of scale need to be considered to understand this difference (see Section 7.1). A more quantitative understanding of the scour behaviour in these layered tests will be developed in the form of a prediction methodology in Section 7.3.

The majority of the layered beds that were tested consisted of a fine sand layer overlying a layer of coarse sand, as has been discussed above. However, three tests were conducted with alternative configurations and these results will now be presented.

For one test (R.6) the sand bed consisted of a layer of coarse sand overlying a fine sand layer so that the layer configuration was reversed compared to that in the tests described above. This layered sand test is shown in Figure 6.15 along with the uniform fine and coarse sand tests under the same flow conditions. Note that this test was conducted as part of the preliminary test series (P-2) and the fine sand test used in the comparison was affected by ripples in the later stages of the test, which explains the reduction and subsequent increase in scour depth in the 2nd half of the curve. As was discussed in Section 4.1 the effects of ripples were removed in the main test series.

It is clear in Figure 6.15 that the scour development through the upper layer, which in this test is the coarse sand, closely matches that in the uniform coarse sand case, demonstrating that the lower sand layer does not influence scour behaviour in the upper layer of a layered bed, in agreement with the findings for the layered tests with fine sand overlying coarse sand.

Interestingly, the opposite result to the layered cases with a lower layer of coarse sand is shown for scour development through the fine sand lower layer of the layered test in Figure 6.15. In the lower layer of fine sand, the scour development is slower and the quasi-equilibrium depth is smaller compared to scour in the uniform fine sand test. Therefore, prediction methods based on the uniform fine and coarse sand scour curves would result in over-conservative predictions in this case. This result is in agreement with the literature for bed armouring (see Section 2.4.4).

The scour depth in the lower fine sand layer actually closely matches the continuing coarse sand curve at this depth. As only one test with this layer configuration was conducted, further investigation would be needed to ascertain if this is a significant result that is applicable to a range of conditions or if it is specific to the particular flow velocity and layer depth chosen for this test.

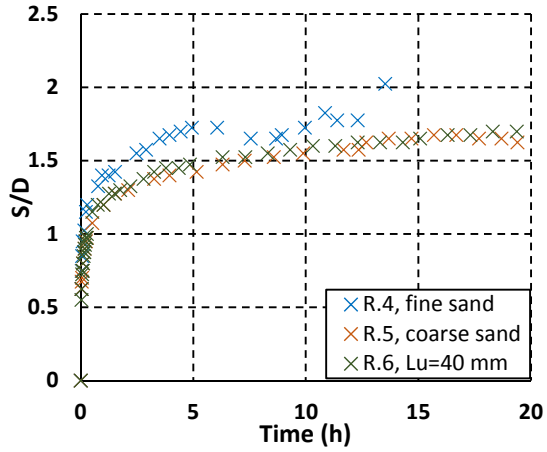

Figure 6.15 Comparison of scour development in uniform fine and coarse sands with a layered bed of coarse sand overlying fine sand under unidirectional current in the small flume, V=25.3 cm/s, 40mm pile.

Two further layered bed configurations were tested. In these cases the number of layers was increased to three. The first case consisted of an upper layer of fine sand, a thin (10 mm) middle layer of coarse sand, and a lower layer of fine sand. In the second case the order of the layers was reversed so that the upper and lower layers were made up of the coarse sand with the middle layer being fine sand. These tests are plotted along with the uniform fine and coarse sand tests in Figure 6.16.

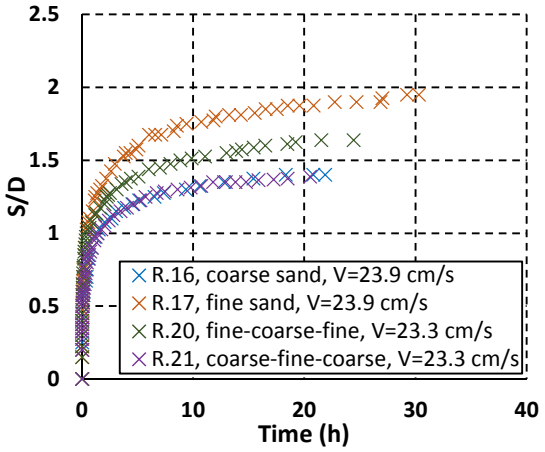

Figure 6.16 Layered beds with three sand layers, 40-10-50 mm thick, plotted alongside the uniform fine and coarse sand tests under unidirectional current in the small flume, with 40 mm pile.

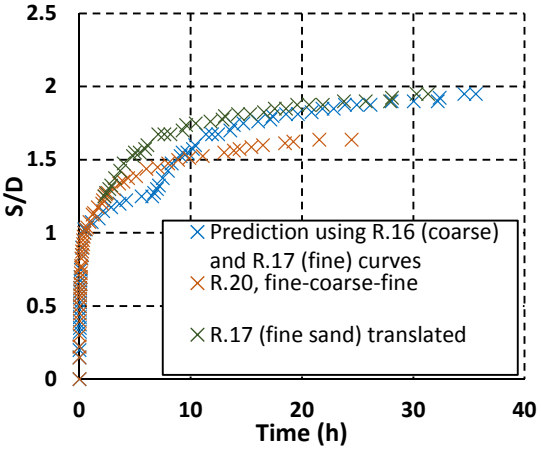

Figure 6.17 Comparison of fine-coarse-fine sand layered test with superposed fine and coarse sand curves for the relevant layers (under unidirectional current in the small flume).

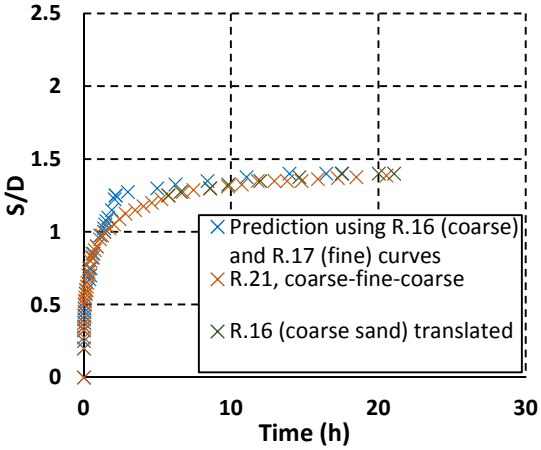

Figure 6.18 Comparison of coarse-fine-coarse sand layered test with superposed fine and coarse sand curves for the relevant layers (under unidirectional current in the small flume).

From Figure 6.16 it can be seen that there is very close agreement between the uniform coarse sand test and the layered coarse-fine-coarse sand test, indicating that the thin middle layer of fine sand has had little influence on the scour time development. However, the fine-coarse-fine

layered test curve lies in-between the uniform fine and coarse sand test curves demonstrating that in this case the thin middle layer of coarse sand has had a significant effect on the scour development.

In order to better understand the scour behaviour in these tests, the two 3-layered tests are plotted separately in Figures 6.17 and 6.18. In each of these figures the predicted trend based on the uniform coarse and fine sand test curves for scour through each layer of the 3-layered sand tests is shown. This makes it clear that similarly to the layered sand tests with two layers the scour does not follow the trend derived from the uniform tests.

In Figure 6.17 the fine-coarse-fine sand layered test is in close agreement with the uniform fine sand test in the upper layer. Once scour reaches the second layer, the scour progress is considerably quicker than in the uniform coarse sand test at that depth. When scour reaches the 3rd layer it slows down in comparison to the scour development at the same depth in the uniform fine sand test. Note that the uniform fine sand curve has been translated in Figure 6.17 to help make the comparison of scour in the lower layer clearer, in a similar manner to the approach in Figures 6.8-6.11 for the 2-layered tests. Therefore, the scour behaviour in all three layers for this 3-layered test is consistent with the trends found for the two-layered tests. A layer of fine sand overlying coarse sand results in an increase in scouring in the coarse sand layer, while a layer of coarse sand overlying fine sand results in a decrease in scour compared to the uniform case.

Figure 6.17 shows the coarse-fine-coarse sand layered test in comparison with the superimposed uniform fine and coarse sand curves. As with the other layered tests discussed there is no difference between scour development in the uppermost layer (coarse sand) of the layered test and that in the uniform coarse sand test. In the second layer (fine sand), scour is much slower than in the uniform fine sand test in agreement with the previous findings. A different result is found for the third layer (coarse sand), as there is no increase in the scour rate compared to the uniform coarse sand test at this depth. Instead the scour development in this layer is in close agreement with that in the uniform coarse sand test. This is probably due to bed armouring induced by the uppermost coarse sand layer and this will be discussed further in Section 7.2.1.

6.1.3 Mixed sand tests

This section presents the results from scour testing in mixed sand beds under unidirectional current. The mixed sand tests from the small and large flumes are shown in Figures 6.19-6.21. A key result is observed when considering the scour time development in these tests. While some of the tests in both flumes do follow the expected scour development trend, there are a number of tests which demonstrate a departure from this shape of curve. This is most noticeable in tests R.T.8 and R.T.11 (Figure 6.20) and R.18 (Figure 6.19), all of which are 50% fine - 50% coarse sand mixtures. After an initial section which closely follows an exponential function, a linear trend then prevails for a substantial portion of these tests, before the curves flatten off as equilibrium scour depth is approached. Interestingly, this trend does not occur in all

of the 50%-50% mixed sand tests. Tests R.T.8, R.T.11 and R.18, were run at fairly low flow velocities, but the 50%-50% mixed bed tests run at higher flow velocities (tests C.90.13, C.20.13, R.14, R.15) exhibited only the standard scour development trend (decreasing gradient as scour depth increases). Therefore, the unusual linear scour development trend appears to be connected to the flow velocity (or flow intensity) and hence is likely to be related to the magnitude of the bed shear stress.

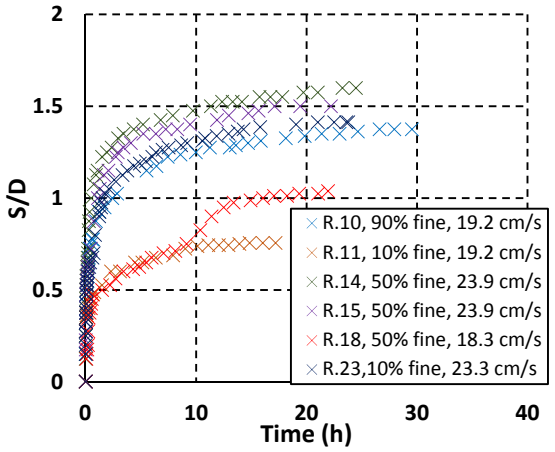

Figure 6.19 Unidirectional current scour tests in the small flume in fine-coarse mixed sand beds, with 40 mm pile.

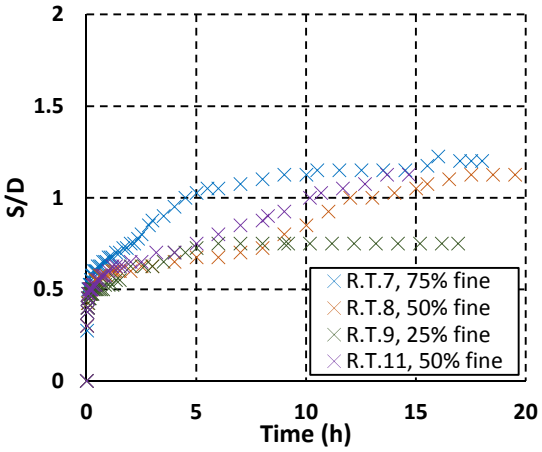

Figure 6.20 Unidirectional current scour tests in the small flume in fine-coarse mixed sand beds, test series T-1, 40mm pile, 19.2 cm/s.

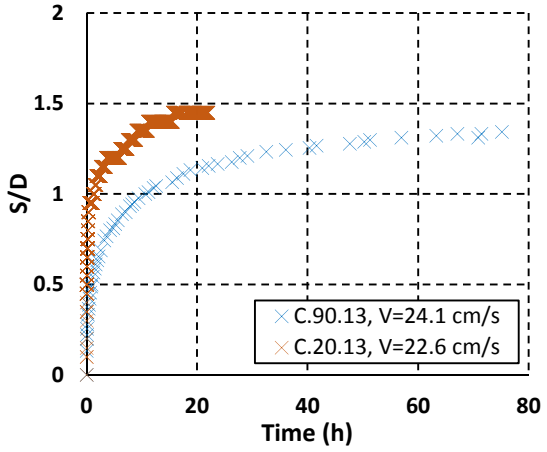

Figure 6.21 Unidirectional current scour tests in the coastal flume in 50%-50% fine-coarse sand mixed beds, 90 and 20 mm piles.

The 3-part scour development trend consisting of curved, linear, and equilibrium sections is also present but to a lesser extent in tests R.T.7 and R.T.9. These tests were also conducted at a lower flow velocity, but the proportion of the fine and coarse sands in the sediment bed differed

(75%-25% and 25%-75% fine-coarse sand respectively). In these tests the section of the curve that fits a linear trend lasts for a shorter duration. For the tests with the very lowest and highest percentages of fine sand in the mixture i.e. 10% and 90% fine sand, tests R.11 and R.14, and indeed in the uniform sand tests the trend follows the usual exponential expression under the same flow conditions. This implies that the 3-part trend is dependent on the proportion of fine to coarse sand in the mixture. As the grain size distribution varies so will the resistance to erosion due to changes in bed structure and interaction effects between the grains. The ratio of horseshoe vortex strength to the sand's resistance to erosion may also be important in terms of the dependence of the linear trend on flow velocity (see Section 7.2.2 for further discussion of these points).

It should be noted that test R.18 was used to verify the results from the R.T test series. R.18 was run in a different test programme at a slightly lower flow velocity than that used in the R.T series, and so the fact that the same trend was found is strongly indicative that this unusual change to the scour development curve is a repeatable and significant result.

The scour development curves in Figures 6.19-6.21 show that in general scour depth increases with increasing proportion of fine sand compared to coarse sand within the mixture and also that the scour depth in the mixed sand tests increases with flow velocity. To study this aspect in greater detail the quasi-equilibrium scour depth for each test is plotted against the proportion of fine sand in the mixture in Figure 6.22. The uniform fine and coarse sand tests are included in Figure 6.22 with the uniform coarse sand plotted at 0% on the x-axis and the uniform fine sand marked at 100% on the x-axis. There are four sets of tests in Figure 6.22 distinguished by the flow velocity. Figure 6.22 demonstrates in general the trend of increasing scour depth with increasing proportion of fine sand, and increasing scour depth with flow velocity. However, there are two notable exceptions to this.

Firstly the similarity of two of the test sets despite different flow velocities is likely to be explained by the change in scale between these tests (i.e. they were conducted in different flumes).

Secondly it is clear in Figure 6.22 that two of the mixed sand tests (R.11 and R.T.9), consisting of a low proportion of fine sand compared to coarse sand, actually resulted in a smaller quasi-equilibrium scour depth than in the uniform coarse sand test. This unexpected result was first found in test R.T.9. A further mixed sand test was conducted with similar results, R.11. A repeat run of the coarse sand test was also conducted, test R.12, to check for consistency across the test programme. The two coarse sand tests and the two mixed sand cases are plotted together in Figure 6.23.

It is clear in Figure 6.23 that there is poor agreement between the two uniform coarse sand tests. This discrepancy is substantially greater than the level of uncertainty found in the majority of the test programme (see Section 6.10). The scour development is unusual in test R.12 as there is a sharp increase in scour depth towards the end of the test, which brings the final scour depth in this test close to that in the original coarse sand test R.T.4. The final scour depths in

tests R.12 and R.T.4 are within 0.05 S/D, which is well within the expected measurement uncertainty discussed in Section 6.10. However, prior to the sudden increase in scour depth the scour development in test R.12 is significantly reduced compared to that in test R.T.4.

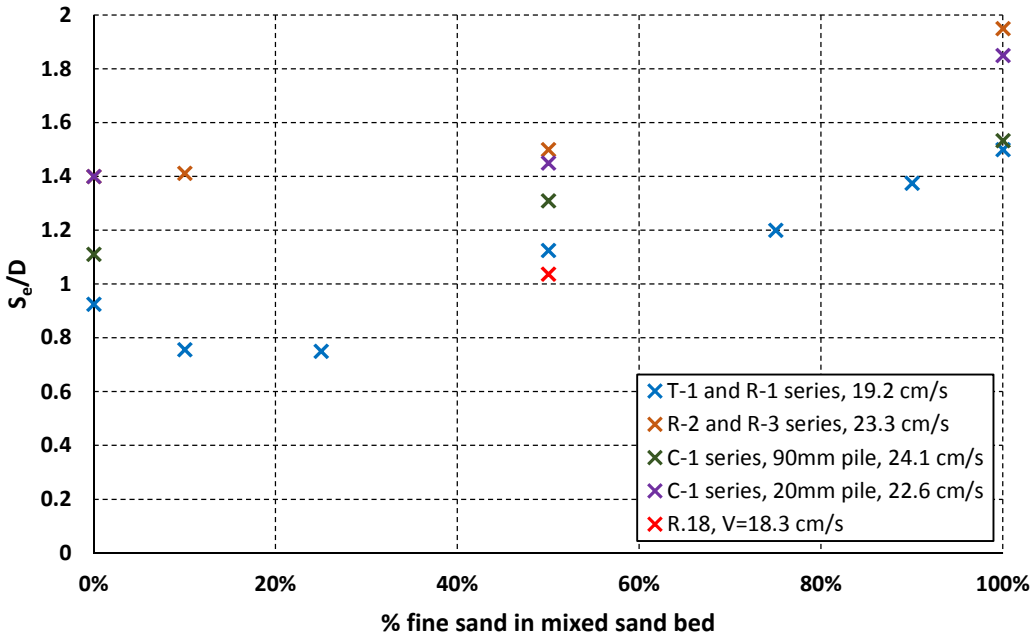

Figure 6.22 Quasi-equilibrium scour depth plotted against percentage of fine sand in the fine-coarse mixed beds under unidirectional current, with uniform coarse and fine sands plotted at 0% and 100% respectively.

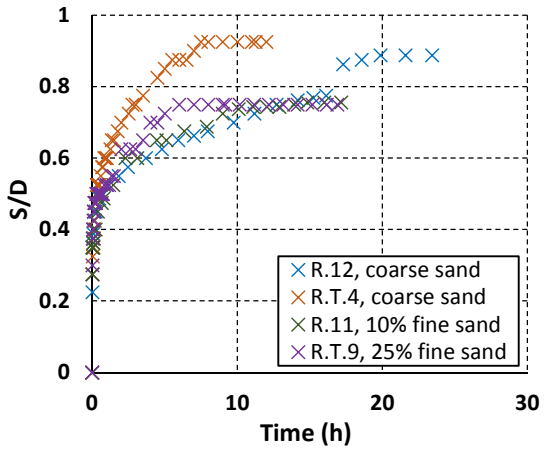

Figure 6.23 Comparison of repeated coarse sand tests and scour in mixed beds with low proportion of fine sand compared to coarse sand (unidirectional current, small flume), V=19.2 cm/s.

The two mixed sand cases, tests R.T.9 and R.11, contain different proportions of fine sand, yet follow similar curves and reach very similar end scour depths in Figure 6.23. Furthermore this end scour depth closely matches the R.12 curve prior to the sudden increase in scour depth. The curve for test R.11 is also in very close agreement with test R.12 from the start of the test up to the sudden increase in scour depth. As the sand bed in test R.11 consisted of 90% coarse sand, intuitively it follows that the scour curve in this mixture would be similar to that in the uniform coarse sand. This makes it difficult to ascertain from this comparison if the scour depth in the mixed sand tests is truly reduced compared to scour in a uniform bed of the coarse sand.

To improve understanding of the scour behaviour in these mixed sands, a 90% coarse sand test (R.23) was run at a higher flow velocity. Figure 6.24 shows the scour development in this mixed sand test compared to the uniform coarse sand test conducted in the same flow conditions. As can be seen in Figure 6.24 there is close agreement between the 90%-10% coarse-fine mixed sand test and the uniform coarse sand test. This indicates that the addition of 10% fine sand to the coarse sand has had negligible effect on scour behaviour compared to that in the uniform coarse sand, in contrast with the results at the lower flow velocity which indicated that the mixtures with a small percentage of fine sand may result in a smaller scour depth than in the uniform coarse sand. However, it is possible that different scour behaviours could occur at different flow velocities, in a similar manner to the scour time development curves switching between linear and exponential expressions.

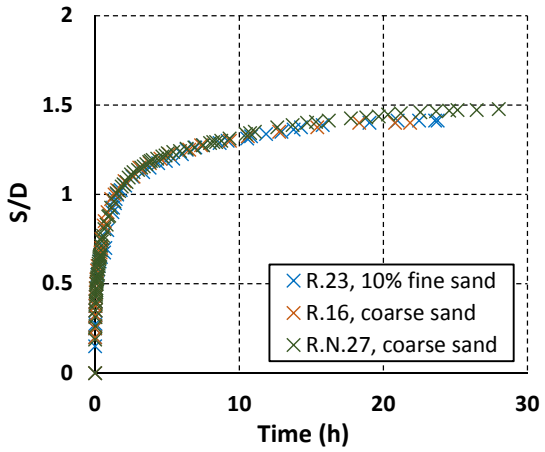

Figure 6.24 Comparison of scour development in uniform coarse sand and a mixed bed with low percentage fine sand (10%), at higher flow velocity (V=23.3 cm/s).

Careful consideration of the reasons for the differences in the scour curves in the two coarse sand tests in Figure 6.23 is required before firm conclusions can be drawn about whether scour depth in these mixed sands is smaller or about the same as the scour depth in a uniform bed of the coarse sand. This is accomplished in Section 7.2.2 where a wider range of results including measurements of the sediment properties presented in Section 6.8 are used to shed light on

this issue. The possibility for errors to have occurred in the experimental procedure are assessed and an alternative explanation is formulated; that potentially the scour behaviour is more variable at lower flow velocities due to instabilities in the flow-seabed interactions due to the lengthening of the initial stages of horseshoe vortex development.

While some of the findings from the mixed tests require further analysis and clarification, what is clear is that the make-up of the mixed sediment bed has had a significant influence on scour depth development in terms of the trend produced and the final scour depth reached. The reasons for these results are discussed in greater detail in Section 7.2.2, where links between the sediment properties and the scour behaviour are considered. The scour development in these types of sand mixtures is also compared with scour data in non-uniform sediments presented in the literature to assess the influence of the bimodal distribution of these mixed sands on scour behaviour.

6.1.4 Dense sand test

One test, R.28, was conducted in order to investigate the effect of sediment bulk density on scour depth in unidirectional current. A concrete poker was used to increase the density of the sand in the flume, as discussed in Section 4.1.1 of the methodology. The dense sand test in comparison with a standard coarse sand test is shown in Figure 6.25. The scour depth is a little smaller as scour progresses in the dense bed, but the results are for the most part within the measurement uncertainty (see Section 6.10). This shows that the difference in scour depth is at most, small for this change in density (see Section 6.8.1 for measurements of the sand density in this test).

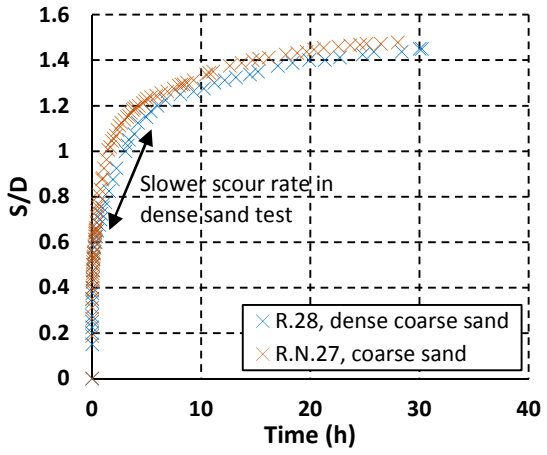

Figure 6.25 Comparison of scour in uniform coarse sand bed and dense coarse sand bed, under unidirectional current in the small flume, V=23.3 cm/s

One section of the curve does show a difference between the tests of greater than the measurement uncertainty. In this section, marked on the graph, the maximum difference between the curves is approximately 0.175 S/D, which is outside the expected measurement uncertainty of 0.1 S/D although not by a huge margin. This may be indicative of a lengthening of

the scour timescale which would account for the closer agreement between the curves in the later stage of the test.

Further tests would be needed to verify this result and to explore the relationship between scour depth and bulk density, especially by extending the work to even denser sand beds where the effects may be more apparent.

The lack of sensitivity of scour depth to this change in density and the different methodology used for preparing the sand bed in this test compared to the other tests indicates that for a given uniform sand it is unlikely that the method of preparing the sand bed is having much of an impact on the tests, at least at this small scale in the laboratory. This gives confidence in the standard methodology used in this project for preparing the test beds.

6.2 Tidal current tests (all sediment types)

In order to develop a more thorough understanding of scour in complex sediments, it is important to consider a range of flow cases, including tidal flows and waves as would be more representative of the marine environment in which offshore wind turbines are situated. However, as discussed in Section 2.3.2 knowledge is limited in these conditions even for scour in uniform sands.

A simple approximation of a tidal flow is obtained by periodically reversing the direction of a flow with constant depth-averaged velocity (square wave signal). This has the advantage of introducing only one additional variable, the flow direction, so that all other parameters can be identical to those in the unidirectional current case. A set of these tests were conducted in the larger flume, where it was more practical to reverse the flow direction, for four bed configurations: uniform coarse sand, uniform fine sand, 50%-50% mixed sand, and a layered bed with fine sand overlying coarse sand.

These tests are shown in Figures 6.26-6.29. The scour development curves are plotted in a different colour in each flow direction to distinguish between the ‘flood’ and ‘ebb’ half cycles, with the initial flow direction defined as the flood flow for each test. The scour depth was measured at the upstream face of the pile for each flow direction (i.e. the measurements switch sides after each flow reversal).

The typical exponential expression used to model scour development is in reasonable agreement with the curves in Figures 6.26-6.28 for the large pile. In contrast, for the tests at the small pile there is a significant discrepancy in scour depth between the flood and ebb directions which is not present to such an extent in the larger pile tests. This makes it difficult to fit an exponential expression to the small pile tests. In test C.20.14 the difference in scour depth under the flood and ebb flows reduces as the test continues, however this is not the case in test C.20.18 where a large difference persists throughout the test. It is also interesting that where there is a discrepancy between scour depth in the flood and ebb directions in the small pile tests it is the scour depth in the ebb direction that is consistently the smaller of the two. In contrast, in the tests at the larger pile, the scour depth is consistently slightly deeper in the ebb flows

compared to in the floods. It is shown in Section 7.2.3 that these differences are linked to a small variation in the velocity profiles in the cross-stream direction and between the flood and ebb directions at the far side of the flume at the small pile resulting in asymmetry in the flow (the velocity measurements are presented in Section 6.7).

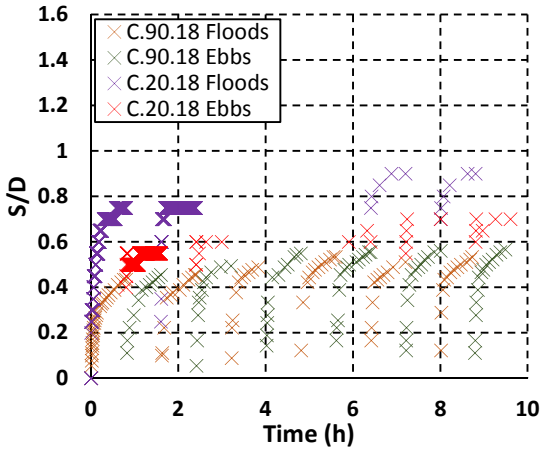

Figure 6.26 Scour development under square wave reversing flow in uniform coarse sand, 90 and 20 mm piles.

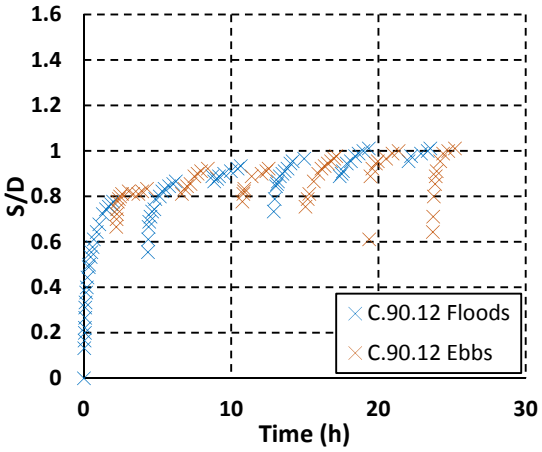

Figure 6.27 Scour development under square wave reversing flow in a layered bed with fine sand overlying coarse sand, L_u=70mm, 90 mm pile.

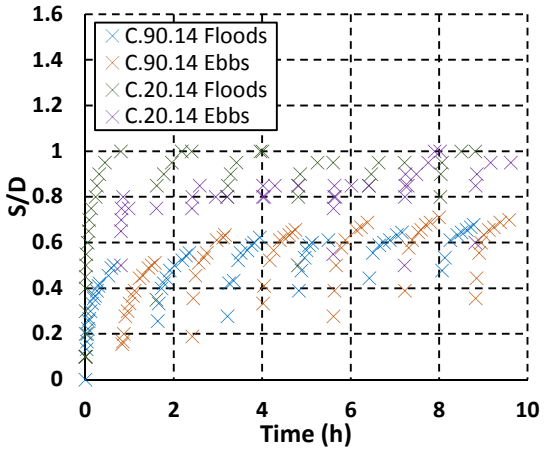

Figure 6.28 Scour development under square wave reversing flow in 50% fine, 50% coarse mixed sand bed, 90 and 20 mm piles.

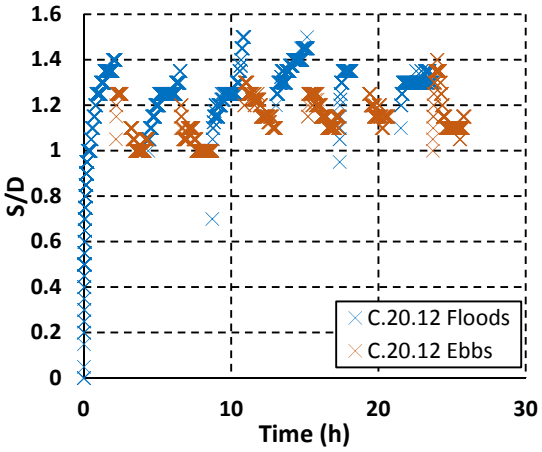

Figure 6.29 Scour development under square wave reversing flow in uniform fine sand, 20 mm pile.

For the small pile tests the scour depth stabilises more quickly than for the larger pile tests. In tests C.20.14 and C.20.12 at the small pile the scour depth does not keep increasing in the later cycles, but either reaches the same maximum in subsequent cycles, or there is a reduction in scour depth in later cycles (test C.20.12) implying that an equilibrium condition has been reached. This could also be argued for test C.20.18 although this is less clear as there is some missing data due to equipment failure between hours 3 and 6.

For all three tests at the larger pile, the scour depth is still increasing after 6 cycles, at least in one of the flow directions. This demonstrates that for these cases at the larger pile equilibrium has not been reached after 6 cycles. This is a key result as it is contrary to many results in the literature where equilibrium is reportedly reached after only a few cycles (see Section 2.3.2). This is probably linked to other studies allowing ripples to influence the tests, which is discussed further in Section 7.2.3. The difference in time to equilibrium between the small and larger pile tests is explained in terms of the ratio between the tidal cycle length and the scour timescale in Section 7.2.3.

In the layered test in Figure 6.27 a longer cycle time was used to ensure that scour would reach the depth of the lower layer prior to the flow reversing. This also enabled investigation of the effect of cycle length on the results, in conjunction with the tests from the small pile (see Section 7.2.3). Flow was reversed every 130 minutes rather than every 48 minutes. Similarly to the other reversing flow tests an equilibrium condition has not been reached after 6 cycles.

Although in general the tests at the larger pile follow the expected scour development trend (scour depth increases but the curve flattens with time), it can be seen when examining the scour development curves in more detail that there is a degree of inconsistency as to how much the scour depth increases between each half cycle. In fact, the scour depth does not necessarily increase between each adjacent half cycle, and in quite a few cases the scour depth actually decreases. However, between each whole cycle, in almost all cases in the large pile tests the scour depth increases.

Within half cycles, in most of the tests in Figures 6.26-6.29 the scour depth remains level or increases; there is no sign of infilling occurring which would be shown by a decrease in scour depth. However, in Figure 6.29 the scour behaviour in the fine sand test at the small pile is quite different to the other reversing flow cases in that the scour depth fluctuates within half cycles. This indicates infilling has occurred in this test. Because this test was run in conjunction with a test at the larger pile it was not possible to smooth out all of the ripples in close proximity to the small pile because the smoothing device could not be brought closer than the edges of the larger pile scour hole which extended beyond that of the small pile. Consequently a portion of the downstream dunes and ripples near the small pile remained in place when the flow was reversed. This has had a significant impact on scour development so that the graph does not display the same trend, and instead infilling occurs. While this practical constraint applied to the other small pile tests, the effect is most significant in the test with the fine sand as this sediment is more mobile. This result is useful as it enables comparison of tests with and without ripples, and indicates that ripples act to decrease the time to equilibrium (see Section 7.2.3 for further discussion).

The effect of the bed layering on scour development is difficult to determine because the test has not reached equilibrium. The coarse sand in the layered test has been scoured to a greater extent than in the uniform coarse sand test. However, it is possible that this is due to a difference in the time development of scour between these tests rather than necessarily signifying an increase in the final equilibrium scour depth that would be attained.

The effect of flow reversal on equilibrium scour depth was investigated in preliminary test C.90.1 in the larger flume. The flow was reversed for the first time at the end of the test i.e. once a quasi-equilibrium condition had been reached under unidirectional flow conditions. The scour depth continued to increase when the flow was reversed at this point into the test (shown in Appendix 3). This may indicate that a flow reversal acts to increase scour depth regardless of the point in time at which it occurs (see further discussion in Section 7.2.3).

6.2.1 Spring-neap tidal tests

While the simple reversing flow tests showed interesting results, the simplicity of this type of test in terms of modelling scour in tidal flow needed to be considered. It was decided to extend this work to investigate scour development under a more realistic tidal flow, with variation in velocity during each cycle, as well as variation in the velocity signal between cycles in the form of a typical semi-diurnal, spring-neap tide. The processing of a suitable signal is discussed in Section 4.2.5 of the methodology.

Two spring-neap tests were conducted in the large flume where flow could be more easily controlled than in the smaller flume. One test was conducted in the coarse sand, and the other in a layered bed, with an upper fine sand layer depth of 70 mm. Due to the extensive duration of these tests it was not possible to also conduct mixed sand tests. The fine sand was tested at the small pile during the layered test at the larger pile.

The scour development in the small and large pile coarse sand tests is plotted in Figure 6.30. The scour development in the layered bed test is plotted in Figure 6.31 and that of the fine sand test in Figure 6.32. Note that the measurement points in each half cycle have been connected up in the figures to indicate the direction of development of scour through each flood and ebb half cycle.

It is immediately clear in these graphs that the standard exponential expression for scour development is not a suitable fit to these tests. There is a significant difference between the flood and ebb scour depths and the shape of the scour development curve varies substantially at different stages within the spring-neap cycle.

First to consider are the two large pile tests. In both the coarse sand and layered sand tests at this pile it is clear that an equilibrium condition has not been reached at the end of the 28 cycle test. In fact there is a significant increase in the scour depth during the last few cycles of both tests. This is a very important result as it demonstrates that the time to equilibrium can be longer than 1 spring-neap cycle, which is contrary to the literature where it is suggested that scour reaches an equilibrium condition in tidal flow after only a few cycles (see Section 2.3.2). In terms of the two small pile tests, the scour depth at the end of each of these tests is less than the scour depth reached near the beginning of the tests. This indicates that an equilibrium condition may have been reached in the small pile tests. A similar difference in the time to equilibrium at the two pile diameters was also noted in the reversing current tests and as mentioned previously this is linked to the relationship between the scour timescale and the tidal cycle duration in Section 7.2.3.

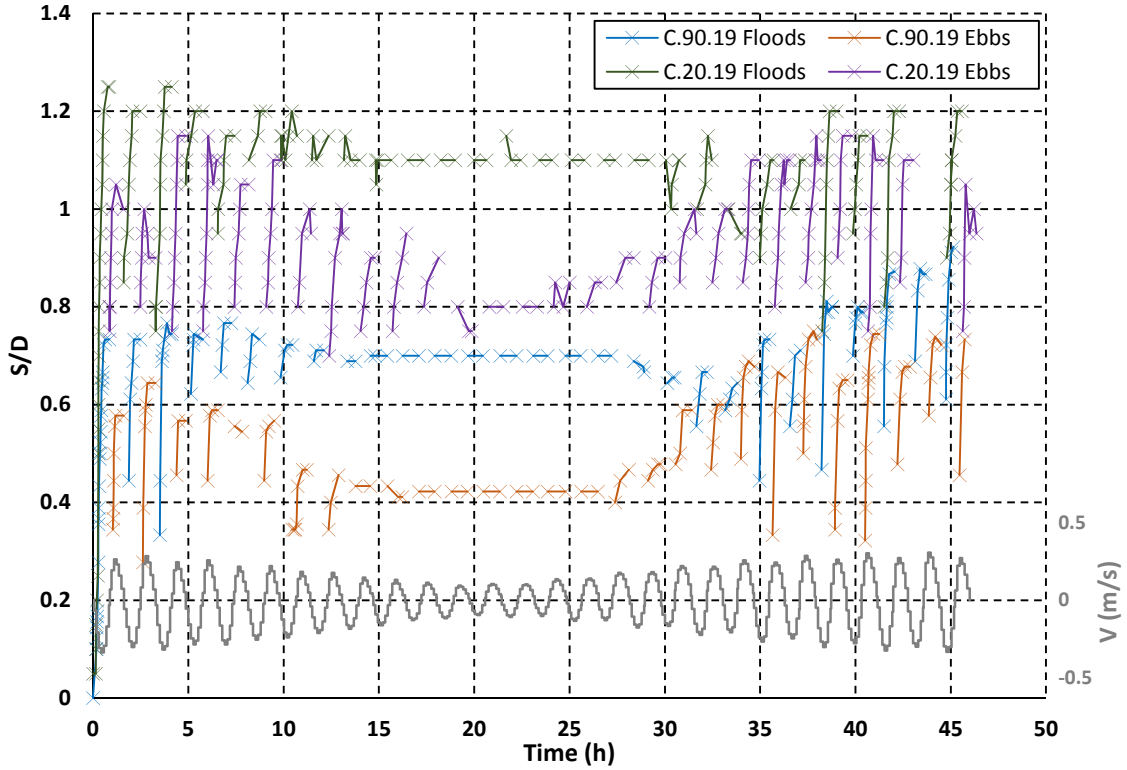

Figure 6.30 Scour development during a spring-neap tidal cycle in uniform coarse sand, with velocity signal (grey) plotted for comparison.

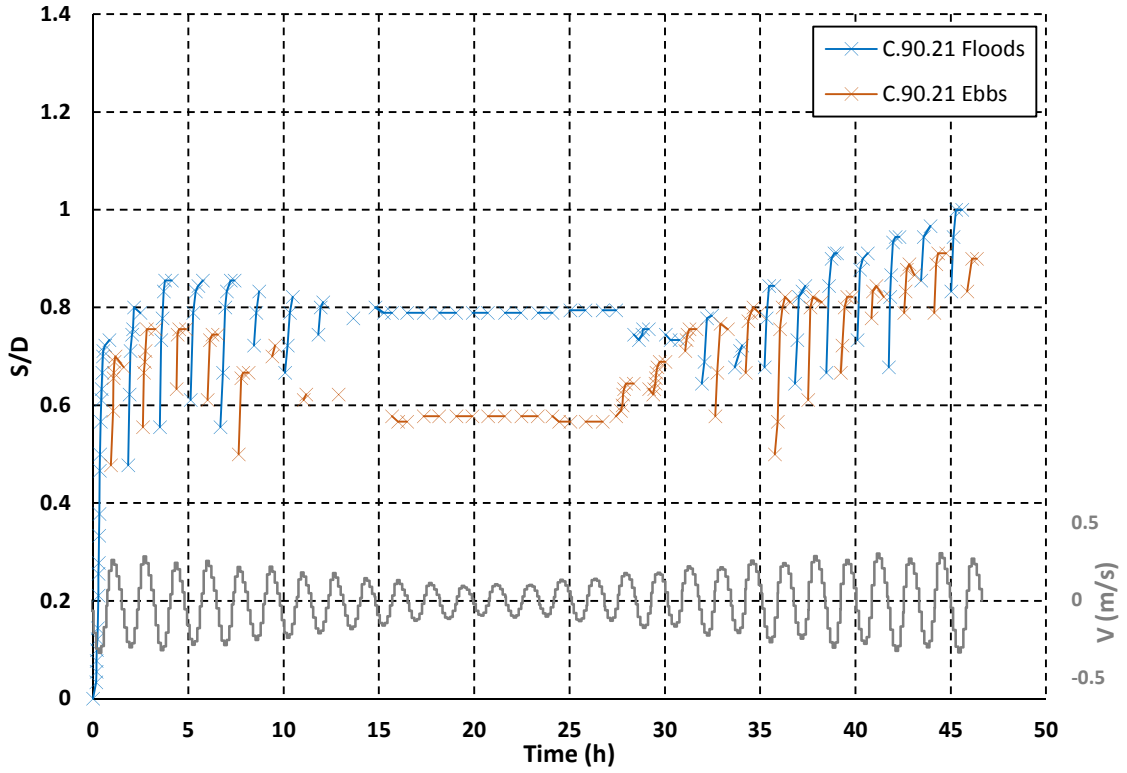

Figure 6.31 Scour development during a spring-neap tidal cycle in a layered bed of fine sand overlying coarse sand, L_u=70mm, with velocity signal (grey) plotted for comparison.

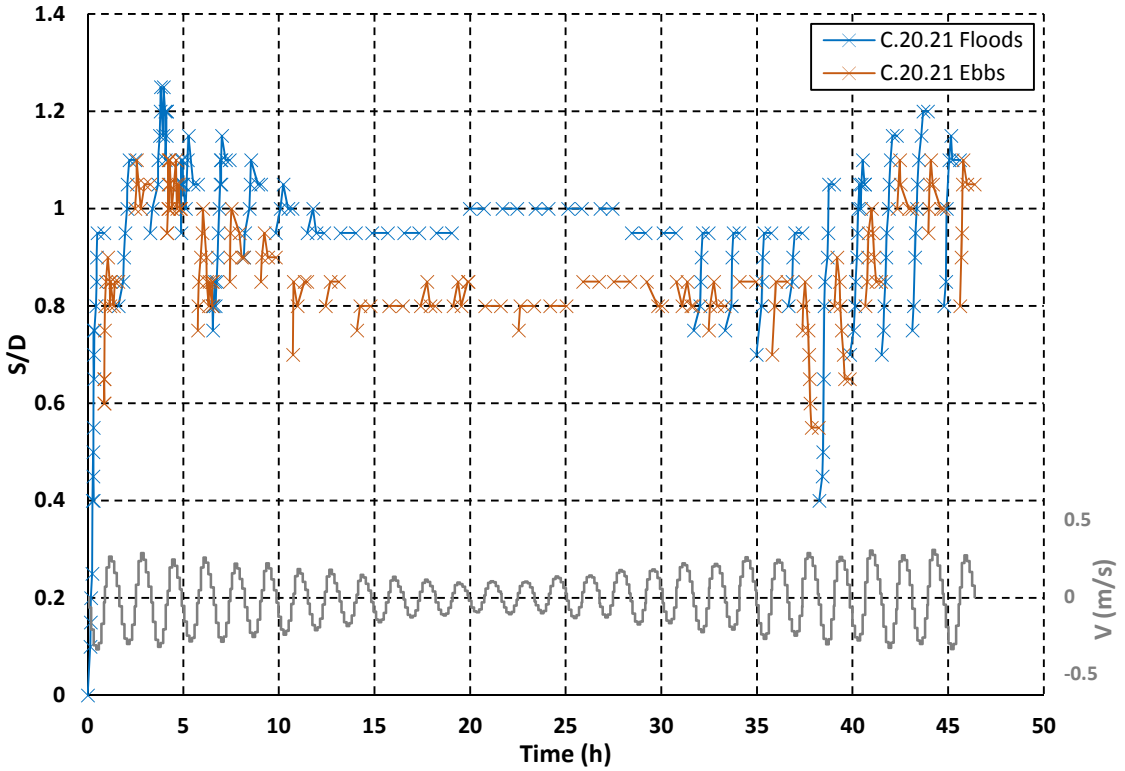

Figure 6.32 Scour development during a spring-neap tidal cycle in a uniform bed of fine sand with velocity signal (grey) plotted for comparison.

Broadly speaking the trend for the tests at both the large and small piles can be described as follows:

- scour depth increases over the first few cycles
- scour then starts to decrease over the next few cycles
- scour depth holds constant for the middle cycles
- scour depth starts to increase again in later cycles
- In the very final cycles the scour behaviour differs between the two piles. For the large pile scour depth continues to increase, but at the small pile the scour depth remains constant or starts to decrease

This trend coincides at least qualitatively with the velocity signal which began in the middle of the spring tides. Therefore, the middle cycles where scour depth holds constant relate to the neap tides. The increase in scour depth in the later cycles is linked to the return of the spring tides.

The lack of movement of the scour depth during the neap tides was to be expected due to the maximum velocity in these cycles being below the theoretical threshold velocity for scouring to occur. This shows that the threshold for scour initiation still holds in these conditions and that the presence of the scour hole and its associated bedforms have not resulted in a change to the threshold velocity.

It should be noted that there is a small amount of variation in scour depth during the neap phase of the fine sand test. This is due to the difficulty of resmoothing the bed in close proximity to the

small pile because of the presence of the larger scour hole around the large pile, as was discussed in relation to test C.20.12 in the previous section. This means that some bedforms close to the scour hole were not smoothed out during the test, which is likely to have contributed to greater variation in the scour depth as sediment ripples migrate through the scour hole. This is also true for the small pile coarse sand test, but the effect is less extensive as the coarser sediment is less mobile.

For the majority of the cycles within each of the four spring-neap scour tests the maximum scour depth in each half cycle is greater in the floods compared to the ebbs. This is interesting as it is the opposite of the trend observed in the reversing flow tests for the large pile. This is probably linked to the asymmetry in the tidal cycle, where the peak ebb velocities are mostly slower than the peak flood velocities (see Section 7.2.3 for further discussion).

The extent of the difference between scour depth in the floods and ebbs varies during the spring-neap cycle and between tests. The difference in scour depth between the floods and ebbs is largest during the neap tides and reduces under the spring tides. In the layered (mostly fine sand) and fine sand tests the difference is generally smaller than in the coarse sand tests where there is a greater difference between the scour depth in the flood and ebb cycles. This is particularly clear during the neaps where for the coarse sand tests the difference is approximately 0.3 S/D but is only 0.2 S/D during the neap section of the fine sand and layered sand tests.

Interestingly, the scour depth was not deeper in the flood half of the cycle in every case. In the coarse sand test at the large pile the scour depth was actually deeper under the ebb flow in the 21st and 23rd cycles. This is probably linked to the velocity signal for these particular cycles having a faster peak velocity in the ebb direction than in the flood direction. However, there are other cycles in the velocity signal such as the 19th and 25th cycles where the peak ebb velocity was greater than the peak flood velocity, but the scour depth was not greater during the ebb half cycle. Similar results are found in the layered case. In this test the scour depth was greater during the ebb half of cycles 19 and 21 but not in the 23rd or 25th cycles. For the coarse sand small pile test scour depth was greater under the ebb flow in cycles 21 and 23. For the small pile fine sand test the scour depth was never greater in the ebb compared to the flood half of the cycle. While this indicates that there is a link between the strength of the peak flow velocity and scour depth, clearly there are other factors of influence.

To better understand the link between flow velocity and scour depth in each half cycle the maximum scour depth is plotted against the maximum velocity in each half cycle for the four tests in Figures 6.33-6.36.

The basic trend in Figures 6.33-6.36 is that peak scour depth increases with peak velocity per half cycle. However there is significant scatter in the data. This results in the greatest scour depth not coinciding with the highest peak velocity in three of the graphs. The scatter also means that several different peak scour depths are observed in the same test under the same flow velocity. This is an important result which is discussed in more detail in Section 7.2.3 in

relation to the influence of ripples on the tests and the changes in the scour behaviour under clear water compared to live bed conditions.

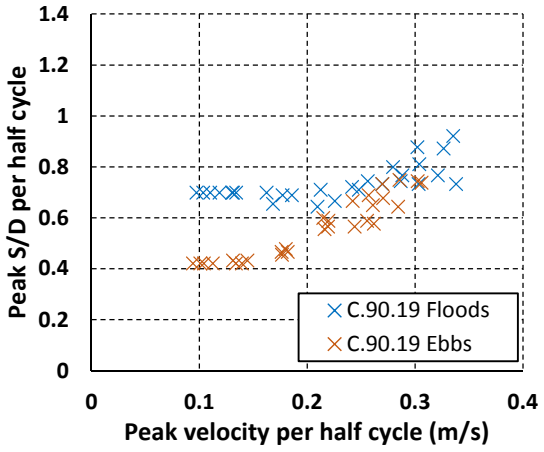

Figure 6.33 Maximum scour depth in each half cycle of spring-neap test plotted against maximum velocity in each half cycle, test C.90.19 (uniform coarse sand, 90 mm pile).

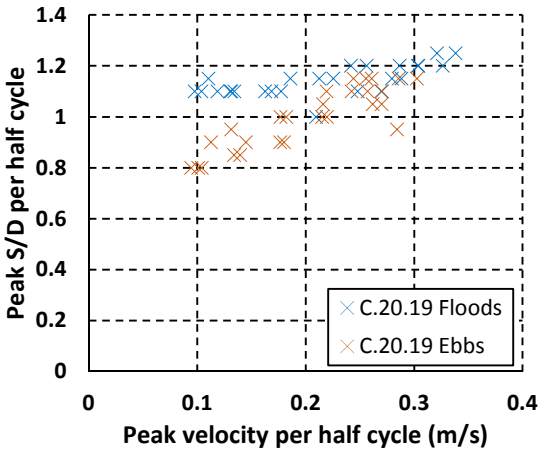

Figure 6.34 Maximum scour depth in each half cycle of spring-neap test plotted against maximum velocity in each half cycle, test C.20.19 (uniform coarse sand, 20 mm pile).

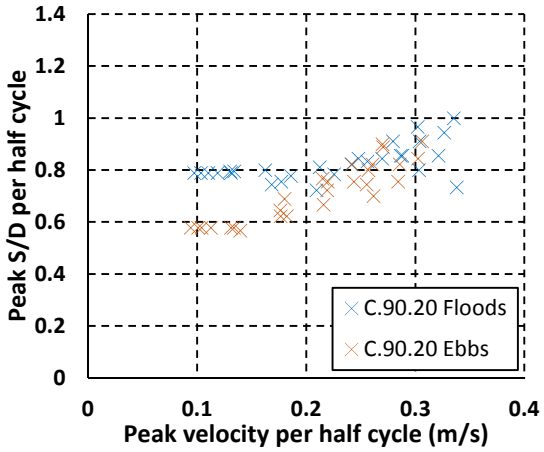

Figure 6.35 Maximum scour depth in each half cycle if spring-neap test plotted against maximum velocity in each half cycle, test C.90.20 (fine over coarse layered bed, 90 mm pile).

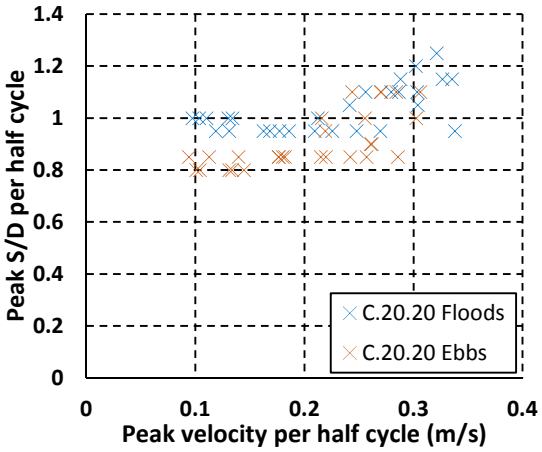

Figure 6.36 Maximum scour depth in each half cycle of spring-neap test plotted against maximum velocity in each half cycle, test C.20.20 (uniform fine sand, 20 mm pile).

The spring-neap test conducted in the layered bed resulted in scour to a greater depth in the coarse sand than at that time in the uniform coarse sand test. However, as these tests did not reach an equilibrium condition, it cannot be determined if ultimately scour in the layered case will be greater than in the uniform coarse sand case. Longer tests would need to be conducted

to determine if the scour enhancement trend found for the layered unidirectional tests is also present under this tidal flow condition.

6.3 Wave tests (all sediment types)

The majority of the tests conducted in waves resulted in very little or no scour developing at the pile. This was anticipated, and was in agreement with the literature because to reduce bed rippling the velocity and hence KC number were limited to low values. More scour occurred at the smaller pile than the larger pile which is consistent with the dependence on KC number shown by other researchers (see Section 2.3.3). A comparison of the wave results with that expected in the literature in terms of the initiation for scouring is given in Appendix 9. See Appendix 3 for the full list of wave tests.

6.4 Wave-current tests (all sediment types)

The main series of wave-current tests were conducted in the clear-water regime with a smaller pile diameter (50 mm) to enable larger KC numbers to be tested within this regime. Figure 6.37 shows the results for these tests in a uniform bed of coarse sand. Three different current velocities were combined with the same wave, tests C.50.26, C.50.27, C.50.28 so that one case had a larger wave component than current component, in one test the components were approximately equal and in the third case the current velocity component was larger than the wave velocity component. It can be seen in Figure 6.37 that the scour depth increased as the current velocity in the wave-current combination increased. Although the scour depths are small for these tests, the general trend of decreasing gradient as scour depth increases is still visible. This is not the case for the scour curve in test C.20.28, Figure 6.37. This test was run under the same flow conditions as test C.50.28, but at the smaller 20 mm diameter pile. Here, the scour development curve is made up of a series of steps. Initially the scour depth increases in the usual way, but the gradient of the curve quickly flattens out. After a time the scour curve starts to increase quite rapidly again before flattening off, and this process continues to repeat. This test could have been stopped based on the stopping criterion at the 5 hour mark, but wasn't because of continuation of scour at this time at the larger pile. Unexpectedly, the scour depth started to increase again quite some time after this point. This demonstrates one of the issues with using stopping criteria in scour tests, as it is shown that it is possible for scour development to be intermittent. This result may be linked to changes in pore pressure affecting the erodibility of the sand in proximity to the pile, see discussion in Section 7.2.4.

Another interesting result is found when comparing the scour development in these wave-current cases to the wave only and current only tests in the coarse sand, where the same wave and current are used in combination or alone. Negligible scour occurred under the wave only case. For the three current cases only the fastest of the three currents produced any scour, and then only at the larger pile where a scour depth of only 0.06 S/D was reached. However, with the wave-current combined, even at the slowest wave-current combination some scour occurred at the larger pile (approximately 0.08 S/D), while 0.15 S/D occurred with the middle current speed plus wave. At the fastest current speed scour was much more significant at 0.5

S/D at the larger pile and 0.75 S/D at the smaller pile. This demonstrates that for these tests the wave-current condition resulted in a greater scour depth than for current alone, so that adding a wave to a current resulted in significantly greater scour, which is a result contrary to that in the literature for live bed scour (see Section 2.3.4).

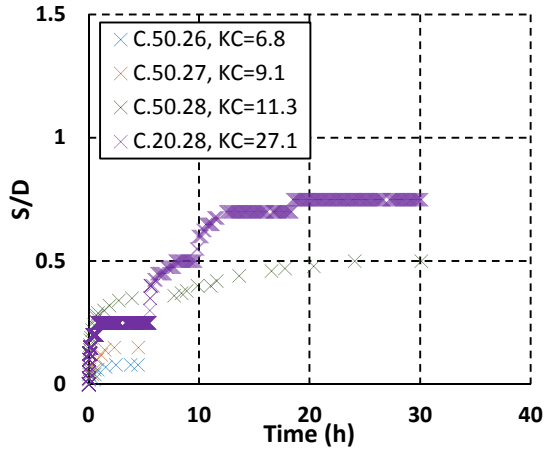

Figure 6.37 Scour development in wave-current tests, uniform coarse sand.

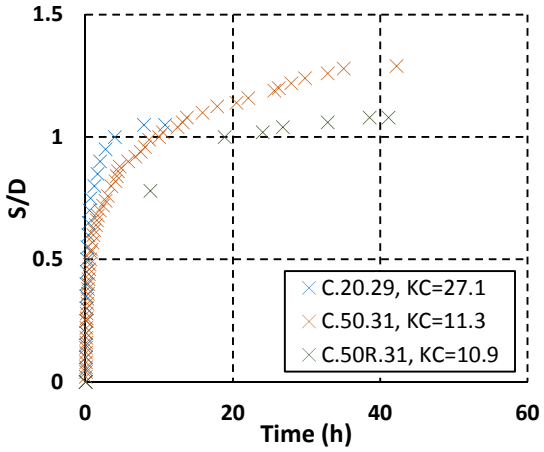

Figure 6.38 Scour development in wave-current tests, uniform fine sand.

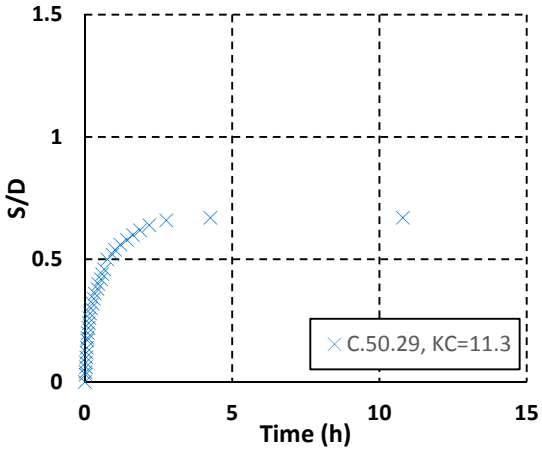

Figure 6.39 Scour development in wave-current tests, fine over coarse sand layered bed, L_u=30mm.

Figures 6.38, 6.39 and 6.42 plot the wave-current tests in the same flow conditions as for test C.50/20.28 (with the fastest of the three current velocities) but with different sand bed configurations. The tests in uniform fine sand are plotted in Figure 6.38, the layered bed test (fine over coarse sand) is plotted in Figure 6.39, and the 50% mixed sand tests are plotted in Figure 6.42. For the fine sand cases in Figure 6.38 the curves follow the usual scour development trend (decreasing gradient as scour depth increases). The short duration of test C.20.28 was dictated by the duration of the layered sand test run in tandem with this test at the larger pile.

Figure 6.39 shows the layered case that was tested under the same wave-current combination as for tests C.50.28-C.50.31. The upper layer was fine sand to a depth of 30 mm, or S/D=0.6. The scour through the upper layer is in close agreement with scour in the uniform fine sand test C.50.31.

Once the interface between the two layers was reached, scour continued a little way into the coarse sand but then soon flattened off with no more scour occurring.

Figure 6.40 shows a comparison of the layered test with the uniform fine and coarse sand wave-current tests. Scour in the uniform coarse sand test did not reach the depth of the layer interface in the layered case. Therefore, any scour beyond the layer interface demonstrates that the scour enhancement effect first discussed in relation to the unidirectional current tests in Section 6.1.2 has occurred. To investigate the extent of the scour enhancement, Figure 6.41 plots the equilibrium scour depths in the uniform fine and coarse sands in comparison with the layered wave-current test following the same method used in Figure 6.14 for the unidirectional current tests. Figure 6.41 shows that the enhancement effect is small in this case which may be due to the large upper layer thickness in comparison to the equilibrium depth reached in the uniform coarse sand test.

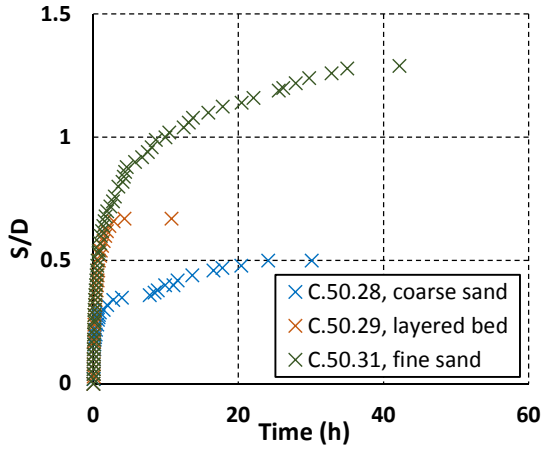

Figure 6.40 Comparison of scour development in uniform fine sand, uniform coarse sand and a fine over coarse sand layered bed, L_u=30mm, in wave-current flow, KC=11.3.

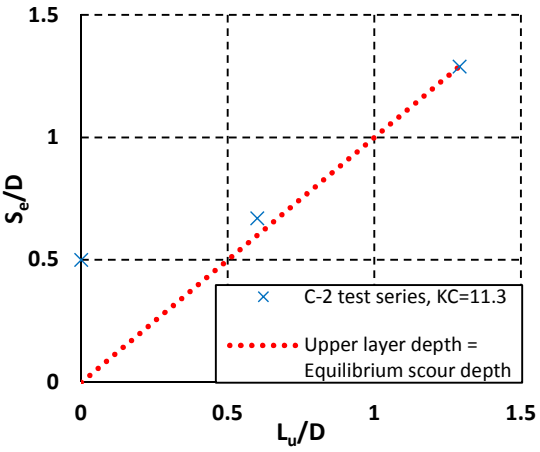

Figure 6.41 Quasi-equilibrium scour depth versus upper layer thickness, comparison of uniform and layered sand tests in wave-current flow, KC=11.3.

The same wave-current case was also conducted with a 50%-50% mixed sand bed. The results for the two piles are shown in Figure 6.42. Interestingly there is a greater difference to the scour development trend for these tests, with the middle sections of each of the curves being more linear, as was found for some of the unidirectional current tests in mixed sands, see Section 6.1.3. The same trend is seen in the wave-current cases as for the unidirectional tests where the initial part of the curve follows the usual exponential expression, then the middle section is linear, before the curve flattens off in the final section. This is a very interesting result as it is

indicating this trend occurs for a different flow condition. It is also the first time this result has been found in the larger flume.

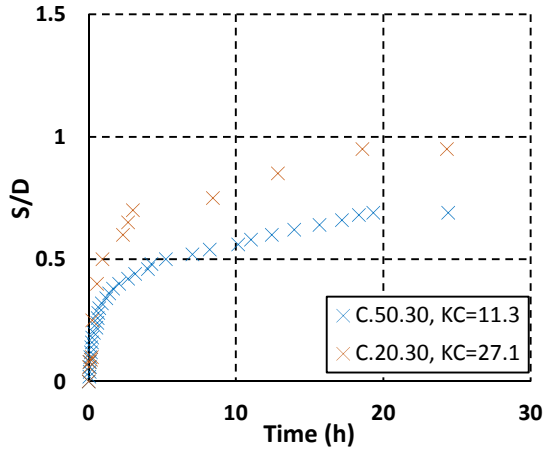

Figure 6.42 Scour development in wave-current tests in 50% fine - 50% coarse sand mixed beds.

6.5 Echosounder results

This section presents the results from the echosounder profiling in the small flume. As a considerable number of profiles were taken, only those pertinent to the discussion will be presented here. For full data see Appendix 7.

The echosounder data enables investigation of the similarities and differences between the scour profiles in the different sand types. This may help to explain the reasons for the differences in scour time development between the uniform, mixed and layered cases (see Sections 7.2.1 and 7.2.2).

Figures 6.43-6.47 show comparisons of scour profiles in uniform coarse and fine sand beds, tests R.16 and R.17, where for each comparison the scour depth at the pile was the same in both tests. Note, therefore, that the time into the tests at which the profiles were taken is different. In Figures 6.43-6.47 the scour depth at the pile ranges from 36 mm to 55 mm.

In each of the figures the upstream parts of the scour hole profiles are in close agreement between the two sands. The small difference is probably due to the issues with measurement accuracy over sharp changes in slope, discussed in Section 4.4.1 and 4.4.5. It seems, therefore, that the development of the upstream scour hole slope is consistent between these two sands.

There is a more significant difference in the downstream sections of the profiles, with the coarse sand having a taller and wider deposition dune than the fine sand, and a smaller downstream scour hole extent. This difference is more pronounced in the comparisons at smaller scour depths, and the differences between the downstream fine and coarse sand profiles are reduced at the larger scour depths, later into the tests.

Note that in Figures 6.43-6.46 the point closest to the pile on the downstream side is artificially high as this does not match with visual observations of the scour hole shape. This is also true for many of the points in the fine sand profile in the 36 mm comparison, Figure 6.43. This is likely due to spurious echoes caused by suspended sediment which is more prevalent for the fine sand, and during the earlier stages of the scour process. This makes comparison of the downstream profiles difficult in Figure 6.43.

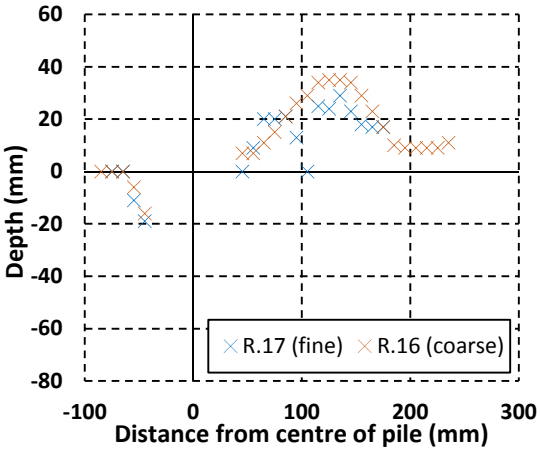

Figure 6.43 Comparison of streamwise echosounder profiles of the scour hole in uniform fine and coarse sand beds, when the scour depth at the pile equalled 36 mm.

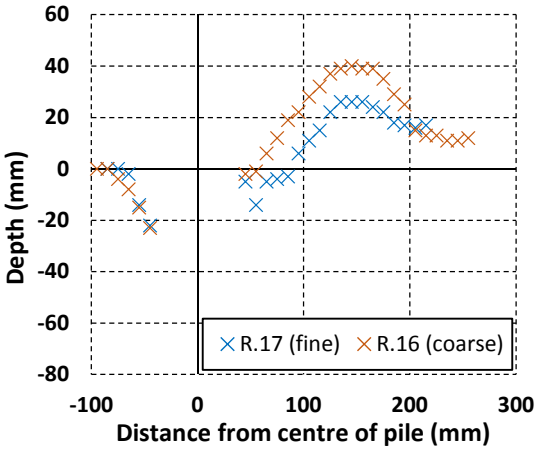

Figure 6.44 Comparison of streamwise echosounder profiles of the scour hole in uniform fine and coarse sand beds, when the scour depth at the pile equalled 43 mm.

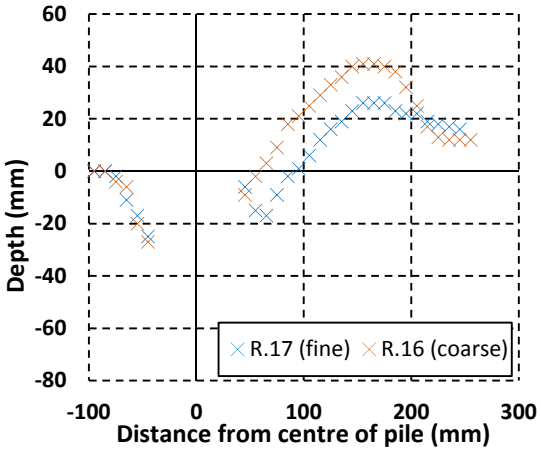

Figure 6.45 Comparison of streamwise echosounder profiles of the scour hole in uniform fine and coarse sand beds, when the scour depth at the pile equalled 46 mm.

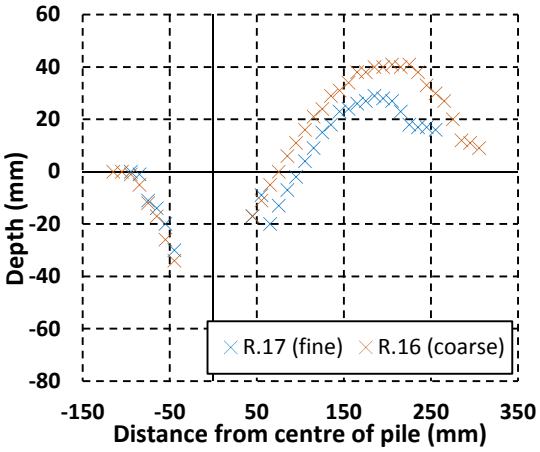

Figure 6.46 Comparison of streamwise echosounder profiles of the scour hole in uniform fine and coarse sand beds, when the scour depth at the pile equalled 52 mm.

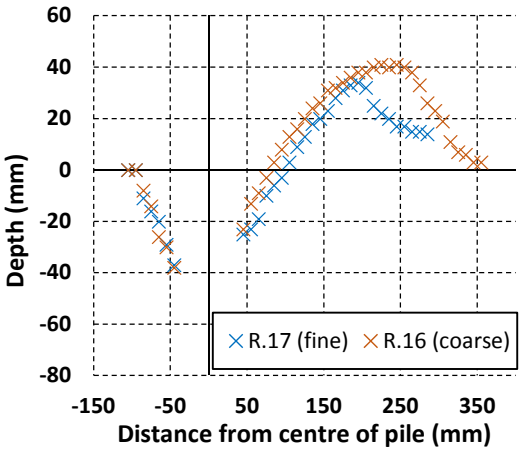

Figure 6.47 Comparison of streamwise echosounder profiles of the scour hole in uniform fine and coarse sand beds, when the scour depth at the pile equalled 55 mm.

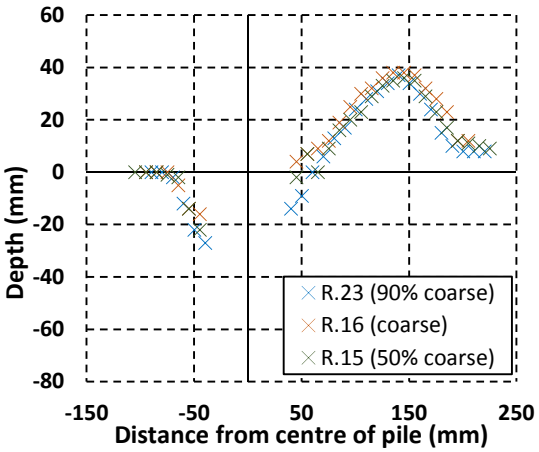

Figure 6.48 Comparison of streamwise echosounder profiles of the scour hole in 50% coarse sand mixed bed, 90% coarse sand mixed bed and uniform coarse sand bed, when the scour depth at the pile equalled 40 mm.

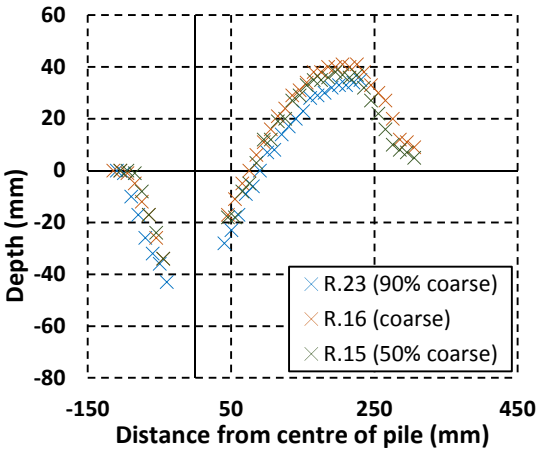

Figure 6.49 Comparison of streamwise echosounder profiles of the scour hole in 50% coarse sand mixed bed, 90% coarse sand mixed bed and uniform coarse sand bed, when the scour depth at the pile equalled 52 mm.

Figures 6.48-6.50 compare sets of scour hole profiles between 50% and 90% coarse sand mixed beds and uniform coarse sand. Similarly to the comparison between the fine and coarse sands (Figures 6.43-6.47), there is good agreement between the upstream profiles in Figures 6.48-6.50, indicating that the scour process is similar on the upstream side of the pile between each of these sands throughout the scour development process. The downstream profiles in Figures 6.48-6.50 are in closer agreement compared to those shown in Figures 6.43-6.47 for

the fine and coarse sand comparisons. In particular the sections of the scour hole slope closest to the pile are in good agreement. There is a greater difference between the peaks of the dunes in each of the sands, but this difference is small compared to that observed in the profiles for the fine and coarse sand comparisons.

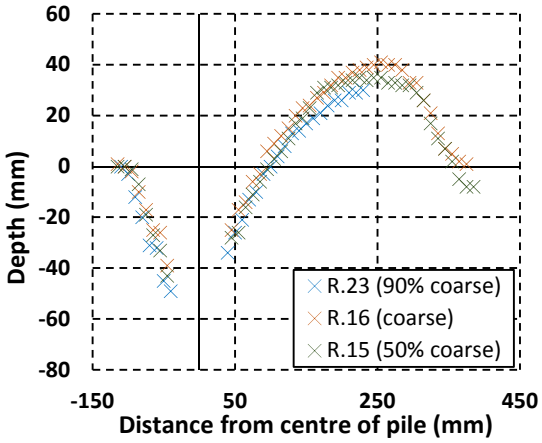

Figure 6.50 Comparison of streamwise echosounder profiles of the scour hole in 50% coarse sand mixed bed, 90% coarse sand mixed bed and uniform coarse sand bed, when the scour depth at the pile equalled 56 mm.

Figure 6.51 compares scour hole profiles for three of the fine over coarse sand layered tests; with 40 mm, 55 mm and 70 mm upper layer depths. Each profile was measured when the scour depth at the pile was 60 mm. Again there is very close agreement between the three profiles on the upstream side of the pile, despite the differences in sand bed configurations between these three tests. On the downstream side there is reasonable agreement between the 40 mm and 55 mm layered tests, but the 70 mm layered test has a slightly steeper slope in the upper extent of the scour hole and a taller deposition dune. The differences in the downstream side may be due to the timescale of scour, with the 70 mm profile being taken much earlier into the test. This would mean that there was less time for the dune to migrate downstream.

In Figures 6.52-6.55 profiles for the uniform fine sand are compared with those from a layered sand bed. As with the previous comparisons, the upstream scour hole profiles are very similar. On the downstream side of the pile, although the scour hole profiles are similar at the smallest scour depth (Figure 6.52), the difference between the two cases increases over time (from Figure 6.52 through to Figure 6.55). This time the uniform fine sand has a taller dune and smaller downstream extent than the layered case. This is likely to be linked to the differences in the timescale of the scour process between these two tests. Scour progresses more slowly in the 40 mm layered test than in the uniform fine sand, however it appears that the time-scale of scour does not influence the speed at which the dunes migrate along the bed. This will be discussed in greater detail in Section 7.2.1.

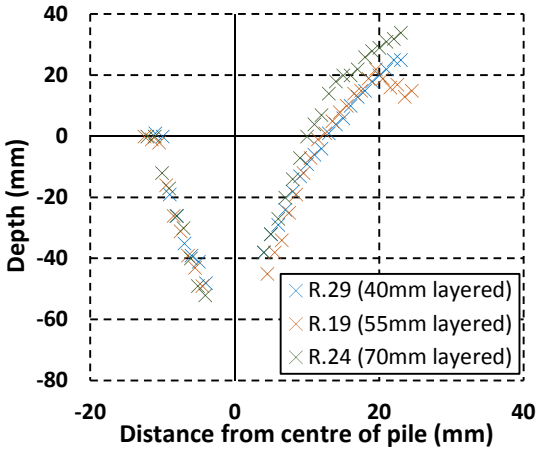

Figure 6.51 Comparison of streamwise echosounder profiles of the scour hole in layered beds (fine sand overlying coarse sand) with 40 mm, 55 mm and 70 mm upper layer thicknesses, when the scour depth at the pile equalled 60 mm.

Note that in Figures 6.52 and 6.53 the first two points of the fine sand profile closest to the downstream edge of the pile are likely to be artificially high due to suspended sediment as discussed previously.

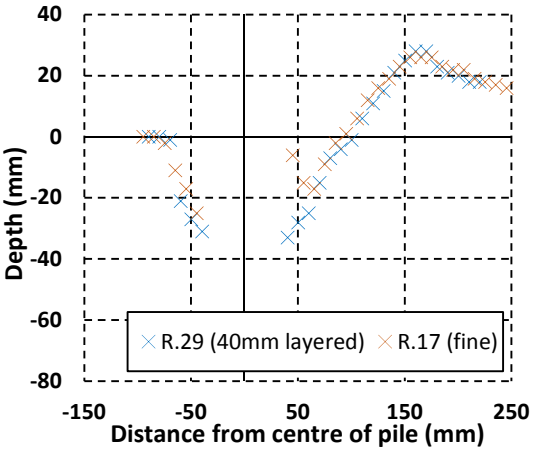

Figure 6.52 Comparison of streamwise echosounder profiles of the scour hole in a uniform fine sand bed and a layered bed (fine sand overlying coarse sand) L_u=40mm, when the scour depth at the pile equalled 45 mm.

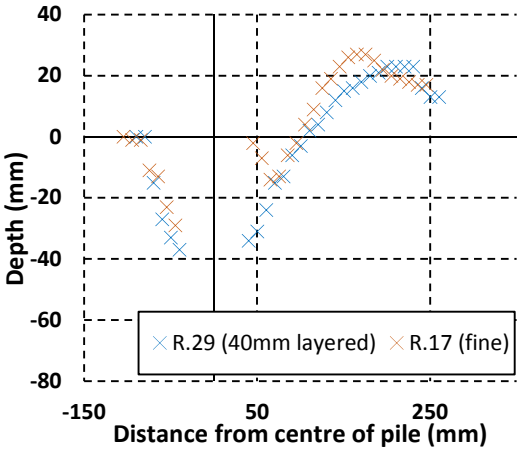

Figure 6.53 Comparison of streamwise echosounder profiles of the scour hole in a uniform fine sand bed and a layered bed (fine sand overlying coarse sand) L_u=40mm, when the scour depth at the pile equalled 50 mm.

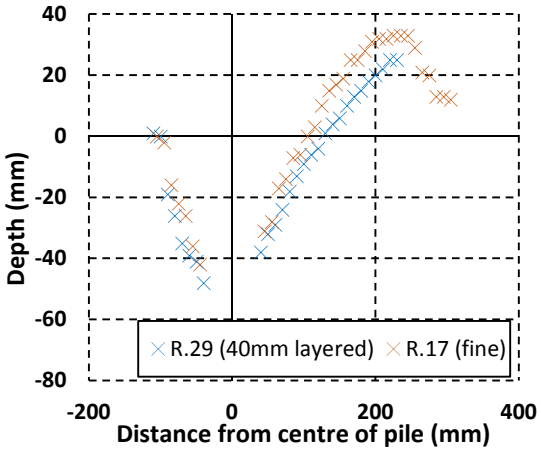

Figure 6.54 Comparison of streamwise echosounder profiles of the scour hole in a uniform fine sand bed and a layered bed (fine sand overlying coarse sand) L_u=40mm, when the scour depth at the pile equalled 60 mm.

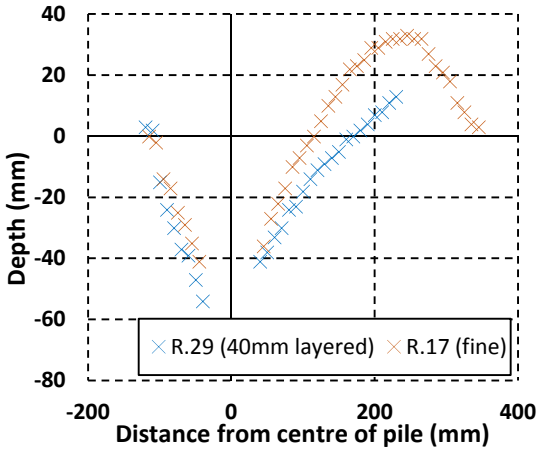

Figure 6.55 Comparison of streamwise echosounder profiles of the scour hole in a uniform fine sand bed and a layered bed (fine sand overlying coarse sand) L_u=40mm, when the scour depth at the pile equalled 64 mm.

In Figure 6.56 two profiles are plotted from tests R.15 and R.18 in the same sand type (50%-50% mixed sand) but at different flow velocities, to determine if the scour hole shape varies with flow condition. This time the agreement is very close in both the upstream and downstream profiles indicating that the scour hole shape is independent of the flow velocity, at least at this scale and under unidirectional current.

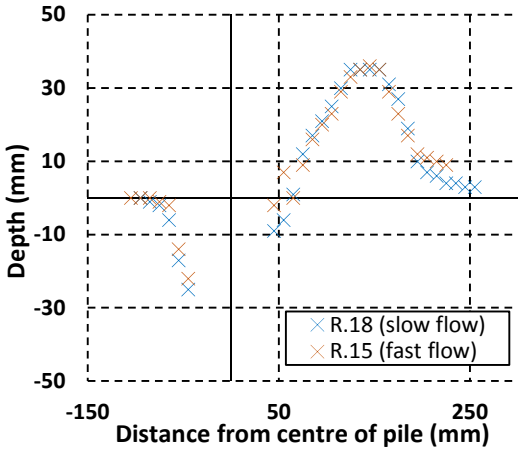

Figure 6.56 Comparison of streamwise echosounder profiles of the scour hole in 50%-50% fine-coarse mixed sand beds at two different flow velocities, when the scour depth at the pile equalled 40 mm.

Figure 6.57 shows all of the echosounder profiles taken during one scour test (R.29.2), so that each profile is at a different stage in time through the test and hence the scour depth at the pile is different. In Figure 6.57 it can be seen that the scour hole widens with time with the upstream profile moving further upstream, and the downstream profile moving further downstream. The slope angle of the upstream slope appears to remain fairly constant over time, although it is difficult to measure this precisely due to the uneven nature of the profiles. On the downstream side, the slope angle appears to become shallower over time, and the dune migrates downstream, reducing in height close to the pile. A similar result is found for the time series of the echosounder profiles for the other tests, and these are shown in Appendix 7.

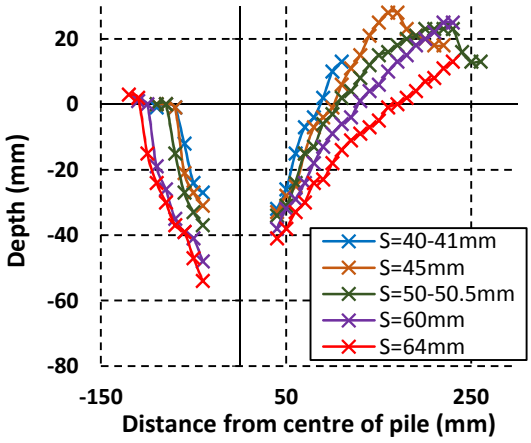

Figure 6.57 Time development of the streamwise scour hole profile through test R.29.2, fine over coarse sand layered bed, L_u=40mm.

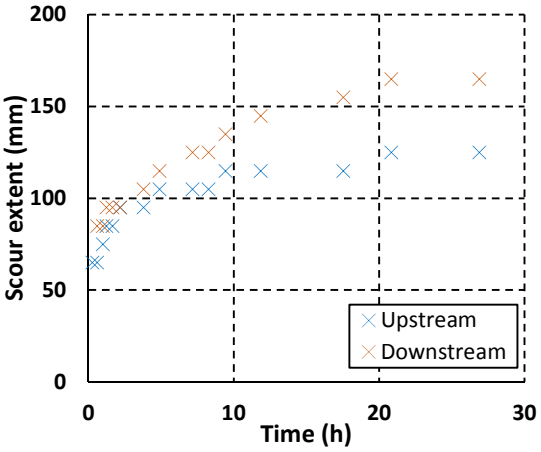

Figure 6.58 Time development of upstream and downstream scour hole extents in uniform fine sand under unidirectional current (test R.17).

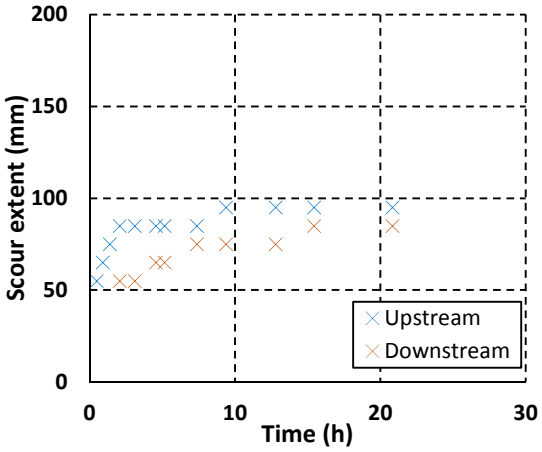

Figure 6.59 Time development of upstream and downstream scour hole extents in uniform coarse sand under unidirectional current (test R.16).

The echosounder profiles allow an estimate to be made of the scour hole extent and its progression through time. This is a further parameter that can be considered in the analysis and thereby provide a greater insight into the scour process.

Estimates of the scour hole extents were obtained from the echosounder profiles, and those for the uniform fine sand and coarse sand tests are plotted in Figures 6.58 and 6.59. The scour hole extent development for the remaining tests is included in Appendix 7. The extent of the scour hole is defined as the horizontal distance from the edge of the pile to the point at which the bed level returns to zero. Note that as the measurement of scour hole extent was not the primary objective of the echosounder measurements, these are approximate values due to interpolation of the profiles. Therefore only the general trends in the scour extents will be identified and discussed qualitatively.

The time development of the upstream scour extent in general seems to follow a similar trend to the scour depth development curve, with the gradient of the curve decreasing as the scour extent increases, and there is little change to the extent in the later stages of the tests. The trend of the downstream extent is more variable, but in many of the tests continues to develop throughout the test. For the predominantly fine sand tests the downstream extent is generally larger than the upstream extent, but for the predominantly coarse sand tests the downstream extent is smaller than the upstream extent. This is indicative of the different rates of ripple migration in the two sands.

6.6 Photogrammetry results

As discussed in the methodology Section 4.4.2 and 4.4.5 the photogrammetry technique was used as the primary measurement of the scour hole profile in the larger flume. Due to the extensive amount of time required to process these data, only key cases were analysed, and in particular the focus was on the reversing and tidal flow cases where it was anticipated that the development of the scour hole shape would be more significant and more influential on the scour process. An evaluation of the photogrammetry technique and the other scour measurement approaches used is given in Section 7.4.3 and options for reducing the processing time are considered in Section 7.5.

Figures 6.60 and 6.61 show 3D scour hole profiles from test C.90.19 (spring-neap tidal cycle over a uniform coarse sand bed). The two profiles were measured at the end of the first half cycle (Figure 6.60) i.e. before the flow has been reversed, and after the end of the 2nd half cycle (Figure 6.61) i.e. flow has been reversed once. It is clear in Figures 6.60 and 6.61 that the deepest part of the scour hole is on the upstream side of the pile in each case so that the scour hole shape close to the pile has reversed in Figure 6.61 compared to that in Figure 6.60. However, the dune created in the first half cycle on the right hand side of Figure 6.60 (downstream of the pile) stays in place under the reversing flow of the next half cycle. This is important because it means that there is no infilling of the scour hole to any great extent from this dune. This is related to the clear water conditions for these tests. On the new downstream side there has been some deposition on the edge of the scour hole in Figure 6.61, but not to

such an extent as in the previous half cycle, indicating that less sediment has been removed from the scour hole during the 2nd half of the cycle, as the scour process slows down.

To gain more of an insight into the differences between the 1st and 2nd half cycles shown in Figures 6.60 and 6.61 a volume change map of the 1st and 2nd half cycles is shown in Figure 6.62. It can be seen that the scour hole has deepened on the new upstream side and become shallower on the new downstream side so that the shape of the scour hole has reversed. This is most noticeable in close proximity to the pile, matching with visual observations of sand being deposited directly adjacent to the new downstream face of the pile after flow reversal so that it does not leave the scour hole. Further away from the pile the differences between the scour hole profiles in the two half cycles are much smaller.

Figure 6.63 shows the final scour hole profile taken from test C.90.19. The deepest part of the scour hole is again on the upstream side of the pile (right hand side at this point in the test). In comparison with the profiles taken at the start of this test (Figures 6.60 and 6.61) it can be seen that the scour hole has deepened, however the scour hole shape is qualitatively similar. The presence of the deposition zone at the initial upstream side is still evident. However, the deposition zone on the left hand side has grown compared to that shown after the first cycle and the scour hole has also widened.

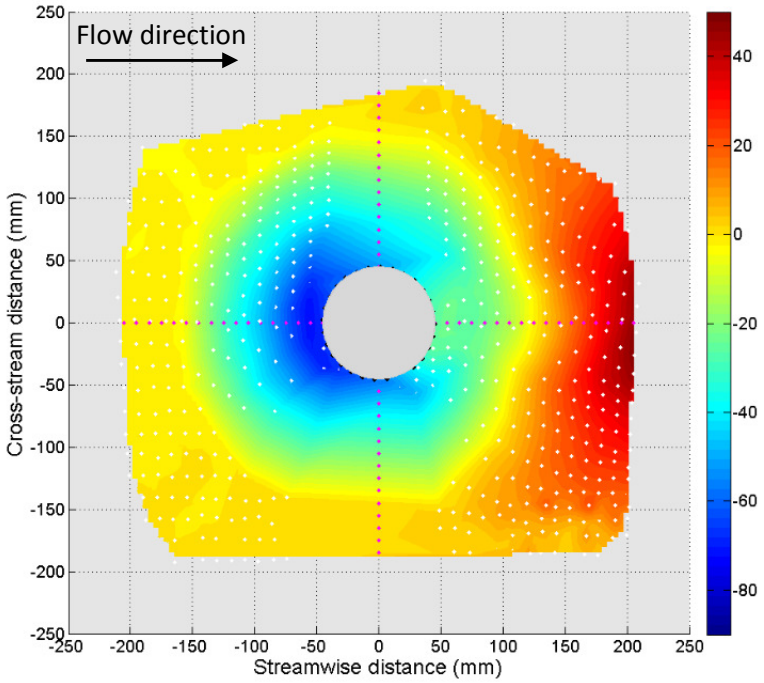

Figure 6.60 Plan view of scour hole profile obtained from the photogrammetry system after the first half cycle prior to flow reversal in test C.90.19, in uniform coarse sand, under spring-neap tidal cycle.

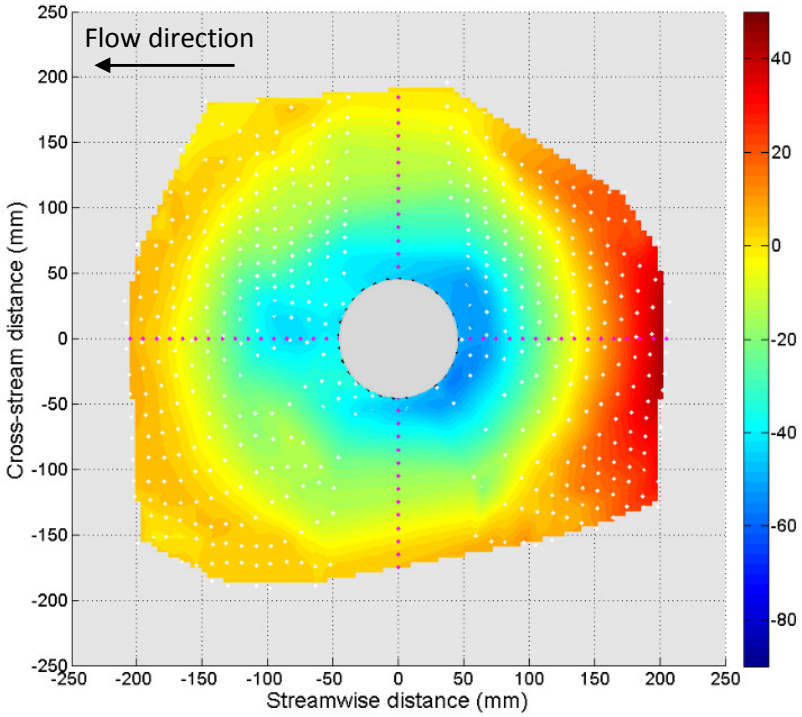

Figure 6.61 Plan view of scour hole profile obtained from the photogrammetry system at the end of the second half cycle in test C.90.19, in uniform coarse sand, under spring-neap tidal cycle.

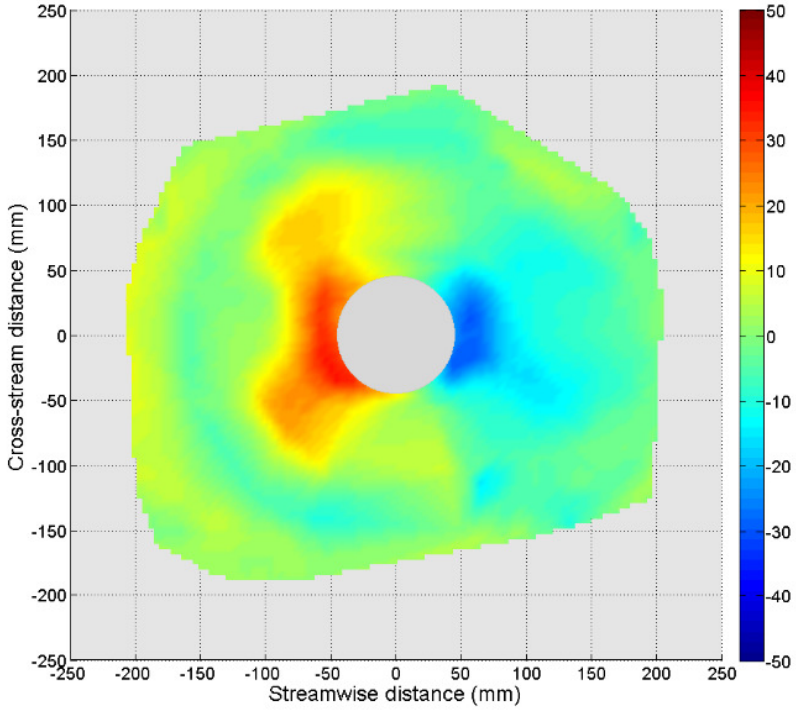

Figure 6.62 Plan view of the change in depth of the scour hole between the 2nd and 1st half cycles shown in Figures 6.61 and 6.60.

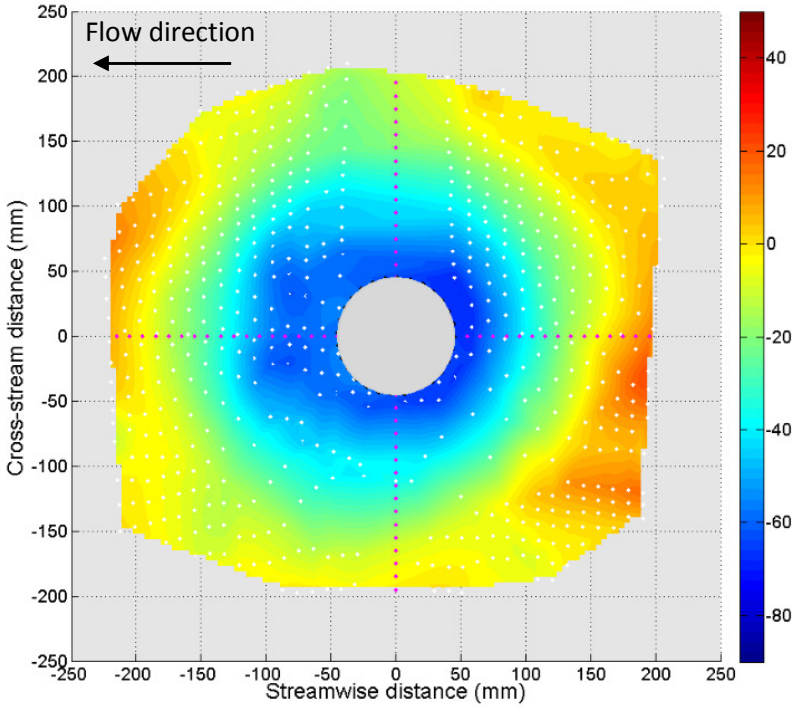

Figure 6.63 Plan view of scour hole profile obtained from the photogrammetry system at the end of test C.90.19, in uniform coarse sand, after one full spring-neap tidal cycle.

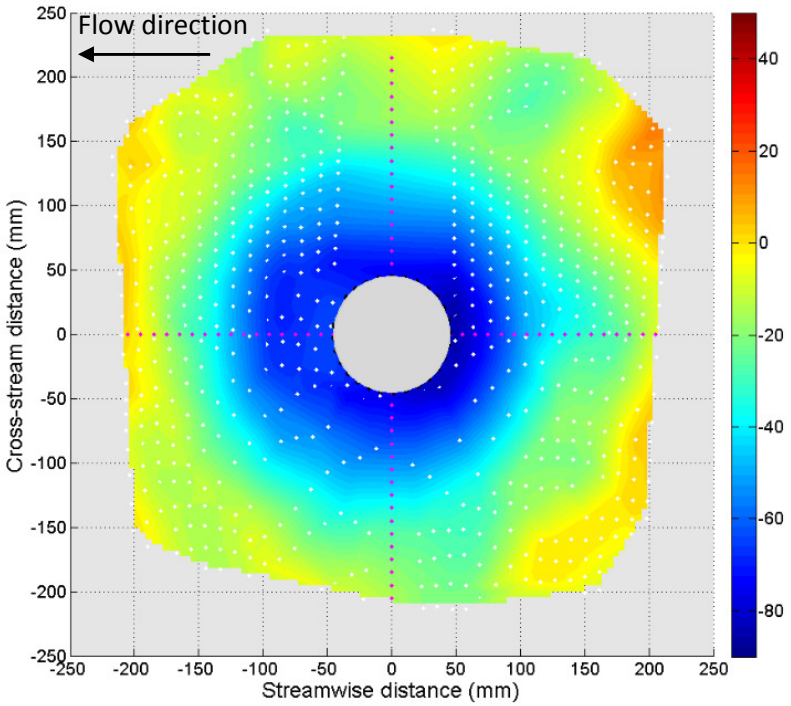

Figure 6.64 Plan view of scour hole profile obtained from the photogrammetry system at the end of test C.90.21, in a layered bed (fine sand overlying coarse sand), after one full spring-neap tidal cycle.

Another interesting comparison is to consider the difference in the scour hole shape between different sand types. In Figures 6.63 and 6.64 the final scour hole profiles are shown from the two spring-neap tests at the large pile, the first in coarse sand, and the second in the layered bed.

Figure 6.64 shows a similar pattern close to the pile to that in Figure 6.63 although the scour hole is deeper and wider. There is greater variation between the two profiles in the outer extremities of the scour hole, with greater fluctuations in the scour depth in this region in Figure 6.64 so that the edges of the scour hole are less well defined, probably due to the higher mobility of the fine sand compared to the coarse sand.

In Figure 6.65 a scour hole profile taken after the first half cycle (prior to flow reversal) of test C.90.18 is shown. This test was conducted under constant reversing flow rather than under the spring-neap cycle so it is interesting to compare this profile with that shown in Figure 6.60 for the same sand type and same stage of the spring-neap test. It can be seen that in comparison the scour hole in Figure 6.65 is significantly shallower and narrower than that in Figure 6.60 which gives an indication of the difference in scour behaviour due to varying flow compared to constant flow (discussed in Section 7.2.3). In Figure 6.65 the deposition zone behind the pile is clearly shown and it can be seen that the shape of the dune is ridged running from the back of the pile downstream.

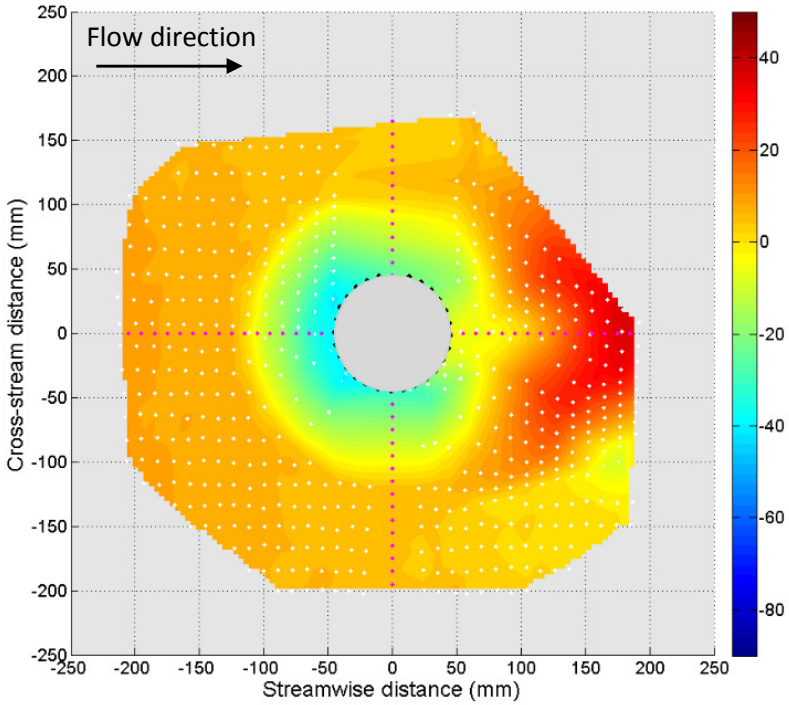

Figure 6.65 Plan view of scour hole profile obtained from the photogrammetry system at the end of the first half cycle (prior to flow reversal) in test C.90.18, in uniform coarse sand under square wave reversing flow.

6.6.1 Scour hole extents and slope angles

In order to analyse the development of the scour hole profile and the differences between the tests, 2D profiles of the scour hole upstream and downstream of the scour hole have been extracted from the photogrammetry data. The available profiles for test C.90.19 are plotted in Figure 6.66, for test C.90.21 in Figure 6.67 and for test C.90.18 in Figure 6.68. In each of the figures a trend line is fitted to the upstream and downstream 2D profiles to obtain estimates of the scour hole slope angles. The slope angles obtained in this way are given in Table 6.1.

Table 6.1 Estimated upstream and downstream scour hole slope angles from the photogrammetry data.

Test	Upstream (°)	Downstream (°)
4.1	31.38 (lhs)	24.70 (rhs)
5.1	33.82 (lhs)	30.96 (rhs)
5.1.5	34.99 (rhs)	28.81 (lhs)
5.28.5	33.42 (rhs)	30.11 (lhs)
7.28.5	33.82 (rhs)	32.62 (lhs)

For each case shown in Table 6.1 the upstream scour hole slope is always slightly steeper than the downstream scour hole slope, although the actual difference in angle is relatively small. There is no clear pattern to the slope angle in terms of a change through time or between the fine and coarse sands, implying that the slope angle remains fairly constant in these types of tests. This is in contrast with the results reported by McGovern et al. (2014) for scour in tidal flow. However, the slope angle is in the region expected for the angle of repose of these sediment sizes in agreement with the findings for unidirectional scour tests (Hoffmans and Verheij, 1997). The difference in the results compared to the study of McGovern et al. (2014) is likely to be a result of the removal of upstream ripples in the present tests and this is discussed in greater detail in Section 7.2.3.

In Figures 6.66-6.68 the scour depth measured using the pile scale is also marked demonstrating the excellent agreement between the two techniques, as was discussed in Section 4.4.5.

Note that the position of the flat bed level on the upstream side of the scour hole in Figure 6.68 is approximately 8 mm above the zero level. This is due to a misalignment between the smoothing level and the level of the base section of the pile. A simple correction could be applied to account for this misalignment by increasing the recorded scour depths by the size of the discrepancy. However, this would not affect the results in relation to the comparison with test C.90.19 as the scour depth after the first half cycle would still be greater in test C.90.19 than in test C.90.18.

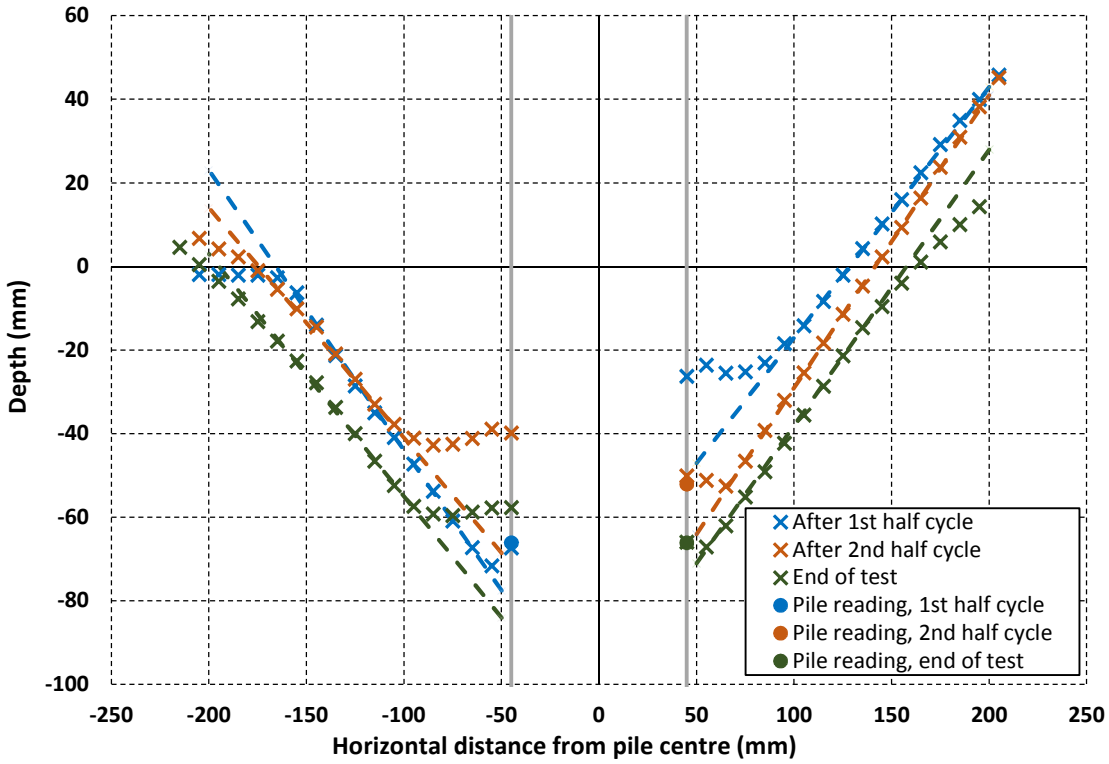

Figure 6.66 Interpolated streamwise scour hole profiles from the photogrammetry data for test C.90.19 (spring-neap test in uniform coarse sand) with fitted lines to estimate upstream and downstream slope angles.

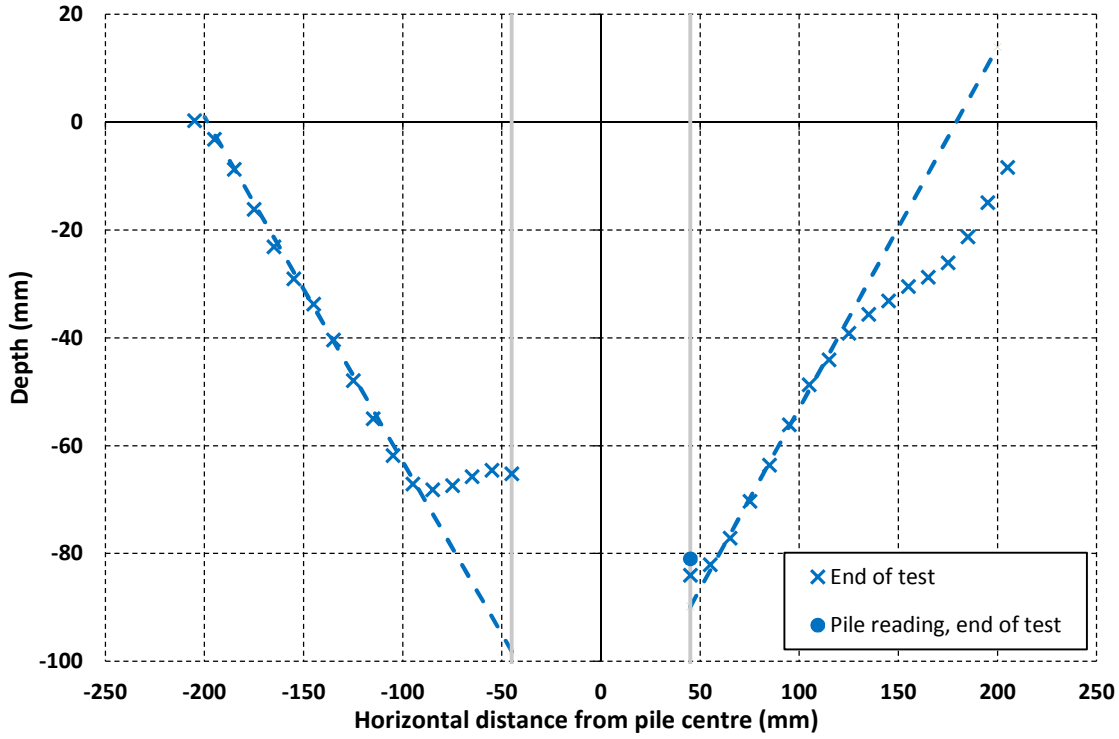

Figure 6.67 Interpolated streamwise scour hole profiles from the photogrammetry data for test C.90.21 (spring-neap test in layered bed) with fitted lines to estimate upstream and downstream slope angles.

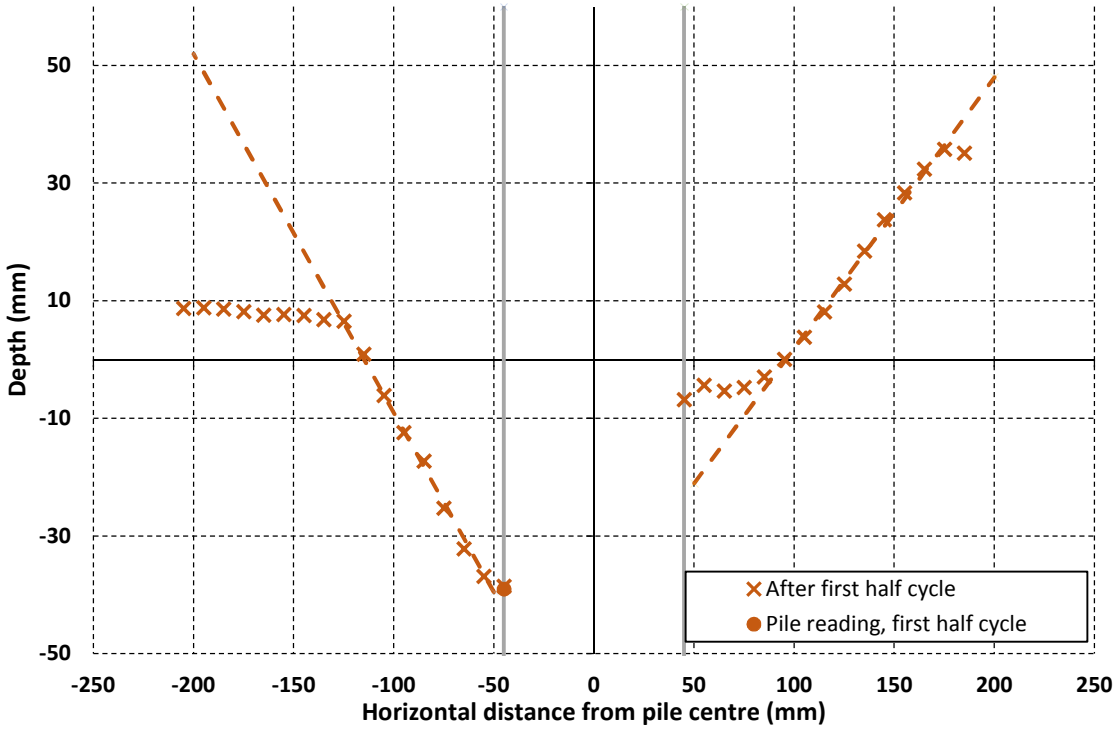

Figure 6.68 Interpolated streamwise scour hole profiles from the photogrammetry data for test C.90.18 (square wave reversing flow in uniform coarse sand) with fitted lines to estimate upstream and downstream slope angles.

6.7 Flow characteristics

This section presents the measurements of the flow velocity and wave heights for the tests. The measurements were predominantly undertaken over a flat sand bed without the pile in place prior to the start of each test series. Therefore, the results are applicable to a set of tests rather than individual cases. The velocity profiles for each test series are shown in Figures 6.69-6.73, and the depth-averaged velocities for each of these as well as the bed shear stress estimated from the profiles are given in Table 6.2. The methodology for estimating bed shear stress is given in Appendix 10.

Figure 6.69 gives the velocity profiles collected for the T-1 test series and tests R.10-R.12, over the fine, coarse and 50% mixed sand beds without the pile in place. There is good agreement between the profiles demonstrating that the velocity profile is consistent between the different sand beds probably because the magnitude of the fixed bed roughness on the upstream false bed over which the boundary layer developed was kept constant between the tests.

Figure 6.70 shows the velocity profiles measured by the LDV probe for tests R.13-R.17. Three profiles were taken and are in excellent agreement. Figure 6.71 gives the LDV velocity profile for test R.18. Again there is excellent agreement between the repetitions.

The velocity profiles in Figure 6.72 relate to tests R.19-R.29. In this figure the profiles are taken at 3 different locations along the flume, 5 cm and 30 cm upstream of the pile centre, and 30 cm downstream of the pile centre, without the pile in place. There is very good agreement between

the profiles. This means that there is no discernible difference in the velocity profile with distance along the flume, in the vicinity of the pile and sand bed. This suggests that the velocity profile is fully developed when it reaches this section of the flume as was the aim in the experiment design.

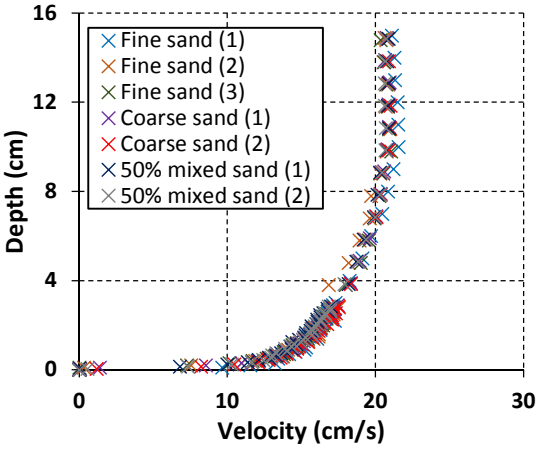

Figure 6.69 LDV streamwise velocity profiles for flow conditions used in the T-1 test series and tests R.10-R.12, small flume.

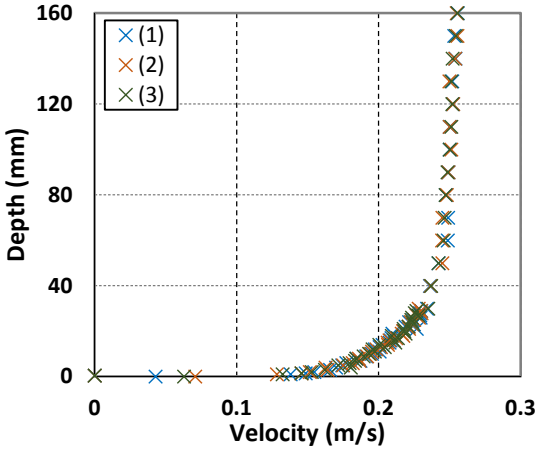

Figure 6.70 LDV streamwise velocity profiles for flow conditions used in tests R.13-R.17, small flume.

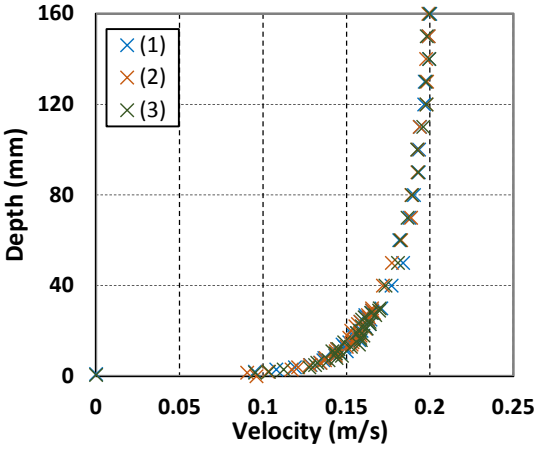

Figure 6.71 LDV streamwise velocity profiles for flow condition used in test R.18, small flume.

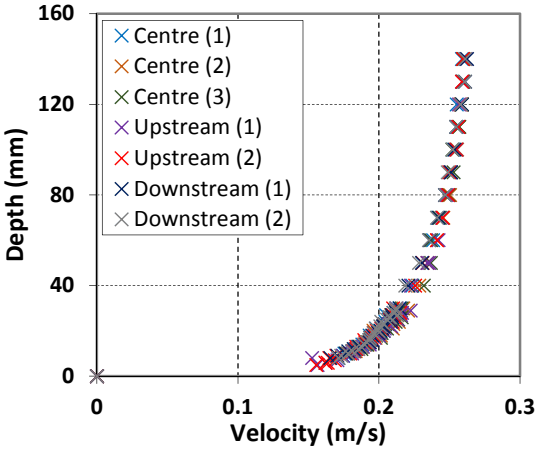

Figure 6.72 LDV streamwise velocity profiles for flow conditions used in tests R.19-R.29, small flume, at three different positions along the flume.

During test series R-3 it was noticed that two different water depths, 16 cm and 16.5 cm could be attained with the same valve positions due to an instability in the flow over the downstream weir gate. LDV profiles were collected for each of these cases to quantify the difference in the velocity profile. There is a noticeable although small difference in velocity due to this seen in Figure 6.73 and the depth-averaged velocity is altered by 0.8 cm/s. Therefore, care was taken to ensure the water level remained constant at the 16 cm depth during the test series.

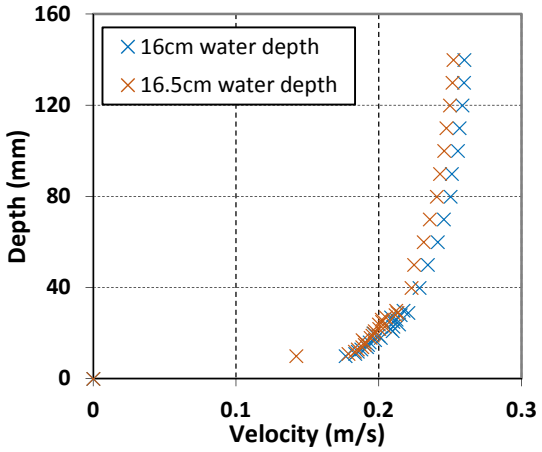

Figure 6.73 Comparison of LDV streamwise velocity profiles with water depths of 16 cm and 16.5 cm in the small flume.

In Table 6.2 it can be seen that the depth-averaged velocity in test series R-2 and R-3 are similar so that direct comparison between these tests may be possible. However, there is greater difference between the estimated bed shear stress for these two test series. Furthermore, test series R-2 has the higher depth-averaged velocity, but lower bed shear stress estimate than test series R-3. This needs to be taken into account when comparing the results from these two test series.

Table 6.2 Depth-averaged velocity and bed shear stress estimates from LDV profiles measured in the small flume.

Test series	Description of profile	Depth-averaged velocity (cm/s)	Depth-averaged velocity per set (cm/s)	u* (m/s)	τ (kg/ms^2)	Average τ per set (kg/ms^2)
R-3	Centre (1)	23.2	23.3	0.013	0.176	0.182
	Centre (2)	23.3		0.014	0.191	
	Centre (3)	23.38		0.013	0.179	
	Upstream (1)	23.5	23.4	0.013	0.182	0.188
	Upstream (2)	23.4		0.014	0.194	
	Downstream (1)	23.2	23.2	0.014	0.190	0.189
	Downstream (2)	23.1		0.014	0.188	
R-2	(1)	23.9	23.9	0.013	0.169	0.163
	(2)	23.9		0.013	0.169	
	(3)	23.9		0.012	0.151	
R-3	16.5 cm water depth	22.5	22.5	0.012	0.155	0.155

R-2, test R.18	(1)	18.4	18.3	0.009	0.087	0.082
	(2)	18.2		0.009	0.079	
	(3)	18.3		0.009	0.080	
T-1 and R-1	Fine (1)	19.6	19.2	0.011	0.125	0.125
	Fine (2)	18.9		0.010	0.105	
	Fine (3)	19.1		0.012	0.135	
	Coarse (1)	19.2	19.2	0.011	0.128	
	Coarse (2)	19.3		0.010	0.108	
	50% mix (1)	19.1	19.1	0.011	0.127	
	50% mix (2)	19.1		0.012	0.147	

Velocity profiles in the larger flume were measured with an ADV probe, due to practical constraints of using the LDV probe in this setting. However, in contrast with the ADV performance in the small flume (see Section 4.5) the noise in the ADV signal was generally acceptable at this larger scale and it was possible to obtain reliable measurements in most cases, although the vertical resolution was not sufficient to obtain estimates of bed shear stress from logarithmic plots of the velocity profiles.

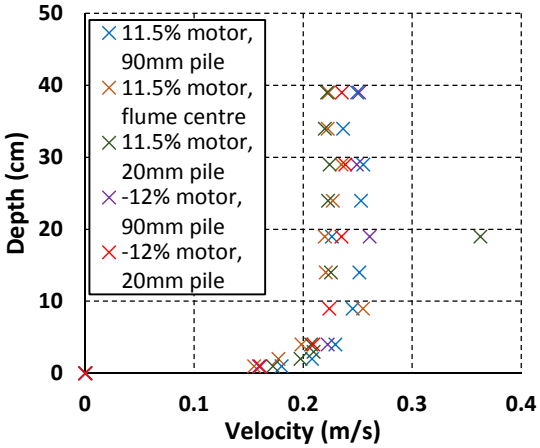

Figure 6.74 ADV streamwise velocity profiles in the coastal flume in the forward and reverse directions, at different locations in the cross-stream direction.

Figure 6.74 shows the velocity profiles measured prior to the scour tests in the larger flume at the two current flow rates that were used predominantly in test series C-1 (flume motor speed set to -12% and +11.5% in the forward and reverse directions respectively). The profiles were taken at different locations in the cross-stream direction and show that there is a certain degree of variation in the flow velocity across the flume. The flow at the location of the small pile is slower compared to that at the larger pile. This will be taken into account when considering these tests in Section 7. Also noticeable in the profiles is the greater deviations in expected profile shape in the positive direction compared to the negative direction. This implies that there

is a greater level of turbulence in the positive flow direction compared to the negative flow direction. There is also an outlier in the small pile 11.5% profile at a depth of 20 cm which is discounted from the depth-averaged velocity calculation for this profile. This outlier is probably due to noise in the ADV signal. It was observed that the ADV signal quality varied with position in the flume, with measurements being difficult at certain locations due to excessive noise, although this occurred to a much lesser extent than in the small flume. The depth-averaged velocities in the forward and reverse directions at the locations of each of the piles computed from these profiles are given in Table 6.3.

Figures 6.75-6.80 show the velocity profiles measured with an ADV probe at the location of each of the piles for the 3 current velocities tested in the C-2 test series in the larger flume. The depth-averaged velocities for each case are given in Table 6.3.

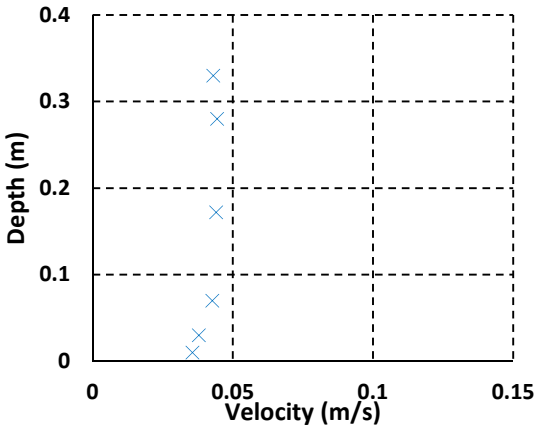

Figure 6.75 ADV streamwise velocity profile at the location of the small pile in the coastal flume, 2.5% motor speed (unidirectional current).

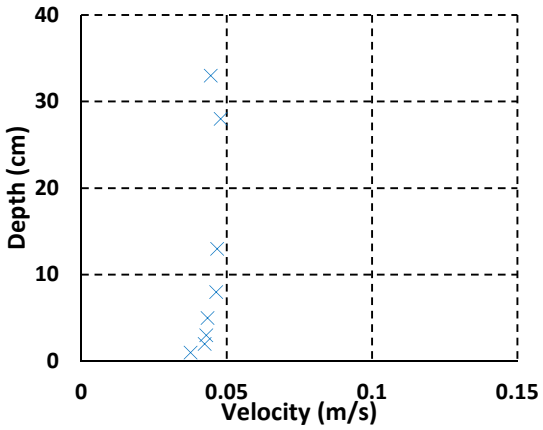

Figure 6.76 ADV streamwise velocity profile at the location of the larger pile in the coastal flume, 2.5% motor speed (unidirectional current).

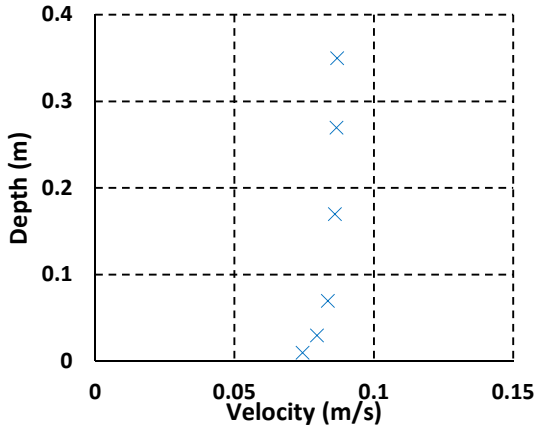

Figure 6.77 ADV streamwise velocity profile at the location of the small pile in the coastal flume, 4.8% motor speed (unidirectional current).

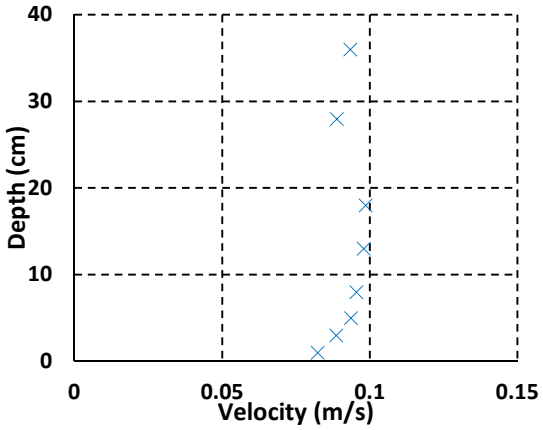

Figure 6.78 ADV streamwise velocity profile at the location of the larger pile in the coastal flume, 4.8% motor speed (unidirectional current).

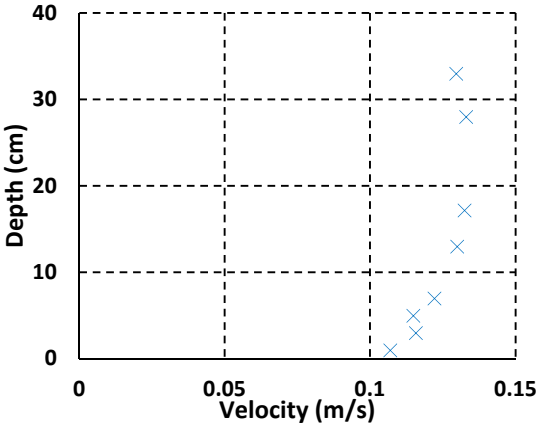

Figure 6.79 ADV streamwise velocity profile at the location of the small pile in the coastal flume, 6.9% motor speed (unidirectional current).

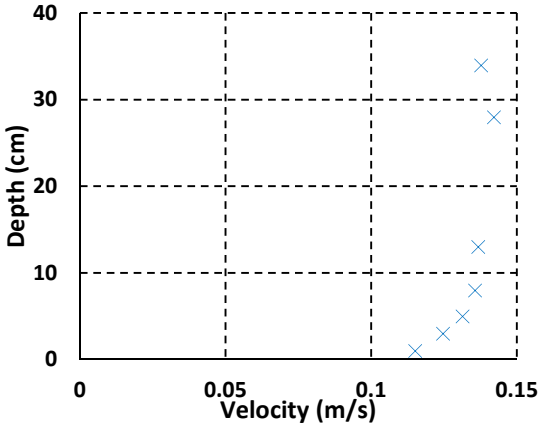

Figure 6.80 ADV streamwise velocity profile at the location of the larger pile in the coastal flume, 6.9% motor speed (unidirectional current).

Figures 6.81-6.87 present the average maximum and minimum velocity profiles under the wave-current and wave alone conditions that were used in the C-2 test series. The depth-averaged velocities and maximum bottom orbital velocity are presented in Table 6.3.

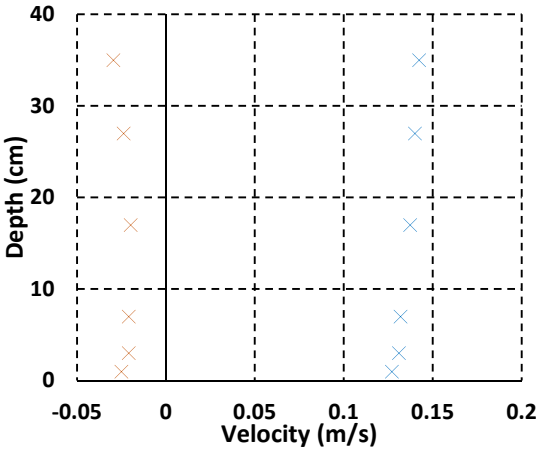

Figure 6.81 Maximum and minimum ADV streamwise velocity profiles at the location of the small pile in the coastal flume in wave-current flow, 2.5% motor speed, 2.5 s wave.

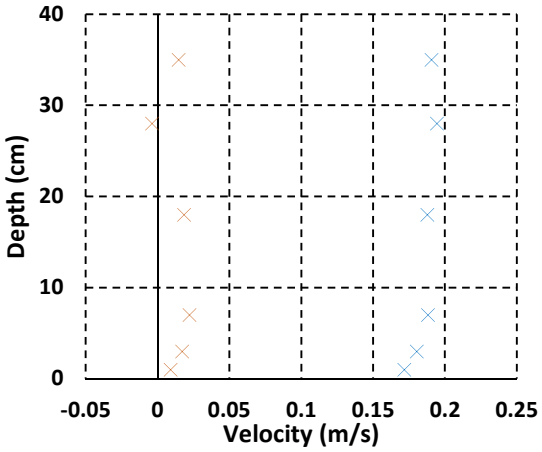

Figure 6.82 Maximum and minimum ADV streamwise velocity profiles at the location of the small pile in the coastal flume in wave-current flow, 4.8% motor speed, 2.5 s wave.

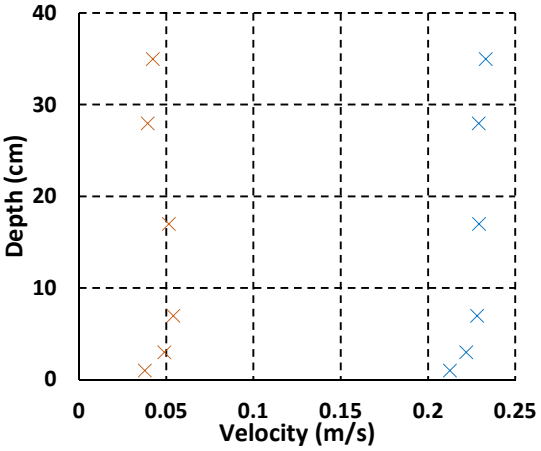

Figure 6.83 Maximum and minimum ADV streamwise velocity profiles at the location of the small pile in the coastal flume in wave-current flow, 6.9% motor speed, 2.5 s wave.

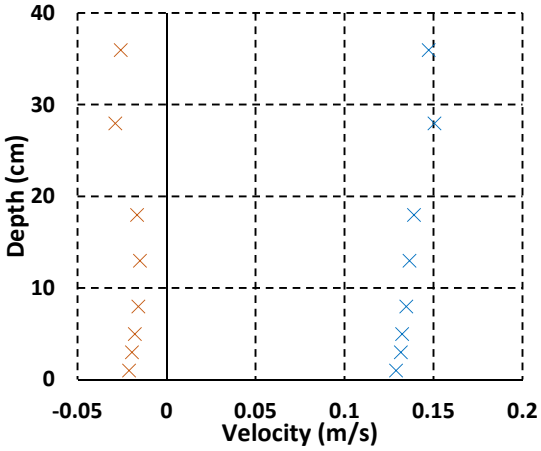

Figure 6.84 Maximum and minimum ADV streamwise velocity profiles at the location of the larger pile in the coastal flume in wave-current flow, 2.5% motor speed, 2.5 s wave.

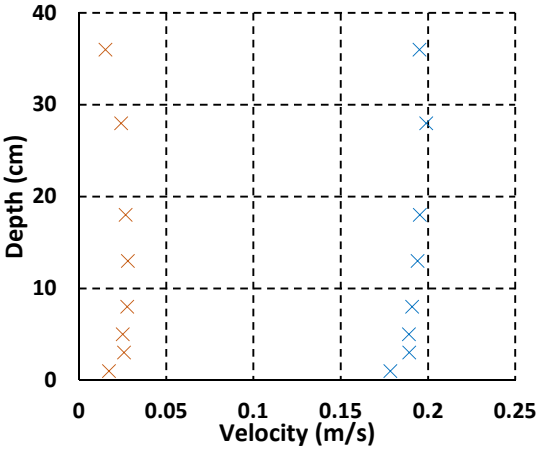

Figure 6.85 Maximum and minimum ADV streamwise velocity profiles at the location of the larger pile in the coastal flume in wave-current flow, 4.8% motor speed, 2.5 s wave.

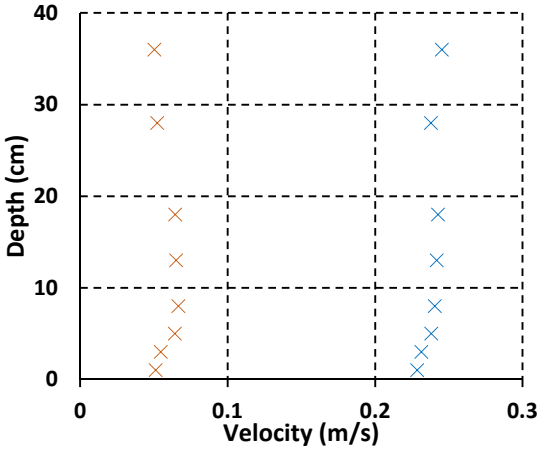

Figure 6.86 Maximum and minimum ADV streamwise velocity profiles at the location of the larger pile in the coastal flume in wave-current flow, 6.9% motor speed, 2.5 s wave.

It is clear in Figures 6.81-6.86 that one of the wave-current tests has a reversal of flow direction, one reduces to just above zero in each half cycle and one remains in the positive flow direction throughout the wave period. This is close to the design objective so that one test is in the wave-dominated regime, one is in the current-dominated regime and one is close to representing the in-between case with approximately equal wave and current contributions.

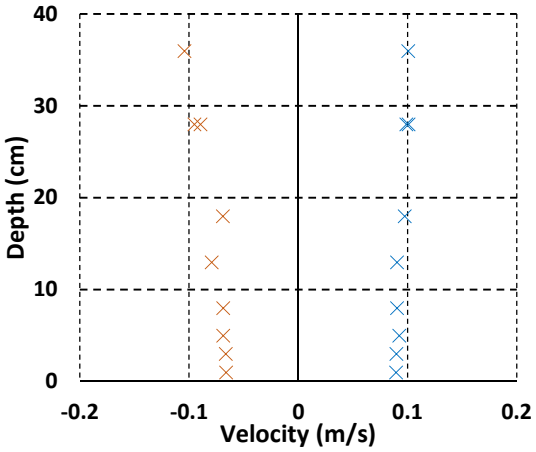

Figure 6.87 Maximum and minimum ADV streamwise velocity profiles in the coastal flume in wave alone (2.5 s wave).

Table 6.3 Flow conditions used in test series C-1 and C-2 in the coastal flume.

Motor speed	Ave. wave height (cm)	Small pile		Larger pile	
		Depth-ave. velocity max; min (cm/s)	U_m	Depth-ave. velocity max; min (cm/s)	U_m
11.5%	-	21.7	-	23.9	-
-12%	-	22.6	-	24.1	-
2.5% current	-	4.2	-	4.5	-
4.8% current	-	8.4	-	3.4	-
6.9% current	-	12.7	-	13.5	-
Wave only	4.7	9.5; -8.4	9.0	9.5; -8.4	9.0
Wave and 2.5% current	4.5	13.6; -2.4	12.7	14.0; -2.2	12.9
Wave and 4.8% current	4.3	18.7; 1.5	17.2	19.2; 2.2	17.8
Wave and 6.9% current	4.3	22.6; 4.5	21.2	23.8; 5.6	22.8

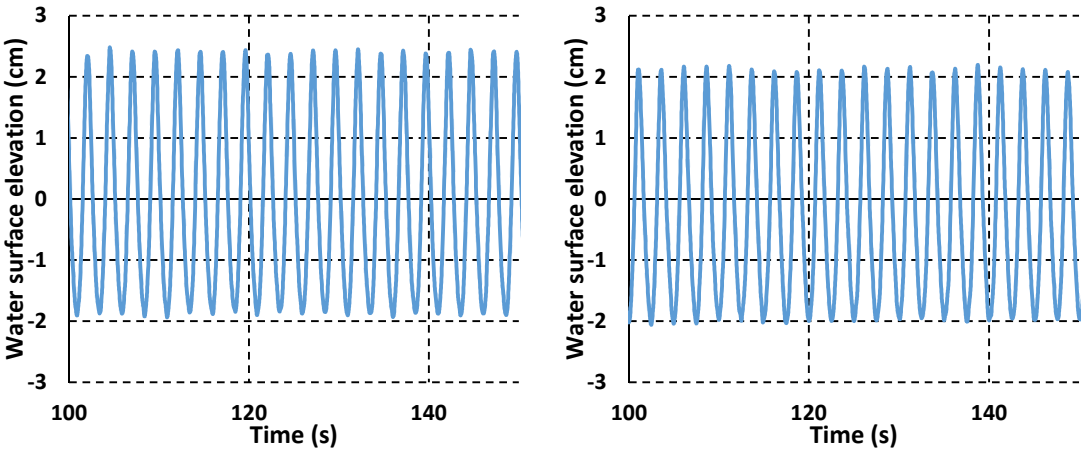

a) b)

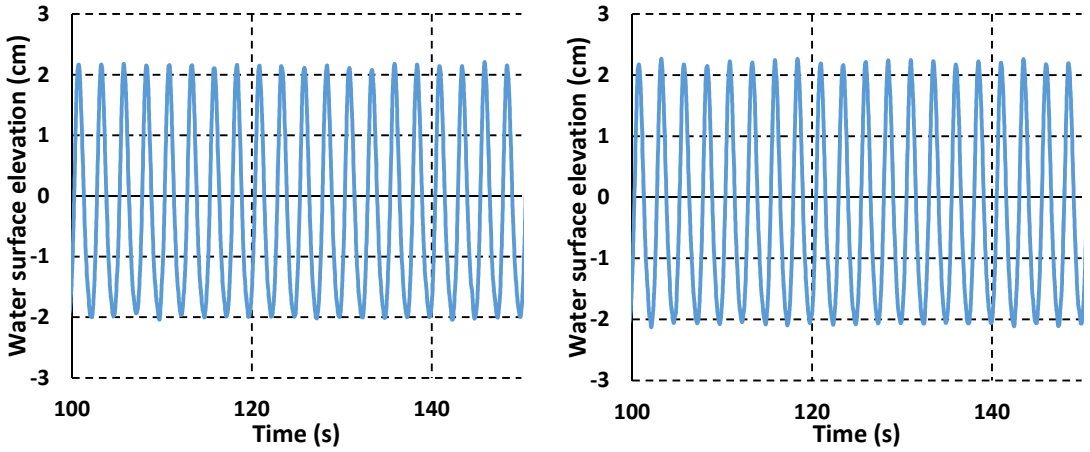

c) d)

Figure 6.88 Typical water surface elevation upstream of the pile a) wave alone b) wave and 6.9% current c) wave and 4.8% current d) wave and 2.5% current.

The typical water surface profile for the wave is shown in Figure 6.88a. There was some variation in the wave height along the flume (see Appendix 9) and the average wave height between the 5 probes was 4.7 cm. The water surface elevation is similar in the three wave-current combinations, Figures 6.88b, 6.88c and 6.88d.

6.7.1 Flow visualisation

Flow visualisation was conducted during test R.24, with a uniform coarse sand bed. While the original objective was to conduct flow visualisation in a range of test conditions, this was not possible due to the filters becoming blocked with the seeding particles during this test (see Appendix 3). However, the results from the visualisation (Figure 6.89) are useful in that they provide a picture of the flow around the pile and enable the key flow features to be identified and compared with the literature. On the left hand side (upstream) of the pile the particle streaks are aligned horizontally, but start to bend downwards as they approach the pile, defining the downflow (see Figure 6.89a). The downflow profile is also shown as the particles bend to a greater extent nearer to the bed. On the left hand side of the pile (upstream side) there is a clear distinction between the uniform particle streaks above the level of the scour hole and the vortex flow in the scour hole. The horseshoe vortex is clearly visible in Figures 6.89b and 6.89d and is present along the entire upstream scour hole slope, although the main vortex core is closer to the pile. In Figure 6.89b the horseshoe vortex is most clear and is made up of at least 3 smaller interacting vortices the positions of which match that described by Dargahi (1989). On the right hand side of the pile the streaks are more chaotic, indicating the wake, and there are clear vertical components to the flow (see Figure 6.89a).

The lip in the upstream scour hole slope is also clearly visible at the bottom of the scour hole (Figures 6.89a and 6.89b), indicating the presence of the vortex on the bed which results in the entrainment of sediment and instigates avalanching effects on the slope as the strength of the vortex fluctuates.

In Figures 6.89c and 6.89d the laser sheet was repositioned to the nearside of the flume so there is no gap in the flow visualisation. Here the horseshoe vortex can still be seen on the upstream side of the pile and deflection of the flow around the pile sides can be observed.

a)

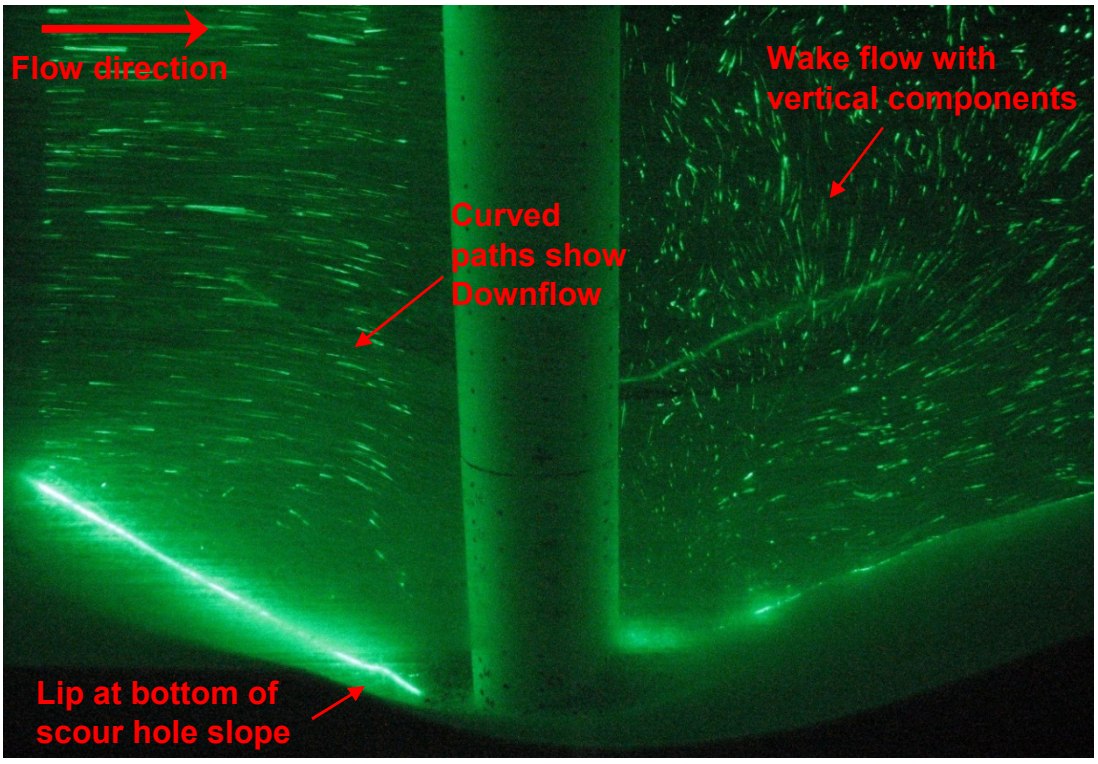

b)

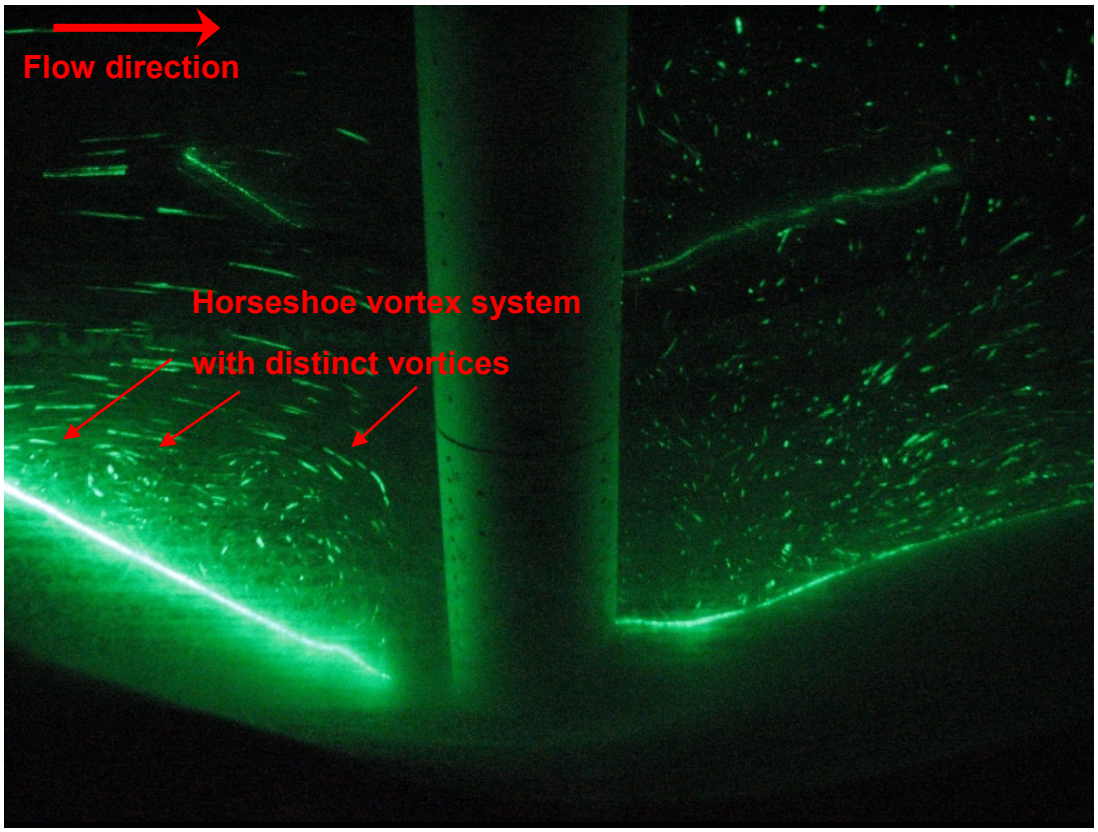

c)

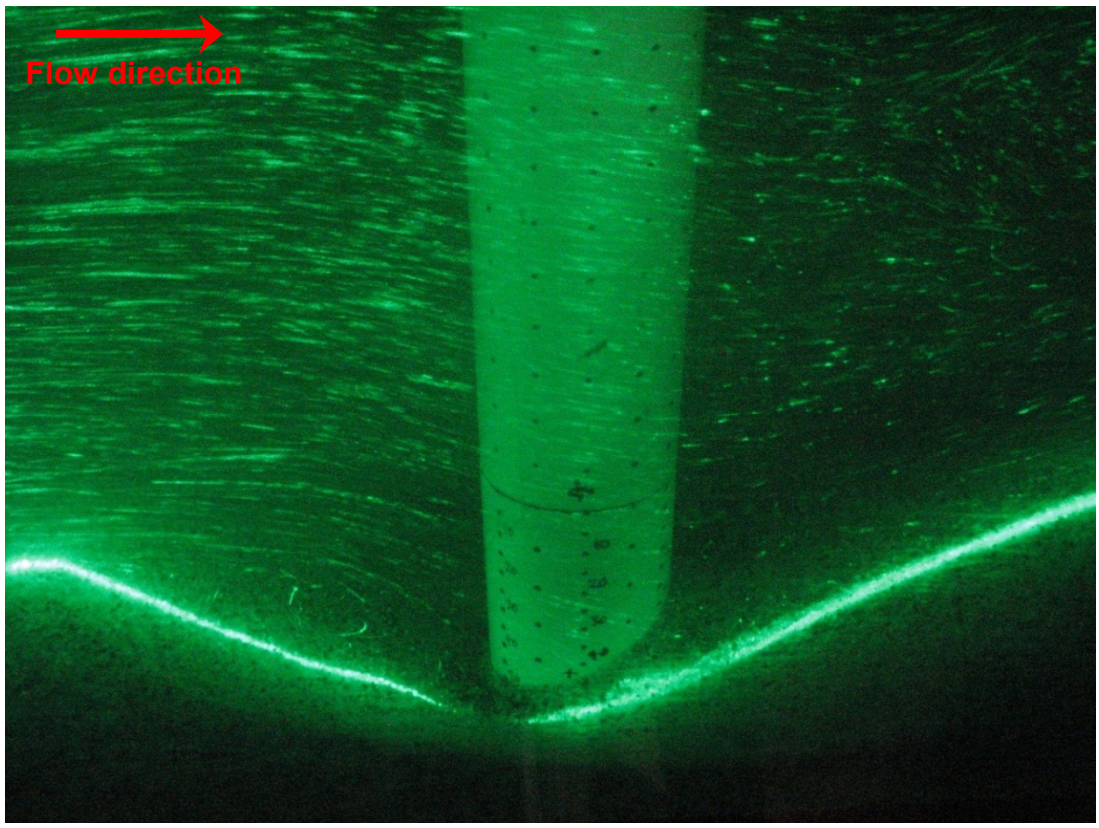

d)

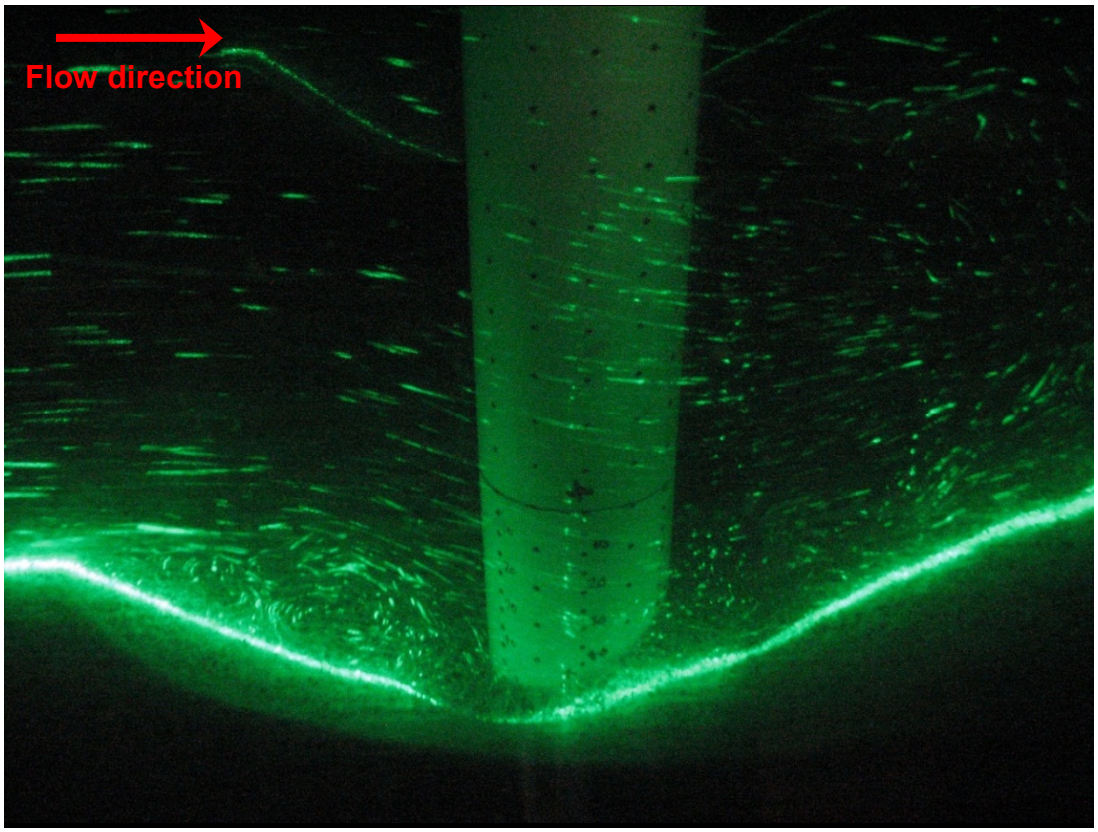

Figure 6.89 Flow visualisation technique of flow in the scour hole around the pile in the streamwise direction in the small flume, a) and b) laser sheet positioned along centreline of scour hole, c) and d) laser sheet positioned to the side of the pile in the cross-stream direction.

6.8 Sediment properties

Additional measurements were collected in relation to the properties of the sediments. This section discusses the sieve analysis of the different sands, the bulk density and permeability measurements. The results from the core sampling technique are discussed in Section 6.9.

6.8.1 In-situ sediment density

The density of the sand bed was measured in four tests, R.25, R.26, R.N.27 and R.28. As described in the methodology Section 4.3.2, plastic pots were located at nine different positions in the bed, at three different depths. The general layout of these is shown in Section 4.3.2 and the exact locations in each of the tests are given in Appendix 5. The aim of these measurements was firstly to get an indication of the variability in the bulk density across the bed, and secondly to ascertain the difference in bulk density between tests. Table 6.4 shows the bulk density measured from the pots at each of the depths. Tests R.25, R.26 and R.27 were set up with a 'loose' sand bed following normal procedures, whereas in test R.28 a concrete poker was used to create a denser sand bed as discussed in Section 4.1.1.

Table 6.4 Bulk density measured in the flume test bed during tests R.25, R.26, R.N.27 and R.28 in uniform coarse sand in the small flume.

	Bulk density, ρ_b (g/cm^3)			
Depth above flume bottom (cm)	**R.25**	**R.26**	**R.N.27**	**R.28**
0	1.55	1.52	1.56	1.71
0	1.53	1.52	1.59	1.70
0	1.54	1.522	1.55	1.72
2	1.51	1.52	1.58	1.71
2	1.53	1.53	1.59	1.72
2	1.55	1.51	1.57	1.69
4	1.52	1.52	1.62	1.71
4	1.55	1.51	1.57	1.71
4	1.55	1.50	1.58	1.71
Average	**1.54**	**1.52**	**1.58**	**1.71**

It can be seen from Table 6.4 that the density difference between the pot locations and depths is small for each test indicating that the density is reasonably homogenous across the bed.

The density is very similar between tests R.25, R.26 and R.N.27. The slightly higher average density in test R.N.27 (Table 6.4) may be due to the test bed preparation being undertaken by a different operator (see Appendix 3). However, the difference in density between these three tests is small, meaning that the test methodology is reasonably consistent, at least for this flume. It is clear in Table 6.4 that using the concrete poker has resulted in a denser sand bed in Test R.28. However, the sand in test R.28 would still be considered a 'loose' sand compared to typical values for dense sand given in the literature. According to Subramanian (2010) a more

typical bulk density for 'dense' sand would be around 2 g/cm^3, and loose sand typically has a bulk density of 1.7-2 g/cm^3, while the bulk density of dense sand is typically 1.9-2.2 g/cm^3. Therefore the increase in density in Test R.28 is relatively small, and this should be borne in mind when considering the scour development results for this test.

6.8.2 Ex-situ bulk density

The dry bulk density of samples of each of the uniform and mixed sands was also measured. Figure 6.90 shows the density measurements for these samples. For the fine and coarse sands, initial density measurements were taken for both loose and shaken samples, before developing a more consistent method for measuring the density of dry, loose samples for all of the sand types, as detailed in Section 4.3.2. It can be seen in Figure 6.90 that the initial loose samples gave similar results to those obtained using the refined methodology, indicating that the results are fairly insensitive to the differences in these methodologies. It can be seen that after shaking the samples the bulk density increases by the order of 0.1 g/cm^3 but this is still well within the range considered 'loose' in the literature (see above).

For the fine sand, the dry density of a saturated sample was also collected. Again, the loose sample is in close agreement with the other two loose samples for this sand, indicating that this has little effect on the bulk density. A shaken wet sample was also tested which gave a similar result to the dry shaken sample. As there was little difference between saturated and dry samples, further wet samples for the other sands were not collected.

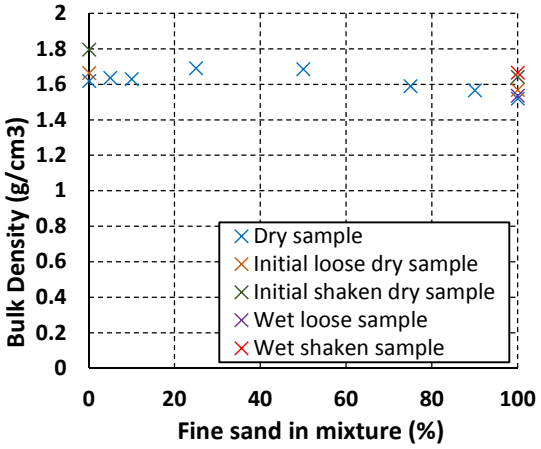

Figure 6.90 Ex-situ bulk density measurements of samples of the mixed and uniform sands.

When comparing the mixed sand samples and the uniform samples in Figure 6.90 there is only a very small variation in density between the sand types. The most non-uniform mixtures have the highest bulk density, which is in agreement with Subramanian (2010) who states that well graded, non-uniform sands will have a higher bulk density than poorly graded, more uniform sands. However, the difference in bulk density is still small so it is unlikely that this parameter has much of a bearing on scour behaviour in the mixed compared to uniform sands.

Another point to note from Figure 6.90 is that the sand with the lowest density is the uniform fine sand. This is in agreement with the factory bulk density data where the loose bulk density of the fine sand is quoted as 1.43 g/cm^3 compared to 1.569 g/cm^3 for the coarse sand. Although these figures are lower than the measurements in Figure 6.90 probably due to differences in the testing methodologies, it is consistent that the fine sand has the lower density. The difference in density between the fine and coarse sands is related to the variability of other properties such as the shape parameters of the particles.

Importantly, the density of the dry sand samples is in the same region as the in-situ density measurements discussed in the previous section. This helps to validate the methodology for density measurement.

6.8.3 Permeability

To help to improve understanding of scour processes in the mixed sands, the permeability of each of the mixtures was measured in a permeameter, following the method discussed in Section 4.3.3. Figure 6.91 shows the results for both constant head and falling head tests. It is clear from the graph that there is very good agreement between these test types which provides confidence in the results.

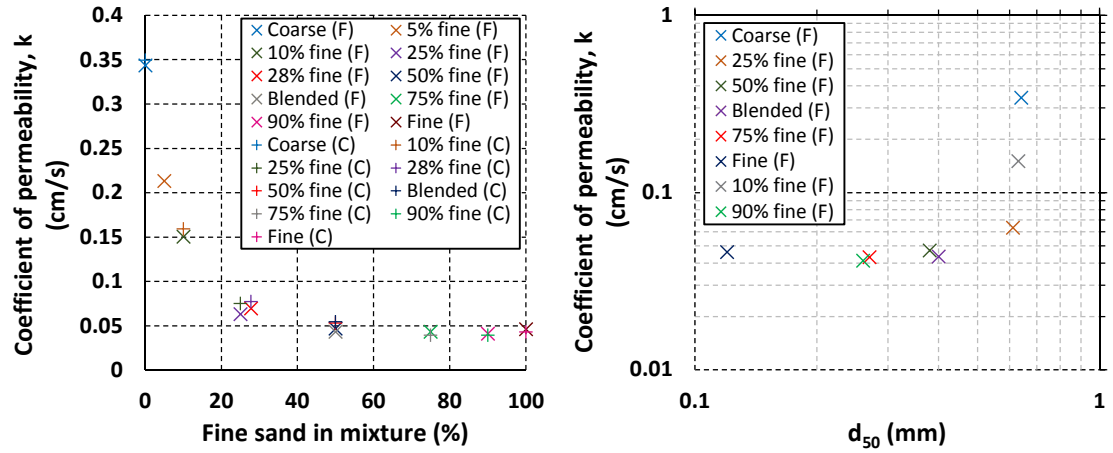

a) b)

Figure 6.91 Permeability of the mixed and uniform sands, (F) falling head test, (C) constant head test a) plotted against percentage of fine sand in the mixture b) plotted against median grain size with logarithmic axes.

Figure 6.91a shows that as the proportion of fine sand in the mixture increases (and hence d_{50} decreases) the permeability decreases. This is as expected from the literature (Blanco, 2003) as the smaller grains in fine sands make it more difficult for water to find paths through. The permeability drops off exponentially as a small percentage of fine sand is added to the coarse sand, and hence there is a relatively large difference in permeability between the coarse sand and the 10% fine, 90% coarse sand mixture. There is little change in permeability beyond a percentage of 50% fines in the mixture.

It should be noted that in comparison to other materials, the difference in permeability between these sands is relatively small. For example the typical permeability of silts and clays is several orders of magnitude lower than the permeabilities for these sands which are of a similar order of magnitude to each other. However, the permeability drops by over half between the coarse sand and the 10% fine sand mixture. It should be considered whether this may be significant enough to have an impact on scour development, and this will be discussed further in Section 7.2.2 in relation to scour in the mixed sands with low percentage of fine sand. The permeability drops by almost half again between the 10% and 25% fine sand mixtures before levelling off for the remaining mixtures.

According to Shepherd (1989) the variation in permeability with grain size should form a straight line on a log-log plot with permeability increasing with grain size. However, considerable scatter is expected in the data due to the other parameters that are known to affect permeability. The data are shown in this format in Figure 6.91b. The significant deviation from the straight line for this data set shows the extent of the effect of other factors (i.e. the sediment non-uniformity) on the permeability characteristics of these sands.

6.8.4 Grading curves

The grain size distribution of each of the uniform and mixed sands was measured in order to quantify the key parameters such as the mean particle size and the sediment uniformity.

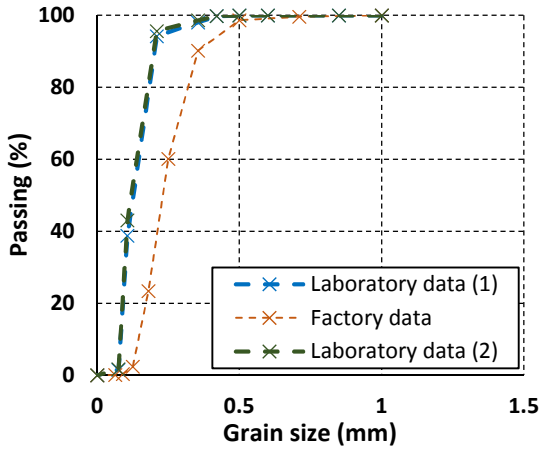

Figure 6.92 Fine sand grain size distribution, comparison of laboratory measurements with factory data sheet.

Figure 6.92 shows a comparison of the factory-provided data for the fine sand with the sand distribution measured in the laboratory following the methodology in Section 4.3.1. There is quite a difference between the two. To check the validity of the in-house measurement, a second sample was sieved, also shown in Figure 6.92. The two measurements in-house show very close agreement. The difference between these results and the factory results may be due to the use of different test procedures. However, one would expect the sieving conducted in the

laboratory to represent the sand as a coarser distribution, so that the curve would be to the right of the factory data in Figure 6.92, as in the laboratory the sieving process was completed by hand and so it is likely that not all of the grains would fall through the appropriate sieve size in the limited time. In an automated sieving test, the sieves would be shaken at higher frequency and for a longer time until no further grains pass through the sieves, which would result in a shift of the curve to the left as a greater proportion of grains pass through the sieves. The factory data being on the right hand side suggests that either the factory methodology was more approximate than the laboratory method, or that there is some variation in the sand being collected from the quarry. As it is unclear as to the assumptions and methods used by the factory, the quantification of the sand parameters will be taken from the laboratory data, which relates to the actual sand used in the scour tests. This means that despite ordering a sediment that would have a d_{50} of 0.2 mm, the fine sand actually has a d_{50} of 0.12mm. The uniformity parameter of the fine sand, however, is similar between the in-house and factory data.

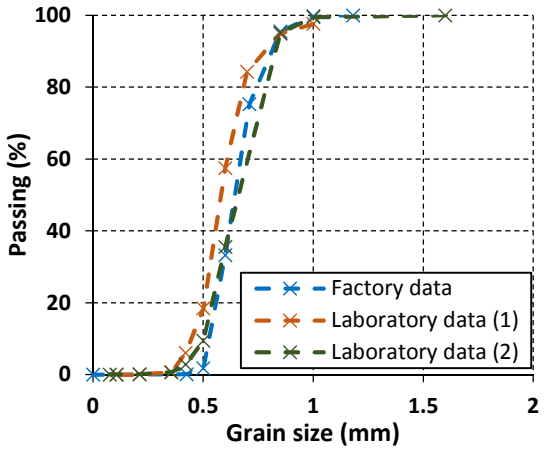

Figure 6.93 Coarse sand grain size distribution, comparison of laboratory measurements with factory data sheet.

As with the fine sand, the coarse sand grain size distribution was checked in the laboratory. In Figure 6.93 the factory data is shown along with two sieve analyses completed in the laboratory for different samples of the coarse sand. The agreement between all three curves is very reasonable. However, the sieve analysis in the laboratory showed that the sand contained slightly more fines than the factory data suggested, making it a little less uniform than the factory data. The laboratory data are used in the analysis instead of the factory data for the same reasons as discussed for the fine sand.

Figure 6.94 shows two sieve analyses for the 50% mixed sand. The two curves were measured at different times, with different samples, but the agreement is very good, indicating consistency in the methodology for sieving, and consistency in the sample preparation of the mixed sand.

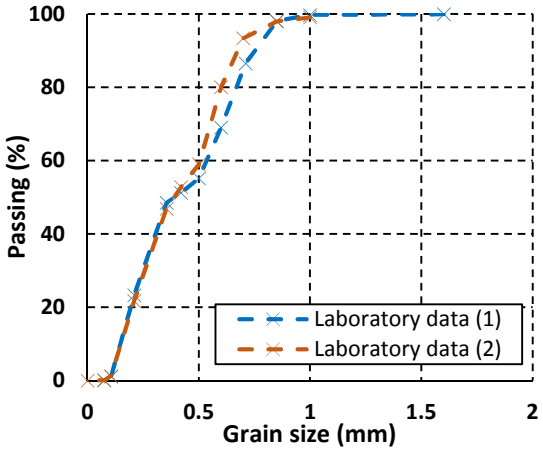

Figure 6.94 50% fine, 50% coarse mixed sand grain size distribution.

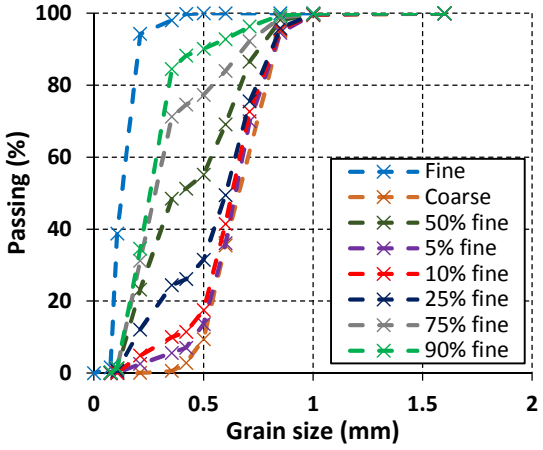

Figure 6.95 Grain size distributions for each of the mixed and uniform sands.

Figure 6.95 shows the grading curves measured in the laboratory for each of the sand mixtures along with the standard fine and coarse sands, and these curves were used to obtain the sediment grading properties given in Table 6.5. The curves in Figure 6.95 clearly show the bi-modal nature of the mixtures by the inflection in the middle of these curves. This is most pronounced for the 50% mixture and least so for those mixtures with less even proportions of fine to coarse sand.

Note the inclusion of a 5% fine sand mixture in Table 6.5. This mixture was not used in the scour tests but was added for the grain size distribution, permeability and bulk density measurements to better define the trends and improve understanding of scour behaviour for mixtures with a low percentage of fine sand.

Table 6.5 Key parameters of the grain size distributions for each of the mixed and uniform sands including median grain size and geometric standard deviation.

Grain size	coarse	coarse factory data	5% fine	10% fine	25% fine	50% fine	75% fine	90% fine	fine	fine fact. data	Ave. fine sand
d_{50}	0.58	0.64	0.64	0.63	0.61	0.38	0.27	0.26	0.12	0.23	0.18
d_5	0.41	0.51	0.32	0.22	0.14	0.13	0.12	0.12	0.08	0.14	0.11
d_{10}	0.46	0.54	0.47	0.35	0.19	0.15	0.14	0.14	0.09	0.15	0.12
d_{16}	0.49	0.55	0.51	0.49	0.25	0.18	0.16	0.15	0.09	0.17	0.13
d_{25}	0.52	0.58	0.56	0.54	0.36	0.22	0.19	0.18	0.1	0.18	0.14
d_{60}	0.61	0.67	0.67	0.66	0.64	0.54	0.31	0.28	0.14	0.25	0.20
d_{75}	0.66	0.71	0.73	0.72	0.71	0.63	0.43	0.33	0.16	0.29	0.23
d_{84}	0.7	0.75	0.78	0.77	0.76	0.69	0.6	0.35	0.18	0.33	0.26
d_{90}	0.75	0.79	0.81	0.8	0.8	0.74	0.68	0.5	0.19	0.35	0.27
d_{95}	0.85	0.84	0.85	0.85	0.84	0.8	0.76	0.66	0.22	0.4	0.31
$C_u=d_{60}/d_{10}$	1.33	1.24	1.43	1.89	3.37	3.6	2.21	2	1.65	1.67	1.67
$\sigma_g=d_{84}/d_{50}$	1.21	1.17	1.22	1.22	1.25	1.82	2.22	1.35	1.50	1.43	1.47
$\sigma_g=d_{50}/d_{16}$	1.18	1.16	1.25	1.29	2.44	2.11	1.69	1.73	1.33	1.35	1.34
$\sigma_g=0.5(d_{84}/d_{50}+d_{50}/d_{16})$	1.20	1.17	1.24	1.25	1.84	1.96	1.95	1.54	1.42	1.39	1.41
$\sigma_g=\sqrt{(d_{84}/d_{16})}$	1.20	1.17	1.24	1.25	1.74	1.96	1.94	1.53	1.41	1.39	1.41

Two measures of grain size uniformity which are frequently used in the literature to define sands have been included in Table 6.5, namely the coefficient of uniformity and the geometric standard deviation. These give different results because of the shift in the shape of the distribution between the mixtures. Three definitions of σ_g are used in the literature (see Section 2.4.1). Each of these are included in Table 6.5. It can be seen that there is good agreement between these for the more uniform sand mixtures but for the sands with greater bimodality (25%, 50% and 75% fine sand mixtures) there is a significant difference between the values. This demonstrates the difficulty of defining non-uniformity of sands with complex distribution shapes and this will be discussed further in Section 7.3.2 with respect to scour modelling techniques in non-uniform sands.

6.9 Core samples

Core samples were taken at the end of a selection of tests to analyse the variation in the grain size distribution with depth at different locations in the scour hole. The core sample methodology underwent considerable development as discussed in Section 4.3.4 and the processing was a delicate operation as well as being time consuming. Consequently, it was not possible to obtain data for all tests, and there was quite a high rate of data loss due to issues with the methodology; in particular it was easy for samples to be destroyed during several of the processing stages (i.e. during removal of samples from the flume, removal of the samples from the tubes, and during oven drying). The data that were collected and processed are discussed in this section. Not every sample is included here, but only those pertinent to the discussion. The full data sets are given in Appendix 6 along with diagrams of the measured sample locations for each test.

It is important to bear in mind that the methodology for the core sampling technique was designed to enable a primarily qualitative analysis, and consequently there are a variety of factors such as compression of the samples and displacement of sand along the edges of the tube that mean that a quantitative analysis would not be appropriate. It is clear from the data that the samples give a reasonable representation of the general trends, as the key features that are expected to be seen in the data are present, such as the interface of the two sands in the layered tests, and intact sand in the bottom sections of the samples which have not been affected by the scour process. There is also good agreement in the representation of the uniform fine and coarse sands at different depths within samples, and between different samples and tests, demonstrating the consistency of the methodology.

6.9.1 Variability of intact mixed sands

One way in which the core samples are useful is to assess the degree of homogeneity of the sediment in the sand test bed, in particular for the mixed sand cases. While the samples indicate that the uniform coarse sand is reasonably homogenous, see Appendix 6, it is clear that there is greater variation in the mixed sediments compared to their design values. Table 6.6 shows the maximum difference in the proportion of fine sand to coarse sand in the mixed cases within and between samples. Note that in Table 6.6 the values do not include the top layer(s) of the samples where these may not be representative of the original sediment mixture due to the scour and sediment transport processes during a test.

The results in Table 6.6 show that the proportion of fine to coarse sand in a mixed bed can vary locally by up to 18% from the expected value. Although the proportions of fine and coarse sands were measured out carefully in order to construct the mixed sands, when the mixed sands were placed in the flume the actual proportion of fine to coarse sand varied quite substantially through the bed. It was observed during the test set-up that the fine sand in the mixed cases had the tendency to settle out of the mixture due to its slower settling velocity in water and this made it difficult to ensure an even mixture in the flume. It can be seen in Table 6.6 that there is slightly greater variability in the mixtures in the larger flume where the sediment bed is deeper

and at a larger scale, so there is more opportunity for the sediment to separate out, and it is more difficult to re-mix the sediment during filling of the flume test bed. The greater degree of fluctuation in the mixed test scour curves and the repeatability of these tests may be linked to the degree of heterogeneity of the bed and this is discussed in Section 7.2.2.

Table 6.6 Variability in the mixed sand distributions with depth in the scour test bed.

Test	Minimum coarse sand %	Maximum coarse sand %	Maximum percentage difference from design value
10% coarse R.10	7	13	3
75% coarse R.T.9	63	77	12
50% coarse R.T.11	47	63	13
50% coarse R.T.8	39	55	11
C.90.13 (50%)	36	60	14
C.90.14 (50%)	32	63	18

6.9.2 Preferential scouring and bed armouring

A second way in which the core samples allow insight to be gained into the scour processes in the mixed and layered sand beds is that any changes to the sediment grading distribution in the top layers of the samples compared to the initial bed configuration can be determined.

A significant result from this relating to the mixed sand tests is that the samples consistently show that there is little change from what would be expected initially in the top layer (see Figure 6.96 and Appendix 6). This is a key result because it indicates that in the mixed cases there is not preferential scouring of the fine sand particles from in-between the coarser material; if this were in fact the case, the top layer of the core samples would show an increase in the proportion of the coarse sand as a result of the coarse sand remaining in the scour hole while the fine sand was scoured. Critically, this means that the greater scour depth measured in the mixed cases compared to the uniform coarse sand tests is a result of both the fine and coarse sand proportions scouring, and the configuration of the mixed sand bed is enabling coarser particles to be eroded under the same flow conditions compared to in a uniform coarse sand bed.

In some of the samples (Figure 6.97 and Appendix 6) there is a small increase in the proportion of the coarsest grain size banding in the top layer of the sample. This is in agreement with visual observations of a thin armour layer forming in the scour hole over time. What is clear from the core samples is that the armouring process has only affected the very largest particles, so that the majority of the coarse sand particle sizes have been scoured along with the fine sand in the mixed bed tests.

It was observed that the scour depth continued to develop after the armour layer formed, indicating that the armour layer was not thick enough to prevent further scouring, and preferential scouring of particles smaller than the armour layer occurred (including the majority of the coarse sand particle sizes). This type of bed armouring was observed in a range of test

types including the uniform sands, not just in the mixed sand tests. This implies that it is a more general process rather than being specific to the sediment mixtures.

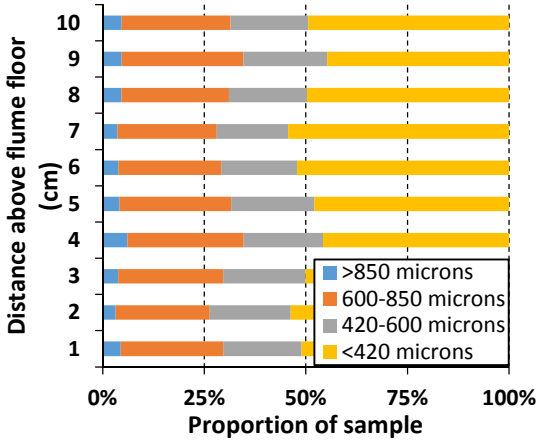

Figure 6.96 Core sample taken at end of test C.90.13 (50%-50% mixed sand) from the deepest part of the scour hole, directly upstream of the pile.

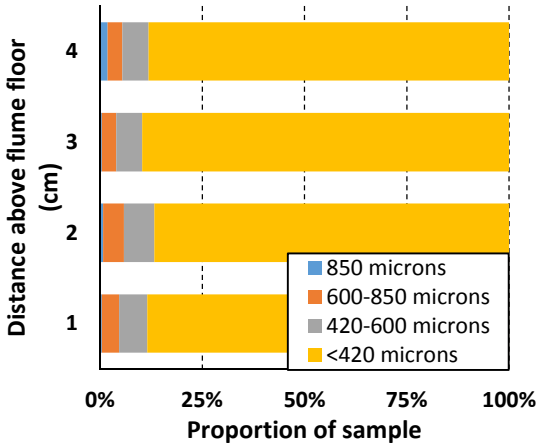

Figure 6.97 Core sample taken at end of test R.10 (90%-10% fine-coarse sand mix) from the deepest part of the scour hole, directly upstream of the pile.

Bed armouring identified by a greater proportion of the coarsest size banding (>850 microns) is not observed in all of the mixed sand samples. In fact many of the samples show no evidence of bed armouring. This lack of consistency may be due to limitations in the methodology rather than providing a true representation of the scour process. Therefore, the core sample analysis is focused on the general trends shown, and what is consistent between the samples for the mixed sand tests is the absence of any significant increase in the overall proportion of the coarse sand in the top layer of the samples, indicating that there has been no preferential scouring of the fine sand.

An interesting result is seen in the core sample shown in Figure 6.98, test C.90.13, as it has greater proportions of all bands of the coarse sand in the top centimetre than would be expected in the initial distribution. This sample was collected from far downstream of the scour hole where it was noticeable in the photographs that the fine and coarse sands were separating out, see Figure 6.99. This is due to dune formation and resultant sediment transport along the bed and shows the different rate of transport between the fine and coarse sands. Therefore, the result does not contradict the finding discussed previously in this section.

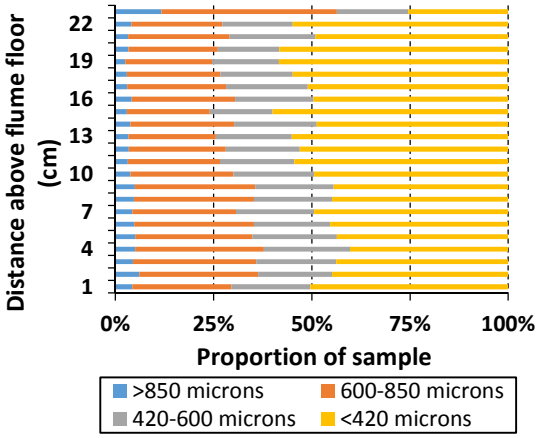

Figure 6.98 Core sample taken at end of test C.90.13 (50%-50% mixed sand) from the dune downstream of the scour hole.

a)  b) 

Figure 6.99 Separation of mixed sands downstream of the pile a) coastal flume test b) small flume test.

6.9.3 Sediment mixing

In terms of the layered sand tests, it is interesting to consider to what extent the two layers have remained separate or become mixed as a result of the scour process.

The samples from the layered tests collected from the deepest part of the scour hole, closest to the upstream pile face (see Figures 6.100 and 6.101), consistently show similar patterns in the

top layer of the sample. At this depth into the bed, the coarse sand layer has been reached, so the initial configuration of the sample at this depth would only consist of coarse sand. However, Figures 6.100 and 6.101 show a small increase in the proportion of fine sand in the top layer of the sample. Based on visual observations this fine sand probably falls in to the scour hole once the flow is stopped and the vortex suspending sediment collapses on the scour hole slope. However, it is possible that the increased proportion of fine sand indicates some level of mixing between the fine and coarse sands within the top centimetre. It is difficult to draw further conclusions about the sediment interaction in the top layer of the samples at this location in the scour hole because it is difficult to quantify and separate the effects of the deposition of the fine sand that was observed. If there are any mixing processes occurring these are confined to the top centimetre, as there is no change to the sand distribution in the lower centimetres.

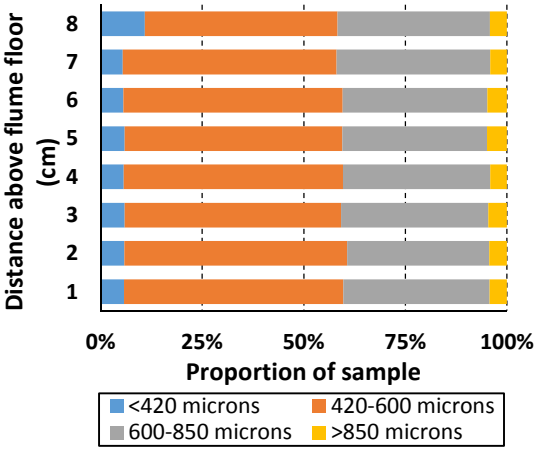

Figure 6.100 Core sample taken at end of test C.90.11 (layered bed with fine sand overlying coarse sand) from the deepest part of the scour hole, directly upstream of the pile.

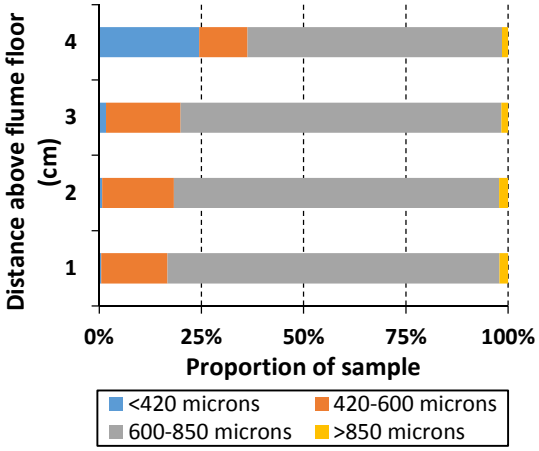

Figure 6.101 Core sample taken at end of test R.29.3 (layered bed, fine sand overlying coarse sand) from the deepest part of the scour hole, directly upstream of the pile.

The core samples show some interesting results in the layered tests under reversing flow. In these cases there is clear evidence of sediment mixing processes occurring. In Figure 6.102, the core sample is taken from the downstream scour hole slope and it can be seen that while the top two centimetres consist mostly of the fine sand as would be expected based on the initial bed configuration at this location and scour depth, there is also a notable proportion of coarse sand in both of these centimetre sections, indicating that mixing has occurred. Similarly in the sample in Figure 6.103 mixing of the fine and coarse sands has happened in the upper four centimetres. The mixture is quite heterogeneous as shown by the wide variation in proportion of fine to coarse sands in the four centimetres. This sample was collected from within the scour hole, adjacent to the pile face on the left hand side of the pile, which was the downstream side for the final half cycle. As discussed in Sections 6.6 and 7.2.3 the deposition zone within the scour hole directly downstream of the pile is shifted to the opposite side of the pile with each reversal of flow direction. The core sample results indicate that this process has

resulted in the fine and coarse sands becoming mixed. This means that the scour development at the pile is actually through a mixed material each time the flow is reversed, not a uniform sand, and this is likely to alter the rate of scour development.

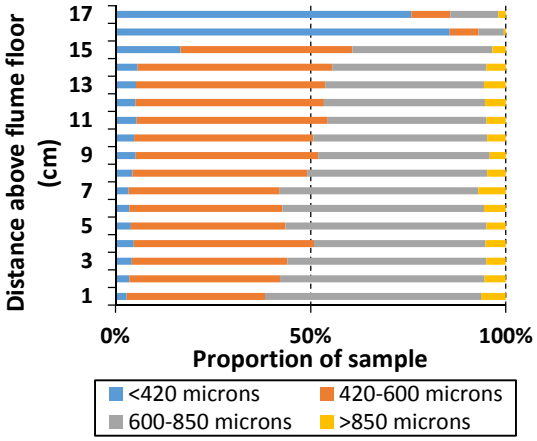

Figure 6.102 Core sample taken at end of test C.90.12 (layered bed, fine sand overlying coarse sand) under square wave reversing current taken from the scour hole slope on the last downstream side.

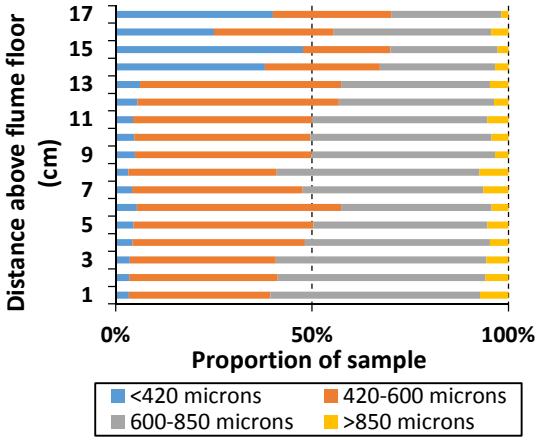

Figure 6.103 Core sample taken at end of test C.90.12 (layered bed, fine sand overlying coarse sand) under square wave reversing current taken directly adjacent to the pile on the last downstream side.

6.10 Test repeatability

This section seeks to understand the measurement uncertainty in the scour development curves. The uncertainty in the laboratory measurements can be quantified where tests were repeated. However, due to the long duration of the scour tests it was only practical to repeat tests to clarify unexpected results or where a fault in the test procedure occurred. An assessment of the repeatability of the data can instead be made through comparison of partial repetitions of tests. For example, scour in the upper sand layer of the layered tests provided a repeated section of test for comparison with the start of the equivalent uniform sand test.

A set of layered sand tests were also conducted where the same test conditions were repeated four times but the tests were stopped at different points in time so that core samples could be taken at different stages of scour development (see Appendix 3). Figure 6.104 shows a comparison of these four tests. There is very good agreement between the curves, showing that the errors due to the experimental methodology and measurement technique are small. For this set of four tests the maximum difference between scour depth measurements is 0.08 S/D, with the majority of points within 0.04 S/D. The largest difference occurred very near the start of the tests where recording scour depth was more difficult due to the high speed of erosion, making measurement error more likely.

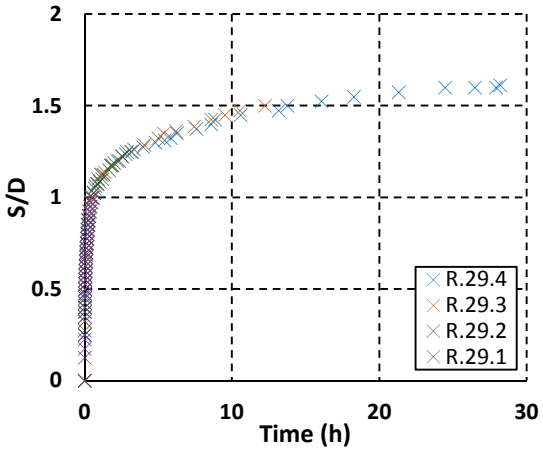

Figure 6.104 Comparison of scour development in tests R.29.1, R.29.2, R.29.3, R.29.4 under same flow conditions in small flume, layered bed with 40 mm upper fine sand layer.

Table 6.7 Comparisons of parts of tests conducted under the same conditions in the small flume.

Tests compared	Maximum difference in S/D
R.29.1, R.29.2, R.29.3, R.29.4	0.08
R.1 and R.2	0.05
R.4 and R.7	0.175* see main text
R.5 and R.6	0.08
R.19, R.20 and R.24	0.08
R.17 and R.19, R.20, R.24	0.13* see main text
R.16 and R.21, R.N.27	0.075

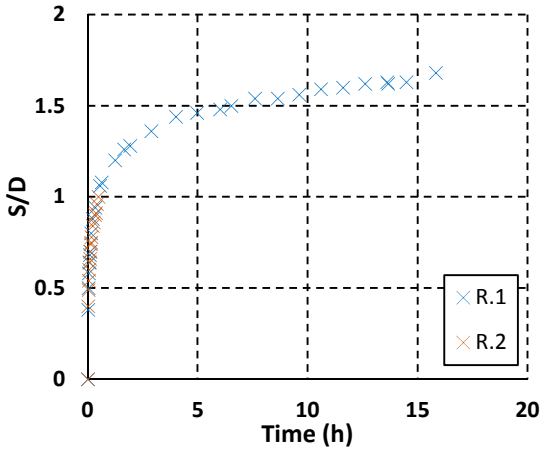

Figure 6.105 Comparison of scour development in tests R.1 and R.2 under same flow conditions in small flume (fine sand).

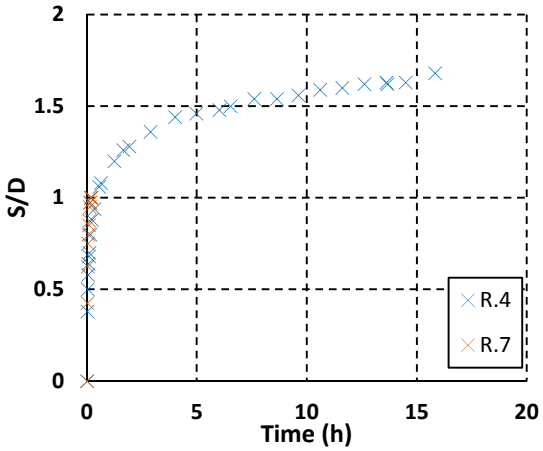

Figure 6.106 Comparison of scour development in tests R.4 and R.7 under same flow conditions in small flume (fine sand).

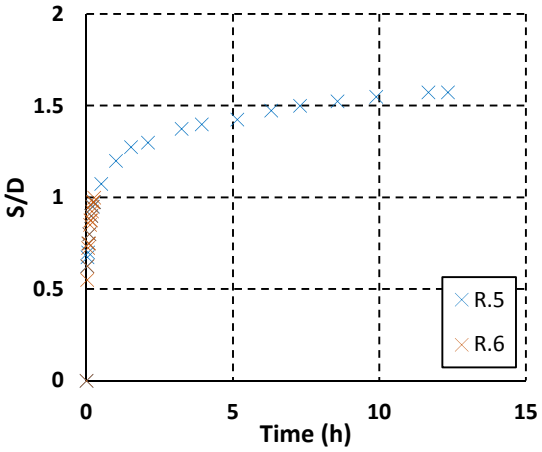

Figure 6.107 Comparison of scour development in tests R.5 and R.6 under same flow conditions in small flume (coarse sand).

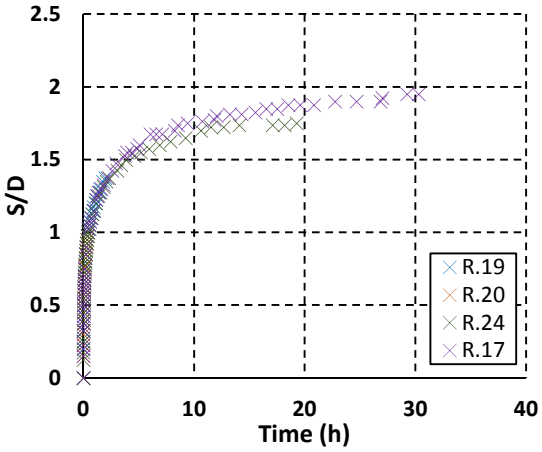

Figure 6.108 Comparison of scour development in tests R.19, R.20, R.24, R.17 under approximately the same flow conditions in the small flume (fine sand).

In Figures 6.105-6.109 the remaining comparisons between the relevant parts of tests conducted in the small flume used to assess the measurement uncertainty are shown. The maximum difference between the curves in each comparison are given in Table 6.7.

The maximum difference between the scour curves in Figure 6.106 is larger than in most of the other comparisons. In Figure 6.106 the maximum difference is approximately 0.175 S/D. However, there is only a small section for comparison as these tests were conducted at the fastest flow velocity used in the test programme. The high speed of the scour process in the initial stage of the test increases the uncertainty in the scour measurements. Furthermore, these tests were part of the preliminary test series, P-2, so the test methodology was less refined at this point. These factors are likely to contribute to the increased difference between the tests, and therefore, the larger measurement uncertainty between these tests will not be considered as standard.

In Figure 6.108, while the difference between the R.19, R.20 and R.24 curves is small, the difference between test R.17 and these three tests is larger than most of the comparisons with a maximum difference of 0.13 S/D. However, test R.17 was conducted during a different test series than the other three tests i.e. several months before, under a slightly different flow velocity. The difference in the velocity between these tests is given in Section 6.7. While the difference in the tests is therefore not related to the measurement uncertainty, it is interesting to include here because it demonstrates the sensitivity of the scour tests to the velocity parameter. Only a small change in velocity is needed to have a noticeable effect on the scour curve.

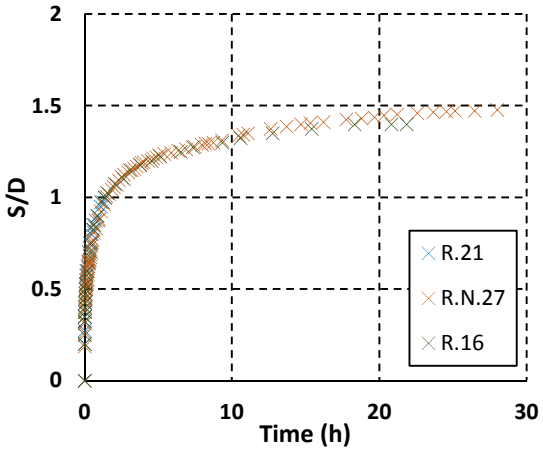

Figure 6.109 Comparison of scour development in tests R.21, R.N.27, R.16 under approximately the same flow conditions in the small flume (coarse sand).

Table 6.8 Comparisons of parts of tests conducted under the same conditions in the coastal flume.

Tests compared	Maximum difference in S/D
C.90.10 and C.90.18	0.06
C.20.10 and C.20.18	0.125 * see main text
C.90.11, C.90.12, C.90.15	0.06
C.20.11, C.20.12, C.20.15	0.2 * see main text
C.90.28 and C.90.30	0.08
C.90.13 and C.90.14	0.05
C.20.13 and C.20.14	0.05

Similarly to Figure 6.108 in Figure 6.109 test R.16 was conducted some months prior to the other tests in the comparison, so the differences between these tests are due to the small change in velocity between the two test series. The change in velocity has had less of an effect on the difference in the scour curves compared to those in Figure 6.108 as the curves are within the measurement uncertainty identified from the other comparisons. This may be linked to the different flow intensity parameters between these two comparisons.

In the larger flume there are also some tests that can be compared to assess the test repeatability, see Figures 6.10-6.116. The maximum difference between the tests in each comparison is given in Table 6.8.

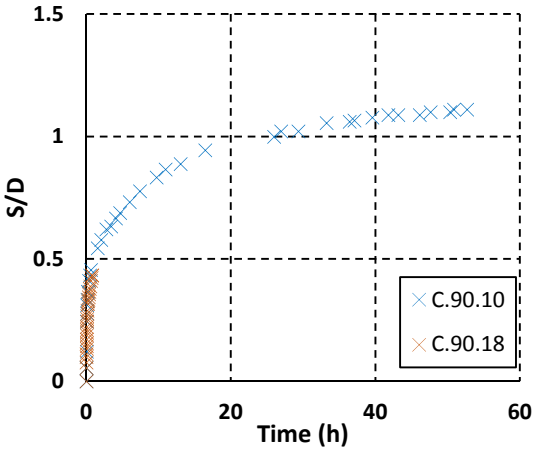

Figure 6.110 Comparison of scour development in tests C.90.10 and C.90.18 under the same flow conditions in the coastal flume (coarse sand).

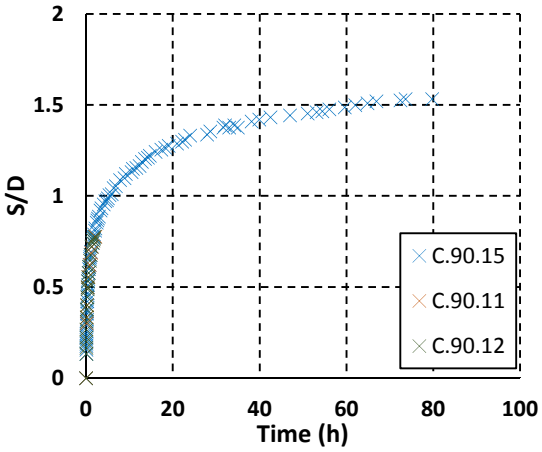

Figure 6.111 Comparison of scour development in tests C.90.15, C.90.11 and C.90.12 under the same flow conditions in the coastal flume (fine sand).

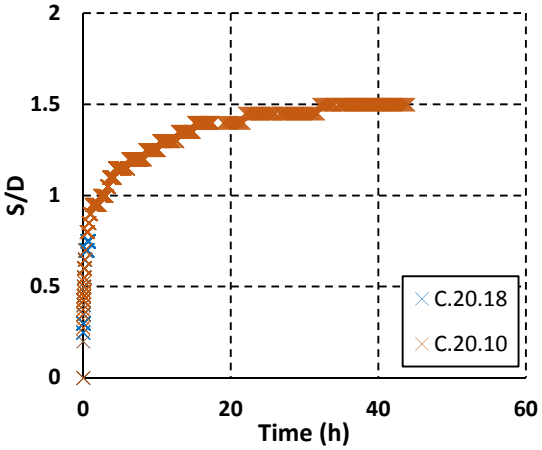

Figure 6.112 Comparison of scour development in tests C.20.10 and C.20.18 under the same flow conditions in the coastal flume (coarse sand).

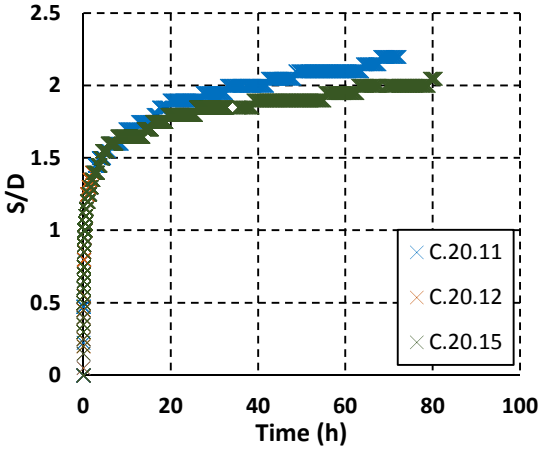

Figure 6.113 Comparison of scour development in tests C.20.11, C.20.12 and C.20.15 under the same flow conditions in the coastal flume (fine sand).

In Figure 6.112 and Figure 6.113 the maximum difference between the curves is higher at 0.125 S/D and 0.2 S/D respectively. Both of these comparisons relate to tests at the small pile in the larger flume. The measurement uncertainty is expected to be higher for this pile due to the coarser resolution of the measurement scale compared to the pile diameter. Consequently the repeatability of these tests will be treated separately from those at the larger pile diameters.

Figure 6.114 shows a comparison of scour development in wave-current scour tests rather than unidirectional current flow as has been discussed previously in this section. In Figure 6.114 the

difference between the two curves is still within the variability expected based on the unidirectional current test data, indicating that the variability in the wave-current scour depth data is no different to the unidirectional current cases.

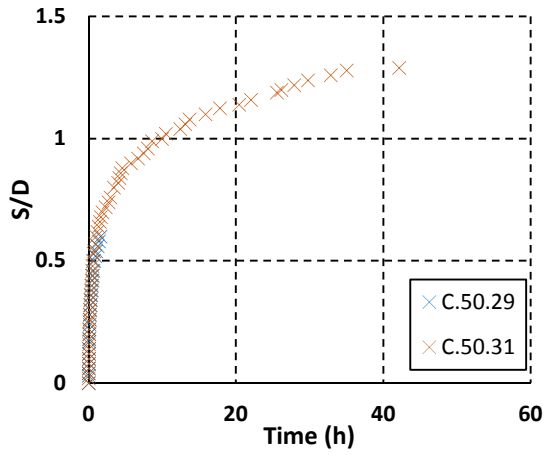

Figure 6.114 Comparison of scour development in tests C.50.29 and C.50.31 under the same wave-current flow in the coastal flume (fine sand).

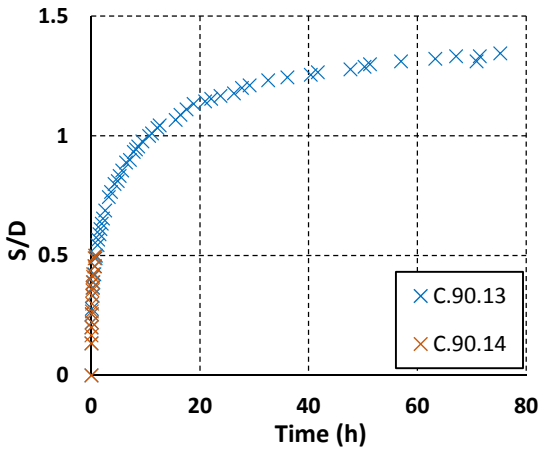

Figure 6.115 Comparison of scour development in tests C.90.13 and C.90.14 under the same current in the coastal flume (mixed sand).

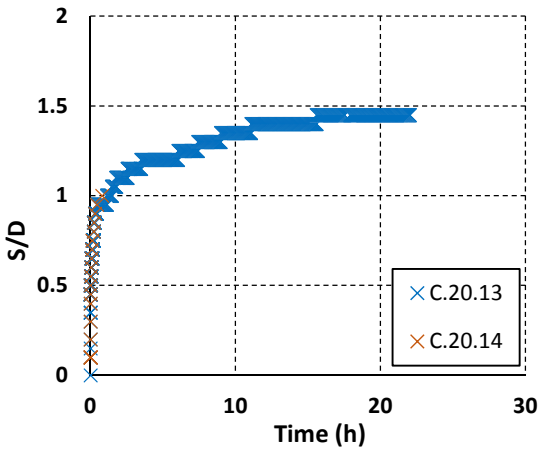

Figure 6.116 Comparison of scour development in tests C.20.13 and C.20.14 under the same current in the coastal flume (mixed sand).

There are two comparisons available for the mixed sand tests. These are shown in Figures 6.115 and 6.116 with the maximum difference between the curves shown in Table 6.8. The repeatability of the mixed sand tests in the larger flume appears to be in the same region as the uniform sand tests. However, only two cases were available for comparison.

Two further cases to discuss are the tests which were repeated in the R.T test series. R.T.2 was a repeat of test R.T.1, and test R.T.11 was a repeat of test R.T.8. Figures 6.117 and 6.118 compare the repeated tests in each case.

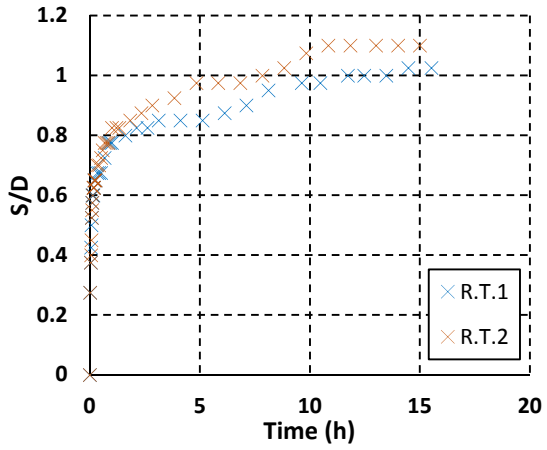

Figure 6.117 Comparison of repeated tests with 25% fine sand, 75% coarse sand mixed bed in the small flume (unidirectional current).

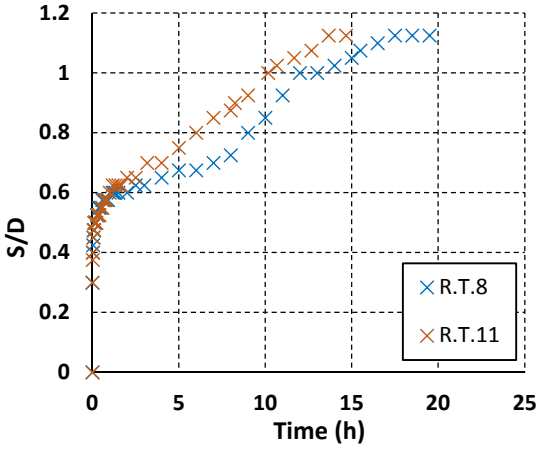

Figure 6.118 Comparison of repeated tests with 50% fine sand, 50% coarse sand mixed bed in the small flume (unidirectional current).

In both cases in Figures 6.117 and 6.118, the largest difference between the repeated tests is a little higher than the expected maximum difference between tests due to the measurement uncertainty; the difference is as much as 0.15 S/D in Figure 6.118. This implies that there may be other factors affecting the scour development in these tests. It is important to note that these tests were the earliest mixed sand tests that were run in the small flume (and these were undertaken primarily by Ferradosa, 2012) and therefore the methodology followed was slightly different and somewhat less developed than in later test series, which may partially account for the larger differences between the tests in Figures 6.117 and 6.118. In addition, the effect of the heterogeneity of the sand mixtures on scour development is considered in Section 7.2.2, as well as the potential for variation in the flow conditions; both are factors that may explain the differences in these tests.

To conclude, the difference between scour depths is mostly well under 0.1 S/D, and therefore this will be taken as the nominal value for the measurement uncertainty. In the few comparisons where the difference between scour depths was greater than 0.1 S/D it was demonstrated that larger measurement errors were likely to be specific to these cases. In general when comparing different scour cases, the effect of the parameter under consideration on the scour development will be deemed to be of significance if the difference in scour depths is greater than 0.1 S/D.

7. Discussion

Following the presentation of the results, this section provides a more detailed examination of the key findings. Analysis of the uniform sand tests in relation to a range of parameters and comparison with the literature is given in Section 7.1 to better understand the baseline cases and assess scale effects in the laboratory, before discussing the novel findings in the layered and mixed cases, as well as under the more complex wave-current and tidal flow conditions in Section 7.2. In Section 7.3 an assessment is made of existing prediction equations for determining scour time development and equilibrium scour depth in the uniform sands. The most promising methods from this investigation are then used to develop approaches for modelling scour behaviour in the complex sediment beds. In the final Sections 7.4 and 7.5 an evaluation of the test methodology and measurement techniques is presented, and recommendations for future work are provided. The main conclusions from the project are then summarised in Section 8.

7.1 Uniform sand, unidirectional current tests

In this section a range of parameters are discussed in comparison with the literature to better understand their relationships with scour depth in the uniform sand tests. Dimensional and non-dimensional parameters related to the flow velocity, sand grain size, pile diameter, water depth and scour timescale are discussed.

7.1.1 Scour relationship with flow velocity and V/V_{cr}

According to the scour literature (see Section 2.2.2) in the clear water regime equilibrium scour depth increases linearly with flow velocity up to the critical velocity of the sediment. By plotting S_e/D against V/V_{cr} for the unidirectional current tests in the uniform sands, Figure 7.1, the data for the different pile diameters and grain sizes should plot to the same line. It can be seen in Figure 7.1 that there is, for the most part, good agreement with this trend. The close fit demonstrates that the scour process is highly sensitive to the V/V_{cr} parameter, as more scatter in the data would imply a greater level of dependency on the other variables in the tests.

However, it is evident in Figure 7.1 that the two uniform sand tests conducted at the 20 mm pile in the larger flume do not fit the trend so closely. These tests resulted in a deeper scour depth at a given value of V/V_{cr} compared to the other tests. For these tests the pile diameter changed but all other dimensional parameters remained constant relative to the larger pile tests conducted in the same flume. Therefore, to understand this difference, the changes in the ratios of parameters as a result of the decrease in pile diameter need to be considered. Possible causes are the increase in grain size relative to pile diameter (which is thought to induce ‘scale effects’ resulting in deeper scour at relatively smaller piles, Lee and Sturm, 2008), or changes in the relationship between the flow parameters and the pile diameter represented by the pile Reynolds number or Euler number (Ettema et al. 1998). These aspects will be considered in more detail in the following sections. A separate trendline has been added to Figure 7.1 for the tests at the 20 mm pile to enable quantification of the increase in scour depth compared to that in the other test cases. It is estimated from Figure 7.1 that an increase of approximately 0.4 S/D for a given V/V_{cr} value has occurred.

There is good agreement between the 90 mm pile tests in the larger flume and the 40 mm pile tests in the smaller flume in Figure 7.1, which indicates that there are no significant scale effects between these tests despite the different flume dimensions and pile diameters. Similar scaling parameters were used for these test sets, but the same sands were used in both flumes so the D/d_{50} ratio was not held constant. The good agreement between the tests in Figure 7.1 indicates that this parameter has not had a significant influence on the scour depth. The D/d_{50} parameter is discussed in more detail in Section 7.1.3.

There is some additional scatter in the data apart from that relating to the 20 mm pile tests. In particular the scour depth in the 19 cm/s fine sand test (R.T.6) is about 0.2 S/D greater than expected. This test was conducted as part of test series T-1 and these tests were completed by Ferradosa (2012). It is possible that small differences in flow velocity occurred between tests in this series as the upper valve was used to control the flow rather than the lower valve, which may have resulted in small changes in the V/V_{cr} parameter. An increase of depth-averaged velocity of only 1 cm/s would bring this test much closer in line with the trendline.

Similarly, test R.5 plots above the trendline. This was conducted as part of preliminary test series P-2. As noted in Section 4.5 the velocity measurement for this series were completed with an ADV system rather than the LDV system and so the measurements were at a much lower resolution and affected by noise due to the proximity of the flume walls. These factors will have reduced the accuracy of the ADV measurements. In this case an increase of only 0.5 cm/s in the depth-averaged velocity would bring it in line with the other tests in Figure 7.1.

Scatter is also likely to be induced where tests were ended before the stopping criterion (preliminary test series P-1, P-2 and series T-1), or may be due to limitations in the stopping criterion to represent comparable points across all of the tests. An evaluation of the stopping criterion is given in Section 7.1.9.

The definition of the V_{cr} parameter also induces some uncertainty. Although a consistent theoretical approach was used in this study, the theoretical approaches are limited as they were developed for uniform particle shapes and grain distributions, and the relationships between parameters in the equation are modelled with a degree of empiricism (see Section 2.1.1).

Scatter in the data may also be the result of parameters other than flow intensity affecting scour development, although the good agreement indicates that the influence of other parameters for these test cases is likely to be small, apart from for those tests conducted with the 20 mm pile in the larger flume. To better understand effects of other flow and sediment parameters on the tests these are discussed in turn in the following sections.

Note that in Figure 7.1 tests R.1 and R.3 from preliminary test series P-1 have been plotted separately to the other data, in order to determine the flow intensity parameter in these tests because reliable velocity measurements were not collected during this test series (see Section 4.5). An estimate of the flow velocity for these tests has been obtained by fitting the data to the trendline in Figure 7.1. Good agreement is obtained for both tests at a velocity of 21.5 cm/s. This also fits well with observations of slower ripple formation than in the P-2 test series with faster

flow, and the scour time development curves for these tests fit in between the faster and slower tests (Appendix 3). As tests R.1 and R.3 have been fitted to the trend they have not been used to define the trend itself.

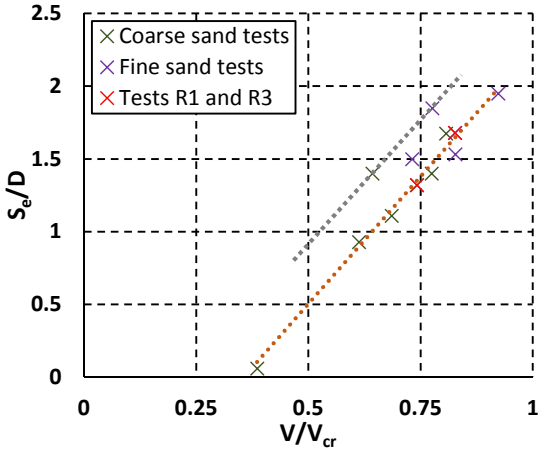

Figure 7.1 Non-dimensionalised quasi-equilibrium scour depth versus flow intensity for uniform fine and coarse sand tests in unidirectional current.

A direct comparison with data in the literature is shown in Figure 7.2 where the present test data is plotted alongside the laboratory data reported in Sheppard et al. (2011a) from a wide range of studies.

There is considerably more scatter in the published data in Figure 7.2 than in the data from the present study, showing that scour depth is dependent on a range of other factors. The scatter makes it difficult to observe a linear trend in the clear water regime.

The data from this project fit in the middle range of the literature data in Figure 7.2. The excellent fit of the test data within the range of values in the literature provides confidence in the methodology and standard of the experiments in this project.

The trendline from Figure 7.1 for the present data is included in Figure 7.2 as well as a trendline taking all of the plotted data into account. The trendline based on the full data set has a much shallower gradient due to a number of tests with small scour depths recorded at high flow intensity values. This appears to have skewed the best fit line so that it does not appropriately model the data, as the point of interception with the x axis is not at a sensible value (i.e. at the threshold for scour to occur).

Tests conducted at low flow velocities in the larger flume as part of test series C-2, enable a comparison to be made of the threshold V/V_{cr} parameter for scour to occur. The calculated threshold V/V_{cr} value is approximately 0.5, based on the condition of Whitehouse (1998) that scour initiates when $\tau/\tau_{crit}>0.25$. Other research suggests that initiation of scour occurs between 0.3-0.6 V/V_{cr} (see Section 2.2.2). From Figure 7.2 the trendline for the present data indicates that scour initiates somewhere in the region of $V/V_{cr}=0.35$, which is in agreement with the literature

data in Figure 7.2 where the threshold value is somewhere between 0.3-0.5. The wide spread of V/V_{cr} for initiation of scour in the data suggests that scour initiation is dependent on a wider range of factors than are currently taken into account in prediction methodologies, so further research is needed to properly define the threshold for scouring over a range of conditions.

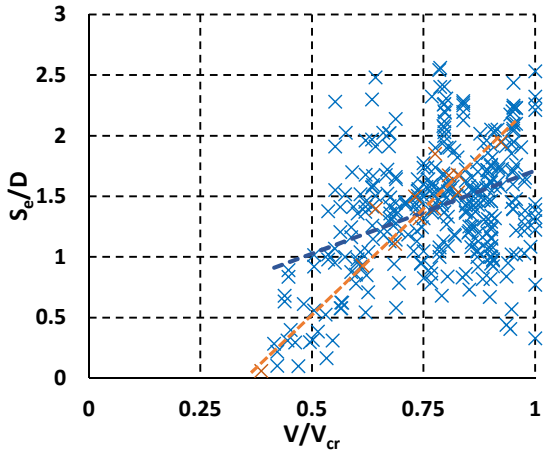

Figure 7.2 Comparison of data given in Sheppard et al. (2011a) (blue) and present study (orange), S_e/D versus V/V_{cr}, uniform fine and coarse sands in unidirectional current.

7.1.2 Pile diameter

In the literature it is widely reported that scour depth scales with pile diameter. In Figure 7.1 the consistency of the data when plotting S_e/D versus V/V_{cr} demonstrates that the main sets of tests conducted at the 40 mm and 50 mm piles in the small flume and at the 90 mm pile in the large flume scale satisfactorily with pile diameter.

As already discussed, this was not the case for the 20 mm pile tests in the larger flume, where the scour depth was increased relative to the pile diameter, mirroring the outcome of laboratory scale effects reported in the literature (see Section 2.7.4).

An additional assessment of scale effects was made during the test programme in the small flume through a comparison of scour development at 25, 40 and 50 mm piles under the same flow conditions, Figure 7.3. Note that due to time constraints tests R.8 and R.9 were not run to equilibrium. In Figure 7.3 the 40 mm and 50 mm pile tests show excellent agreement when the results are plotted with the scour depth normalised by the pile diameter. However, this is not the case for the 25 mm pile in this flume, where scour depth is greater than in the other tests when normalised by pile diameter. This indicates that the reduction in pile diameter while maintaining constant flow conditions has resulted in a significant change in terms of the ratios of one or more parameters compared to the pile diameter thereby influencing scour behaviour. The influence of a range of parameter ratios on scour depth are considered in the following sections in order to establish the causes of this result and that of the enhanced scour depth at the small pile in the larger flume.

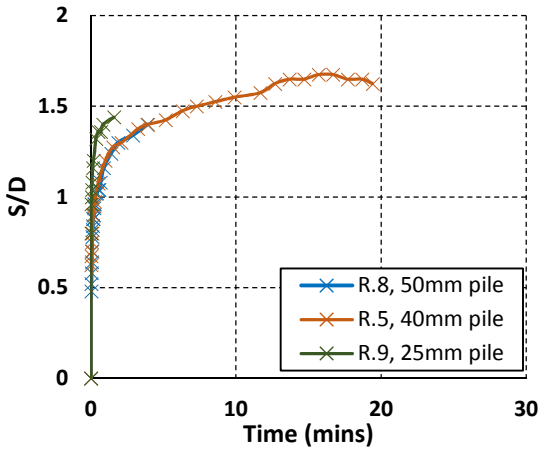

Figure 7.3 Scour development at different pile diameters in the small flume under the same flow conditions (coarse sand).

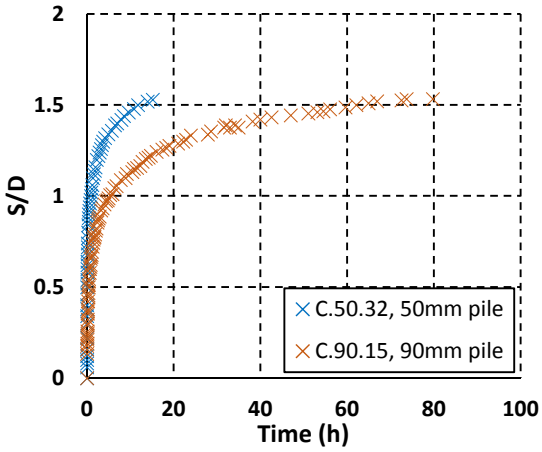

Figure 7.4 Scour development at different pile diameters in the coastal flume under the same flow conditions (fine sand).

In the larger flume three different pile diameters were employed during the test programme, namely 20, 50 and 90 mm. However, due to the discrepancy in the flow velocity between the near and far side of the flume (see Section 6.7), only one direct comparison between tests under exactly the same flow condition is available, between tests at the 50 mm and 90 mm piles which were conducted at the same location in the flume. These tests (C.90.15 and C.50.32) are plotted in Figure 7.4. Note that time constraints meant that test C.50.32 could not be run to equilibrium. It is clear in Figure 7.4 that similarly to the results in Figure 7.3 scour depth does not scale with pile diameter between these two cases, with the smaller pile resulting in greater S_e/D than at the larger pile.

In Figure 7.5 a comparison is made of tests conducted at the 20, 50 and 90 mm pile diameters in the larger flume in fine sand. Note that for the 20 mm test (C.20.15) the depth-averaged velocity is reduced by approximately 1.5 cm/s compared to the other tests. However, in Figure 7.5 it can be seen that the scour depth relative to the pile diameter is already greater at the 20 mm pile than at the 50mm pile despite the lower flow velocity, so it is clear that the relative scour depth increases with decreasing pile diameter when all other parameters remain constant.

A correction for the velocity difference for the 20 mm pile tests can be determined using the trendlines in the V/V_{cr} versus S_e/D graph in Figure 7.1. This indicates that the scour depth has been reduced by approximately 0.1 S/D, and hence the increase in scour depth is estimated as 0.4 S/D if the tests were conducted under the same flow velocity (as discussed in the previous section).

It is more difficult to estimate the size of the scale effect at the 50 mm pile in the larger flume and at the 25 mm pile in the small flume because these tests were not run to equilibrium scour depth, and extrapolation methods are not suited to short duration tests (Simarro-Grande and Martin-Vide, 2004).

Considering the scour curves in Figures 7.3 and 7.5 the effects due to the reduction in pile diameter are less apparent at the 25 mm pile in the small flume than at the 50 mm or 20 mm piles in the larger flume tests where there is a greater difference in terms of S/D between these curves and that at the 90 mm pile.

It is possible that the difference in the scour curves in the initial stage of the tests in Figure 7.3 is due to a difference in the timescale parameter for scour, which is not normalised in the figures, as opposed to indicating an increase in the relative equilibrium scour depth, but the short duration of the tests prevents further investigation of this aspect.

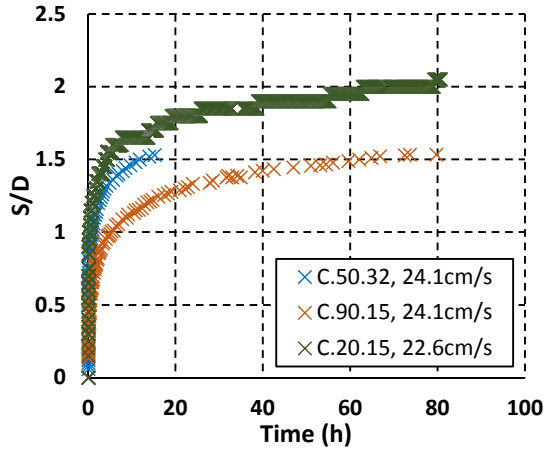

Figure 7.5 Comparison of scour development at the three pile diameters used in the coastal flume in unidirectional current, fine sand

7.1.3 Grain size and D/d_{50}

One parameter that is reported to induce scale effects in the laboratory is the ratio of pile diameter to grain size (Lee and Sturm, 2008). Grains smaller than about 0.1 mm exhibit cohesive properties imposing a limit on the geometric scaling of sediment, so that it is often not possible to keep the ratio of D/d_{50} constant when scaling scour tests. This section will evaluate the effect of this parameter on the tests to help determine the cause of the relatively higher scour depths at the smaller pile diameters in the present study.

As discussed in Section 2.2.4 of the literature review, Lee and Sturm (2009) presented a detailed analysis of the relationship between S_e/D and D/d_{50}. S_e/D is expected to increase with D/d_{50} up to D/d_{50}=25. However not all of the literature is in agreement with the trend identified by Lee and Sturm (2009) once D/d_{50}>25. Some researchers have reported that S_e/D is independent of D/d_{50} after this point, whereas Lee and Sturm (2009) found that S_e/D decreases as D/d_{50} increases from 25 up to around 200 when S_e/D becomes independent of D/d_{50}. The decrease in S_e/D with increasing D/d_{50} implies that S_e/D will be greater when the sand grains are larger compared to the pile diameter, which potentially would account for the greater scour depth at the smaller piles.

The D/d_{50} values for each test condition are given in Table 7.1. Note that D/d_{50} is greater than 25 in every case, so for these tests it is expected that S_e/D will either decrease with increasing D/d_{50} or be independent of this parameter.

Table 7.1 D/d_{50} parameter for each combination of pile diameter and uniform sediment used in the test programme.

Condition	D/d_{50}
Large flume, 90mm pile, coarse sand	150
Large flume, 90mm pile, fine sand	900
Large flume, 50mm pile, fine sand	500
Large flume, 20mm pile, coarse sand	33.33
Large flume, 20mm pile, fine sand	200
Small flume, 50mm pile, coarse sand	83.33
Small flume, 40mm pile, coarse sand	66.67
Small flume, 40mm pile, fine sand	400
Small flume, 25mm pile, coarse sand	41.67

The lowest value of D/d_{50} relates to the coarse sand test at the 20 mm pile in the larger flume. However, the fine sand test at the 20 mm pile does not equate to the 2nd smallest value of D/d_{50}. In fact there are four other test conditions that result in smaller D/d_{50} values than in the case of the fine sand test at the 20 mm pile. Therefore, if scale effects at the small pile are dependent on the D/d_{50} parameter then it would be expected also to see scale effects in these other tests, which is not the case in Figure 7.1. Furthermore, D/d_{50}=200 for the fine sand test at the 20 mm pile, which is close to the expected range for independence of this parameter as shown by Lee and Sturm (2009). When considering the 50 mm pile in the larger flume the D/d_{50} ratio is even larger than that at the 20 mm pile, yet the relative scour depth was still increased compared to that at the 90 mm pile. Therefore, the D/d_{50} parameter does not account for the higher values of S_e/D observed at these piles.

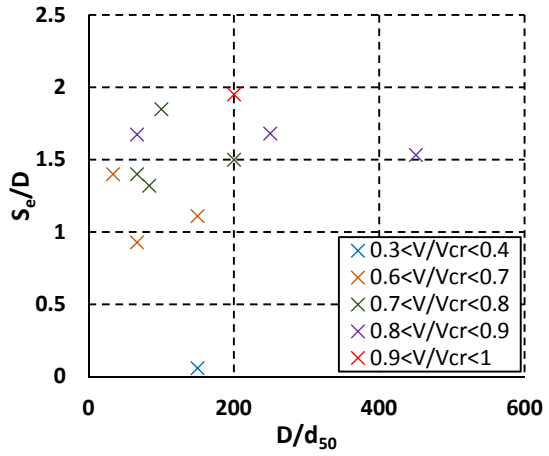

Figure 7.6 Relationship between relative grain size and non-dimensionalised equilibrium scour depth in the uniform sand tests.

To make this clearer, in Figure 7.6 S_e/D is plotted against the D/d_{50} parameter. Tests conducted at approximately the same V/V_{cr} are identified on the graph but there is no obvious relationship between these parameters in Figure 7.6, and S_e/D does not appear to increase with decreasing D/d_{50}. Therefore, these test results are more in agreement with the findings of Raudkivi and Ettema (1983) and Raikar and Dey (2005) that S_e/D is independent of D/d_{50} within the range tested. While Lee and Sturm's analysis applied corrections to the data for V/V_{cr}, h/D, pile shape and alignment, there is still a considerable amount of scatter in their data compared to the trend they identifed between S_e/D and D/d_{50}. Clearly there are other factors of importance, and the scatter indicates that the dependence on the D/d_{50} parameter is fairly weak in the available data to Lee and Sturm (2009).

7.1.4 Water depth and h/D

Another parameter considered to influence scour depth in the literature is the water depth relative to the pile diameter. It is generally concluded in the literature that this parameter is only important for low values of h/D, and scour is thought to be independent of h/D for h/D>3 or 4 (see Section 2.2.3). For this reason the h/D parameter for these tests was set above this value. Table 7.2 shows the h/D values for each test condition in the two flumes.

Table 7.2 h/D parameter for each pile diameter used in the test programme

Condition	h/D
Large flume, 90mm pile	5
Large flume, 50mm pile	9
Large flume, 20mm pile	22.5
Small flume, 50mm pile	3.2
Small flume, 40mm pile	4
Small flume, 25mm pile	6.4

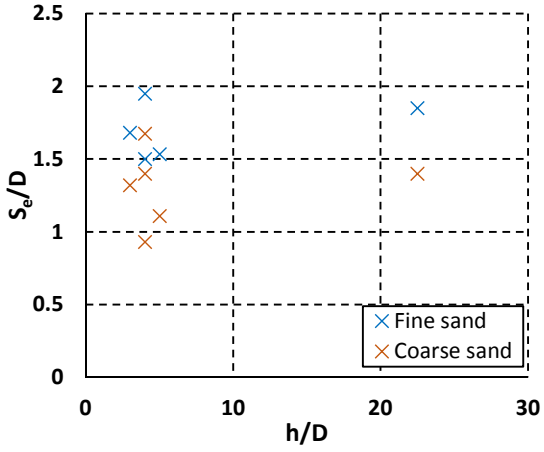

Figure 7.7 Relationship between relative water depth and non-dimensionalsied equilibrium scour depth in the uniform sands.

In Figure 7.7 S_e/D is plotted against h/D for the test series, but the results do not show a strong dependence on this parameter.

In Figure 7.1 the 40 and 50 mm piles in the small flume and the 90 mm pile in the larger flume were shown to be in good agreement in terms of the expected trend between S_e/D and V/V_{cr}. This implies that there is no influence of the h/D parameter between these tests, which is in the range 3.2-5. However, for the tests in which equilibrium scour depth did not scale with pile diameter in a consistent manner, the h/D parameter increases with the observed increase in S/D i.e. from the 25 mm pile test in the small flume, to the 50 mm pile and then to the 20 mm pile in the larger flume.

This apparent link with water depth may indicate a change in the flow patterns relative to the pile diameter as water depth is not expected to directly influence scour behaviour in deeper water once interaction between the surface and horseshoe vortices ceases (see Section 2.2.3).

7.1.5 Froude number

The potential link of S_e/D with water depth discussed in the previous section will be considered further in terms of other flow related parameters that may better represent this apparent effect across the test series. The effects of Froude, Reynolds and Euler number are addressed in turn.

In some scour studies the Froude number has been considered an important parameter for scour, while others have not discussed it. In the scour prediction methods that do include Froude number scour depth is expected to increase with Froude number in the subcritical range.

The Froude number is a characteristic of the flow and water depth so is not related to the pile diameter or sediment properties. Consequently in these tests it is a function of the flume size (as this resulted in a change in the water depth), and flow velocity. Therefore, the Froude number was constant in the larger flume, but varied with flow velocity in the small flume. Table 7.3 presents the Froude number for the lowest and highest velocities tested in the small flume along with the Froude number for the tests in the larger flume.

Table 7.3 Froude number in the laboratory studies in each flume

Condition	Froude
Coastal flume	0.11
Small flume, fastest velocity	0.20
Small flume, slowest velocity	0.15

The Froude number is smallest in the coastal flume, and largest for the fastest flow velocity in the small flume. However, the difference in Froude number between these cases is relatively small. If this difference in Froude number was significant there would be a systematic change in the scour behaviour between the two flumes in terms of S_e/D versus V/V_{cr} (Figure 7.1). However, this is not the case and so it can be concluded that Froude number is not significant over this small range tested.

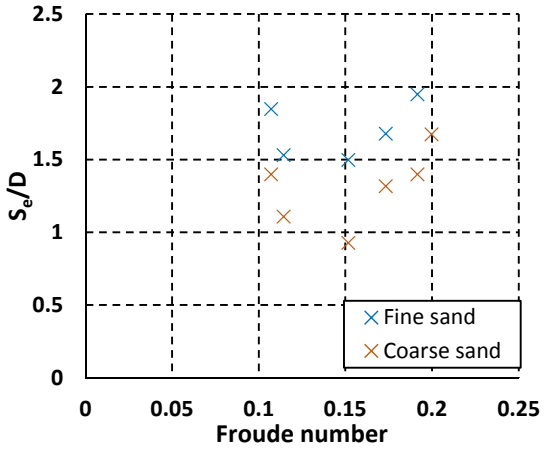

Figure 7.8 Relationship between Froude number and non-dimensionalised equilibrium scour depth in the uniform sands.

In Figure 7.8 the Froude number for each test is plotted against S_e/D. It is clear that for the small flume tests in the range Fr=0.15-0.2 S_e/D increases with Froude number, in agreement with the literature. However, this trend is not continued to the larger flume tests at lower Froude numbers. The apparent trend in the small flume tests is really a proxy for the V/V_{cr} parameter which for these particular tests increases directly with Froude number, and it can be seen that the fine and coarse sand tests are separated in Figure 7.8 because Froude number does not take into account the sediment parameters. This indicates that the dependence on Froude number is weak, and because the Froude number is smallest for the tests at the 20 mm pile in the larger flume this parameter does not explain the higher value of S_e/D seen in these tests.

7.1.6 Sensitivity to V^2/gD parameter

Another parameter that has been used to understand scale effects in scour experiments by Ettema et al. (1998) is V^2/gD (Euler number). This parameter describes the ratio of the stagnation pressure at the structure to the pile diameter. As the pile diameter decreases V^2/gD increases and this means that the gradient in the flow increases at the pile, increasing the downflow and horseshoe vortex strength relative to the pile diameter and as a result increasing S_e/D. The V^2/gD parameter is linked to the apparent increase in S_e/D with water depth in the tests at the smaller pile diameters, because it was the pile diameter that was reduced to increase the ratio of h/D. This resulted in an increase in the V^2/gD parameter because the flow velocity remained constant as the pile diameter decreased.

Table 7.4 displays the values of V^2/gD for the tests and the data are plotted in Figure 7.9 in terms of S_e/D against V^2/gD. The V^2/gD parameter is greatest for the 20 mm pile in the larger flume, which helps to explain the larger S_e/D parameter at this pile.

Table 7.4 Euler number for each test condition

Condition	V^2/gD
Large flume, 90mm pile	0.065
Large flume, 50mm pile	0.117
Large flume, 20mm pile	0.258
Small flume, 50mm pile, 25cm/s	0.127
Small flume, 40mm pile, 25cm/s	0.159
Small flume, 25mm pile, 25cm/s	0.255
Small flume, 40mm pile, 19cm/s	0.092

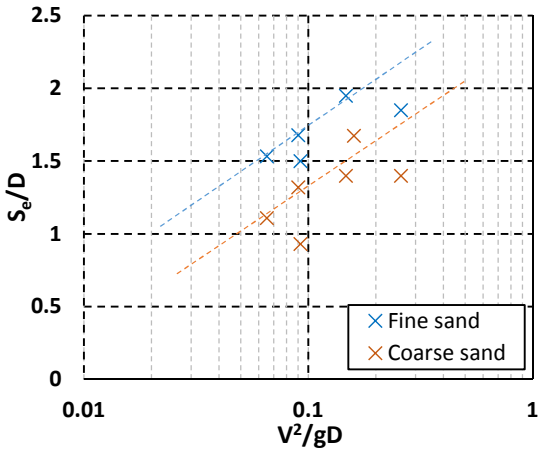

Figure 7.9 Relationship between Euler number and non-dimensionalised equilibrium scour depth in the uniform sands.

Ettema et al. (1998) found that S_e/D increased linearly with V^2/gD when plotted on a semi-log graph. The present test data in Figure 7.9 is in agreement with this trend. Separate trendlines are shown in Figure 7.9 for the fine sand and coarse sand tests as the V^2/gD parameter does not take sediment properties into account. There is still some scatter in the data however, with the 19 cm/s tests in the small flume and the 20 mm pile tests in the larger flume having smaller S_e/D values than would be expected from the trend. This indicates that the increase in S_e/D at the small pile should be even larger based purely on this parameter, and therefore other factors may be influencing the S_e/D parameter in these tests.

The V^2/gD parameter does not uniquely account for the higher S_e/D values at the smaller pile diameters because the 25 mm pile in the small flume had a similar V^2/gD parameter to that at the 20 mm pile in the larger flume, but S_e/D was increased by a smaller amount. Also, the V^2/gD parameter for the 50 mm pile in the larger flume was smaller than in other tests which did scale consistently with the pile diameter.

7.1.7 Pile Reynolds number

Another flow parameter that can influence S_e/D is the pile Reynolds number, as discussed in Section 2.2.6 of the literature review. Table 7.5 presents the pile Reynolds number for each set of tests. It can be seen that the 20 mm pile in the larger flume and the 40 mm pile in the small flume in a current of 19 cm/s have small pile Reynolds numbers, which may link with the relatively smaller scour depth plotted for these tests compared to the trend on the V^2/gD graph (Figure 7.9). Furthermore the difference from the expected trend in Figure 7.9 is greater for the 20 mm pile in the larger flume which is consistent with the pile Reynolds number being lower in these tests compared to those under 19 cm/s flow in the small flume.

Table 7.5 Pile Reynolds number for each test condition.

Condition	Pile Reynolds number
Large flume, 90mm pile	21600
Large flume, 50mm pile	12000
Large flume, 20mm pile	4500
Small flume, 40mm pile, 19cm/s	7600
Small flume, 40mm pile, 25cm/s	10000
Small flume, 25mm pile, 25cm/s	6250

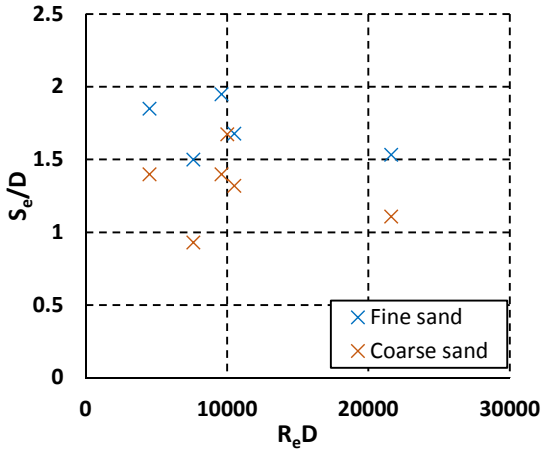

Figure 7.10 Relationship between pile Reynolds number and non-dimensionalised equilibrium scour depth in the uniform sands.

In Figure 7.10 the pile Reynolds number is plotted against S_e/D. However, it is difficult to identify a relationship between the parameters for the range of Reynolds number tested, suggesting that the influence of Re_D on S_e/D is small for these tests in the subcritical regime in agreement with the literature.

7.1.8 Timescales of scour

The time development of scour is difficult to quantify, because there is no universally accepted parameter to describe this. Several researchers have developed definitions of a scour 'timescale' parameter, T_c, and a non-dimensional form of this, T*, (see Section 2.6.5 of the literature review). However, these definitions vary between authors and are essentially empirical in nature. Therefore, in this section the timescale of scour is discussed in a more fundamental sense, using a parameter that can be more universally defined directly from the test data, the time to equilibrium. This parameter enables comparison between these tests with the expected trends in the literature, but does not allow assessment of the rate of change of scour during the test and how this changes with different test conditions. The shape of the scour curve and hence the rate of change of scour is discussed in the second part of this section following discussion of the time to equilibrium parameter.

a) Time to equilibrium

As a starting point for investigating the relationship between scour timescale and scour depth, in Figure 7.11 the equilibrium time is simply plotted against the equilibrium scour depth. Figure 7.11 shows that there is a linearly increasing trend of scour depth with time to equilibrium, so that the deeper the equilibrium scour depth, the longer the process takes. This is in agreement with the literature where the scour process in larger scale tests and in the field have longer timescales than those at small scale in the laboratory.

There is some scatter in the data however, especially for the 20 mm pile tests in the larger flume, indicating that other parameters are important for the timescale of scour. The 20 mm pile tests have a much slower timescale for scour than expected from the prevalent trend in Figure 7.11. This indicates that the parameters responsible for the higher S_e/D values in the tests at the small pile diameters have also influenced the scour timescale.

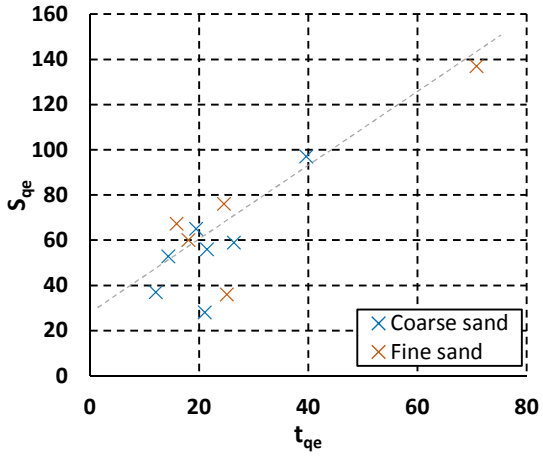

Figure 7.11 Quasi-equilibrium scour depth versus time to quasi-equilibrium in the uniform sands

In the literature it is expected that the time to equilibrium will increase with V/V_{cr}. In Figure 7.12 V/V_{cr} is plotted against time to equilibrium. Although the data appear quite scattered, they can be separated into the tests at the different pile diameters, as the effect of pile diameter is not taken into account in the graph. Once the data are separated in this way it can be seen that the time to equilibrium increases with V/V_{cr} as expected from the literature for each pile diameter. This shows that under the same flow conditions even though the rate of scour may be faster in the fine sand, the time to equilibrium is longer in this sand than in the coarse sand, because a greater volume of material is eroded.

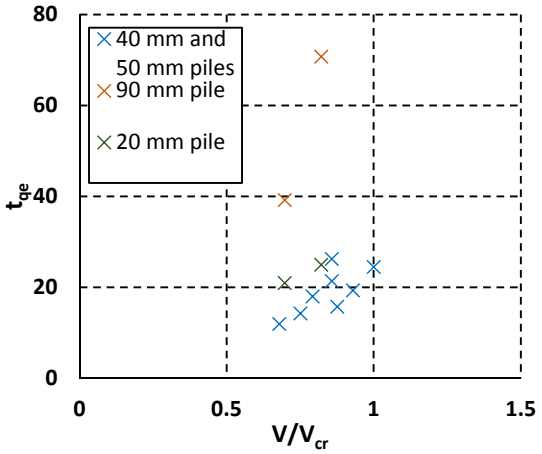

Figure 7.12 Relationship between flow intensity and time to quasi-equilibrium scour depth in the uniform sands.

Some of the scatter in Figures 7.11 and 7.12 may be explained by errors in the definition of t_e for the tests (especially those that were stopped a little short of the test stopping criterion). The t_e parameter as with the S_e parameter for these tests is a measure of a quasi-equilibrium stage and relies on the criterion for stopping tests being suitably defined and consistent across the tests (see Section 7.1.9 for further discussion of this).

b) Scour time development and rate of change of scour

In order to compare the shape of the scour curve between tests and study the differences in the rate of change of scour under the various test conditions, in Figure 7.13 the scour time development curves are normalised by the equilibrium scour depth and the time to equilibrium parameters.

Figure 7.13a indicates that while many of the tests show qualitatively good agreement in terms of the shape of the curve, there is some variation between the tests. For example in the larger flume there is a consistent difference between the fine and coarse sand curves, with a faster rate of scour in the fine sand. Similarly there is a difference between tests at the two pile diameters in the larger flume with a faster scour rate at the 20 mm pile. In the small flume, the curves from the T-1 test series have slower scour development in the first section, but the shape of the curves for the fine and coarse sands are fairly similar to each other. These differences may be indicating a

weak dependence on the V/V_{cr} parameter, with increasing scour rate of change with V/V_{cr}, so that at high V/V_{cr} the curve is steeper in the first section and flatter in the second section compared to a curve at lower V/V_{cr} where the curve is less steep in the first part, but then flattens off less quickly in the final section.

This is in agreement with the literature such as Melville and Chiew (1999) who also plotted S/S_e versus t/t_e and reported an influence of V/V_{cr} on the S/S_e versus t/t_e curve. They plotted the data on a log-log plot, so for direct comparison with their data, in Figure 7.13b the test data is plotted in a similar manner. In this format they plotted a set of linear trends for S/S_e versus t/t_e with a greater proportion of the equilibrium scour depth being obtained at a given value of t/t_e for tests with higher V/V_{cr} values. Similarly, in Figure 7.13b test R.5 has the highest V/V_{cr} parameter and plots as the uppermost line. The T-1 test series and the 90 mm pile coastal flume tests had lower V/V_{cr} values and plot towards the bottom of Figure 7.13b.

There is scatter in the data, and this is also true in the data of Melville and Chiew (1999), where there is considerable overlap in the curves for different V/V_{cr} values. The scatter in the data is an indication of the effects of other variables on the rate of change of scour development. However, it is anticipated that much of the scatter is due to experimental uncertainty depending on the method of identifying the S_e and t_e parameters. This probably explains why the T-1 test curves are similar despite the difference in V/V_{cr}, as the test stopping criterion was not followed in this test series.

The 20 mm pile tests in the larger flume do not fit the expected trend in Figure 7.13. These showed a faster scour rate than at the 90 mm pile despite a similar V/V_{cr} value. Therefore, for the 20 mm pile tests in the coastal flume, S_e/D, t_e and the rate of scour have all been altered relative to the tests at the larger piles. This is probably related to the steeper gradient in the downflow and higher frequency of eddies relative to the pile diameter discussed in Sections 2.2.6 and 2.7.4. Where these have not remained in proportion with the geometric scaling between the piles, but have actually increased relative to the pile diameter then the V/V_{cr} parameter will not be representative of the actual capacity for scour at the pile. Instead scour will be more representative of that under a larger V/V_{cr} value, which is then consistent with the higher placement of the 20 mm pile scour time development curves in Figure 7.13b compared to those at the 90 mm pile.

In terms of the shape of the curves, Melville and Chiew (1999) found that 50% of equilibrium scour occurred within 0.1-10% of the time to equilibrium, and 80% of the scour process was completed in 5%-40% of the equilibrium time, which demonstrates that there can be considerable variation in the scour rate. In Figure 7.13 50% of the scour process occurred in 5% of the time to equilibrium and 80% of the scour depth occurred within 10%-30% of the equilibrium time, in agreement with Melville and Chiew (1999), although the range is larger for the data of Melville and Chiew (1999) because this covered a wider range of V/V_{cr} values from scour threshold up to critical velocity for the sediment.

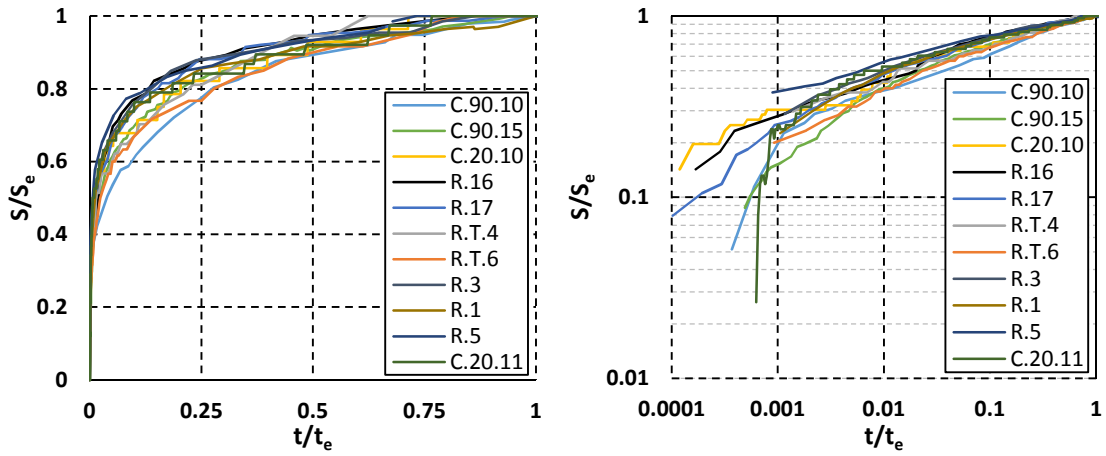

a) b)

Figure 7.13 Scour development plotted as normalised scour depth versus normalised time a) normal plot b) log-log plot.

7.1.9 Test stopping criteria

One aspect that has become evident in the discussion above is that the tests may be showing sensitivity to the definition of the t_e parameter. This section, therefore, discusses the test stopping criterion in more detail.

One interesting result shown in Section 6.1.1 was that even in the very longest duration tests compared to the expected timescale of scour, a true equilibrium condition was not reached - scour depth continued to increase, albeit slowly. This demonstrates the need for the use of stopping criteria, not only to curtail the tests for practical reasons, but also because it may otherwise be very difficult to determine if a test has truly stopped, as a gradual creep in scour depth may continue for an extended period.

For the longest duration test (C.20.15), which was at the 20 mm pile in the coastal flume in uniform fine sand, a range of criteria found in the literature can be applied and compared. Table 7.6 shows the results for eight different stopping criteria (which were discussed in Section 2.7.4) in comparison with the criterion used in this study. The range in definition of equilibrium scour depth and time to equilibrium from these different approaches is significant and illustrates the issues that this will cause when comparing data in the literature due to a lack of consistency when only equilibrium parameters are reported, or where these are used to inform prediction equations, without explicitly stating the stopping methodology, or indeed making available the full data to enable other criteria to be applied.

From Table 7.6 it can be seen that relying purely on a change in slope in a log plot of scour depth versus time is not a reliable method as several changes in slope are recorded during a test, as was found by Simarro et al. (2011). This method is likely, therefore, significantly to underestimate S_e and t_e. Using a criterion of $<d_{50}$ per hour also resulted in much smaller S_e and t_e parameters compared to the other criteria. Due to the short time period used in this criterion, natural variation in the scour rate through the curve is not taken into account with this approach so that it is more

likely that this criterion will assume equilibrium has been reached when it has not. The criteria of Lança et al. (2013a) and Melville and Chiew (1999) give the same S_e parameter, and the criterion used in this project results in a similar scour depth to these methods. However the time to equilibrium parameter is significantly different between these three approaches. This gives confidence in using the methodology employed in the present study for obtaining a reasonable estimate of the S_e parameter, but implies there may be significant error in the t_e parameter, which helps to explain the scatter in the figures in Section 7.1.8.

Table 7.6 Comparison of different test stopping criteria with results from test C.20.15.

Stopping criteria	**Author**	**S_e/D**	**t_e**
<d_{50} per hour	Link et al. (2006)	1.65	13.7
<2d_{50} in 24 hours	Fael et al. (2006)	Criteria not reached	
Check for flat slope on semi-log plot	Cardoso and Bettes (1999)	1	0.19
>7 day test duration	Lança et al. (2013a); Lança et al. (2013b);	Criteria not reached	
<2mm in 24 hours	Lança et al. (2013a)	1.9	43
<0.05D/3 in 24 hours	Grimaldi et al. (2009)	Criteria not reached	
<0.05D in 24 hours	Melville and Chiew (1999)	1.9	55.2
Test run for 1-2 weeks	Simarro et al. (2011)	Criteria not reached	
<0.025D in 6 hours	Criteria used for these tests	1.8	25

The Lança et al. (2013a) and Melville and Chiew (1999) methods result in a t_e parameter approximately twice as long as that in the criterion used in this project. These criteria would simply not have been practical to use in this study as each test would have taken over a week of working hours to run, even in the small flume. Furthermore, the test used in the comparison in Table 7.6 was not run for long enough to apply three of the criteria to it. These criteria, although more accurate would be very difficult to follow due to practical reasons (no overnight testing, sharing facilities with others).

The final scour depth recorded in the test was 2.05 at 80.7 hours, so the longest criterion that can be applied to this test, that of Melville and Chiew (1999), underestimates S_e/D by 7% and the equilibrium time by 32% compared to the end values, which are still not the equilibrium values. This indicates that the stopping criteria that were not applied to this test because it was not run for long enough will have a significantly larger t_e parameter compared to the other criteria in Table 7.6, but less of a difference in the S_e/D parameter. This is a very important result in terms of predictive methods for scour, because many rely on a t_e parameter and therefore will be constrained by the consistency of its definition. Predictive methods are discussed in greater detail in Section 7.3.

What is clear from this analysis is that a consistent approach is particularly important in order to understand the trends and relationships between parameters for scour. It would be beneficial for different researchers to use the same criteria (standardised approach) to enable inter-test comparison. At the least researchers should clearly report the definition they used, or make

available the full time development curves. Definition of a quasi-equilibrium criterion would be useful to enable laboratory testing to be practical, if this could then be linked to a final equilibrium criterion. However, in order to do this some very long duration testing would be needed.

7.1.10 Final remarks on scale effects

No scale effects were observed between the tests at the 90 mm pile in the larger flume and the 40 mm pile in the small flume. This is consistent with these tests being scaled from similar field parameters so that the small differences in parameter ratios between these tests were not significant, and the different scale ratios of 1:55 and 1:125 for the tests in the two flumes are equally valid in terms of quantifying the S_e/D parameter. Scour depth did not scale with pile diameter when the pile diameter was reduced. This was not found to be related to the ratio of D/d_{50} but instead due to a lack of similarity in the flow patterns in the vicinity of the pile.

In the tests in the larger flume the flow velocity and water depth parameters remained constant for the tests at the different pile diameters. A smaller pile in the same flow results in a relatively stronger gradient upstream of the pile, as the pile causes less of an obstruction to the flow. This means there is a change in the dimensions of the flow patterns relative to the pile, resulting in a relatively stronger downflow and horseshoe vortex, causing an increase in the S_e/D parameter. This effect is quantified by the V^2/gD parameter, however, this parameter did not fully account for the smaller scale effects at the 25 mm pile in the small flume compared to the tests in the larger flume.

In terms of the scour timescale in the larger flume tests, this was also influenced by the reduction in pile diameter, with the time to equilibrium becoming relatively longer compared to the pile diameter. This may be similarly linked to the change to the dimensions of the flow patterns relative to the pile.

It is plausible that there are also Reynolds number and Froude number effects in these tests, as the scour behaviour at the smaller pile diameters could not be fully accounted for by the Euler number. However, further testing would be needed to investigate this, by running a test series where Fr, Re_D and V^2/gD are varied independently, over a wider range of values, in order to understand fully the effects of Froude number, pile Reynolds number and V^2/gD on scour behaviour.

7.2 Discussion of key results: layered and mixed sands, tidal and wave-current flow

This section develops explanations for the novel results obtained from the layered, mixed, tidal and wave-current test programmes.

7.2.1 Layered tests

An extensive comparison of the layered tests with literature data is not possible because few studies have been conducted in similar sediment beds. However, the small number of studies identified in the literature review, Section 2.4, to be similar to this work are compared with the present data in the first part of this section, before the new findings from the test programme are discussed in the second part of the section.

a) Comparison of layered test results with literature

In the literature review, Section 2.4.4, it was found that a small number of studies have been conducted in layered sand beds with coarse sand overlying fine sand in the context of understanding the bed armouring process. These studies can be compared with the coarse over fine sand layered test that was conducted as part of the P-2 test series. Studies by Raudkivi and Ettema (1985) and Dey and Raikar (2007b) found that the equilibrium scour depth reached in this type of layered bed depended on a range of parameters and the flow regime (clear water or live bed), so that in some cases the scour depth was less in the layered bed than it would be without the armour layer, but under other conditions scour was actually deeper than without the presence of the armour layer (see Section 2.4.4 for further details). In this project the coarse over fine sand layered test resulted in the former result, because the V/V_{cr} parameter for this test was well within the clear water condition for both of the sand layers.

For the case of fine sand overlying coarse sand, only one study was available for comparison at a similar structure. Gjunsburgs et al. (2014) investigated scour in a bed of fine sand overlying coarse sand at an abutment as well as in a bed with the layers reversed so that coarse sand overlaid the fine sand (see Section 2.4.5 for further details). While they concluded that scour in these layered beds could be predicted by superposition of the uniform sand tests, on closer inspection of their data it is clear that in the bed of fine sand overlying coarse sand the scour depth is increased in the lower coarse sand layer compared to scour in a uniform bed of the coarse sand. In the coarse sand overlying fine sand bed, the scour depth is reduced in the lower layer compared to in a uniform bed of fine sand, in agreement with the findings of the present study. This gives confidence in the present results and indicates that they apply to a wider range of structures as a similar result can also be seen in Govsha and Gjunsburgs (2012) relating to guide banks in rivers.

b) Explanation of key results from layered tests

The key finding from the layered tests was that scour development in the lower sand layer did not follow the same trend as that in a uniform sand bed of the lower layer sand type. In a bed of fine sand overlying coarse sand, scour development was enhanced in the lower coarse sand layer, whereas in a bed of coarse sand overlying fine sand, scour in the lower fine sand layer was suppressed compared to a uniform bed of the same sand. In this section a physical explanation of these results is developed by considering the mechanisms which may be responsible.

A change in scour development through the lower sand layer suggests that there has been a change to one of two aspects due to a difference in the sand type overlying the lower sand layer. Either the layered bed configuration has resulted in a change to the flow patterns in the scour hole compared to those over a uniform bed of the lower layer sand type, or the layered configuration has resulted in different behaviour of the sediment in terms of its resistance to erosion.

The first of these can be considered by investigating the scour hole shape in the two sands using the results from the echosounder profiling (Section 6.5). A difference in scour hole shape between

the two sand types for a given depth of scour at the pile would result in different flow patterns within the scour hole. This would mean that when the two sands are placed in a layered configuration the coarse sand as the lower layer feels different flow conditions compared to when it is in a uniform bed of coarse sand.

However, as was shown in Section 6.5, the upstream scour hole profile is unaffected by sand type, flow velocity, layer configuration or time into the test, only depending on the scour depth at the pile. The upstream slope angle is generally thought to be linked to the angle of repose of the sediment, and as there is no difference between the slopes in the two sand types this indicates that the two sands have a similar angle of repose, which is conceivable considering the difference in grain size is relatively small.

In contrast, there was some variation in the downstream scour hole profiles in the echosounder results. The change in downstream profile was shown in Section 6.5 to be a function of time into the test in terms of different dune migration rates of the two sand types because of the different V/V_{cr} parameters for the two sands under a given flow condition, rather than being a function of scour depth. As shown in Section 6.5 this difference in downstream dune is most prevalent during the early stages of the tests. Later into the tests there is less difference in dune shape between the two sands. Towards the start of the tests the coarse sand dune slope is approximately 3 cm closer to the downstream edge of the pile and about 1 cm higher at its peak than that in the fine sand. The coarse sand is less mobile than the fine sand so it is deposited more quickly, closer to the back of the pile to form a higher dune. More of the fine sand will be deposited further downstream, and the dune will migrate faster downstream due to its greater mobility under the same flow velocity.

The downstream dune will create a flow blockage causing acceleration of flow around it and deceleration of flow upstream of it. However, these changes to the flow patterns can be expected to be small in the tests because the downstream dune is located in the pile wake region, in an area of lower velocity (see flow visualisation Section 6.7.1). Also, the dune only presents a small area of blockage to the flow as it does not extend throughout the full water column. A larger dune would have more of an influence on the flow as it would require greater flow acceleration around its sides due to presenting a larger blockage area. Although it seems unlikely that this would be having an effect on the horseshoe vortex behaviour at the pile, to investigate this further the time development of the dune can be considered. If the larger dune in the coarse sand acted to hinder scour development due to deceleration of flow in front of it interacting with the horseshoe vortex system, over time this influence would diminish as the dune migrates downstream, becoming flatter and further away from the pile. This would therefore, at best affect the timescale of scour, not the ultimate scour depth reached, as once the influence of the dune has disappeared the horseshoe vortex can continue unhindered. In the layered test both the timescale and the ultimate scour depth reached in the lower coarse sand layer are altered, so this cannot be accounted for by the differences in the scour hole shape downstream of the pile between the two sand types.

This explanation is also consistent with test R.N.27 where the downstream dune was resmoothed once quasi-equilibrium scour depth was reached (see Appendix 3). There was no observed effect

on the scour depth at the pile due to the disappearance of the downstream dune. While this does not allow information to be obtained in terms of an influence on time development of scour depth during earlier stages of the test, this does show that the flattening of the dune has no impact on the ultimate scour depth in terms of the presence of the dune preventing scour to any extent.

If it is not the scour hole shape or downstream deposition dune shape that is responsible for the change in scour development in the lower sand layer then by elimination it is likely to be due to interactions at the grain scale between the two sands.

Possible mechanisms relating to grain interactions for the layered case with fine sand overlying coarse sand can be developed from observations of the tests. The presence of the vortex at the base of the upstream scour hole slope is visible due to the suspension of sand particles within it. In the fine over coarse sand tests the sand in the vortex appeared to be predominantly the fine sand (see Figure 7.14). The strength of the vortex fluctuates and hence the sand suspended in it is frequently deposited and re-entrained allowing interaction between the overlying fine sand and the underlying coarse sand in the scour hole close to the pile.

Potentially this could result in a mixing process as the vortex strength fluctuates that helps mix the fine and coarse sands together, causing a change to the grain distribution and structure of the surface layer of sand in the scour hole. This in turn would make the coarse sand particles more susceptible to erosion due to greater exposure of the grains, resulting in an increase in scour depth compared to that in a uniform bed of the coarse sand. This mechanism of increased erosion of coarse grains depending on the grain distribution and bed structure is similar to the mechanism for scour in the mixed sand tests which will be discussed in the next section. This mixing effect would be local to the vortex at the base of the upstream scour hole slope and would only affect the surface layer of sediment, as from the core samples it was found that any mixing between the sands was contained well within 1 cm beneath the sand-water interface (see Section 6.9.3).

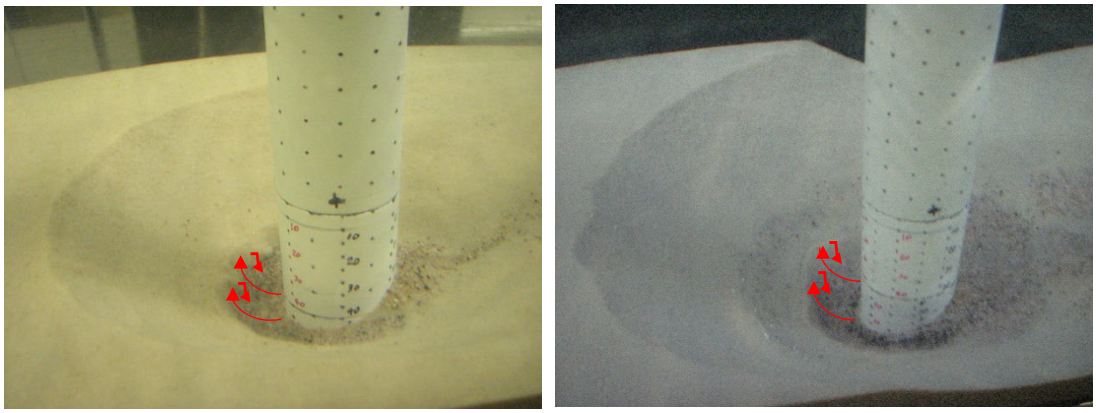

Figure 7.14 Observations of the vortex at the base of the scour hole slope in fine sand overlying coarse sand layered tests.

A second mechanism could be that rather than mixing the fine and coarse sands, the fine sand particles being more mobile and hence more numerous in the vortex collide with the coarse sand particles on the bed when they drop out of suspension due to fluctuations in the strength of the vortex, and the particles being at higher velocity give the coarse particles momentum to erode

more so than when in a bed of coarse sand where fewer particles are entrained and suspended within the vortex.

Another aspect of the fine over coarse sand layered test findings is why the behaviour changes with layer depth, and in particular why there is a point at which scour no longer occurs in the lower layer of coarse sand as the upper layer thickness is increased. The transition point between whether scour occurs in the lower layer of coarse sand or not is linked to the layer depth and hence to the strength of the horseshoe vortex. As scour depth increases, the horseshoe vortex strength weakens (see Section 2.1.3). This means that the mechanism for scour enhancement in the lower layer is reduced because the vortex next to the pile cannot entrain the fine sand as much and consequently the interactions between the fine and coarse grains will be less prevalent.

In the case of the coarse sand overlying fine sand test the suppression of scour in the lower fine sand layer can be attributed to bed armouring effects whereby the larger grains from the coarse sand provide a protective layer over the fine sand, anchoring the fine sand grains in place and preventing them from being eroded, as was discussed in relation to the literature at the start of this section (also see Sections 2.4.1 and 2.4.4).

Now that the mechanisms have been described for both layer configurations of fine sand overlying coarse sand and coarse sand overlying fine sand, it is interesting to compare this with the results from the tests with a 3-layered bed. In test R.20 with a fine-coarse-fine layered bed the scour in the second layer of coarse sand behaved in a similar way to the 2-layered tests. Scour in the 3rd layer of fine sand was then supressed compared to scour development at that depth in a uniform bed of fine sand, again repeating the previous trend. However, this result was interesting, because much of the overlying material for the 3rd layer was actually fine sand. This indicates that bed armouring effects are independent of much of the overlying material. Instead it appears that what is important under these clear water conditions is the sand that is interacting within the scour hole, close to the pile. In the 3-layered test with coarse-fine-coarse layers (test R.21), scour in the middle layer of fine sand was supressed, consistent with findings for the other tests. However, there was no enhancement of scour in the 3rd layer of coarse sand despite a layer of fine sand above it. This suggests that the mechanism associated with the fine sand interacting with the coarse sand was not strong enough to overcome the effects of bed armouring resulting from the uppermost coarse sand layer.

7.2.2 Mixed tests

This section focuses on the tests in the mixed sands. These tests are first compared with the literature available on scour in non-uniform sediments, before the novel results in terms of equilibrium scour depth and scour time development are discussed in detail in the second part of the section.

a) Comparison with literature

Although few researchers have reported tests in bimodal sands, the mixed sand tests can be compared to literature trends for non-uniform sediments more generally.

In Figure 7.15 the S_e/D values in the mixed sand tests are plotted against the V/V_{cr} parameter, along with the uniform sand tests plotted previously in Figure 7.1. The V_{cr} parameter was obtained using the d_{50} value for each sediment mixture as determined from the laboratory sieve analysis (see Section 6.8.4).

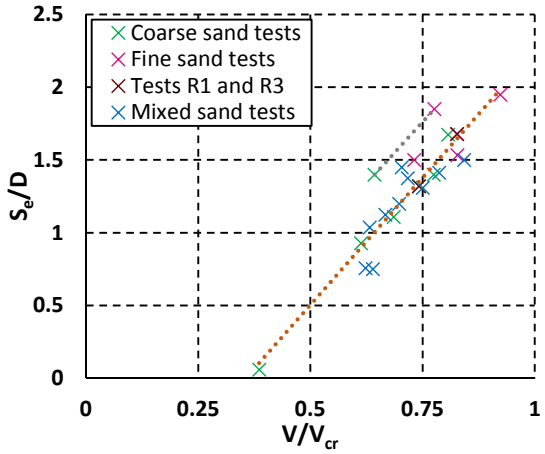

Figure 7.15 Comparison of mixed sand tests with uniform sand tests in terms of the relationship between flow intensity and non-dimensionalised equilibrium scour depth.

Interestingly there is good agreement between the uniform and mixed sands, with most of the mixed tests following the straight line trend of increasing S_e/D with V/V_{cr}. Furthermore, the mixed sand test conducted at the 20 mm pile in the larger flume shows a similar level of increase in the S_e/D parameter as in the uniform sand cases. This indicates that the effect of sediment non-uniformity on equilibrium scour depth is insignificant in these cases.

Exceptions to this are found at each extreme of the V/V_{cr} range. At low values of V/V_{cr} the 75% and 90% coarse sand tests resulted in smaller scour depth than expected, indicating that the sediment distribution is affecting the scour process under these conditions. This will be discussed in the second part of this section.

The test run at the highest value of V/V_{cr} also deviates from the trendline in Figure 7.15, with a reduction in scour depth. This could be due to bed armouring becoming more important as V/V_{cr} increases which is in agreement with the findings of Melville (2008) (see Section 2.4.1). This test (R.14) had a 50%-50% fine-coarse mixed sand bed, and bed armouring is expected to be the most prevalent in this mixture because it has the largest σ_g parameter. However, the sediment non-uniformity parameters are relatively small for all of the mixtures which helps to explain the close agreement between most of the mixed and uniform sand tests. Because of this it should be possible to predict the equilibrium scour depth in most of the mixed tests using the same scour equations as for the uniform cases. A bed armouring factor may need to be introduced in order to model correctly the tests at higher V/V_{cr}. Also, an additional factor would be needed for the

small percentage fine sand tests at low V/V_{cr} values to model correctly this behaviour. Further discussion of scour prediction in the mixed sands is included in Section 7.3.

b) Explanation of key results

In Section 6.1.3 three new findings were discussed for the mixed sand tests: that tests under lower flow velocities exhibited a linear trend for part of the time development curve, that the mixtures with a small percentage of fine sand resulted in a reduction in the equilibrium scour depth, and that these trends varied with the flow velocity.

Following the discussion of the layered sand tests in Section 7.2.1 it is understood that the scour hole shape was similar under the different flow velocities and sand types, so that the approach velocity profile and local flow patterns within the scour hole are also expected to be similar between the tests. A key result from the core sample data was that there was no preferential scouring of fine sand particles compared to the coarse sand particles in the mixed sand beds. This means that, as with the layered cases, the changes to the scour process are related directly to differences in the interactions between the sand particles because of the alterations to the sediment grain distribution for these tests. This section will discuss the mechanisms for the grain-grain interactions and influence on scour depth for the different test conditions, in order to explain the causes of the three identified observations.

Firstly, the linear trend will be considered. In the 25%, 50% and 75% mixed sand tests at low flow velocities a clear change to the scour development trend with time was observed, with the curve initially following the expected non-linear trend with decreasing gradient as the scour depth increases, before the curves started to follow a linear trend.

A change in trend in the scour development curve has also been reported in the literature (see Section 2.6.5) for uniform sand tests where the scour process may be best modelled by applying different functions to different stages of the curve with time, and Talebi et al. (2004) and Chang et al. (2004) even reported that the very initial stage of scour appeared to follow a linear trend. However, a linear trend in the very initial stage of scour is probably due to the horseshoe vortex maintaining its strength while the scour depth is still small relative to the pile diameter so is unlikely to be related to the linear trend found in these tests which is sustained for longer and to a deeper scour depth.

In Section 7.1.8 it was noted that a low V/V_{cr} parameter results in a slower rate of change of scour. Observations showed that the initial stages of the scour process described by Unger and Hager (2007) where the scour hole is deepest at the side of the pile rather than directly upstream of the pile persisted for longer during these tests. This delay in the scour process gives more time for instabilities to occur and asymmetry in the scour hole shape to develop which was observed in some (uniform sand) tests. In relation to the mixed sand tests, this may enable sediment interaction effects to be more prevalent, which would partly explain why this trend is not seen at higher flow velocities (see later in this section for further discussion). Particles are less erodible under weaker flow so sediment entrainment is likely to be more sensitive to grain-grain interactions such as how the bed is structured. For example the hiding and exposure of grains

can make a significant difference to the erodibility of individual grains (Shen and Lu, 1983), see Section 2.4.3.

The linear trend seen in the scour development curves is less steep compared to the expected scour development curve that can be modelled with an exponential function which suggests that the grain-grain interaction effects are inhibiting scour development compared to the usual scour mechanism relating to the diminishing strength of the horseshoe vortex with increasing scour depth. The trend in the initial part of the mixed sand scour curves coincides with when the horseshoe vortex is strongest, and so it follows that at this stage of the process the vortex is strong enough to overcome any increase in resistance to erosion due to the sediment interaction effects, so that the strength of the horseshoe vortex is the limiting factor for scour development. As scour depth increases and the horseshoe vortex weakens, the grain-grain interaction effects become relatively stronger, inhibiting scour progress. This means that further weakening of the horseshoe vortex with depth no longer affects the scour process because the limiting factor instead is the rate at which the mixture can be entrained into the flow. Consequently a linear trend is found.

As the proportion of fine to coarse sand in the mixture varies, the gradient and duration of the linear section changes. The structure of the sediment will be altered due to the change in proportion of fine to coarse sand in the mixture so that the resistance to erosion is also likely to change, dictating the gradient of the straight line section. There is also a change in the V/V_{cr} parameter as the distribution of the mixture varies, changing the relationship between the strength of the horseshoe vortex compared to the erodibility of the sand. At a higher V/V_{cr} parameter it would be expected that the duration of the linear trend would be shorter and start later into the test as is seen in Section 6.1.3 because the horseshoe vortex will be relatively stronger compared to any grain-grain interaction effects.

For several of the mixed sand tests the grain-grain interaction effects only influence the rate of scour development, not the equilibrium scour depth reached. However, in the tests conducted at low flow velocity in the mixed sand beds consisting of a small proportion of fine sand compared to coarse sand, the equilibrium scour depth did appear to be affected. This suggests that an additional scour mechanism may be present. A difference in density for these mixtures was ruled out, as the measured change in density between the mixtures was small (see Section 6.8.1), and in test R.28 where a higher density sand bed was tested this had little effect on scour development. However, the permeability tests showed approximately 50% reduction between the uniform coarse sand test and the 90% coarse sand test (see Section 6.8.3). This change in permeability without a significant change in bulk density demonstrates that there has been a change to the arrangement of the sand grains within the bed. While the overall volume of voids within a sample remains constant, the distribution of voids within the sample has changed so as to have a greater number of small gaps between particles compared to fewer larger gaps in a more permeable mixture. This change in particle arrangement may act to reduce the erodibility of the sand mixture due to its effect on the flow-particle interactions, with smaller, more numerous

voids distributed through the sample acting to break up the flow reducing the drag forces on the grains.

It was noted in Section 6.1.3 that further discussion is needed to assess the certainty of this finding relating to the small percentage fine sand tests. As detailed in Section 6.1.3 there is some conflicting evidence as to whether this result is supported across all tests, due to discrepancies between the two coarse sand tests conducted under the same flow conditions (tests R.T.4 and R.12). Understanding the possible reasons for the lack of agreement between these two tests will help to assess the likelihood of this finding being genuine and repeatable.

In Section 6.1.3 the unusual increase in scour depth in test R.12 was found to occur soon after the test was paused overnight. This suggests that the unusual scour development curve may be due to a change in the flow parameters during the restart procedure. This could be due to the restart being completed too quickly, which can cause a surge of water down the flume and a temporary increase in velocity. However, this is unlikely because the restart procedure was developed to prevent this from occurring, and this would probably show itself as a more sudden increase in scour depth immediately following the restart in the scour curve.

Another explanation is that at this lower flow velocity, as the initial scour stage lasts for longer, the scour process may be more unstable and potentially more sensitive to fluctuations in the flow and the pause-restart procedure. The observed asymmetry in the scour hole shape prominent in test R.12 is probably linked to the slower scour timescale at low V/V_{cr} so that the scour hole assumes its predominant shape with the deepest scour depth at the front of the pile much later into the test. With the deepest part of the scour hole remaining at the side of the pile for a considerable length of time the asymmetry between either side of the pile will be prolonged and significant. This asymmetry only reduced as the point of deepest scour reached the front of the pile which coincided with the increase in scour depth towards the end of test R.12. Only once the horseshoe vortex weakened enough at the far side of the pile because of the increase in scour depth could the scour depth at the nearside of the pile begin to catch-up. Figure 7.16 shows the scour hole when the deepest part of the scour hole was at the pile side, and with the deepest part of the scour hole at the pile front. Asymmetry in the scour hole shape was not observed in all tests in this flow condition. It may be that asymmetry is induced at the start of the test due to natural fluctuations in the flow. If no asymmetry occurs in the initial phase of scouring then the scour hole can develop more uniformly under the same flow condition.

The repeatability for test series T-1 was in general shown to be poorer than for other test series (see Section 6.10). While this may partly be a result of inhomogeneity in the sand mixtures (see discussion later in this section) it may also be linked to the slower rate of scour prolonging this initial phase of scour and the scour hole shape remaining in the initial, more unstable phase for longer.

a) 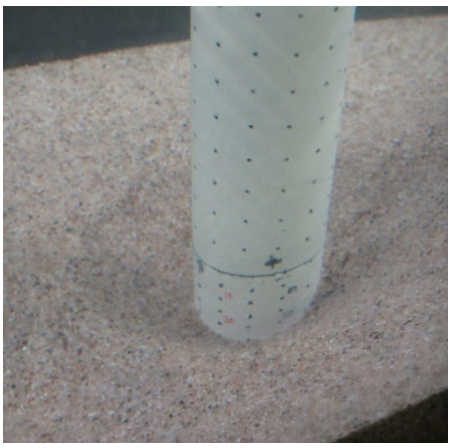 b) 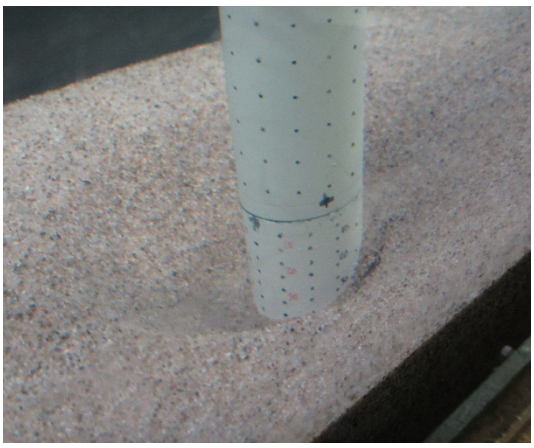

Figure 7.16 Scour hole with deepest point at a) pile side (cross-stream direction) b) pile front (upstream).

While this discussion is intended to provide plausible explanations of this unusual test result, it is clear that further testing would be needed in order to understand conclusively the result. In order to come to a provisional conclusion about this result the evidence for and against can be weighed up. Evidence to suggest that the scour depth may not be smaller in these cases than in the uniform sand test is that the mixed and uniform curves from tests R.11 and R.12 are in very close agreement for the first section. This matches with tests R.23 and R.N.27 conducted at higher V/V_{cr} where the scour curves also matched between the mixed and uniform sands. Evidence to suggest that the scour depth is genuinely less in these tests is the link with a reduction in permeability, that the equilibrium scour depth in the two coarse sand tests (R.T.4 and R.12) is approximately equal, and that this equilibrium depth is in good agreement with the V/V_{cr} trend in Figure 7.1.

Interestingly even if the true result is that the uniform curve and the mixed curves are the same, this is still indicating a small reduction in scour depth from what would be expected in the mixed tests, because these sands have an increased V/V_{cr} parameter compared to the coarse sand.

Another significant result from the mixed tests to discuss is the apparent dependence of the scour time development trend on the flow velocity. The tests which displayed a linear trend occurred at approximately $V/V_{cr}<0.7$. This suggests that there is a critical value of V/V_{cr} where the behaviour changes, which can be linked to the ratio of the strength of the horseshoe vortex compared to the sediment resistance to erosion. The core samples demonstrated that all particle sizes were scoured regardless of flow velocity implying that the scour mechanism is the same under the different flow conditions. The structure of the sediment bed in the mixed sands has resulted in the larger particles being more erodible but at the same time the larger particles protect the finer particles from being entrained.

It has not been tested as to whether the trends discussed above are related to the specific distributions of the mixtures and the degree of bimodality. That these trends have not been reported in the literature for non-uniform sands may be indicative that this is related only to the specific mixtures tested in this project or perhaps to bimodal sediments in general. Further

evidence to support this is that the most bimodal distribution (50% mixture) had the scour curves with the longest linear trend sections indicating that the grain-grain interactions are dependent on the grain distribution and may be linked to a lack of intermediate grain sizes, so that hiding-exposure of grains is more apparent. Further testing would be needed of a greater range of sediment distributions with bimodal and normal distributions to progress understanding of this.

One interesting observation from the core samples was the inherent inhomogeneity of sediment distribution in the mixed tests (shown in Section 6.9.1). It seems likely that this will affect the scour development, seeing as the scour development is known to be sensitive in general to grain size and distribution from these and other tests. This looks to be evident where the scour development curves are less smooth in some of the tests.

7.2.3 Tidal tests: explanations of results and comparison with literature

This section focuses on the tidal flow tests presented in Section 6.2 in order to provide a better understanding of the scour process under the uniform reversing flow and spring-neap cycle tests. The reasons for the differences in the scour behaviour under these different flow conditions, in the different sands and at the different pile diameters are explored. In these tests the differences in scour development will be predominantly explained by considering the key parameters that affect the rate of scour development under these flow conditions. It is anticipated that the main parameters are the flow velocity and sand type, the scour depth at the start of the half cycle, and the duration of the half cycle.

First to be considered are the tests conducted with a constant velocity in the flood and ebb directions. If it is assumed that the scour process is roughly similar to that in unidirectional flow, so that the scour time development curve in each half cycle follows a similar trend to the relevant part of the scour curve obtained in unidirectional flow depending on the parameters listed above, then it would be expected that the scour depth would increase between each half cycle up to an equilibrium scour depth. However, because there is a difference in scour depth between the upstream and downstream sides of the pile due to scour being concentrated at the front of the pile and deposition of sand immediately downstream of the pile, there will be a setback of the scour time development curve when flow is reversed. Some of the time at the start of the half cycle will be used to clear this deposited material, before scour can then continue beyond the depth obtained under the previous half cycle. If scour development follows broadly the same scour rate of change curve as in unidirectional flow from a given depth then the scour depth would still be expected to increase between each half cycle, but because of the offset in scour depth this would result in a slower rate of change in (peak) scour over consecutive cycles. A schematic of this proposed scour behaviour is given in Figure 7.17. This explanation fits well with the scour development observed in tests C.90.18, C.90.12 and C.90.14 (Figures 6.26, 6.27 and 6.28).

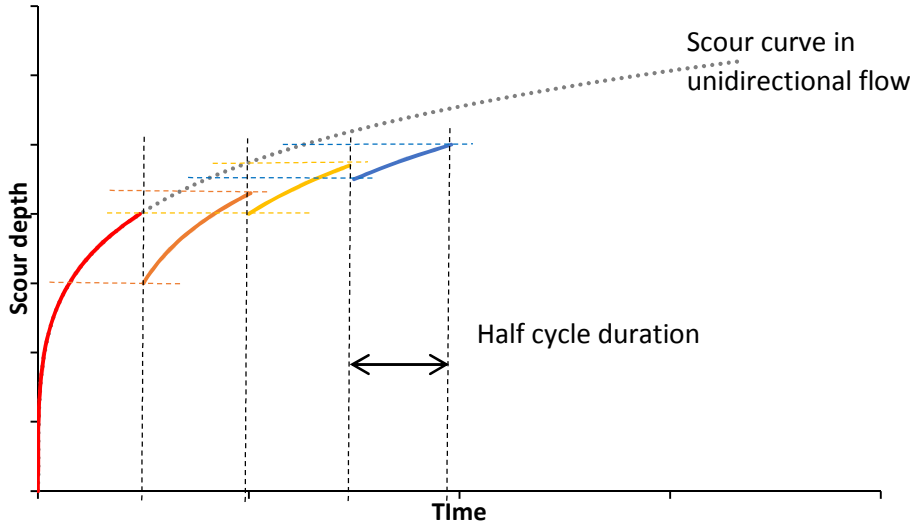

Figure 7.17 Schematic of scour development under symmetric reversing flow.

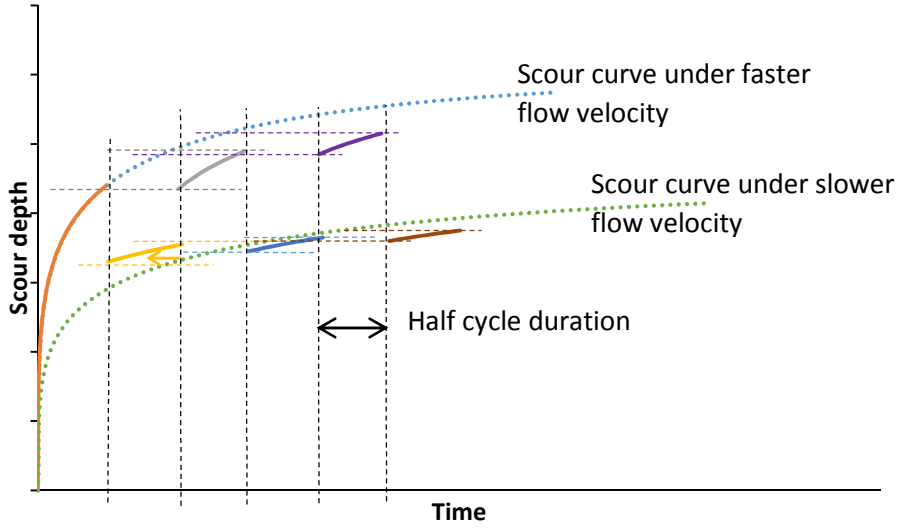

Figure 7.18 Schematic of scour development under asymmetric reversing flow.

A second case to consider is the scour behaviour under asymmetric reversing flow. If the flow velocity in the reverse (ebb) direction is slower than in the flood direction then the rate of scour will also be slower on reversal. This means that because the half cycle time is constant, less scour would be able to occur in a half cycle in the ebb direction than in the flood direction. Depending on the difference in scour rate between the two directions, and because of the deposited material having to be scoured at the start of the cycle, the scour depth may not be able to exceed that obtained in the previous half cycle. This will result in a clear difference in peak scour depth obtained in the flood and ebb half cycles, which is evident in the spring-neap tests. Although tests C.20.18, C.20.12 and C.20.14 were designed to be conducted under constant flow velocity, the velocity profiles (Section 6.7) demonstrated that the flow in the ebb direction was actually reduced by 1 cm/s compared to the flow in the flood direction at the location of the 20 mm pile at the far

side of the flume. Therefore, the gap between scour in the flood and ebb directions seen in these tests (Figures 6.26, 6.28 and 6.29) is also consistent with this explanation.

Under asymmetric flow, if the scour rate is slower in the ebb direction, then less material will be deposited at the downstream side of the pile during the ebb half cycles. When the flow reverses back to the flood direction, there will then be less of a set-back in scour depth. Consequently the scour process can proceed beyond the previous peak scour depth at an earlier stage in the half cycle, further exacerbating the difference in scour depth between the flood and ebb directions. In Figure 7.18 a diagram of the scour development under asymmetric flow is given.

A greater difference in the scour depth in the flood and ebb directions was observed in the coarse sand compared to the fine sand beds in the spring-neap tests. The same velocity signal was used for the tests in the different sands, so the V/V_{cr} parameter was reduced in the coarse sand tests. In Section 7.1.8 it was seen that the shape of the scour time development curve in unidirectional flow varies with V/V_{cr} and at lower values of V/V_{cr} the rate of change of scour is slower in the first half of the curve. The equilibrium time is also reached more quickly than in tests conducted at higher values of V/V_{cr}. This means that for a given asymmetric flow conducted at lower values of V/V_{cr} i.e. in coarser sand, the portion of the curve that equates to scour from a given depth under the slower flow velocity in the ebb half cycle will be relatively closer to equilibrium time than the relevant portion of the curve in tests at higher V/V_{cr}. Therefore, there will be a bigger difference in the scour rate between the flood and ebb directions in the coarse sand tests.

The explanations so far would suggest that the equilibrium condition under symmetric reversing flow is more predictable than under unidirectional flow, as it will be controlled by the half cycle length relative to the rate of scour. Scour will not be able to continue once the rate of scour is slower than the half cycle time. Because the cycle time remains constant through a test, less and less scour can occur in a half cycle as scour depth increases. It can be foreseen that eventually under each flow reversal only the deposited material from the previous half cycle will be scoured, resulting in an equilibrium condition. This implies that the equilibrium depth reached would be less than in unidirectional tests, but depends on the length of the cycle, with a longer cycle enabling greater equilibrium depth (in agreement with Escarameia and May, 1999).

In regards to test C.90.1 where the flow was reversed once a quasi-equilibrium condition had been reached, scour was able to continue after flow reversal, because the flow was run for a substantial length of time in the reverse direction, so that the half cycle time was not a limiting factor for scour progress in this test.

In both the reversing and spring-neap tests an equilibrium condition appeared to be reached in the small pile tests but not in the large pile tests, where scour depth continued to increase substantially at the end of the cycle. The smaller pile diameter results in a shorter time to equilibrium compared to at the larger pile (see Section 2.2.1) so the timescale of reversal is effectively different at the two piles because the cycle time is constant, and so at the small pile a greater proportion of the scour curve is completed prior to flow reversal. The limiting case would be when the entire scour curve is completed in one half cycle. This would mean that no further

scour could occur in the reverse direction, assuming the limit for scouring is the same in both directions and purely a function of V/V_{cr}, not scour hole shape, etc. If a greater proportion of the scour curve occurs in the first half cycle, it will take fewer cycles to reach equilibrium than if less of the scour curve occurs in the first half cycle. This is why an equilibrium condition is reached in fewer cycles at the small pile than at the larger pile. It should be noted that bed ripple effects were also present in the small pile tests which provide an additional mechanism for the equilibrium condition to be reached more quickly/in fewer cycles.

In terms of the spring-neap tests there are several interesting findings to discuss further. One aspect is the stability of the scour hole under the neap section of the cycle. It was anticipated that scour would not continue under the neap cycles because the theoretical threshold velocity for scour initiation was not surpassed. The expected threshold velocity for scour from theory was 0.18 m/s in test C.90.19 (see Appendix 2). In general this coincides with the point at which scour occurs, although in some cycles (second half of 17th cycle and first half of 19th cycle) scour occurred despite the peak velocity being just under the critical value. This is most likely due to the limitations in the theory in terms of correctly modelling the relationship between bed shear stress and depth-averaged velocity. Bed ripples are known to cause a change to the initiation of motion on a flat bed, so it is plausible that the presence of the deposition dune upstream of the scour hole when the flow reverses would also result in a difference in the initiation condition for scour. However, the general agreement with the theoretical condition indicates that there has not been a change to the initiation of scour and this also supports the discussion in Section 7.2.1 where changes in scour hole shape in the layered and mixed beds were not thought to have had an effect on the scour process.

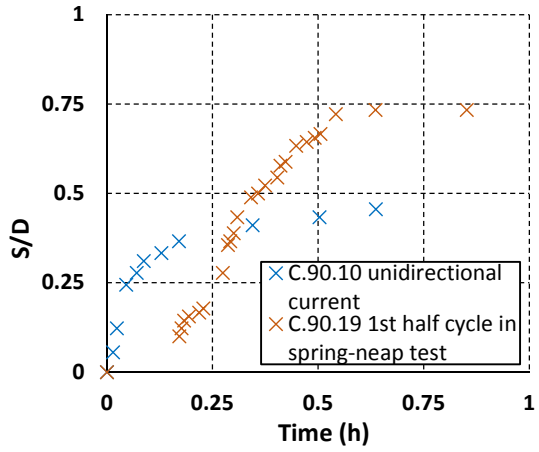

Figure 7.19 Comparison of scour development in first half cycle of spring-neap tidal cycle with unidirectional current test (coarse sand).

A comparison of the initial stage of the unidirectional current test and the first half cycle of the spring neap test in the same sand shows the significance of the scour timescale parameter on the scour process (Figure 7.19). In the spring-neap test where the velocity varies within the half

cycle this results in a deeper scour depth even though the average velocity during this half cycle is slightly lower than in the unidirectional current and reversing flow tests. In the spring-neap test the average velocity in the first half cycle is 22 cm/s, whereas in the unidirectional and reversing current tests it is 24 cm/s. The increase in scour depth under velocity varying flow is a result of the increase in the rate of scour under a higher V/V_{cr} parameter. If this difference in the scour timescale is not taken into account when comparing velocity varying flow tests with constant flow tests then the conclusions may not be valid, as the comparison will not be between like-for-like cases. However, it is difficult to determine a suitable method to normalise the scour timescale, as discussed in Sections 2.6.5 and 7.1.8 and this is something that requires further work.

Another interesting result discussed in Section 6.2.1 was the complexity of the relationship between the peak velocity and peak scour depth per half cycle, so that the scour depth was not always deepest under the half cycles with the fastest peak velocity, and a reversal in asymmetry in the flow so that the flow was stronger in the ebb compared to the flood half of the cycle did not necessarily result in a greater scour depth in the ebb half of the cycle compared to in the flood half. These results indicate that the history of the scour depth development over several previous cycles may be important for determining scour behaviour in future cycles. Scour depth is not purely dictated by the velocity within a given half cycle, but may also be influenced by the scour hole shape and extent, deposition zone, and scour depth at the end of the previous cycle. This helps to explain in more detail the scour development in the square wave reversing tests at the larger pile where there was a small amount of deviation compared to the model shown in Figure 7.17 in terms of the change in scour depth per half cycle.

These results also demonstrated that a range of peak scour depths were obtained under half cycles with the same peak flow conditions. It is possible in the clear water regime to have a different scour depth under the same stable conditions (below the threshold velocity for scour) because of different historical drivers for scour development, and the lack of infilling of the scour hole from the surrounding sediment bed. This means that the scour hole may be deeper than the expected equilibrium depth under a particular flow condition. Conversely in the live bed regime, Sumer et al. (2013) found that this is not the case because ultimately the scour depth tended to a constant value under a given flow condition owing to the combination of the scour and backfilling processes.

In the clear water regime, the scour depth is likely to reflect some of the worst flow conditions in its history (as no infilling occurs), although note that a small reduction in scour depth is seen from the worst cases under the first set of springs compared to under the neaps because the deposited material adjacent to the downstream pile face cannot be completely shifted under the lower flow conditions. However, this still results in the recorded scour depth being much deeper than predicted for the lower flow condition.

In terms of the expected trends in the literature for tidal scour, it is generally reported that an equilibrium condition will be obtained after only a few cycles (McGovern et al., 2014; Escarameia, 1998). However, this was not the case for most of the tests in this series where an equilibrium condition was not reached after many cycles. A key difference between this test series and many

of the studies in the literature (Escarameia, 1998; Jensen et al., 2006; Margheritini et al., 2006; McGovern et al., 2014) is that these tests were conducted in the clear water regime, and that the influence of upstream bed ripples was removed (note that the deposition dune was left intact). The removal of ripples mitigated the scale effects caused by ripples on the flat bed section being much larger compared to the pile than they would be in the field. This unique test methodology compared to other studies has had a significant impact on the results, increasing the number of cycles to equilibrium, lengthening the timescale of the scour process and potentially increasing the equilibrium scour depth. Importantly it was observed that by using this methodology it meant that infilling of the scour hole did not occur, despite the position of the deposition dune upstream of the scour hole. Without infill the scour process can continue more readily after each flow reversal. In contrast in live bed conditions the deposition dune in combination with bed ripples play a significant role in the scour development at the pile, with the backfilling process inhibiting further scour development so that an equilibrium condition is reached more quickly. Escarameia (1998) also reported that bedforms have a significant effect on scour development under reversing flow. They attributed the reduction in scour depth in their tests compared to unidirectional flow tests to the presence of the bedforms upstream of the pile after flow reversal.

Another comparison with the literature can be made in terms of the measured slope angles in Section 6.6.1 as Mcgovern et al. (2014) also measured this parameter. They found that the slope angle was much shallower in tidal than unidirectional flow, and that the downstream slope was shallower than the upstream slope in unidirectional flow, but about equal in tidal flow. The bed profiles in the unidirectional tests in Section 6.5 are in agreement with Mcgovern et al. (2014). The downstream profile is shallower than the upstream profile and the upstream slope angles are in a similar range in the order of 30 degrees. The slope angle is linked to the angle of repose, and the sand used in the Mcgovern et al. (2014) study was of a similar size to that in this project. In the spring-neap tests the slope angle was more similar between the upstream and downstream sides than in the unidirectional tests, but the downstream profile was still slightly shallower. As the equilibrium condition was not reached in these tests the slope angle may continue to even out over time to give a similar result in clear water tidal tests to that in Mcgovern et al. (2014). However, there is a large difference between the slope angle of 30 degrees compared to 11 degrees in the tidal tests of Mcgovern et al. (2014). As mentioned previously a key difference between the tests was the propagation of ripples in the live bed tests. This is likely to affect the scour hole shape and slope angle due to the migration of ripples through the scour hole.

7.2.4 Wave-current scour

This section provides a comparison with the literature of core parameters related to scour development under wave and wave-current flows (KC number, U_{cw}, θ/θ_{crit}) before elaborating further on the novel findings from test series C-2. Note that a discussion of the initiation of motion in the wave tests is included in Appendix 9.

Test series C-2 was designed to produce equilibrium scour depth data unaffected by ripples or bed lowering, being in the clear water regime for scour. Therefore, it is possible to make

comparison of these results with the literature in terms of equilibrium scour depth and scour timescale.

a) Influence of KC number, θ and U_{cw} on scour depth

As mentioned in the previous section the KC parameter is thought to have a strong influence on scour development in wave and wave-current flows. In Figure 7.20 S_e/D is plotted against KC_{wave} for the test series. There are relatively few data in the literature regarding scour in wave-current flows but that which could be obtained are also plotted in Figure 7.20. Note that due to the lack of data in the literature collected under clear water conditions the published data plotted in Figure 7.20 relates to live bed conditions. Therefore, it is important to remember the difference in regime between the test data and literature data when making this comparison.

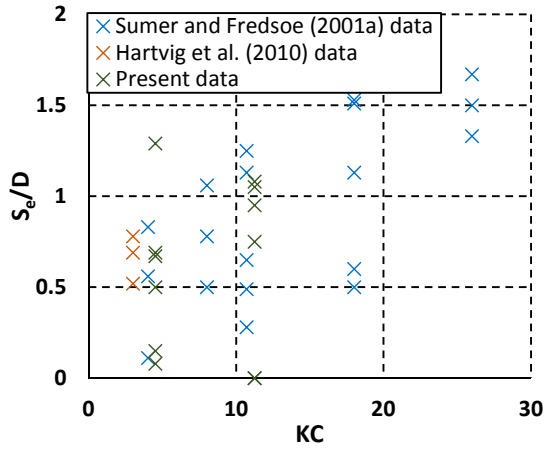

Figure 7.20 Comparison of the present data (clear water) with the data of Sumer and Fredsøe (2001a) and Hartvig et al. (2010) (live bed) in terms of the relationship between non-dimensionalised equilibrium scour depth and KC number based on the wave component of wave-current flow.

In Figure 7.20 there is considerable scatter in the data, suggesting a relatively weak dependence on KC_{wave} number. This scatter reflects the other parameters of influence such as U_{cw} and θ/θ_{crit} (see discussion later in the section). A broad trend of increasing scour depth with increasing KC number is evident, which is in agreement with the expected trend (see Section 2.3.4). The test data fit reasonably well with the range on the graph, demonstrating that live bed and clear water tests can give comparable scour depths. However, the scour depth at the 50 mm pile in the fine sand is actually greater compared to this literature data despite the low value of KC_{wave} for this test. This result may indicate that deeper scour depths can be achieved in the clear water regime than in live bed conditions, in a similar manner to scour in unidirectional current, due to bedforms passing through the scour hole in the live bed regime limiting the scour depth. The influence of ripples may be different in the live bed regime for wave-current flow compared to under unidirectional current because of the effect of flow oscillations on the formation and migration of

the ripples. As with scour in unidirectional flow, the worst case for scour in wave-current flows may be near critical velocity for the sediment, and at high KC number. However, in practice this condition may not be realised, as a high KC_{wave} number in the context of offshore wind turbine foundations would often coincide with the flow velocity being above critical for the sediment.

Another parameter considered to be important for wave-current scour is the ratio of the wave velocity to the current velocity. Sumer and Fredsøe (2001a) investigated this relationship for live bed tests and developed a relationship between these parameters and KC number, where the KC number is that for the wave component of the combined wave-current flow. In the live bed regime the scour depth is expected to increase with U_{cw} for a given KC number from the wave alone case, but always to be less than the steady current value. In Figure 7.21 the test data are plotted in terms of U_{cw} versus S_e/D and the trends of Sumer and Fredsøe (2002a) are added to the figure. Note that these trends are valid for KC>6 in the live bed regime so may not be applicable to the present test data in the clear water regime. There is a lack of literature data for wave-current tests in clear water conditions, and a comparison with the live bed tests will enable any similarities and differences in wave-current scour between the two regimes to be identified.

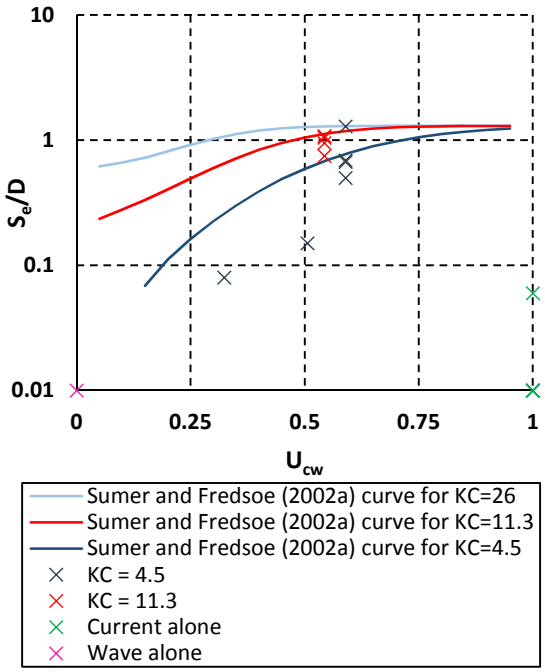

Figure 7.21 Comparison of the present data (clear water) with the trend lines derived by Sumer and Fredsøe (2002a) for live bed conditions to represent the relationship between non-dimensionalised equilibrium scour depth and ratio of wave and current components in wave-current flow.

The general trend of the data plotted in Figure 7.21 is that scour depth increases with U_{cw}, which is in agreement with the results of Sumer and Fredsøe (2001a). However, the scour depth in the wave-current tests is much greater than in the corresponding current alone case which is a

fundamentally different result to that of the trends of Sumer and Fredsøe (2002a) in the live bed regime. Therefore, for the clear water regime a modification is needed on the right hand side of the graph to account for the drop in scour for the current only case. Further testing would be needed to fully understand this section of the trend over a range of parameters in the clear water regime.

Sumer and Fredsøe found that with a KC_{wave} number less than about 6 little or no scour occurred. However, significant scour has occurred for all of the tests at KC_{wave}=4.5 in the clear water regime. This is an important result because it demonstrates a difference in the relationship between the core parameters and scour in the clear water compared to live bed regime, probably because of the increased importance of the θ/θ_{crit} parameter in the clear water regime. The relationship with θ/θ_{crit} is discussed further shortly.

In Figure 7.21 the fine sand scour test with KC=4.5 results in a significantly greater scour depth than the other tests so that it is in line with the curve for KC=26. The KC versus U_{cw} graph does not take into account differences in the sediment properties which results in the observed scatter in the data.

The reason that scour occurred at lower KC numbers in the clear water regime compared to the live bed regime may be due to the presence of bedforms in the live bed regime. In the clear water regime, no infilling of the scour hole occurred under the wave-current flows.

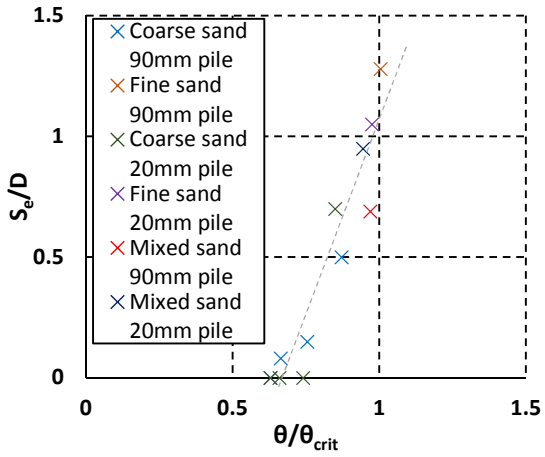

Figure 7.22 Relationship between θ/θ_{crit} and non-dimensionalised equilibrium scour depth for the wave-current tests in test series C-2.

In Figure 7.22 the θ/θ_{crit} parameter is plotted against S_e/D for each of the tests. A linear trend of increasing S_e/D with θ/θ_{crit} is present, in agreement with the unidirectional flow tests in Figure 7.1, and with the findings of Eadie and Herbich (1986) for wave-current scour. This trend extends throughout the clearwater regime from initiation of scour up to the critical Shields parameter at the transition from clear water to live bed conditions in the wave-current flow tests.

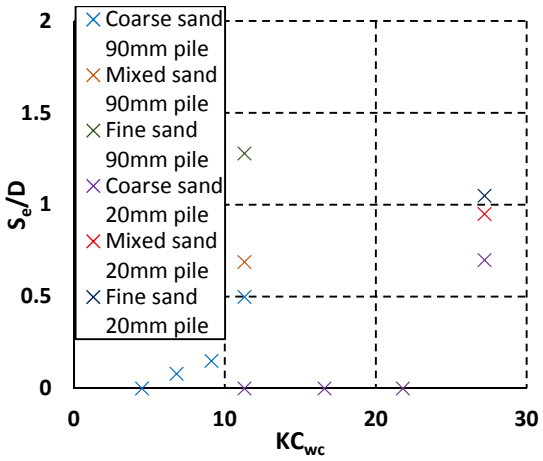

Figure 7.23 Relationship between combined KC number for the wave-current tests in series C-2 and non-dimensionalised equilibrium scour depth.

The wave-current data are more scattered in Figure 7.22 than in Figure 7.1 for the unidirectional current data. This may be linked to the short duration of some of the wave-current tests compared to the stopping criteria usually employed, due to time constraints for the test series. In the fine sand tests at the two piles an unusual result is that the deeper scour depth was actually at the larger pile. This may again be due to the short duration of the test at the small pile. There is also scatter in terms of the threshold condition for scour, and an unusual result is found when comparing tests C.50.26 with C.20.27 and C.50.27 with C.20.28 at the 20 and 50 mm piles where scour occurred at the larger pile but not at the small pile under a similar θ/θ_{crit} value. This result is discussed further in the final part of this section.

In Figure 7.23 the combined KC_{wc} value for the wave-current flows is plotted against S_e/D. This is in comparison with Figures 7.20 and 7.21 where the KC number based on the wave component of the combined flow was plotted, following the procedure of Sumer and Fredsøe (2001a). Using the KC_{wc} parameter enables more of the wave-current tests to have unique parameter values, rather than all of the tests in this series being described by one of two KC_{wave} numbers. There is considerable scatter in Figure 7.23 compared to that in the θ/θ_{crit} graph in Figure 7.22 indicating as with the KC_{wave} parameter there is also less dependence on KC_{wc} than on θ/θ_{crit}.

In Figure 7.23 when comparing the same sediment types there is an increase in scour depth in most cases between the larger and smaller piles which demonstrates an increasing trend of S_e/D with KC_{wc}. The only tests that do not fit this trend are the fine sand tests where S_e/D was larger at the 50 mm pile, but this is probably due to the short duration of the fine sand test at the 20 mm pile, which is discussed further in the final part of this section. Also this figure illustrates that the results for the tests at the small pile where no scour was observed are unusual and do not fit the trend. These will also be analysed in the final part of this section.

b) **Timescale of scour**

In Figure 7.24 θ/θ_{crit} for the wave-current tests is plotted against time to equilibrium. It is seen that in general the time to equilibrium increases with increasing θ/θ_{crit}. This is in agreement with the

tests in unidirectional current. However, for scour in live bed wave-current tests Petersen et al. (2012) found that the timescale decreased with increasing θ.

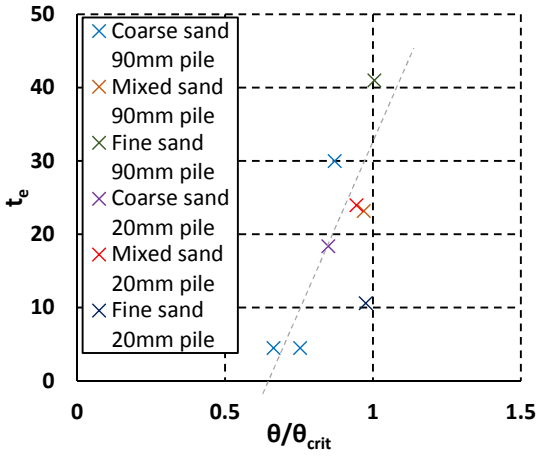

Figure 7.24 Relationship between θ/θ_{crit} and time to equilibrium in the wave-current tests, series C-2.

In Figure 7.25 the combined KC_{wc} number is plotted against the time to equilibrium. The dependence on θ/θ_{crit} in Figure 7.24 is much clearer than the dependence of equilibrium time on KC_{wc}. The relationship between KC number and t_e is also more difficult to understand in Figure 7.25 because fewer distinct values of KC_{wc} are available in the test series than for θ/θ_{crit}. Two different trends are seen in Figure 7.25. Firstly looking at the three wave-current tests conducted in the coarse sand at the 50 mm pile, t_e appears to increase with KC number. For these three tests the Shields parameter also increases in this order and therefore, because of the greater dependence on the Shields parameter this is probably dominating the relationship between t_e and KC_{wc} for these three tests.

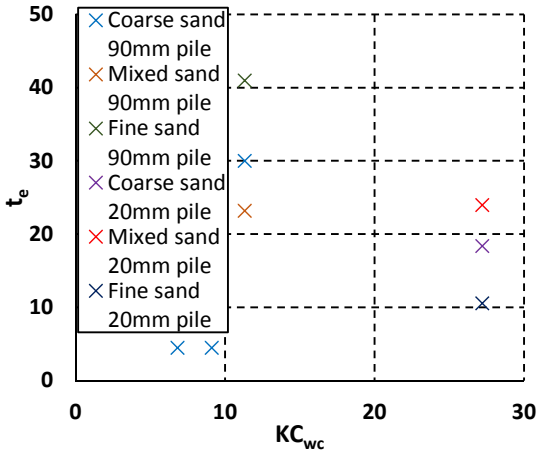

Figure 7.25 Relationship between combined KC number for the wave-current tests, series C-2 and time to equilibrium.

Conversely when comparing the tests under the same flow conditions and sand type at the two piles so that only KC_{wc} varies between the tests, t_e decreases with increasing KC_{wc} for the fine

and coarse sand tests, but increases very slightly at the small pile in the mixed sand. The different trend in the mixed tests is probably a result of not consistently following the stopping criterion in some of the tests in this series.

One final aspect relating to the timescale of scour in wave-current tests is to consider the rate of change of scour through the tests. In Figure 7.26 the scour time development curve is normalised by the equilibrium time and equilibrium scour depth, as was done in Figure 7.13 for the unidirectional current tests. In Figure 7.26 the tests at the 50 mm pile for the fine and coarse sands are plotted. The rate of change of scour i.e. the shape of the curve in Figure 7.26 is very similar between the two sands for the same wave-current condition, and furthermore these look to be similar to the shape of the other test curves under unidirectional flow demonstrating that the scour process is similar in the different flow conditions in these wave-current tests. There are however, some more unusual scour development curves in the data set which are discussed below.

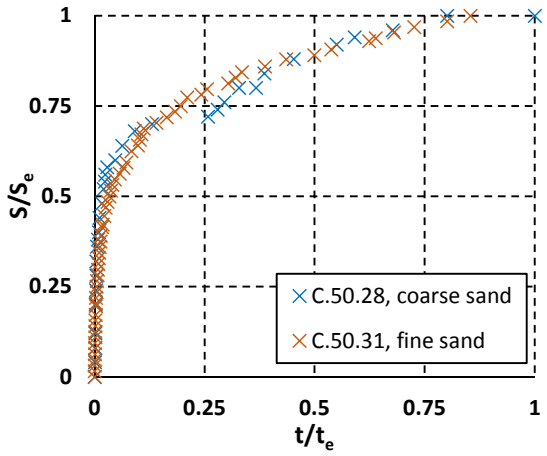

Figure 7.26 Normalised scour depth against normalised time for wave-current tests.

c) Wave-current test explanations

One aspect discussed above that did not fit the expected trends and requiring further explanation is the wave-current tests at the three piles in the fine sand. The large pile unusually resulted in the largest S_e/D value, while the 50 mm rough pile and 20 mm small pile tests gave about the same scour depth, although with different timescales.

It is shown in Appendix 3 that pile roughness did not have an effect on scour, so the reduction in scour depth for the rough 50 mm pile compared to the smooth 50 mm pile can be accounted for by the reduction in flow velocity at the far side of the flume. For the small pile, however, it was expected that the scour depth would be greater because of the higher KC number, which would be in accordance with the results for the other sand types where scour depth was increased at the smaller pile. To understand this result, the 20 mm and 50 mm pile fine sand tests are plotted together in Figure 7.27. It can be seen in the figure that the small pile fine sand test was stopped after a much shorter time into the test than at the larger pile. This is due to the small pile test being conducted alongside the layered test at the larger pile, with the layered test being the primary test dictating the stopping point.

In Figure 7.27 it can be seen that initially the rate of scour is quicker at the 20 mm pile, but then the scour depth flattens off. This unusual drop in scour rate earlier than expected was also observed in tests C.50.28 and C.20.28 which were the wave-current tests at each pile in the coarse sand. These tests are shown in Figure 7.28.

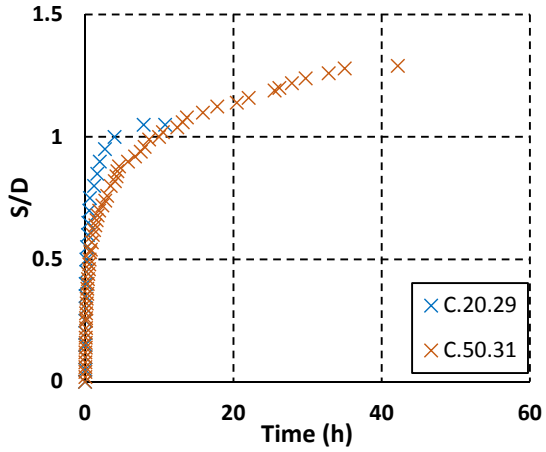

Figure 7.27 Scour development in wave-current flow in uniform fine sand at the two different piles (20 mm and 50 mm).

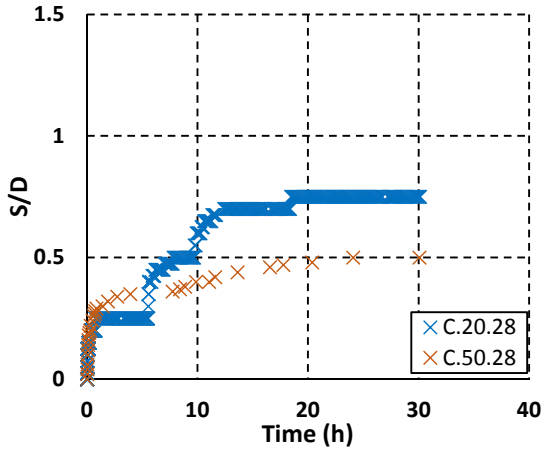

Figure 7.28 Scour development in wave-current flow in uniform coarse sand at the two different piles (20 mm and 50 mm).

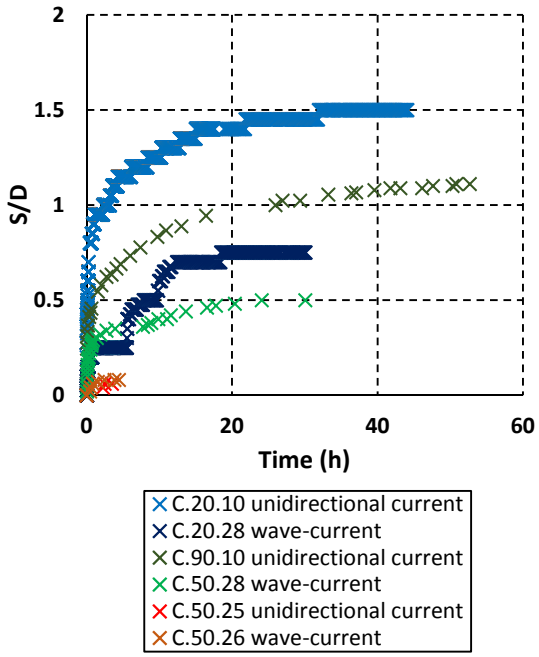

Figure 7.29 Comparison of scour development in wave-current flow with that in unidirectional current with velocity equal to the maximum combined velocity in the wave-current case, coarse sand.

In both of these tests, but especially at the 20 mm pile the scour development curve consists of clear cycles of a step-like form, where the scour depth increases, but the gradient of the curve decreases, before flattening off for a time. Then the process picks up again with another increasing section before another flatter section. It is possible that this pattern would also have been observed in the fine sand 20 mm pile curve if the test was run for longer, and this would explain why the curve flattens off more quickly than expected at the point at which it was stopped. In the coarse sand test at the larger pile, one step-like feature is present, but the curve flattens more gently before the scour rate picks up again after about 8 hours.

This unusual scour time development in the coarse sand may be caused by the influence of the waves on the pore pressures in the sand. As discussed in Section 2.4.6 waves can have a significant effect on pore pressures, with the continuous loading and unloading resulting in a build-up in the pore pressure which can eventually lead to liquefaction. In relation to these tests, it does not seem likely that the bed is fully liquefying as under this situation much more rapid scour would occur. It is possible instead that the pressures build up and dissipate in a cyclic fashion without reaching the point of liquefaction, resulting in the more gentle change in scour behaviour in Figure 7.28. This would need to be investigated further by conducting tests in which the pore pressures in the bed were measured, in order to understand the differences in the scour development curves in the different sand types and at the different piles.

Some of the differences in the scour curves between the different pile diameters in Figure 7.28 may be indicative of differences in the interactions between the wave pressures and the flow structures and vortices around the pile. The flow patterns are not scaled identically between the two pile diameters (see scale effects Section 2.7.4). Therefore, the different KC numbers and ratios of flow velocity to pile diameter mean that the vortex shedding frequency and flow patterns will be quite different. Also the scale of the wave for the 20 mm pile is larger which means that the wave induced flow will be relatively stronger compared to the size and strength of the downflow and horseshoe vortex system at the 20 mm pile.

Another unusual result to discuss further is the lack of scour at the small pile while scour occurred at the larger pile in the wave-current tests in uniform coarse sand. One explanation for this is due to the limitations of the measurement system. The scour depth at the 50 mm pile was small in these tests, and at the 20 mm pile the scour depth in millimetres would be even smaller, less than 5 mm. This would have been difficult to detect at the small pile especially because the first scale marking (at 5 mm) would not yet be visible.

One of the key findings from this set of tests presented in Section 6.4 was that scour depth was increased by adding a wave to a current, which is the opposite result to that reported for live bed scour. However, it is unclear if this is a like-for-like comparison, and others in the literature have used different methods. One of these is comparing a wave-current case to a unidirectional current test with velocity equal to the maximum combined velocity under the wave-current flow. In this set of tests it is possible to make two comparisons using this method. The smallest current and wave combination can be compared with the largest of the three currents on its own, and the largest wave-current combination can be compared with the 24 cm/s current test in the coastal flume, for

the two pile diameters tested. In the first case, the scour depth was very similar between the wave-current and current flows. This may be because of the proximity to the threshold condition for scour, which may be reduced due to the wave component of the flow. In the second case however where conditions were significantly above the threshold for scour the current alone test gave the greater scour depth for both pile diameters, see Figure 7.29.

For the second comparison case the greater scour depth under unidirectional current indicates that the change to the flow patterns caused by the wave has acted to reduce scour depth, rather than simply slow down the timescale of scour and reach ultimately the same equilibrium condition as would be expected if scour depth was purely a function of the maximum velocity, as has been shown under unidirectional current conditions. This is in agreement with the findings of Niedoroda and Dalton (1982); that the waves prevent full formation of the boundary layer, reducing the downflow strength at the pile.

In terms of the literature, the more common approach is to compare the current alone case to the wave added to that current (Sumer and Fredsøe, 2001a; Breusers, 1971; Eadie and Herbich, 1986; Kawata and Yoshito, 1988; Bijker and Bruyn, 1988; Rudolph and Bos, 2006; Chen et al., 2012; Qi and Gao, 2014b). When considering the tests from this perspective the wave clearly enhanced the scour depth compared to the current alone. This implies that the increase in maximum velocity has been more important than the reduction in downflow strength caused by the wave orbital motion. The increase in the V/V_{cr} parameter due to the addition of the wave is unique to clear water conditions and demonstrates a dependence on V/V_{cr} similar to that in unidirectional current. This appears more important than the KC number, as the results are in disagreement with the lower limit for scour set in the literature for KC number and this result is fundamentally different to those in the live bed regime for wave-current scour where scour depth is expected to be reduced by the addition of a wave to a current.

Another aspect that was intended to be studied in this set of tests was the influence on the scour process of having either a wave-dominated or current-dominated flow, and especially, if there was any interesting effect on scour when the current and wave velocities were equal, at a combined KC number of about 10 where the unique vortex patterns may enhance sediment transport. The influence of this was assessed by considering the U_{cw} parameter. However, no effect was apparent in Figure 7.21. As the V/V_{cr} parameter increased between the cases, this may have been the dominating factor compared to any influence of the KC number and U_{cw} combination. Therefore, to investigate this further, tests would need to be conducted where the V/V_{cr} parameter was fixed, for example by also changing the sediment parameters.

7.3 Curve fitting and scour prediction

This section provides an analysis and evaluation of existing prediction equations, firstly for time prediction of scour development, and secondly for equilibrium scour depth. The focus is somewhat more on modelling scour time development because of the interesting findings regarding this in the test series. Furthermore, it was found in the literature review (Section 2.6.5)

that comparison of time development equations has been less extensive than comparison of equilibrium scour predictors.

For the scour time development and scour equilibrium predictors, a selection of key formulae have been chosen for the analysis. These are based on those reported in the literature review, and the selection is chosen to cover a range of approaches. For the equilibrium scour predictors, close attention was paid to the extensive study of Sheppard et al. (2011a), and the selection of scour predictors was partly based on their findings in terms of the best performing equations.

7.3.1 Comparison of scour time development equations

Eleven scour time prediction equations have been chosen for comparison with the test data. The focus is primarily on uniform sands, but the most promising technique will also be compared to some of the more complex flow and sediment cases.

The range of approaches can be classified into those which are primarily curve fitting techniques, compared to those with fully defined input parameters based on the sediment and flow properties. The latter are obviously more useful for true scour prediction. However, inclusion of the former may help to improve understanding of the fundamental trends in the data and aid the selection of the most appropriate form of the equation for future development of prediction equations.

In Appendix 4 each of the equations is compared with the scour curves from a range of tests. In Table 7.7 the results of the comparison are summarised and the equations giving the best and worst fits to the test data for a typical scour curve (test R.17) are given in Figures 7.31 and 7.30 respectively. In order to compare the predicted scour trend to that in the data on a more detailed level, the comparisons are also shown on a semi-log plot in Figures 7.30b and 7.31b so that the fit to the data can be more clearly seen at the start of the curve where the scour rate is very rapid.

In Table 7.7 and Figures 7.30 and 7.31 (and Appendix 4) it is clear that the equations based on the approach of Sumer and Fredsøe (2002a) (Rudolph et al., 2008; Borghei et al., 2012; Lança et al., 2013a) give a poor fit to the data. Fundamentally the form of these equations doesn't correctly model the shape of the scour curve through time, regardless of the values given to the fitting parameters. Sumer's approach is one of the earlier published methods, providing a baseline for further research and development of more refined prediction equations, although it is still used quite extensively in the literature. This comparison suggests that other approaches are now more suitable.

Of the other curve fitting techniques, the one that gives the best fit across the set of tests is that of Guo (2014). However, this type of approach can only be useful for scour prediction if a link can be found between the curve fitting parameters and the physical parameters that define the scour process.

Only a few approaches enable full prediction of the scour development curve (Chang et al., 2014b; Oliveto and Hager, 2002; Lança et al., 2013a; Melville and Chiew, 1999). In these methods all parameters in the formulae are fully defined by known parameters. However, in general these methods do not give as good a fit to the data as the curve fitting methods. The equation of Chang

et al. (2014b) results in a poor fit for the middle section of the scour curve. The approach of Oliveto and Hager (2002) significantly over-predicts scour depth. The method of Melville and Chiew (1999) also over-predicts scour depth but to a lesser extent. The Lança et al. (2013a) equation gives a reasonable fit to the data if the S_e parameter is set equal to a somewhat larger value than that given by the quasi-equilbrium scour depth measured in the tests, indicating that the definition of the equilibrium scour depth condition is important to express as part of the equation. For the Melville and Chiew (1999) and Oliveto and Hager (2002) equations an extra factor can be included in the equation to reduce the over-prediction. However, Melville's equation gives a better fit using this approach than Oliveto and Hager's method. Therefore, the three most promising techniques are those of Melville and Chiew (1999) with an additional correction factor, Lança et al. (2013a) and the curve fitting technique of Guo (2014). These were, therefore, considered in greater detail through assessment of the input parameters.

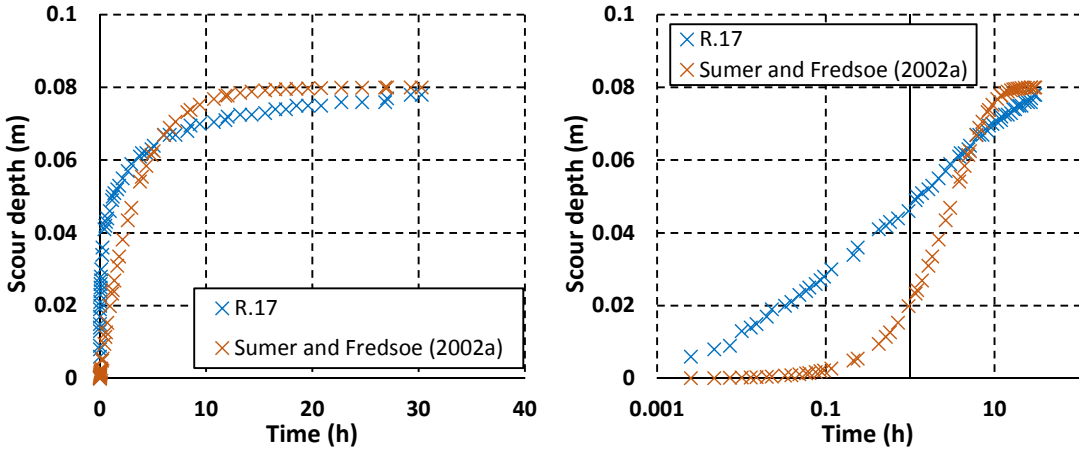

a) b)

Figure 7.30 Predicted scour time development compared with present test data for the worst fitting equation (Sumer and Fredsøe, 2002a) a) normal plot b) logarithmic plot.

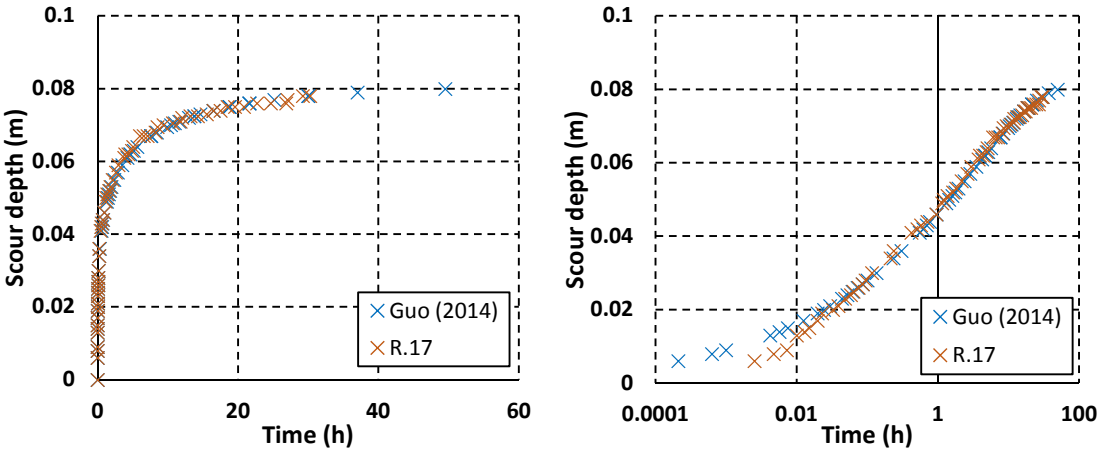

a) b)

Figure 7.31 Predicted scour time development compared with present test data for the best fitting equation (Guo, 2014) a) normal plot b) logarithmic plot.

Table 7.7 Evaluation of different scour time prediction equations.

Author	Fitting parameters	Description of fit to present data
Sumer and Fredsøe (2002a)	**(S_e), (T_c), P**	Poor fit to all parts of curve. In the first stage scour is under-predicted. Scour is over-predicted in the later stages
Melville and Chiew (1999)	**none**	This approach does not require knowledge of t_e or S_e but the method over-predicts the data. A better fit is achieved by including an extra factor, but the fit is still poor at the start of the curve
Sheppard et al. (2004) a	**a_1, a_2, a_3, a_4**	The fit is reasonable to the second part of the curve but not to the first part
Sheppard et al. (2004) b	**a_1, a_2, a_3, a_4**	Gives poor fit to all parts of curve, being initially too slow, and then flattening off too quickly
Guo (2014)	**T_c, (S_e)**	Close fit to data in all parts of curve. The approach is suited to modelling up to a quasi-equilibrium stage and extrapolation much beyond the present curves was not possible
Zhao et al. (2012)	**(S_e) and T_c**	A reasonable fit is achieved although the prediction curve flattens off too quickly in the later stages and is too steep in the first section
Oliveto and Hager (2002)	**none**	Although this approach does not require curve fitting, the equation significantly over-predicts scour development. The empirical factor in the formula can be altered to achieve a better fit, although the scour rate is too fast for the first half of the curve and flattens off too quickly in the final stages
Lança et al. (2013a) after Franzetti et al. (1989)	**(S_e)**	The gradient is too steep in the latter part of the curve, but a good fit is achieved in the first part
Chang et al. (2014b)	**(S_e), t_e**	The use of three separate functions qualitatively matches the shape of the scour curve in a logarithmic plot. A good fit can be achieved in the first or third sections but not at the same time. The second function results in steeper scour development than in the test data
Borghei et al. (2012)	**S_e, t_e, a_1, a_2**	Equation provides a good fit to data if the a_1 and a_2 constants are altered. However, when using a logarithmic plot, the fit is very poor in the initial stage of the curve
Rudolph et al. (2008)	**S_e**	Scour development is overestimated and the equilibrium depth is reached much more quickly (similar issues to original Sumer equation). The authors note this is an order of magnitude approach

For the approach of Guo (2014), T_c and S_e parameters are required as inputs. In Table 7.8 the T_c and S_e parameters that gave the best fit to the test data are presented so that the consistency of these parameters over a range of test conditions can be evaluated. In Table 7.8 it can be seen that the S_e parameters that gave the best fit to the test data were a little larger than the quasi-equilibrium scour depths measured in the tests. From Table 7.8 the S_e parameter is about 5-10% larger than the quasi-equilibrium condition. The difference between S_e and the measured quasi-equilibrium depth was fairly consistent across the range of tests. Small variations in this are probably due mostly to inconsistencies in applying the stopping criterion. Therefore, the S_e parameter seems to be reasonably definable for this approach and should be calculable based on an equilibrium scour depth equation, see next Section (7.3.2).

This consistency is not present in the T_c parameter in Table 7.8. In the small flume tests the T_c parameter is consistently larger in the fine sand tests compared to the coarse sand tests under the same flow conditions, which is consistent with the time to equilibrium being longer for higher values of V/V_{cr}. However, in the larger flume tests T_c is greater in the coarse sand tests. T_c is smaller at the 20 mm pile than at the 90 mm pile which fits with the difference in scour timescale. Determining a link with the quasi-equilibrium time parameter measured in the tests is more difficult because as was shown in Section 7.1.9 the stopping criteria resulted in a less consistent definition of this parameter across the tests. There does not seem to be a consistent link between T_c and flow velocity as tests R.1 and R.3 have the smallest values of T_c but were not run at the lowest flow velocities. The T_c parameter is probably accounting for more than just the scour timescale; also accommodating variation in terms of the rate of change of scour. That there are some trends evident in the T_c parameter is encouraging and indicates that further research would be worthwhile to develop this equation into a more physically based approach.

Table 7.8 Best fit parameters for Guo (2014) equation.

		Best fit parameters		Experiment parameters		Prediction	Experiment	Prediction/ Experiment
Sand	Test	T_c	S_e	t_e (quasi)	S_e (quasi)	S_e/D	S_e/D	S_e/D_{pred} / S_e/D_{exp}
fine	R.17	19	81	24.5	76	2.0	1.9	1.07
coarse	R.16	10	57	21.4	56	1.4	1.4	1.02
fine	R.1	9	86	15.8	85	1.7	1.7	1.01
coarse	R.3	7	68	14.3	66	1.4	1.3	1.03
fine	R.T.6	30	69	18	60	1.7	1.5	1.15
coarse	R.T.4	16	42	12	37	1.1	0.9	1.14
coarse	C.90.10	115	120	39.3	97	1.3	1.1	1.24
fine	C.90.15	95	154	70.8	138	1.7	1.5	1.12
coarse	C.20.10	25	31	21	28	1.55	1.4	1.11
fine	C.20.15	16	38	25	36	1.9	1.8	1.06

Table 7.9 Best fit parameters for Melville and Chiew (1999) equation.

Sand	Test	Extra factor required
fine	R.17	0.91
coarse	R.16	0.8
fine	R.1	0.95
coarse	R.3	0.86
fine	R.T.6	0.91
coarse	R.T.4	0.73
coarse	C.90.10	0.7
fine	C.90.15	0.8
coarse	C.20.10	0.93
fine	C.20.15	none

Table 7.10 Best fit parameters for Lança et al. (2013a) equation.

Sand	**Test**	**S_e best fit**	**S_e (quasi)**	**S_e/D (model)**	**S_e/D (exp)**	**S_e/D_{pred} / S_e/D_{exp}**
fine	R.17	100	76	2.5	1.9	0.76
coarse	R.16	90	56	2.3	1.4	0.62
fine	R.1	120	85	2.4	1.7	0.71
coarse	R.3	105	66	2.1	1.3	0.63
fine	R.T.6	83	60	2.1	1.5	0.72
coarse	R.T.4	58	37	1.4	0.9	0.64
coarse	C.90.10	130	97	1.4	1.1	0.75
fine	C.90.15	150	138	1.7	1.5	0.92
coarse	C.20.10	36	28	1.8	1.4	0.78
fine	C.20.15	45	36	2.3	1.8	0.8

In Table 7.9 the factor added to the equation of Melville and Chiew (1999) to achieve the best fit with the data is listed for each of the tests. The coarse sand tests needed a greater adjustment than the fine sand tests, but interestingly this difference in the adjustment is quite consistent for the different pairs of tests, being approximately 0.1, apart from in tests R.T.6 and R.T.4 which were stopped sooner than the criterion. The tests at the 20 mm pile in the larger flume needed less adjustment probably due to the scale effect in these tests not being modelled in the approach of Melville and Chiew (1999). However, there is little consistency in the factors when comparing between the tests conducted at different flow velocities.

In Table 7.10 the S_e parameters used in the Lança et al. (2013a) equation to obtain the best fit for each test are compared. The S_e parameter values are fairly consistent compared to the measured quasi-equilibrium scour depths, if small inconsistencies in the stopping criterion are taken into account. As mentioned previously the S_e parameter for this approach appears to be related to the expected final equilibrium value for these tests, so is somewhat larger compared to S_{qe} than in the Guo (2014) method. This result means that this approach is likely to give the best predictive results, as it is purely based on inputting S_e (i.e. no T_c parameter is required), and no correction factors are needed. Although the fit to the data was not as good in terms of the shape of the scour development curve, this method would give a reasonable approximation of the scour curve shape and time to equilibrium parameter.

Despite the issues with linking the equation input parameters to physical parameters in the tests, the analysis of the time prediction equations showed that the Guo (2014) approach gave the best match to the shape of the scour time development curve across the full range of test cases. This indicates that the Guo (2014) approach fundamentally is the right, or closer to the right function form. Therefore, this may provide a good starting point from which to develop a more physically based prediction equation.

The Guo (2014) equation also provides a reasonable fit to the wave-current tests where the standard scour development trend (increasing function with decreasing gradient) was prevalent (in fine sand), indicating that these wave-current scour curves are of a similar form to the unidirectional current tests in agreement with the S/S_e versus t/t_e curves in Section 7.2.4. Figure 7.32 shows a comparison of the Guo (2014) approach with a wave-current test.

The equation does not provide such a good fit if directly applied to the layered tests, due to the change in the rate of scour between the two layers. However, a good fit can be obtained by adjusting the T_c and S_e parameters for each sand layer, so for a two-layered bed a two part equation is needed. The start time for the 2nd part of the curve in the lower layer is then matched to the end time of the first part of the curve, for the upper layer. For the upper layer, the T_c and S_e parameters are equal to those in a bed of uniform sand. For the second layer the S_e parameter matches the S_e for the layered bed. A method for obtaining this parameter is discussed in the following section where a new prediction equation for layered beds is proposed. In Figure 7.33 this method is shown compared to test data for a layered bed.

The Guo (2014) equation also provides a good fit to those mixed sand tests which followed the standard scour development trend (i.e. the mixed tests run at higher V/V_{cr}). The fit was based on using the d_{50} for the mixture from the sieve analysis. This works for the 10% coarse, 90% coarse, and 50% coarse mixtures in the small flume, and for the 50% mix at the 90 mm pile in the larger flume. Similarly to the uniform sand tests, the key to utilising this approach as a prediction method is the determination of the T_c parameter. What this comparison shows is that the curve shape is controlled by the same structure of equation in these different cases. A comparison of the Guo (2014) equation with a mixed sand test is given in Figure 7.34.

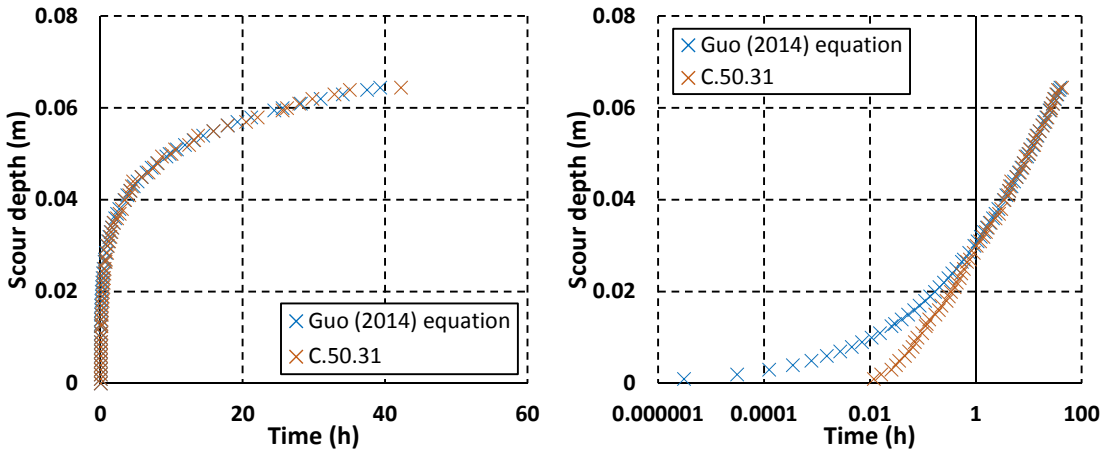

Figure 7.32 Predicted scour time development using the Guo (2014) equation compared with present test data for scour in wave-current flow.

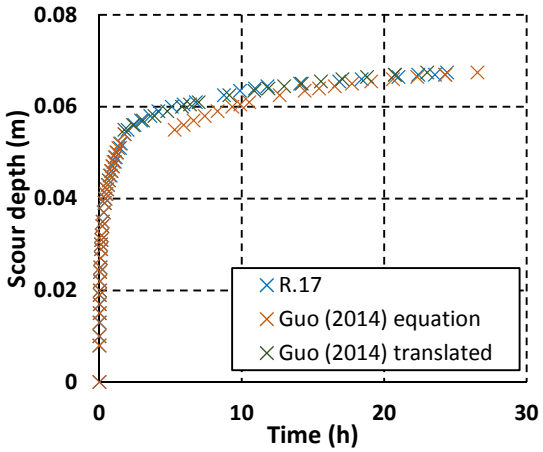

Figure 7.33 Modelling scour development in layered beds with the Guo (2014) equation.

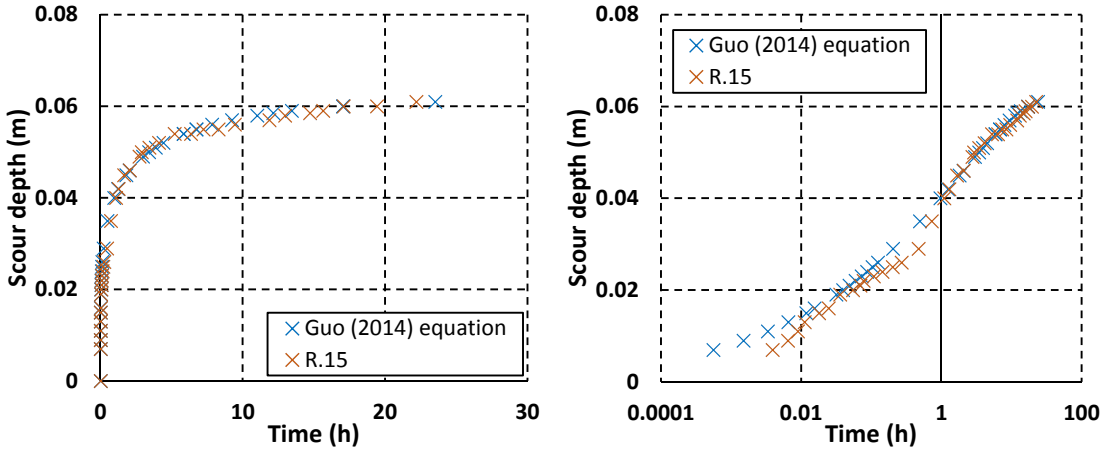

a) b)

Figure 7.34 Predicted scour development using the equation of Guo (2014) compared with scour in mixed sand bed (unidirectional current) a) normal plot b) logarithmic plot.

For the mixed sand tests at lower flow velocities a modification is needed to the Guo (2014) approach to better model the linear trend. These curves can be modelled in three stages. The Guo (2014) equation gives a good fit to the initial scour stage. The second part follows a linear trend, and the final stage is approximated to equal the equilibrium scour depth which gives a reasonable fit to the data in most cases. It is difficult to provide a comprehensive methodology here due to the small number of cases tested (because this trend was only found under some of the test conditions), so this should not be considered as a final equation, but more of a starting point or framework that can be refined with further data. The three parts of the equation are defined as follows:

For $t < t_B$: use standard scour time development equation such as Guo (2014)

For $t_e > t \geq t_B,\ S < S_e$:

$$\frac{S}{D} = A_1(t - t_B) + A_2\frac{S_e}{D} \tag{7.1}$$

For $t \geq t_e$:

$$S = S_e \tag{7.2}$$

where t_B is the time at which $S/D = A_2 S_e/D$, and t_e is the time at which equilibrium scour depth is reached. Based on the limited test data, A_1=0.03-0.1 in current, A_1=0.015 in wave-current, and A_2=0.5 in current, 0.7 in wave-current, and A_2=0.67 for small percentage fine sand mixed beds in current. In order to make this equation applicable to a wider range of tests further work would be needed to define A_1 and A_2, preferably in terms of parameters rather than constants through extended laboratory testing of different sediment mixtures under a variety of flow conditions. Figure 7.35 shows a comparison of this prediction method to a mixed test displaying the linear trend.

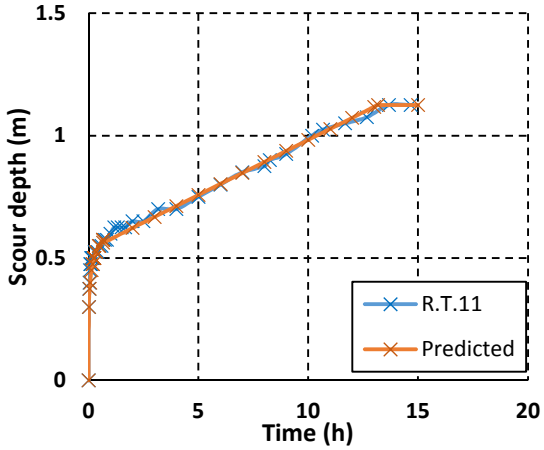

Figure 7.35 Comparison of prediction of linear trend in mixed sand bed with laboratory data.

7.3.2 Comparison of equilibrium scour prediction equations

Seven equations for equilibrium scour prediction were selected for comparison with the test data. These were chosen to include the most popular methods used in the literature and industry (Richardson and Davis, 2001 (HEC-18); Breusers et al, 1977; Melville and Sutherland, 1988), the most promising from the analysis of Sheppard et al. (2011a) (S/M equation) and to cover a range of approaches (i.e. based on either pile Reynolds number, Froude number or V/V_{cr}). Equations which allow prediction of scour in non-uniform sand were also included for comparison with the mixed sand tests (Molinas, 2003; Melville and Sutherland, 1988). For a more extensive comparison of S_e predictors in general, see Sheppard et al. (2011a) and Section 2.6.1 of the literature review.

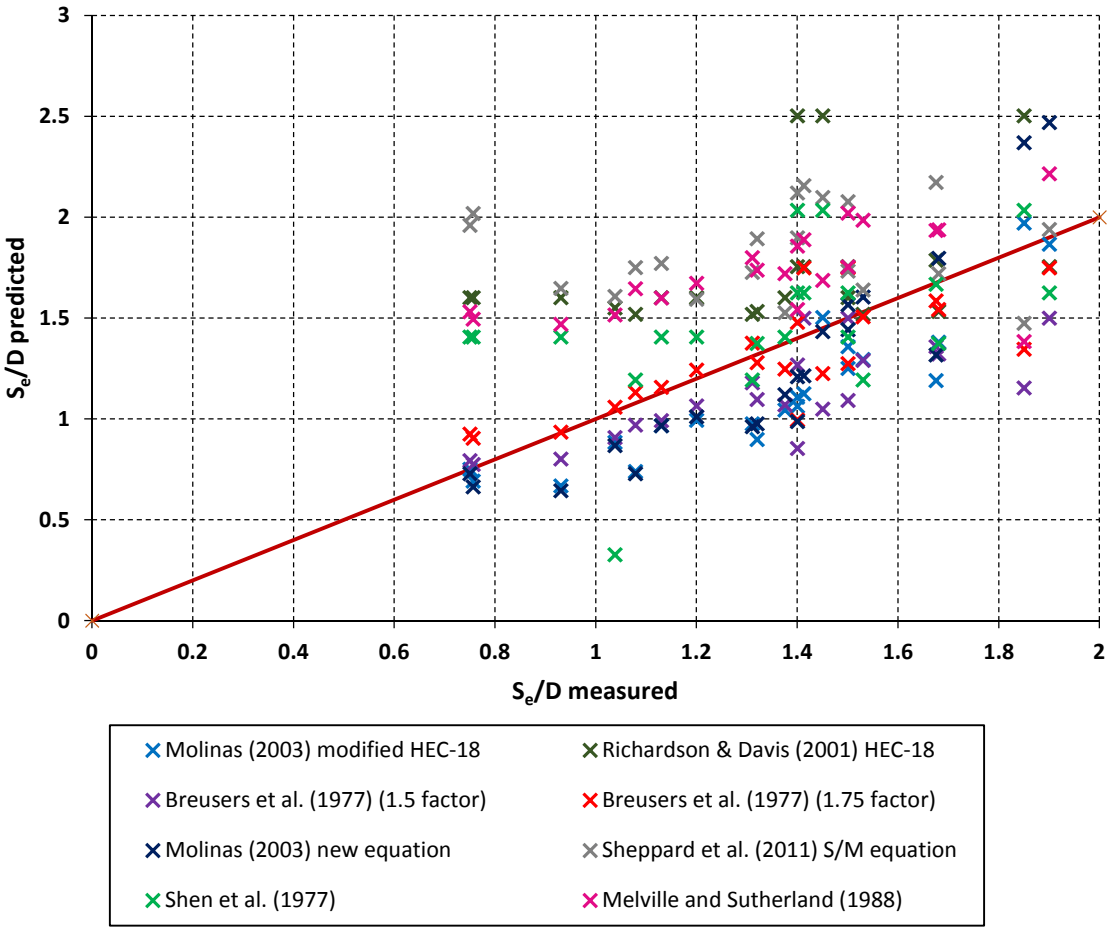

Figure 7.36 Equilibrium scour depth equations: comparison of key methods for uniform sands and mixed sands using the present data.

In Figure 7.36 S_e/D in the uniform and mixed sand tests under unidirectional current in both flumes is plotted against the predicted S_e/D for each of the seven equations. There is a large amount of scatter in the predictions, and the data are both over and under-predicted by the range of approaches.

The S/M, HEC-18 and Melville and Sutherland (1988) equations have a tendency to over-predict scour depth in Figure 7.36, but for each of these equations there is at least one test which is

under-predicted, so the conservative nature of these equations is not guaranteed. The fit of the S/M and HEC-18 equations to the data is generally better at higher values of S_e/D, where the conservatism of these approaches is reduced under conditions close to the worst case for scour. The most substantial over-predictions are given by the S/M equation for tests R.T.9 and R.11 (low percentage fine sand mixed tests, at low flow velocity) which are over-predicted by more than 1 S_e/D which is of the same order of magnitude as a typical value of S_e/D. This demonstrates the real need for improvement of scour prediction methods, as this level of error means that foundation designs cannot be tailored in a sophisticated way to account for scour depth at the pile.

The two Molinas (2003) equations and Breusers' approach with a 1.5 factor predominantly under-predict the data in Figure 7.36. It is perhaps surprising that the equations under-predict the data seeing as only a quasi-equilibrium scour depth was achieved in the tests. This may indicate that other researchers have similarly defined scour depth at a quasi-equilibrium condition.

The data modelled by Shen's equation are quite scattered in Figure 7.36, so that scour depth is both over and under-predicted. This approach, as with the HEC-18 equation does not take into account the effect of sediment properties. This causes a high level of scatter when compared to data containing a range of sand types, even though the difference in grain size between the tests was relatively small.

The equations which give the best fit to the shape of the identity line are those which include the V/V_{cr} parameter (Breusers et al., 1977; Melville and Chiew, 1999; Molinas, 2003), rather than being based on pile Reynolds number or Froude number, which is in agreement with the observed stronger relationship between V/V_{cr} and S_e/D in Section 7.1.1.

Overall, the method of Breusers et al. (1977) with an extra factor of 1.75 gives the best fit to the data out of the 7 methods. For this approach the greatest deviation from the identity line is for the tests at the 20 mm pile in the larger flume, which Breusers' method under-predicts. This shows that Breusers' approach does not take scale effects into account (i.e. the pile diameter was small relative to the water depth and grain size), which may be considered acceptable as these effects should not be present in the field. The majority of the tests demonstrate a reasonably good fit between this equation and the data, especially for the tests with lower S_e/D values.

Interestingly this includes the mixed sand tests where the fit is as good for the mixed sands as it is for the uniform sands. An exception to this is seen in tests R.T.9 and R.11 for the small percentage fine sand mixtures at low V/V_{cr} where an unusually small scour depth was recorded. Breusers' method does not model this effect, consequently over-predicting S_e/D for these two tests. It was not expected that Breusers' approach would be successful at modelling the mixed tests. However, it appears that simply using the d_{50} parameter for the mixture in a uniform sand equation is adequate for most of these tests. This may be linked to the fairly small σ_g values and lack of bed armouring processes observed in Figure 7.15. However, it should be noted that many authors would classify the mixed tests as non-uniform based on the σ_g value.

Of the approaches that were designed to take into account differences in the sediment distribution, Molinas (2003) uses a definition for bed armouring in terms of a D_{cfm} parameter which defines the median grain size of the coarsest part of the sediment grading curve:

$$D_{cfm} = \frac{d_{85}+2d_{90}+2d_{95}+d_{99}}{6} \quad (7.3)$$

For the mixed sediments the D_{cfm} parameters are given in Table 7.11.

Table 7.11 D_{cfm} parameter for the mixed and uniform sands used in the test programme.

Test	D_{cfm}
Fine	1.70
75% fine	2.32
50% fine	2.42
25% fine	1.48
Coarse	1.30

In Table 7.11 the 50% mixed sand has the largest value of D_{cfm}, followed by the 75% mixture so bed armouring should be most prevalent in these sands. This is qualitatively in agreement with Figure 6.22 where S_e/D was plotted against the percentage of fine sand in the mixture, as these two mixtures showed the biggest drop in scour depth compared to a linearly increasing trend. However, use of the D_{cfm} parameter in the equation results in too large a reduction in scour depth in Figure 7.36 for these tests, implying that bed armouring effects are less severe in these sands than is expected for standard non-uniform sediments with the same σ_g value and D_{cfm} parameter.

The approaches of Melville and Chiew (1999) and Molinas (2003) resulted in a worse prediction of the mixed sand tests when non-uniformity parameters were taken into account than if they were not included. This means that consistently across the approaches bed armouring was less severe in the mixed sediments than expected. This is likely attributable to the bimodal nature of the mixtures. Further work would be needed to select parameters that would better represent these distributions and their effects on scour, through testing of a wider range of bi-modal and normally distributed sands. For these tests specifically it is concluded that uniform sand predictors are adequate to obtain the equilibrium scour depth, except in the low percentage fine sand mixtures under low flow velocity. To improve the prediction of S_e/D in the low percentage fine sand mixtures at low flow velocity a reduction factor can be applied to the equilibrium scour depth prediction for a uniform bed of the coarse sand type in the mixture under the same flow condition:

$$\frac{S_{e,m}}{D} = 0.8\frac{S_{e,uc}}{D} \quad \text{for} \quad \frac{V}{V_{cr}} < 0.7, \qquad Fine\ sand\ fraction < 25\% \quad (7.4)$$

where $S_{e,m}$ is the equilibrium scour depth in mixed sand, and $S_{e,uc}$ is the equilibrium scour depth in uniform coarse sand. However, this preliminary model is specific to tests R.T.9 and R.11 as a more general model was not possible because of the limited number of tests.

Approaches for scour prediction in layered beds were discussed in Section 2.6.3 of the literature review. As few studies are available, also few prediction methods are available. The one

described by Gjunsburgs et al. (2014) does not take into account the observed interaction effects in this study and the limitations in their model were discussed in Section 7.2.1 in that there was actually a noticeable difference in the layered bed scour development curves to that based on the uniform fine and coarse sand scour curves. Another prediction methodology for layered beds is that of Annandale (2006). However, for these tests the difference in the sediment properties between the fine and coarse sands is too small to be taken into account in Annandale's approach. The approaches of Briaud (2001) and Briaud (2002) also address scour in layered sediment beds. However, this is a more complex approach requiring erosion jet testing making it less practical. Therefore, there are no suitable predictors currently available to model the findings in this project. Instead a preliminary predictor has been formulated based on the present data.

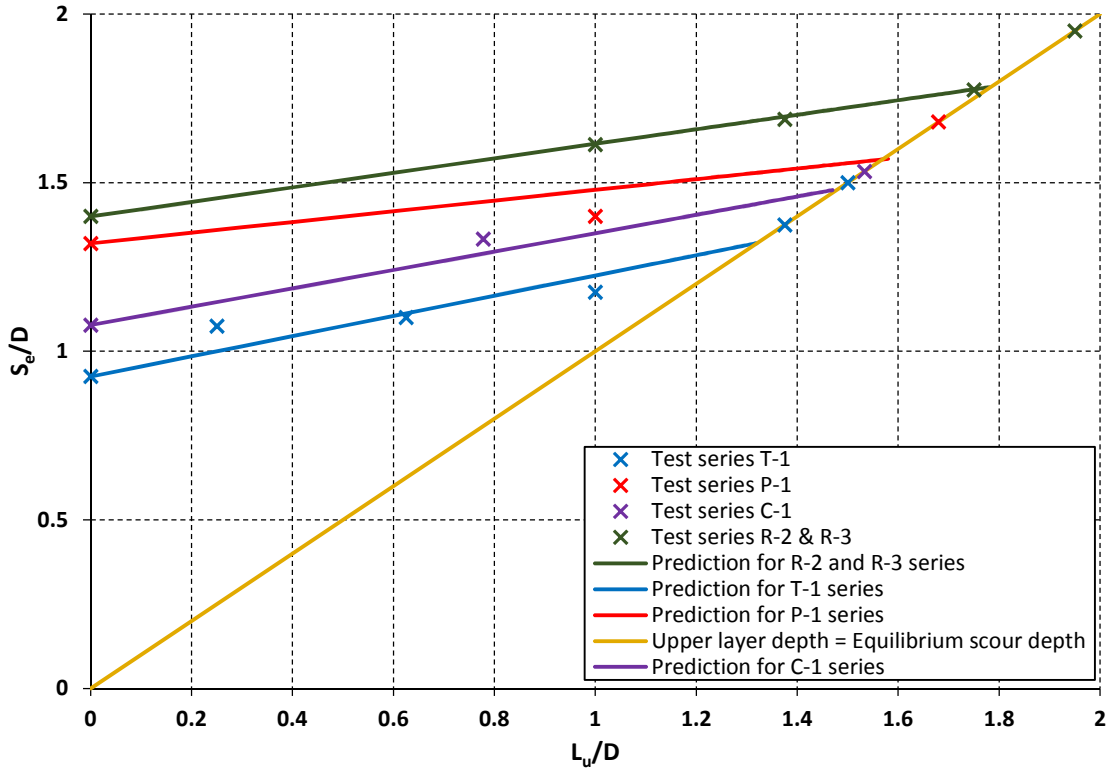

Figure 7.37 Prediction of quasi-equilibrium scour depth in the layered tests with a range of upper layer thicknesses (L_u) with fine sand overlying coarse sand compared with the experimental data.

An empirical equation has been formulated to predict equilibrium depth in a two layered bed of fine sand overlying coarse sand. The equation describes the equilibrium scour depth depending on the upper layer depth. The prediction is based on prior calculation of the equilibrium scour depths in the individual sand types i.e. from other prediction methods under the same flow conditions, and utilises the V/V_{cr} and h/D parameters. The prediction equation is split into two parts depending on the depth of the upper layer. The first part covers the cases with smaller upper layer depths where scour is enhanced in the lower coarse sand layer, and the second part covers the cases with larger upper layer depths where scour depth coincides with the depth of the interface between the layers so that no scour occurs in the lower layer.

An empirical approach was used to obtain the best fitting form of equation using these parameters. This is a first attempt and based on limited data so it is expected that this equation would be refined with additional data. The equation is as follows:

$$\frac{S_{e,layered}}{D} = \frac{S_{e,Ll}}{D}\left(1 + \frac{L_u}{DK_A}\right),\ \frac{L_u}{D} < 0.9\frac{S_{e,Lu}}{D} \tag{7.5}$$

$$\frac{S_{e,layered}}{D} = \frac{L_u}{D},\ \frac{L_u}{D} \geq 0.9\frac{S_{e,Lu}}{D} \tag{7.6}$$

$$K_A = \frac{14.3}{\left(\frac{S_{e,Lu}}{D} - \frac{S_{e,Ll}}{D}\right)}\frac{D}{h}\left(\frac{V}{V_{cr}}\right)^3 \tag{7.7}$$

where L_u is the upper layer thickness, subscript Lu relates to the upper fine sand layer and subscript L_l relates to the lower coarse sand layer.

Figure 7.37 shows the equation fitted to the present test data for the four different sets of tests. An excellent fit is achieved with the tests in series R-3. The fit is less good for test series T-1 and preliminary set P-1, which may be due to the effects of ripples and lack of consistency in stopping the tests. For the tests in series C-1 in the larger flume the fit is good for the coarse sand and layered test, but the fine sand test plots lower than would be expected. This test also plotted on the low side in Figure 7.1 for S_e/D versus V/V_{cr}, so this may also be an issue with consistency in the stopping criteria. The 0.9 factor used to identify the transition point between the two conditions would probably be better represented as a dependent variable, but with only a few data points, this could not be determined in greater detail.

Prediction of the equilibrium scour depth in the wave-current tests is more difficult because there is a lack of equilibrium scour equations presented in the literature that are valid for wave-current scour in the clear water regime. A wider test programme would be needed in order to develop a new prediction equation for these tests.

Equilibrium scour prediction equations for the tidal tests are not considered because an equilibrium condition was not reached in the majority of the tests.

7.4 Evaluation of test methodology and areas for development

This section provides an evaluation of the test methodology and measurement techniques used in the project, to provide assurance of the quality of the data, and to help improve future experiment design for scour testing in the laboratory. In regards to future work, the final part of the discussion section (Section 7.5) makes a broader assessment of aspects that would be interesting to study further, and that would complement and extend the work in this project.

7.4.1 Test set-up and operation

The test methodology that was designed and used in this project has been shown to be successful due to the consistency and repeatability of the results from the majority of the tests and the excellent agreement with the literature. The discrepancies from the expected trends for a small number of tests have been successfully explained and accounted for (see Appendix 3).

One limiting factor of the test procedure was the limited duration of the scour tests, as was discussed in relation to test stopping criteria in Section 7.1.9. The long timescale of the scour process combined with the finite laboratory time available resulted in a compromise between the length of individual tests and the number of different tests that could be run. Therefore, in future test programmes further consideration should be given to the feasibility of running the equipment overnight, in terms of health and safety, and in terms of the design of automated monitoring systems. Based on the results in this project and in the literature (Simarro et al., 2011) the scour depth continues to increase even after considerable time, yet the final scour stage is little studied due to the time issues discussed. A methodology that enabled full scour curves to be obtained would be a valuable contribution to understanding the scour process.

7.4.2 Sources of error

One potential source of error in the test procedure was the low resolution of the pile scale. This will have the most significant effect on the data for the 20 mm pile, but less so at the larger pile diameters, where the 5 mm resolution is smaller compared to the pile diameter. A 5 mm scale was used because it was more visible to the cameras, and it is possible to obtain a reasonable estimate by eye of the scour depth to the nearest mm from a 5 mm scale.

In the small flume, one source of error is likely to be due to the difficulty of consistently re-setting the flow velocity between tests and after a test is paused. This is an inherent property of the flume and its mechanics, but this was minimised through the establishment of consistent start-up procedures based on the experiences from the preliminary sets of tests.

Errors induced by differences in the sand bed set-up were also found to be small, as the scour process was insensitive to small changes in density (test R.28). Furthermore, the sand bed set-up procedure was reasonably consistent between tests, shown by the good agreement between the core sample distributions and in-situ density measurements for tests R.25, R.26, R.N.27 and R.28 in the uniform coarse sand.

A greater level of variability was found for the mixed sand tests in terms of the grain size distribution in the test bed, which was linked to greater variability in the scour curves (see Section 7.2.2). This interesting effect on the scour process may be more representative of field conditions so does not have to be thought of as an error. However, further thought should be given as to how to either measure the variability in the bed, or instead how to improve the uniformity of the mixture to enable better quantification of the test parameters in future tests.

The range of errors was more prominent during the preliminary test series in the project where the methodology was still being refined, for example the effects of ripples were removed in later tests, better start up and pausing procedures were developed and those parts of the test procedure reliant on human operation became more consistent. These aspects have been presented openly, to better inform others of best practices for these types of tests but should not detract from the reliability of the results. Instead careful assessment has been made of each test, and these have been shown either to agree with the expected trends or have been disregarded

with specific reasons given. The key results in the early tests have been replicated in later tests with the most developed methodology.

While it is important to assess the shortcomings and areas for improvement in the methodology, this should not overshadow the overall success of the test programme. On the contrary, in comparison with the literature there is excellent agreement with the core trends for the baseline cases. This gives validation to the measurement techniques and experimental set-up, providing confidence in the results for the novel tests where comparisons with the literature are not available.

7.4.3 Scour measurement

A key part of this project was researching and developing scour measurement techniques, as discussed in Sections 2.7.3 and 4.4. Therefore, it is important to review the success of these and outline areas for further development.

While both the echosounder and photogrammetry techniques worked well in the small flume, and the results showed excellent agreement between these (Section 4.4.5), the slower processing time for the photogrammetry data resulted in the echosounder being the preferred system for collecting 2D profiles.

In the larger flume there was a significant deterioration in the echosounder data due to the larger scale and faster traversing speed. While the accuracy could be increased by collecting a greater number of measurements at each position in the matrix, the time taken to complete a profile would be increased and would likely be too long compared to the rate of scour in the earlier stages of the tests. To obtain a level of accuracy similar to that in the small flume the echosounder device would need to be placed closer to the bed, creating an unacceptably large disturbance to the flow. In this environment the photogrammetry technique is much more promising. The key advantages of the photogrammetry technique are its quick and practical set-up and operation in flume, the high level of accuracy in the processed results, and the excellent spatial coverage and resolution of the measurement points. These aspects make it a favourable technique compared to other options such as echosounder and laser scanners due to its high level of accuracy but much smaller cost compared to these systems.

Compromises had to be made in the final photogrammetry set-up so that measurements could only be collected when the flow was paused, and the slow processing time for obtaining the results was a disadvantage. Ways to improve the technique to mitigate these disadvantages are discussed in the following section.

7.5 Further work

One area for further development relates to the measurement techniques. The photogrammetry technique was found to be promising but further development would be useful, particularly at the larger scale where the echosounder technique was found to be less practical. Two areas for development have been identified:

- improving the set-up so that non-intrusive measurements can be obtained without pausing the flow
- development of the post-processing technique to speed up the analysis

A set of underwater cameras could be positioned close to the water surface downstream of the pile to enable in-test operation of the system without pausing the flow. However, the cameras would need to be considerably smaller in size compared to the one used in this project so that the level of disturbance to the flow would be small. Compatibility with the existing synchronisation system would need to be considered for the new cameras. It would also need to be tested if a suitable field of view of the scour hole could be obtained from this set-up. This could initially be tested with larger cameras to assess the viability of the approach. It would also need to be considered how this system could be operated in tidal flow or wave flow. In waves, the submergence depth may need to be increased, so the size of the cameras would be critical to ensuring the flow disturbance is small. In tidal flow the cameras would have to be repositioned with each flow reversal. A simple rig could be manufactured to enable the cameras to be swapped to either side of the pile.

In order to improve the data processing methodology, a different technique for dot projection could be employed, with each dot given a unique colour or shape to make the identification of dots easier in the photographs. This would also possibly help to improve the success of automatic detection algorithms, but at least would greatly aid the human operator.

Another development path for the photogrammetry technique would be to redevelop the code based on alternative photogrammetric algorithms as discussed in Section 2.7.3 of the literature review and to investigate if any of these enable a reasonable estimate of the scour hole coordinates with the cameras positioned outside of the flume. The success of this method would be less certain and considerably more time consuming than to build on the existing approach that has been developed in this project.

The small amount of further work necessary to employ smaller waterproof cameras linked to a synchronisation system along with an improved methodology for identification of the marker points in the images is likely to result in a useful system for scour measurement that would also be transferable to other applications.

In terms of identifying areas for focusing further scour research, this project has shown that study of the effects of the sediment bed configuration and its properties is key to improving understanding of the scour process. It would be interesting to study the effect of bulk density further. Improvement of the test methodology so that a greater increase in the bed density could be achieved and consistency of the density was ensured across the bed would enable this aspect to be more comprehensively investigated. It would also be interesting to delve further into other sediment properties and the effects of these on the scour process. This would require extensive measurement technique development in order to monitor grain-grain interaction effects such as particle collisions, as well as investigating the arrangement of grains and pore pressures within the bed. It would also be useful to conduct experiments to study in more detail the sediment

transport processes in mixed sands and the properties that affect the erodibility of different sand mixtures under a variety of flow conditions.

Further investigation of the flow structures within the scour hole would help to develop the analytical and numerical approaches to modelling scour development. Considering analytical approaches in tandem with experimental work would improve understanding of the relationship of the downflow/horseshoe vortex strength variation with parameters such as water depth and pile diameter which would help to quantify scale effects improving the link between scour in the laboratory and scour in the field. Consideration would need to be given to the measurement techniques employed in order to monitor the 3D flow patterns around the pile dynamically during scour testing.

While a fairly wide range of flow conditions and sediment bed configurations have been tested in this project, extension of the work to live bed conditions, and testing of sand bed configurations using a greater number of layers, different sediment grain sizes, and a wider range of distribution shapes in the mixed sands would extend understanding of scour in complex sediment beds. This would enable refinement of the definitions of the factors in the prediction equations developed in Section 7.3.2.

8. Conclusions

The objective of this thesis was to improve understanding of the scour process in mixed and layered sand beds. This was achieved through an extensive laboratory test programme to examine the effects of a range of sediment bed configurations and flow conditions on the scour process. During the design process, measurement techniques for scour monitoring were researched and developed. Baseline cases were included in the laboratory testing to enable comparison with the literature to assess the suitability of the methodology. Excellent agreement was found with trends in the literature, showing that the methodology was robust and provided repeatable and comparable results. This gives confidence in the results of the laboratory tests for new cases where no comparisons were available. The analysis of the laboratory data led to identification of new trends for scour development and equilibrium scour depth in layered and mixed sands, as well as furthering understanding of scour in the more complex flow conditions of tidal cycles and wave-current combinations. A comparison of the data with predictions gave an assessment of the suitability of existing prediction techniques, and led to development of new approaches to model scour development in layered and mixed sands (see Section 7.3). The main findings for each of these aspects are as follows:

1. Layered beds – scour can be increased by up to 0.3 S/D when a layer of fine sand overlies coarse sand, depending on the thickness of the upper layer, compared to scour in a uniform bed of the underlying sand type (coarse sand). This contrasts with the reduction in scour depth due to the bed armouring effect that can occur when coarse sand overlies fine sand. The increase in scour depth is linked to the fluctuations in vortex strength in the scour hole instigating grain-grain interaction effects between the two sediment layers.

2. Bimodal sands – in most cases these can be treated similarly to other types of non-uniform sediments and equilibrium scour depth can be predicted based on the d_{50} value of the mixture. There was a reduction in the rate of scour time development at lower flow velocities where a linear trend was observed for part of the scour curve. This may be explained by an increased resistance to erosion relative to the strength of the horseshoe vortex due to the configuration of the grains in mixed sand beds.

3. Tidal scour – scour development does not fit the standard scour prediction model of an increasing function with decreasing gradient (exponential expression) under a spring-neap cycle. Equilibrium scour depth was not reached after one full spring-neap cycle and it is likely that scour depth would continue to increase over several cycles. The longer timescale of the scour process is in contrast with existing studies and this difference is attributed to the removal of ripples that developed on the flat bed during the test which do not scale correctly in the laboratory.

4. Wave-current scour – adding a wave to a current can increase the scour depth in clear water conditions, contrary to research in the live bed regime. This is attributable to the strong dependence on θ/θ_{cr} in this regime, with a similar relationship to scour under unidirectional current.

5. Scour prediction – existing equations do not perform satisfactorily to predict scour equilibrium depth or time development in standard cases let alone in complex sediments or hydrodynamic conditions. Modifications have been suggested to incorporate some of the aspects discussed.

6. Scour measurement techniques – photogrammetry is a promising technique for accurate scour measurement in the laboratory, which significantly out-performs echosounder devices but requires further development to obtain dynamic measurements.

These results are significant because they show that even in simple sediment bed configurations consisting of only two different sands, the effects on the scour process can be substantial. It is concluded that the interaction effects at the sediment grain scale in layered and non-uniform sediment beds have a significant impact on scour development. Further research is warranted in this regard to extend the scope of the current project to a wider range of sand bed configurations and to verify the scour mechanisms identified from this investigation (see Section 7.5 for detailed recommendations for future work). This would be a worthwhile endeavour as it would help to reduce empiricism in current modelling approaches, and increase the direct applicability to real field sites. Furthermore, it is anticipated that a greater variety of interesting results and interaction effects would be discovered as the complexity of the sediment beds is expanded, and a greater variety of sediment properties are investigated.

This project is highly relevant to the offshore wind energy industry, because the findings are not currently taken into account in design methods for foundations. This work should increase awareness in academia and industry of the existence of novel effects on scour due to complexities in the sediment and flow conditions and the potential for improving design approaches through further research into these aspects. Reducing the costs of renewable energy technology is critical for meeting EU and UK government targets for reducing carbon emissions and improving energy security. Optimised foundation design can be achieved by decreasing the uncertainty in scour prediction, facilitating a substantial reduction in project costs especially when considering sites with multiple turbines. Investment in further scour research which would lead to improvement in prediction approaches can be justified by these cost savings and would help to establish the industry as a viable and cost competitive option for energy generation in the future.

References

ABPmer Ltd et al. (2010). *A further review of sediment monitoring data*. Commissioned by COWRIE Ltd (proj. ref. ScourSed-09).

Agrawal, A., Ramalingam, S., Taguchi, Y. and Chari, V. (2012). A theory of multi-layer flat refractive geometry, *Proc. Computer Vision and Pattern Recognition*, Providence, USA, 3346-3353.

Ahmed, F. and Rajaratnam, N. (1998). Flow around bridge piers, *J. Hydraul. Eng.*, **124:3**, 288-300.

Akib, S., Mohammadhassani, M. and Jahangirzadeh, A. (2014). Application of ANFIS and LR in prediction of scour depth in bridges, *Computers & Fluids*, **91**, 77-86.

Annandale, G. W. and Smith, S. (2001). *Calculation of bridge pier scour using the erodibility index method*, Dept. of Transport, USA, Report No. CDOT-DTD-R-2000-9.

Annandale, G. W., Wittler, R. J., Ruff, J. F. and Lewis, T. M. (1998). Prototype validation of erodibility index for scour in fractured rock media, *Proc. Water Res. Conf.*, Tennessee, USA.

Annandale, G. W. (2006). Quantification of the erosive capacity of water, *Proc. GeoCongress*, Atlanta, USA, 1-6.

Apsilidis, N., Diplas, P., Dancey, C. L., Vlachos, P. P. and Raben, S. G. (2010). Local scour at bridge piers: the role of Reynolds number on horseshoe vortex dynamics, *Proc. 5th Int. Conf. on Scour and Erosion*, San Francisco, USA, 86-94.

Apsilidis, N., Khosronejad, A., Sotiropoulos, F., Dancey, C. L. and Diplas, P. (2012). Physical and numerical modeling of the turbulent flow field upstream of a bridge pier, *Proc. 6th Int. Conf. on Scour and Erosion*, Paris, France, 181-188.

Arkhipov, G. A. (1984). Consideration of sediment transport when calculating local scour, *Gidroteknicheskoe Stroitel'stvo*, **4**, 14-16.

Ataie-Ashtiani, B. and Beheshti, A. A. (2006). Experimental investigation of clear-water local scour at pile groups, *J. Hydraul. Eng.*, **132:10**, 1100-1104.

Ayoubloo, M. K., Etemad-Shahidi, A. and Mahjoobi, J. (2010). Evaluation of regular wave scour around a circular pile using data mining approaches, *Applied Ocean Research*, **32**, 34-39.

Azamathulla, H. Md., Ghani, A. A., Zakaria, N. A. and Guven, A. (2010). Genetic programming to predict bridge pier scour, *J. Hydraul. Eng.*, **136:3**, 165-169.

Babu, M. R., Rao, S. N. and Sundar, V. (2002). A simplified instrumentation for measuring scour in silty clay around a vertical pile, *Applied Ocean Res.*, **24**, 355-360.

Babu, M. R., Rao, S. N. and Sundar, V. (2003a). Current-induced scour around a vertical pile in cohesive soil, *Ocean Eng.*, **30**, 893-920.

Babu, M. R., Sundar, V. and Rao, S. N. (2003b). Measurement of scour in cohesive soils around a vertical pile-simplified instrumentation and regression analysis, *IEEE J. Oceanic Eng.*, **28:1**, 106-116.

Baglio, S. and Foti, E. (2003). Non-invasive measurements to analyse sandy bed evolution under sea waves action, *IEEE Transactions on Instrumentation and Measurement*, **52:3**, 762-770.

Baglio, S., Faraci, C., Foti, E. and Musumeci, R. (2000). Stereo vision for non-invasive dynamic measurements of the scour process around a circular cylinder in an oscillating flow, *Proc. IEEE Conf. and Exhibition*, Providence, USA, **2**, 987-992.

Baglio, S., Faraci, C., Foti, E. and Musumeci, R. (2001). Measurements of the 3-D scour process around a pile in an oscillating flow through a stereo vision approach, *Measurement*, **30**, 145-160.

Baglio, S., Foti, E. and Musumeci, R. E. (2005). Measuring the effects of wave action around piers, *IEEE Instrumentation & Measurement Magazine*, **8:5**, 28-33.

Baker, C. J. (1979). The laminar horseshoe vortex, *J. Fluid. Mech.*, **95:2**, 347-367.

Baker, C. J. (1980). The turbulent horseshoe vortex, *J. of Wind Eng. and Industrial Aerodyn.*, **6**, 9-23.

Baker, C. J. (1985). The position of points of maximum and minimum shear stress upstream of cylinders mounted normal to flat plates, *J. of Wind Eng. and Industrial Aerodyn.*, **18**, 263-274.

Ballio, F. and Radice, A. (2003). A non-touch sensor for local scour measurements, *J. of Hydraul. Res.*, **41:1**, 105-108.

Ballio, F., Teruzzi, A. and Radice, A. (2009). Constriction effects in clear-water scour at abutments, *J. Hydraul. Eng.*, **135:2**, 140-145.

Baranya, S., Olsen, N. R. B., Stoesser, T. and Sturm, T. W. (2014). A nested grid based computational fluid dynamics model to predict bridge pier scour, *Proc. Inst. Civ. Eng., Water Management*, **167:WM5**, 259-268.

Barbhuiya, A. K. and Dey, S. (2003). Vortex flow field in a scour hole around abutments, *Int. J. Sediment Res.*, **18:4**, 310-325.

Bateni, S. M., Jeng, D. and Melville, B. W. (2007). Bayesian neural networks for prediction of equilibrium and time-dependent scour depth around bridge piers, *Advances in Eng. Software*, **38**, 102-111.

Beg, M. (2010). Mutual interference of bridge piers on local scour, *Proc. 5th Int. Conf. on Scour and Erosion*, San Francisco, USA, 76-85.

Beheshti, A. A. and Ataie-Ashtiani, B. (2008). Analysis of threshold and incipient conditions for sediment movement, *Coastal Eng.*, **55**, 423-430.

Bell, P. S. and Thorne, P. D. (1997). Application of a high resolution acoustic scanning system for imaging sea bed microtopography, *Proc. 7th Int. Conf. on Elec. Eng. in Oceanography*, Southampton, UK, 128-133.

Best, J. and Ashworth, P. (1994). A high-resolution ultrasonic bed profiler for use in laboratory flumes, *J. Sedimentary Res.*, **64:3a**, 674-675.

Bettess, R. (2002). A review of predictive methods for general scour, *Proc. 1st Int. Conf. on Scour of Foundations*, November 17-20, 162-174.

Bijker, E. W., and de Bruyn, C. A. (1988). Erosion around a pile due to current and breaking waves, *Proc. 21st Int. Conf. Coastal Eng.*, Malaga, Spain, 1368-1381.

Bilgili, M., Yasar, A. and Simsek, E. (2011). Offshore wind power development in Europe and its comparison with onshore counterpart, *Renewable and Sustainable Energy Rev.*, **15:2**, 905-915.

Blanco, B. L. D. S. R. (2003). *Dynamics of gravel and mixed, sand and gravel, beaches*, Thesis, Dept. Civ. Enviro. Eng., Imperial College London, UK.

Bonakdari, H., Lipeme-Kouyi, G. and Asawa, G. L. (2014). Developing turbulent flows in rectangular channels: a parametric study, *J. Applied Res. in Water and Wastewater*, **1:2**, 53-58.

Borah, D. K. (1989). Scour-depth prediction under armoring conditions, *J. Hydraul. Eng.*, **115:10**, 1421-1425.

Borghei, S. M., Kabiri-Samani, A., Banihashem, S. A. (2012). Influence of unsteady flow hydrograph shape on local scouring around bridge pier *Proc. Inst. Civ. Eng., Water Management*, **165**, 473-480.

Boukhanovsky, A. V., Lopatoukhin, L. J. and Soares, C. G. (2007). Spectral wave climate of the North Sea, *App. Ocean Res.*, **29**, 146-154.

Breusers, H. N. C. (1971). Local scour near offshore structures, *Proc. Symposium on Offshore Hydrodynamics*, Wageningen, The Netherlands.

Breusers, H. N. C., Nicollet, G. and Shen, H. W. (1977). Local scour around cylindrical piers, *J. Hydraul. Res.*, **15:3**, 211-252.

Briaud, J. L., (2002).The SRICOS-EFA Method, *Proc. 1st Int. Conf. on Scour and Erosion*, Texas, USA, 57-69.

Briaud, J. L., Ting, F. C. K., Chen, H. C., Guadavalli, R., Perugu, S. and Wei, G. (1999). SRICOS: Prediction of scour rate in cohesive soils at bridge piers, *J. Geotech. Geoenvrion. Eng.*, **125:4**.

Briaud, J. L., Ting, F. C. K., Chen, H. C., Cao, Y., Han, S. W. and Kwak, K. W. (2001). Erosion function apparatus for scour rate predictions, *J. Geotech. Geoenvrion. Eng.*, **127:2**, 105-113.

Briaud, J., Gardoni, P. and Yao, C. (2014). Statistical, risk and reliability analyses of bridge scour, *J. Geotech. Geoenvrion. Eng.*, **140**.

Buscombe, D. and Conley, D. C. (2012). Effective shear stress of graded sediments, *Water Resources Res.*, **48:5**.

Calappi, T., Miller, C. J. and Carpenter, D. (2010). Revisiting the HEC-18 scour equation, *Proc. 5th Int. Conf. Scour and Erosion*, California, USA, 1102-1109.

Campbell, L., McEwan, I., Nikora, V., Pokrajac, D., Gallagher, M. and Manes, C. (2005). Bed-load effects on hydrodynamics of rough-bed open-channel flows, *J. Hydraul. Eng.*, **131:7**, 576-585.

Cardoso, A. H. and Bettess, R. (1999). Effects of time and channel geometry on scour at bridge abutments, *J. Hydraul. Eng.*, **125:4**, 388-399.

Carreiras, J., Larroude, P., Seabra-Santos, F., Mory, M. (2000). Wave scour around piles, *Proc. 27th Int. Conf. Coastal Eng.*, Sydney, Australia, 1860-1870.

Chang, W., Lai, J., and Yen, C. (2004). Evolution of scour depth at circular bridge piers, *J. Hydraul. Eng.*, **130:9**, 905-913.

Chang, W., Lai, J., Yu, T., Lin, F., Lee, L., Tsai, W. and Loh, C. (2014a). Pier scour monitoring system by bed-level image tracking, *Int. J. Sediment Res.*, **29:2**, 269-277.

Chang, W., Lin, F., Lai, J., Lee, L., Tsai, W., Loh, C. (2014b). Multi-lens pier scour monitoring and scour depth prediction, *Proc. Inst. Civ. Eng., Water Management*, **167:WM2**, 88-104.

Chari, V. and Sturm, P. (2009). Multi-view geometry of the refractive plane, *Proc. British Machine Vision Conf.*, London, UK, 56.1-56.11.

Chaudhuri, S. and Debnath, K. (2013). Observation on initiation of pier scour and equilibrium scour hole profiles in cohesive sediments, *J. Hydraul. Eng.*, **19:1**, 27-37.

Chen, H., Yang, R., Kuo, P. and Hwung, H. (2012). Physical modelling study on scour and scour countermeasure for sea-crossing bridge piers, *Proc. 33rd Conf. Coastal Eng.*, Santander, Spain.

Cheng, L., An, H., Luo, C., Brown, T., Draper, S., White, D. J., (2014a). UWA's O-tube facilities: Physical modelling of fluid-structure-seabed interaction, *Proc. 8th Int. Conf. Phys. Modelling in Geotech.*, **1**, Leiden, The Netherlands, 3-20.

Chiew, Y. M. (1984). *Local scour at bridge piers*, Dept. Civil Eng., Auckland Uni., NZ.

Chiew, Y. M. and Melville, B. W. (1989). Local scour at bridge piers with non-uniform sediments, *Proc. Instn Civ. Engrs. Part 2*, **87**, 215-224.

Chiew, Y. M., (2008). Scour and scour countermeasures at bridge sites, *Trans. Tianjin Univ.*, **14:4**, 289-295.

Chreties, C., Simarro, G. and Teixeira, L. (2008). New experimental method to find equilibrium scour at bridge piers, *J. Hydraul. Eng.*, **134:10**, 1491-1495.

Chreties, C., Simarro, G. and Teixeira, L. (2013). Influence of flow conditions on scour hole shape for pier groups, *Proc. Inst. Civ. Eng., Water Management*, **166:WM3**, 111-119.

Coleman, S. E. and Melville, B. W. (1996). Initiation of bed forms on a flat sand bed, *J. Hydraul. Eng.*, **122:6**, 301-310.

Coleman, S. E. and Melville, B. W. (2001). Case study: New Zealand bridge scour experiences, *J. Hydraul. Eng.*, **127:7**, 535-546.

Coleman, S. E., Lauchlan, C. S. and Melville, B. W. (2003). Clear-water scour development at bridge abutments, *J. Hydraul. Res.*, **41:5**, 521-531.

Cooper, M. A. R. and Robson, S. (1996). Theory of close range photogrammetry. In Atkinson, K. B. (ed.), *Close range photogrammetry and machine vision*, 9-51, Whittles Publishing, Caithness.

Dalrymple, R. A. and Kirby, J. T. (1986). Water waves over ripples, *J. Waterway, Port, Coastal, Ocean Eng.*, **112:2**, 309-319.

Dargahi, B. (1989). The turbulent flow field around a circular cylinder, *Experiments in Fluids*, **8**, 1-12.

Dargahi, B. (1990). Controlling mechanism of local scouring, *J. Hydraul. Eng.*, **116:10**, 1197-1214.

De Jong, C. D., Lachapelle, G., Skone, S. and Elema, I. A. (2002). *Hydrography*, VSSD Delft University Press, Delft, Netherlands

De Vos, L., Rouck, J. D., Troch, P. and Frigaard, P. (2011). Empirical design of scour protections around monopile foundations, *Coastal Eng*, **58:6**, 540-553.

De Vriend, H. J. and Barends, F. B. J. (2006). Scour and erosion: common ground between hydraulics and geotechnics, *Proc. 3rd Int. Conf. on Scour and Erosion*, Amsterdam, The Netherlands.

Debnath, K. and Chaudhuri, S. (2010). Bridge pier scour in clay-sand mixed sediments at near-threshold velocity for sand, *J. Hydraul. Eng.*, **136:9**, 597-609.

Debnath, K. and Chaudhuri, S. (2011). Effect of suspended sediment concentration on local scour around cylinder for clay-sand mixed sediment beds, *Eng. Geology.*, **117**, 236-245.

DECC. (2008). *Dynamics of scour pits and scour protection – synthesis report and recommendations (Milestones 2 and 3)*, Final Report.

DECC. (2011). *UK Renewable Energy Roadmap Department of Energy and Climate Change, London*. [Online] Available from: https://www.gov.uk/government/uploads/system/uploads/attachment_data/file/48128/2167-uk-renewable-energy-roadmap.pdf [Accessed 18 Sept 2015].

Den Boon, J. H., Sutherland, J., Whitehouse, R., Soulsby, R., Stam, C. J. M., Verhoeven, K., Høgedal, M. and Hald, T. (2004). Scour behaviour and scour protection for monopile foundations of offshore wind turbines, *Proc. of the European Wind Energy Conf.*, Aalborg, Denmark.

Deng, L. and Cai, C. S. (2010). Bridge scour: prediction, modelling, monitoring, and countermeasures-review, *Practice periodical on Structural Design and Construction*, **15:2**, 125-134.

Dey, S. (1996). Sediment pick up for evolving scour near circular cylinders, *Appl. Math. Modelling*, **20**, 534-539.

Dey, S. and Barbhuiya, A. K. (2005). Time variation of scour at abutments, *J. Hydraul. Eng.*, **131:1**, 11-23.

Dey, S. and Raikar, R. V. (2007a). Characteristics of horseshoe vortex in developing scour holes at piers, *J. Hydraul. Eng.*, **133:4**, 399-413.

Dey, S. and Raikar, R. V. (2007b). Clear-water scour at piers in sand beds with an armor layer of gravels, *J. Hydraul. Eng.*, **133:6**, 703-711.

Dey, S., Chiew, Y. and Kadam, M. S. (2008). Local scour and riprap stability at an abutment in a degrading bed, *J. Hydraul. Eng.*, **134:10**, 1496-1502.

Dey, S., Sumer, B. M. and Fredsøe, J. (2006). Control of scour at vertical circular piles under waves and current, *J. Hydraul. Eng.*, **132:3**, 270-279.

Diab, R., Link, O. and Zanke, U. (2008). Measuring developing scour holes in gravel, *Proc. 4th Int. Conf. on Scour and Erosion,* Tokyo*,* Japan*,* 486-490.

Diab, R., Link, O. and Zanke, U. (2010). Geometry of developing and equilibrium scour holes at bridge piers in gravel, *Can. J. Civ. Eng.*, **37**, 544-552.

Dingler, J. R., Boylis, J. C. and Lowe, R. L. (1977). A high-frequency sonar for profiling small-scale subaqueous bedforms, *Marine Geology*, **24**, 279-288.

Dixen, F. H., Dixen, M., Pedersen, J. and Dahl, J. F. (2012a). Scour development around offshore wind turbine foundation: field measurement and analysis, *Proc. 6th Int. Conf. on Scour and Erosion,* Paris, France, 1441-1447.

Dong, Z., Wang, J., Chang-Zhi, C. and Zhen-Huan, X. (1992). Hydraulic characteristics of open channel flows over rough beds, *Science in China*, **35:8**, 1007-1016.

Eadie and Herbich (1986). Scour about a single cylindrical pile due to combined random waves and a current, *Proc. 20th Conf. Coastal Eng.*, Taipei, Taiwan.

Elliot, K. R. and Baker, C. J. (1985). Effect of pier spacing on scour around bridge piers, *J. Hydraul. Eng.*, **111:7**, 1105-1109.

Escarameia, M. (1998). Laboratory investigation of scour around large structures in tidal waters, *Proc. 3rd Int. Conf. Hydroscience and Eng.*, Cottbus/Berlin, Germany.

Escarameia, M. and May, R. W. P. (1999). *Scour around structures in tidal flows*, HR Wallingford Ltd., UK, Report SR 521.

Estaban M. D., Diez, J. J., López, J. S. and Negro, V. (2011). Why offshore wind energy? *Renewable Energy*, **36:2**, 444-450.

Ettema, R., Kirkil, G. and Muste, M. (2006). Similitude of large-scale turbulence in experiments on local scour at cylinders, *J. Hydraul. Eng.*, **132:1**, 33-40.

Ettema, R., Melville, B. W. and Barkdoll, B. (1998). Scale effect in pier-scour experiments, *J. Hydraul. Eng.*, **124:6**, 639-642.

European Commission. (2014). *A policy framework for climate and energy in the period from 2020 to 2030.* [Online] Available from: http://eur-lex.europa.eu/legal-content/EN/TXT/PDF/?uri=CELEX:52014DC0015 [Accessed 18 Sept 2015].

EWEA. (2015). *The European offshore wind industry – key trends and statistics 2014*. [Online] Available from: http://www.ewea.org/fileadmin/files/library/publications/statistics/EWEA-European-Offshore-Statistics-2014.pdf [Accessed 18 Sept 2015].

Fael, C. M. S., Simarro-Grand, G., Martin-Vide, J. P. and Cardoso, A. H. (2006). Local scour at vertical-wall abutments under clear-water flow conditions, *Water Resources Research*, **42**, W10408, 1-12.

Faraci, C., Foti, E. and Baglio, S. (2000). Measurements of sandy bed scour processes in an oscillating flow by using structured light, *Measurement*, **28**, 159-174.

Yang, F., Liu, X., Cao, S. and Huang, E. (2010). Bed load transport rates during scouring and armouring processes, *J. Mt. Sci.*, **7**, 215-225.

Ferradosa, T. J. F. (2012). *Scour around marine foundations in mixed and layered sediments*, Thesis, University of Porto, Portugal.

Foti, E., Rabionet, I. C., Marini, A., Musumeci, R. E. and Sánchez-Arcilla, A. (2011). Experimental investigations of the bed evolution in wave flumes: performance of 2D and 3D optical systems, *Coastal Eng.*, **58**, 606-622.

Fowler, J. E. (1993). *Coastal scour problems and methods for prediction of maximum scour*, Coastal Engineering Research Centre, U.S. Army Corps of Engineers, Technical Report CERC-93-8.

Franzetti, S., Larcan, E., and Mingosa, P. (1982). Influence of tests duration on the evaluation of ultimate scour around circular piers. *Proc. Int. Conf. on the Hydraulic Modelling of Civ. Eng. Structures*, Cranfield, UK.

Fredsøe, J., Andersen, K. H. and Sumer, B. M. (1999). Wave plus current over a ripple-covered bed, *Coastal Eng.*, **38**, 177-221.

Froehlich, D. C. (1995). Armor-limited clear-water contraction scour at bridges, *J. Hydraul. Eng.*, **121:6**, 490-493.

Ghosn, M. and Wang, J. (2003). Reliability model for bridge scour analysis, *Life-cycle performance of deteriorating structures*, 238-246.

Gjunsburgs, B., Govsha, J. and Lauva, O. (2014). Scour at layered river bed: reason of the structures failure, *Proc. 9th Int. Conf. Environ. Eng.*, Vilnius, Lithuania.

Goda, Y. and Suzuki, T. (1976). Estimation of incident and reflected waves in random wave experiments, *Proc. 15th Conf. Coastal Eng.*, Hawaii, USA, 828-845.

Gomez, B. (1994). Effects of particle shape and mobility on stable armor development, *Water Resources Res.*, **30:7**, 2229-2239.

Govindasamy, A. V., Briaud, J., Chen, H., Delphia, J., Elsbury, K., Gardoni, P., Herrman, G., Kim, D., Methewson, C. C., McClelland and M., Olivera, F. (2008). Simplified method for estimating scour at bridges, *GeoCongress*, Atlanta, USA, 385-393.

Govsha, E. and Gjunsburgs, B. (2012). Effect of the river bed stratification on scour at guide banks, *Proc. 6th Int. Conf. on Scour and Erosion,* Paris, France, 729-737.

Graf, W. H. and Istiarto, I. (2002). Flow pattern in the scour hole around a cylinder, *J. Hydraul. Res.*, **40:1**, 13-20.

Graf, W. H. and Yulistiyanto, B. (1998). Experiments on flow around a cylinder; the velocity and vorticity fields, *J. Hydraul. Res.*, **36:4**, 637-654.

Grass, A.J., Simons, R.R. and Cavanagh, N.J. (1985). Fluid loading on horizontal cylinders in wave type orbital oscillatory flow, *Proc. 4th Int. Symposium on Offshore Mech. and Arctic Eng.*, Dallas, USA.

Green, R. and Vasilakos, N. (2011). The economics of offshore wind, *Energy Policy*, **39:2**, 496-502.

Greenwood, B., Richards, R. G. and Brander, R. W. (1993). Acoustic imaging of sea-bed geometry: a high resolution remote tracking sonar (HRRTS II), *Marine Geology*, **112**, 207-218.

Grimaldi, C., Gaudio, R., Calomino, F. and Cardoso, A. H. (2009). Control of scour at bridge piers by a downstream bed sill, *J. Hydraul. Eng.*, **135:1**, 13-21.

Guney, M. S., Aksoy, A. O. and Bombar, G. (2011). Experimental study of local scour versus time around circular bridge pier, *Proc. 6th Int. Adv. Technologies Symposium*, Elaziğ, Turkey, 135-137.

Guney, M. S., Bombar, G. and Aksoy, A. O. (2012). Experimental investigation of time-dependent clear water scour around bridge pier due to a trapezoidal hydrograph, *World Environ. And Water Resources Congress*, New Mexico, USA, 2538-2545.

Guo, J. (2012). Pier scour in clear water for sediment mixtures, *J. Hydraul. Res.*, **50:1**, 18-27.

Guo, J. (2014). Semi-analytical model for temporal clear-water scour at prototype piers, *J. Hydraul. Res.*, **52:3**, 366-374.

Guo, J., Kerenyi, K., Suaznabar, O., Shan, H., Shen, J. J. and Xie, Z. (2012). Updating pier scour equations for coarse bed material, *Proc. 6th Int. Conf. on Scour and Erosion,* Paris*,* France, 761-768.

GWEC. (2015). *Global wind report annual market update 2014*. [Online] Available from: http://www.gwec.net/wp-content/uploads/2015/03/GWEC_Global_Wind_2014_Report_LR.pdf [Accessed 18 Sept 2015].

Hager, W. H. (2007). Scour in hydraulic engineering, *Proc. Inst. Civ. Eng., Water Management*, **160:WM3**, 159-168.

Hager, W. H., Unger, J. and Oliveto, G. (2002). Pier and abutment scour-new laboratory data, *Proc. First Int. Conf. on Scour of Foundations*, Texas, USA, 774-784.

Hancu, S. (1971). Sur le calcul des affouillements locaux dans la zone des piles des ponts, *14th Int. Assoc. of Hydraul. Congress*, Paris, France, 299-313.

Harris, C. K. (2003). *Sediment transport processes in coastal environments*, [Lecture], Virginia Inst. Of Marine Science, MS698-3, Lecture 1.

Harris, J. M. and Whitehouse, R. J. S. (2012). Scour management – a risk based approach, *Proc. 5th Int. Conf. on Scour and Erosion*, San Francisco, USA, 1511-1518.

Harris, J. M. and Whitehouse, R. J. S. (2014). Marine scour: Lessons from nature's laboratory, *Proc. 7th Int. Conf. on Scour and Erosion*, Perth, Australia, 19-31.

Harris, J. M., Whitehouse, R. J. S. and Benson, T. (2010a). The time evolution of scour around offshore structures, *Proc. Inst. Civ. Eng., Maritime Eng.*, **163:MA1**, 3-17.

Harris, J. M., Whitehouse, R. J. S. and Sutherland, J. (2010b). Scour assessment in complex marine soils – an evaluation through case examples, *Proc. 5th Int. Conf. Scour and Erosion*, San Francisco, USA, 450-459.

Harris, J. M., Whitehouse, R. J. S. and Sutherland, J. (2011). Marine scour and offshore wind – lessons learnt and future challenges, *Proc. 30th Int. Conf. Ocean, Offshore and Arctic Eng.*, Rotterdam, The Netherlands, 450-459.

Hartvig, P. A., Thomsen, J. M., Frigaard, P. and Andersen, T. L. (2010). Experimental study of the development of scour and backfilling, *Coastal Eng. J.*, **52:2**, 157-194.

Hatton, K. A. (2006). *Scour and ripple migration offshore of a vertically mounted pile subjected to irregular waves*, Thesis, Ohio State University, USA.

Heibaum, M. H. (2002). Geotechnical parameters of scouring and scour countermeasures, *Mitteilungsblatt der Bundesanstalt für Wasserbau*, **85**, 59-70.

Heller, V. (2011). Scale effects in physical hydraulic engineering models, *J. Hydraul. Res.*, **49:3**, 293-306.

Hoffmans, G. J. C. M. and Verheij, H. J. (1997). *Scour Manual*, CRC Press, USA.

Høgedal, M. and Hald, T. (2005). Scour assessment and design for scour for monopile foundations for offshore wind turbines, *Proc. Copenhagen Offshore Wind*, Copenhagen, Denmark.

Hong, J., Goyal, M. K., Chiew, Y. and Chua, L. H. C. (2012). Predicting time-dependent pier scour depth with support vector regression, *J. Hydrology*, **468-469**, 241-248.

Hossain, M. M. and Sarker, L. K. (2006). A laboratory study on incipient motion of nonuniform sediment mixtures, *Proc. 3rd Int. Conf. on Scour and Erosion*, Amsterdam, The Netherlands.

Huang, M. Y. F., Huang, A. Y. L. and Capart, H. (2010). Joint mapping of bed elevation and flow depth in microscale morphodynamics experiments, *Exp. Fluids*, **49**, 1121-1134.

Huang, W., Yang, Q. and Xiao, H. (2009). CFD modelling of scale effects on turbulence flow and scour around bridge piers, *Computers & Fluids*, **38**, 1050-1058.

Hughes, S.A. (1993). *Physical Models and Laboratory Techniques in Coastal Engineering*, *Volume 7 of Advanced series on ocean engineering*, World Scientific, Singapore.

IHB (2005). *Manual on hydrography*, International Hydrographic Bureau, Monaco, Publication M-13.

Imberger, J., Alach, D. and Schepis, J. (1982). Scour behind circular cylinders in deep water, *Proc. 18th Conf. Coastal Eng.*, Cape Town, South Africa, 1522-1554.

Ismail, A., Jeng, D., Zhang, L. L. and Zhang, J. (2013). Predictions of bridge scour: application of a feed-forward neural network with an adaptive activation function, *Eng. Applications of Artificial Intelligence*, **26**, 1540-1549.

Isiarto, I (2001). *Flow around a cylinder in a scoured channel bed*, École Polytechnique Fédérale de Lausanne, Switzerland, Thesis 2368.

Istiarto, I. and Graf, W. H. (2001). Experiments on flow around a cylinder in a scoured channel bed, *Int. J. Sediment Res.*, **4**.

Jain, S. C. (1981). Maximum clear-water scour around circular piers, *J. Hydraul. Division*, **107:HY5**, 611-626.

Jehanno, P., Marcellin, L. and Guilbaud, C. (2012). Laboratory scouring measurements: lessons learned regarding classic methods and recent or new methods, *Proc. 6th Int. Conf. on Scour and Erosion,* Paris, France, 371-378.

Jensen, M. S., Larsen, B. J., Frigaard, P., De Vos, L., Christensen, E. D., Hansen, E. A., Solberg, T., Hjertager, B. H. and Bove, S. (2006). *Offshore wind turbines situated in areas with strong currents*, Offshore Center Denmark, Aalborg University.

Jetté, C. D. and Hanes, D. M. (1997). High-resolution sea-bed imaging: an acoustic multiple transducer array, *Meas. Sci. Technol.*, **8**, 787-792.

Johnson, P. A. (1995). Comparison of pier-scour equations using field data, *J. Hydraul. Eng.*, **121:8**, 626-629.

Kantoush, S. A., Bollaert, E. F. R., Boillat, J., Schleiss, A. J. and Uijttewaal, W. S. J (2006). Experimental study of suspended sediment transport and deposition in a rectangular shallow reservoir, *River Flow*, Taylor and Francis Group, 1623-1631.

Kawata, Y. and Tsuchiya, Y. (1988). Local scour around cylindrical piles due to waves and currents combined, *Proc. 21st Conf. Coastal Eng.*, Torremolinos, Spain.

Kaya, A. (2010). Artificial neural network study of observed pattern of scour depth around bridge piers, *Computers and Geotechnics*, **37**, 413-418.

Khalfin, I. Sh. (2007). Modeling and calculation of bed score around large-diameter vertical cylinder under wave action, *Water Resources*, **34:1**, 49-59.

Kirkil, G., Constantinescu, G. and Ettema, R. (2007). Interaction of horseshoe vortex, detached shear layers, and near-wall turbulence during scour at a bridge pier, *Proc. Int. Conf. on Civ. and Enviro. Eng.*, Higashi-Hiroshima, Japan.

Kirkil, G., Constantinescu, S. G. and Ettema, R. (2008). Coherent structures in the flow field around a circular cylinder with scour hole, *J. Hydraul. Eng.*, **134:5**, 572-587.

Kirkil, G., Ettema, R. and Muste, M. V. (2004). *Similitude of coherent turbulence structures in flume studies of bridge scour*, *Proc. 2nd Int. Conf. on Scour and Erosion*, Meritus Mandarin, Singapore.

Kobayashi, Y. and Oda, K. (1994). Experimental study on developing process of local scour around a vertical cylinder, *Proc. 24th Conf. Coastal Eng.*, Kobe, Japan.

Kong, X., Cai, C. S. and Hou, S. (2013). Scour effect on a single pile and development of corresponding scour monitoring methods, *Smart Mater. Struct.*, **22**, 1-13.

Kothyari, U. C. and Kumar, A. (2012). Temporal variation of scour around circular compound piers, *J. Hydraul. Eng.*, **138:11**, 945-957.

Kothyari, U. C., Garde, R. J. and Raju, K. G. R. (1992). Temporal variation of scour around circular bridge piers, *J. Hydraul. Eng.*, **118:8**, 1091-1106.

Kotowski, R. (1988). Phototriangulation in multi-media photogrammetry, *Int. Archives of Photogrammetry and Remote Sensing*, **27**, 324-334.

Kuhnle, R. A. (1993). Fluvial transport of sand and gravel mixtures with bimodal size distributions, *Sedimentary Geo.*, **85**, 17-24.

Kuhnle, R. A., Alonso, C. V. and Shields Jr., F. D. (1999). Geometry of scour holes associated with 90° spur dikes, *J. Hydraul. Eng.*, **125:9**, 972-978.

Kumar, A., Kothyari, U. C. and Raju, K. G. R. (2012). Flow structure and scour around circular compound bridge piers – a review, *J. Hydro-environment Res.*, **6**, 251-265.

Lança, R. M., Fael, C. S., Maia, R. J., Pêgo, J. P. and Cardoso, A. H. (2013a). Clear-water scour at comparatively large cylindrical piers, *J. Hydraul. Eng.*, **139:11**, 1117-1125.

Lança, R. M., Fael, C. S., Maia, R. J., Pêgo, J. P. and Cardoso, A. H. (2013b). Clear-water scour at pile groups, *J. Hydraul. Eng.*, **139:10**, 1089-1098.

Larsen, B. J., De Vos, L. and Frigaard, P. (2004). *Scour around offshore wind turbine foundations*, Hydraulics and Coastal Engineering No. 9, Aalborg University, 1-53.

Laucelli, D., Giustolosi, O. (2011). Scour depth modelling by a multi-objective evolutionary paradigm, *Enviro. Modelling & Software*, **26**, 498-509.

Le Roux, J. P. (2005). Grains in motion: a review, *Sedimentary Geology*, **178**, 285-313.

Lee, S. O. and Sturm, T. (2008). Scaling issues for laboratory modelling of bridge pier scour, *Proc. 4th Int. Conf. on Scour and Erosion,* Tokyo*,* Japan*,* A-2, 111-115.

Lee, S. O. and Sturm, T. W. (2009). Effect of sediment size scaling on physical modelling of bridge pier scour, *J. Hydraul. Eng.*, **135:10**, 793-802.

Lee, S. O., Sturm, T. W., Gotvald, A., and Landers, M. (2004). Comparison of laboratory and field measurements of bridge pier scour, *Proc. 2nd Int. Conf. on Scour and Erosion*, Meritus Mandarin, Singapore, 231-239.

Li, Y., Briaud, J., Chen, H., Nurtjahyo, P. and Wang, J. (2002). Shear stress approach to pier scour predictions, *Proc. 1st Int. Conf. on Scour of Foundations*, Texas, USA, 156-161.

Li, Y., Wang, J., Wang, W., Briaud, J. and Chen, H. (2002). Flume Tests Results *Proc. 1st Int. Conf. on Scour of Foundations*, Texas, USA, 1208-1221.

Lim, S. (1997). Equilibrium clear-water scour around an abutment, *J. Hydraul. Eng.*, **123**, 237-243.

Lin, Y., Chen, J., Chang, K., Chern, J. and Lai, J. (2005). Real-time monitoring of local scour by using fiber Bragg grating sensors, *Smart Mater. Struct.*, **14**, 664-670.

Link, O. (2006). Time scale of scour around a cylindrical pier in sand and gravel, *Proc. Third Chinese-German Joint Symposium on Coastal and Ocean Eng.*, Tainan, Taiwan.

Link, O. and Zanke, U. (2004a). Influence of flow depth on scour at a circular pier in uniform coarse sand, *Proc. 2nd Int. Conf. on Scour and Erosion*, Meritus Mandarin, Singapore.

Link, O. and Zanke, U. (2004b). On the time-dependent scour-hole volume evolution at a circular pier in uniform coarse sand, *Proc. 2nd Int. Conf. on Scour and Erosion*, Meritus Mandarin, Singapore.

Link, O., Gobert, C., Manhardt, M. and Zanke, U. (2008). Effect of the horseshoe vortex system on the geometry of a developing scour hole at a cylinder, *Proc. 4th Int. Conf. on Scour and Erosion*, Tokyo, Japan, A-10, 162-168.

Link, O., Pfleger, F. and Zanke, U. (2006). Automatic non-intrusive measurement of scour hole geometry, *Proc. 3rd Int. Conf. on Scour and Erosion*, Amsterdam, The Netherlands

López, G., Teixeira, L., Ortega-Sánchez, M. and Simarro, G. (2014). Estimating final scour depth under clear-water flood waves, *J. Hydraul. Eng.*, **140:3**, 328-332.

Lu, J., Hong, J., Su, C., Wang, C. and Lai, J. (2008). Field measurements and simulation of bridge scour depth variations during floods, *J. Hydraul. Eng.*, **134:6**, 810-821.

Mackwood, P. R., Bearman, P. W. and Graham, J. M. R. (1997). *Wave and current flows around circular cylinders at large scale*, Health and Safety Executive, Offshore Technology Report OTH 491.

Margheritini, L., Frigaard, P., Martinelli, L. and Lamberti, A. (2006). Scour around monopile foundations for off-shore wind turbines, *Proc. 1st Int. Conf. on the Application of Phys. Modelling to Port and Coastal Protection*, Porto, Portugal.

Marszalec, J.A. and Marszalec, E. (1994). *Integration of lasers and fiber optics into robotic systems*, The International Society for Optical Engineering, Washington, USA.

Matutano, C., Negro, V., López-Gutiérrez, J., Esteban, M. D. (2013). Scour prediction and scour protections in offshore wind farms, *Renewable Energy*, **57**, 358-365.

May, R. W. P. and Escarameia, M. (2002). Local scour around structures in tidal flows, *Proc. First Int. Conf. on Scour of Foundations*, Texas, USA, 320-336.

McGovern, D., Ilic, S., Folkard, A., McLelland, S. and Murphy, B. (2012). Evolution of local scour around a collared monopile through tidal cycles, *Proc. 33rd Int. Conf. Coastal Eng.*, Santander, Spain.

McGovern, D., Ilic, S., Folkard, A., McLelland, S. and Murphy, B. (2014). Time development of scour around a cylinder in simulated tidal currents, *J. Hydraul. Eng.*, **140:6**, 1-12.

McLachlan, A. and Brown, A. C. (2006). *The ecology of sandy shores*, Academic Press, Waltham, USA.

Melville, B. W. (1975). *Local scour at bridge sites*, School of Engineering, University of Auckland, New Zealand.

Melville, B. W. (1984). Live-bed scour at bridge piers, *J. Hydraul. Eng.*, **110:9**, 1234-1247.

Melville, B. W. (2002). Local scour depths at bridge foundations: New Zealand methodology, *Proc. First Int. Conf. on Scour of Foundations*, Texas, USA, 120-139.

Melville, B. W. (2008). The physics of local scour at bridge piers, *Proc. 4th Int. Conf. on Scour and Erosion,* Tokyo, Japan, K-2, 28-40.

Melville, B. W. and Chiew, Y. (1999). Time scale for local scour at bridge piers, *J. Hydraul. Eng.*, **125:1**, 59-65.

Melville, B. W. and Coleman, S. E. (2000). *Bridge Scour*, Water Resources Publication, LLC, Colorado, USA.

Melville, B. W. and Sutherland, A. J. (1988). Design method for local scour at bridge piers, *J. Hydraul. Eng.*, **114:10**, 1210-1226.

Mengé, P. and Gunst, N. (2008). Gravity base foundations for the wind turbines on the Thorntonbank – Belgium, *Proc. 15th Innovatieforum Geotechniek*, Antwerp, Belgium.

Mia, Md. F. and Nago, H. (2003). Design method of time-dependent local scour at circular bridge pier, *J. Hydraul. Eng.*, **129:6**, 420-427.

Mikhail, E. M., Bethel, J. S. and McGlone, J. C. (2001). *Introduction to modern photogrammetry*, John Wiley & Sons, Inc., New Jersey, USA.

Miller Jr., W. and Sheppard, D. M. (2002). Time rate of local scour at a circular pile, *Proc. 1st Int. Conf. on Scour of Foundations*, Texas, USA, 827-841,

Mlaenik, J., Vosnjak, S. and Klasinc, R. (2004). Mapping of river bed – methods for hydraulic modelling, *Proc. 2nd Int. Conf. on Scour and Erosion*, Meritus Mandarin, Singapore.

Molinas, A. (2003). *Bridge scour in nonuniform sediment mixtures and in cohesive materials: synthesis report*, Federal Highway Administration, U.S. Dept. of Transportation, Publication No. FHWA-RD-03-083.

Molinas, A. and Noshi, H. M. (1999). *Effects of gradation and cohesion on bridge scour Vol. 2. Experimental study of sediment gradation and flow hydrograph effects on clear water scour around circular piers*, Federal Highway Administration, U.S. Dept. of Transportation, Publication No. FHWA-RD-99-184

Mueller, D. S. and Wagner, C. R. (2002). Analysis of pier scour predictions and real-time field measurements, *Proc. 1st Int. Conf. on Scour of Foundations*, Texas, USA, 257-271.

Mulsow, C. (2010). A flexible multi-media bundle approach, *Int. Archives of the Photogrammetry, Remote Sensing and Spatial Information Sciences*, **38:5**, 472-477.

Murthy, V. N. S. (2002). *Geotechnical engineering: principles and practices of soil mechanics and foundation engineering*, CRC Press, USA.

Najafzadeh, M., Barani, G. and Hessami-Kermani, M. (2013). Group method of data handling to predict scour depth around vertical piles under regular waves, *Scientia Iranica A*, **20:3**, 406-413.

Neill, C. R. (1973). *Guide to bridge hydraulics*, Roads and Transportation Assoc. Canada, University of Toronto Press, Canada.

Niedoroda, A. W. and Dalton, C. (1982). A review of the fluid mechanics of ocean scour, *Ocean Eng.*, **9:2**, 159-170

Nielsen, A. W., Sumer, B. M., Ebbe, S. S. and Fredsøe, J. (2012). Experimental study on the scour around a monopile in breaking waves, *J. Waterway, Port, Coastal and Ocean Eng.*, **138:6**, 501-506.

Olabarrieta, M., Medina, R. and Castanedo, S. (2010). Effect of wave current interaction on the current profile, *Coastal Eng.*, **57**, 643-655.

Oliveto, G. and Hager, W. H. (2002). Temporal evolution of clear-water pier and abutment scour, *J. Hydraul. Eng.*, **128:9**, 811-820.

Ong, M. C., Myrhaug, D. and Hesten, P. (2012). Scour around vertical pile foundations for offshore wind turbines due to long-crested and short-crested nonlinear random waves plus a current, *Proc. 6th Int. Conf. on Scour and Erosion,* Paris*,* France, 791-798.

Ong, M. C., Myrhaug, D. and Hesten, P. (2013). Scour around vertical piles due to long-crested and short-crested nonlinear random waves plus a current, *Coastal Eng.*, **73**, 106-114.

Pal, M., Singh, N. K. and Tiwari, N. K. (2012). M5 Model tree for pier scour prediction using field dataset, *KSCE J. Civ. Eng.*, **16:6**, 1079-1084.

Paphitis, D. (2001). Sediment movement under unidirectional flows: an assessment of empirical threshold curves, *Coastal Eng.*, **43**, 227-245.

Payne, G. (2008). *Guidance for the experimental tank testing of wave energy converters*, SuperGen Marine, The University of Edinburgh, UK, Version 01b.

Petersen, T. U., Sumer, B. M. and Fredsøe, J. (2012). Time scale of scour around a pile in combined waves and current, *Proc. 6th Int. Conf. on Scour and Erosion,* Paris*,* France, 981-988.

Porter, K. (2011). *Scour around complex foundations*, [MRes dissertation], Dept. Civ. Enviro. & Geomat. Eng., University College London, UK.

Prendergast, L. J. and Gavin, K. (2014). A review of bridge scour monitoring techniques, *J. Rock Mech. and Geotech. Eng.*, **6:2**, 138-149.

Prepernau, U., Grune, J., Sparboom, U., Schmidt-Koppenhagen, R., Wang, Z. and Oumeraci, H. (2008). Large-scale model study on scour around slender monopiles induced by irregular waves, *Proc. 31st Int. Conf. Coastal Eng.*, Hamburg, Germany, 2707-2716.

Qi, W., Gao, F., Han, X. and Gong, X. (2012). Local scour and pore-water pressure around a monopile foundation under combined waves and currents, *Proc. 22nd Int. Offshore and Polar Eng. Conf.*, Rhodes, Greece, 159-165.

Qi, W. and Gao, F. (2014a). Equilibrium scour depth at offshore monopile foundation in combined waves and current, *Science China, Technological Sciences*, **57:5**, 1030-1039.

Qi, W. and Gao, F. (2014b). Physical modelling of local scour development around a large-diameter monopile in combined waves and current, *Coastal Eng.*, **83**, 72-81.

Raaijmakers, T. and Rudolph, D. (2008). Time-dependent scour development under combined current and waves conditions – laboratory experiments with online monitoring technique, *Proc. 4th Int. Conf. on Scour and Erosion,* Tokyo*,* Japan*,* A-9, 152-161.

Raaijmakers, T. C., van Oeveren, M. C., Rudolph, D., Leenders, V. and Sinjou, W. C. P. (2010). Field performance of scour protection around offshore monopiles, *Proc. 5th Int. Conf. Scour and Erosion*, California, USA, 428-439.

Raaijmakers, T., Liefhebber, F., Hofland, B. and Meys, P. (2012). Mapping of 3D-bathymetries and structures using stereophotography through an air-water-interface, *Proc. 4th Int. Conf. on the App. of Phys. Modelling to Port and Coastal Protection*, Ghent, Belgium, 390-399.

Raikar, R. V. and Dey, S. (2005). Clear-water scour at bridge piers in fine and medium gravel beds, *Can. J. Civ. Eng.*, **32**, 775-781.

Raikar, R. V. and Dey, S. (2009). Maximum scour depth at piers in armor-beds, *J. Civ. Eng.*, **13:2**, 137-142.

Raudkivi, A. J. (1986). Functional trends of scour at bridge piers, *J. Hydraul. Eng.*, **112:1**, 1-13.

Raudkivi, A. J. (1998). *Loose boundary hydraulics*, CRC Press, USA.

Raudkivi, A. J. and Ettema, R. (1983). Clear-water scour at cylindrical piers, *J. Hydraul. Eng.*, **109:3**, 338-350.

Raudkivi, A. J. and Ettema, R. (1985). Scour at cylindrical bridge piers in armoured beds, *J. Hydraul. Eng.*, **111:4**, 713-731.

Remondino, F. and Fraser, C. (2006). Digital camera calibration methods: considerations and comparisons, *IAPRS*, **36**, 266-272.

RenewableUK. (2015). *Offshore Wind Project Timelines 2015*. [Online] Available from: http://www.renewableuk.com/en/publications/index.cfm/Offshore-Wind-Project-Timelines-2015 [Accessed 18 Sept 2015].

Richardson, E. V. and Davis, S. R. (2001). *Evaluating scour at bridges 4th edition*, Federal Highways Administration, U.S. Dept. Transportation, Publication No. FHWA NHI 01-001.

Robson, S. and Shortis, M.R. (2012). Vision Measurement System (version 8.5) [Computer program]. Geometric Software P/L, 15 Maranoa Crescent, Coburg, 3058, Australia, www.geomsoft.com.

Rosier, B., Boillat, J. and Schleiss, A. (2004). Mapping of bed morphology for lateral overflow using digital photogrammetry, *Proc. 2nd Int. Conf. on Scour and Erosion*, Meritus Mandarin, Singapore.

Roulund, A., Sumer, B. M., Fredsøe, J. and Michelsen, J. (2005). Numerical and experimental investigation of flow and scour around a circular pile, *J. Fluid Mech.*, **534**, 351-401.

Rudolph, D. and Bos, K. J. (2006). Scour around a monopile under combined wave-current conditions and low KC-numbers, *Proc. 3rd Int. Conf. Scour and Erosion*, Amsterdam, The Netherlands.

Rudolph, D., Raaijmakers, T. and Stam, C. (2008). Time-dependent scour development under combined current and wave conditions - hindcast of field measurements, *Proc. 4th Int. Conf. on Scour and Erosion,* Tokyo, Japan, B-15, 340-347.

Saadi, Y. (2008). Fractional critical shear stress at incipient motion in a bimodal sediment, *Civ. Eng. Dimension*, **10:2**, 89-98.

Salvi, J., Armangué, X. and Batlle, J. (2002). A comparative review of camera calibrating methods with accuracy evaluation, *Pattern Recognition*, **35**, 1617-1635.

Sarpkaya, T. and Isaacson, M. (1981). *Mechanics of wave forces on offshore structures,* Van Nostrand Reinhold Co., New York, USA.

Selley, R. C. (2000). *Applied sedimentology*, Academic Press, Waltham, USA.

Shen, H. W. and Lu, J. (1983). Development and prediction of bed armouring, *J. Hydraul. Eng.*, **109:4**, 611-629.

Shen, H.W., Schneider, V. R., and Karaki, S. S. (1969). Local scour around bridge piers, *J. Hydraul. Div. ASCE*, **95:HY11**, 1919-1940.

Shepherd, I. E. (1996). The measurement of bed form shapes in hydraulic models, *Proc. 25th Int. Conf. Coastal Eng.*, Florida, USA, 3169-3182.

Shepherd, R. G. (1989). Correlations of permeability and grain size, *Ground water*, **27:5**, 633-638.

Sheppard, D. M. (2003). *Large scale and live bed local pier scour experiments*, Florida Dept. Transportation, USA, FDOT Contract No. BB-473.

Sheppard, D. M. and Miller Jr., W. (2006). Live-bed local pier scour experiments, *J. Hydraul. Eng.*, **132:7**, 635-642.

Sheppard, D. M., Demir, H. and Melville, B. W. (2011a). *Scour at wide piers and long skewed piers*, Transportation Research Board, Washington D.C., NCHRP Report 682.

Sheppard, D. M., Melville, B. W. and Demir, H. (2011b). Evaluation of existing equations for local scour at bridge piers, *J. Hydraul. Eng.*, **140:1**, 14-23.

Sheppard, D. M., Odeh, M. and Glasser, T. (2004). Large scale clear-water local pier scour experiments, *J. Hydraul. Eng.*, **130:10**, 957-963.

Sheppard, D. M., Odeh, M., Pritsivelis, A. and Glasser, T. (2000). Clearwater local scour experiments in a large flume, *Joint Conf. on Water Resource Eng. and Water Resources Planning and Mgmt.*, Minnesota, USA, 1-9.

Shields, I., translated by Ott, J. and Martin-Vide, J. (1936). Anwendung der Aehnlichkeitsmechanik und der Turbulenzforschung auf die Geschiebebewegung. [English title: Application of similarity principles and turbulence research to bed-load movement], *Preussische Versuchsanstalt für Wasserbau und Schiffbau*, **26**, 524-526.

Simarro, G., Fael, C. M. S. and Cardoso, A. H. (2011). Estimating equilibrium scour depth at cylindrical piers in experimental studies, *J. Hydraul. Eng.*, **137:9**, 1089-1093.

Simarro-Grande, G. and Martin-vide, J. P. (2004). Exponential expression for time evolution in local scour, *J. Hydraul. Res.*, **42:6**, 663-665.

Simons, R., Weller, J. and Whitehouse, R. (2007). Scour development around truncated cylindrical structures, *Proc. 5th Int. Conf. Coastal Structures*, Venice, Italy, 1881-1890.

Sørensen, S. P. H., Ibsen, L. B. and Frigaard, P. (2012). Relative density of backfilled soil material around monopiles for offshore wind turbines, *Proc. 22nd Int. Offshore and Polar Eng. Conf.*, Rhodes, Greece, 177-183.

Soulsby, R. L. (1997). *Dynamics of Marine Sands*, Thomas Telford, London, UK.

Soulsby, R. L. and Clarke, S. (2005). *Bed shear-stresses under combined waves and currents on smooth and rough beds*, HR Wallingford, UK, Report TR 137.

Stahlmann, A. and Schlurmann, T. (2010). Physical modelling of scour around tripod foundation structures for offshore wind energy converters, *Proc. 32nd Conf. Coastal Eng.*, Shanghai, China.

Stancanelli, L. M., Musumeci, R. A., Marini, A., Foti, E., Rabionet, I. C. and Sanchez-Arcilla, A. (2010). Optical techniques for measuring swash zone morphodynamics, *Proc. 32nd Conf. Coastal Eng.*, Shanghai, China.

Sturm, T. W. and Janjua, N. S. (1994). Clear-water scour around abutments in floodplains, *J. Hydraul. Eng.*, **120:8**, 956-972.

Subramanian, N. (2010). *Design of Steel Structures*, Oxford University Press India, India.

Sumer, B. M. (2004). Physical and mathematical modelling of scour, *Proc. 2nd Int. Conf. on Scour and Erosion*, Meritus Mandarin, Singapore, 29-46.

Sumer, B. M. (2007). Mathematical modelling of scour: A review, *J. Hydraul. Res.*, **45:6**, 723-735.

Sumer, B. M. (2008). Coastal and offshore scour/erosion issues – recent advances, *Proc. 4th Int. Conf. on Scour and Erosion,* Tokyo, Japan, K-6, 85-94.

Sumer, B. M. and Fredsøe, J. (1997). *Hydrodynamics around cylindrical structures*, *Volume 12 of Advanced series on ocean engineering*, World Scientific, Singapore.

Sumer, B. M. and Fredsøe, J. (1998). Wave scour around group of vertical piles, *J. Waterway, Port, Coastal and Ocean Eng.*, **124:5**, 248-256.

Sumer, B. M. and Fredsøe, J. (2001a). Scour around pile in combined waves and current, *J. Hydraul. Eng.*, **127:5**, 403-411.

Sumer, B. M. and Fredsøe, J. (2001b). Wave scour around a large vertical circular cylinder, *J. Waterway, Port, Coastal and Ocean Eng.*, **127:3**, 125-134.

Sumer, B. M. and Fredsøe, J. (2002a). *The mechanics of scour in the marine environment*, *Volume 17 of Advanced series on ocean engineering*, World Scientific, Singapore.

Sumer, B. M. and Fredsøe, J. (2002b). Time scale of scour around a large vertical cylinder in waves, *Proc. 12th Int. Offshore and Polar Eng. Conf.*, Kitakyushu, Japan, 55-60.

Sumer, B. M. and Fredsøe, J. (2006). *Hydrodynamics around cylindrical structures (revised edition)*, *Volume 26 of Advanced series on ocean engineering*, World Scientific, Singapore.

Sumer, B. M. and Nielsen, A. W., (2013). Sinking failure of scour protection at wind turbine foundation, *Proc. ICE Energy*, **166:4**, 170-188.

Sumer, B. M., Christiansen, N. and Fredsøe, J. (1993). Influence of cross section on wave scour around piles, *J. Waterway, Port, Coastal and Ocean Eng.*, **119:5**, 477-495.

Sumer, B. M., Fredsøe, J. and Christiansen, N. (1992). Scour around vertical pile in waves, *J. Waterway, Port, Coastal and Ocean Eng.*, **118:1**, 15-31.

Sumer, B. M., Hatipoglu, F. and Fredsøe, J. (2004). Wave scour around a vertical circular pile in silt, *Proc. 2nd Int. Conf. on Scour and Erosion*, Meritus Mandarin, Singapore, 498-505.

Sumer, B. M., Hatipoglu, F., Fredsøe, J. (2007). Wave scour around a pile in sand, medium dense and dense silt, *J. Waterway, Port, Coastal and Ocean Eng.*, **133:1**, 14-27.

Sumer, B. M., Hatipoglu, F., Fredsøe, J. and Hansen, N. O. (2006a). Critical flotation density of pipelines in soils liquefied by waves and density of liquefied soils, *J. Waterway, Port, Coastal and Ocean Eng.*, **132:4**, 252-265.

Sumer, B. M., Hatipoglu, F., Fredsøe, J. and Sumer, S. K. (2006b). The sequence of sediment behaviour during wave-induced liquefaction, *Sedimentology*, **53**, 611-629.

Sumer, B. M., Petersen, T. U., Locatelli, L., Fredsøe, J., Musumeci, R. E. and Foti, E. (2013). Backfilling of a scour hole around a pile in waves and current, *J. Waterway, Port, Coastal and Ocean Eng.*, **139:1**, 9-23.

Sumer, B. M., Whitehouse, R. J. S. and Tørum, A. (2001). Scour around coastal structures: a summary of recent research, *Coastal Eng.*, **44**, 153-190.

Sutherland, J. and Whitehouse, R. J. S. (1998). *Scale effects in the physical modelling of seabed scour*, HR Wallingford Ltd., UK, Report TR 64.

Talebi, S., Minor, H. E. and Ortmanns, CH. (2004). Evaluating the time effect on scour and comparing the different experimental and semi-experimental formulas, *Proc. 2nd Int. Conf. on Scour and Erosion*, Meritus Mandarin, Singapore, 146-153.

The Crown Estate. (2015). *Energy and infrastructure key facts 2015-2016*. [Online] Available from: http://www.thecrownestate.co.uk/energy-and-infrastructure/offshore-wind-energy/ [Accessed 18 Sept 2015].

Thompson, D. M. and McCarrick, C. R. (2010). A flume experiment on the effect of constriction shape on the formation of forced pools, *Hydrol. Earth Syst. Sci.*, **14**, 1321-1330.

Thorne, P. D. and Hanes, D. M. (2002). A review of acoustic measurement of small-scale sediment processes, *Continental Shelf Res.*, **22**, 603-632.

Tian, Q., Lowe, K. T. and Simpson, R. L. (2010). A laser-based optical approach for measuring scour depth around hydraulic structures, *Proc. 5th Int. Conf. on Scour and Erosion*, San Francisco, USA, 787-796.

Ting, F. C. K., Briaud, J., Chen, H. C., Gudavalli, R., Perugu, S. and Wei, G. (2001). Flume tests for scour in clay at circular piers, *J. Hydraul. Eng.*, **127:11**, 969-978.

Umeda, S. (2011). Scour regime and scour depth around a pile in waves, *J. Coastal Res.*, **SI64**, 845-849.

Umeda, S., Yamazaki, T. and Ishida, H. (2008). Time evolution of scour and deposition around a cylindrical pier in steady flow, *Proc. 4th Int. Conf. on Scour and Erosion,* Tokyo, Japan, A-7, 140-146.

Umeda, S., Yamazaki, T. and Yuhi, M. (2010). An experimental study of scour process and sediment transport around a bridge pier with foundation, *Proc. 5th Int. Conf. on Scour and Erosion,* San Franciso, USA, 66-75.

Unger, J. and Hager, W. H. (2005). Discussion of 'The mean characteristics of horseshoe vortex at a cylindrical pier' by Muzzammil, M. and Gangadhariah, T., *J. Hydraul. Res.*, **43:5**, 584-587.

Unger, J. and Hager, W. H. (2007). Down-flow and horseshoe vortex characteristics of sediment embedded bridge piers, *Exp. Fluids*, **42**, 1-19.

Van Der Tempel, J., Zaaijer, M. B., and Subroto, H. (2004). The effects of scour on the design of offshore wind turbines, *Proc. 3rd Int. Conf. on Marine Renewable Energy*, London, UK, 27-35.

Veerappadevaru, G., Gangadharaiah, T., Jagadeesh, T. R. (2011). Vortex scouring process around bridge pier with caisson, *J. Hydraul. Res.*, **49:3**, 378-383.

Veerappadevaru, G., Gangadharaiah, T., Jagadeesh, T. R. (2012). Temporal variation of vortex scour process around caisson piers, *J. Hydraul. Res.*, **50:2**, 200-207.

Wei, G. and Ma, S. D., (1994). Implicit and explicit camera calibration: theory and experiments, *IEEE Transactions on Pattern Analysis and Machine Intelligence*, **16:5**, 469-480.

WenGang, Q. and FuPing, G. (2014). Equilibrium scour depth at offshore monopile foundation in combined waves and current, *Science China, Technological Sciences*, **57:5**, 1030-1039.

White, C. (1940). The equilibrium of grains on the bed of a stream, *Proc. Royal Soc. London Series A, Mathematical and Phys. Sci.*, **174:958**, 322-338.

Whitehouse, R. J. S. (1998). *Scour at marine structures*, Thomas Telford, London, UK.

Whitehouse, R. J. S. (2006). Scour at coastal structures, *Proc. 3rd Int. Conf. on Scour and Erosion*, Amsterdam, The Netherlands.

Whitehouse, R. J. S., Harris, J. M., Mundon, T. R. and Sutherland, J. (2010a). Scour around offshore structures, *Proc. 5th Int. Conf. on Scour and Erosion*, San Francisco, USA.

Whitehouse, R. J. S., Harris, J. M., Sutherland, J. and Rees, J. (2008). An assessment of field data for scour at offshore wind turbine foundations, *4th Int. Conf. on Scour and Erosion,* Tokyo*,* Japan*,* B-13, 329-335.

Whitehouse, R. J. S., Harris, J. M., Sutherland, J. and Rees, J. (2011). The nature of scour development and scour protection at offshore windfarm foundations, *Marine Pollution Bulletin*, **62:1**, 73-88.

Whitehouse, R. J. S., Lam, C., Richardson, S. and Keel, P. (2010b). Evaluation of seabed stability and scour control around subsea gravity protection structures, *Proc. OMAE*, Shanghai, China.

Whitehouse, R. J. S., Sutherland, J. and O'Brien, D. (2006). Seabed scour assessment for offshore windfarm, *Proc. 3rd Int. Conf. on Scour and Erosion*, Amsterdam, The Netherlands.

Wilcock, P. R. (1993). Critical shear stress of natural sediments, *J. Hydraul. Eng.*, **119:4**, 491-505.

Wilcock, P. R. (2001). Experimental study of the transport of mixed sand and gravel, *Water Resources Res.*, **37:12**, 3349-3358.

Wolf, J. and Prandle, D. (1999). Some observations of wave-current interaction, *Coastal Eng.*, **37**, 471-485.

Woolf, D. K., Cotton, P. D. and Challenor, P. G. (2003). Measurements of the offshore wave climate around the British Isles by satellite altimeter, *Phil. Trans. R. Soc. Lond. A*, **361**, 27-31.

Wörman, A (1992). Incipient motion during static armouring, *J. Hydraul. Eng.*, **118:3**, 496-501.

Wu, B., Molinas, A. and Julien, P. Y. (2004). Bed-material load computations for nonuniform sediments, *J. Hydraul. Eng.*, **130:10**, 1002-1012.

Yanmaz, A. M. and Altinbilek, H. D. (1991). Study of time-dependent local scour around bridge piers, *J. Hydraul. Eng.*, **117:10**, 1247-1268.

Yoon, T. H. (2004). Bed form deformation due to upstream group piles, *Proc. 2nd Int. Conf. on Scour and Erosion*, Meritus Mandarin, Singapore, 70-76.

Younkin, B. D. and Hill, D. F. (2009). Rapid profiling of an evolving bed form using planar laser sheet illumination, *J. Hydraul. Eng.*, **135:10**, 852-856.

Zanke, U. C. E. (2003). On the influence of turbulence on the initiation of sediment motion, *Int. J. Sediment Res.*, **18:1**, 17-31.

Zanke, U. C. E., Hsu, T., Roland, A., Link, O. and Diab, R. (2011). Equilibrium scour depths around piles in noncohesive sediments under currents and waves, *Coastal Eng.*, **58**, 986-991.

Zdravkovich, M. M. (1987). The effects of interference between circular cylinders in cross flow, *J. Fluids and Structures*, **1**, 239-261.

Zevenbergen, L. W., Lagasse, P. F. and Edge, B. L. (2004). *Tidal hydrology, hydraulics and scour at bridges*, Federal Highway Administration, U.S. Dept. Transportation, Publication No. FHWA-NHI-05-077.

Zhao, M., Cheng, L. and Zang, Z. (2010). Experimental and numerical investigation of local scour around a submerged vertical circular cylinder in steady currents, *Coastal Eng.*, **57**, 709-721.

Zhao, M., Zhu, X., Cheng, L. and Teng, B. (2012). Experimental study of local scour around subsea caissons in steady currents, *Coastal Eng.*, **60**, 30-40.

Zhao, X. and Wang, X. (2009). Simulation of piles in hydraulic model and experiment study on local scour at pile foundation in offshore wind farm, *Proc. Int. Conf. on Sustainable Power Generation and Supply*, Nanjing, China.

Zhao, X., Ma, J. and Chen, Z. (2003). Model studies on local scour in the regulation project of the deep channel in the Changjiang estuary, *Int. Conf. on Estuaries and Coasts*, Hangzhou, China, 531-536.

Appendix 1 - Measurement technique tables

Table A1.1 Pile scales and rules.

Paper	Method of measurement	Vertical resolution and accuracy	Spatial coverage	Time resolution
Roulund et al. (2005)	Scale marked onto pile	Scale marked in 1cm intervals with depth on a 10cm diameter pile	Marked around entire pile circumference	
Chaudhuri and Debnath (2013); Debnath and Chaudhuri (2010); Debnath and Chaudhuri (2011)	Graduated measurement tapes glued inside perspex pile and monitored by camera on a traverse inside the pile to give vertical and rotational movement.	Inch scale with 1/8 inch markings (approx. 3 mm)	4 scales at 90 degree intervals around pile circumference	Camera records one scale at a time at regular intervals
Chang et al. (2014a); Chang et al. (2014b)	Camera driven by motor along rail inside pile (or multiple cameras in fixed positions), and Scour depth computed from image recognition of the interface between sand and water with scale on inside of pile for image calibration. Automatic feedback to move camera to keep in-line with interface.	1 mm scale	1 scale at upstream side of pile, and no rotational capability of the camera system.	
Sheppard et al. (2004); Sheppard et al. (2000)	Measuring tapes attached to inside of pile with 2 video camera inside pile on vertical traverse.		2 scales at upstream face of pile, approx. 15 degrees either side of centre	Continuous
Kawata and Yoshito (1988)	Fibre optic sensors placed in a vertical line on the inside of the pile and monitored with video camera. Scour depth determined from number of visible lights.		Adjacent to pile	Continuous
Lin et al. (2005); Kong et al. (2013)	FBG sensors arranged in series along optical fibre on a cantilever beam attached to outside of pile. Response changes as the sensors emerge from the sediment bed as scour increases		1 scale	
Babu et al. (2002); Babu et al. (2003a); Babu et al. (2003b)	Pairs of 2mm diameter steel wires vertically attached to the pile in grooves. The depth is measured by recording the change in electrical current.		4 scales at 90 degree intervals around pile circumference	Continuous
Sumer and Fedsøe (2001b)	Calibrated measurement pins of 3mm diameter placed in the bed, monitored by eye or video camera		Discrete points anywhere on the bed	Continuous

Table A1.2 Echosounder measurement techniques

Paper	Method of measurement	Sensor dimensions and submergence depth	Sensor resolution/beam footprint (horizontal)	Spatial coverage	Flow paused?	Time resolution
Dingler et al. (1977)	Mounted on instrument carriage.	2.5cm diameter transducer Submerged below water surface, depth unknown.		yes		
Best and Ashworth (1994)						20 pulses per second, reading output each 0.5s as average of 10 pulses
Greenwood et al. (1993)	Traversed over sea-bed attached to a platform (~0.25x0.10m)	Sensor designed for use in field. Sensor of the order of 10 cm diameter. Max. distance 5m	small beam footprint 0.74 degrees beam angle gives footprint of 0.006m at distance of 0.75m.	3m of sea bed in 10 mins		
Bell and Thorne (1997)	Mounted on stepper motor to move it to different angles – rotating sensor with 400 angular positions instead of horizontal positioning.	0.5-1m above seabed	1 degree beam width.			
Coleman et al. (2003)	Positioned sensor at the point that maximum scour depth expected to occur.			Single point		Scour depth recorded at varying time intervals 10-60s then 10-30min.
Sheppard et al. (2000); Sheppard (2003); Sheppard and Miller (2006)	Attached 3 transducers to pile, one upstream, and one on each side of pile, mounted close to water surface. Each transducer has 4 crystals i.e. four separate measurements taken with each transducer.	Close to the bed. Sensors stick out from pile quite a way but are thin in vertical. The crystals are 2.5cm in diameter and 8cm distance from each other, for smaller scale testing the crystals were 4 cm apart, located approx. 10 cm below water surface.	In large scale experiments transducer located 0.915m from bed has 5 cm diameter beam footprint.	12 measurement points around pile		Measured every 600 seconds.

Jetté and Hanes (1997)	multiple transducer array – 37 elements avoiding need for traversing the equipment	Spacing 1.2 centre to centre of the transducers. Dimensions of array is 50x8.5x5cm	2cm horizontal resolution Half beam angle = 0.9 degrees			Transducers fired sequentially 5 seconds to do one scan.
Kantoush et al. (2006)	Sensor on traverse to take bed profiles					Parts of bed profile measured every 20mins
Stahlmann and Schlurmann (2010)	Used abs (acoustic back scatter probes) as single beam echosounder attached to tripod structure, a few each at different locations	ABS fully submerged				
Guney et al. (2011)	transducers in different fixed positions two upstream, 6.3 and 12cm from centre of pile, and one at side 7cm from centre of pile	only 2 cm above the initial bed surface				
Guney et al. (2012)	Used ultrasonic velocity profiler sensors to measure scour depth – position 3 around the pile, upstream, downstream and one side	2cm above initial bed surface				4MHz
Chen et al. (2012)	Ultrasonic profiles on traverse					before and after tests only
McGovern et al. (2012)	Used 12 sensors 3 at each side of the pile closest ones 6.5 cm from pile then spaced at 10cm radially.	all on one bar to hold them so significant amount of equipment in water. No dimensions given				Depth recorded at 1s interval took average of 20 readings, discarding 3 highest and 3 lowest
WenGang and FuPing (2014)	attached two ultrasonic distance sensors to the pile upstream and downstream	Attached to pile submerged				

Kawata and Tsuchiya (1988)	used ultrasonic depth sounder to measure ripple heights and lengths but not scour					
Kuhnle et al. (1999)	SedBed monitor – mounted on instrument carriage 24 streamwise transects 3.6 long collected at 5cm intervals A full grid	Operates underwater			no	approx. 30 minutes for each full profile. Collected before start of test then during test, frequent intervals at start then not so frequent at end. Initial profile was with flume drained (measured with an acoustic sensor that works in air). Measurements taken during scouring – flow not paused
Lee and Sturm (2009)	Uses adv mounted on carriage rail	5cm above bed	Diameter 4.5-6mm			Before and after test

Table A1.3 Point gauge techniques

Paper	Method of measurement	Sensor dimensions and submergence depth	Sensor resolution/beam footprint (horizontal)	Vertical resolution and accuracy	3D measurements?	Flow paused or drained?	Time resolution
Akib et al. (2014)	digital point gauge						1min x 10, 10min x 10, 100min x 5
Sturm and Janjua (1994)	Point gauge with a blunt tip attached to an instrument carriage (traverse).	Water drained					Only measured bed profile at end of test with water drained.
Lança et al. (2013a)	Measured scour hole depth with an 'adapted' point gauge			to accuracy of ±1mm.			approx. every 5 minutes during first hour

Cardoso and Bettess (1999)	Scour depth measured with point gauge with a tip painted with luminous red paint – put the red tip into the sand until it could no longer be seen			error of 1mm.			
Borghei et al. (2012)	Point gauge to measure scour depth and water depth.			accuracy of 1mm			
Hager et al. (2002)	Sediment surface measured with a 'shoe gauge' they reckon this makes measurements simpler than with conventional point gauge. They took various points including scour extent, max scour, and points of interest.	5mm length and 2mm width		Accuracy was about 0.5d50 = 1mm		Sounds like measurements taken during test running	Frequency of readings slowed as test progressed starting at 1,3,6,10,20 minutes then hours etc.
Li et al. (2002)	Electronic point gauge. Needle attached to a vertical ruler. As soon as tip of needle touches surface of bed get a sudden change in volt reading on the meter	The needle is thin so that it does not damage the bed even when it penetrates it.		Resolution is ±1mm.	They employed a method of searching for the deepest point in the scour hole when visually could not be seen. Measured point of deepest scour, but took several measurements at different points in order to find the deepest point.	used to measure scour depth without interrupting the test.	It took 1 minute to take one reading and 10 minutes to collect one data set for a single pier.

Whitehouse et al. (2006)	Bed profiles measured along 8 radial lines using a 'touch-sensitive bed profiler'. Top of pile removed so could use pile level as baseline (0 depth)	water was drained				yes	final bed profile and initial profiles before test.
Eadie and Herbich (1986)	points taken over a rectangular grid	water was drained				yes	after each test
Simons et al. (2007)	laser pointer external to the flume and a projected grid through a Perspex sheet on the water surface. The laser pointer is lined up with each grid crossing in turn to take measurements.				Yes	No	5 mins for 60 mins, then 15 mins. Depth and extent measured at end
Ballio and Radice (2003)	fibre optic probe attached to a 3D traverse Measures reflected infrared light that it emits. Automatically Positioned in the vertical until it reaches point of selected sensing distance which equals a specific light intensity.	Probe has 3mm tip diameter and 10mm normal diameter (100cm long). Sensing distance about 15mm from bed	Measurement spotlight on bed is about 3-4mm diameter for operating distance of 10-20mm	accuracy 0.1mm			
Thompson and McCarrick (2010)	Digital point gauge, 5cm intervals line profile, also grid profile on some tests						End of test only
Babu et al. (2002)	Point gauge for bed profiling					Flume drained	Equilibrium only
Debnath and Chaudhuri (2010)	Point gauge on graduated traverse					Flume drained	Equilibrium only

Table A1.4 Laser techniques

Paper	Method of measurement	Sensor dimensions and submergence depth	Sensor resolution/beam footprint (horizontal)	Vertical res/accuracy	3D measurements?	Flow paused?	Time resolution
Stahlmann and Schlurmann (2010)	Laser distance sensor Attached to traverse	laser was submerged				looks like flow paused at certain points during test to take profiles	
Link (2006); Link and Zanke (2004b); Diab et al. (2008); Diab et al. (2010)	laser distance sensor placed inside Plexiglas pier taking horizontal measurements. Radial and vertical position of laser moved with precision step motors	non-intrusive measurements	20-30points measured in vertical, 24 different radial positions.	accuracy ± 0.4mm. Motors had accuracy of ±0.1mm vertical, ±0.5degrees radial or 0.65m with accuracy ± 0.3 mm.			Full scour hole topography measured in 2 minutes. 70hz freq of data capture. A full profile took about 30s in the initial scour stages and about 180s at the end
Mlaenik et al. (2004)	Time of flight laser distance sensor attached to traverse for horizontal 2d movement						
Margheritini et al. (2006)	laser profiler Laser on a traverse	Didn't have to drain the water				yes	Mostly used at end of tests. 35 minutes to take grid of measurements in 1.5cm intervals. Used it to measure profiles each time flow reversed in tidal tests (every half hour)

Jensen et al. (2006)	Same Laser profiler as Margheritini et al (2006) 1.5x1.5cm grid	Some drained, some not Note that the dimensions of the sensor look to be pretty large.				yes	I.e after 30min wet, after 1h dry, after 2h dry.
Hartvig et al. (2010)	Same Laser profiler as Margheritini et al (2006)	Not drained	Horizontal about 0.3mm	Vertical accuracy of ± 1mm		yes	
Zhao et al. (2010)	laser profile laser fixed to traverse time of flight	Drained. Sensor has large dimensions relative to model	Traverse accurate to ± 0.2mm				End of test speed up to 5m/s
Unger and Hager (2007)	Laser distance sensor on traverse			±0.5mm accuracy		yes	during the test
Shepherd (1996)	Laser distance sensor uses scattered reflected infra-red light.	Laser is put in waterproof housing to take measurements underwater. Can keep sensor at large distance from bed and don't need to adjust vertical position of the sensor.	excellend horizontal res due to 1mm diameter spot2mm horizontal res,	. <0.1vertical res			

Table A1.5 photogrammetry techniques

Paper	Method of measurement	Interfaces	Resolution and accuracy	3D measurements?	Flow paused and/or drained?	Time resolution	Method for accounting for refraction
Umeda et al. (2008)	Four perspectives with camera above flume	none	1mm accuracy	Yes	drained	Equilibrium only	Not necessary as no interface
Rosier et al. (2004)	Camera 6.5m above flume	none		Yes	drained		Not necessary as no interface

Umeda et al. (2010)	Four external cameras	Air-water	1mm accuracy	Yes	paused		Not accounted for but water depth was shallow so loss of accuracy was small
Raaijmakers at al. (2012)	Two cameras 200mm apart	Air-water		yes	paused		Accounted for using Muslow's method
Foti et al. (2011)	Laser grid and camera in plexiglass box	Air-glass		Yes			
Stancanelli et al. (2010)	Laser grid and camera	Air-glass	1mm	Yes	no	5mins	
Baglio et al. (2000); Baglio et al. (2001); Baglio and Foti (2003); Baglio et al. (2005)	Pair of video cameras and structured light grid	Air-glass-water	~1mm	Yes	no		No lens distortion or refraction effect has been accounted for in the computation.
Sumer et al. (2013)	Two external upstream cameras and laser grid	Air-glass-water		yes			Includes lens distortion correction, but no explicit correction for refraction due to air-glass-water interface
Hatton (2006)	Underwater video camera and laser light sheet	none		2D – line profile			Rectify image using known geometry/coordinates
Younkin and Hill (2009)	Camera outside of flume, perpendicular to flume wall	Air-glass-water	1-2mm			0.67Hz	Geometry of camera minimises refraction and means that it is symmetrical
Huang et al. (2010)	Camera above flume with laser sheet	Air-water		2D line profile but scanned to get 3D profile over a finite time.			Physical correction for refraction (Snell's law) by assuming camera is perpendicular to laser sheet.
Tian et al. (2010)	2D laser line recorded with camera	Air-water	1mm	2D line profile but scanned to get 3D profile over a finite time.			

Faraci et al. (2000);	Video camera and laser sheet	Air-glass	1mm	Yes			Neglected corrections because of position of laser and small dimensions of measurement region. i.e. image plane parallel to laser sheet
Baglio and Foti (2003)	Video camera and light sheet	Air-glass-water	1mm	2D	no		

Appendix 2 - Test design and parameter selection

Sediment trap design

Sediment traps are necessary in the larger flume to prevent sediment from entering the pumps. The trap design is complicated in this model because of the need for a symmetrical false bed layout to accommodate tidal flows. Therefore, consideration needs to be given as to how to limit the influence of the trap on the flow over it.

By placing the sediment traps as far away from the pile as possible it is assumed that most of the sediment will be travelling as bedload once it reaches the traps as most of the suspended load under the wake should have settled out. To ensure that the sediment is travelling as bedload under waves, the trap also needs to be wider than the maximum horizontal excursion under the waves.

Based on the length of the flume and the length of the false bed section on either side of the test section, the sediment trap was set to 30 cm width, starting 30 cm from the edge of the ramp.

A calculation was also completed to assess the height at which suspended particles in the water column starting just downstream of the pile would still be captured by the trap. This estimate ignores pile wake effects and is based on the settling velocity of the sediment and the critical flow velocity. This enables the distance to the point at which the sediment settles on the bed to be determined, which must be less than the distance to the trap (3.7 m from location of the pile). The calculation is summarised in Table A2.1.

Table A2.1 Maximum height of suspended sediment at pile to settle out before reaching trap.

d_{50} m	0.0002	0.0006
w_s m/s	0.026	0.085
max height at pile (m) to settle out before trap	0.32	0.45
V_{cr}	0.29	0.35
Downstream distance to settle (m)	3.55	1.85

Table A2.1 shows that fine sand in the bottom 71% of the water column will settle out before the start of the trap, but coarse sand will settle out from 100% of the water column, ignoring wake effects that may keep sediment in suspension for longer. Table A2.1 shows that the coarse sand has ample settling time before reaching the trap, but that there is less margin for error for

the fine sand. However, most sediment will be confined to lower down in the water column, probably in the bottom 50%.

Therefore, caution is needed using fine sand in the large flume if in live bed conditions as the traps would not be expected to capture all of the suspended sand under these conditions. However, as the main test series was designed for clear water conditions the sediment trap design was found to be more than adequate for trapping both fine and coarse sediments.

Critical velocity calculations

The critical Shields parameter for each sand type was calculated using the dimensionless grain size, D*, following the method of Soulsby (1997):

$$\text{For } D^* < 10,\ \theta_{crit} = \frac{0.3}{1+1.2D^*} + 0.055\left[1 - e^{(-0.02D^*)}\right] \quad \text{(A2.1)}$$

$$\text{For } D^* > 10,\ \theta_{crit} = \frac{0.24}{D^*} + 0.055\left[1 - e^{(-0.02D^*)}\right] \quad \text{(A2.2)}$$

$$D^* = d_{50}\left(\frac{(s-1)g}{v^2}\right)^{\frac{1}{3}} \quad \text{(A2.3)}$$

The clear water or live bed regime was determined by calculating the Shields parameter for the test condition and comparing it to the critical Shields parameter calculated from above.

Following the method of Soulsby and Clarke (2005), in unidirectional current the Shields parameter was calculated from:

$$\theta = \frac{\tau}{(\rho_s - \rho)g d_{50}} \quad \text{(A2.4)}$$

$$\text{Where } \tau_{current} = \rho C_D V^2 \quad \text{and} \quad C_D = \left(\frac{0.4}{\ln(h/z_0)-1}\right)^2, \quad z_0 = 2.5\frac{d_{50}}{30} \quad \text{(A2.5)}$$

In waves the Shields parameter was calculated as above but with the following definition of bed shear stress:

$$\tau_{wave} = 0.5\rho f_w {U_w}^2, \quad f_w = 1.39\left(\frac{A}{z_0}\right)^{-0.52}, \quad A = \frac{U_w T}{2\pi} \quad \text{(A2.6)}$$

In combined wave-currents the Shields parameter was calculated based on the following definition of bed shear stress:

$$\tau_{max} = ([\tau_{mean} + \tau_{wave}\cos(\phi)]^2 + [\tau_{wave}\sin\phi]^2)^{0.5} \quad \text{(A2.7)}$$

$$\text{where } \tau_{mean} = \tau_{current}\left\{1 + 1.2\left(\frac{\tau_{wave}}{\tau_{wave}+\tau_{current}}\right)^{3.2}\right\} \quad \text{(A2.8)}$$

Note that ø is the angle between the wave and current direction, which was zero for the present tests.

Wave and wave-current test series design

The wave-current tests were designed based on linear wave theory with consideration of the critical velocity in order to remain in the clear water regime.

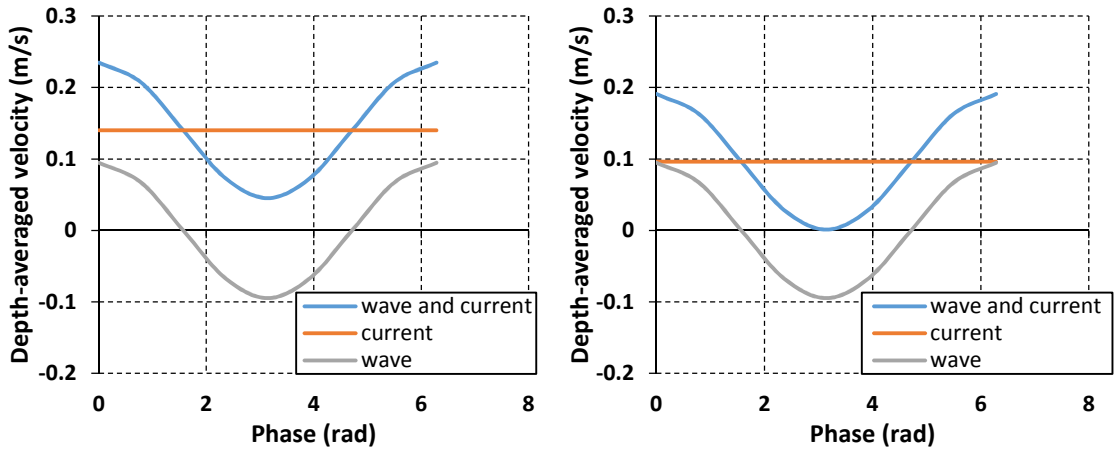

a) b)

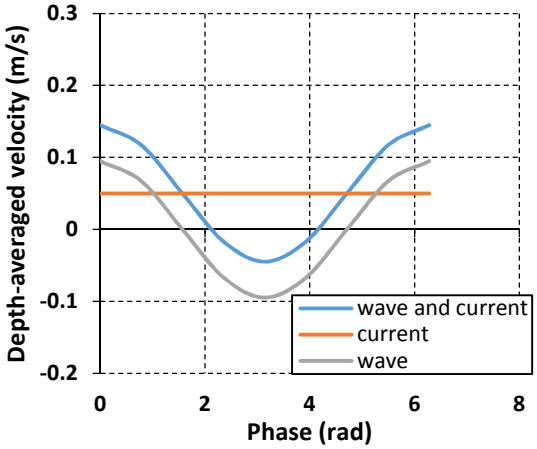

c)

Figure A2.1 a) Largest wave-current combination b) middle wave-current combination c) smallest wave-current combination.

The wave for test series C-2 was designed to have a 2.5 s period and 4.5 cm wave height. The three currents chosen to combine with the wave had depth-averaged velocities of 5 cm/s, 9.6 cm/s and 14 cm/s to achieve 1) wave dominated, 2) equal wave-current components and 3) current dominated cases.

Appendix 3 – Scour depth experimental data

a) Quality control

Note that while all tests during the project are included in the last part of this appendix, not all of the tests were selected for the main analysis. The following provides a summary of the excluded tests:

Large flume tests assessment:

- Preliminary large flume test series did not have final test methodology so monitoring was not fully in place, also meshes were used to cover inlets which caused varying flow velocity.
- Preliminary wave tests excluded because very small scour depths occurred
- Preliminary wave-current tests were affected by general bed lowering and/or were affected by bed ripples. It is difficult to correct for bed lowering because of the presence of bedforms which make the bed level difficult to determine.

Small flume tests assessment:

- Preliminary tests R.2, R.4, R.5, R.7 were affected by bed ripples
- Preliminary tests R.2 and R.5 were affected by poor re-start procedures towards the end of the tests
- Test R.25 had unstable flow conditions due to clogging of the filters by polystyrene balls used for flow visualisation. Note that the test following R.25, R.26 also had an unusual scour development curve (discussed in more detail below)
- Test R.13 had an issue with velocity consistency at the start of the test and was therefore repeated (test R.14) (also discussed below)
- The scour depth was smaller than expected in test R.22 (discussed further below)

Additionally note that:

- Some tests have missing data for sections of the test due to equipment malfunction (i.e. the cameras suffered from loss of data in transfer)
- Test R.12 had an unexpected increase in scour depth which was not immediately explainable and this is discussed in detail in the main report
- The agreement between repetitions of 3 tests was poorer than expected. These are discussed below. The pairs of tests affected are R.T.2 and R.T.1, R.T.11 and R.T.8, and R.T.4 and R.12.

Test R.13 result explanation

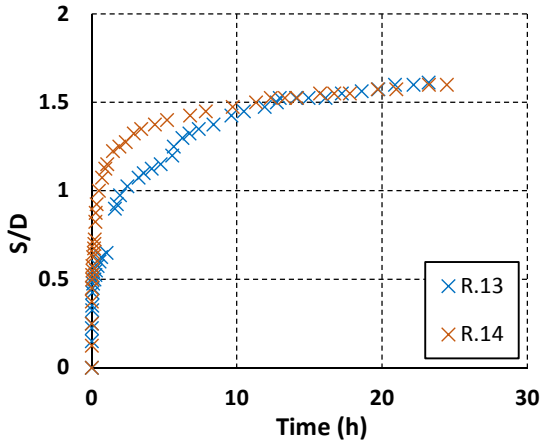

Figure A3.1 Scour development curves for tests R.13 and R.14 in the small flume, coarse sand.

The scour development curves for tests R.13 and R.14 are shown in figure A3.1. These two curves are for the same sand but there was an issue with maintaining a consistent velocity in the flume at the start of test R.13. This is shown by the initially slower and less smooth curve for test R.13. The same end scour depth is reached in both tests once the flow conditions were stabilised.

Test R.22 result explanation

An unexpected result was found in test R.22 where the scour depth was a little shallower than anticipated. This layered test with a 70 mm thick upper layer of fine sand was repeated in test R.24 as it was suspected that the fine sand had been contaminated with (a small amount of) coarse sand in test R.22 prior to running the test, resulting in the shallower scour depth (see Figure A3.2).

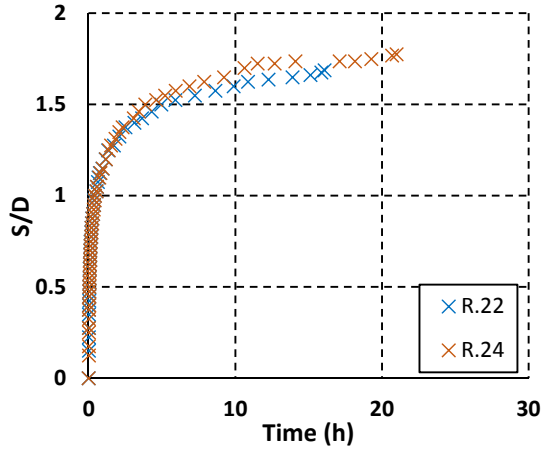

Figure A3.2 Scour development curves for tests R.22 and R.24, fine over coarse sand layered tests, L_u=70 mm.

A sieve analysis was undertaken in order to determine whether the fine sand in test R.22 had been contaminated with coarse sand prior to the test. Three samples were taken from the undisturbed bed at the end of the test and sieved, and the results are shown in Figure A3.3. The distributions from the three samples from test R.22 are plotted alongside the fine sand distribution. It can be seen that the samples from test R.22 are considerably coarser than the fine sand, indicating that the sand was indeed contaminated by coarse sand, changing the grading distribution and increasing the d_{50} value to around 0.2 mm rather than approximately 0.1 mm. This resulted in a reduction in scour depth at the pile.

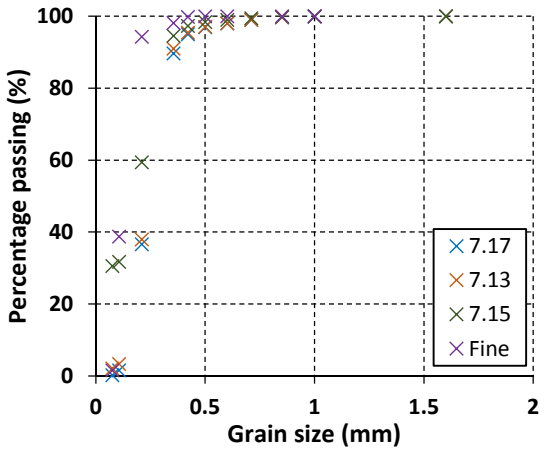

Figure A3.3 Grain size distributions for test R.22 contaminated sand analysis.

Test R.25 result explanation

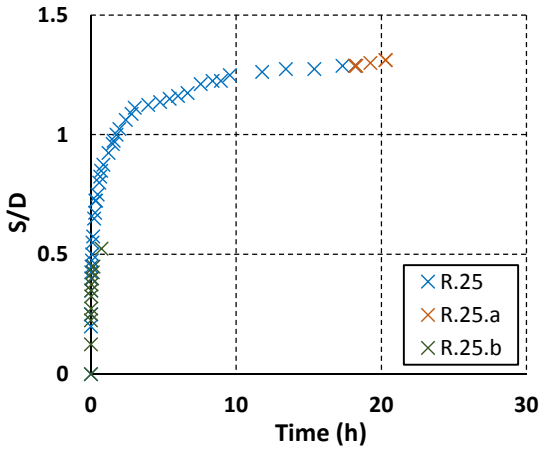

Figure A3.4 Scour development curves for tests R.25, R.25.a, R.25.b, small flume, coarse sand.

The use of polystyrene balls for the flow visualisation tests resulted in filter blockage in Test R.25. This caused the flow properties to vary over time during this test. The difference in the

flow velocity between the start and end of the test is shown by test R.25.b, Figure A3.4, where the test was restarted and shows significantly slower scour due to the slower flow.

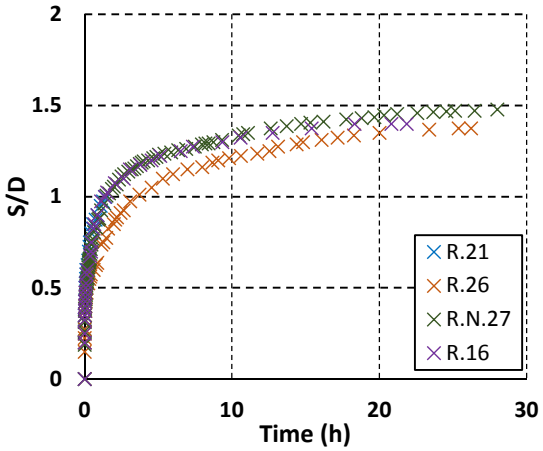

Figure A3.5 Scour development curves for coarse sand tests before and after flow visualisation testing

The filters were cleaned as a result of test R.25, prior to running further tests. The next test that was run was test R.26. However, the results from this test showed slower scour development than expected (Figure A3.5). Despite showing slower scour development in the first stages, the equilibrium depth reached in this test is similar to that in R.16. It is possible that the flow was adjusting during the first part of the test due to the cleaning of the filters and further declogging of the filters may have occurred due to the flow through them during the first stages of the test.

b) Additional results

Rough pile tests

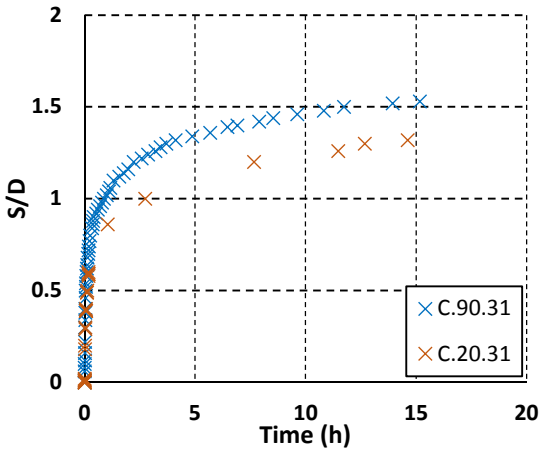

Figure A3.6 Scour development curves for rough and smooth 50mm piles in the coastal flume, under unidirectional current

Figure A3.6 shows a comparison of tests conducted simultaneously in the coastal flume, with the same pile diameter of 5 cm, but where one pile was coated with sand grains to make a 'rough' pile, and the other was a smooth plastic pile as was used for the rest of the tests. In figure A3.6 there is a significant difference of over 0.2 S/D between these cases, where test C.20.31 is the rough pile which has the smaller scour depth. However, when the velocity in the flume was measured, there was a clear difference in velocity at the position of the far pile, relative to the pile on the near side of the flume. Therefore, in order to determine if the pile roughness has had any measurable effect, first, the influence of the different velocity must be taken into account.

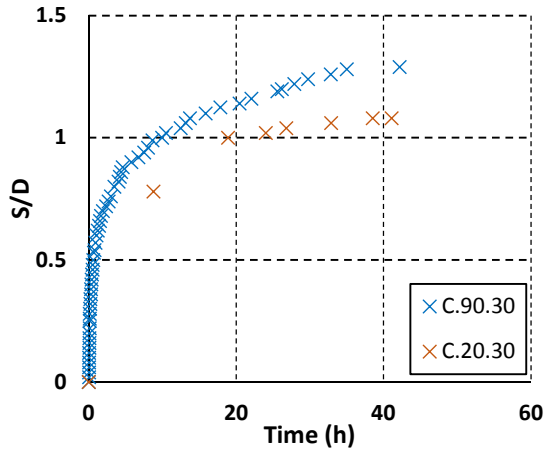

Figure A3.7 Scour development curves for rough and smooth 50 mm piles in the coastal flume, under wave-current flow

Figure A3.7 shows a second comparison of rough and smooth piles, this time in wave-current flow. Again the velocity difference needs to be considered before further conclusions can be drawn. What is noticeable in figures A3.6 and A3.7 is that in both the unidirectional and wave-current cases the difference in scour depth between the smooth and rough piles is similar at about 0.2 S/D.

A velocity correction was determined using the trendlines in Figure 7.1. This makes the expected scour depth on the far side of the flume approximately 0.2 S/D less than that at the nearside for these test cases. This accounts for the difference between the rough and smooth pile scour curves, bringing the two curves together within the measurement uncertainty. This indicates that the pile roughness has not had an effect in these tests.

An increase in pile roughness may cause the critical Reynolds number to be reached at lower flow velocity than with a smooth pile, changing the boundary layer regime at the cylinder, and hence the separation point and wake dimensions. This has the potential to affect the scour depth, although few studies are available to confirm this. Sumer and Fredsøe (2006) provide a graph of the change in Strouhal number with Reynolds number. For a smooth cylinder in the subcritical range, the Strouhal number is constant with Reynolds number. This means that if the

pile diameter is decreased while keeping the flow velocity constant then the frequency of vortex shedding will increase. This is one reason why there may be a pile Reynolds number dependence on scour depth as the flow patterns around the cylinder are altered as the ratio of inertial to viscous forces changes.

At the end of the subcritical range a jump in Strouhal number occurs at the critical Reynolds number. Sumer and Fredsøe (2006) show how the critical Reynolds number varies with pile roughness, with the jump in Strouhal number moving to lower pile Reynolds number as the surface roughness increases. However, for the size of roughness in these tests the critical point is not expected to be reached at the pile Reynolds number the test was conducted at. Therefore, as the same flow regime is expected at both the smooth and rough piles, as they were both under the same scaling conditions (same pile diameter, and approximately same flow velocity, pile Reynolds and Strouhal numbers), there is no effect due to pile roughness.

Preliminary layered sand tests

These figures are included to provide additional evidence of the scour enhancement in the lower layer of coarse sand in fine overlying coarse sand layered beds. This result was found in both preliminary test series (P-1 and P-2).

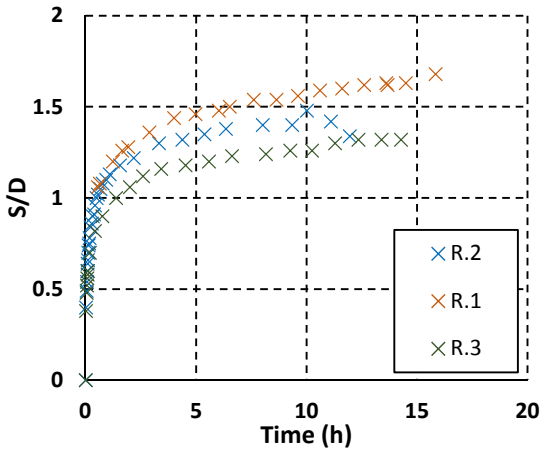

Figure A3.8 Uniform and layered bed scour development curves for test series P-1.

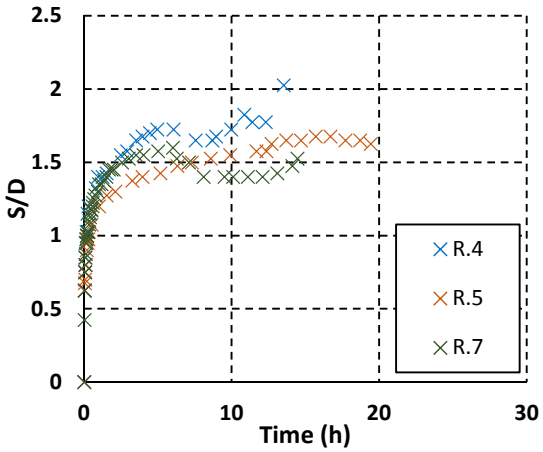

Figure A3.9 Uniform and layered bed scour development curves for test series P-2.

Preliminary tests large flume

Figure A3.10 shows an important result that when the flow direction was reversed after an equilibrium condition had been reached, scour depth continued to increase.

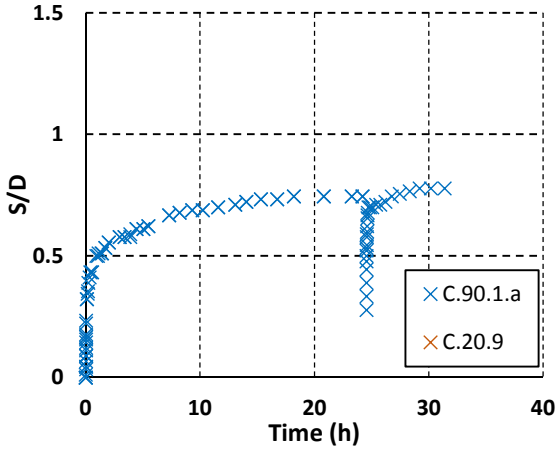

Figure A3.10 Scour development curve in coarse sand, with flow reversal after equilibrium scour depth was reached.

Comparison of factory blended and in house mixed sands

In figure A3.11, a comparison is given of the scour development in the factory blended 50% sand with the laboratory prepared 50% mix. While these two sands should theoretically be of the same grading distribution, the maximum difference between these two curves is 0.275 S/D. This indicates that the difference in the two mixes is large enough to cause a noticeable change to the scour depth. However, large sections of the curves have a difference of around 0.1 S/D or less and in general it can be said that the difference in the composition of these two sands is small enough for the effect of this on the scour development to be insignificant.

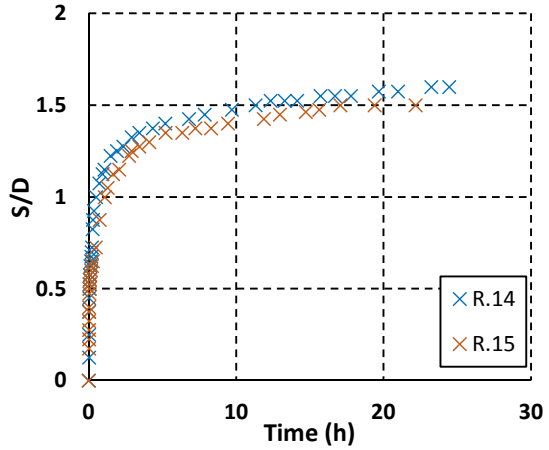

Figure A3.11 Comparison of scour development in off-site blended and in-house blended sands

c) Scour curve and test description for each test:

P-1 Series - Preliminary Small Flume Tests

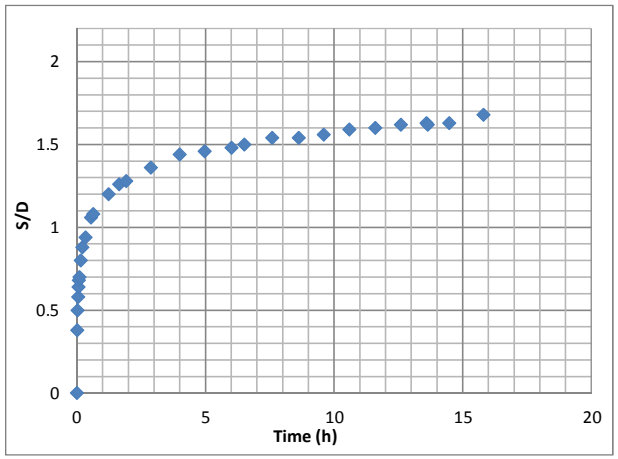

Test Number	R.1
Date	17/08/2011
Test description	Unidirectional current
Flume	Reversing current flume
Pile Diameter (mm)	50
Water depth (m)	0.16
Current depth averaged velocity (cm/s)	21.5
Sand configuration	uniform (original fine sand)
Notes	Initial methodology (water drains overnight, pile in place at start,scour depth read from nearside etc.) Scoured to flume base

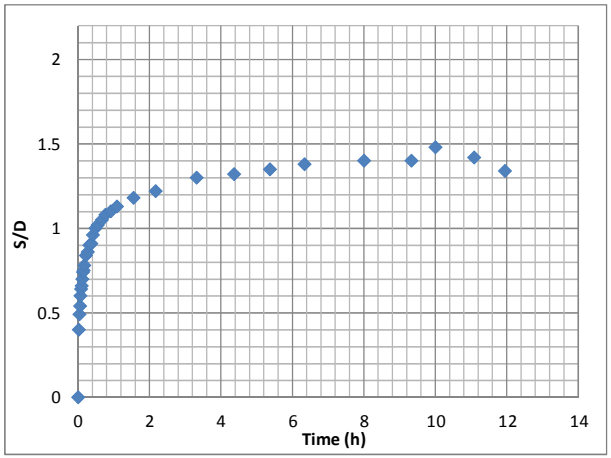

Test Number	R.2
Date	24/08/2011
Test description	Unidirectional current
Flume	Reversing current flume
Pile Diameter (mm)	50
Water depth (m)	0.16
Current depth averaged velocity (cm/s)	21.5
Bed description	layered fine sand upper 50mm
Notes	Initial methodology (water drains overnight, pile in place at start,scour depth read from nearside etc.) Migrating dunes

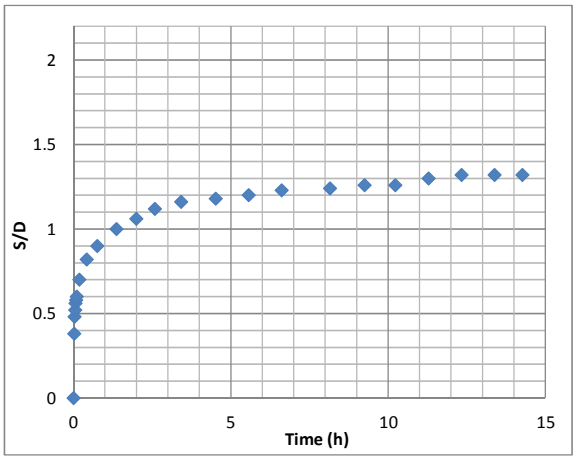

Test Number	R.3
Date	28/09/2011
Test description	Unidirectional current
Flume	Reversing current flume
Pile Diameter (mm)	50
Water depth (m)	0.16
Current depth averaged velocity (cm/s)	21.5
Bed description	uniform coarse sand
Notes	Initial methodology (water drains overnight, pile in place at start,scour depth read from nearside etc.)

P-2 Series - Preliminary Small Flume Tests

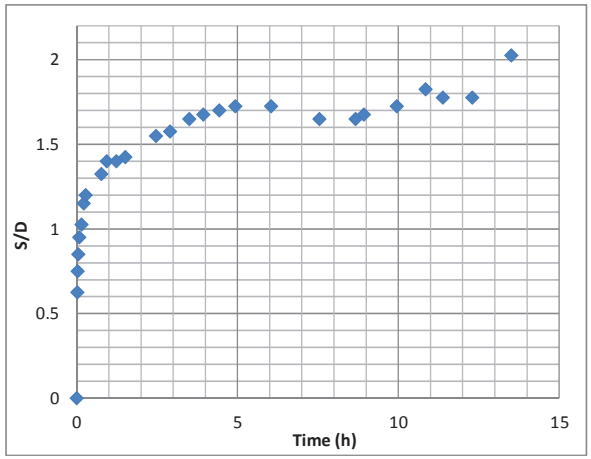

Test Number	R.4
Date	30/01/2012
Test description	Unidirectional current
Flume	Reversing current flume
Pile Diameter (mm)	40
Water depth (m)	0.17
Current depth averaged velocity (cm/s)	25.3
Bed description	uniform fine sand
Notes	Later section of test influenced by ripples

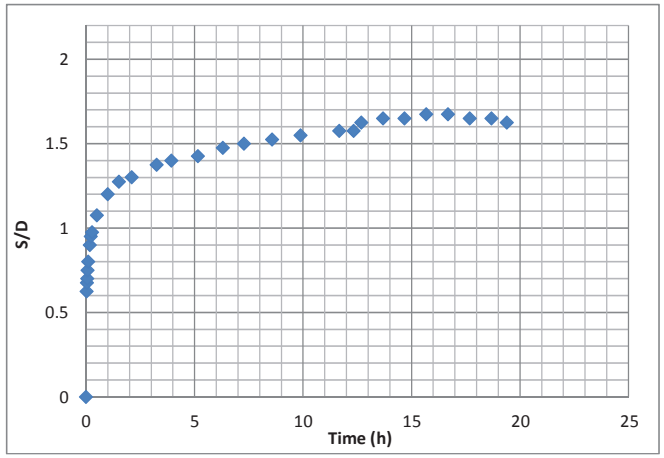

Test Number	R.5
Date	02/02/2012
Test description	Unidirectional current
Flume	Reversing current flume
Pile Diameter (mm)	40
Water depth (m)	0.17
Current depth averaged velocity (cm/s)	25.3
Bed description	uniform coarse sand
Notes	

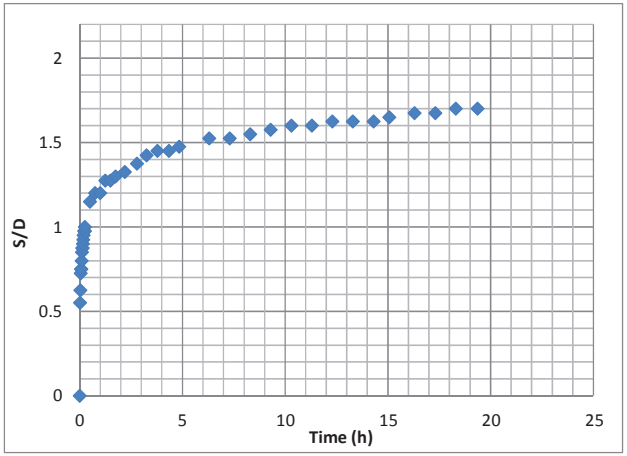

Test Number	R.6
Date	08/02/2012
Test description	Unidirectional current
Flume	Reversing current flume
Pile Diameter (mm)	40
Water depth (m)	0.17
Current depth averaged velocity (cm/s)	25.3
Bed description	Layered upper coarse 40mm
Notes	

P-2 Series - Preliminary Small Flume Tests

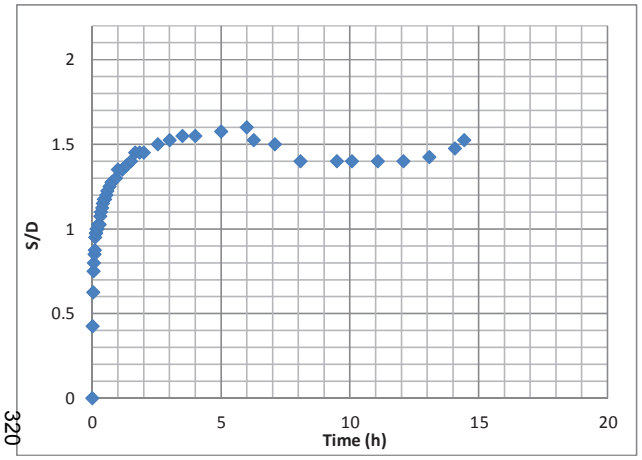

Test Number	R.7
Date	12/02/2012
Test description	Unidirectional current
Flume	Reversing current flume
Pile Diameter (mm)	40
Water depth (m)	0.17
Current depth averaged velocity (cm/s)	25.3
Bed description	layered upper fine 40mm
Notes	

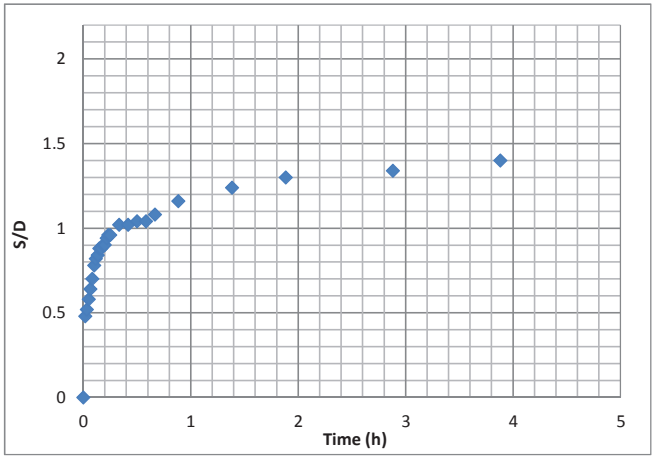

Test Number	R.8
Date	12/02/2012
Test description	Unidirectional current
Flume	Reversing current flume
Pile Diameter (mm)	50
Water depth (m)	0.17
Current depth averaged velocity (cm/s)	25.3
Bed description	uniform coarse sand
Notes	

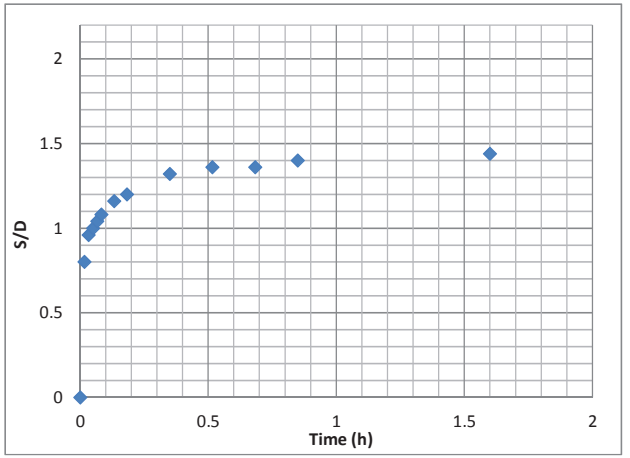

Test Number	R.9
Date	12/02/2012
Test description	Unidirectional current
Flume	Reversing current flume
Pile Diameter (mm)	25
Water depth (m)	0.17
Current depth averaged velocity (cm/s)	25.3
Bed description	uniform coarse sand
Notes	

R-1 Series - Small Flume Tests

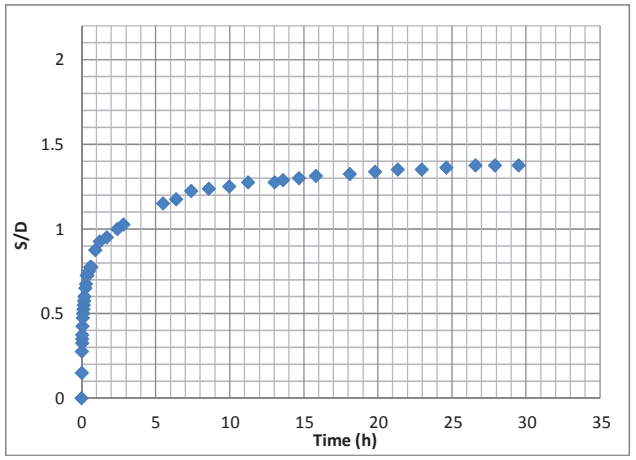

Test Number	R.10
Date	06/06/2012
Test description	Unidirectional current
Flume	Reversing current flume
Pile Diameter (mm)	40
Water depth (m)	0.16
Current depth averaged velocity (cm/s)	19.2
Bed description	mixed, 90% fine
Notes	

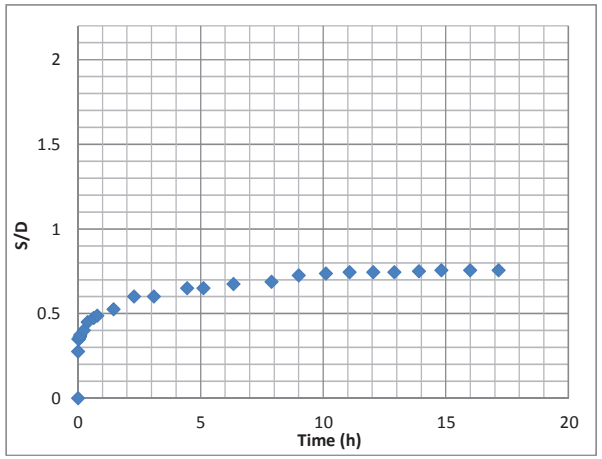

Test Number	R.11
Date	
Test description	Unidirectional current
Flume	Reversing current flume
Pile Diameter (mm)	40
Water depth (m)	0.16
Current depth averaged velocity (cm/s)	19.2
Bed description	mixed, 90% coarse
Notes	

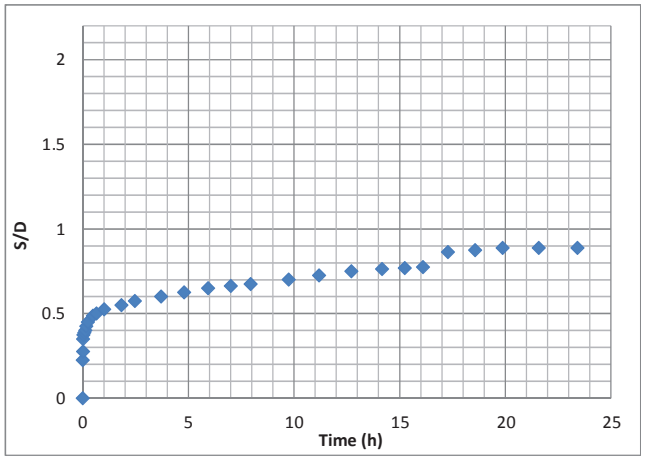

Test Number	R.12
Date	15/06/2012
Test description	Unidirectional current
Flume	Reversing current flume
Pile Diameter (mm)	40
Water depth (m)	0.16
Current depth averaged velocity (cm/s)	19.2
Bed description	uniform coarse sand
Notes	

R-2 Series - Small Flume Tests

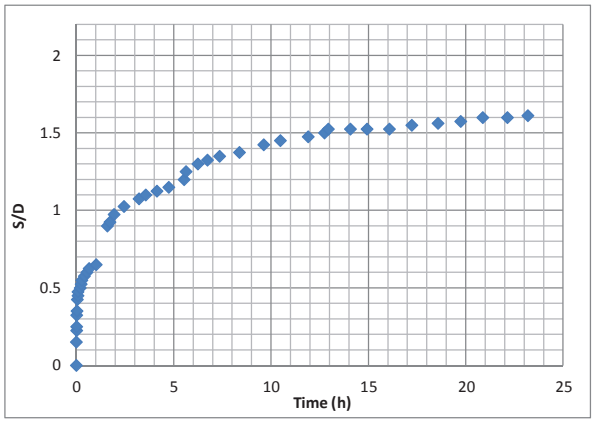

Test Number	R.13
Date	25/10/2012
Test description	Unidirectional current
Flume	Reversing current flume
Pile Diameter (mm)	40
Water depth (m)	0.17
Current depth averaged velocity (cm/s)	23.9
Bed description	blended sand (50%)
Notes	offsite blend, restart/velocity issues

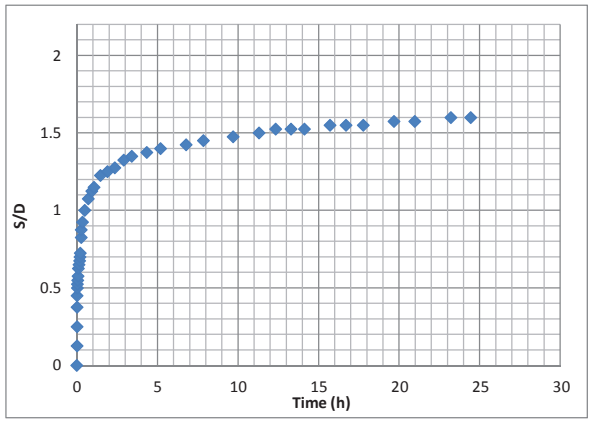

Test Number	R.14
Date	30/10/2012
Test description	Unidirectional current
Flume	Reversing current flume
Pile Diameter (mm)	40
Water depth (m)	0.17
Current depth averaged velocity (cm/s)	23.9
Bed description	blended sand (50%)
Notes	offsite blend, repeat of R.13

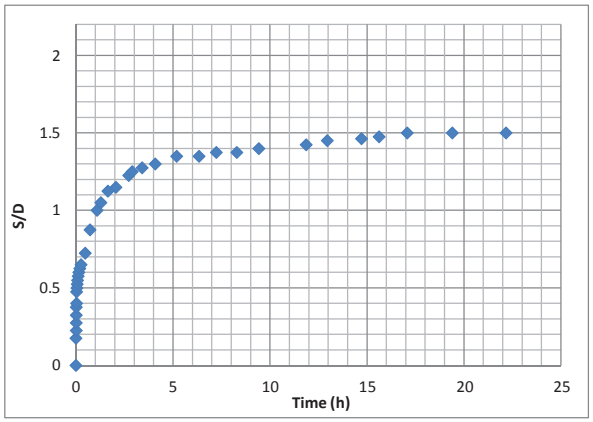

Test Number	R.15
Date	07/11/2012
Test description	Unidirectional current
Flume	Reversing current flume
Pile Diameter (mm)	40
Water depth (m)	0.175
Current depth averaged velocity (cm/s)	23.9
Bed description	Mixed sand 50%
Notes	inhouse mixed, same as used previously

R-2 Series - Small Flume Tests

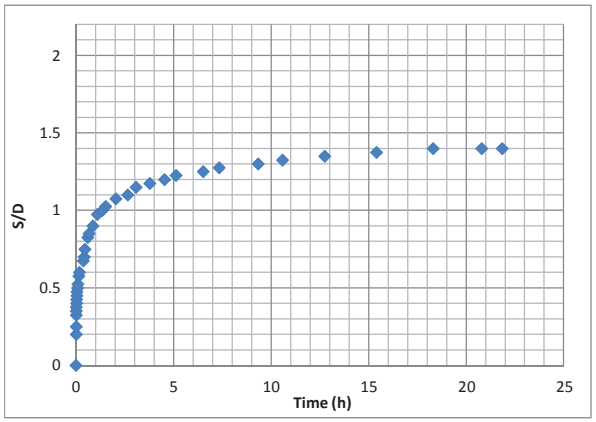

Test Number	R.16
Date	14/11/2012
Test description	Unidirectional current
Flume	Reversing current flume
Pile Diameter (mm)	40
Water depth (m)	0.175
Current depth averaged velocity (cm/s)	23.9
Bed description	coarse sand
Notes	(unused coarse sand)

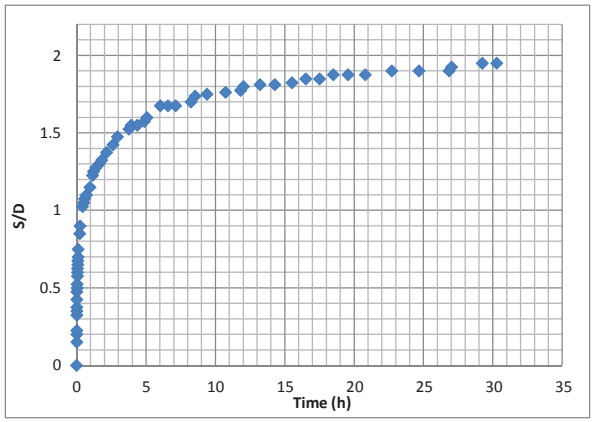

Test Number	R.17
Date	19/11/2012
Test description	Unidirectional current
Flume	Reversing current flume
Pile Diameter (mm)	40
Water depth (m)	0.175
Current depth averaged velocity (cm/s)	23.9
Bed description	Fine sand
Notes	

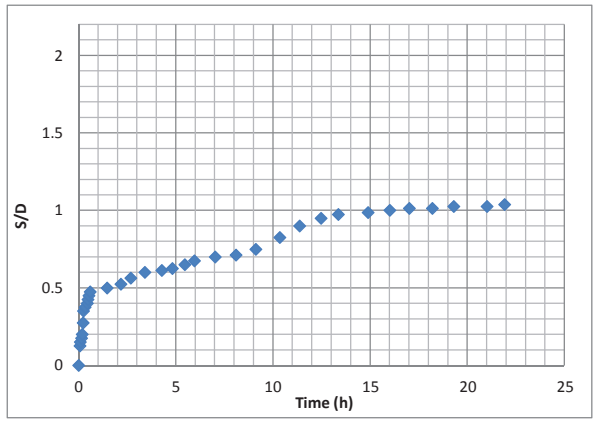

Test Number	R.18
Date	19/11/2012
Test description	Unidirectional current
Flume	Reversing current flume
Pile Diameter (mm)	40
Water depth (m)	0.175
Current depth averaged velocity (cm/s)	18.3
Bed description	blended sand 50%
Notes	

R-3 Series - Small Flume Tests

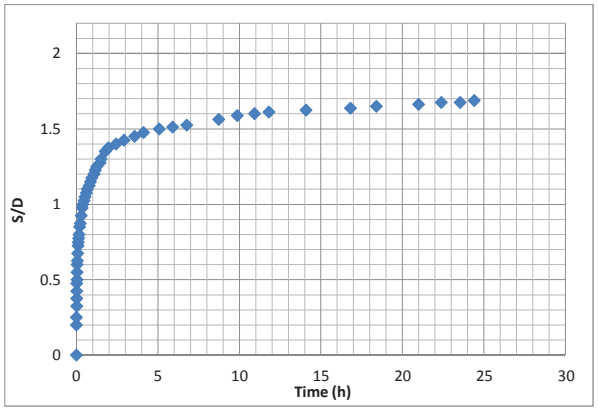

Test Number	R.19
Date	12/09/2013
Test description	Unidirectional current
Flume	Reversing current flume
Pile Diameter (mm)	40
Water depth (m)	0.165
Current depth averaged velocity (cm/s)	23.3
Bed description	layered upper fine 55mm
Notes	

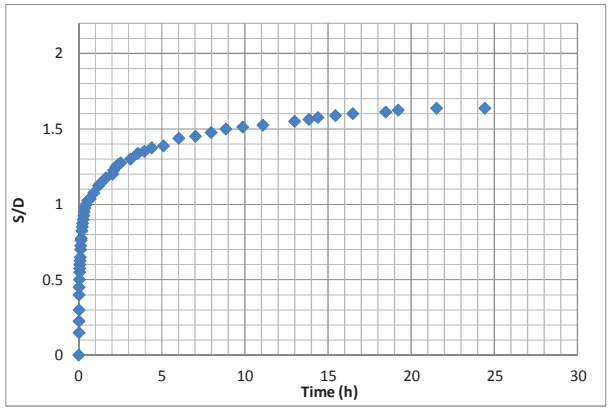

Test Number	R.20
Date	
Test description	Unidirectional current
Flume	Reversing current flume
Pile Diameter (mm)	40
Water depth (m)	0.165
Current depth averaged velocity (cm/s)	23.3
Bed description	fine 40mm, coarse 10mm, fine 50mm
Notes	

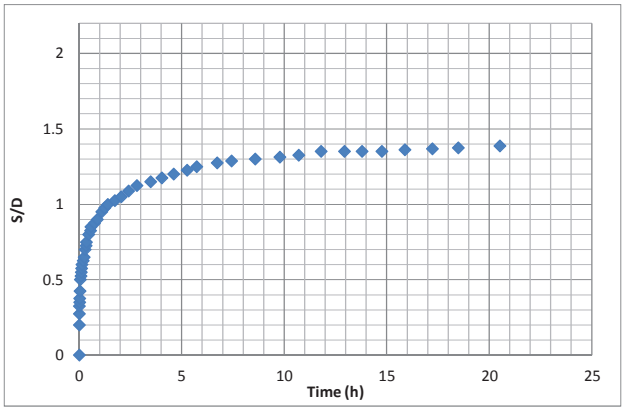

Test Number	R.21
Date	
Test description	Unidirectional current
Flume	Reversing current flume
Pile Diameter (mm)	40
Water depth (m)	0.165
Current depth averaged velocity (cm/s)	23.3
Bed description	Coarse 40mm, fine 10mm, coarse 50mm
Notes	

R-3 Series - Small Flume Tests

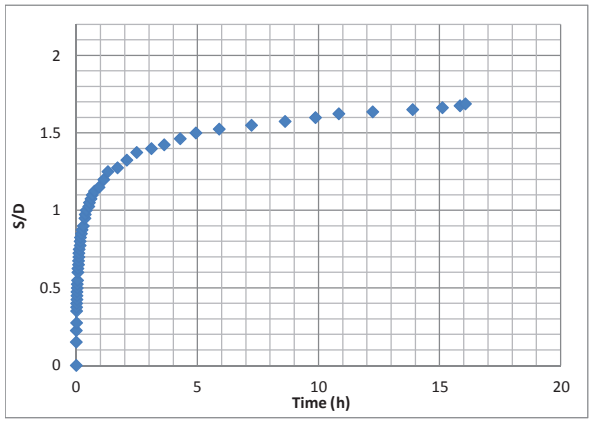

Test Number	R.22
Date	
Test description	Unidirectional current
Flume	Reversing current flume
Pile Diameter (mm)	40
Water depth (m)	0.165
Current depth averaged velocity (cm/s)	23.3
Bed description	layered upper fine 70mm
Notes	contamination of fine with coarse apparent

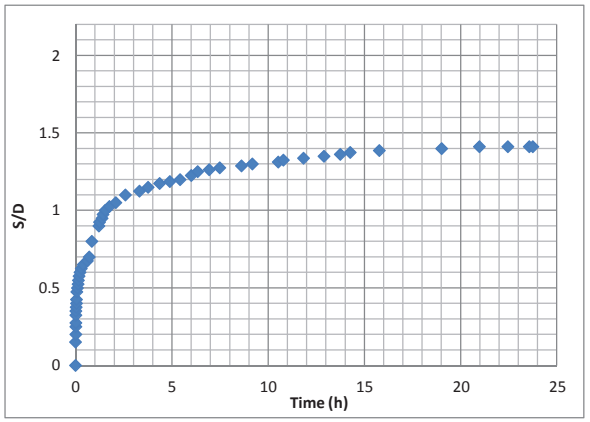

Test Number	R.23
Date	
Test description	Unidirectional current
Flume	Reversing current flume
Pile Diameter (mm)	40
Water depth (m)	0.165
Current depth averaged velocity (cm/s)	23.3
Bed description	mixed 90% coarse
Notes	new in house blend

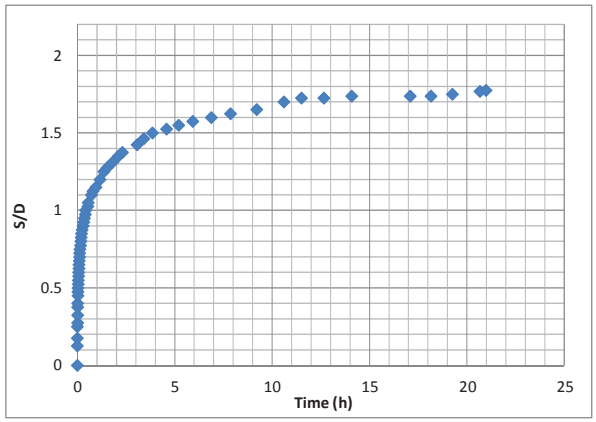

Test Number	R.24
Date	
Test description	Unidirectional current
Flume	Reversing current flume
Pile Diameter (mm)	40
Water depth (m)	0.165
Current depth averaged velocity (cm/s)	23.3
Bed description	layered upper fine 70mm
Notes	repeat of R.22

R-3 Series - Small Flume Tests

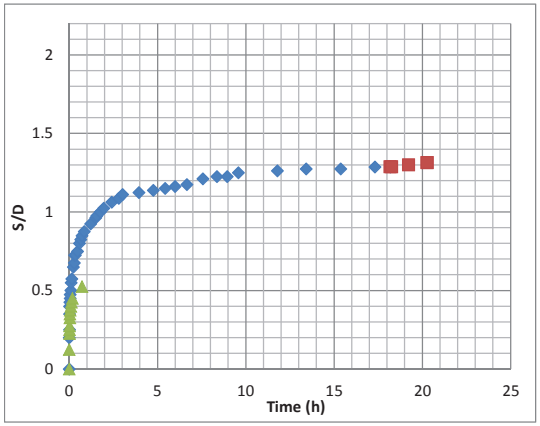

Test Number	R.25, R.25.a, R.25.b
Date	
Test description	Unidirectional current
Flume	Reversing current flume
Pile Diameter (mm)	40
Water depth (m)	0.165
Current depth averaged velocity (cm/s)	?
Bed description	coarse
Notes	velocity issue. Unidirectional current, downstream resmooth at end test, full bed resmooth for downstream resmooth during test (ended due to WL rise)

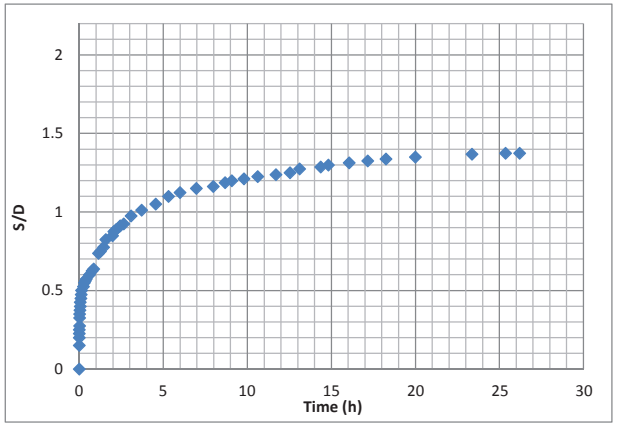

Test Number	R.26
Date	
Test description	Unidirectional current
Flume	Reversing current flume
Pile Diameter (mm)	40
Water depth (m)	0.165
Current depth averaged velocity (cm/s)	22.5
Bed description	coarse
Notes	coarse repeat (with cleaned filter)

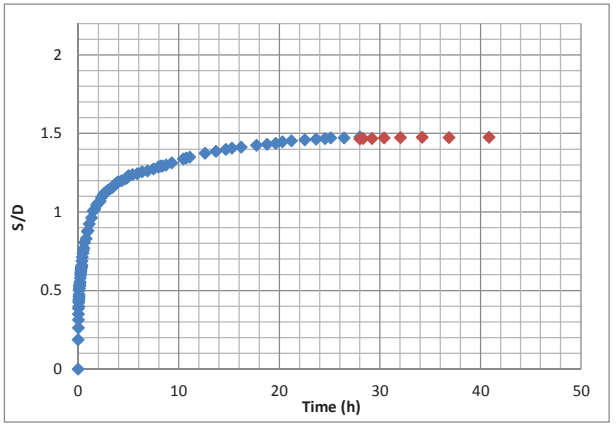

Test Number	R.N.27 and R.N.27a
Date	
Test description	Unidirectional current
Flume	Reversing current flume
Pile Diameter (mm)	40
Water depth (m)	0.16
Current depth averaged velocity (cm/s)	23.3
Bed description	coarse
Notes	Unidirectional, then downstream resmoothed and test continued

R-3 Series - Small Flume Tests

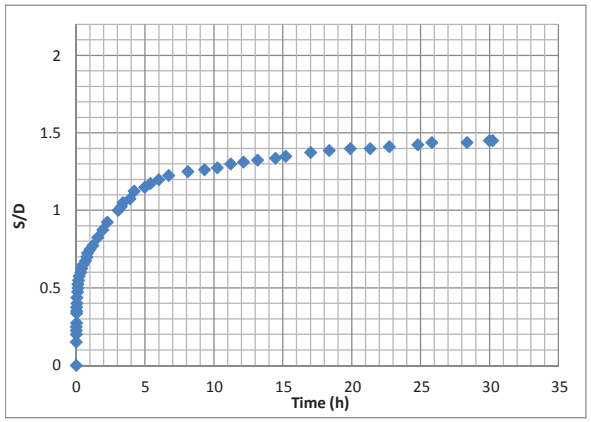

Test Number	R.28
Date	02/12/2013
Test description	Unidirectional current
Flume	Reversing current flume
Pile diameter (mm)	40
Water depth (m)	0.16
Current depth averaged velocity (cm/s)	23.3
Bed description	Coarse (dense)
Notes	dense bed (vibrated in situ with concrete poker, then surface compacted with 5kg weight)

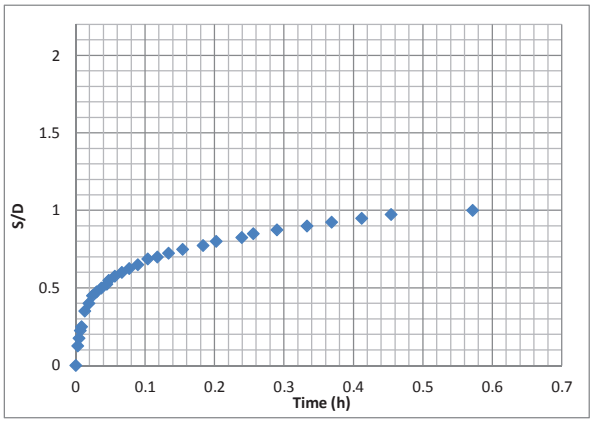

Test Number	R.29.1
Date	13/12/2013
Test description	Unidirectional current
Flume	Reversing current flume
Pile Diameter (mm)	40
Water depth (m)	0.16
Current depth averaged velocity (cm/s)	23.3
Bed description	layered upper fine 40mm
Notes	stopped at 40mm

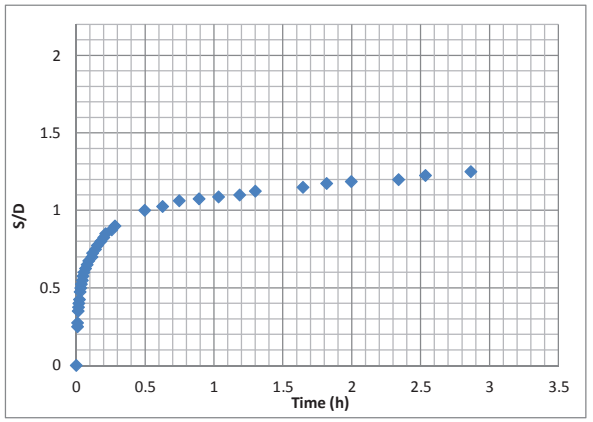

Test Number	R.29.2
Date	06/01/2014
Test description	Unidirectional current
Flume	Reversing current flume
Pile Diameter (mm)	40
Water depth (m)	0.16
Current depth averaged velocity (cm/s)	23.3
Bed description	layered upper fine 40mm
Notes	stopped at 50mm

R-3 Series - Small Flume Tests

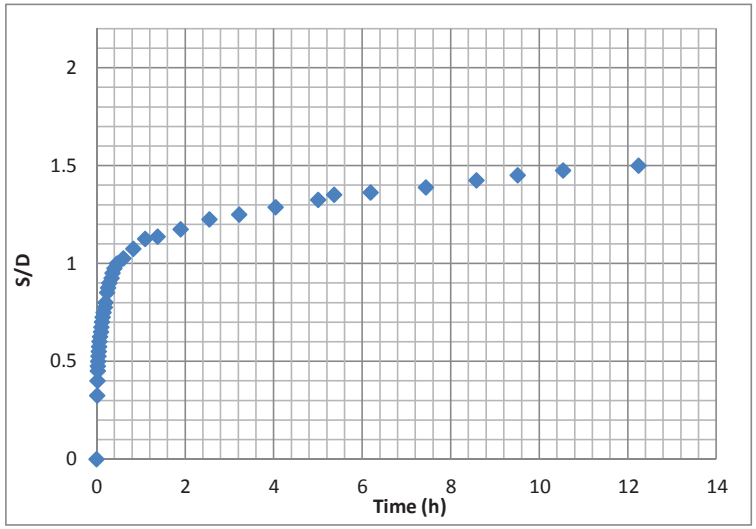

Test Number	R.29.3
Date	02/01/2014
Test description	Unidirectional current
Flume	Reversing current flume
Pile Diameter (mm)	40
Water depth (m)	0.16
Current depth averaged velocity (cm/s)	23.3
Bed description	layered upper fine 40mm
Notes	stopped at 60mm

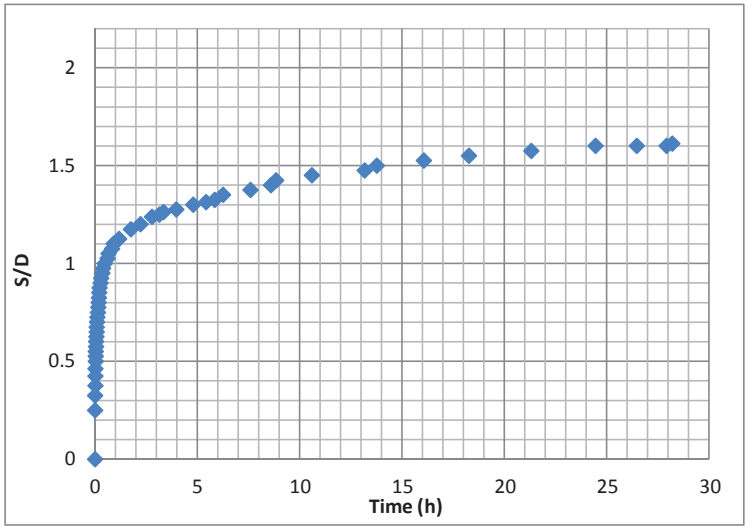

Test Number	R.29.4
Date	16/12/2013
Test description	Unidirectional current
Flume	Reversing current flume
Pile Diameter (mm)	40
Water depth (m)	0.16-0.161
Current depth averaged velocity (cm/s)	23.3
Bed description	layered upper fine 40mm
Notes	stopped at equilibrium

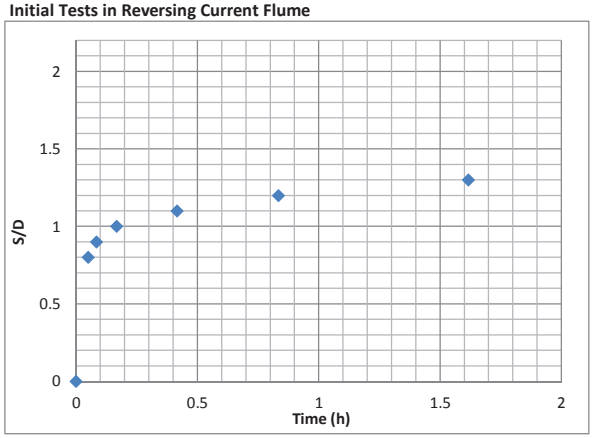

Test Number	R.X.1
Date	
st d criptio n	Unidirectional current
Flume	Reversing current flume
Pile Diameter (mm)	50
Water depth (m)	0.16
Current depth averaged velocity (cm/s)	20-21
Bed description	fine
Notes	Initial test

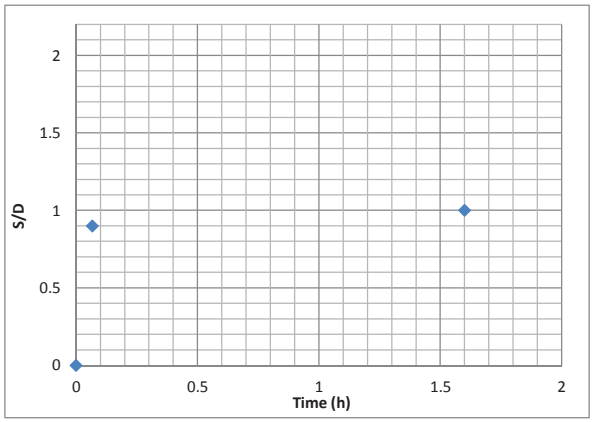

Test Number	R.X.2
Date	
Test description	Unidirectional current
Flume	Reversing current flume
Pile Diameter (mm)	50
Water depth (m)	0.16
Current depth averaged velocity (cm/s)	13-14
Bed description	fine
Notes	Initial test

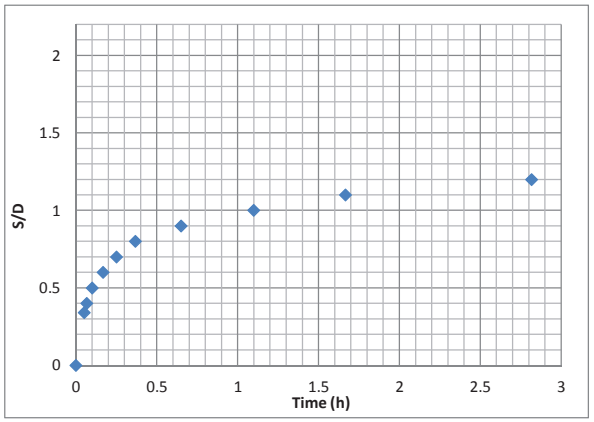

Test Number	R.X.3
Date	
Test description	Un directio al current
Flume	Reversing current flume
Pile Diameter (mm)	50
Water depth (m)	0.16
Current depth averaged velocity (cm/s)	17-18
Bed description	fine
Notes	Initial test

T-1 Series

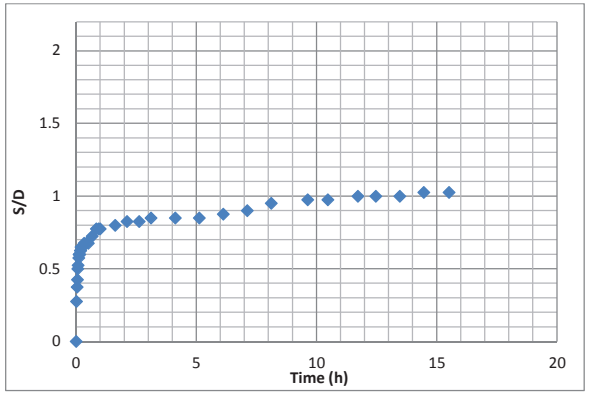

Test Number	R.T.1
Test description	Unidirectional current
Flume	Reversing current flume
Pile Diameter (mm)	40
Water depth (m)	0.16
Current depth averaged velocity (cm/s)	19.2
Bed description	layered upper fine 25mm
Notes	

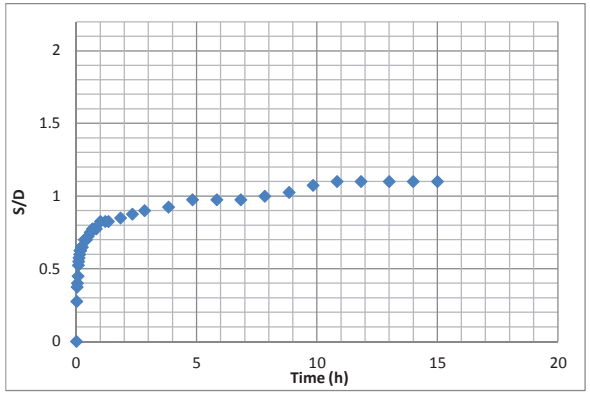

Test Number	R.T.2
Test description	Unidirectional current
Flume	Reversing current flume
Pile Diameter (mm)	40
Water depth (m)	0.16
Current depth averaged velocity (cm/s)	19.2
Bed description	layered upper fine 25mm
Notes	repeat of R.T.1

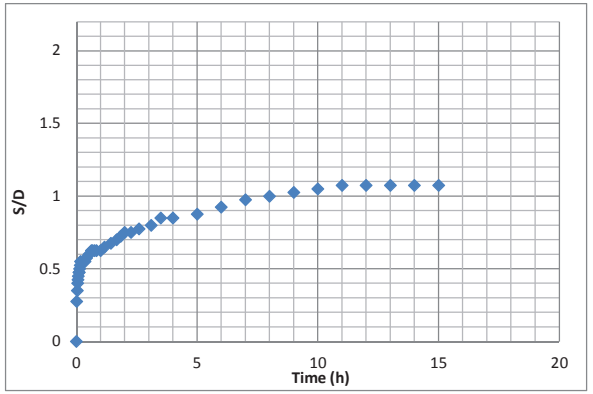

Test Number	R.T.3
Test description	Unidirectional current
Flume	Reversing current flume
Pile Diameter (mm)	40
Water depth (m)	0.16
Current depth averaged velocity (cm/s)	19.2
Bed description	layered upper fine 10mm
Notes	

T-1 Series

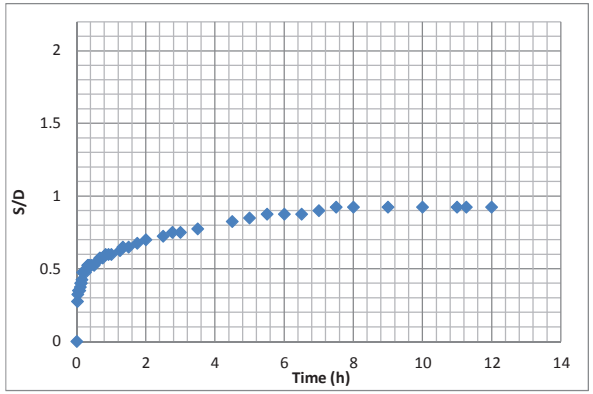

Test Number	R.T.4
Test description	Unidirectional current
Flume	Reversing current flume
Pile Diameter (mm)	40
Water depth (m)	0.16
Current depth averaged velocity (cm/s)	19.2
Bed description	uniform coarse
Notes	

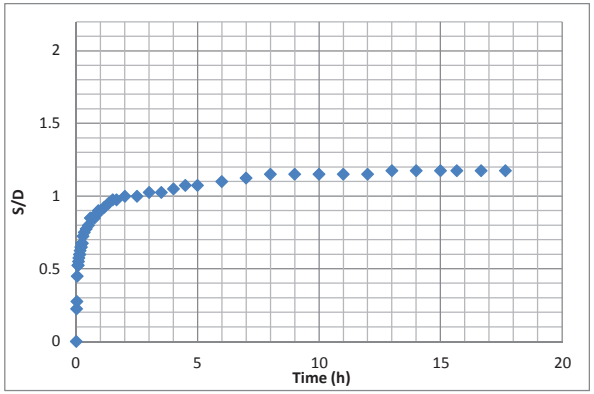

Test Number	R.T.5
Test description	Unidirectional current
Flume	Reversing current flume
Pile Diameter (mm)	40
Water depth (m)	0.16
Current depth averaged velocity (cm/s)	19.2
Bed description	layered upper fine 40mm
Notes	

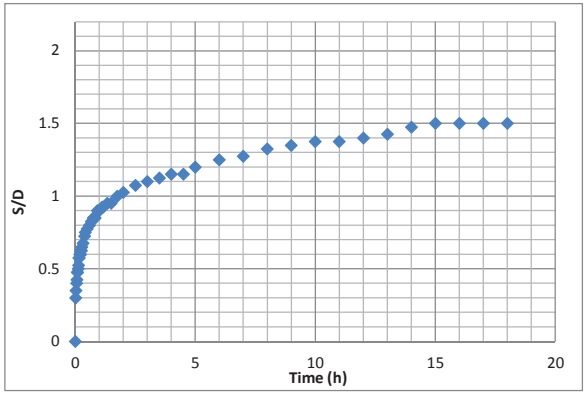

Test Number	R.T.6
Test description	Unidirectional current
Flume	Reversing current flume
Pile Diameter (mm)	40
Water depth (m)	0.16
Current depth averaged velocity (cm/s)	19.2
Bed description	uniform fine
Notes	

T-1 Series

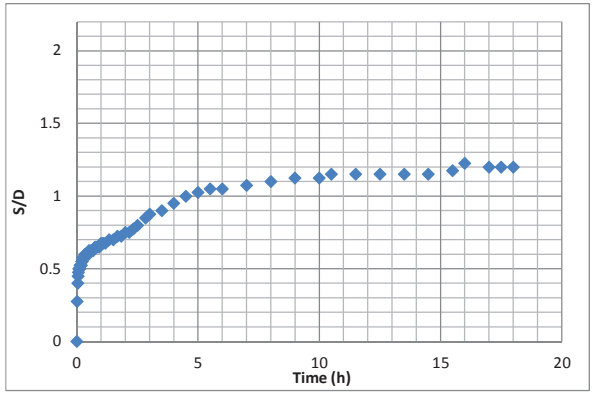

Test Number	R.T.7
Test description	Unidirectional current
Flume	Reversing current flume
Pile Diameter (mm)	40
Water depth (m)	0.16
Current depth averaged velocity (cm/s)	19.2
Bed description	25% coarse
Notes	

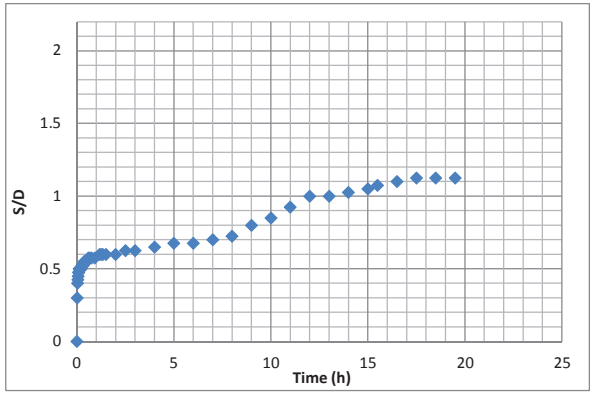

Test Number	R.T.8
Test description	Unidirectional current
Flume	Reversing current flume
Pile Diameter (mm)	40
Water depth (m)	0.16
Current depth averaged velocity (cm/s)	19.2
Bed description	50% coarse
Notes	

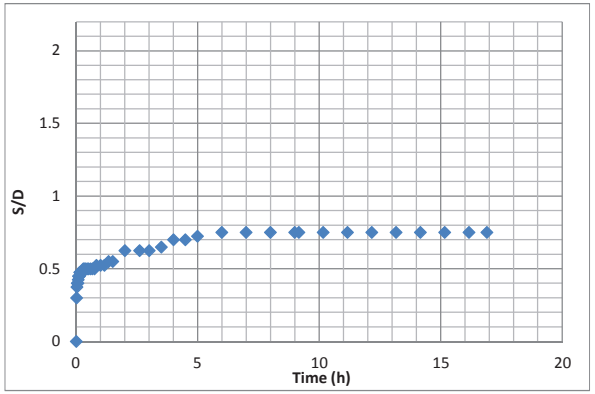

Test Number	R.T.9
Test description	Unidirectional current
Flume	Reversing current flume
Pile Diameter (mm)	40
Water depth (m)	0.16
Current depth averaged velocity (cm/s)	19.2
Bed description	75% coarse
Notes	

T-1 Series

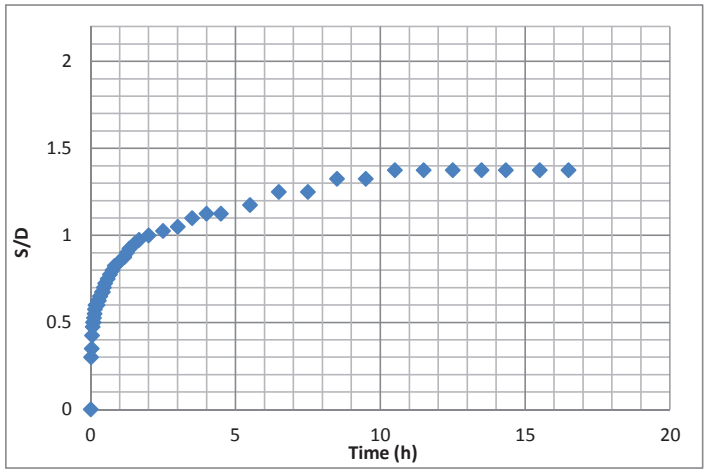

Test Number	R.T.10
Test description	Unidirectional current
Flume	Reversing current flume
Pile Diameter (mm)	40
Water depth (m)	0.16
Current depth averaged velocity (cm/s)	19.2
Bed description	layered upper fine 55mm
Notes	

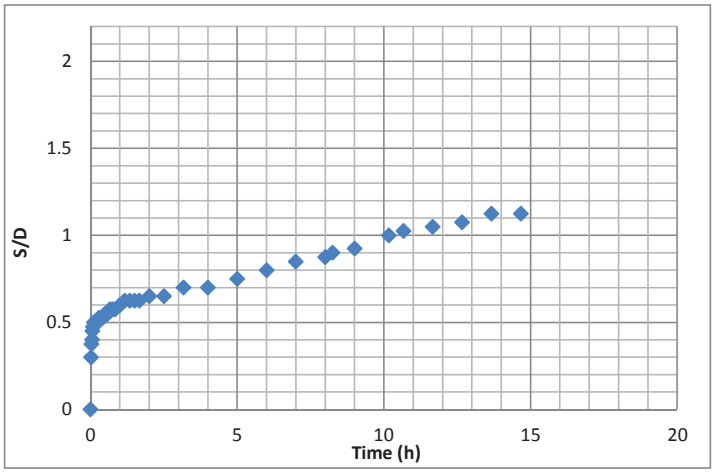

Test Number	R.T.11
Test description	Unidirectional current
Flume	Reversing current flume
Pile Diameter (mm)	40
Water depth (m)	0.16
Current depth averaged velocity (cm/s)	19.2
Bed description	50% coarse
Notes	repeat of test R.T.8

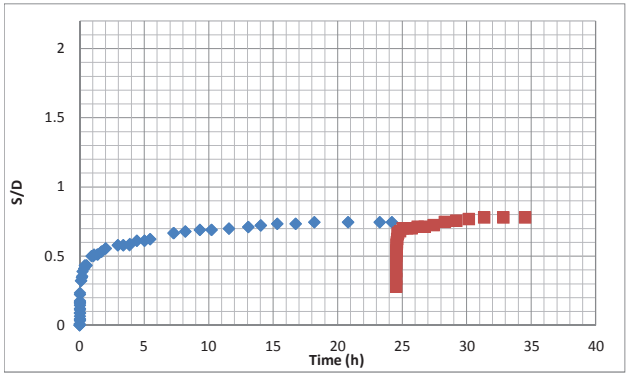

Test Number	C.90.1 and C.90.1.a
Date	25/11/2011
Test description	Large pile, unidirectional current, flow reversal at end of test
Flume	Coastal
Pile Diameter (mm)	90
Water depth (m)	0.45
Current velocity (cm/s)	22cm/s (but variable during test)
motor speed	15%, -15%
current direction	Right to left then left to right
Wave period (s)	-
Wave amp (cm)	-
Sand d_{50} (mm)	0.64
Bed description	uniform coarse sand
Notes	Velocity issue due to wire mesh

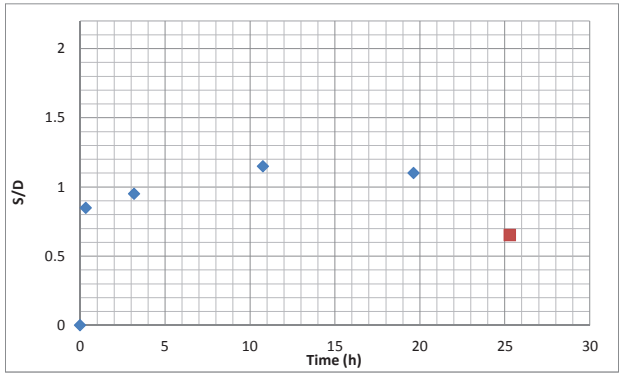

Test Number	C.20.1 and C.20.1.a
Date	25/11/2011
Test description	Small pile, unidirectional current, flow reversal at end of test
Flume	Coastal
Pile Diameter (mm)	20
Water depth (m)	0.45
Current velocity (cm/s)	22cm/s (but variable during test)
motor speed	15%, -15%
current direction	Right to left then left to right
Wave period (s)	-
Wave amp (cm)	-
Sand d_{50} (mm)	0.64
Bed description	uniform coarse sand
Notes	unidirectional current, flow reversal at end test, pile scale not visible in photos Discrepancy between photo obs and visual obs

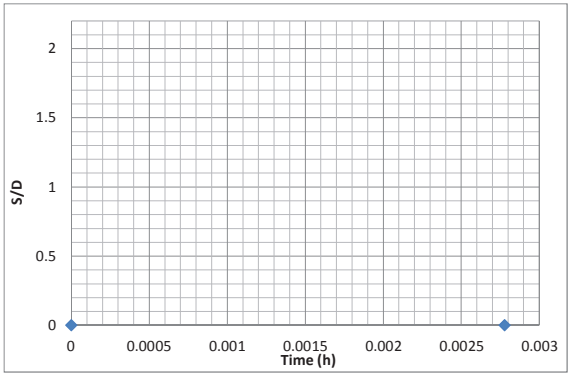

Test Number	C.90.2
Date	30/11/2011
Test description	Large pile, wave test
Flume	Coastal
Pile Diameter (mm)	90
Water depth (m)	0.45
Current velocity (cm/s)	-
motor speed	-
current/wave direction	right to left
Wave period (s)	1
Wave amp (cm)	0.01
Sand d_{50} (mm)	0.64
Bed description	uniform coarse sand
Notes	no scour

P-3 Series - Preliminary Coastal Flume Tests

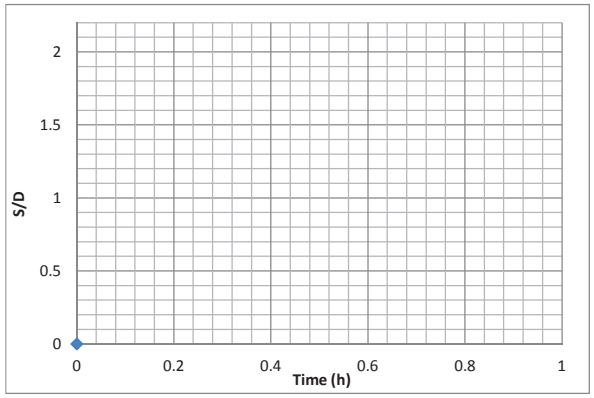

Test Number	C.20.2
Date	30/11/2011
Test description	Small pile, wave test
Flume	Coastal
Pile Diameter (mm)	20
Water depth (m)	0.45
Current velocity (cm/s)	-
motor speed	-
current/wave direction	right to left
Wave period (s)	1
Wave amp (cm)	0.01
Sand d_{50} (mm)	0.64
Bed description	uniform coarse sand
Notes	No data

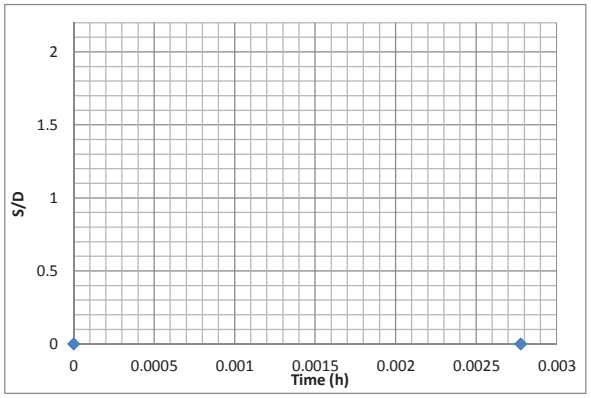

Test Number	C.90.3
Date	30/11/2011
Test description	Large pile, wave test
Flume	Coastal
Pile Diameter (mm)	90
Water depth (m)	0.45
Current velocity (cm/s)	-
motor speed	-
current/wave direction	right to left
Wave period (s)	2
Wave amp (cm)	0.01
Sand d_{50} (mm)	0.64
Bed description	uniform coarse sand
Notes	no scour

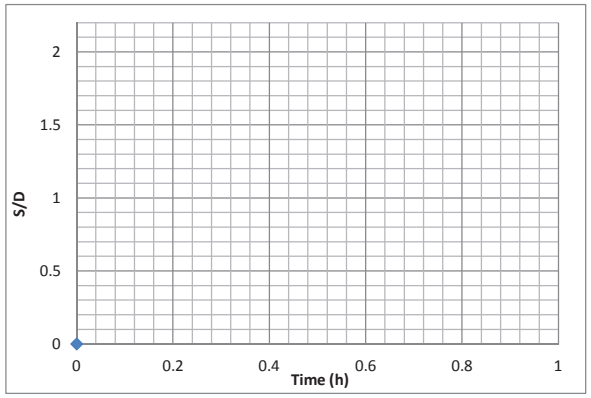

Test Number	C.20.3
Date	30/11/2011
Test description	Small pile, wave test
Flume	Coastal
Pile Diameter (mm)	20
Water depth (m)	0.45
Current velocity (cm/s)	-
motor speed	-
current/wave direction	right to left
Wave period (s)	2
Wave amp (cm)	0.01
Sand d_{50} (mm)	0.64
Bed description	uniform coarse sand
Notes	No data

P-3 Series - Preliminary Coastal Flume Tests

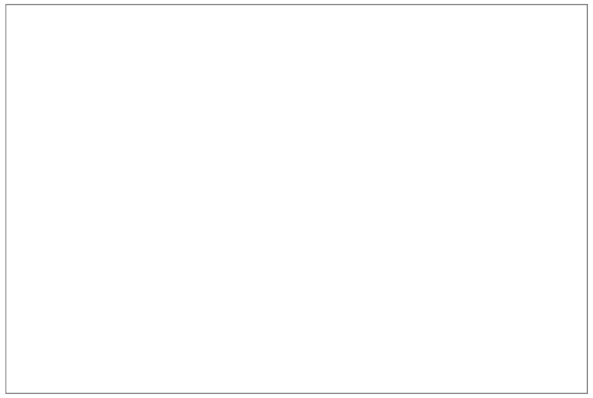

Test Number	C.90.4
Date	30/11/2011
Test description	Large pile, wave test
Flume	Coastal
Pile Diameter (mm)	90
Water depth (m)	0.45
Current velocity (cm/s)	-
motor speed	-
current/wave direction	right to left
Wave period (s)	2.941176471
Wave amp (cm)	0.01
Sand d_{50} (mm)	0.64
Bed description	uniform coarse sand
Notes	small amount of scour approx couple millimeters No data

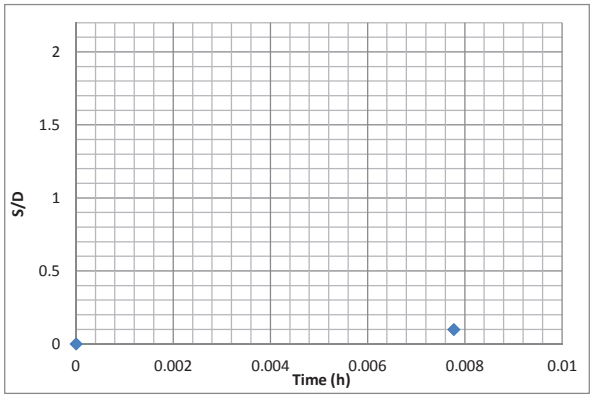

Test Number	C.20.4
Date	30/11/2011
Test description	Small pile, wave test
Flume	Coastal
Pile Diameter (mm)	20
Water depth (m)	0.45
Current velocity (cm/s)	-
motor speed	-
current/wave direction	right to left
Wave period (s)	2.941176471
Wave amp (cm)	0.01
Sand d_{50} (mm)	0.64
Bed description	uniform coarse sand
Notes	small amount of scour approx couple millimeters

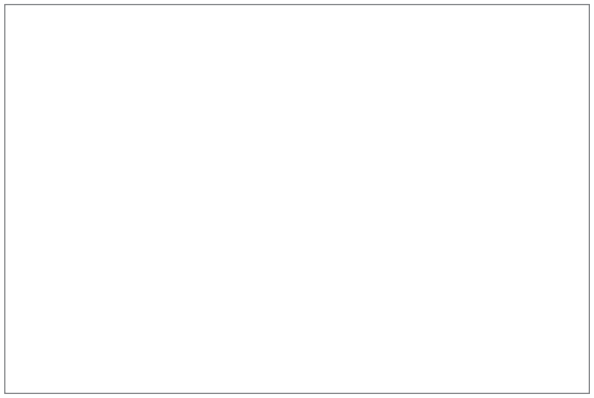

Test Number	C.90.5
Date	
Test description	Large pile, wave test
Flume	Coastal
Pile Diameter (mm)	90
Water depth (m)	0.45
Current velocity (cm/s)	-
motor speed	-
current/wave direction	right to left
Wave period (s)	1.724137931
Wave amp (cm)	0.02
Sand d_{50} (mm)	0.64
Bed description	uniform coarse sand
Notes	small amount of scour. Conditions appear in clear water regime No data

P-3 Series - Preliminary Coastal Flume Tests

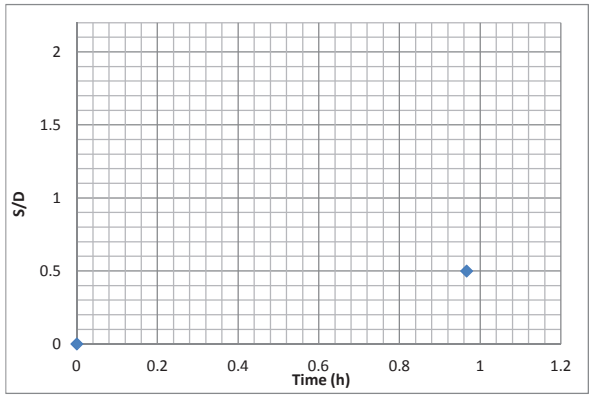

Test Number	C.20.5
Date	
Test description	Small pile, wave test
Flume	Coastal
Pile Diameter (mm)	20
Water depth (m)	0.45
Current velocity (cm/s)	-
motor speed	-
current/wave direction	right to left
Wave period (s)	1.724137931
Wave amp (cm)	0.02
Sand d_{50} (mm)	0.64
Bed description	uniform coarse sand
Notes	note plastic sheet scale became unstuck and created obstacle in scour hole (made scour hole unsymmetrical) - Reject data

Test Number	C.90.6
Date	
Test description	Large pile, wave test
Flume	Coastal
Pile Diameter (mm)	90
Water depth (m)	0.45
Current velocity (cm/s)	-
motor speed	-
current/wave direction	right to left
Wave period (s)	2.631578947
Wave amp (cm)	0.03
Sand d_{50} (mm)	0.64
Bed description	uniform coarse sand
Notes	bed lowered approx 2.3cm No data

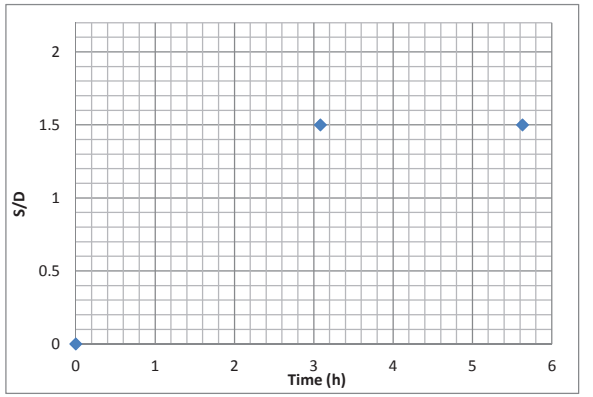

Test Number	C.20.6
Date	
Test description	Small pile, wave test
Flume	Coastal
Pile Diameter (mm)	20
Water depth (m)	0.45
Current velocity (cm/s)	-
motor speed	-
current/wave direction	right to left
Wave period (s)	2.631578947
Wave amp (cm)	0.03
Sand d_{50} (mm)	0.64
Bed description	uniform coarse sand
Notes	bed lowered approx 2.3cm

P-3 Series - Preliminary Coastal Flume Tests

Test Number	C.90.7 and C.90.7a
Date	
Test description	Large pile, random wave tests
Flume	Coastal
Pile Diameter (mm)	90
Water depth (m)	0.45
Current velocity (cm/s)	
motor speed	
current/wave direction	right to left
Wave period (s)	2.5
Wave amp (cm)	0.3, 0.4
Sand d_{50} (mm)	0.64
Bed description	uniform coarse sand
Notes	RANDOM WAVE repeat time 128s, R number = 12, clock freq=32Hz. No data

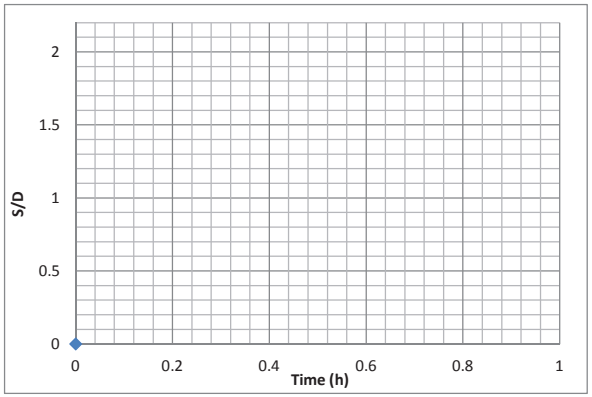

Test Number	C.20.7 and C.90.7a
Date	
Test description	Small pile, random wave tests
Flume	Coastal
Pile Diameter (mm)	20
Water depth (m)	0.45
Current velocity (cm/s)	
motor speed	
current/wave direction	right to left
Wave period (s)	2.5
Wave amp (cm)	0.3, 0.4
Sand d_{50} (mm)	0.64
Bed description	uniform coarse sand
Notes	RANDOM WAVE repeat time 128s, R number = 12, clock freq=32Hz. No data

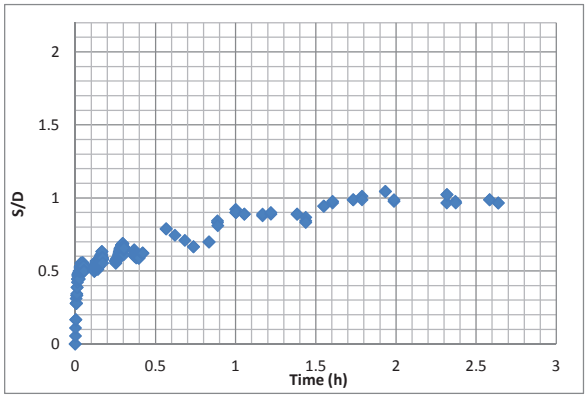

Test Number	C.90.8
Date	04/12/2011
Test description	Large pile, wave and current
Flume	Coastal
Pile Diameter (mm)	90
Water depth (m)	0.45
Current velocity (cm/s)	
motor speed	15%
current/wave direction	right to left
Wave period (s)	2.631578947
Wave amp (cm)	0.03
Sand d_{50} (mm)	0.64
Bed description	uniform coarse sand
Notes	

P-3 Series - Preliminary Coastal Flume Tests

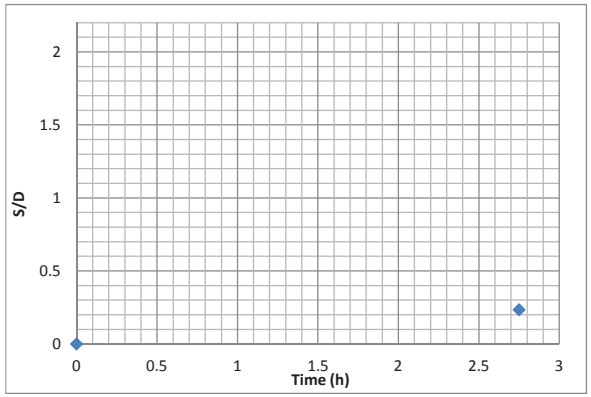

Test Number	C.20.8
Date	04/12/2011
Test description	Small pile, wave and current
Flume	Coastal
Pile Diameter (mm)	20
Water depth (m)	0.45
Current velocity (cm/s)	
motor speed	15%
current/wave direction	right to left
Wave period (s)	2.631578947
Wave amp (cm)	0.03
Sand d_{50} (mm)	0.64
Bed description	uniform coarse sand
Notes	

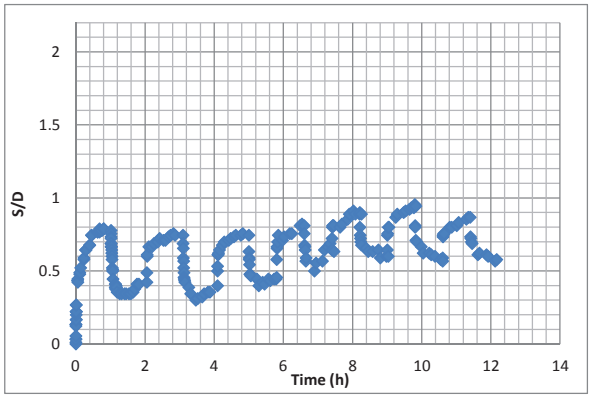

Test Number	C.90.9
Date	05/12/2011
Test description	Large pile, reversing current
Flume	Coastal
Pile Diameter (mm)	90
Water depth (m)	0.45
Current velocity (cm/s)	
motor speed	15%, -15%
current/wave direction	starting right to left
Wave period (s)	-
Wave amp (cm)	-
Sand d_{50} (mm)	0.64
Bed description	uniform coarse sand
Notes	

Test Number	C.20.9
Date	05/12/2011
Test description	Small pile, reversing current
Flume	Coastal
Pile Diameter (mm)	20
Water depth (m)	0.45
Current velocity (cm/s)	
motor speed	15%
current/wave direction	starting right to left
Wave period (s)	-
Wave amp (cm)	-
Sand d_{50} (mm)	0.64
Bed description	uniform coarse sand
Notes	No data

C-1 Series

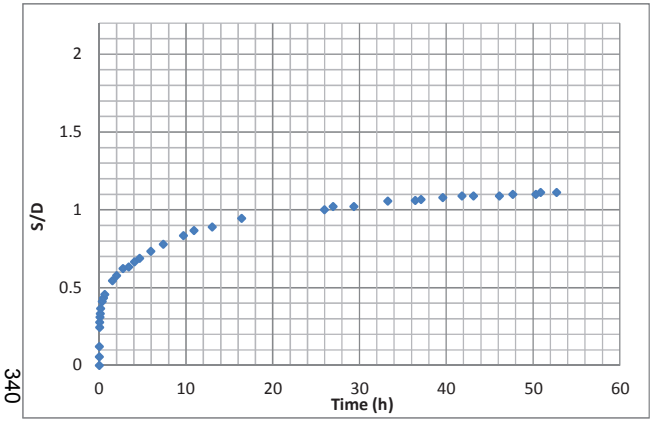

Test Number	C.90.10
Date	13/09/2012
Test description	Large pile, unidirectional current
Flume	Coastal
Pile Diameter (mm)	90
Water depth (m)	0.45
Current velocity (cm/s)	24.1
motor speed	-12%
Bed description	uniform coarse sand
Notes	

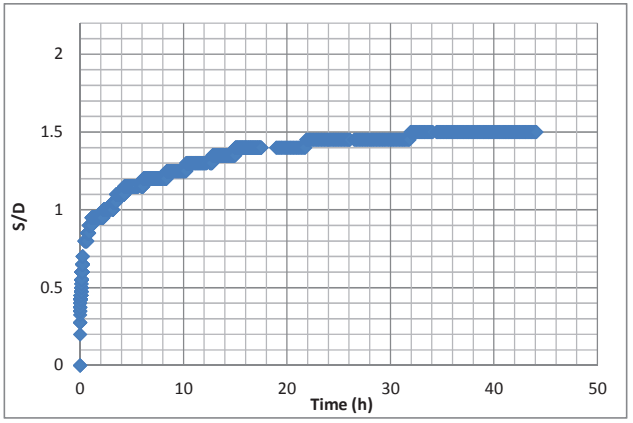

Test Number	C.20.10
Date	13/09/2012
Test description	Small pile, unidirectional current
Flume	Coastal
Pile Diameter (mm)	20
Water depth (m)	0.45
Current velocity (cm/s)	22.6
motor speed	-12%
Bed description	uniform coarse sand
Notes	

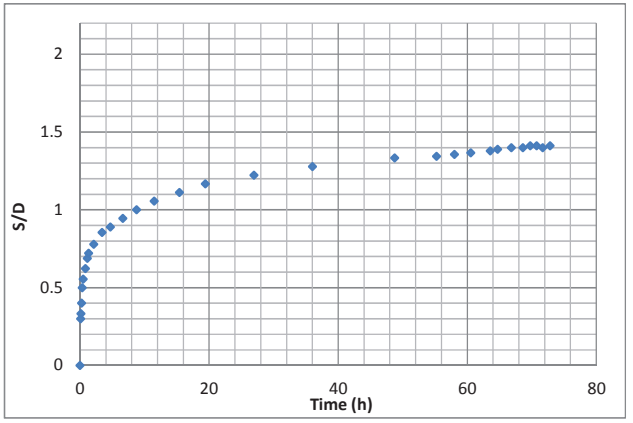

Test Number	C.90.11
Date	21/09/2012
Test description	Large pile, unidirectional current
Flume	Coastal
Pile Diameter (mm)	90
Water depth (m)	0.45
Current velocity (cm/s)	24.1
motor speed	-12%
Bed description	layered upper fine 70mm
Notes	

C-1 Series

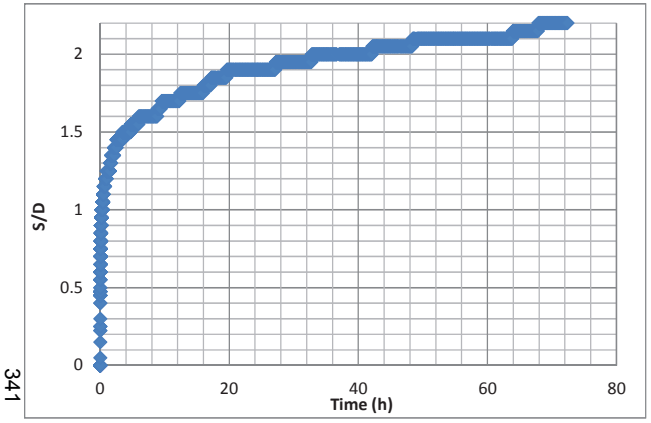

Test Number	C.20.11
Date	21/09/2012
Test description	Small pile, unidirectional current
Flume	Coastal
Pile Diameter (mm)	20
Water depth (m)	0.45
Current velocity (cm/s)	22.6
motor speed	-12%
Bed description	uniform fine
Notes	

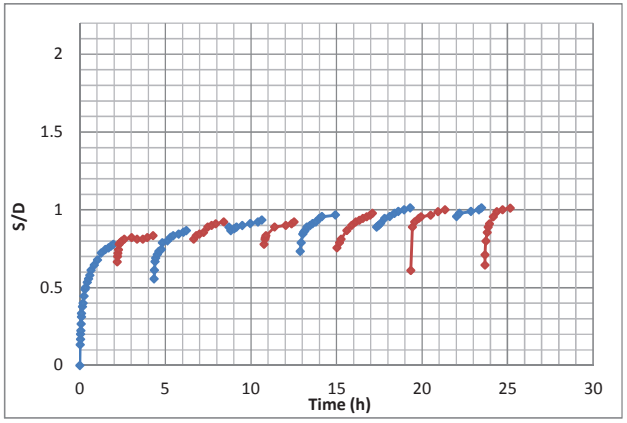

Test Number	C.90.12
Date	28/09/2012
Test description	Large pile, reversing current
Flume	Coastal
Pile Diameter (mm)	90
Water depth (m)	0.45
Current velocity (cm/s)	24.1, 23.9
motor speed	-12%, 11.5%
Bed description	layered upper fine 70mm
Notes	Longer cycle length due to depth of lower layer

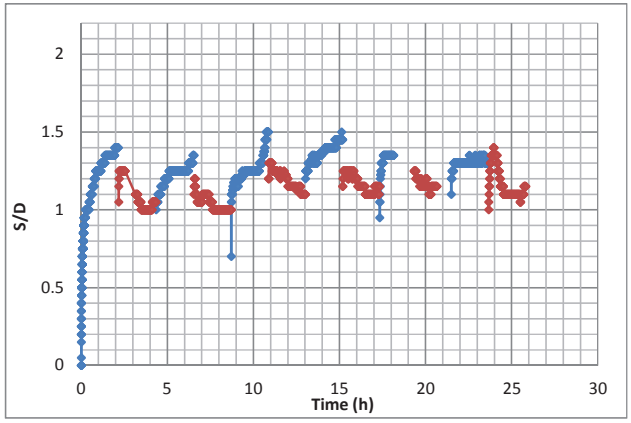

Test Number	C.20.12
Date	28/09/2012
Test description	Small pile, reversing current
Flume	Coastal
Pile Diameter (mm)	20
Water depth (m)	0.45
Current velocity (cm/s)	22.6, 21.7
motor speed	-12%, 11.5%
Bed description	uniform fine sand
Notes	missing data middle run 2 and end run 9

C-1 Series

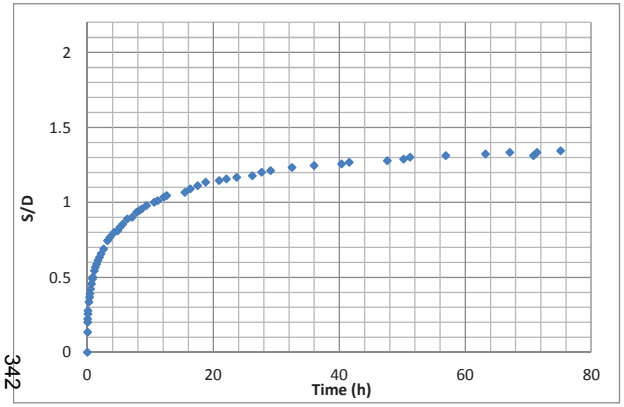

Test Number	C.90.13
Date	02/10/2012
Test description	Large pile, unidirectional current
Flume	Coastal
Pile Diameter (mm)	90
Water depth (m)	0.45
Current velocity (cm/s)	24.1
motor speed	-12%
Bed description	mixed 50%
Notes	

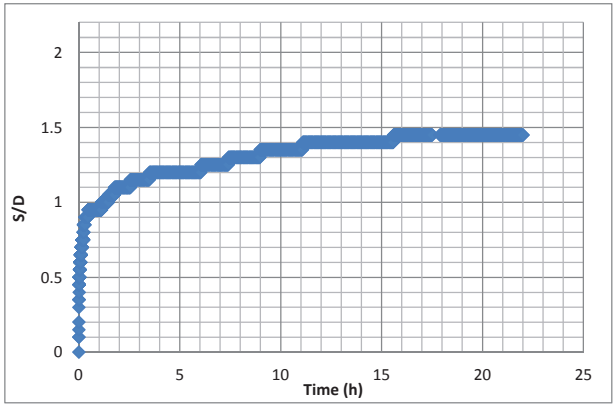

Test Number	C.20.13
Date	02/10/2012
Test description	Small pile, unidirectional current
Flume	Coastal
Pile Diameter (mm)	20
Water depth (m)	0.45
Current velocity (cm/s)	22.6
motor speed	-12%
Bed description	mixed 50%
Notes	

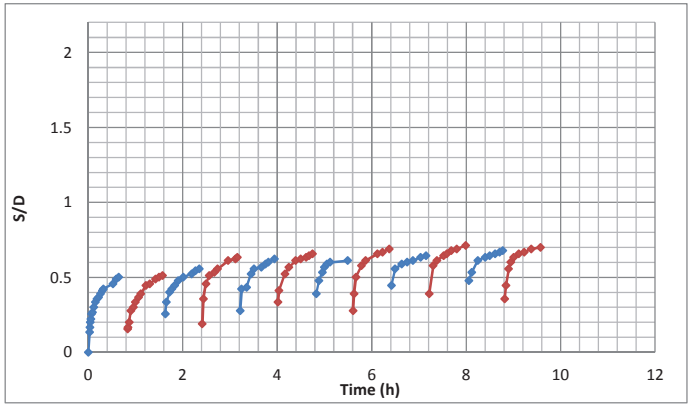

Test Number	C.90.14
Date	07/10/2012
Test description	Large pile, reversing current
Flume	Coastal
Pile Diameter (mm)	90
Water depth (m)	0.45
Current velocity (cm/s)	24.1, 23.9
motor speed	-12%, 11.5%
Bed description	mixed 50%
Notes	

C-1 Series

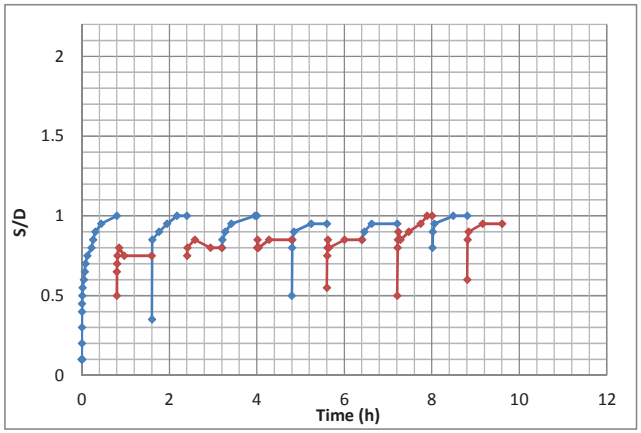

Test Number	C.20.14
Date	07/10/2012
Test description	Small pile, reversing current
Flume	Coastal
Pile Diameter (mm)	20
Water depth (m)	0.45
Current velocity (cm/s)	22.6, 21.7
motor speed	-12%, 11.5%
Bed description	mixed 50%
Notes	

C-1 Series

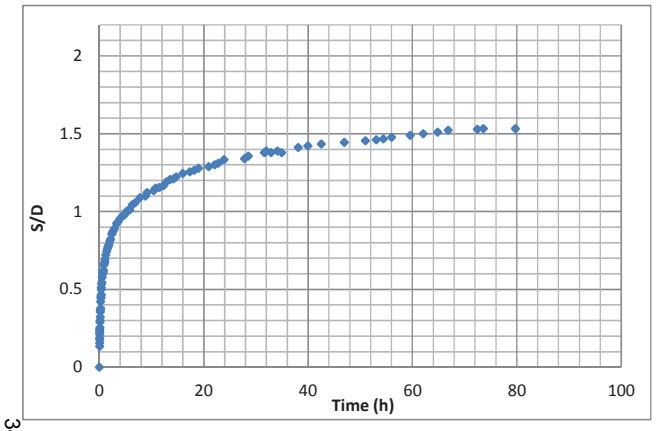

Test Number	C.90.15
Date	30/04/2013
Test description	Large pile, unidirectional current
Flume	Coastal
Pile Diameter (mm)	90
Water depth (m)	0.45
Current depth averaged velocity (cm/s)	24.1
motor speed	-12%
Wave period (s)	-
Wave amp (cm)	-
Bed description	fine sand
Notes	

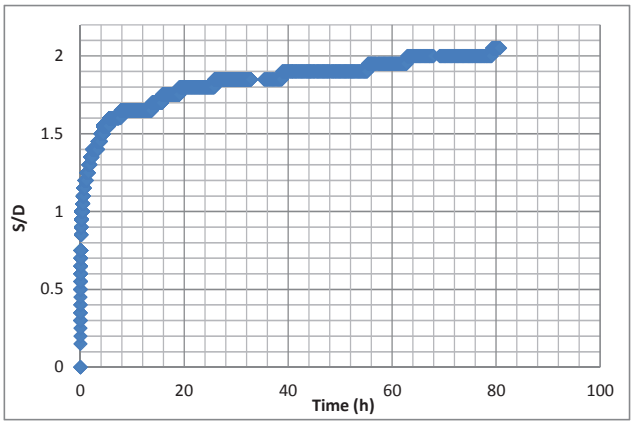

Test Number	C.20.15
Date	30/04/2013
Test description	Small pile, unidirectional current
Flume	Coastal
Pile Diameter (mm)	20
Water depth (m)	0.45
Current depth averaged velocity (cm/s)	22.6
motor speed	-12%
Wave period (s)	-
Wave amp (cm)	-
Bed description	fine sand
Notes	

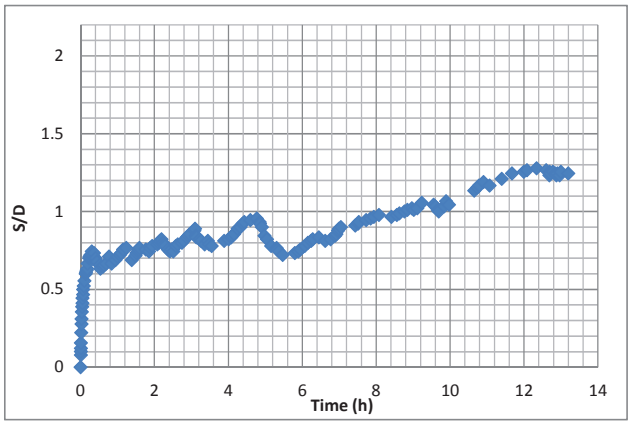

Test Number	C.90.16
Date	
Test description	Large pile, wave and current
Flume	Coastal
Pile Diameter (mm)	90
Water depth (m)	0.45
Current depth averaged velocity (cm/s)	
motor speed	
Wave period (s)	-
Wave amp (cm)	-
Bed description	coarse sand
Notes	

C-1 Series

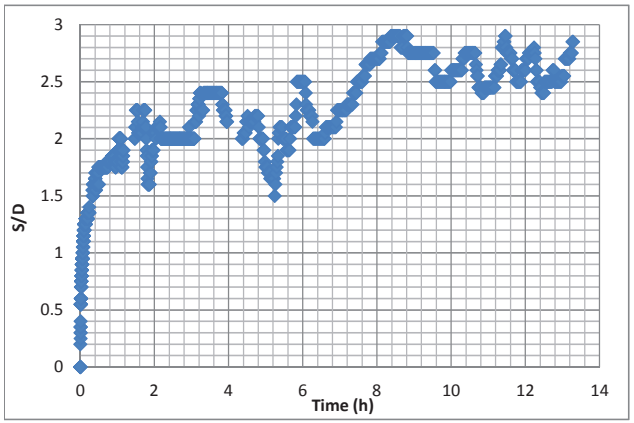

Test Number	C.20.16
Date	
Test description	Small pile, wave and current
Flume	Coastal
Pile Diameter (mm)	20
Water depth (m)	0.45
Current depth averaged velocity (cm/s)	
motor speed	
Wave period (s)	-
Wave amp (cm)	-
Bed description	coarse sand
Notes	

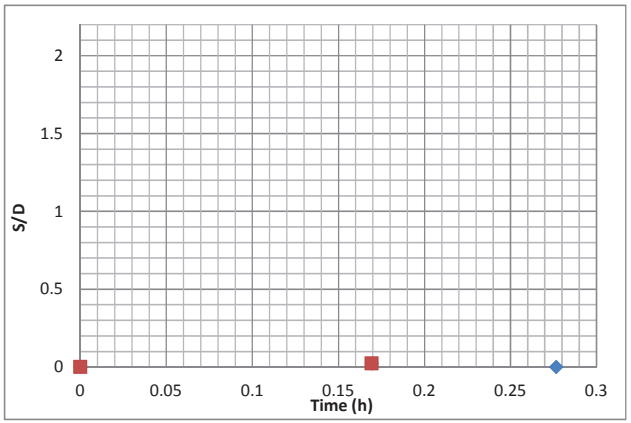

Test Number	C.90.17
Date	14/05/2013
Test description	Large pile, wave
Flume	Coastal
Pile Diameter (mm)	90
Water depth (m)	0.45
Current depth averaged velocity (cm/s)	
motor speed	
Wave period (s)	-
Wave amp (cm)	-
Bed description	coarse sand
Notes	live bed BED BECAME UNATTACHED DURING TEST

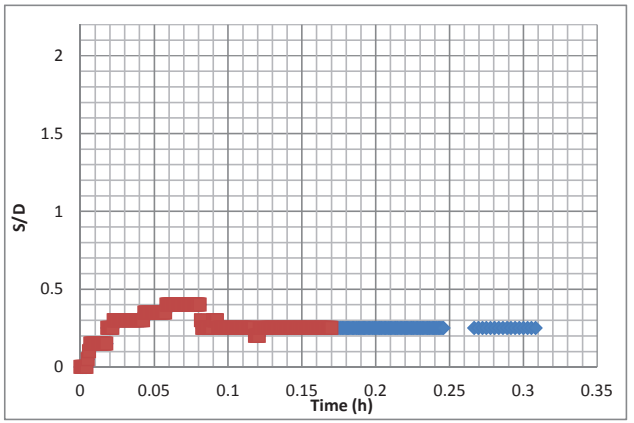

Test Number	C.20.17
Date	14/05/2013
Test description	Small pile, wave
Flume	Coastal
Pile Diameter (mm)	20
Water depth (m)	0.45
Current depth averaged velocity (cm/s)	
motor speed	
Wave period (s)	-
Wave amp (cm)	-
Bed description	coarse sand
Notes	BED BED BECAME UNATTACHED DURING TEST

C-1 Series

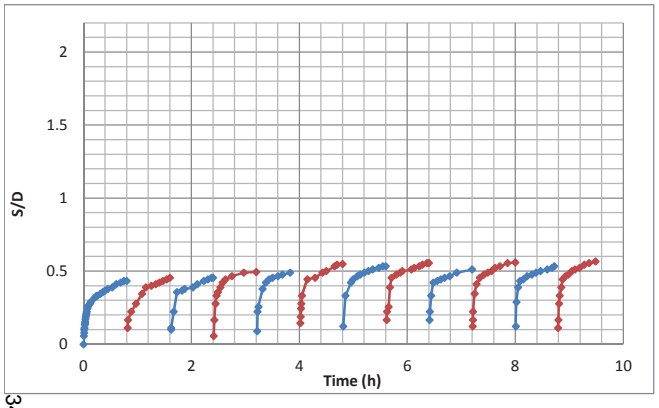

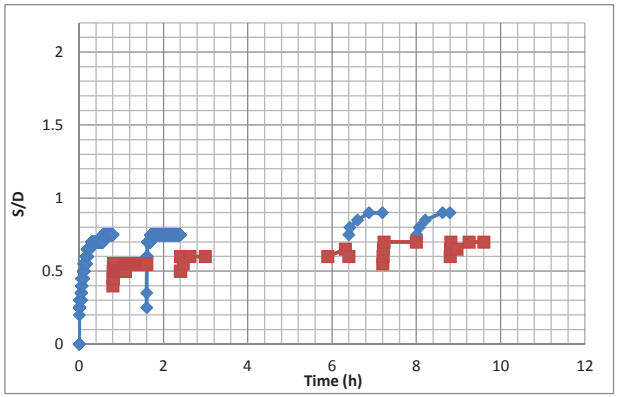

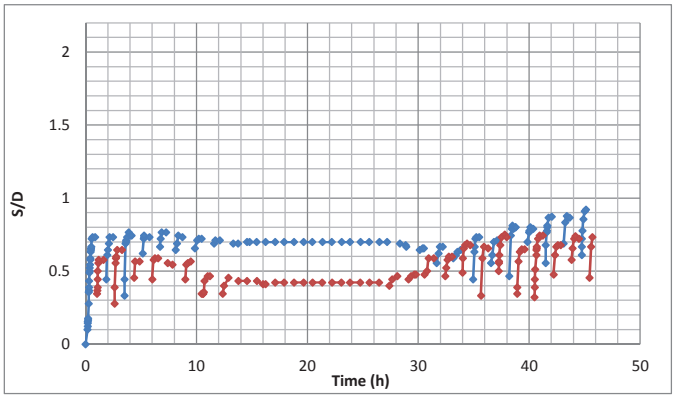

Test Number	C.90.18
Date	16/05/2013
Test description	Large pile, reversing current
Flume	Coastal
Pile Diameter (mm)	90
Water depth (m)	0.45
Current depth averaged velocity (cm/s)	23
motor speed	-12%, +11.5%
Wave period (s)	-
Wave amp (cm)	-
Bed description	Coarse sand
Notes	

Test Number	C.20.18
Date	16/05/2013
Test description	Small pile, reversing current
Flume	Coastal
Pile Diameter (mm)	20
Water depth (m)	0.45
Current depth averaged velocity (cm/s)	
motor speed	
Wave period (s)	-
Wave amp (cm)	-
Bed description	coarse sand
Notes	

Test Number	C.90.19
Date	18/05/2013
Test description	Large pile, spring-neap cycle
Flume	Coastal
Pile Diameter (mm)	90
Water depth (m)	0.45
Current depth averaged velocity (cm/s)	expected between -30.6 and +33.8
motor speed	between -16.6% and +15.3%
Wave period (s)	-
Wave amp (cm)	-
Bed description	coarse sand
Notes	missing video for last 2 reverses

C-1 Series

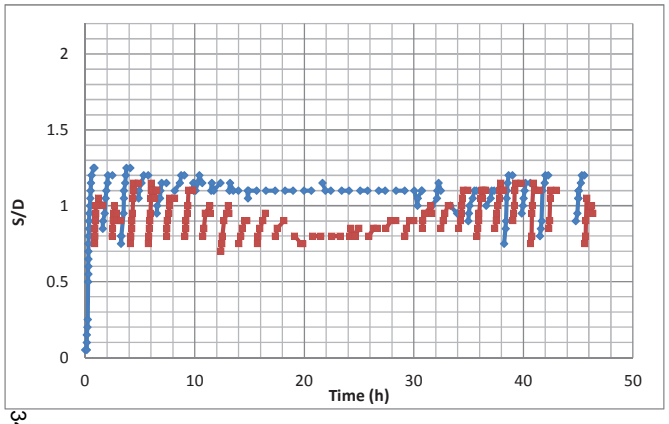

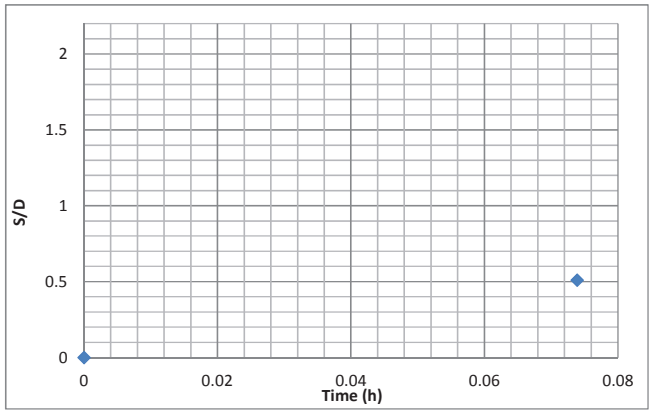

Test Number	C.20.19
Date	18/05/2013
Test description	Small pile, spring-neap cycle
Flume	Coastal
Pile Diameter (mm)	20
Water depth (m)	0.45
Current depth averaged velocity (cm/s)	expected between -30.6 and +33.8
motor speed	variable between -16.6% and +15.3%
Wave period (s)	-
Wave amp (cm)	-
Bed description	coarse sand
Notes	missing reverse 27 and 27.5

Test Number	C.90.20
Date	
Test description	Large pile, wave and current
Flume	Coastal
Pile Diameter (mm)	90
Water depth (m)	0.45
Current depth averaged velocity (cm/s)	
motor speed	
Wave period (s)	
Wave amp (cm)	
Bed description	layered upper fine 70mm
Notes	Test stopped due to too much fine sediment movement towards pump inlet, due to live bed conditions

Test Number	C.20.20
Date	
Test description	Small pile, wave and current
Flume	Coastal
Pile Diameter (mm)	20
Water depth (m)	0.45
Current depth averaged velocity (cm/s)	
motor speed	
Wave period (s)	-
Wave amp (cm)	-
Bed description	layered upper fine 70mm
Notes	No data

C-1 Series

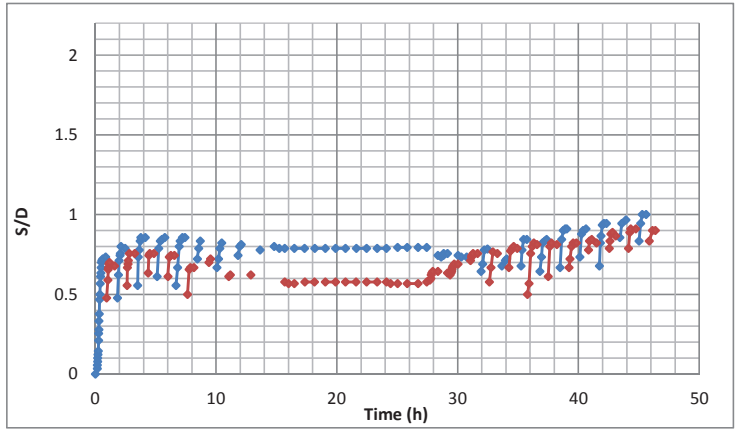

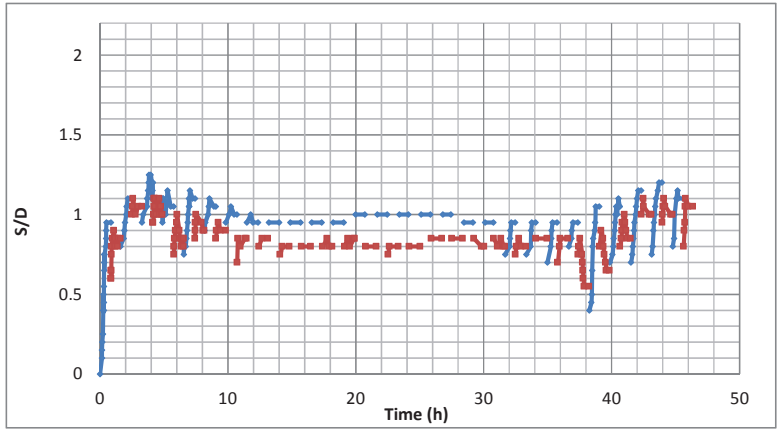

Test Number	C.90.21
Date	30/05/2013
Test description	Large pile, spring-neap cycle
Flume	Coastal
Pile Diameter (mm)	90
Water depth (m)	0.45
Current depth averaged velocity (cm/s)	expected between -30.6 and +33.8
motor speed	between -16.6% and +15.3%
Wave period (s)	-
Wave amp (cm)	-
Bed description	layered upper fine 70mm
Notes	Different timescale of flow reversal between C.90.19 and C.90.12

Test Number	C.20.21
Date	30/05/2013
Test description	Small pile, spring-neap cycle
Flume	Coastal
Pile Diameter (mm)	20
Water depth (m)	0.45
Current depth averaged velocity (cm/s)	expected between -30.6 and +33.8
motor speed	variable between -16.6% and +15.3%
Wave period (s)	-
Wave amp (cm)	-
Bed description	uniform fine sand
Notes	

C-2 Series

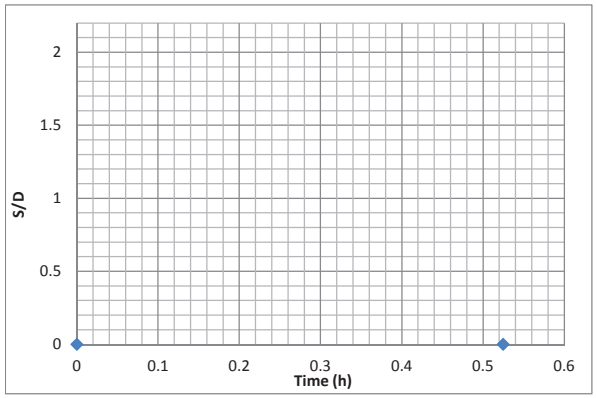

Test Number	C.50.22
Test description	Large pile, wave
Flume	Coastal
Pile Diameter (mm)	50
Water depth (m)	0.45
Current depth averaged velocity (cm/s)	-
motor speed	-
Wave period (s)	2.5
Wave amp (cm)	2.25
Bed description	coarse sand
Notes	No sediment movement visible. Test run over scoured bed from 6.9% current test

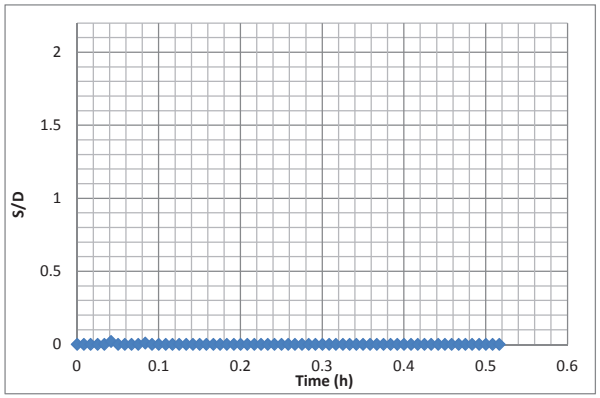

Test Number	C.20.22
Test description	Small pile, wave
Flume	Coastal
Pile Diameter (mm)	20
Water depth (m)	0.45
Current depth averaged velocity (cm/s)	-
motor speed	-
Wave period (s)	2.5
Wave amp (cm)	2.25
Bed description	coarse sand
Notes	No sediment movement visible. Test run over scoured bed from 6.9% current test

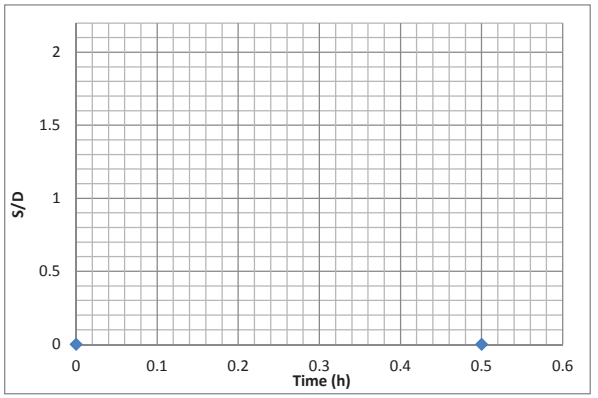

Test Number	C.50.23
Test description	Large pile, unidirecitonal current
Flume	Coastal
Pile Diameter (mm)	50
Water depth (m)	0.45
Current depth averaged velocity (cm/s)	
motor speed	2.5%
Wave period (s)	-
Wave amp (cm)	-
Bed description	coarse sand
Notes	No sediment movement observed

C-2 Series

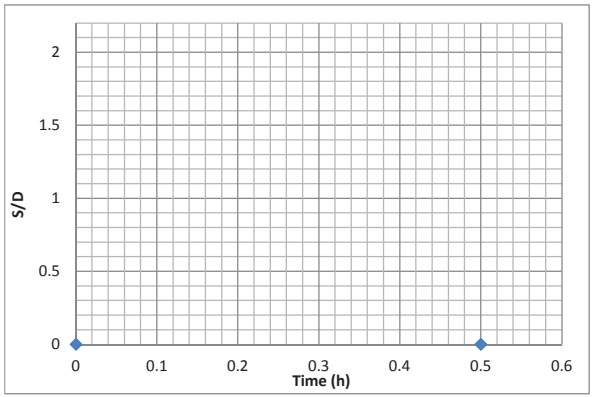

Test Number	C.20.23
Test description	Small pile, unidirecitonal current
Flume	Coastal
Pile Diameter (mm)	20
Water depth (m)	0.45
Current depth averaged velocity (cm/s)	
motor speed	2.5%
Wave period (s)	-
Wave amp (cm)	-
Bed description	coarse sand
Notes	No sediment movement observed

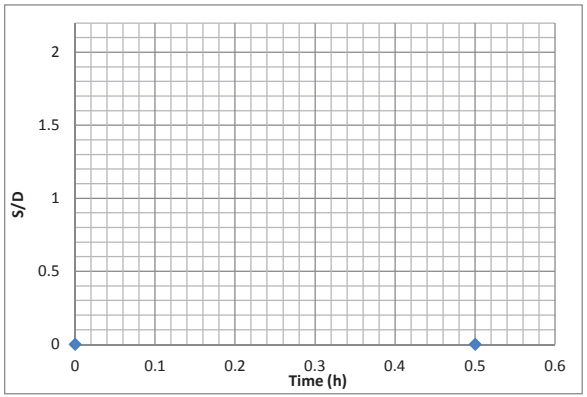

Test Number	C.50.24
Test description	Large pile, unidirecitonal current
Flume	Coastal
Pile Diameter (mm)	50
Water depth (m)	0.45
Current depth averaged velocity (cm/s)	
motor speed	4.8%
Wave period (s)	-
Wave amp (cm)	-
Bed description	coarse sand
Notes	No sediment movement observed

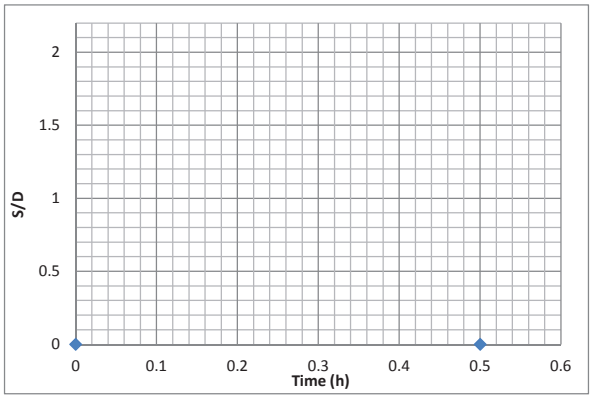

Test Number	C.20.24
Test description	Small pile, unidirecitonal current
Flume	Coastal
Pile Diameter (mm)	20
Water depth (m)	0.45
Current depth averaged velocity (cm/s)	
motor speed	4.8%
Wave period (s)	-
Wave amp (cm)	-
Bed description	coarse sand
Notes	No sediment movement observed

C-2 Series

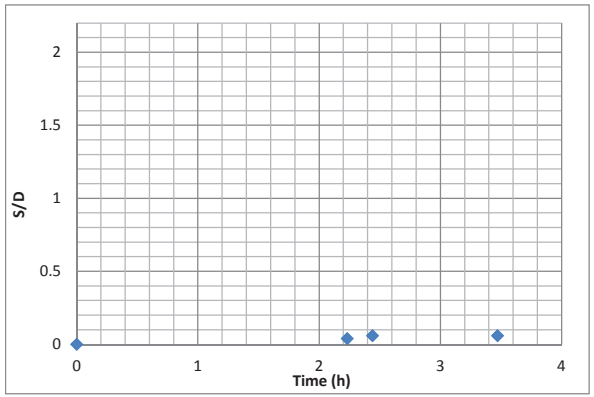

Test Number	C.50.25
Test description	Large pile, unidirecitonal current
Flume	Coastal
Pile Diameter (mm)	50
Water depth (m)	0.45
Current depth averaged velocity (cm/s)	
motor speed	6.9%
Wave period (s)	-
Wave amp (cm)	-
Bed description	coarse sand
Notes	Sediment movement observed, infilling of dip next to pile at downstream side, before some scouring at upstream side.

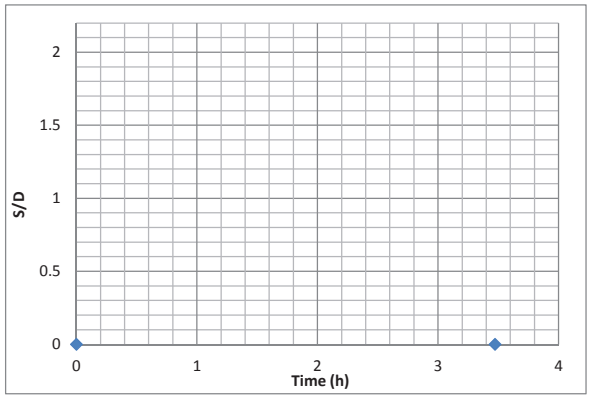

Test Number	C.20.25
Test description	Small pile, unidirecitonal current
Flume	Coastal
Pile Diameter (mm)	20
Water depth (m)	0.45
Current depth averaged velocity (cm/s)	
motor speed	6.9%
Wave period (s)	-
Wave amp (cm)	-
Bed description	coarse sand
Notes	No sediment movement observed

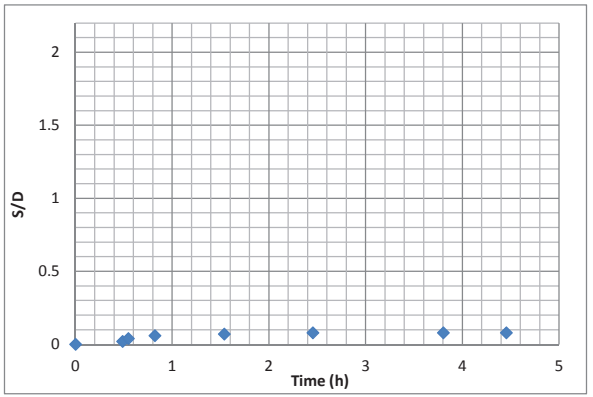

Test Number	C.50.26
Test description	Large pile, wave and current
Flume	Coastal
Pile Diameter (mm)	50
Water depth (m)	0.45
Current depth averaged velocity (cm/s)	
motor speed	2.5%
Wave period (s)	2.5
Wave amp (cm)	2.25
Bed description	coarse sand
Notes	

C-2 Series

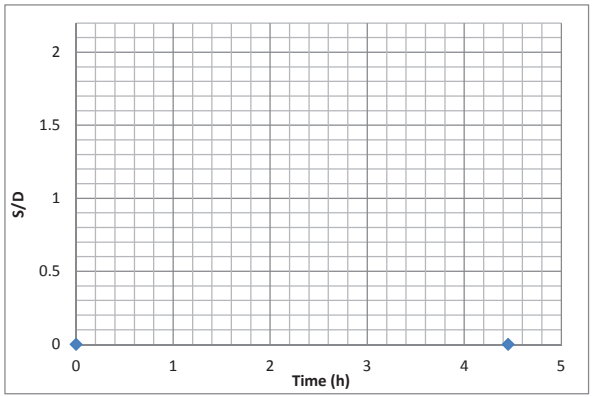

Test Number	C.20.26
Test description	Small pile, wave and current
Flume	Coastal
Pile Diameter (mm)	20
Water depth (m)	0.45
Current depth averaged velocity (cm/s)	
motor speed	2.5%
Wave period (s)	2.5
Wave amp (cm)	2.25
Bed description	coarse sand
Notes	No sediment movement observed

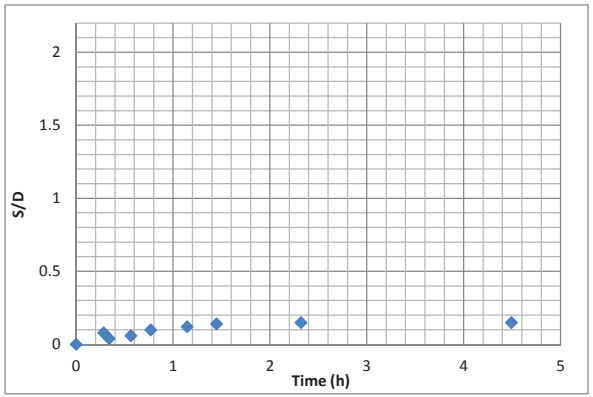

Test Number	C.50.27
Test description	Large pile, wave and current
Flume	Coastal
Pile Diameter (mm)	50
Water depth (m)	0.45
Current depth averaged velocity (cm/s)	
motor speed	4.8%
Wave period (s)	2.5
Wave amp (cm)	2.25
Bed description	coarse sand
Notes	

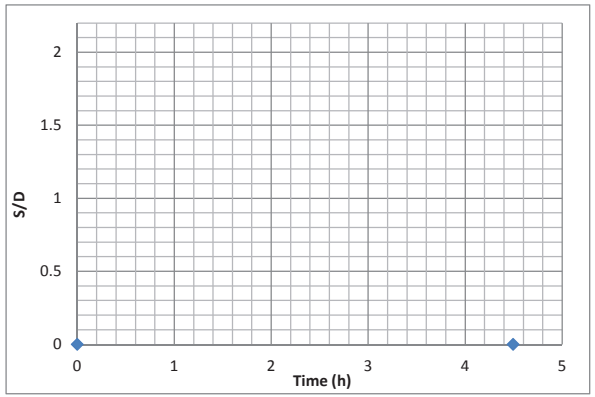

Test Number	C.20.27
Test description	Small pile, wave and current
Flume	Coastal
Pile Diameter (mm)	20
Water depth (m)	0.45
Current depth averaged velocity (cm/s)	
motor speed	4.8%
Wave period (s)	2.5
Wave amp (cm)	2.25
Bed description	coarse sand
Notes	visual obs - no scour at pile, but movement of sand bed in vicinity - two deposition zones and scour pit away from pile

C-2 Series

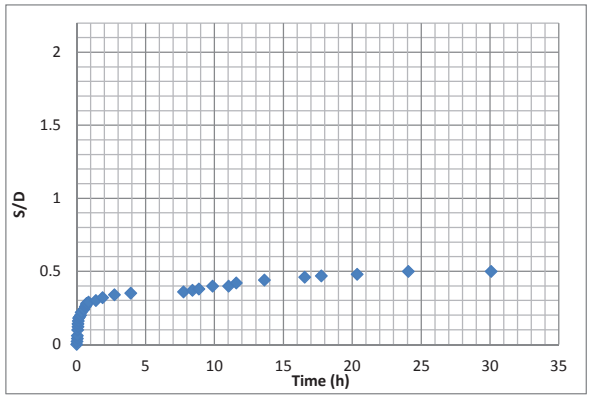

Test Number	C.50.28
Test description	Large pile, wave and current
Flume	Coastal
Pile Diameter (mm)	50
Water depth (m)	0.45
Current depth averaged velocity (cm/s)	
motor speed	6.9%
Wave period (s)	2.5
Wave amp (cm)	2.25
Bed description	coarse sand
Notes	

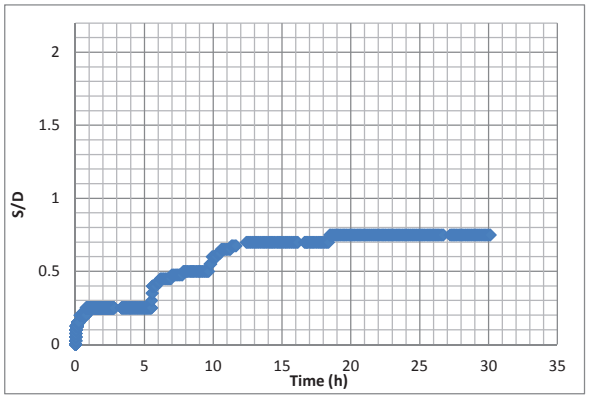

Test Number	C.20.28
Test description	Small pile, wave and current
Flume	Coastal
Pile Diameter (mm)	20
Water depth (m)	0.45
Current depth averaged velocity (cm/s)	
motor speed	6.9%
Wave period (s)	2.5
Wave amp (cm)	2.25
Bed description	coarse sand
Notes	

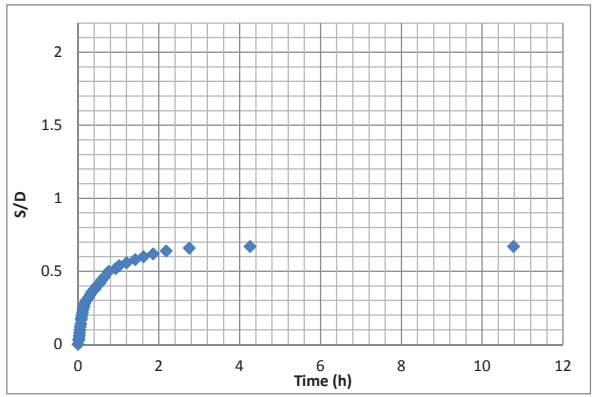

Test Number	C.50.29
Test description	Large pile, wave and current
Flume	Coastal
Pile Diameter (mm)	50
Water depth (m)	0.45
Current depth averaged velocity (cm/s)	
motor speed	6.9%
Wave period (s)	2.5
Wave amp (cm)	2.25
Bed description	layered upper fine 30mm
Notes	

C-2 Series

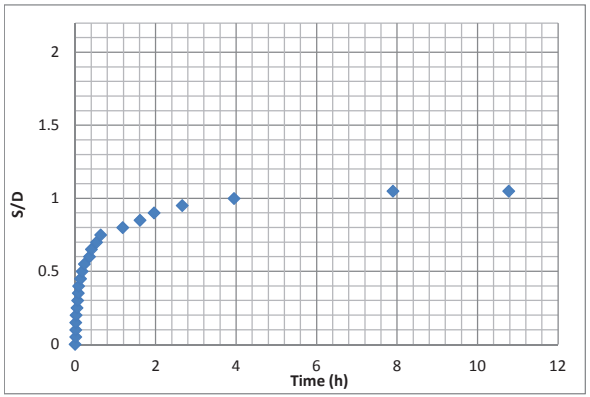

Test Number	C.20.29
Test description	Small pile, wave and current
Flume	Coastal
Pile Diameter (mm)	20
Water depth (m)	0.45
Current depth averaged velocity (cm/s)	
motor speed	6.9%
Wave period (s)	2.5
Wave amp (cm)	2.25
Bed description	fine sand
Notes	

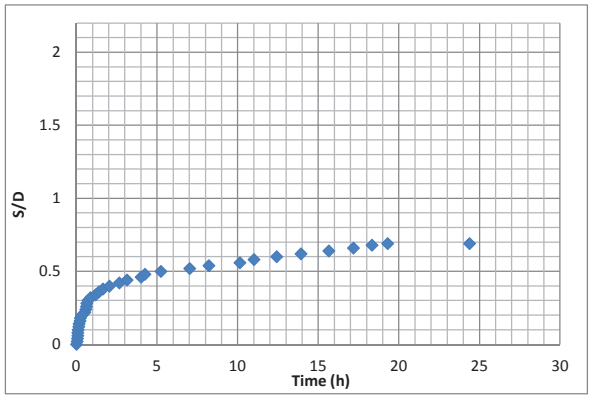

Test Number	C.50.30
Test description	Large pile, wave and current
Flume	Coastal
Pile Diameter (mm)	50
Water depth (m)	0.45
Current depth averaged velocity (cm/s)	
motor speed	6.9%
Wave period (s)	2.5
Wave amp (cm)	2.25
Bed description	mixed 50%
Notes	

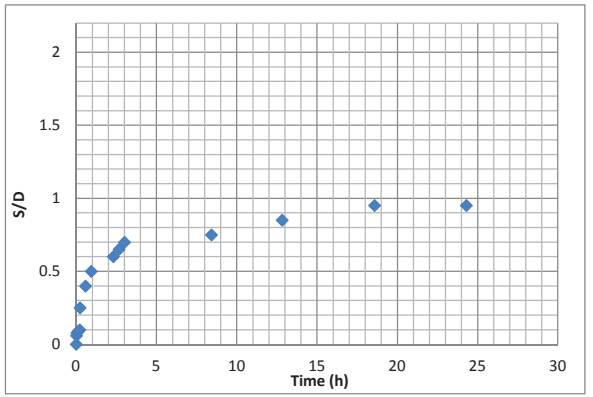

Test Number	C.20.30
Test description	Small pile, wave and current
Flume	Coastal
Pile Diameter (mm)	20
Water depth (m)	0.45
Current depth averaged velocity (cm/s)	
motor speed	6.9%
Wave period (s)	2.5
Wave amp (cm)	2.25
Bed description	mixed 50%
Notes	

C-2 Series

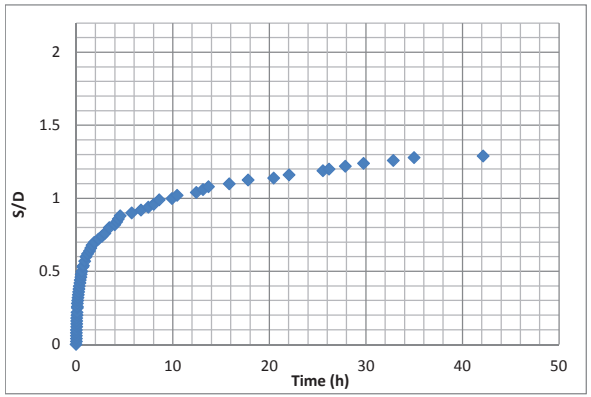

Test Number	C.50.31
Test description	Large pile, wave and current
Flume	Coastal
Pile Diameter (mm)	50
Water depth (m)	0.45
Current depth averaged velocity (cm/s)	
motor speed	6.9%
Wave period (s)	2.5
Wave amp (cm)	2.25
Bed description	fine sand
Notes	

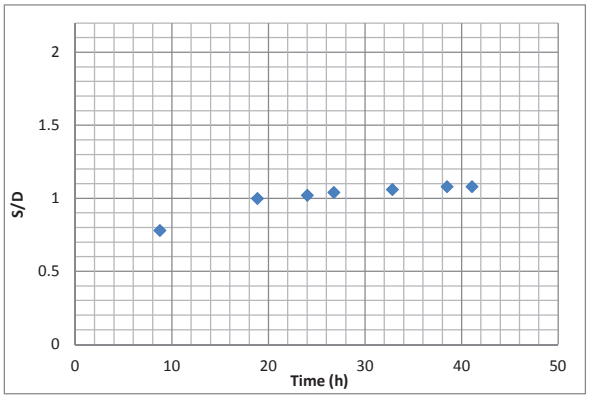

Test Number	C.50R.31
Test description	Small pile, wave and current
Flume	Coastal
Pile Diameter (mm)	50
Water depth (m)	0.45
Current depth averaged velocity (cm/s)	
motor speed	6.9%
Wave period (s)	2.5
Wave amp (cm)	2.25
Bed description	fine sand
Notes	Rough pile

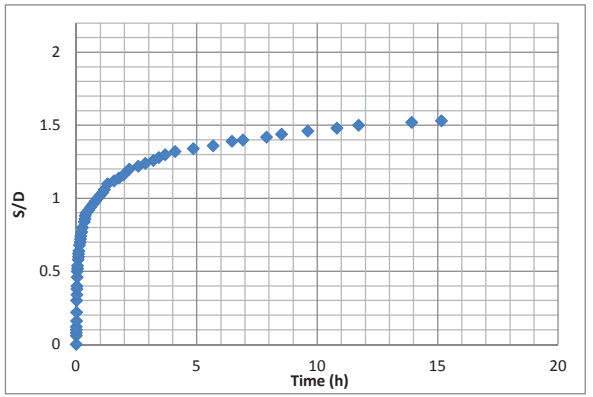

Test Number	C.50.32
Test description	smooth pile , unidirectional current
Flume	Coastal
Pile Diameter (mm)	50
Water depth (m)	0.45
Current depth averaged velocity (cm/s)	
motor speed	-12.0%
Wave period (s)	-
Wave amp (cm)	-
Bed description	fine sand
Notes	

C-2 Series

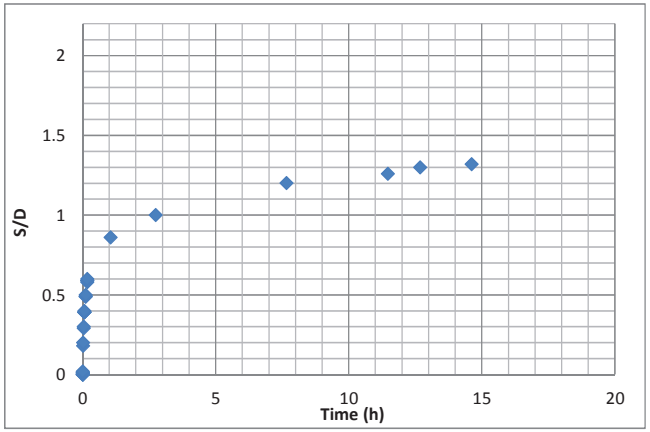

Test Number	C.50R.32
Test description	rough pile, unidirectional current
Flume	Coastal
Pile Diameter (mm)	50
Water depth (m)	0.45
Current depth averaged velocity (cm/s)	
motor speed	-12.0%
Wave period (s)	-
Wave amp (cm)	-
Bed description	fine sand
Notes	Rough pile

Appendix 4 - Scour prediction

Equilibrium scour depth equations:

Hancu (1971):

$$\frac{S_e}{D} = 2.42K_v\left(\frac{V^2}{gD}\right)^{1/3} \quad \text{(A4.1)}$$

$$For\ \frac{V}{V_{cr}} < 0.5, K_v = 0 \quad \text{(A4.2)}$$

$$For\ 0.5 < \frac{V}{V_{cr}} < 1, K_v = \frac{2V}{V_{cr}} - 1 \quad \text{(A4.3)}$$

$$For\ \frac{V}{V_{cr}} > 1, K_v = 1 \quad \text{(A4.4)}$$

Breusers et al. (1977):

$$\frac{S_e}{D} = K_v\left[2\tanh\left(\frac{h}{D}\right)\right]K_1K_2 \quad \text{(A4.5)}$$

K_v is defined as above.

Melville and Sutherland (1988):

$$\frac{S_e}{D} = K_vK_hK_dK_\sigma K_sK_\alpha \quad \text{(A4.6)}$$

K factors for flow intensity, flow depth, sediment size, sediment gradation, pier shape and alignment.

Sheppard et al. (2011):

$$\frac{S_e}{D} = 2.5K_1K_2K_3, for\ 0.4 < \frac{V}{V_{cr}} < 1 \quad \text{(A4.7)}$$

$$\frac{S_e}{D}K_1\left[2.2\left(\frac{\frac{V}{V_{cr}}-1}{\frac{V_{lp}}{V_{cr}}-1}\right) + 2.5K_3\left(\frac{\frac{V_{lp}}{V_{cr}}-\frac{V}{V_{cr}}}{\frac{V_{lp}}{V_{cr}}-1}\right)\right], for\ 1 < \frac{V}{V_{cr}} < \frac{V_{lp}}{V_{cr}} \quad \text{(A4.8)}$$

$$\frac{S_e}{D} = 2.2K_1, for\ \frac{V}{V_{cr}} > \frac{V_{lp}}{V_{cr}} \quad \text{(A4.9)}$$

$$K_1 = \tanh\left[\left(\frac{h}{D}\right)^{0.4}\right] \quad \text{(A4.10)}$$

$$K_2 = \left\{1 - 1.2\left[\ln\frac{V}{V_{cr}}\right]^2\right\} \quad \text{(A4.11)}$$

$$K_3 = \left[\frac{\left(\frac{D}{d_{50}}\right)}{0.4\left(\frac{D}{d_{50}}\right)^{1.2} + 10.6\left(\frac{D}{d_{50}}\right)^{-0.13}}\right] \quad \text{(A4.12)}$$

Richardson and Davis (2001) (HEC-18):

$$\frac{S_e}{D} = 2.0 K_1 K_2 K_3 K_4 \left(\frac{h}{D}\right)^{0.35} Fr^{0.43} \quad \text{(A4.13)}$$

Correction factors are for pier shape, angle of attack, bed condition, bed armouring (gradation). Covers both live bed and clear water regimes. K_1 and K_2=1 for circular pier. K_3=1.1 for clear water conditions. For K_4, if d_{50}<2 mm and d_{95}<20 mm, K_4=1. Otherwise K_4 is a function of the scour initiation velocity, critical velocity for each of the d_{50} and d_{95} sediment sizes and the actual flow velocity.

Equilibrium scour equations in waves/wave-current

Sumer et al. (1993):

$$\frac{S_e}{D} = 1.3\left[1 - e^{-0.03(KC-6)}\right], for\ KC \geq 6 \quad \text{(A4.14)}$$

Petersen et al. (2012):

$$\frac{S_e}{D} = \frac{S_c}{D}\left[1 - e^{-A_1(KC-A_2)}\right] \quad \text{(A4.15)}$$

$$A_1 = 0.03 + \frac{3}{4} {U_{cw}}^{2.6} \quad \text{(A4.16)}$$

$$A_2 = 6e^{(-4.7U_{cw})} \quad \text{(A4.17)}$$

$$U_{cw} = \frac{U_c}{U_c + U_m} \quad \text{(A4.18)}$$

where S_c is calculated for current alone, and KC is calculated for wave alone.

Scour time development prediction equations

Sumer and Fredsøe (2002) and Whitehouse (1998):

$$S(t) = S_e\left[1 - \left(e^{-t/T_c}\right)^n\right] \quad \text{(A4.19)}$$

$$T^* = \frac{\left(g(s-1){d_{50}}^3\right)^{0.5}}{D^2} T_c \quad \text{(A4.20)}$$

Rudolph et al. (2008):

$$\frac{S}{S_e} = 1 - e^{\left(-\frac{t}{T_c}\right)} \quad \text{(A4.21)}$$

where for waves:

$$T_{c,waves} \approx 10^3 D^2 {U_{bed}}^{-3} K_{mob} \quad \text{(A4.22)}$$

and for currents:

$$T_{c,current} \approx 10^3 D^2 V^{-3} K_{mob} \quad \text{(A4.23)}$$

$K_{mob}=1+10(\theta_{crit}/\theta)^2$. (A4.24)

Sheppard et al. (2004):

$$S(t) = a_1\left[1 - \frac{1}{(1+a_1 a_2 t)}\right] + a_3\left[1 - \frac{1}{(1+a_3 a_4 t)}\right] \quad \text{(A4.25)}$$

Or

$$S(t) = a_1[1 - e^{-a_2 t}] + a_3[1 - e^{-a_4 t}] \quad \text{(A4.26)}$$

Chang et al. (2004):

$$S = 0.08 K_\sigma K_v {T_c}^{-1.3} \frac{t}{t_e}, for\ 0 \le \frac{t}{t_e} \le T_c \quad \text{(A4.27)}$$

$$S = S_e - 0.27 K_\sigma K_v \left(\left(\frac{t}{t_e}\right)^{-1.3} + 0.41\right), for\ T_c \le \frac{t}{t_e} \le 0.04 \quad \text{(A4.28)}$$

$$S = S_e - 1.1 K_\sigma K_v \left(\frac{t}{t_e} - 2.22\left(\frac{t}{t_e}\right)^{0.45} + 1.22\right), for\ 0.04 \le \frac{t}{t_e} \le 1 \quad \text{(A4.29)}$$

where

$$T_c = \left(\frac{S_e}{0.35 K_\sigma K_v} - 0.31\right)^{-3.33} \quad \text{(A4.30)}$$

K_σ=1 for uniform sand

$$K_v = \frac{V}{V_{cr}} - 0.4 \quad \text{(A4.31)}$$

Melville and Chiew (1999):

$$S = K_{hD} K_v K_d K_s K_\alpha K_G K_t \quad \text{(A4.32)}$$

where the K factors are derived from envelope curves fitted to lab data.

$$K_t = exp\left\{-0.03\left|\frac{V_{cr}}{V} ln\left(\frac{t}{t_e}\right)\right|^{1.6}\right\}, for\ \frac{V}{V_{cr}} \le 1 \quad \text{(A4.33)}$$

There are two equations for t_e depending on the ratio of h/D. Both are for $V/V_{cr}>0.4$.

$$t_e(days) = 48.26\frac{D}{V}\left(\frac{V}{V_{cr}} - 0.4\right), for\ \frac{h}{D} > 6 \quad \text{(A4.34)}$$

$$t_e(days) = 30.89\frac{D}{V}\left(\frac{V}{V_{cr}} - 0.4\right)\left(\frac{h}{D}\right)^{0.25}, for\ \frac{h}{D} < 6 \quad \text{(A4.35)}$$

$$K_{hD} = 2.4D, for\ \frac{D}{h} < 0.7 \quad \text{(A4.36)}$$

$$K_v = \frac{V-(V_a-V_{cr})}{V_{cr}}, for\ \frac{V-(V_a-V_{cr})}{V_{cr}} < 1 \quad \text{(A4.37)}$$

$K_d=1$ *for* $D/d_{50}>25$ (A4.38)

Oliveto and Hager (2002):

$$Z = 0.068NF_d{}^{1.5}\log(T_c), for\ F_{di} < F_d < F_{dt} \quad \text{(A4.39)}$$

where

$$T_c = \left[\sigma_g{}^{1/3}\left((s-1)gd_{50}\right)^{1/2}/D^{2/3}h^{1/3}\right]t \quad \text{(A4.40)}$$

N=1 for a pier, F_d is the densimetric particle Froude number:

$$F_d = \frac{\sigma_g{}^{-1/3}V}{((s-1)gd_{50})^{1/2}} \quad \text{(A4.41)}$$

F_{di} is inception densimetric particle Froude number and F_{dt} is the threshold densimetric particle Froude number.

Z is relative scour depth defined as $Z = \frac{S}{(D^{2/3}h^{1/3})}$

Lança et al. (2013):

$$\frac{S}{S_e} = 1 - e^{[-a_1(Vt/D)^{a_2}]} \quad \text{(A4.42)}$$

$$a_1 = 1.22\left(\frac{D}{d_{50}}\right)^{-0.764} \quad \text{(A4.43)}$$

$$a_2 = 0.09\left(\frac{D}{d_{50}}\right)^{0.244} \quad \text{(A4.44)}$$

Zhao et al. (2012):

$$S(t) = S_e\frac{t}{t+T_c} \quad \text{(A4.45)}$$

Comparison of scour time prediction equations with experimental data

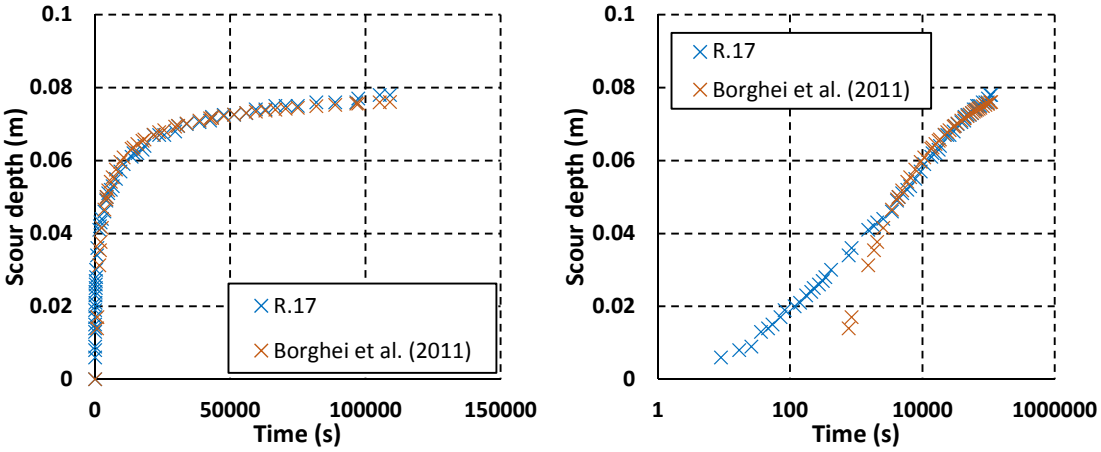

Figure A4.1 Linear and logarithmic plots of Borghei et al. (2011) equation compared to test R.17

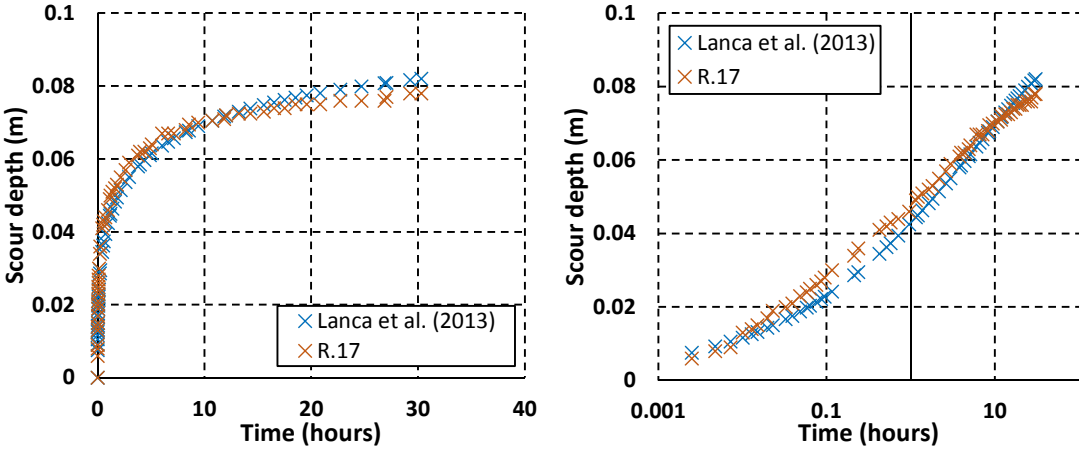

Figure A4.2 Linear and logarithmic plots of Lanca et al. (2013) equation compared to test R.17

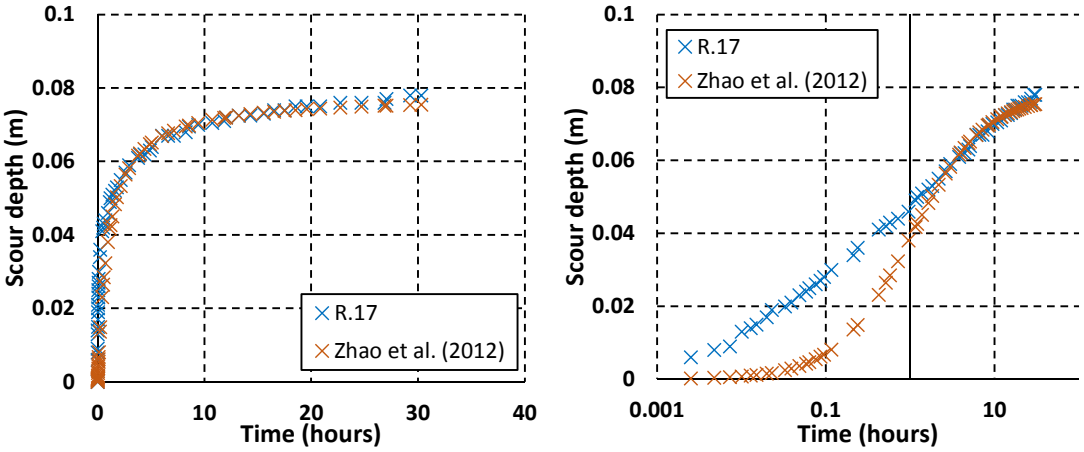

Figure A4.3 Linear and logarithmic plots of Zhao et al. (2012) equation compared to test R.17

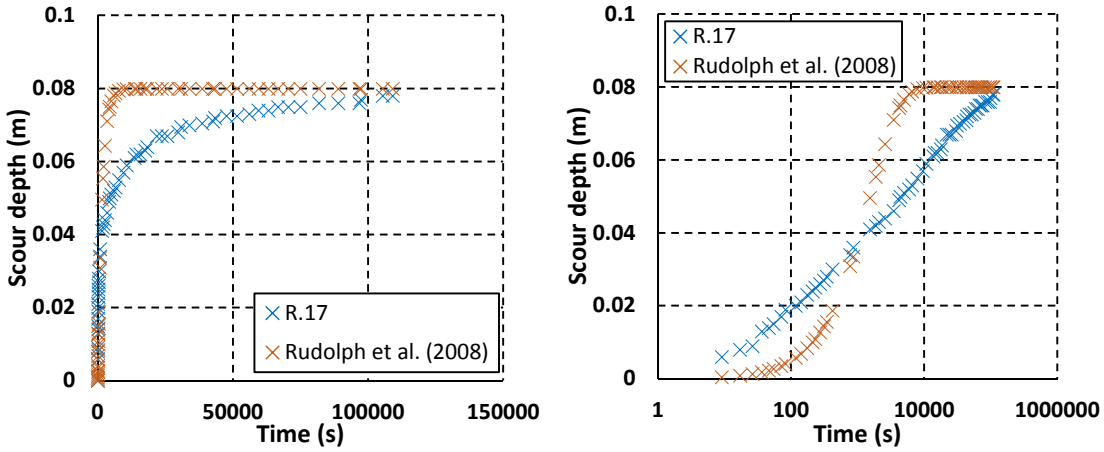

Figure A4.4 Linear and logarithmic plots of Rudolph et al. (2008) equation compared to test R.17

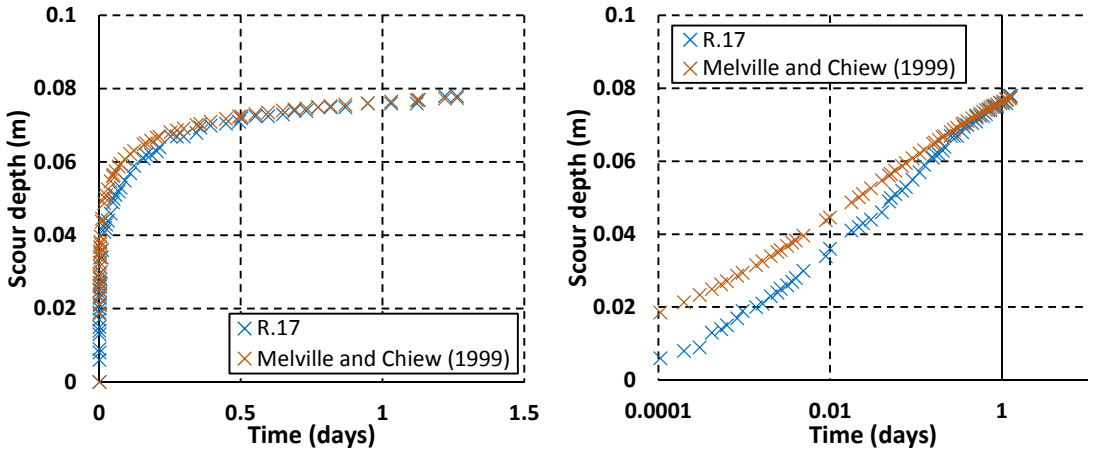

Figure A4.5 Linear and logarithmic plots of Melville and Chiew (1999) equation compared to test R.17

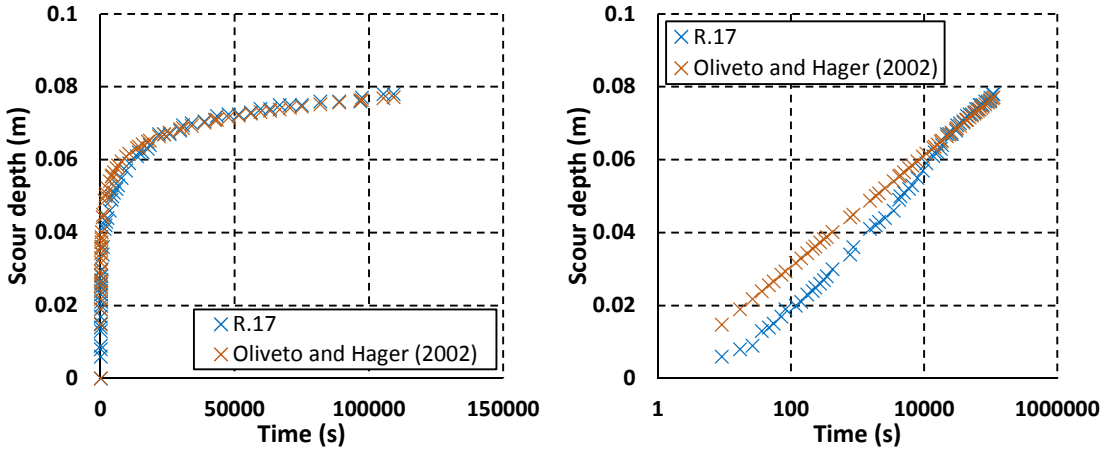

Figure A4.6 Linear and logarithmic plots of Oliveto and Hager (2002) equation compared to test R.17

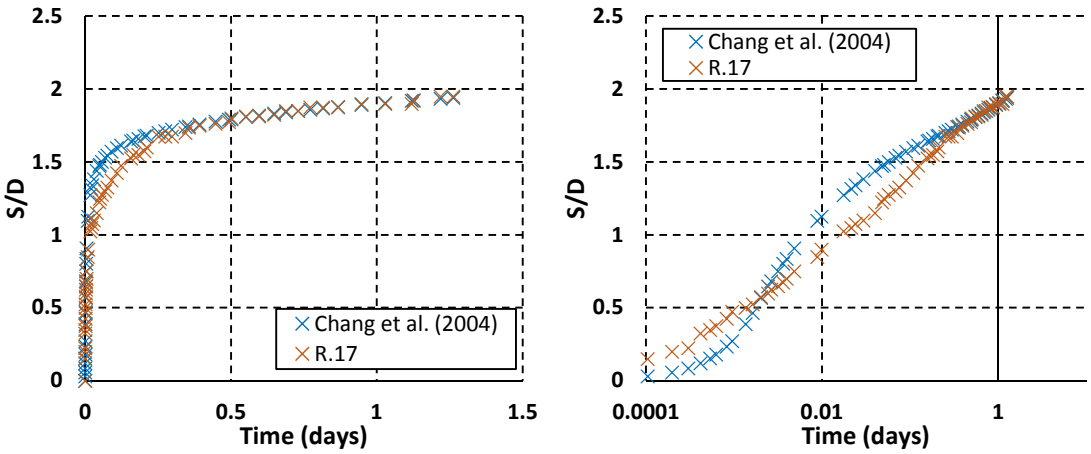

Figure A4.7 Linear and logarithmic plots of Chang et al. (2004) equation compared to test R.17

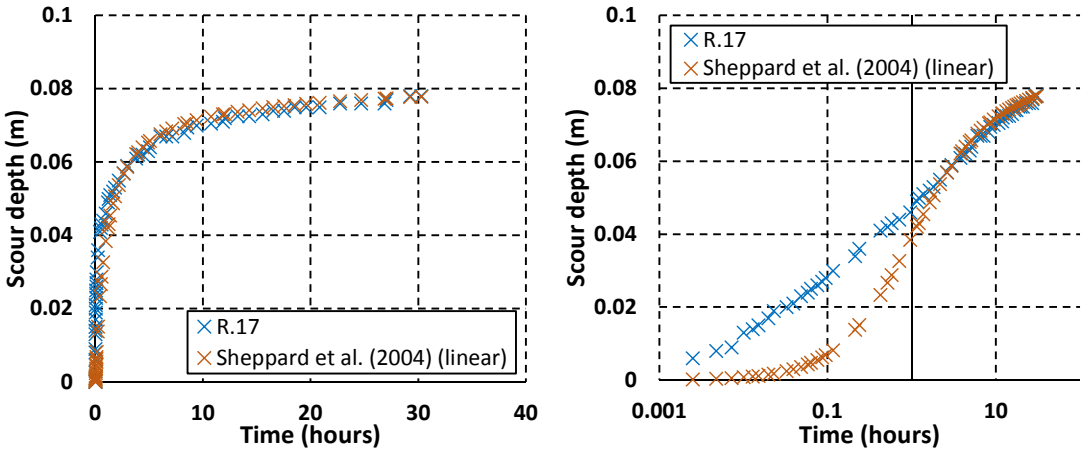

Figure A4.8 Linear and logarithmic plots of Sheppard et al. (2004) linear equation compared to test R.17

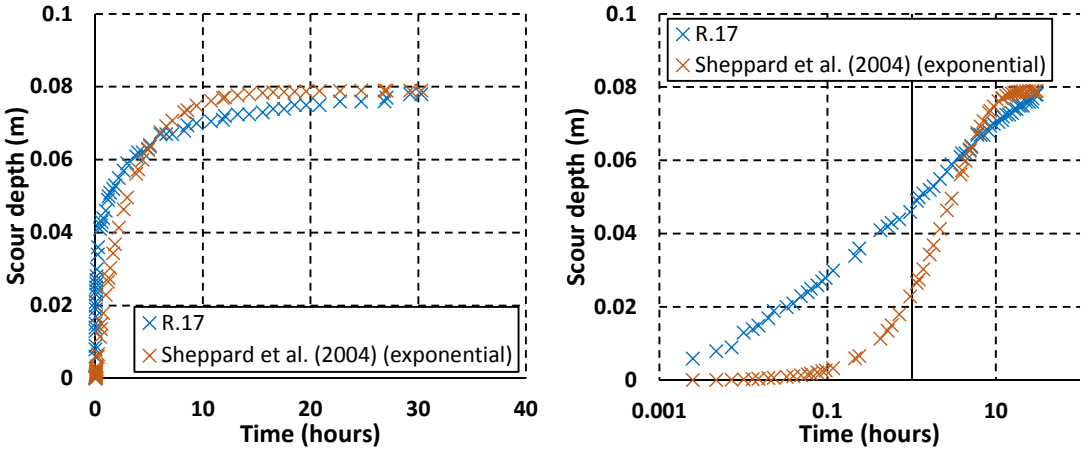

Figure A4.9 Linear and logarithmic plots of Sheppard et al. (2004) exponential equation compared to test R.17

Appendix 5 - Sediment testing

Permeability calculation

Equation for falling head tests:

$$k = \frac{a_x L \ln(h_0/h_1)}{A_x t} \quad \text{(A5.1)}$$

Equation for constant head tests:

$$k = \frac{qL}{A_x \Delta h} \quad \text{(A5.2)}$$

L is length of test section, A_x is cross-sectional area of test section, a_x is the cross-sectional area of the standpipe, h_0 is initial head level, h_1 is final head level, q is flow rate, Δh is head difference, t is time.

Density pot locations

Table A5.1 Test R.26, coarse sand, measurements are to edge of sand (pot inside edge)

pot number	streamwise	str measured to	cross-stream	crs measured to
1	2	farside glass	11.5	join false bed
2	3.1	farside glass	10.2	from pot 1
3	1.3	nearside glass	10.9	join false bed
4	2.5	nearside glass	41.6	join false bed
5	1.7	farside glass	51.4	join false bed
6	2.35	nearside glass	59.2	join false bed
7	8.2	nearside glass	11.9	from pot 8
8	7.8	nearside glass	13.1	from pot 9
9	8.3	nearside glass	13.1	join false bed

Table A5.2 Test R.28 (dense sand)

pot number	streamwise	str measured to	cross-stream	crs measured to
1	15	nearside glass	13	false bed join
2	13.9	farside glass	22.5	false bed join
3	14.5	nearside glass	45.5	false bed join
4	14.5	nearside glass	38.5	false bed join
5	14.4	nearside glass	50.5	false bed join
6	15	farside glass	62.5	false bed join
7	9.1	nearside glass	55	false bed join
8	8	nearside glass	36.5	false bed join
9	8.4	nearside glass	12.5	false bed join

Initial sands used

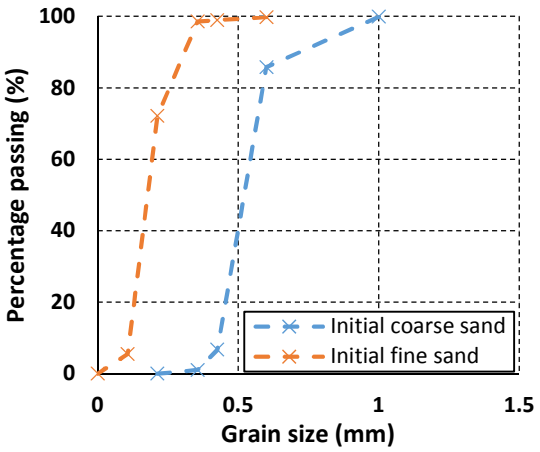

Figure A5.1 initial fine and coarse sand grain size distributions

In the very first tests conducted in the small flume slightly different fine and coarse sands were used. The distributions of these sands are shown in Figure A5.1. These sands were used based on what was available in the laboratory prior to the selection and ordering of sand for the main series of tests. The initial sands were used for test series P-1, and the original fine sand was also used in test series P-2. The sands used in later tests were chosen to have similar grain distributions and median grain size to the initial sands within the constraints of what was available commercially as it was not possible to repurchase the same sand. The parameters of the distributions for the initial sands used are given in table A5.3. The initial fine sand is a little coarser and the coarse sand is a little finer, than the main sands used in the project based on the d_{50} values. The initial sands have larger C_u values than the later sands used but slightly lower geometric standard deviations.

Table A5.3 Grading parameters for initial fine and coarse sands used in small flume

	D50 mm	D90 mm	D10 mm	Uniformity	D84	D16	σ_g
Fine	0.17	0.29	0.116	2.50	0.25	0.13	1.38675
Coarse	0.5	0.63	0.415	1.52	0.58	0.44	1.148121

Factory data for fine and coarse sands used in main test series:

MINERALS MARKETING

17 Carter Close, Nantwich,
Cheshire, CW5 5GD

Email: enquiries@mineralsmarketing.com
Phone: +44 (0) 1270 625573
Fax: +44 (0) 8709 127479

Chelford 16/30 Product Information

Source	**Lower Withington, Cheshire**
Geology	**Glacial Deposit of the Pleistocene Period**
Description	**Washed and Graded High Silica Sand**

Chemical Analysis:

	Typical %
SiO_2	98.31
Fe_2O_3	0.12
Al_2O_3	0.63
K_2O	0.25
LOI	0.26

Physical Analysis:

Microns	Typical % Retained Each Sieve	Limit %	Typical % Cumulative Retained	Limit %	Typical % Cumulative Passing	Limit %
1180	0.0		0.0		100.0	
1000	0.2		0.2	5.0 Max	99.8	95.0 Min
850	4.3		4.5		95.5	
710	20.2		24.7		75.3	
600	42.1		66.8		33.2	
500	31.4		98.2	95.0 Min	1.8	5.0 Max
425	1.7		99.9		0.1	
-425	0.1		100.0		0.0	

	Typical	
Nominal Effective Size	0.53mm	D10
Uniformity Coefficient	1.29	D60/D10
Modal Size	0.64	D60
Grain Shape	Rounded	
Loose Bulk Density	1569	Kg/M3

The information contained in this sheet does not constitute a specification, but is issued in good faith.
A specification can be issued if required.

MINERALS MARKETING

17 Carter Close, Nantwich,
Cheshire, CW5 5GD

Email: enquiries@mineralsmarketing.com
Phone: +44 (0) 1270 625 573
Fax: +44 (0) 8709 127 479

Minerals Marketing RHT Product Information

Source	**Redhill, Surrey**
Geology	**Lower Green Sand from the Cretaceous Period**
Description	**Washed and Graded Silica Sand**

Chemical Analysis:

	Typical %	Limit %
SiO_2	99.50	99.0 Min
Fe_2O_3	0.04	0.05 Max
Al_2O_3	0.09	0.12 Max
K_2O	0.01	
LOI	0.13	

Physical Analysis:

Microns	Typical % Retained Each Sieve	Limit %	Typical % Cumulative Retained	Limit %	Typical % Cumulative Passing	Limit %
1000	0.0		0.0		100.0	
710	0.3		0.3		99.7	
500	1.0		1.3	8.0 Max	98.7	92.0 Max
355	8.5		9.8		90.2	
250	30.0		39.8		60.2	
180	36.8		76.6		23.4	
125	21.0		97.6		2.4	
90	2.0		99.6		0.4	
63	0.3		99.9	99.5 Min	0.1	0.5 Max
-63	0.1	0.5 Max				

	Typical	Range / Limit
Average Grain Size	230 Microns	
Grain Shape	Sub Rounded	
Loose Bulk Density kg/m3	1430	

The information contained in this sheet does not constitute a specification, but is issued in good faith.
A specification can be issued if required.

Appendix 6 - Core Samples

Locations of core samples for each test used in the analysis:

C.90.11

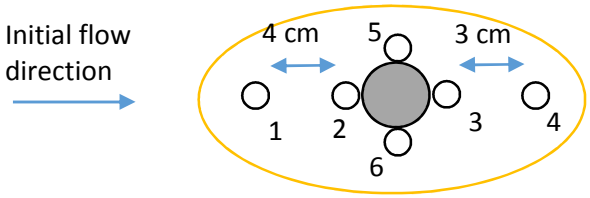

C.90.12

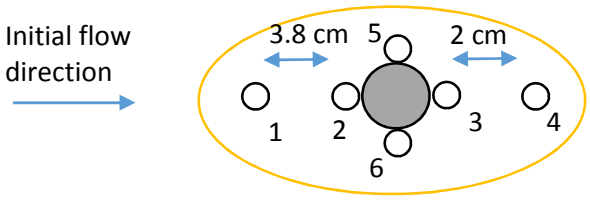

C.90.13

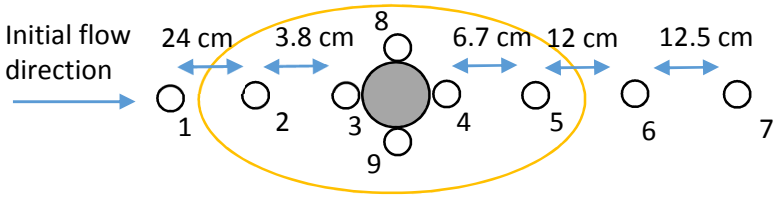

R.29.3

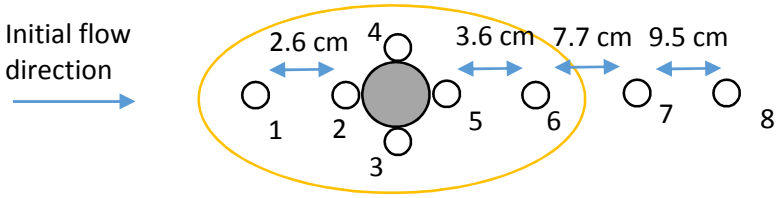

Additional core sample data:

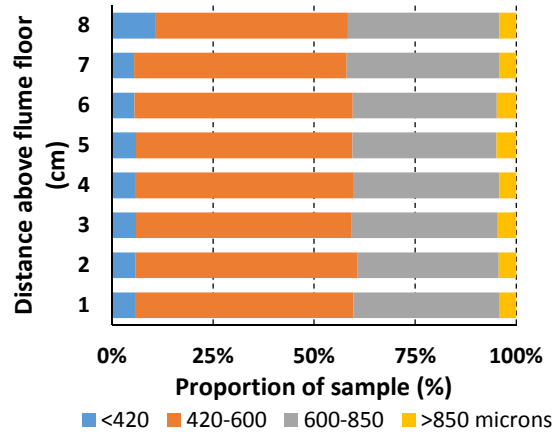

a)

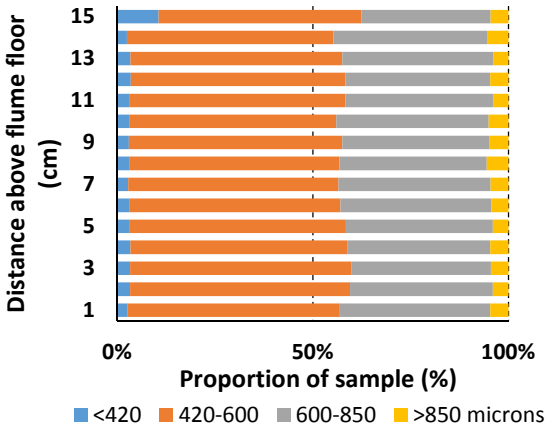

b)

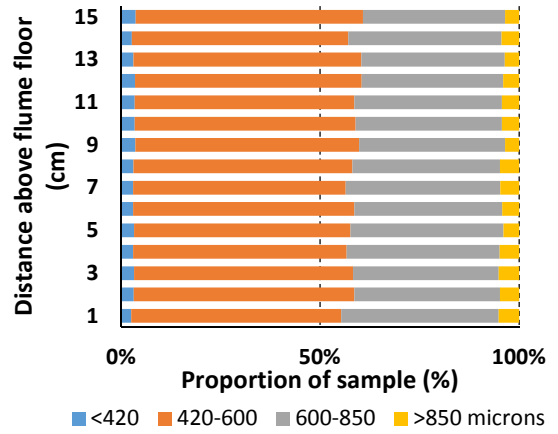

c)

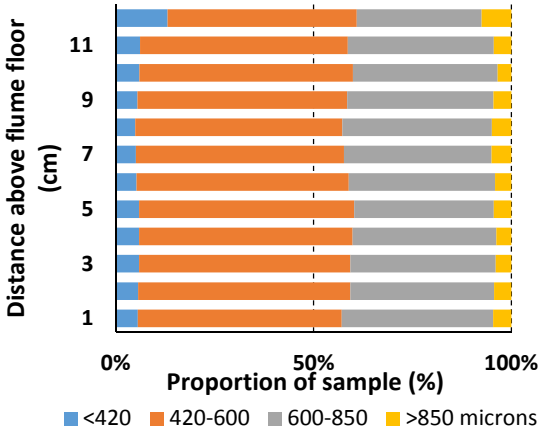

d)

Figure A6.1 core samples for test C.90.11, a) sample 2 b) sample 3 c) sample 4 d) sample 5

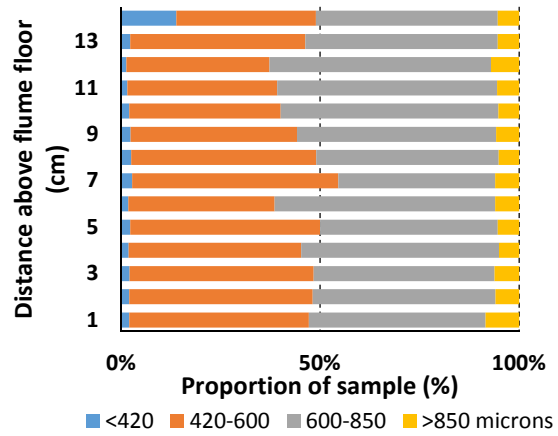

a)

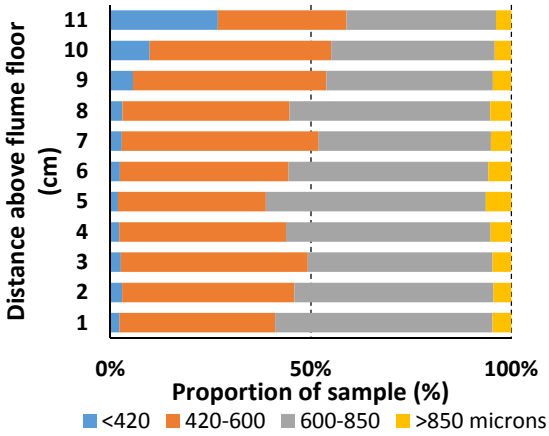

b)

Figure A6.2 core samples for test C.90.12, a) sample 3 b) sample 5

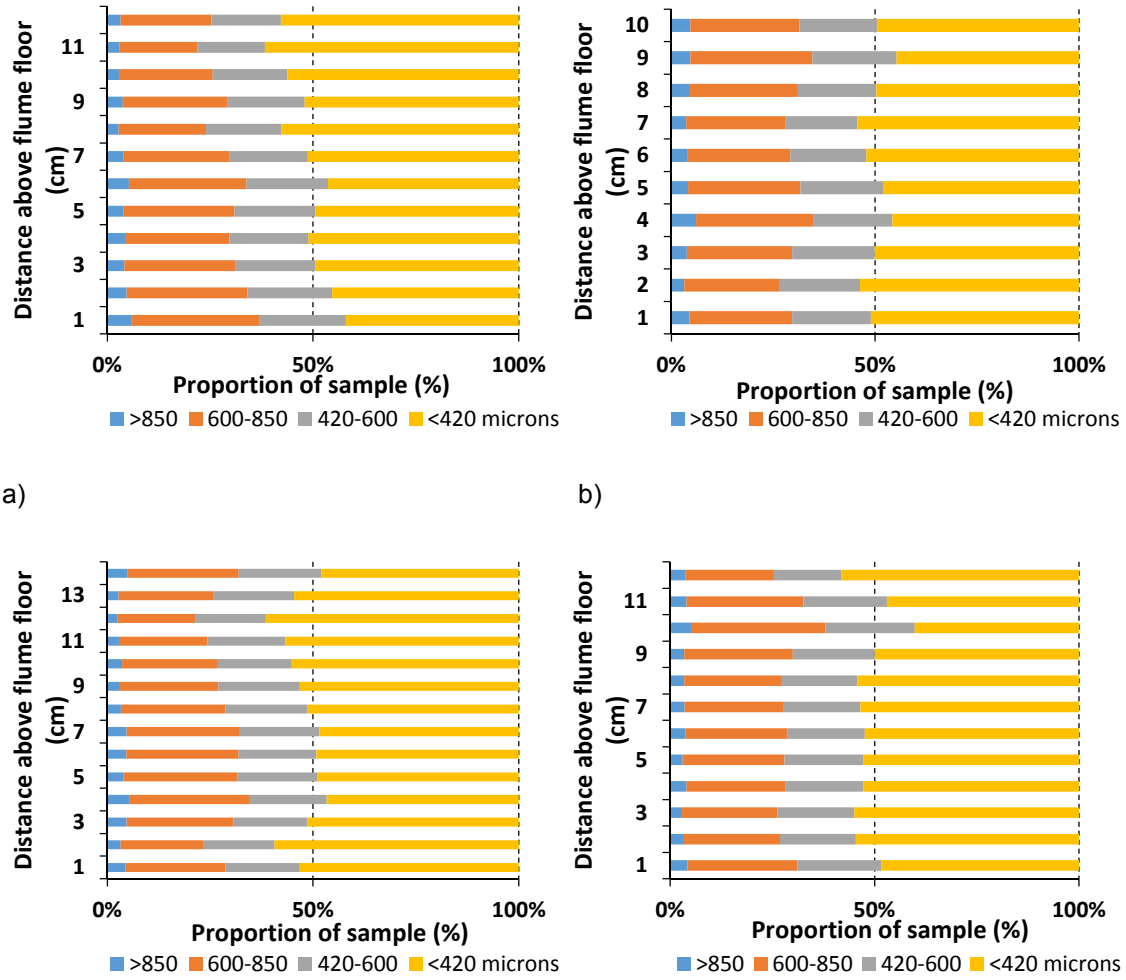

Figure A6.3 Core samples for C.90.13, a) sample 2 b) sample 3 c) sample 4 d) sample 5

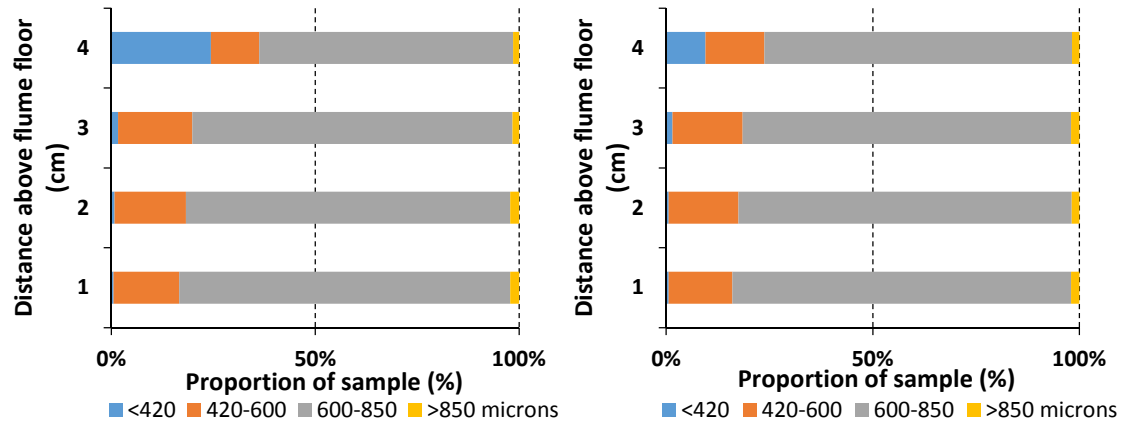

a)

b)

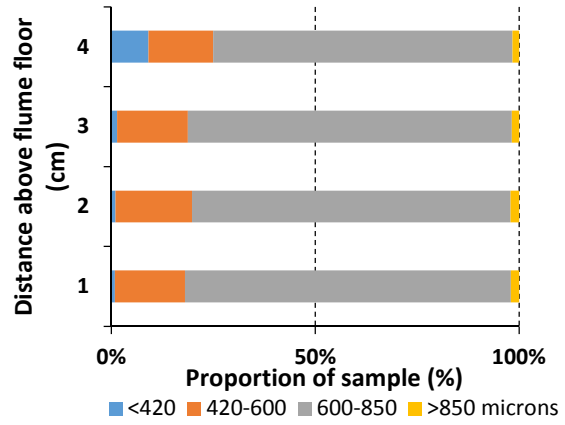

c)

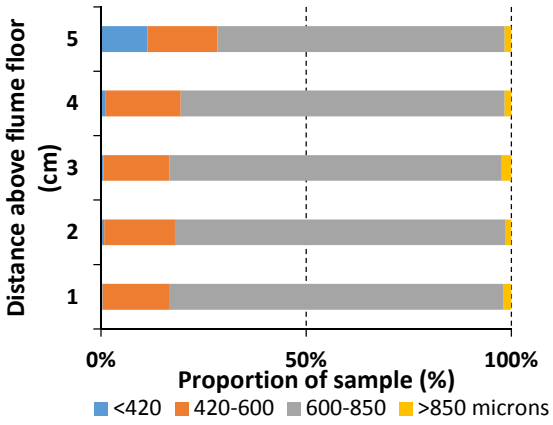

d)

Figure A6.4 core samples for test R.29.3, a) sample 2 b) sample 3 c) sample 4 d) sample 5

Appendix 7 - Echosounder

Echosounder profiles from small flume tests

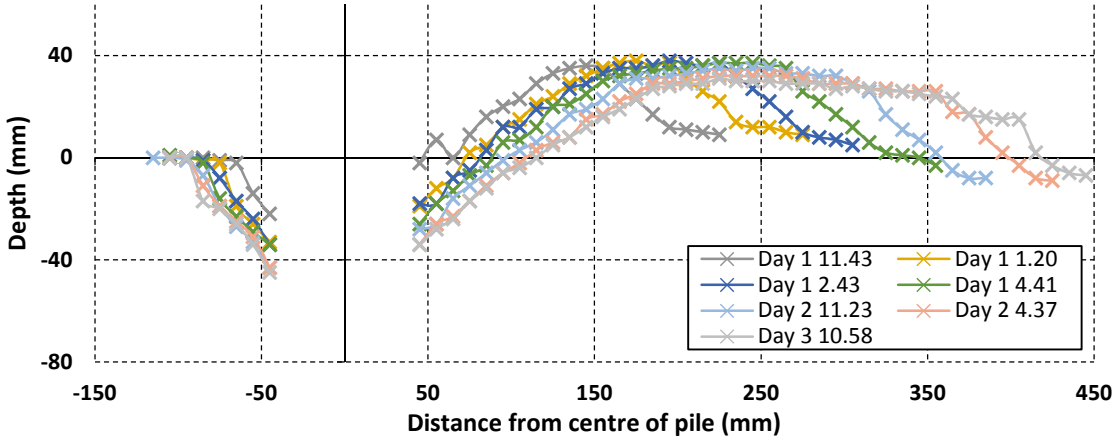

Figure A7.1 50% mixed sand test R.15.

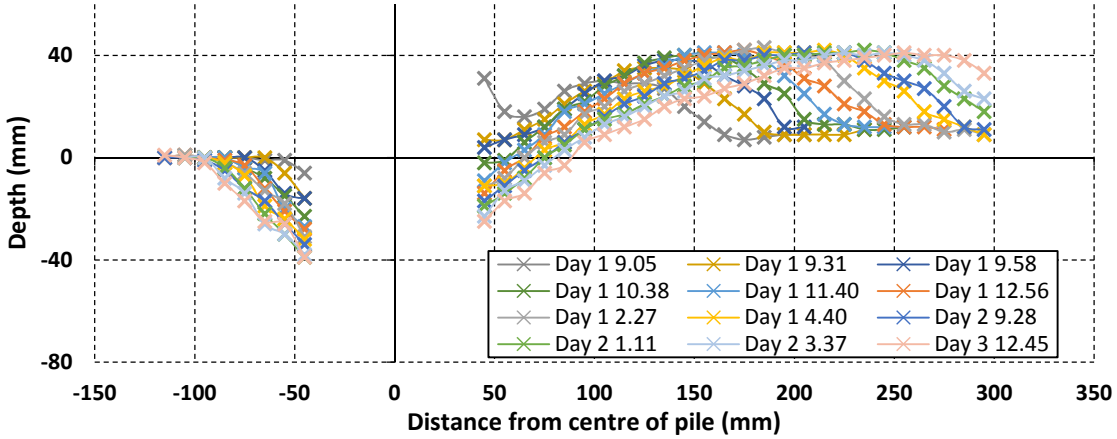

Figure A7.2 Test R.16 coarse sand.

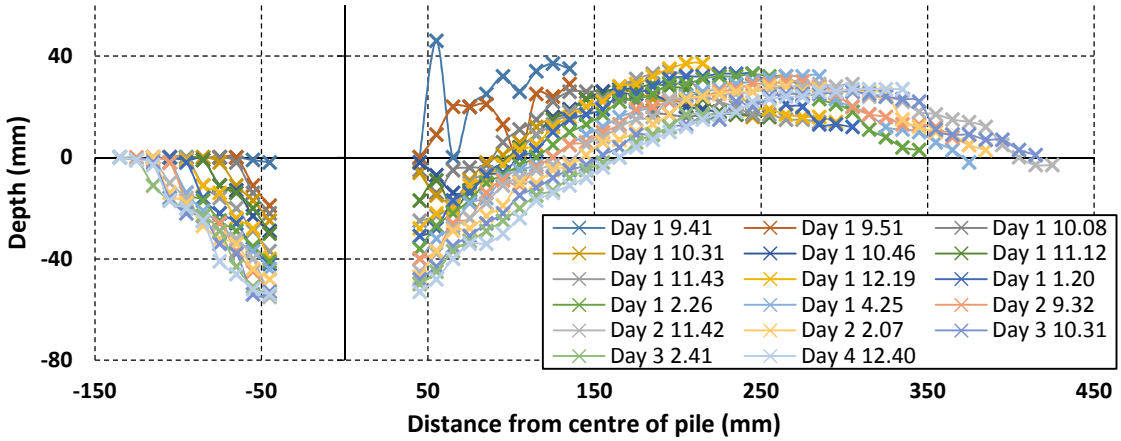

Figure A7.3 Test R.17 fine sand.

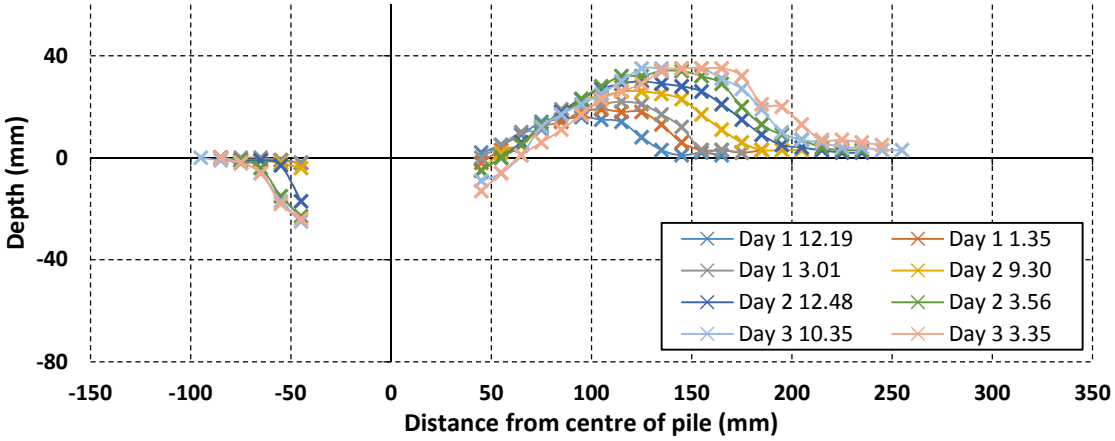

Figure A7.4 Test R.18 slow velocity 50% mixed sand.

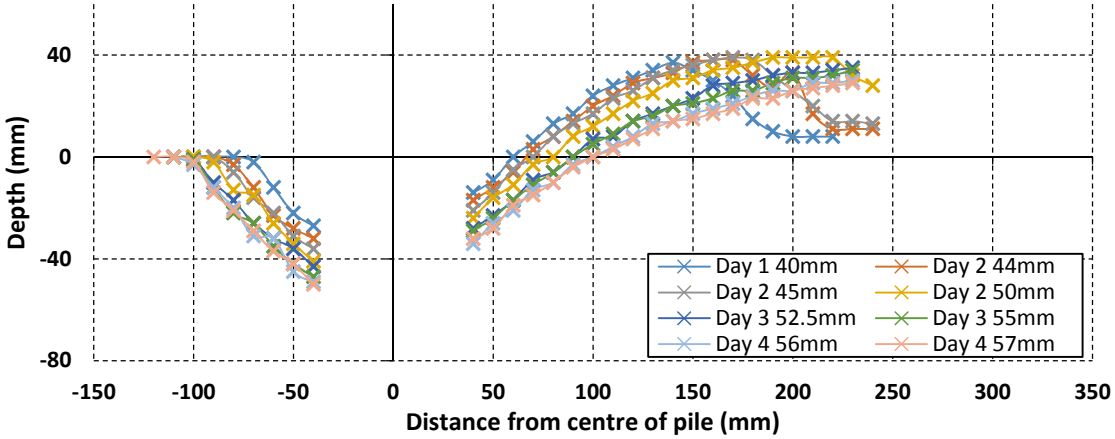

Figure A7.5 90% coarse sand test R.23.

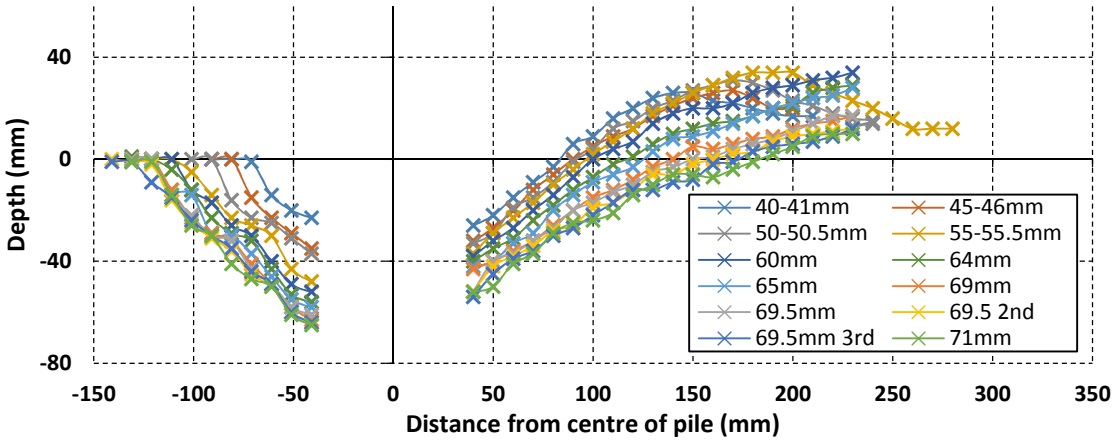

Figure A7.6 Layered 70 mm fine sand layer over coarse sand test R.24.

Repeatability of measurements

In order to assess the quality of the echosounder data a comparison is presented of profiles from tests R.29.1, 2, 3 and 4 which were conducted under the same conditions and which exhibited excellent agreement between the scour time development curves at the pile. Figures A7.7-A7.9 are for stages of the tests when the scour depth at the pile was 40 mm, 50 mm and 60 mm respectively. These figures give an indication of the extent of agreement that can be expected and allow an estimate of the measurement uncertainty to be made. This suggests that the echosounder methodology is repeatable, and that the scour hole shape is not subject to random variation but is directly related to the depth of scour at the pile. Small differences in the two curves are most likely due to the measurement errors caused by spurious echos and sharp changes in the bed profile. Small errors may also be induced by discrepancies in the x-y positioning of the echosounder.

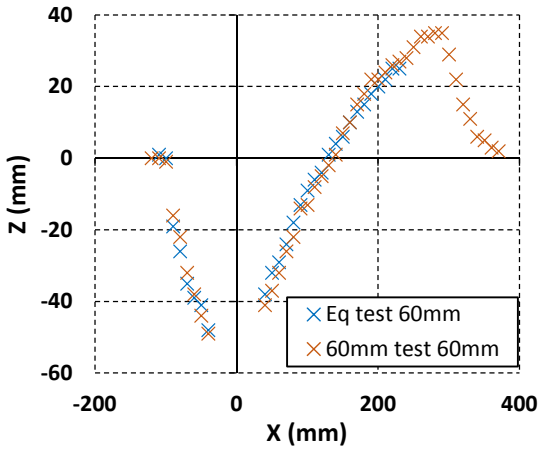

Figure A7.7 Echosounder profiles from end of fine over coarse sand layered test run to S=60 mm, L_u=40 mm, small flume.

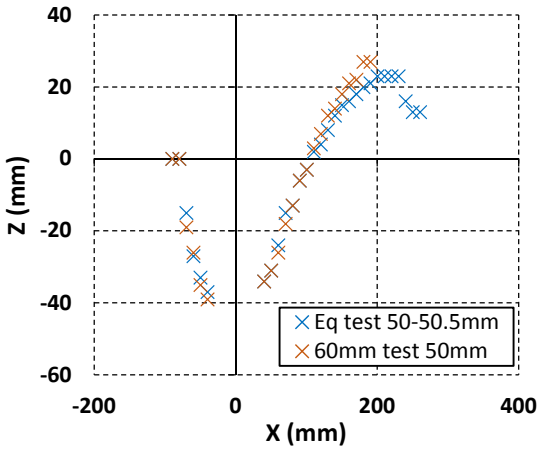

Figure A7.8 Echosounder profiles from end of fine over coarse sand layered test run to S=50 mm, L_u=40 mm, small flume.

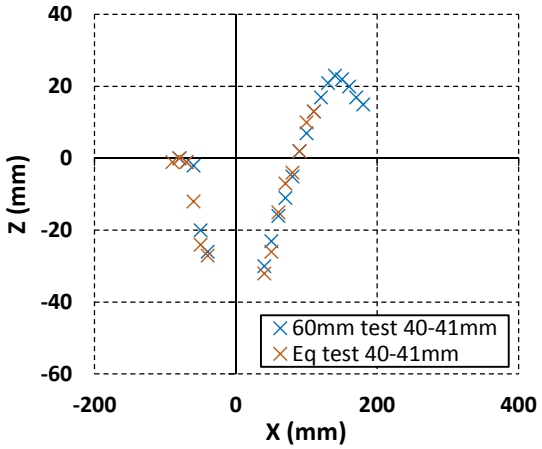

Figure A7.9 Echosounder profiles from end of fine over coarse sand layered test run to S=40 mm, L_u=40 mm, small flume.

Scour extents

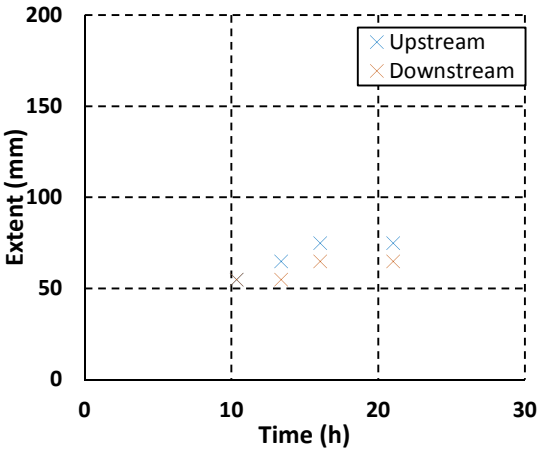

Figure A7.10 Scour extent development, test R.18 slow velocity 50% mixed sand.

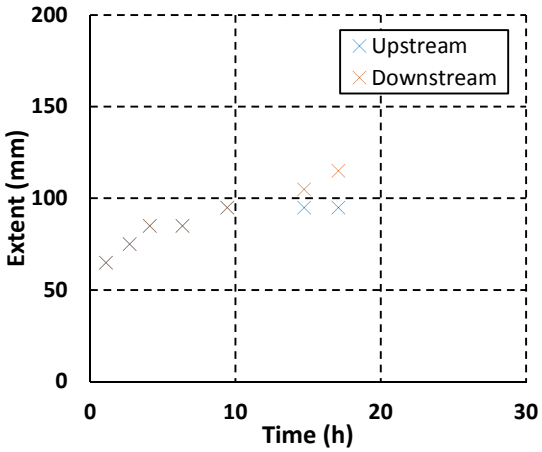

Figure A7.11 Scour extent development, test R.15 50% mixed sand.

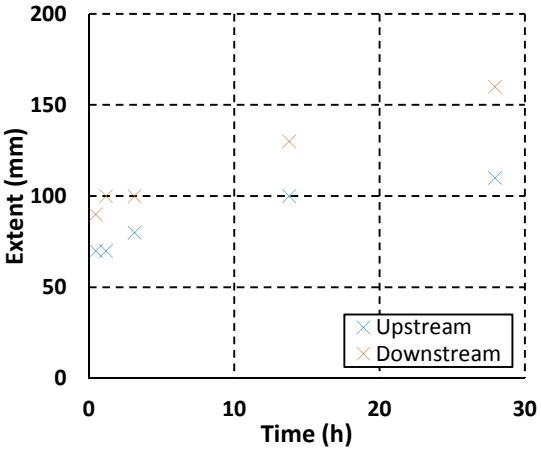

Figure A7.12 Scour extent development, test R.29 40mm layered fine over coarse sand.

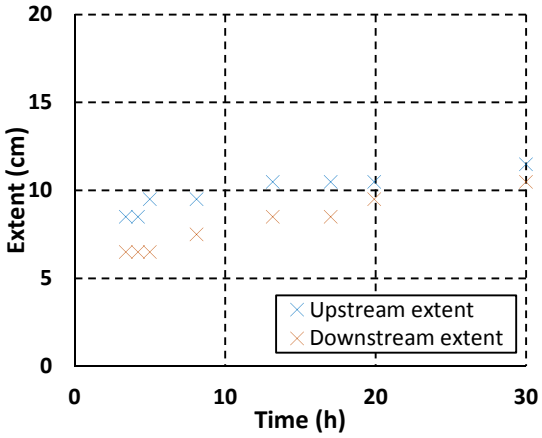

Figure A7.13 Scour extent development, test R.28 dense coarse sand.

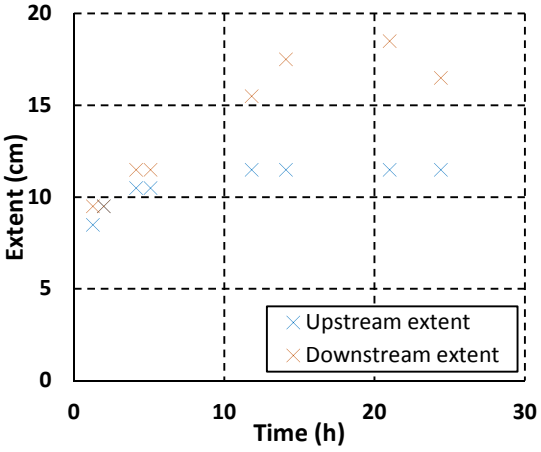

Figure A7.14 Scour extent development, test R.19 55mm layered fine over coarse sand.

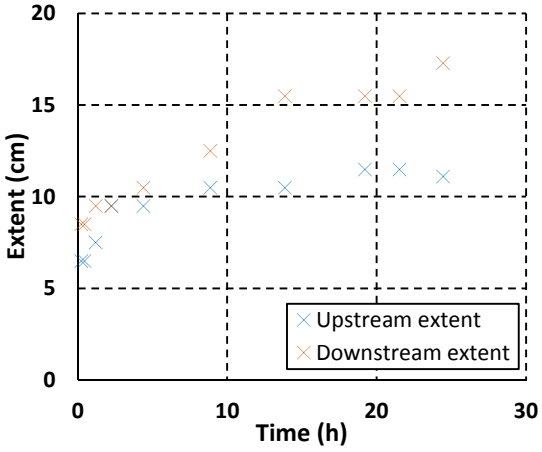

Figure A7.15 Scour extent development, test R.20 fine-coarse-fine layered sand.

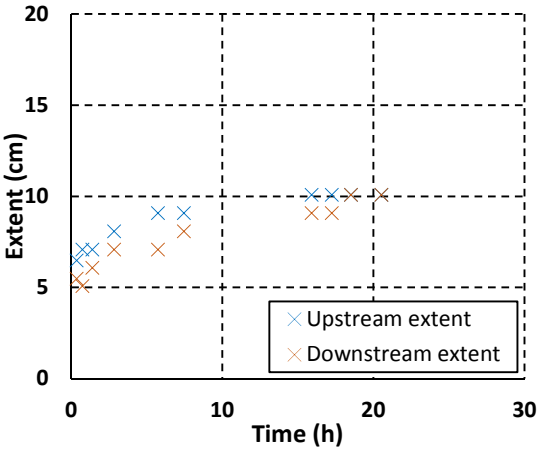

Figure A7.16 Scour extent development, test R.21 coarse-fine-coarse layered sand.

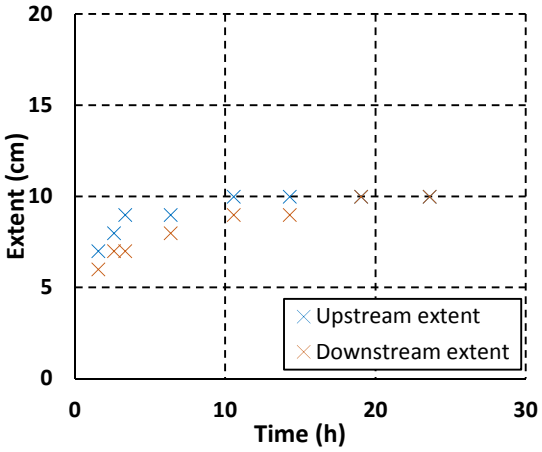

Figure A7.17 Scour extent development, test R.23 90% coarse sand.

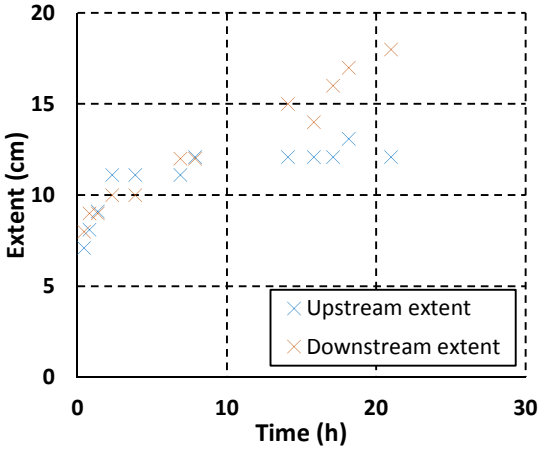

Figure A7.18 Scour extent development, test R.24 layered 70 mm fine sand layer over coarse sand.

Appendix 8 - Photogrammetry

Theory and calibration

Photogrammetry is a technique where 3D measurements of an object are obtained from photographs of the object. Photogrammetry is based on a mathematical model of the optical system between the camera and the object being photographed. The basic model is known as the Pinhole Camera model. A very simple camera can be made by making a pinhole in a sheet of paper, so that only a single (or very few) light rays can pass from each point on the object through the hole. This means that an inverted image of the object is projected onto a sheet placed behind the pinhole. This is only possible because effectively one ray of light has come through the pinhole from each point on the object, thereby enabling an image to be defined. A key feature of this model is that the light travels in a straight line from each point on the object to the corresponding point on the image plane through the pin hole. This condition is true when light travels through a single media, i.e. air where there is no change in refractive index. This characteristic enables the point on an object to be linked through a geometric relationship to its associated point in the image using the principle of colinearity. A more detailed introduction and treatment of this topic can be found in Mikhail et al. (2001) and Cooper and Robson (1996).

Following Cooper and Robson (1996), one method for linking the 3D coordinates of a point in the object space to the 2D coordinates of the equivalent point in the image space is given in equation A8.1. This equation is obtained through the principle of colinearity i.e. that light travels in a straight line between the object point and image point through the pin hole camera (perspective centre). In the object space coordinate system, the point on the object is given by the coordinates of the camera plus the distance vector from the camera position to the point on the object. However, this vector lies on the coplanarity line so it can instead by defined in terms of the vector from the camera to the image plane, and so by measuring the coordinates of the point in the image plane, the points in the object space can be determined.

$$\boldsymbol{X}_A = \boldsymbol{X}_o - \mu \boldsymbol{R}^t \boldsymbol{x}_a \tag{A8.1}$$

where μ is a scaling factor, and

$$\boldsymbol{X}_A = \begin{bmatrix} X_A \\ Y_A \\ Z_A \end{bmatrix} \tag{A8.2}$$

is the 3D coordinates of any point on the object being photographed and

$$\boldsymbol{X}_O = \begin{bmatrix} X_O \\ Y_O \\ Z_O \end{bmatrix} \tag{A8.3}$$

is the 3D coordinates of the camera location at which the image was taken.

$$\boldsymbol{x_a} = \begin{bmatrix} x_a \\ y_a \\ -c \end{bmatrix} \tag{A8.4}$$

is the 2D coordinates of the measurement points in the image plane. C is the principle distance, (usually equal to the focal length).

$$\boldsymbol{R} = \begin{bmatrix} r_{11} & r_{12} & r_{13} \\ r_{21} & r_{22} & r_{23} \\ r_{31} & r_{32} & r_{33} \end{bmatrix} \tag{A8.5}$$

is the rotation matrix for the orientation of the camera where:

$$r_{11} = \cos\varphi \cos\kappa \tag{A8.6}$$
$$r_{12} = \sin\omega \sin\varphi \cos\kappa + \cos\omega \sin\kappa \tag{A8.7}$$
$$r_{13} = -\cos\omega \sin\varphi \cos\kappa + \sin\omega \sin\kappa \tag{A8.8}$$
$$r_{21} = -\cos\varphi \sin\kappa \tag{A8.9}$$
$$r_{22} = -\sin\omega \sin\varphi \sin\kappa + \cos\omega \cos\kappa \tag{A8.10}$$
$$r_{23} = \cos\omega \sin\varphi \cos\kappa + \sin\omega \cos\kappa \tag{A8.11}$$
$$r_{31} = \sin\varphi \tag{A8.12}$$
$$r_{32} = -\sin\omega \cos\varphi \tag{A8.13}$$
$$r_{33} = \cos\omega \cos\varphi \tag{A8.14}$$

and ω, φ, and κ are rotation angles about the x, y and z axes respectively.

To solve equation A8.1 a minimum of 4 known 3D coordinates are needed in the object space. This enables the 6 camera position parameters for each photograph to be determined. A minimum of two photographs taken from different locations are needed in order to then solve for the unknown 3D coordinates of other points in the object space. Determining the camera position parameters is a ‘calibration’ step as known points in the object space are used to determine the extrinsic camera parameters (camera position and rotation). For the known coordinates required in this step a flat plate or 3D object where points on the plate or object have been measured with high precision using another technique are often used. However, calibration can also be completed by having some known coordinates mixed in with the unknown ones desired to be measured, or calibration can be conducted prior to the measurement using a separate calibration object. In this case it is important to keep the intrinsic camera parameters constant (i.e no change to focal length, same camera etc.) between calibration and measurement. Further, the camera should be kept in the same position if the camera orientation (extrinsic) parameters are not wished to be recalculated.

In reality there are some deviations from this mathematical model of the pin hole camera due to the configuration of a real camera. The pinhole camera model assumes perfect central perspective projection, but this may not be quite true in a real camera and light paths will be refracted through the camera lens so that the colinearity condition is not quite true. It also assumes that the plane that the image is projected onto is perfectly flat. These deviations from the model assumptions can be accounted for by adding terms to the model to link the ideal

image coordinate calculated from the method above to the actual measured image coordinate so that:

$$x_{meas} = x_{ideal} + \delta r_x + \delta t_x + a_o y + a_a x \quad \text{(A8.15)}$$

$$y_{meas} = y_{ideal} + \delta r_y + \delta t_y \quad \text{(A8.16)}$$

where a_1 and a_2 are orthogonality and affinity terms, δr_x, δr_y are the radial lens distortions (x and y components of the radial displacement of a point in the image plane). The radial lens distortions have been shown to be closely modelled by a polynomial function:

$$\delta r_x = (K_1 r^3 + K_2 r^5 + K_3 r^7)(x/r) \quad \text{(A8.17)}$$

$$\delta r_y = (K_1 r^3 + K_2 r^5 + K_3 r^7)(y/r) \quad \text{(A8.17)}$$

and δt_x, δt_y are the tangential lens distortions in the x and y directions in the image plane,

$$\delta t_x = P_1(r^2 + 2x^2) + 2P_2 xy \quad \text{(A8.18)}$$

$$\delta t_y = P_2(r^2 + 2y^2) + 2P_1 xy \quad \text{(A8.19)}$$

where K_1, K_2, K_3, P_1 and P_2 are coefficients which depend on the focal length, x and y are the coordinates of the point in the image and r is the radial distance to the point in the image. Remondino and Fraser (2006) discuss the additional parameters in more detail. They note that although lots of different models have been tried, the above is the optimal formulation for digital camera calibration.

Equation A8.1 is solved using an iterative least squares approach and hence the most rigorous solution is obtained by simultaneously processing 3D coordinates of many points in the object space from a large number of photographs taken from different orientations. This is known as bundle adjustment. Remondino and Fraser (2006) note that accuracy increases with the number of measured points on an image (up to a few 10s of points). Also different roll angles, and a large number of well distributed object points are necessary for an accurate solution.

Appendix 9 - Wave data

Calibration graphs for wave probes

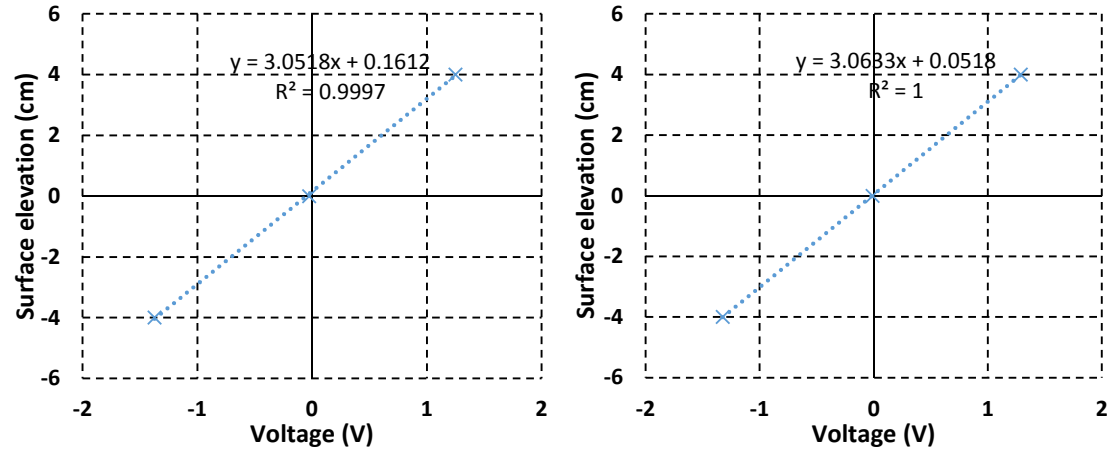

a)

b)

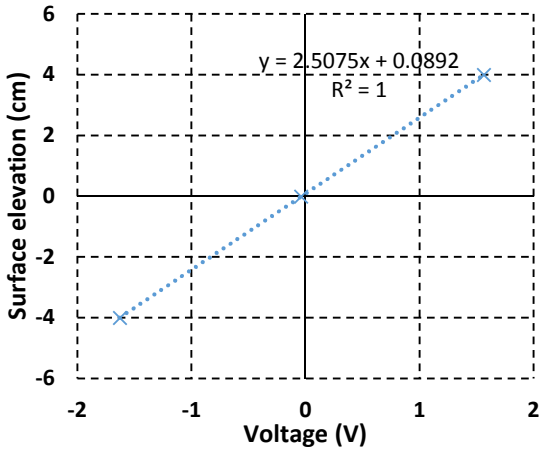

c)

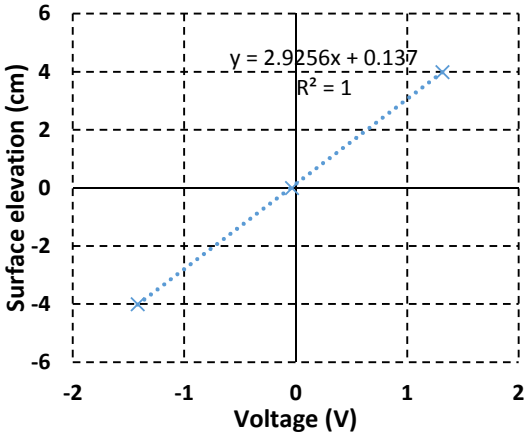

d)

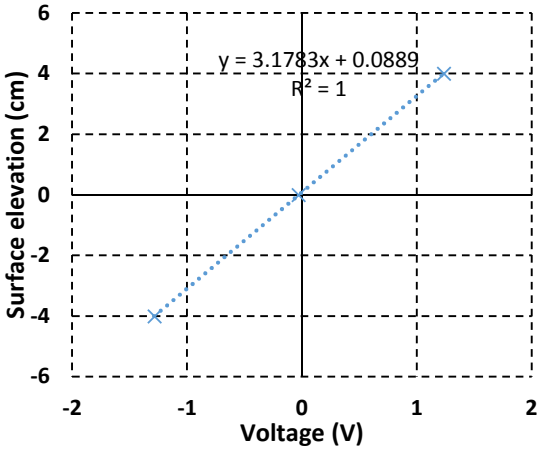

e)

Figure A9.1 Calibration graphs for each probe a) probe 1 b) probe 2 c) probe 3 d) probe 4 e) probe 5.

Wave surface elevation data

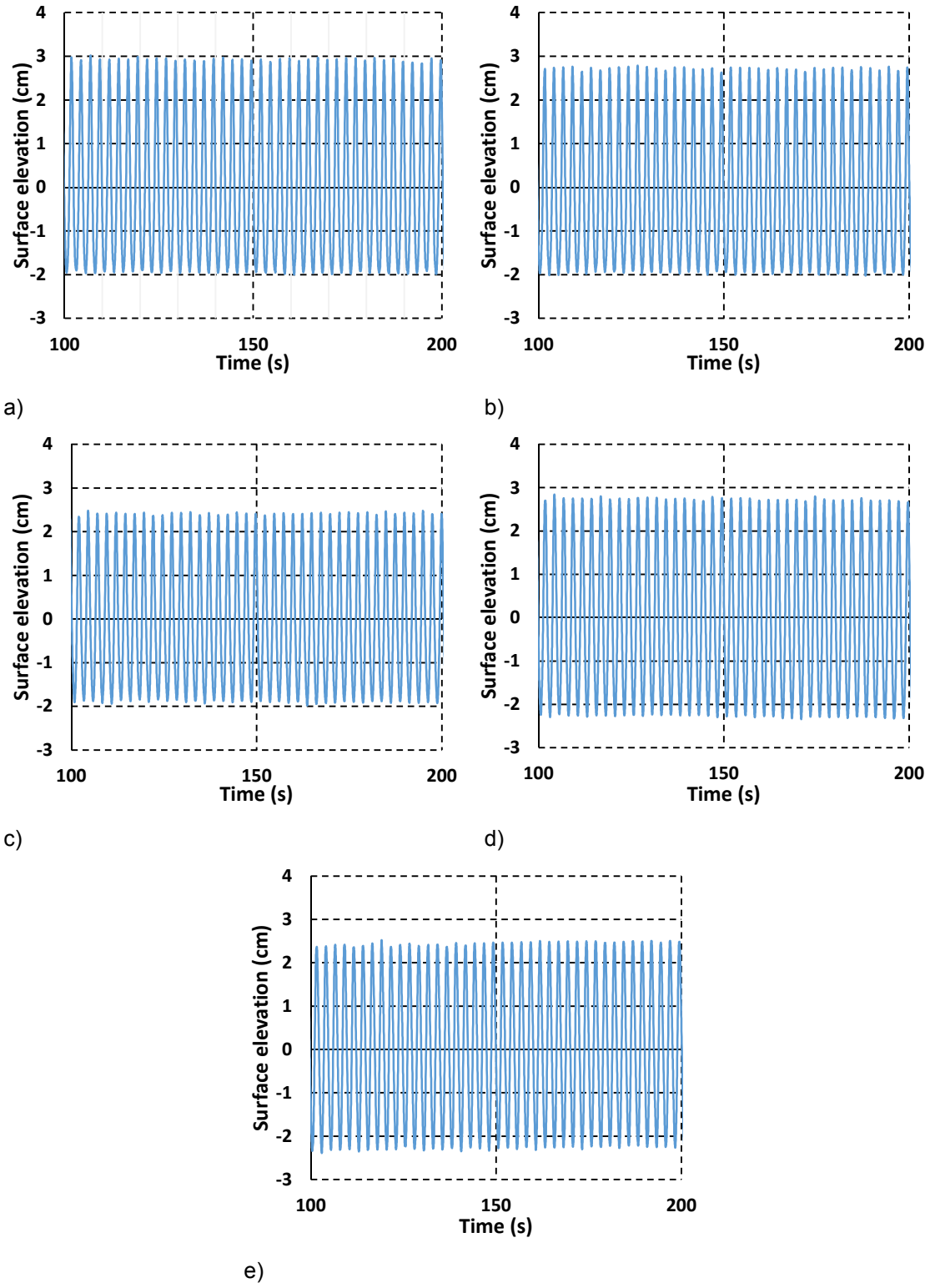

Figure A9.2 Surface elevation for each probe in wave flow used in test series C-2 a) probe 1 b) probe 2 c) probe 3 d) probe 4 e) probe 5

Table A9.1 Average wave height for each probe in Figure A9.2

probe	average wave height
1	4.85
2	4.61
3	4.30
4	5.02
5	4.76
average	4.71

Wave reflection

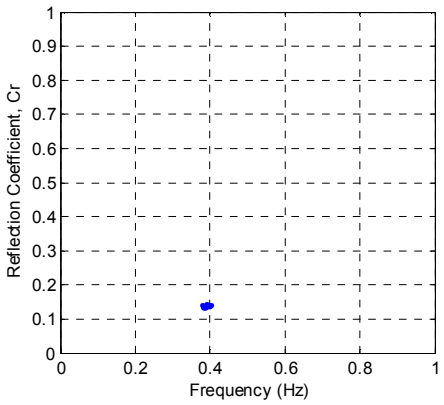

Figure A9.3 Reflection coefficient using probes 4 and 5

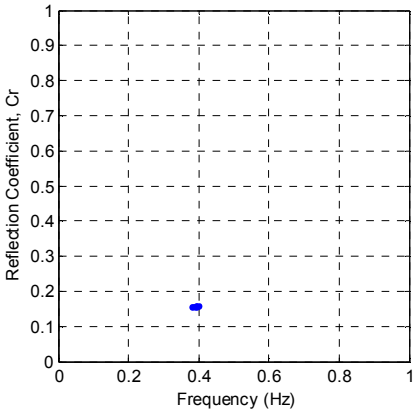

Figure A9.4 Reflection coefficient using probes 3 and 4

Analysis of initiation of motion under waves and wave-current flows

An equilibrium scour depth was not obtained for many of the preliminary wave tests and some of the wave-current tests, due to measurement technique issues, general bed lowering in live bed conditions, or because little or no scour occurred. Instead of focusing on the equilibrium scour depth, one way in which these tests can be interpreted is to consider the conditions for initiation of scour under wave and wave-current flows. In Table A9.2 the key parameters for the wave and wave-current tests are listed along with whether scour occurred. Only those tests conducted in the coarse sand are included as these have the lowest θ/θ_{crit} parameter and because the majority of the preliminary wave tests were conducted in the coarse sand.

According to Sumer et al. (1992) in the live bed regime scour is not expected to occur if the KC number for the wave component of the flow is less than 6. However, some authors have reported small amounts of scour at lower KC numbers (Baglio et al. (2001); Sumer and Fredsøe

(2001b); Sumer and Fredsøe (2002b); Larsen et al. (2004); Khalfin (2007)). In comparison, the data in Table A9.2 does not show a clear link between the initiation of scour and the KC number for the wave. Scour occurs in some of the tests with KC<6, and scour does not occur in some of the tests with KC>6. Using the combined KC number for wave-current flows gives a better fit to the expected relationship between scour threshold and KC number, as KC_{wc} is consistently greater than 6 in Table A9.2 for the wave-current cases in which scour occurred. Therefore, KC_{wc} may be a more suitable parameter for describing the wave-current tests. Using this parameter, the wave and wave-current tests in the live bed regime in Table A9.2 also fit with the criteria for scour occurring only if KC>6.

For the clear water tests in Table A9.2 the threshold for scour appears to be more dependent on the θ/θ_{crit} parameter than on the KC number so that scour does not initiate in some cases with higher KC but low θ/θ_{crit}.

For the wave tests at very low KC numbers and low θ/θ_{crit} parameters where a small amount of scour still occurred, this may be linked to diffraction effects. Sumer and Fredsøe (2001b) found that in the diffraction regime scour was induced by steady streaming effects when KC equalled approximately 1 and $0.15<D/\lambda<0.27$. For the two tests with KC=1.4 the D/λ parameter shown in Table A9.2 is in the right range for steady streaming. According to Sumer and Fredsøe (2001b) the steady streaming results in a significantly larger wave induced velocity near the pile, so that scour will initiate at a lower value of Shields parameter calculated from the far stream flow velocity.

Table A9.2 Comparison of parameters in preliminary and main wave and wave-current tests in uniform coarse sand

Test	U_c	U_m	KC wave	KC combined	θ	θ_{crit}	D/λ	Regime	Scour?
C.90.16 Wave-current (coarse, 90mm pile)	0.24	0.24	5.3	10.6	0.11	0.03		live	yes
C.20.16 Wave only (coarse, 90mm pile)	-	0.24	5.3	-	0.09	0.03		live	no
C.90.20 Wave-current (coarse, 20mm pile)	0.225	0.24	23.7	46.2	0.11	0.03		live	yes
C.20.20 Wave only (coarse, 20mm pile)	-	0.24	23.7	-	0.09	0.03		live	yes
C.50.22 Wave only (coarse, 50mm pile)	-	0.09	4.5	-	0.02	0.03	0.01	clear	no
C.20.22 Wave only	-	0.09	11.3	-	0.02	0.03	0.004	clear	no

(coarse, 20mm pile)									
C.50.26 Wave+2.5%current, Coarse, 50mm pile	0.045	0.09	4.5	6.8	0.02	0.03		clear	Yes (just)
C.50.27 Wave+4.8%current, Coarse, 50mm pile	0.092	0.09	4.5	9.1	0.02	0.03		clear	yes
C.50.28 Wave+6.9%current, Coarse, 50mm pile	0.135	0.09	4.5	11.3	0.02	0.03		clear	yes
C.90.8 coarse sand wave-current	0.28	0.13	3.7	11.9	0.06	0.03		live	yes
C.90.3 wave, coarse sand, 90mm	-	0.04	0.9	-	0.01	0.03		clear	no
C.90.4 wave, coarse sand, 90mm	-	0.04	1.4	-	0.01	0.03	0.015	clear	Just about
C.20.4 wave, coarse sand 20mm	-	0.04	6.4	-	0.01	0.03	0.003	clear	Yes just
C.90.5 wave, coarse sand 90mm	-	0.07	1.4	-	0.02	0.03	0.03	clear	Just about
C.20.5 wave, coarse sand, 20mm pile	-	0.07	6.4	-	0.02	0.03	0.006	clear	Yes

Appendix 10 - Velocity data

Estimating bed shear stress from LDV velocity profiles in the small flume

Bed shear estimates were obtained by plotting the velocity profiles on a semi-log plot and measuring the gradient of the straight line section of the data. The bed shear stress is then estimated using the following equation:

$$u(z) = \frac{2.3u^*}{\kappa}\log_{10}(z/z_0) \quad \text{(A10.1)}$$

Where u* is the shear velocity, κ = 0.4, z is the depth in the water column and u(z) is the average velocity at depth z in the water column. This equation is rearranged to obtain the shear velocity and hence the bed shear stress from

$$\tau = \rho u^{*2} \quad \text{(A10.2)}$$

A typical fitted line to obtain the gradient for computation of bed shear stress is shown in Figure A10.1.

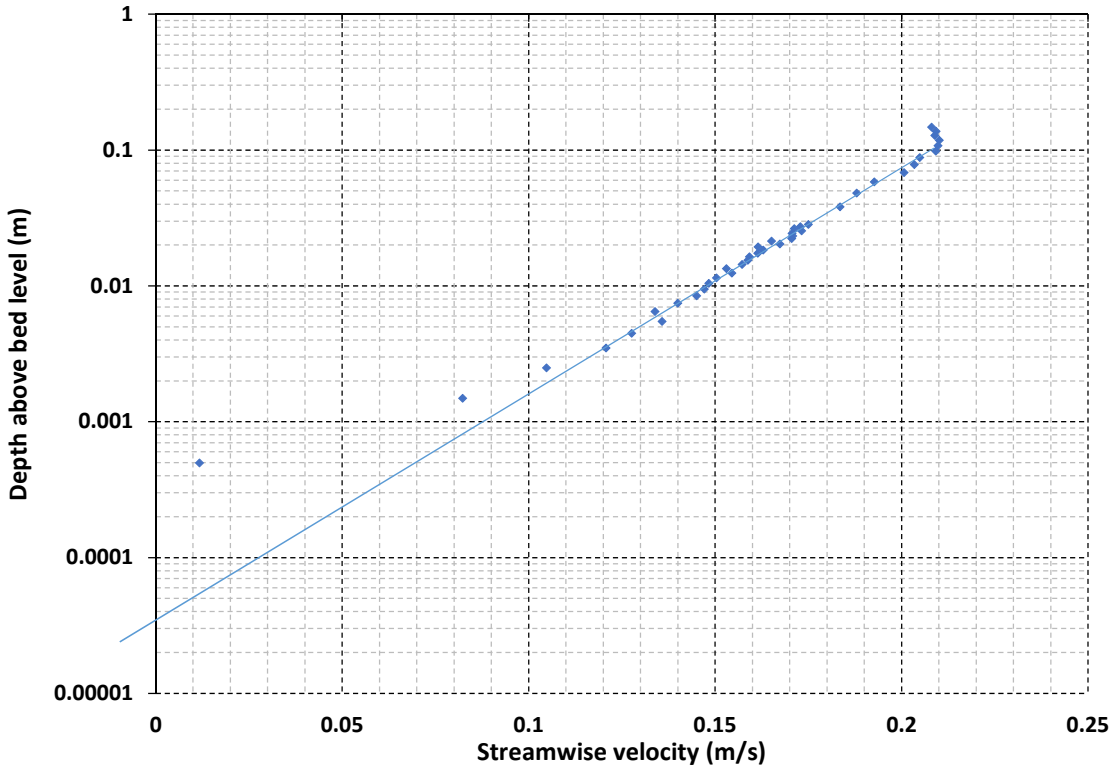

Figure A10.1 Estimate of bed shear stress from LDV data.

Comparison of LDV and ADV measurements in the small flume

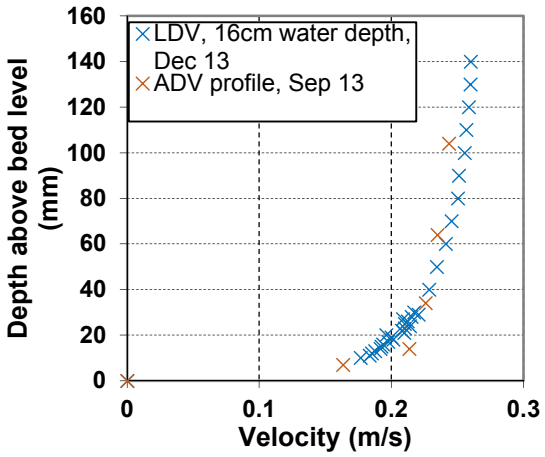

Figure A10.2 Velocity profiles for tests R.19-R.29 measured with LDV and ADV systems.

Figure A10.2 makes a comparison of LDV and ADV velocity profiles measured in the small flume. The resolution is significantly lower using the ADV technique, and the close proximity to the flume walls due to the small scale of the facility resulted in significant noise in the signal. However, the agreement is reasonable between the ADV and LDV measurements.

Preliminary velocity measurements

Note that the velocity profiles for the very first set of tests in the small flume, tests R.1-R.3, were collected with an impeller meter, prior to establishing a preferred methodology for velocity profiling using the LDV system. It was later discovered that the instrumentation was set in cm/s rather than in Hz, and it was unknown if the conversion parameters were correct for the probe used. Therefore, for this first set of tests an estimate of the depth-averaged velocity was made based on a comparison of all of the scour data from this test programme and the expected results from the literature (see Figure 7.1 in Section 7).

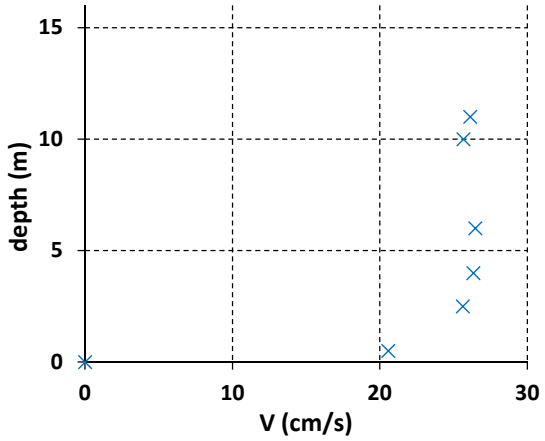

Figure A10.3 ADV velocity profile for tests R.4-R.9

The velocity profile for the second set of preliminary tests completed in the small flume (test series P-2) were collected with an ADV probe. Figure A10.3 shows one of the velocity profiles taken prior to the tests. It was found that the ADV probe was not ideal for use in this flume due to the substantial amount of noise in the signal, even with heavily seeded flow. Therefore, this profile is only an estimate of the flow condition, but is included because for this set of tests this was the primary method of flow measurement. As a result of the noise issues in the ADV signal, future test series in the small flume used the LDV system. Note also that the ADV probe cannot be positioned to measure the top 5 cm of the water column due to the instrument configuration.

Preliminary large flume tests

Note that the ADV signal quality was very poor for the first test (C.90.1) conducted in the larger flume. For the reversing current test, C.90.9, the ADV signal quality was improved and Figure A10.4 shows the average velocity in each half cycle of the test. The slower flow in the negative direction under the same motor percentage is apparent, and this was accounted for in future reversing flow tests by adjusting the motor speed until the velocity profiles matched in both flow directions. The reduction in flow velocity in the final negative half cycle is linked to a change in the position of the mesh covering the inlet for this initial set of tests which was removed for subsequent testing. For this reason this test was not considered in the main analysis.

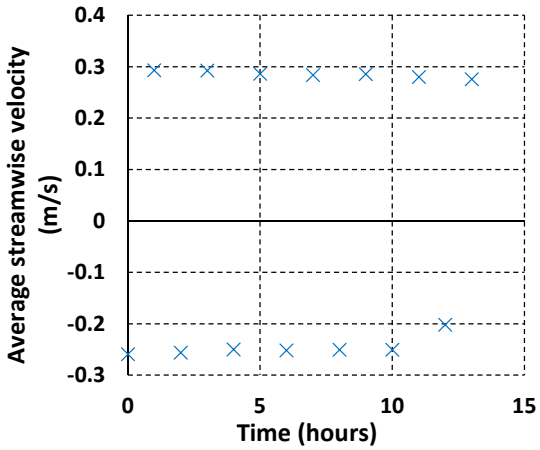

Figure A10.4 Average velocity in each half cycle of test C.90.9 in reversing flow.

Tidal signal calibration

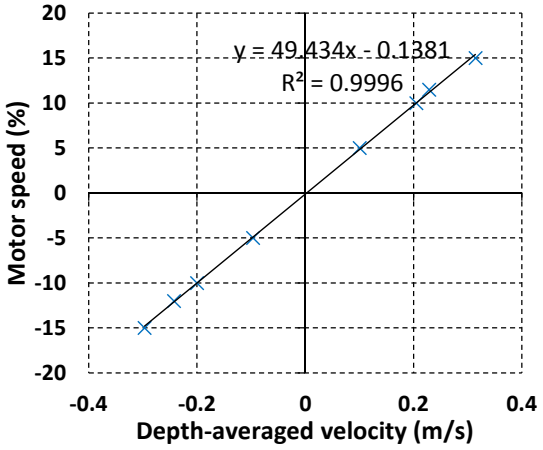

Figure A10.5 Calibration of motor speed with depth-averaged velocity measured in flume.

Comparison of measured velocity with design velocity for spring-neap tidal tests

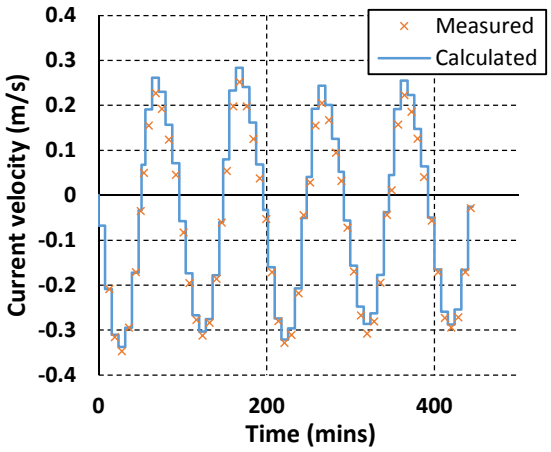

Figure A10.6 Comparison of design flow velocity with measured flow velocity during spring-neap test.

Figure A10.6 shows a comparison of the measured velocity at the depth-averaged position compared to the design velocity obtained from calibration of the motor speed during the first 4 cycles of one of the spring-neap tests. The fit is quite reasonable, although there is some deviation, with the positive velocities generally showing lower values than the predicted signal. However, it should be noted that the quality of the ADV signal was not as high for much of the test compared to the pre-test calibration because the addition of a large quantity of seeding would reduce visibility too much for the scour depth to be observed. Secondly the ADV was positioned downstream of the pile during the negative flow direction half cycles and the pile wake would affect the measurements. In the positive flow direction the ADV probe was far upstream so as not to disturb the scour downstream of it. As a result the flow may not be fully developed or representative of the flow at the scour hole location.